

# **Environmental Science and Technology**

**(2016)**

**Volume 1**

Edited by

**George A. Sorial  
Jihua Hong**

ISBN 978-1-5323-2259-4

Library of Congress Cataloging-in-Publication Data

Environmental Science and Technology 2016 Vol. 1

Proceedings from the 8th International Conference on Environmental Science and Technology, held on June 6-10, 2016 in Houston, Texas, USA

Includes bibliographical references

ISBN: 978-1-5323-2259-4

I. Sorial, George A.

II. Hong, Jihua

III. International Conference on Environmental Science and Technology  
(8th : 2016 : Houston : Texas)

Printed in the United States of America

Copyright © 2016 American Science Press. All rights reserved. This document, or parts thereof, may not be reproduced in any form without the written permission of the American Science Press. Requests for permission or further information should be addressed to the American Science Press, 9720 Town Park Dr. Ste. 18, Houston, TX 77036, USA

Email: [press@AASci.org](mailto:press@AASci.org)

Website: [www.AASci.org/conference/env](http://www.AASci.org/conference/env)

ISBN 978-1-5323-2259-4

© 2016 American Science Press

# **Environmental Science and Technology (2016)**

**Volume 1**

Edited by

George A. Sorial  
Jihua Hong

American Science Press, Houston, USA

# TABLE OF CONTENTS

## INTRODUCTION

<i>George A. Sorial and Jihua Hong</i> .....	1
--	---

## PLENARY SESSION

Geological and Anthropogenic Imprints on Ground Water Quality: Beware of the Anecdotal Models. <i>Barry J. Hibbs</i> .....	4
Who is Responsible for the Environment? <i>Erica Schoenberger</i> .....	5
The Future of Human Environment and Health: Sustainability through Integrated Approach. <i>Momoh A. Yakubu</i> .....	6
Manufactured Nanomaterials: New Emerging Contaminants and Their Potential Impact to Drinking Water Resources. <i>Endalkachew Sahle-Demessie</i> .....	7

## WATER POLLUTION AND WATER QUALITY

### *Rivers, Lakes and Estuary Systems*

Sustainable River bank Erosion Management by Soft Engineering Approach: A Case Study of the Brahmaputra. <i>Prashanta Kumar Bordoloi</i> .....	9
Freshwater Mussels of the Upper San Antonio River Watershed and Lower Cibolo Creek in Bexar, Guadalupe, Wilson, and Karnes Counties: Abundance and Densities. <i>Larry Larralde</i> .....	10
Bioaccumulation of Arsenic, Cadmium, Mercury, and Lead in Fishes of the Daliao River Estuary, China. <i>Chunye Lin, Kai Lei, Deqi Jiao, Mengchang He</i> .....	12
Nitrification and Denitrification by Algae-Attached and Free-Living Microorganisms during Cyanobacterial Bloom in Lake Taihu. <i>Xiaofeng Chen, Haiyang Jiang, Liuyan Yang</i> .....	13

### *Watershed Management*

Tailings Storage Facilities and Environmentally Sustainable Mining. <i>Erica Schoenberger</i> .....	14
State Approaches to Watershed-Based Permitting. <i>Danielle Stephan, Greg Currey</i> .....	15
Rain Harvesting for Sustainable Watershed Management – Local Water Supply and Regional Water Quality Improvement. <i>Neal Shapiro</i> .....	16
Impact of Watershed Management Activities in Land Use Pattern and People's Livelihood in Nepal. <i>Ajay Karki</i> .....	17

### *Water Resources and Assessment*

Natural Attenuation of Indicator Bacteria in Natural Water Systems. <i>Amin Kiaghadi and Hanadi S. Rifai</i> .....	18
--	----



Survey of Physical-Chemical Quality of Superficial Waters at the Surrounding Area of the Sebkha Basin (Moknine, Tunisia). <i>Taoufik Naamoun</i> . ....	25
Assessment of Water Balance in the South-West Coastal Region of Bangladesh. <i>Nepal C Dey, Mohmood Parvez, Nur A. Khondaker</i> . ....	26

### Groundwater

Application of Water Quality Index for Groundwater Quality Assessment of Nanded Tehsil, (M.S.) India. <i>Vasant Wagh, Dipak Panaskar, Ranjitsinh Pawar, Aniket Muley and Shrikant Mukate</i> . ....	27
Hydrochemical Characterization of Groundwater in Bhokar Taluka of Nanded District, Maharashtra, India. <i>Dipak B. Panaskar, Vasant M. Wagh and Ranjitsinh S. Pawar</i> . ....	32
Modelling of Arsenic Removal from Groundwater by Electrodialysis. <i>Rose Marie O. Mendoza, Meng-Wei Wan, Chi-Chuan Kan, Maria Lourdes P. Dalida</i> . ....	39
Phosphate Removal from Synthetic Groundwater by Mixed Algae Culture. <i>Eda Tuna Öztürk, Güneş Özden, and Serdar Göncü</i> . ....	51
Groundwater Pollutant Loading in Urban Watersheds along Lined and Unlined Channels. <i>Barry Hibbs</i> . ....	56

### Drinking Water

Arsenic Content in Drinking Water and Occurrence of Cancer in Nalbari and Kamrup District, Assam. <i>Dipali Das Deka and Jogen Chandra Kalita</i> . ....	57
Simultaneous Nitrate and Phosphate Removal from Drinking Water Using Immobilized Polyethyleneimine. <i>Enrico T. Nadres, Debora F. Rodrigues</i> . ....	62
Suspended Bacteria Community of Processing Units in the Typical Drinking Water Treatment Plant of China. <i>Weiying Li, Feng Wang, Junpeng Zhang and Wanqi Qi</i> . ....	63
Full-Scale Studies of Factors Related to Biological Stability of Water Distribution System in South China. <i>Weiying Li, Junpeng Zhang, Feng Wang and Wanqi Qi</i> . ....	64
Options for the Removal of Arsenic from Drinking Water in Rural Areas of Bihar, India. <i>Nityanand Singh Maurya, Astha Kumari, Sudhir Nigam</i> . ....	65
Pond-Wetland Complexes as Processor of Drinking Water Source. <i>Weidong Wang and Chengqing Yin</i> . ....	66
Interaction between Hydrolysis and Flocculation, and Its Influence on Generation of Disinfection By-Products with Aluminum. <i>Hong Shen, Xin Chen, Hongbin Chen</i> . ....	67
Defluoridation Potential of Vermiculite Modified with Hexadecyltrimethylammonium. <i>Tayo Oladipo Ologundudu, John Ogony Odiyo, Georges-Ivo Ekosse</i> . ....	68

### Water Quality Assessment/Management

Evaluation of Water Quality of the ASI (Orontes) River between 1997 and 2008. <i>Hasan Goksel Ozdilek, Mustafa Kemal Sangun, Ziya Sedat Çetiner</i> . ....	69
Water Quality Assessment for Melen Watershed in the Marmara Region, Turkey. <i>Atilla Akkoyunlu, Ersin Orak</i> . ....	77
Analysis of Elevated Concentrations in Trace Elements and Nutrients in Urban Creek. <i>Michael Harrison and Barry Hibbs</i> . ....	84
Influence of Pollutant Process Uncertainty on the Prediction of Stormwater Quality in Urban Catchments. <i>Buddhi Wijesiri, Prasanna Egodawatta, James McGree, Ashantha Goonetilleke</i> . ..	89

Contaminant Reduction by Pervious Concrete Pavement and Bamboo Bioretention Basin. <i>Vincent Hwang, Amber Masters, Evelyn Montalvo, Sangchul Hwang.</i> .....	95
Toxicology of Azo Dyes with Respect to Their Metabolically Produced and Chemically Related Aromatic Amines. <i>King-Thom Chung</i> . .....	96
Significance and Application of the Global Drinking Water Quality Index: Lebanon Case Study. <i>Mey Jurdi, Sami Ramia, Samira Korfali, Nabil Amacha, Joumana Nasr, Rola Ajib and Sara Chehab.</i> .....	97
Coliform Counts and Plankton Species in Lawaye River, Batangas as Indicators of Pollution. <i>Natividad F. Lacdan, Jose Rafael L.Lopez, and Renz Michael F.Pasilan.</i> .....	98

### ***Nitrogen-Phosphorus Wastewater Treatment / Sludge Treatment***

Effects of Supersaturation Control Strategies on Hydroxyapatite (HAP) Crystallization Process for Phosphorus Recovery from the Wastewater. <i>Hongliang Dai and Xiwu Lu.</i> .....	99
Phytoremediation of Nutrient-rich Wastewaters Using Duckweed. <i>Summer Lentini, Emily Smith, David Petrik, and Sara Arana.</i> .....	110

### ***Sludge Treatment***

Effects of Anaerobic Digestion on the Combustion of Sewage Sludge. <i>Emrehan Berkay Çelebi, Aysegül Aksoy and F. Dilek Sanin.</i> .....	111
Change of pH and ORP with Applied DC on Leachate Activated Sludge, <i>Gülizar Kurtoğlu Akkaya, Elif Sekman, Selin Top, Senem Yazici Guvenc, Ece Sagir, Mahir Ince and Mehmet Sinan Bilgili.</i> .....	116
Combustion 641. Characteristics and Kinetics of the Pulping Effluent Sludge using Thermogravimetric Analysis. <i>Kanhaiya Lal, Anurag Garg.</i> .....	117
Reduced Sludge Growth at High Bulk Liquor DO Induced by Increased Maintenance. <i>Anwar Khursheed, Meena Sharma, Rubia Z. Gaur, Abid Ali Khan, Vinay Kumar Tyagi, A. A. Kazmi...</i> .....	118
Effect of Thermal-alkaline Pretreatment on Microbial Communities in an Anaerobic Digestion of High-solid Sludge. <i>Wang Tao, Gao Peng, and Dai Xiaohu.</i> .....	119
Efficient Anaerobic Production of Volatile Fatty Acids from Sewage Sludge by Alkyl Polyglucose. <i>Jingyang Luo, Leiyu Feng, Yinglong Su, Yinguang Chen.</i> .....	120

### ***Municipal Wastewater Biotreatment***

Pretreatment Performance of a Novel AWFR for Decentralized Domestic Wastewater. <i>Juan-hong Li, Xi-wu Lv.</i> .....	121
A Comparative Study on Light Grey Water from Buildings with Different Functions. <i>Giresunlu, E., Beler-Baykal, B, Afacan, E.</i> .....	127
A Pilot-Scale Study of a Modified Wastewater Treatment Process Using the Sludge Reduction Effect. <i>Chenyi Shi, Yushan Wang, Xiang Wei, Wuzhen Guo, Meishan Lin, Jinxin Tan and Lianpeng Sun.</i> .....	134
Dissolved Methane Recovery from Anaerobic Attached Growth Reactor Treating Synthetic Domestic Wastewater. <i>Brian Crone, George Sorial, Jay Garland.</i> .....	140
A Novel and Cost-Effective Sewage Treatment Process with Energy Recovery and Autotrophic Nitrogen Removal. <i>Dawen Gao.</i> .....	141
Enrichment of Denitrifying Methanotrophic Bacteria of the NC10 Phylum from Activated Sludge. <i>Shubham Singh and Jih-Gaw Lin.</i> .....	142

### Industrial Wastewater Biotreatment

Surface Engineered Green Polymers for Enhanced Water Decontamination. <i>Moushumi Ghosh</i> . .....	143
Volatile Fatty Acid Production during Acidification of Olive Mill Wastewater, <i>Havva BAG, Secil ERDEM, Canan Can Yarimtepe, Orhan Ince and Nilgün AYMAN OZ</i> . .....	154
Decolorization of Anaerobically Digested Molasses Spentwash by Fungal Strain: Isolation and Screening of Strains. <i>Mrityunjay Singh Chauhan, Anil K. Dikshit</i> . .....	159
Improvement of Bacterial Biodemulsifier Biosynthesis in Permeabilizing Agent-Enhanced Utilization of Rape Oil. <i>Yuyan Zhang, Kaiming Peng, Yansong Wei, and Xiangfeng Huang</i> . .....	160

### Adsorption/Desorption for Wastewater Treatment

Surfactant Removal by Metal Oxides and Adsorbilization of Organics in Exhausted Material. <i>Suman Koner, Anjali Pal, Asok Adak</i> . .....	161
A Comparative Study on Production of Activated Carbon from Hardwood Chips and Pellets. <i>Hafiz Ahmad, Jordan Mayers and Brandon Madden</i> . .....	167
Molecular Simulation and Validation Studies of Resorcinol Adsorption on Ordered Mesoporous Carbon. <i>Bing Chao, Zaki Uddin Ahmad, and Daniel Dianchen Gang</i> . .....	173
Phenol Removal from Water Using Biochar and Activated Carbon from Albizia: An Invasive Plant Evaluation. <i>Hafiz Ahmad, Korhan Adalier, Brandon Madden and Douglas Brown</i> . .....	179
Experimental Study of Congo Red and Direct Red 80 Adsorption from Water onto Carbon Nanotubes. <i>Madhu Agarwal and Priti Kumari</i> . .....	185
Copper (II) Biosorption Characteristics of A Novel Biosorbent Combination: Fungus and Agriculture Waste. <i>Jingyao Wang and Chongwei Cui</i> . .....	191
Sun-Coral Powder as Adsorbent for Phosphorus Removal in Wastewater. <i>M.T.G Vianna and Marcia Marques</i> . .....	199
Comparative Study of Adsorption of Dyes onto Activated Carbon and Chitosan Impregnated Activated Carbon. <i>Pratyusha Reddy Reddy, George A. Sorial</i> . .....	206
Natural Iron-Based Material As a Cost-Effective Solution for the Treatment of Arsenic Contaminated Waters from Gold Mine. <i>Małgorzata Szlachta and Patryk Wójtowicz</i> . .....	207
Conversion of Black Liquor into Activated Carbon for Ciprofloxacin Removal from Wastewater. <i>Anirudh Gupta</i> . .....	208
Multiwalled Carbon Nanotubes as a Novel Solid-Phase Extraction Adsorbent for TPH Determination in Contaminated Water. <i>Akinpelu A Adeola, Ilyas Muhammad, Ahsan M Shemsi</i> . .....	209
Ammonia Nitrogen Adsorption by Zeolite and Wetland Soils Under Different Temperatures. <i>Wei Huang and Weidong Wang</i> . .....	210
Heterogeneous catalytic degradation of acetaminophen and simultaneous oxidation/adsorption of arsenite by Cu-Zn-Fe-LDH <i>Hongtao Lu, Zhiliang Zhu, Jianyao Zhu</i> . .....	211
Electrospraying <i>Saccharomyces cerevisiae</i> Immobilized Onto Composite Nanofibrous Mats for Heavy Metals Adsorption. <i>Hongbing Deng, Xiaodan Qiu, Zhaoyang Zeng</i> . .....	212
Synergistic Adsorption and Degradation of Aqueous Contaminants Using Magnetic Mesoporous Adsorbent. <i>Yaocheng Deng, Lin Tang, Jingjing Wang</i> . .....	213

### Physico-chemical Wastewater Treatment

Persulfate activation in the Presence of Formic Acid for Carbon Tetrachloride and Chromium (VI) Removal. <i>Xiaogang Gu and Shuguang Lu</i> . .....	214
---	-----

Enhanced Settling of Suspended Solids in Olive Mill Wastewater by Application of High Frequency Ultrasound . <i>Alev Cagla Uzun, Nilgün Ayman Oz and Canan CAN YARIMTEPE</i> . ....	220
Study of a Fluidized Bed Reactor for Phenol Photocatalysis. <i>Guillermo Rincon and Enrique La Motta</i> . ....	225
Development of BiVO <sub>4</sub> Photoanode for Degrading Pollutants. <i>Qin Shi, Hui Wang, and Zhaoyong Bian</i> . ....	226
Optimization of Operating Parameters on Reactive Black 5 Dye Removal by Electrocoagulation Process and Energy Consumption. <i>Mook Wei Tze, Mohamed Kheireddine Aroua and Małgorzata Szlachta</i> . ....	227
Quartz Sand Filter Medium for Oily Wastewater by Hydrophobic Modification. <i>Wei Bigui</i> . ....	228
Construction of Fe-TAML Activator Systems to Degrade Sulfur-Containing Contaminants in Waters. <i>Qingquan Liu and Xiyun Cai</i> . ....	229
p-AgI Anchored on n-Bi <sub>2</sub> O <sub>2</sub> CO <sub>3</sub> Sheets by Co-Crystallization with Excellent Photocatalytic Performances under Visible Light. <i>Lili Zhang, Chun Hu</i> . ....	230
Cost Analysis of Electro Dialysis Cell for Desalinating Brackish Water. <i>Naglaa M. Eid</i> . ....	231
Mixed Metal Oxides Derived from Ce-Doped Zn-Al Layered Double Hydroxide: Synthesis, Characterization and Photocatalytic Activity. <i>Jianyao Zhu, Zhiliang Zhu, and Hongtao Lu</i> . ...	232
A Novel Process by A Small Molecule Enhanced Effective Degradation for Methyl Orange Dye in Aqueous Solutions under UV-VIS Irradiation. <i>Jingjing Wang, Renbi Bai</i> . ....	233
Physico-Chemical Qualities of the Treated Final Effluent Discharges of Some Wastewater Treatment Plants in Buffalo City Municipality, Eastern Cape, South Africa. <i>T Kulati, OO Okoh and AI Okoh</i> . ....	234
Application of Electrohydrolysis Process for Vinegar Wastewater and Municipal Wastewater Mixture. <i>Faruk Hakan Canbaz, Canan Can YARIMTEPE, Rabia ERARSLAN, Elif ERDOGAN and Nilgun Ayman OZ</i> . ....	235

### Reactions and Degradation of Wastewater Contaminants

Removal and Degradation Pathway of Sulfamethoxazole from Municipal Wastewater Treatment by Anaerobic Membrane Bioreactor. <i>Chun-Hai Wei, Claudia Sanchez Huerta, and TorOve Leiknes</i> . ....	236
OH Radical Formations in Phyto-Fenton Reactions: Detection and Application, <i>Shigeki Nara, Yoshihiko Inagaki and Yutaka Sakakibara</i> . ....	242
Continuous Treatment of Wastewaters Containing PPCPs by an Electrochemical Advanced Oxidation Process, <i>Junya Suzuki, Eiji Kawada, Taiki Maehata and Yutaka Sakakibara</i> . ....	247
Acute Toxicity of Graphene Nanoplatelet to Bacterial Communities in Activated Sludge. <i>Hang Ngoc Nguyen and Debora Frigi Rodrigues</i> . ....	253
Isolation of Bacteria from Lake Waters Associated with Wastewater Effluents Capable of Degrading Various Pharmaceuticals. <i>Noreen Gallagher and Dr. Jeff Lodge</i> . ....	254
Characterization and Quantification of DOM in Wastewater and its Interaction with Pharmaceuticals. <i>Sanjeeb Mohapatra, Neha Sharma, Suparna Mukherji and Lokesh P. Padhye</i> . ....	255
Deep Insights into the Mechanism of 2,4-Di-tert-butylphenol(2,4-D) Degradation by Using UV/persulfate with a New Model. <i>Qiongfang Wang, Yisheng Shao, Naiyun Gao and Xiang Shen</i> . ....	256

### Nanotechnology Applications

Removal of Estriol in Water Using Sequentially Coupled Membrane Filtration/TiO <sub>2</sub> Photocatalytic Processes. <i>Irwing Ramírez, Ashantha Goonetilleke, Erick R. Bandala</i> . ....	257
---	-----

Study on the Influence of Addition of Acids on Particle Size and Surface Area of Titanium Dioxide Photocatalyst. <i>Padmini Ellappan and Lima Rose Miranda</i> . ....	263
Interaction of Engineered Materials with Microbial Biofilms and Its Potential Applications. <i>Hengye Jing, George A. Sorial, and Endalkachew Sahle-Demessie</i> . ....	269
Understanding the Formation of Naturally Occurring Silver Nanoparticles in Aquatic Environment. <i>Nathaniel F. Adegboyega</i> . ....	270
Optimized Synthesis of Polymer-based Graphene Oxide Nanocomposites for Heavy Metal Adsorption using Response Surface Methodology. <i>Jem Valerie D. Perez and Maria Lourdes P. Dalida, Debora F. Rodrigues</i> . ....	271
Organic Radical Intermediate-Sparked Highly Fenton-Catalytic Efficiency of Dandelion-Like TiCuAl-SiO <sub>2</sub> Nanospheres from Organic Contaminant Degradation. <i>Lai Lyu, Lili Zhang, and Chun Hu</i> . ....	272
Electrospun Rectorite/TiO <sub>2</sub> /Polymer Nanofibrous Mats for Adsorption of Heavy Metals, <i>Yingfei Zhan and Hongbing Deng</i> . ....	274
Multifunctional Graphene-Based Nanocomposite Modified Membrane Filters for Heavy Metals and Bacteria Removal from Water. <i>Yvonne Ligaya F. Musico and Maria Lourdes P. Dalida, Debora F. Rodrigues and Catherine M. Santos</i> . ....	275
Study on the Photocatalytic Degradation of Microcystins by TiO <sub>2</sub> Immobilized on Fiberglass Cloth. <i>Deqiang Chen, Yiqun Chen</i> . ....	276
Electrospun Carbon Nanofibers with Zero Valent Iron Nanoparticles (ZVINPs@ECNFs) for Heavy Metals Remediation in Ground and Wastewater. <i>Nikhil. R. Mucha, Ramesh Ravella, Muchha, R. Reddy, Lifeng Zhang</i> . ....	277

## AIR POLLUTION AND AIR QUALITY CONTROL

### Aerosol

PM <sub>2.5</sub> Chemical Constituents at Rural Site, Agra in Indo-Gangetic Plain: Sources and Transport. <i>Aparna Satsangi, Nidhi Verma, Anita Lakhani, K. Maharaj Kumari</i> . ....	279
An Innovative Approach to Use MODIS AOD Data for PM <sub>2.5</sub> Monitoring. <i>Zhiming Yang, Harris Williams</i> . ....	286
Study on Aerosol Formation Properties in Ammonia-based WFGD Processes. <i>Huang Rongting, Pan Danping, and Yang Linjun</i> . ....	292

### Air Quality Assessment

Air Flow Simulation around Aircraft. <i>Jianfeng Liu, Baoqing Wang, Ronghui Chen and Zihui Ren</i> . ....	293
Black Carbon and Size-resolved Particle Number Concentrations during Open-field Burning of Corn Straw. <i>Yu-Hsiang Cheng and Li-Sing Yang</i> . ....	297
Integrated Assessment of Particulate Matter in KPK and Baluchistan by Using GAINS- South Asia Model. <i>Sheikh Saeed Ahmad and Aisha Khan</i> . ....	302
Heavy Metals in Road Dust from Xiandao District, Changsha City, China: Haracteristics, Health Risk Assessment and Integrated Source Identification. <i>Jingdong Zhang, Fei Li and Jun Yang</i> . ..	319
Chlorinated Paraffins in Canadian House Dust and NIST SRM 2585 (Organic Contaminants in House Dust). <i>Xinghua Fan, Hongtao Shang, Cariton Kubwabo, and Pat E. Rasmussen</i> . ....	304
Beijing Dust Storm in Spring Season and Its Source Apportionment. <i>Yan-Ju Liu</i> . ....	305

Observable Characteristics of Cloud-To-Ground Lightning Induced NO <sub>x</sub> and O <sub>3</sub> over the PRD Region, China. <i>Yonglin Liu, Xinhui Bi, L. Y. Chan, Qinhao Lin, Leilei Fei, Xinming Wang, Ping'an Peng and Guoying Sheng.</i> .....	306
Atmospheric Aerosol Compositions and Sources at Two National Background Sites in Northern and Southern China. <i>Qiao Zhu, Ling Yan He and Xiao Feng Huang.</i> .....	307
Decreasing Emission Factor of Pollutants in Abadan Refinery by Renovating the Furnace Design. <i>Abbas Zabihi and Mohammad Raazi Tabari.</i> .....	308

### **Transport of Pollutants**

Modelling Ground-Level Ozone Concentration Using Improved Data-Mining Algorithms. <i>S. Mohan and P. Saranya.</i> .....	309
---	-----

### **Waste Gas Control Techniques**

Advanced Buffer Materials for CO <sub>2</sub> Control: Improved Air Quality and Energy Conservation in Commercial Buildings. <i>Pavithra Rajan, Glenn Morrison, Fateme Rezaei.</i> .....	310
Amine Impregnated Activated Carbon is a Novel Material for CO <sub>2</sub> Capture. <i>Dipa Das, Debi Prasad Samal, and B. C. Meikap.</i> .....	320
Catalytic Oxidation of VOCs and CO over Octahedral Layered Birnessites Synthesized by Different Methods. <i>Zhidan Fu, Qing Ye, Heng Lu, Shuiyuan Cheng, Wang Dao.</i> .....	327
Photocatalytic Oxidation of Fuel Vapors: A Novel Method for Reducing Fuel Vapor Emissions from Automobiles. <i>Catherine B. Almquist.</i> .....	328
Synthesis of LiAl <sub>2</sub> -layered Double Hydroxides for CO <sub>2</sub> Capture over a Wide Temperature Range. <i>Liang Huang, Junya Wang, Yanshan Gao, Yaqian Qiao, Qianwen Zheng and Qiang Wang, Zhanhu Guo, Yufei Zhao, Dermot O'Hare</i> .....	329
Novel DeNO <sub>x</sub> and DeSO <sub>x</sub> Technologies for Flue gas Treatment for Boilers and Furnaces. <i>Jian Luo and Qiuhua Zhang.</i> .....	330
Immobilization of Self-Stabilized Plasmonic Ag-AgI on mesoporous Al <sub>2</sub> O <sub>3</sub> for NO Elimination under LED Illumination. <i>Chun He, Xiuqin Tan, Jiawei Zeng, Yaohua Hou, and Dong Shu.</i> .....	331
Target-specific Capture of Relevant Gaseous Pollutants Using Biodegradable Polymeric Nanoparticles. <i>Fernanda Delbuque Guerra, McKenzie L. Campbell, Daniel C. Whitehead and Frank Alexis.</i> .....	332
Water Scrubbing of H <sub>2</sub> S Gas in Dual-Flow Sieve Plate Column Scrubber. <i>Swamy Kurella, Pavan Kishan, Bhukya and B. C. Meikap.</i> .....	333

### **Air Pollutant Monitoring**

Industrial Air Pollution in Saudi Arabia and the Influence of Meteorological Variables. <i>Jamal A. Radaideh.</i> .....	334
Monitoring of Hazardous Atmospheric Releases under Emergency Situation by Radar Tracer Method. <i>Boris S. Yurchak.</i> .....	346
An Alternative On-Line Method for Evaluating Brown Carbon in the Atmosphere. <i>Guohua Zhang, Xinhui Bi, Xinming Wang, and Guoying Sheng.</i> .....	352
Environmental Impact of Biomass Burning For Civil Uses onto a Mountain Area. <i>F. Petracchini, C. Balducci, M. Perilli, A. Cecinato, F. Liotta, V. Paolini, L. Paciucci.</i> .....	353
A Preliminary Assessment of Major Air Pollutants in the City of Urumqi, China. <i>Francesco Petracchini, Angelo Cecinato, Lucia Paciucci, Valerio Paolini and Flavia Liotta.</i> .....	354

Methodologies for a Better Interpretation of the Preliminary Assessment: IAPMS Pančevo. <i>Lucia Paciucci, Francesco Petracchini, Angelo Cecinato, Paola Romagnoli, Valerio Paolini, Flavia Liotta, Francesca Vichi and Micol Biscotto.</i> .....	355
---	-----

### **Hazardous Gas Biofiltration / Catalysts for Reducing Emission**

Biological Treatment of Chloroform in a Controlled Aerobic Trickle Bed Biofilter. <i>Keerthisaranya Palanisamy*, Bineyam Mezgebe and George A. Sorial, Endalkachew Sahle-Demessie.</i> .....	356
Effect of Methanol and Toluene on Removal of Trichloroethylene in a Fungi seeded Biotrickling Filter. <i>Dhawal Chheda and George Sorial.</i> .....	358
Evaluations of the Removal of Trihalomethanes by Two independent Bio-trickling filters under Different Operating Conditions. <i>Bineyam Mezgebe, George Sorial, Keerthisaranya Palanisamy, Endalkachew Sahle-Demessie</i> .....	359
Removal of Vapour Phase Methanol in the Presence of Thiosulphate Using Anaerobic Biotrickling Filter. <i>Mekonnen Maschal Tarekegn, Eldon Raj Rene Jack van de Vossenbergh and Piet N. L. Lens.</i> .....	360
Interface Effects for CO <sub>2</sub> Hydrogenation on Pt <sub>4</sub> /γ-Al <sub>2</sub> O <sub>3</sub> . <i>Yulu Liu, Wanglai Cen and Jianjun Li.</i> ....	361
A Novel SnO <sub>2</sub> -CoO <sub>x</sub> Catalyst for NO Oxidation with H <sub>2</sub> O. <i>Huazhen Chang, Mingguan Li, Junhua Li.</i> .....	362
Environment-Friendly and Highly Efficient Rare Earth Based Catalyst for Selective Catalytic Reduction of NO <sub>x</sub> . <i>Shemin Zhu, Yuesong Shen, Zhiwei Xue, Zhimin Wang.</i> .....	363

### **Fuel Gas DeSO<sub>x</sub>, DeNO<sub>x</sub>, and Metal Removal**

Influence of Fe Loadings on Desulfurization Performance of Activated Carbon Treated By Nitric Acid. <i>Jiaxiu Guo, Song Shu and Xiaoli Liu.</i> .....	364
---	-----

### **Air Pollution Prevention and Management**

Minimizing Environmental Pollution and the effects in Nigeria through Green Design and Green Buildings. <i>Iwuagwu, Ben Ugochukwu; Onyegiri, Ikechukwu; Iwuagwu, Ben Chioma.</i> .....	365
Enhancing the Algal Biohydrogen Production using Flue Gas Derived Bicarbonate and Nutrient Limitation Methods. <i>Sai Sameer Pusapaty and K.Sata Sathasivan.</i> .....	371
How Do Plant Leaves Remove Dust and its Attached Metals on the Roadside of Beijing? <i>Zheng Yang, Yan-Ju Liu</i> .....	379
Future Perspective and Mitigation Options for Atmospheric Mercury (Hg) Emissions in China. <i>Qingru Wu, and Shuxiao Wang.</i> .....	380

## **BIO-ASSESSMENT AND TOXICOLOGY**

### **Human Exposure**

Respiratory System Emergency Service Visits in Adana, Turkey (2007-2011). <i>Ertan KARA, Hasan Göksel ÖZDİLEK, Emine Erman KARA.</i> .....	382
Carcinogenicity and Mutagenicity Assessments of Dietary Exposure to PAHs in Imported Fish Products in Nigeria. <i>Nsikak U. Benson, Akan B. Williams, Winifred U. Anake, Kelechi P. Eke, Adebayo E. Adedapo and Abaas A. Olajire</i> .....	388

Dose Response Curves Derived from Clinical Ozone Exposures Can Inform Public Policy. <i>Sabine Lange, Ge Tao, Lorenz Rhomberg, Julie Goodman, Michael Dourson, Michael Honeycutt.</i> .....	389
Mitochondrial Injury-Regulated Joint Hepatotoxicity Induced by Combined Exposure of PCB77 and Cd. Mitochondrial Injury-Regulated Joint Hepatotoxicity Induced by Combined Exposure of PCB77 and Cd. <i>CUI Jiansheng GAO Yu WANG Lixin.</i> .....	390
Protective Role of Cichorium Intybus against Manganese Toxicity in Liver and Kidney. <i>Ram Prakash</i> .....	391
Urinary Metabolomics Revealed Arsenic Exposure-Related Metabolic Alteration: A Proof-Of-Concept Study in a Chinese Male Cohort. <i>Jie Zhang, Weipan Xu, Heqing Shen.</i> .....	392
Assessing Occupational Exposure in Black Hair Salons. <i>Sarah Lemelman, Raymond Trott, Anna Abrams, Allison Marill, Alexis J. Cooper, Ramya Ramakrishna, Jay Feinstein, Teleah Slater, Annie Fortnow, Cassidy Tatum, Omkar Kulkarni, Sandra Watemberg, Laura J. Goldin, Theodore A. Myatt, Joseph G. Allen, James H. Stewart, Matthew A. Fragala .</i> .....	393
Dioxin-like Rather Than Non Dioxin-Like PCBs Promote the Development of Endometriosis through the Stimulation of Immune-Endocrine Interaction. <i>Qiansheng Huang, Yajie Chen, Sijun Dong.</i> .....	394
Bactericidal and Antioxidant Properties of Essential oils of the Fruits <i>Dennettia tripetala</i> G. Baker. <i>Sunday O. Okoh, B.C. Iweriebor, O.O. Okoh and U.U. Nwodo and A. I. Okoh.</i> .....	395

### **Bio-response and Ecotoxicology**

Aflatoxin Contamination of Some Edible Grains from Lagos and Ota Markets, <i>Nigeria. Mary Oloyede, Akan Williams, and Nsikak Benson.</i> .....	396
Genotoxic Effects of Coal Fly Ash in <i>Trigonella Foenum Graceum</i> (L.). <i>Rucha U. Raval, Kailash P. Patel and Mariya J. Jairajpuri.</i> .....	400
Histological Effects of Bisphenol A on Gills, Digestive Glands and Adductor Muscles of Laboratory-Reared <i>Corbicula fluminea</i> Linn. <i>Kimberly B. Benjamin, Jessmine L. Competente and Dyan Gabrielle H. de.</i> .....	405
Bio-Assessment and Toxicological Effects of Biolarvicides on Target and Non-target Organisms in Rivers State, Nigeria. <i>Wachukwu, C.K., Ollor, O.A., Ganabel, C.B, and Azike, C. A.</i> .....	412
Enantioselective Phytotoxicity of $\gamma$ -Hexabromocyclododecane Enantiomers to Maize. <i>CUI Jiansheng, LIU Ying, WU Tong.</i> .....	413
Effects on Length, Weight and Orientation Responses of Earthworms Exposed to Man-Made Electromagnetic Noise. <i>Şükran Yalçın Özdilek , Sevil Yalçın and Rukiye Altaş.</i> .....	414
Assessment of Pollution Biomarker and Stable Isotope Data in <i>Mytilus Galloprovincialis</i> Tissues. <i>Şükran Yalçın Özdilek and Neslihan Demir.</i> .....	415
Graphene Induced Epithelial-Mesenchymal Transition in A549 Cells <i>In Vitro.</i> <i>Yanyan Liao, Ziyang Zhang.</i> .....	416
Developing an Association Network from Proteome Changes to Root Phenotypic Properties for Aluminum Tolerance in Switchgrass. <i>Mahesh Rangu, Zhuji Ye, Theodore W. Thannhauser, Sarabjit Bhatti, Suping Zhou.</i> .....	417

### **Bioavailability and Bio-accumulation**

Site-Specific Soil Arsenic Bioavailability: the 21 <sup>st</sup> Century Nexus between Site Characterization and Risk Assessment. <i>N.T. Basta, S.D. Whitacre, V. M. Hanley, P. Myers, A.L. Foster, and S.W. Casteel.</i> .....	418
--	-----



Comprehensive Evaluation of in vitro Bioaccessibility Methods to Predict Bioavailability of Arsenic in Contaminated Soils. <i>Brooke N Stevens, Nicholas T Basta, Shane D Whitacre, Aaron R Betts, Kirk G Scheckel, and Karen D Bradham.</i> .....	419
--	-----

### **Microbiology and Microbial Degradation**

Increased Enzyme Activity during Antagonistic Invasion Interaction of Fungi Grown on Corn Cob. <i>Grace Nkechinyere Ijoma, Memory Tekere.</i> .....	420
Anaerobic Biodegradation of Para-Toluene Sulfonic Acid, Sulfanilic Acid and Thiophene-2-Acetic Acid by the Sulfate Reducing Bacterium <u>Desulfovibrio psychrotolerans</u> , Strain JS1 <sup>T</sup> in Liquid Cultures, Soil and Sludge Microcosms. <i>Sasikala, Ch., Sasi Jyothsna, Ch. V Ramana.</i> .....	432
Relation among Triphenyltin Recognition, Degradation, Ion Metabolism and Effective Proteins of <u>Bacillus Thuringiensis</u> . <i>Jinshao Ye and Linlin Wang.</i> .....	444
Bacterial Community Structure Corresponds To Performance in A Microaerophilic Sulfate and Nitrate Co-Reduction System. <i>Xi-Jun Xu, Chuan Chen*, Ai-Jie Wang, Duu-Jong Lee, and Nan-Qi Ren.</i> .....	450
A New AHL Molecule Generated by Nitrite-oxidizing Bacteria. <i>Jie Gao, and Guoqiang Zhuang.</i> .....	451
Evidence of Quorum Quenching and Inhibition of Biofilm Formation in <u>Sphingomonas</u> Spp. <i>Parul Gulati and Moushumi Ghosh.</i> .....	452
Identification of Fungal Endophytes from Maize Shoots with Biotechnological Potential in Agriculture. <i>Mashiane R.A and Adeleke R.A, Bezuidenhout C.C.</i> .....	453
Pectinase from <u>Bacillus subtilis</u> strain Btk-27: Optimizaton of Cultural Conditions and Application in Coffee Processing. <i>Oliyad Jeilu Oumer and Dawit Abate.</i> .....	454



## **INTRODUCTION**

The Eighth International Conference on Environmental Science and Technology 2016 was held in Houston, Texas, USA, June 6-10, 2016. The Program included 16 sections, containing 60 sessions with approximately 600 platform and poster presentations. This conference series strives to provide a platform for an extremely diverse group of environmental topics for engineers and scientists from around the world.

Authors of the presentations accepted for the program were invited to submit their papers to the Conference Organizing Committee. More than 120 papers were received and then reviewed by the editors, session chairs, and the members of the Scientific/Technical Committee of the conference. Those papers and abstracts accepted for publication were assembled into two volumes.

Sections are arranged basically according to their order listed in the original program except the sessions entitled Land (Soil, Waste Solid) Pollution and Remediation. This exception was made to balance the length of the two volumes. The conference also consisted of having a plenary session with four speakers from different universities at the United States and other countries.

Environmental Science and Technology 2016 (Volume 1) contains the following sections:

- Plenary Presentation
- Water Pollution and Water Quality Control
- Air Pollution and Air Quality Control
- Bio-Assessment and Toxicology

Sections included in Environmental Science and Technology 2016 (Volume 2) are as follows:

- Land (Soil, Waste Solid) Pollution and Remediation
- Ecosystem Assessment and Restoration
- Bio-Assessment and Toxicology
- Wetlands and Sediments
- Global Warming and Climate Change
- Metals (Distribution, Removal, Remediation, Speciation, and Phytoremediation)
- Chlorinated and Other Persistent Organic Compounds
- Modeling
- GIS for Environmental Assessment, Database, and Remote Sensing Applications
- Environmental Analysis and Measurements
- Society and the Environment
- Environmental Planning and Management

- Renewable Energy Development

We would like to especially thank the session chairs who were instrumental in the success of the conference. The Conference was sponsored and organized by the American Academy of Sciences, with financial contributions from the co-sponsors and supporting organizations.

The papers in these proceedings represent the authors' results and opinions. No sponsors, cosponsors, participating organizations or editors should be construed as endorsing any specific contents or conclusions in the proceedings.

George A. Sorial, Ph.D.

University of Cincinnati

Jihua Hong, Ph. D.

American Academy of Sciences

## **PLENARY PRESENTATION**

## **GEOLOGICAL AND ANTHROPOGENIC IMPRINTS ON GROUND WATER QUALITY: BEWARE OF THE ANECDOTAL MODELS**

***Barry J. Hibbs***

(Department of Geosciences and Environment, California State University, Los Angeles, 5151 State University Drive, Los Angeles, CA 90032, USA. bhibbs@exchange.calstatela.edu)

Geological and mineralogical associations have been used to determine baseline water quality variations in aquifers for well over a century. Geological factors can be misidentified and misunderstood in establishing water quality relationships in aquifers however, especially in groundwater basins undergoing rapid development. The problem is particularly acute when time series and spatial changes in aquifer water quality occur. Time series and spatial changes in groundwater quality may be related to physical changes in aquifer dynamics that are either natural or anthropogenic.

The effectiveness of a generic, but widely accepted model in explaining water quality in one aquifer may be a weak analog for explaining water quality variations in another, apparently similar aquifer. Too often interpreters grasp at the most simple or apparent explanation for a process based on anecdotal evidence; e.g., "agriculture creates the elevated salinity," "industrial activity is the source of the elevated trace elements in the aquifer." A possible misinterpretation might arise merely on account of the fact that there is substantial agricultural or industrial activity in the groundwater basin. Reasons for misidentifying processes related to water quality is often due to a poor understanding of the geologic history of the groundwater basin, mischaracterization and misidentification of flow processes/hydraulics, and incomplete knowledge of the primary and secondary mineralogical assemblages in the aquifer. Insufficient training in evaluating the geological, hydraulic, and water/rock/soil interactions is another factor that comes into play.

The purpose of this presentation is to summarize our workgroup studies where earlier anecdotal models of water quality did not account for the actual water quality processes in the aquifers. These studies will serve as examples of flagrant risks associated with accepting anecdotal models to explain water quality variations in aquifers.

**WHO IS RESPONSIBLE FOR THE ENVIRONMENT?**

***Erica Schoenberger***

(Department of Geography and Environmental Engineering, The Johns Hopkins University, 3400 N.  
Charles Street, Baltimore, MD 21218, USA. ericas@jhu.edu)

We are all in some sense responsible for the environmental damages humans have inflicted on the earth. At the same time, none of us is exactly responsible for those harms. I contribute to those damages by living my ordinary life, and if I ceased living tomorrow, the harms would continue to accumulate. What is the nature of responsibility in such a situation? What kinds of choices are open to us and how may we tilt the system in the direction of clean and away from dirty?

## **THE FUTURE OF HUMAN ENVIRONMENT AND HEALTH: SUSTAINABILITY THROUGH INTEGRATED APPROACH**

***Momoh A. Yakubu***

(Department of Environmental and Interdisciplinary Sciences, College of Science, Engineering and Technology, Texas Southern University, 3100 Cleburne Avenue, Houston, TX 77004, USA.  
Yakubu\_ma@tsu.edu)

Environmental health concern brings together experts, researchers, scholars and students from diverse backgrounds. These experts are working so hard in their respective fields to protect the human environment from the devastation and calamity that is waiting to befall it. Despite these efforts and colossal resources expended over these years, we are still faced with bad news of the impending doom for the human environment and health. Recently, our young generations are increasingly diagnosed with devastating diseases like dementias, Parkinson, infertility, attention deficit disorder, Alzheimer's, diabetes, etc. at very tender age. Some of these diseases have been linked to the quality of our environment and the increasing concentrations of disrupting chemical in our water. The fear of climate change is real, the recorded increase in global temperature with the attending droughts, heat waves, intense rainfalls resulting in floods, loss of vegetation and deforestations. The oceans are warming up and glaciers are melting with increasing sea levels. All of these attest to this fear. Despite advances in our understanding of our environment and the dangers locking around it – we are still on a crazing speed to self-destruction. There is therefore, the need to harness and integrate the various efforts of environmental-natural scientists along with others and stake holders – activists, government and global agencies, community leaderships, regulators, developed and developing nations to work seamlessly together to protect and sustain the future of human environment. NOW, we have the need to create a new generation of scientists to integrate a rigorous discipline depth with the ability to interact with other disciplines and work in an increasingly interdisciplinary, collaborative team to serve our global and human environment. This is more urgent as knowledge creation and innovation frequently occur at the interface of diverse disciplines.



**MANUFACTURED NANOMATERIALS: NEW EMERGING CONTAMINANTS AND THEIR  
POTENTIAL IMPACT TO DRINKING WATER RESOURCES**

***Endalkachew Sahle-Demessie***

(U.S. EPA, Office of Research and Development, National Risk Management Laboratory, 26 W. Martin Luther King Drive, Cincinnati, OH 45268, USA. Sahle-demessie.endalkachew@epa.gov)

As nanomaterials become increasingly part of everyday consumer products, it is imperative to measure their potential release during production, use, and disposal, and assess their impact on the health of human and the ecosystem. This compels the research to better understand how the properties of manufactured nanomaterials (MNMs) lead to their accumulation and redistribution in the environment whether they could become emerging pollutants or can affect the mobility and bioavailability of other toxins. If nanoparticles are released from their matrix, the high surface to volume ratio and reactivity of MNMs makes them highly dynamic in environmental systems. The resulting transformations of the MNMs affect their fate, transport, and toxic properties. Photodegradation of nanocomposites in the environment during the use or end-of-life could release of MNM. This study aims in better understanding of the human and environmental risks of using consumer products, such as polymer nano-composites.

This presentation focuses on the characterization, occurrence in the environment, detection and analysis, toxicity, fate and transport of MNM and the efficacy of water treatment methods in removing them from drinking water supplies.

**WATER POLLUTION  
AND  
WATER QUALITY CONTROL**

**SUSTAINABLE RIVER BANK EROSION MANAGEMENT BY SOFT ENGINEERING  
APPROACH: A CASE STUDY OF THE BRAHMAPUTRA**

***Prashanta Kumar Bordoloi***

(Department of Civil Engineering, The Assam Kaziranga University, NH37, Karaikhowa, Jorhat-785006,  
Assam, India)

The Brahmaputra River basin (catchments area 924,000 km<sup>2</sup>), the least studied one in Asia, is currently experiencing severe river bank erosion, of its reach 640 km resulting from climatic and ecological changes in the basin. The Brahmaputra valley receives in average 2000mm of rainfall annually, 65% of which is received within four summer months from June to September leading to flooding and erosion of the river banks. Since the formation Task Force Against Erosion in 1964, 0.4 million square kilometer land is eroded by the river causing agony to the inhabitants. Government has taken up hard engineering measure like flood proofing with embankment and deflecting flow from eroded reach by structural measures like spurs with mixed result. Mostly erosion is caused by the auxillary channels. In 2009, soft engineering measures were taken at vulnerable areas of Jhanjimukh for containing erosion to minimum with people's participation with great success. The measure consists of initiation of siltation in the auxiliary channel launching porcupine like RCC fencing post, and planting riverine plants with elasticity property to retard the flow velocity on the eroded reach. Silt deposition has been a continuous process on the eroded reach. Locally available elastic planting materials are planted on the fresh sedimentation on the eroded reach, which is protected by the plants in a sustainable way. This paper discusses the potential of containing river bank erosion with unique soft engineering technique in a sustainable way and its prospect of wider adaptability in the alluvial world.

**FRESHWATER MUSSELS OF THE UPPER SAN ANTONIO RIVER WATERSHED AND  
LOWER CIBOLO CREEK IN BEXAR, GUADALUPE, WILSON, AND KARNES COUNTIES:  
ABUNDANCE AND DENSITIES**

***Larry Larralde***

(San Antonio River Authority, 600 E. Euclid Street, San Antonio, Texas 78283, USA)

Three mussel species under review for federal listing under the United States Endangered Species Act (ESA) and legally threatened in the State of Texas have historically been found in the San Antonio River (SAR) basin. One species, golden orb *Quadrula aurea* has been recently found in numerous locations in the San Antonio River and its tributaries (Lower Cibolo Creek). Previous efforts to survey the lower Cibolo Creek watershed began in the early 1990's and no records have been located regarding the West Side Creeks. Therefore, the San Antonio River Authority (SARA) proactively decided that basin wide monitoring efforts be implemented as soon as possible.

Sample data included baseline demographics such as density, richness, diversity, and age-class structure for the native mussel community. Data will be collected and distributed to regulatory agencies to assist in the decision making process for listing or delisting candidate species of concern. Sample efforts for 2014-2015 included the West Side Creeks of the Upper San Antonio Watershed from the Texas Commission on Environmental Quality (TCEQ) segment 1911, and the Lower Cibolo Creek, TCEQ segment 1902. Quantitative sample methods (Systematic Sampling) were implemented with a 0.25m<sup>2</sup> quadrat and catchment along with qualitative timed visual and tactile searches conducted at 46 collection sites across five lower Cibolo Creek sample reaches.

Qualitative-catch-per-unit-efforts (CPUE no. /h) under visual timed searches was the preferred and only method utilized for the West Side Creeks. Qualitative results from all four creeks yielded one native mussel species, paper pondshell *Utterbackia imbecillis*, from Martinez Creek. The CPUE for Martinez creek was 0.83/h., and overall, five live specimens were collected with a CPUE estimate of 0.26/h mussels for all four creeks. The total area searched and total search time were 2,762m<sup>2</sup> over 19 search hours. Quantitative results from lower Cibolo Creek yielded a total of eighty – one observed individuals and a population(s) estimate (n=78) representative of five native species (species richness, n=5), yellow sandshell *Lampsilis teres* (n=38), golden orb *Quadrula aurea*, (n=32), paper pondshell *Utterbackia imbecillis* (n=3), pistolgrip *Quadrula verrucosa* (n=7), and Louisiana fatmucket *Lampsilis hydiana* (n=1). Non-native asian clam, *corbicula* spp. were common across all reaches. Species richness per site ranged from 0 - 2 species at 0.83 ± 0.12 (mean ± SE), with the highest (2 spp.) occurring at 10 sites and the lowest (no catch) at 22 sites. Species richness in quadrat samples and species richness in timed searches were found to be significantly correlated (Spearman's rho, r=0.36, P = 0.01). The range of quadrats per sample site (n = 13-17) was a contributing factor for the total number of quadrats (n=720) aimed at providing for good spatial coverage and estimating for precise densities. Only one fourth (26%) of our overall quantitative sample had measurable data indicative of low mussel densities at most sites that ranged from 0.0m<sup>2</sup> – 0.024m<sup>2</sup>. Quantitative mean mussel densities for all sites was 0.034m<sup>2</sup> ± 0.01 and seemed to be the standard. Our species of conservation concern, golden orb, was collected at 35% of all our sample sites in low densities and represented by thirty - two specimens. The mean CPUE for golden orb for all sites was 0.13/h ± 0.05. Qualitative timed searches were more successful and exhibited mussel presence 52% of the time whereas quantitative efforts were at 26%.

A Paired 2 Sample t-test was ran to test the Null hypothesis comparing the effectiveness of quantitative (quadrat) and qualitative (timed searches) mussel surveys and results were significant at the <.05 level (P = 0.008 ) thus rejecting the null hypothesis. Qualitative results produced an overall CPUE range of 0.0 – 2.33 /h and a mean CPUE for the community from all sites of 0.40/h ± 0.08. Shell lengths were measured to provide insight on community size class structure, however, class estimates could be biased due to a small sample size. Louisiana fatmucket and pistolgrip lacked representative juveniles, and conversely all other species except paper pondshell were represented by medium to large sized adults. Golden orb was represented by only a few juveniles and more representative in the 31-40mm class. The

largest class was represented by pistolgrip, yellow sandshell, and golden orb in moderation, however, there are also some recent recruitment issues from several species. Habitat utilization was dominated by golden orb and yellow sandshell located in glide and run combinations. There also seemed to be disjointed mussel community where no individuals were located in the farthest upstream reach and just below the middle reach where very few were found. The lower Cibolo creek mussel community has high species richness however densities are relatively low and evenness among species is lacking. The Golden orb is a state threatened mussel found in relatively low abundance throughout the San Antonio River and its tributaries, therefore, this mussel and the watershed that it is found should obtain focused conservation efforts to protect it.

## **BIOACCUMULATION OF ARSENIC, CADMIUM, MERCURY, AND LEAD IN FISHES OF THE DALIAO RIVER ESTUARY, CHINA**

Chunye Lin, Kai Lei, Deqi Jiao, Mengchang He

(State Key Joint Laboratory of Environmental Simulation and Pollution Control, School of Environment, Beijing Normal University, Beijing 100875, China)

The contamination of toxic metals in the coastal aquatic ecosystem is extensively concerned owing to their high bioaccumulation in marine products and potential risks to human health through seafood consumption. As an important industrial base with oil, chemical, and steel factories in the northeast part of China, the Liao River Watershed has been subjected to heavy anthropogenic influences as a result of rapid economic developments in the past ca. 50 years. This has resulted in significant stress to the Daliao River Estuary in the Liaodong Bay of Bohai Sea (China). In this research, sediment, water, and fishes were sampled in the Daliao River Estuary. The concentrations of As, Cd, Hg, and Pb in the sediment, water, fish were determined. The bioaccumulation factor and hazard quotient via fish consumption were calculated. The results indicated that the concentrations of As, Cd, Hg, and Pb in fishes were 0.57~8.18, 0.01~3.33, 0.01~8.29, 0.07~1.71 mg/kg, respectively. The concentrations of As, Cd, Hg, and Pb in sediment were 4.61~11.41, 0.05~0.67, 0.01~0.10, and 16.57~39.18 mg/kg, respectively; while their concentrations in water were 3.84~9.12, 0.05~0.64, 0.01~0.05, and 0.69~4.37  $\mu$ g/L. The bioaccumulation factor revealed that heavy metals were more accumulated in the liver and intestine of fishes. Hg and Cd showed the high bioaccumulation level in the fishes. Hazard quotient showed that fish consumption may pose a health risk to local residents, primarily due to the high concentration of As in the fishes.

**NITRIFICATION AND DENITRIFICATION BY ALGAE-ATTACHED AND FREE-LIVING MICROORGANISMS DURING CYANOBACTERIAL BLOOM IN LAKE TAIHU**

*Xiaofeng Chen*, Haiyang Jiang (Yangzhou University, Yangzhou, China)  
Liuyan Yang (Nanjing University, Nanjing, China)

Cyanobacterial bloom may stimulate the epiphytic and pelagic microorganisms to take great roles in nitrification and denitrification process. In order to validate this hypothesis, a 4-weeks floating mesocosms experiment, involved cyanobacterial decay-growth-decay period, was performed at Lake Taihu. In addition to conventional detection of the physical and chemical properties, quantitative real-time PCR was used for the determination of nitrification and denitrification genes (AOA, AOB, nirS and nirK). Results showed that total nitrogen removed from the treatment with cyanobacteria added was about 3.62 mg L<sup>-1</sup>, 40% of which was organic nitrogen, indicating a nitrogen transformation and removal mechanism occurred in the system. Variations of the biogeochemical properties suggested that remineralization and coupling nitrification and denitrification was the primary pathway that nitrogen removed. This study reveals that algal bloom can accelerate nitrogen removal efficiency in lake ecosystem.

## **TAILINGS STORAGE FACILITIES AND ENVIRONMENTALLY SUSTAINABLE MINING**

***Erica Schoenberger***

(The Johns Hopkins University, Baltimore, MD USA)

Tailings dam failures account for about three-fourths of major mining-related disasters. Tailings dams are not built like water retention dams. They are constructed from mine wastes and built up as mining proceeds. Nevertheless, water management is the critical problem. Tailings storage facilities (TSF) must be maintained in perpetuity. The technical challenges of constructing a TSF that can withstand extremes of climate, seismic events and often difficult terrain are substantial. I argue, however, that the principal cause of TSF failures is political and economic rather than technical.

When mining companies are held to the highest standards, they can and do meet them. Whether or not they are held to those standards depends in part on the regulatory environment. How exigent are the regulations, how comprehensive are they, and how well are they enforced? The answers to these questions have in part to do with the influence of the industry in particular jurisdictions compared with other land-intensive uses, especially as this bears on regulatory capacity and competence. Second, the social composition of the surrounding population also matters. Local populations with political and financial resources will have a much greater chance of escaping environmental disasters than those without such resources. Third, building the design of the TSF into the design of the mine and submitting the design for peer review provides important safeguards.

In this paper, I analyze the performance of three mines. Two of them suffered major TSF dam collapses with widespread and continuing environmental damage: the Ok Tedi mine in Papua New Guinea (PNG), and the Mount Polley mine in British Columbia. The third mine – the McLaughlin mine in Northern California – is a rare success story in which all of the environmental dislocations necessarily associated with mining were confined on site and, to a significant degree, remediated after active mining ceased.

The environmental damages of mining are closely linked to social harms (through impacts on livelihoods, exposure to environmental toxins and the like), so it is particularly worthwhile getting at the causes of both success and failure in an effort to determine whether mining can increasingly be done in a way that contains and remediates environmental harms.



## **STATE APPROACHES TO WATERSHED-BASED PERMITTING**

**Danielle Stephan** (US Environmental Protection Agency, 1200 Pennsylvania Ave, NW, Washington, DC 20460)

Greg Currey (Tetra Tech, Inc., 10306 Eaton Place, Suite 340, Fairfax, VA 22030)

The United States Environmental Protection Agency (USEPA) has been an advocate for State Permitting Authorities to consider using a Watershed-based Permitting approach where pollution is a result from a variety of sources within a defined watershed. The primary difference between this approach and the traditional approach to permitting is the consideration of watershed goals and the impact of multiple pollutant sources and stressors, including nonpoint source contributions rather than a focus on a single point source. Watershed-based permitting may encompass a variety of activities ranging from synchronizing permits within a basin to developing water quality-based effluent limits using a multiple-discharger modeling analysis. The types of permitting activities will vary from watershed to watershed, depending on the unique circumstances in the watershed and the sources affecting watershed conditions. The ultimate goal of watershed-based NPDES permitting, however, is to develop and issue NPDES permits that consider the conditions of the entire watershed and address the diverse sources within the watershed.

Several states have emerged as champions of the watershed-based Permitting approach, and EPA has developed a variety of case studies to demonstrate real world examples of how the watershed-based permitting approach can be used to address pollution problems in a given watershed. This presentation will discuss the concepts of a watershed permitting analytical approach and an NPDES watershed framework as they relate to state approaches to watershed planning and permitting. Specifically, the presentation will describe the drivers, processes and outcomes of a number of state watershed permitting approaches. Examples of cases studies that will be presented may include the following:

- 1) *Tualatin River Watershed Permit for Clean Water Services in Portland, Oregon*: This case study focuses on the components of the watershed-based permit issued to Clean Water Services (CWS), a public utility in Portland, Oregon. The permit incorporates the NPDES requirements for all four of CWS's advanced wastewater treatment facilities, its two industrial storm water permits, and its municipal separate storm sewer permit into a single permit and includes provisions for water quality credit trading involving temperature (thermal load), biochemical oxygen demand (BOD), and ammonia.
- 2) *Neuse River Watershed Permit, North Carolina* - This case study focuses on the components of the watershed-based permit issued to the Neuse River Compliance Association and the group compliance mechanisms used by the co-permittees to meet the terms of the permit.
- 3) *General Permit for Nitrogen and Phosphorus Dischargers to the Chesapeake Bay Watershed in the Commonwealth of Virginia* - This case study focuses the general permit issued to approximately 180 significant and new and expanding municipal dischargers of nitrogen and phosphorus in the Commonwealth of Virginia discharging to the Chesapeake Bay watershed.

## **RAIN HARVESTING FOR SUSTAINABLE WATERSHED MANAGEMENT – LOCAL WATER SUPPLY AND REGIONAL WATER QUALITY IMPROVEMENT. NEAL SHAPIRO**

Neal Shapiro

(Santa Monica City, Office of Sustainability & the Environment, Santa Monica, CA, USA)

Throughout the United States, water quality and adequate water supplies are worsening. Around the world, rising population demand is using freshwater supplies faster than can be replenished by nature or society, resulting in short-term deficits and long-term unreliability; millions of people die or suffer health impacts from unsafe or inadequate water supplies; climatic oscillations in temperature gradients and precipitation from what civilization has considered “normal” for the last 50 years will make long-term, reliable storage management more challenging; water quality of surface water bodies are degrading from more intense stormwater runoff pollution; and energy costs to move surface water hundreds of miles through aging infrastructure from distant watersheds to consumers are unsustainable; such infrastructure is exposed to natural disasters which would disrupt water flow to urbanized centers. The clean water supply pie shrinks, yet water demand grows. The solution is to grow the supply pie in a sustainable way to keep pace with demand while also managing water demand to be as efficient as technically possible.

With the participation of water consumers, water management professionals must implement a new sustainable water demand and supply side management approach, including well-tested scientific and technical products focused increasingly on non-traditional, local non-potable water resources, such as rainwater. Such solutions exist, and are proven and working today to improve water supply and quality.

Why rainwater? Rain harvesting has many benefits: it is a local, independent supply, e.g. water security and resiliency; it eliminates stormwater, and stormwater pollution; it reduces combined sanitary sewer overflows, helping to comply with Clean Water Act NPDES regulations; and it lowers the use of municipal water, such that more freshwater can be left in stressed surface waters and aquifers. Onsite rain harvesting effectively delivers a water supply to an end use at an acceptable water quality and minimal energy cost. By keeping rainwater onsite, less pollution enters surface water bodies, where water-quality violations can occur.

Rain harvesting technology has been around for decades, but has improved dramatically over the last 10 years. These systems are safe and reliable, and modular and scalable. Such systems use the appropriate harvesting and treatment technologies to meet appropriate end uses of non-potable and even potable.

The national leader for rain harvesting is the American Rainwater Catchment Systems Association. ARCSA’s mission is to promote sustainable rain and stormwater harvesting practices to help solve potable, non-potable, stormwater, water quality and energy challenges throughout the world. ARCSA is in the forefront in seeking, producing and implementing solutions, nationally and internationally, fostering integration and transfer of the latest scientific research and engineering applications. With partners, ARCSA produced plumbing design standards documents and recently a comprehensive rainwater harvesting manual.

Innovative rain harvesting case studies demonstrate the effectiveness of this sustainable, low impact development and green infrastructure strategy. From using rainwater and stormwater for irrigation to indoor flushing, these examples show how the technology works, how economies grow, how pollution is kept out of the aquatic environment and how local water supply is increased.

## **IMPACT OF WATERSHED MANAGEMENT ACTIVITIES IN LAND USE PATTERN AND PEOPLE'S LIVELIHOOD IN NEPAL**

Ajay Karki

(Department of Soil Conservation and Watershed Management, Po Box 4719, Babarmahal, Kathmandu, Nepal)

This paper examines the impact of watershed management activities on landuse pattern and livelihood upliftment, implemented by Department of Soil Conservation and Watershed Management in Kaski District of western Nepal. An JICA funded development project was implemented in Kaski district for five years. Main objective of the project was to improve the watershed condition by making (bio)/engineering structures and to uplift the people's livelihood by implementing the income generation activities. Baseline data and report of the project were used mainly to prepare this paper. Following are the main result of the project:

1. Irrigated area increased significantly
2. Green coverage area increased
3. River bank cut off decreased and rehabilitated area increased
4. Landslide decreased, soil erosion decreased
5. Income of people increased

## NATURAL ATTENUATION OF INDICATOR BACTERIA IN NATURAL WATER SYSTEMS

*Amin Kiaghadi* and Hanadi S. Rifai (University of Houston, Houston, TX, USA)

**ABSTRACT:** The presence of pathogens in surface water bodies is considered to be the main cause of several different types of diseases worldwide. Monitoring for Fecal Indicator Bacteria (FIB) in water bodies has conventionally relied on *E. coli* and Enterococci for fresh and marine waters, respectively. High concentrations of FIB in rivers, bays and estuaries, including in Galveston Bay near Houston, Texas where this study was undertaken, have been extensively documented in the general literature. While FIB concentrations are relatively high in Galveston Bay (Texas, USA), they are much lower when compared to FIB concentrations in the Houston Metropolitan area. This result could be explained by considering the Houston Ship Channel (HSC) as a treatment reactor that naturally attenuated the bacterial loads emanating from the Houston Metropolitan watersheds. Higher salinity, lower velocities, larger flows in the HSC, and tidal influences from Galveston Bay support this assumption. There are no studies to date which investigate the concept of natural attenuation of pathogenic pollutants in surface waters. The main purpose of this study is to address this deficiency and introduce the term “natural attenuation” for pathogenic pollutants in natural water systems. The fate and transport of the bacterial load transportation within the HSC can be categorized into three mechanisms: 1) reactive- dilution mixing of fresh and marine water, 2) advective-reactive transport along the HSC, and 3) dilution mixing with Galveston Bay water. This study investigates whether each of the aforementioned attenuating mechanisms is responsible for reducing FIB concentrations and loads into Galveston Bay. Several lines of evidence are presented that demonstrate natural attenuation of FIBs within the HSC: 1) lower Enterococci concentrations in tributary tidal waters compared to those in fresh waters for the tributaries discharging into the HSC, 2) 70% reduction in bacterial loads within the Channel itself, 3) a general decreasing trend in Enterococci geometric means from upstream to downstream within the HSC, and 4) lower Enterococci concentrations in Galveston Bay at the confluence with the HSC.

## INTRODUCTION

The presence of pathogens in surface water bodies is considered to be the main cause of several different types of diseases worldwide. The annual cost of marine-born microbial contamination in the U.S. alone exceeds \$900 million (Dwight et al. 2005, Ralston et al. 2011). Elevated Fecal Indicator Bacteria FIB levels in natural water systems are typically associated with urbanization, storm water discharges, releases from wastewater plants, illegal dumping, and domestic and wildlife animals. Ingestion or inhalation of water during recreational activities, consumption of raw seafood, and contaminated water contact with open wounds are the main causes of diseases. Monitoring for FIB in water has been widely used to reduce the cost of marine-born microbial contamination (Desai et al. 2010, Goodwin et al. 2012). For this purpose, fecal coliform, and more recently *E. coli* for fresh waters and Enterococci for marine waters have been suggested as measures of pathogenic contamination (Ostrolenk et al. 1947, Cabelli et al. 1979). Different environmental factors can affect FIB concentrations including physico-chemical conditions such as salinity, pH, Dissolved Oxygen (DO), and water temperature, and biological-environmental conditions such as microbial predation and the effect of sunlight (Anderson et al. 2005, Mill et al. 2006).

In 2010, Desai et al. reported elevated levels of *E. coli* in almost all of the Houston Metropolitan area bayous (Desai et al. 2010). Waters originating from Houston watersheds discharge to the Houston Ship Channel (HSC), a 55 mi navigational man-made tidal channel, and eventually to Galveston Bay and its recreational beaches. Elevated values of FIBs in Galveston Bay have been reported by several public agencies such as the Texas Commission on Environmental Quality (TCEQ) and the Texas Department of State Health Services (TDSHS). To date, the sources of FIB contributing to Upper Galveston Bay have not been elucidated. However, a rational hypothesis would associate bacterial loads from Houston area watersheds to the presence of FIB in Galveston Bay. However, FIB concentrations in Galveston Bay are significantly lower when compared to the FIB concentrations in Houston area watersheds. This change

could be explained by considering the HSC as a treatment reactor that naturally attenuates the bacterial loads emanating from Houston watersheds. Higher salinity, lower velocities, larger flows in the HSC, and tidal influences from Galveston Bay support this observation. This concept is novel for FIB, and to the best of the knowledge of the authors has yet to be addressed in this context.

Natural attenuation is defined as “observed reduction in contaminant concentrations as contaminants migrate from the source in environmental media due to a number of fate and transport processes” (Wiedemeier et al. 1999). Most of the research related to natural attenuation has been mostly completed in ground water systems and groundwater-surface water interactions (Kao et al. 2010, Ouyard et al. 2013, Freitas et al. 2015). Very little research has been done on the concept of natural attenuation for surface water; most has focused on Uranium and pharmaceuticals and in wetlands for nutrients (Casey and Klaine 2001, Manaka et al. 2007, Acuna et al. 2015). There are no studies to date to investigate the natural attenuation of pathogenic pollutants in surface waters. The main purpose of this study is to fill this gap and analyze the “natural attenuation” for pathogenic pollutants in natural water systems. This research relies on statistical methods to study the role of the tidally influenced HSC in naturally attenuating bacterial loads from the Houston Metropolitan area.

## MATERIALS AND METHODS

**Study Area Data.** The HSC is tidally influenced and begins at the Port of Houston, near downtown Houston, Texas, extends through Galveston Bay and enters the Gulf of Mexico. The average depth and width of the channel are 13.7 and 162 m respectively. In this study, a total length of 46 km upstream of Morgan’s Point (the inlet to Galveston Bay) was studied (**Error! Reference source not found.**). The Texas Commission on Environmental Quality (TCEQ) Surface Water Quality Web Reporting Tool was used to obtain the water quality data for the HSC. Thirteen water quality monitoring (WQM) stations in the HSC, one in Upper Galveston Bay, and nineteen additional stations in bayous were used in the study (Figure 1). The period of record covers the years 2000-2013 since there was no available data for Enterococci prior to 2000. As noted previously, *E.coli* and Enterococci are the FIB for fresh and marine waters respectively. Thus, stations above the tide line (see Figure 1) have *E.coli* data while the tidal stations contain Enterococci data. Flow and rainfall data were compiled from the USGS and the Harris County Flood Control District database (HCFCD, 2014), respectively. Hourly tide data at Morgan’s Point were obtained from the National Oceanic and Atmospheric Administration (NOAA) Center for Operational Oceanographic Products and Services (CO-OPS, 2014) tides and currents database.

**Conceptual Model of Natural Attenuation in the Study Area.** Galveston Bay is an estuarine system with relatively low tide height and the HSC is considered a pathway for bacteria loads that emanate from Houston area watersheds to Galveston Bay (**Error! Reference source not found.**). The fate and transport of FIB loads within the HSC can be categorized into three mechanisms: 1) reactive-dilution mixing of bayou fresh water with HSC marine water, 2) advective-reactive transport along the Channel, and 3) dilution mixing with Galveston Bay water (**Error! Reference source not found.**). The HSC has long travel and residence times due to the very low advective flows within the channel. Consequently, the HSC can be considered as a series of mixing reactors with natural attenuation capacities that reduce the bacterial contamination. However, bacteria loads from Houston area watersheds and other sources such as leakage in large barge sewage systems and bird feces can counteract the aforementioned capacity and increase the bacteria concentration.

To demonstrate the effect of the first mechanism (dilution-mixing with HSC water), in a given tributary, one should be able to observe 1) a noteworthy change in FIB concentrations between two WQM stations located above and below the tide line, respectively, and 2) a significant reduction in the HSC bacteria loads discharged to Galveston Bay when compared to the cumulative input loads from Houston area watersheds. The first observation was tested by converting the freshwater *E. coli* data at WQMs above the tide line into saline Enterococci-equivalents. The conversion ratio was obtained by applying a linear regression to the data from 8 WQM stations near the tidal boundaries where both indicator data were available. For the second observation, an existing Environmental Fluid Dynamics Code (EFDC) simulation of the HSC developed by Howell (2012) was used to obtain the discharge flows from the HSC at Morgan’s

Point (station 11252, see Figure 1). The FIB load for the HSC was calculated by multiplying the geometric mean concentration of Enterococci at station 11252 with the extracted discharge rate from EFDC. Input loads from Houston area watersheds were calculated using flow data from USGS gages and the converted Enterococci-equivalents data from non-tidal WQM stations (except for Goose and Vince bayous where the closest WQM stations to the tidal boundaries were used). The calculated HSC load was then compared to the FIB input loads from Houston.

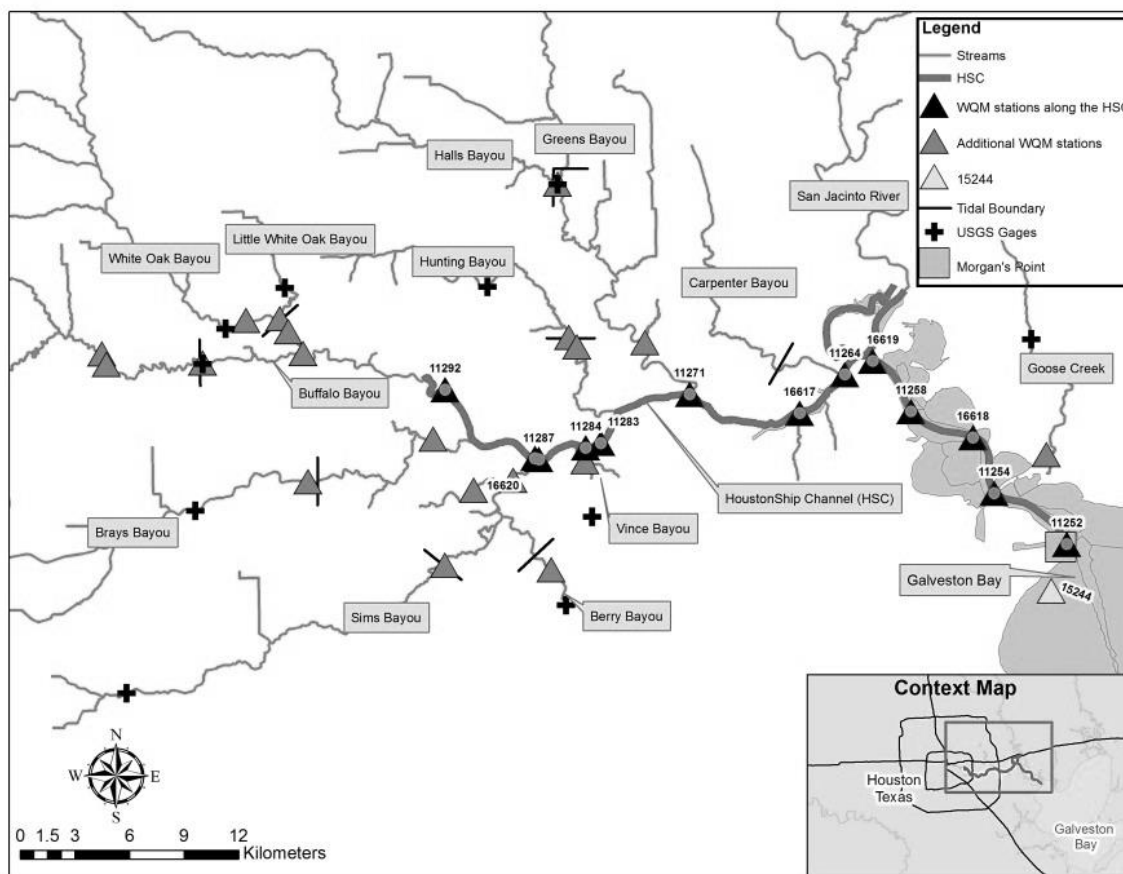


Figure 1- Houston Ship Channel (HSC), USGS gages and Water Quality Monitoring Stations

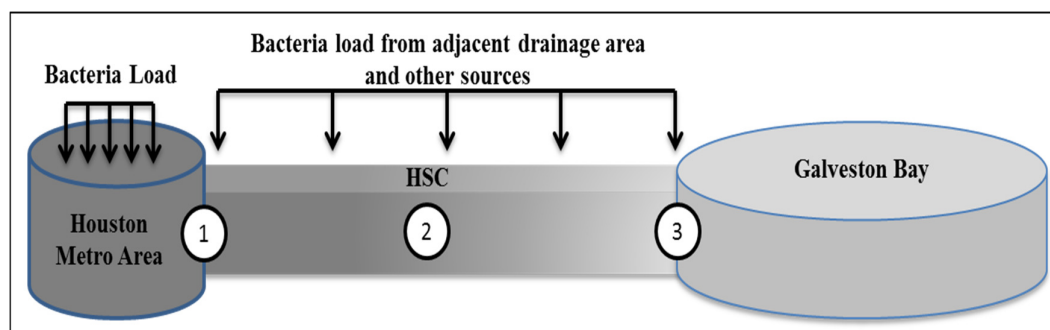


Figure 2- Bacteria load pathway from Houston Metropolitan area through the HSC leading to Galveston Bay

Different components of natural attenuation can occur during the advective-reactive transport along the channel (second mechanism) that can be attributed to variation in the volume of water (dilution), tide

effects, and ambient environmental factors. Thus, a spatial analysis for FIB concentrations within the HSC was undertaken in addition to a correlation analysis between FIB concentrations and tides and ambient environmental factors.

Lastly, and to assess attenuation of FIB due to dilution-mixing with Galveston Bay waters (third mechanism), FIB concentrations in the WQM station located at the mouth of the HSC (station 11252) were compared to those at the WQM station located in Upper Galveston Bay (station 15244).

**Statistical Analyses.** Normality and log-normality tests were conducted using SPSS software via Kolmogorov-Smirnov and Shapiro-Wilk methods. The results showed that none of the water quality data sets used in this study were normal or log-normal ( $P\text{-Value} < 0.05$ ) for any station. Therefore, in this study, geometric mean and median instead of mean; Mann-Whitney U test instead of t-test; and Spearman correlation test instead of Pearson Correlation test were used. To find any possible correlation between concentrations/values of FIB and other environmental variables and also with distance from the channel outlet (Morgan's Point), visual analysis, regression analysis and Spearman's correlation test were used.

## RESULTS

The average log-scale conversion ratio between Enterococci and *E. coli* was found to be 0.78, which is comparable to the 0.73 value obtained by taking the ratio of the EPA standards for the two FIBs ( $\log 35 / \log 126$  MPN/dL).

### Reactive-Dilution Mixing of Bayou Fresh Water with HSC Marine Water

**Relationship between FIB in tributaries and the receiving HSC.** As shown in Figure 3, a rapid drop in Enterococci geometric mean concentrations is observed when comparing the fresh water (above the tide line) segments of tributaries with their saline water (tidal) counterparts for all tributaries. This observation has also been confirmed using the Mann-Whitney U test which showed a significant difference in Enterococci bacteria concentrations between fresh and saline waters in all tributaries except for Greens Bayou ( $P\text{-value} = 0.09$ ). The Greens Bayou anomaly can be explained by the fact that the distance between the tidal and above tide line WQM stations is relatively longer in comparison to the other tributaries. Moreover, the above tide line WQM station is located at the confluence of Greens and Halls Bayous causing some uncertainties due to rapid mixing.

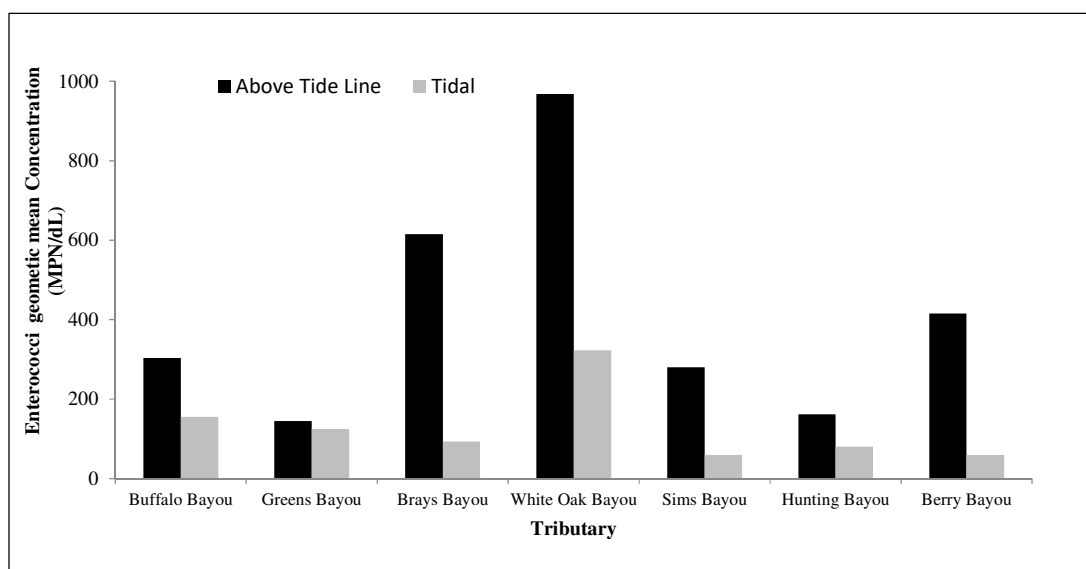


Figure 3- Enterococci geometric mean concentration before and after tide line in different tributaries

**Input and output bacterial loads.** Although White Oak, Brays, and Little White Oak bayous had the highest Enterococci concentrations, the variation in Enterococci geometric mean concentrations did not exceed an order of magnitude in the different tributaries. For the flow, however, the variation was up to three orders of magnitude: Greens, Buffalo, and Brays had the highest flows whereas the lowest flows were found in Goose, Vince and Berry bayous. The highest load contributions were calculated for Greens, Buffalo, and Brays bayous with median loads of 11, 7.4, and 2 trillion MPN per day, respectively.

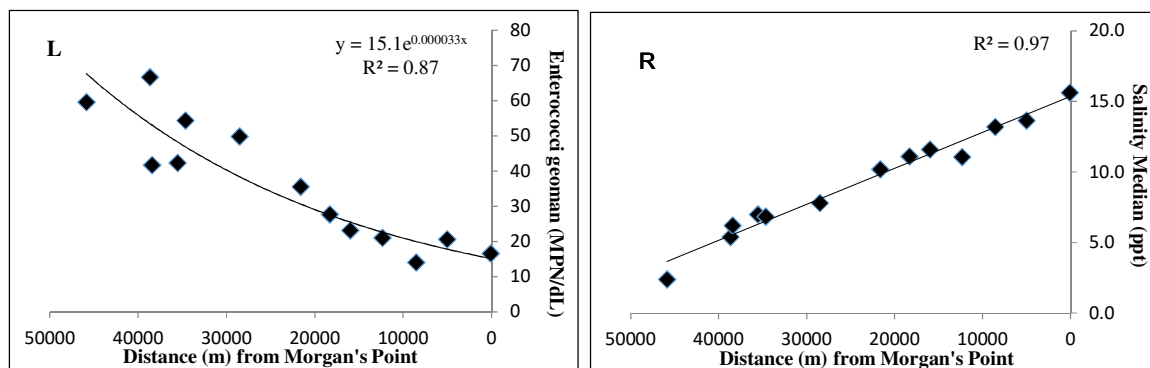


Figure 4- Enterococci geometric mean concentrations (L) and Salinity median values (R) as a function of distance from outfall of Channel into Galveston Bay

The sum of all bacteria loads discharging to the HSC was estimated to be 21.6 trillion MPN per day. EFDC model results at Morgan's Point (**Error! Reference source not found.**) show a median advective velocity of 0.108 m/s. A flow rate of 444 m<sup>3</sup>/s was estimated by multiplying the aforementioned velocity with the HSC cross sectional area obtained using ArcGIS (Version 10.1, ESRI, Redlands, California), Digital Elevation Model (DEM) data and the EFDC model grid. Finally, by considering the Enterococci geometric mean concentration of 17 MPN/dL at Morgan's Point (station 11252, see **Error! Reference source not found.**) the total output bacteria load from the HSC was estimated to be 6.5 trillion MPN per day, a 70% reduction when compared to the input load.

#### Advective-Reactive Transport along the Channel

Along the channel (in 13 WQM stations), Enterococci concentrations ranged from non-detect ( $\leq 10$  MPN/dL) to more than 24,000 MPN/dL. As demonstrated in **Error! Reference source not found.**, a general decreasing trend can be observed in Enterococci geometric mean concentrations from upstream to downstream in the HSC. This trend has also been confirmed using Spearman's correlation test ( $P$ -value  $< 0.05$ ). A curvilinear regression analysis showed that an exponential trend ( $P$ -value  $< 0.05$ ,  $R^2 = 0.87$ ) achieved the best fit for the data. The observed decreasing trend supports the occurrence of natural attenuation of FIB within the HSC.

The median for salinity increases as the flow moves towards the mouth of the HSC as would be expected due to the mixing of fresh and marine water from Galveston Bay (see **Error! Reference source not found.**). Significant negative correlation between salinity and Enterococci concentration ( $P$ -value  $< 0.05$ ) was confirmed using Spearman's correlation test. A stronger correlation was obtained by analyzing median concentrations of salinity and geometric means of Enterococci at WQM stations. The Mann-Whitney U test was applied to evaluate the effect of tide conditions on Enterococci concentrations. The results showed Enterococci concentrations were significantly lower ( $P$ -Value  $< 0.05$ ) in samples collected in ebb (receding) tides compared to ones collected in higher when the tide is rising.

#### Dilution Mixing with Galveston Bay Water

The results of the Mann-Whitney U test for Enterococci data from the two WQM stations located at the entrance of the HSC into Galveston Bay (station 11252 within the HSC and 15244 in Galveston Bay, see Figure 1) indicated a significant difference between them. Additionally, for the samples collected in flood tides. This is in agreement with what would be expected as salinity is Galveston Bay (WQM 15244),



81% of the samples had a value below the detection limit. This number was only 35% in station 11252 that is located only 3.5 km upstream of station 15244. Lastly, the Enterococci geometric mean concentration for station 15244 was found to be 7 MPN/dL, a value that is less than half of the 17 MPN/dL reported for station 11252. It can be concluded that dilution-mixing is occurring as HSC water mixes into Galveston Bay.

## DISCUSSION

In natural water systems, coastal estuaries can be characterized as a transitional phase for bacteria loads from fresh waters to their destination saline receptors. Such tidal systems have normally higher salinities compared to the fresh water streams that discharge bacteria loads but lower salinities than the terminal receptor, in this case, Galveston Bay. The reduction in FIB concentrations in estuary systems compared to fresh waters that have been reported widely in the literature (McLaughlin et al. 2007, Lewis et al. 2013) can be attributed to the natural attenuation capacities of these sentry water bodies such as the HSC.

Enterococci concentrations along the HSC showed a high degree of spatial variability in keeping with similar trends reported by others (Cui et al. 2013, De Luca-Abbott et al. 2000). Mixing marine waters from Galveston Bay with fresh waters emanating from the greater Houston Metropolitan area can significantly change the physico-chemical characteristics of water. Salinity and tide oscillations were the most important variables affecting the reduction of FIBs within the HSC; confirming similar findings by Mill et al. 2006, Johnston et al. 2015.

In fresh water streams, Desai and Rifai (2013) showed a Bacteria Diurnal Sag (BDS) in a non-tidal urban watershed in Houston caused by changes in water temperature and solar radiation intensities. They concluded that time and numbers of samples were the most important factors in water-quality monitoring. In an estuary system, tidal mechanisms can cause significant variation in the salinity and consequently affect FIB concentrations at different times of the day suggesting that FIB measurements in WQM stations are highly sensitive to the time of sampling. Thus, for a tidal system such as the HSC, the time of sampling should also be adjusted to the tide mechanisms that could vary from month to month different in different months.

## CONCLUSION

Several lines of evidence were presented that demonstrate natural attenuation of FIBs within the HSC: 1) lower Enterococci concentrations in tributary tidal waters compared to those in fresh waters for the tributaries discharging into the HSC, 2) a 70% reduction in bacteria loads within the Channel itself, 3) a general decreasing trend in Enterococci geometric means from upstream to downstream within the HSC, and 4) lower Enterococci concentrations in Galveston Bay at the confluence with the HSC.

Water bodies similar to the HSC with natural attenuation capacities can act as sentries for coastal pathogenic contamination by reducing overall bacteria loads to receiving bays and estuaries thus reducing the risk of diseases. It would be important to maintain relatively high water quality in such systems in order to sustainably use their natural attenuation capacities for bay protection. In addition, bacteria concentrations should be monitored relatively frequently to capture the inherent variabilities in FIB levels caused by sunlight, temperature, and tide effects.

## AKNOWLEDGMENTS

The research was funded by the Texas Commission on Environmental Quality and the U. S. EPA; their support is gratefully acknowledged.

## REFERENCES

- Acuna, V., von Schiller, D., Garcia-Galan, M.J., Rodriguez-Mozaz, S., Corominas, L., Petrovic, M., Poch, M., Barcelo, D. and Sabater, S. (2015) Occurrence and in-stream attenuation of wastewater-derived pharmaceuticals in Iberian rivers. *Science of the Total Environment* 503, 133-141.
- Anderson, M.L., Whitlock, J.E. and Harwood, V.J. (2005) Persistence and differential survival of fecal indicator bacteria in subtropical waters and sediments. *Applied and Environmental Microbiology* 71(6), 3041-3048.

- Cabelli, V.J., Dufour, A.P., Levin, M.A., McCabe, L.J. Haberman, P.W. (1979) Relationship of microbial indicators to health effects at marine bathing beaches. *American Journal of Public Health* 69(7), 690-696.
- Casey, R.E. and Klaine, S.J. (2001) Nutrient attenuation by a riparian wetland during natural and artificial runoff events. *Journal of Environmental Quality* 30(5), 1720-1731.
- Cui, H.L., Yang, K., Pagaling, E. and Yan, T. (2013) Spatial and Temporal Variation in Enterococcal Abundance and Its Relationship to the Microbial Community in Hawaii Beach Sand and Water. *Applied and Environmental Microbiology* 79(12), 3601-3609.
- De Luca-Abbott, S., Lewis, G.D. and Creese, R.G. (2000) Temporal and spatial distribution of enterococcus in sediment, shellfish tissue, and water in a New Zealand Harbour. *Journal of Shellfish Research* 19(1), 423-429.
- Desai, A.M. and Rifai, H.S. (2013) Escherichia coli Concentrations in Urban Watersheds Exhibit Diurnal Sag: Implications for Water-Quality Monitoring and Assessment. *Journal of the American Water Resources Association* 49(4), 766-779.
- Desai, A.M., Rifai, H., Helfer, E., Moreno, N. and Stein, R. (2010) Statistical Investigations into Indicator Bacteria Concentrations in Houston Metropolitan Watersheds. *Water Environment Research* 82(4), 302-318.
- Dwight, R.H., Fernandez, L.M., Baker, D.B., Semenza, J.C. and Olson, B.H. (2005) Estimating the economic burden from illnesses associated with recreational coastal water pollution - a case study in Orange County, California. *Journal of Environmental Management* 76(2), 95-103.
- Freitas, E.T.F., Montoro, L.A., Gasparon, M. and Ciminelli, V.S.T. (2015) Natural attenuation of arsenic in the environment by immobilization in nanostructured hematite. *Chemosphere* 138, 340-347.
- Goodwin, K.D., McNay, M., Cao, Y.P., Ebentier, D., Madison, M. and Griffith, J.F. (2012) A multi-beach study of Staphylococcus aureus, MRSA, and enterococci in seawater and beach sand. *Water Research* 46(13), 4195-4207.
- Howell, N.L. (2012) Bed and suspended sediments as source and transport mechanisms for polychlorinated biphenyls in HSC estuary system, University of Houston, Houston, TX.
- Johnston, K.K., Dorsey, J.H. and Saez, J.A. (2015) Stratification and loading of fecal indicator bacteria (FIB) in a tidally muted urban salt marsh. *Environmental Monitoring and Assessment* 187(3).
- Kao, C.M., Chien, H.Y., Surampalli, R.Y., Chien, C.C. and Chen, C.Y. (2010) Assessing of Natural Attenuation and Intrinsic Bioremediation Rates at a Petroleum-Hydrocarbon Spill Site: Laboratory and Field Studies. *Journal of Environmental Engineering-Asce* 136(1), 54-67.
- Lewis, D.J., Atwill, E.R., Pereira, M.D.C. and Bond, R. (2013) Spatial and Temporal Dynamics of Fecal Coliform and Escherichia coli Associated with Suspended Solids and Water within Five Northern California Estuaries. *Journal of Environmental Quality* 42(1), 229-238.
- Manaka, M., Seki, Y., Okuzawa, K., Kamioka, H. and Watanabe, Y. (2007) Natural attenuation of dissolved uranium within a small stream of central Japan. *Limnology* 8(2), 143-153.
- McLaughlin, K., Ahn, J.H., Litton, R.M. and Grant, S.B. (2007) Use of salinity mixing models to estimate the contribution of creek water fecal indicator bacteria to an estuarine environment: Newport Bay, California. *Water Research* 41(16), 3595-3604.
- Mill, A., Schlacher, T. and Katouli, M. (2006) Tidal and longitudinal variation of faecal indicator bacteria in estuarine creek in south-east Queensland, Australia. *Marine Pollution Bulletin* 52(8), 881-891.
- Ostrolenk, M., Kramer, N. and Cleverdon, R.C. (1947) Comparative Studies of Enterococci and Escherichia coli as Indices of Pollution. *Journal of Bacteriology* 53(2), 197-203.
- Ouvrard, S., Chenot, E.D., Masfaraud, J.F. and Schwartz, C. (2013) Long-term assessment of natural attenuation: statistical approach on soils with aged PAH contamination. *Biodegradation* 24(4), 539-548.
- Ralston, E.P., Kite-Powell, H. and Beet, A. (2011) An estimate of the cost of acute health effects from food and water-borne marine pathogens in the USA. *Journal of Water and Health* 9(4), 680-694.
- Wiedemeier, T.H., Rifai, H.S., Newell, C.J. and Wilson, J.T. (1999) *Natural Attenuation of Fuels and Chlorinated Solvents in the Subsurface*.

#546

**SURVEY OF PHYSICAL-CHEMICAL QUALITY OF SUPERFICIAL WATERS AT THE  
SURROUNDING AREA OF THE SEBKHA BASIN (MOKNINE, TUNISIA)**

TAOUFIK NAAMOUN (University of Sfax, Faculty of Sciences, Department of Geology, Route de  
Soukra Km 3,5; P.B. 1171, Sfax, 3000, Tunisia)

The present investigation was conducted to control the physical-chemical parameters of superficial waters in the sebkha basin to evaluate their degree of pollution. Also, we aim to study the environmental impacts of the anthropogenic inputs on the different compartments of the sebkha. Twenty two water samples were collected and analyzed. The first results have shown that the obtained temperatures reflect those of the air the days corresponding to the field campaigns. The pH is oscillating between near neutral to slightly basic. The electro conductivity reveals that all samples are excessively mineralized. The salinity ranges from saline to hyper saline. Moreover, most samples contain potential reserves of hazardous metals. However, most of the measured concentrations exceed the limits for cadmium and lead for the sewage. Their concentrations reached 299ppb and 2.58ppm respectively.

## **ASSESSMENT OF WATER BALANCE IN THE SOUTH-WEST COASTAL REGION OF BANGLADESH**

**Nepal C Dey<sup>1\*</sup>**, Mahmood Parvez<sup>1</sup> and Nur A. Khondaker<sup>2</sup>

(<sup>1</sup>Research and Evaluation Division, BRAC, 75 Mohakhali, Dhaka 1212; <sup>\*</sup>Department of Environmental and Occupational Health, George Washington University, USA; <sup>2</sup>FAO Representation in Bangladesh, House # 32, Road # 8, Dhanmondi R/A)

Coastal environment and morphology are relatively less suitable for traditional crop cultivation, mainly because of soil and water salinity and inefficient water management system. As availability of fresh water is a limited resource mainly in the lean period, it is very important to assess how efficiently water can be managed considering development of more conservation sources for rain water harvesting to use in the lean period. This paper has been extracted from the water balance study conducted in South-West Coastal Region of Bangladesh in 2014. The aim of this paper is to make an assessment of utilizable water resources by looking at the inflow-outflow process in the South-West coastal region of Bangladesh. This paper focuses specially on irrigation adoption based on surface water availability in order to propose an effective planning, and on efficient management of the water resources. Assessment of monthly water balance for Khulna, Patuakhali and Barguna districts has been made based on the various inflow and outflow components in the catchment. Groundwater fluctuation method has been applied to estimate the monthly aquifer recharge. Availability of groundwater and surface water has been assessed based on demand and supply of water for the catchment. Temporal and spatial variation of soil and water salinity has been studied thematically. Study shows over 37 percent of total rainfall results into surface-runoff in this region. As distribution of rainfall is not uniform across the study area, situation of water balance also varies in two major districts, Khulna and Patuakhali of the South-West region. Most of the amount of run-off occurs during monsoon season (June to September) when there is relatively low scarcity of irrigation water. On the other hand, there is a lack of availability of irrigation water during dry season. Two different conditions of groundwater resources have been found in the coastal area, declining trend over the last three decades in Khulna area, and increasing trend in Patuakhali-Barguna area. Groundwater table fluctuates within 1-4m from the surface round the year in the coastal area. The salinity level of groundwater remains above the critical (3 ds/m) in most of the months in Khulna region and within the standard level with 1.6-2.0 dS/m throughout the year in Patuakhali region. Water level in major rivers in this region shows an increasing trend over the last three decades. So, sufficient river water is available in this area, but due to high salinity during most of the time surface water irrigation is not very suitable. From water availability analysis it is evident that a significant part of future irrigation water demand can be met by properly conserving the runoff resulting from precipitation using surface structures. The difference in annual irrigation water volume and the surface storable amount (runoff) is the total annual deficit that can be met from other sources, viz. subsurface, improving water productivity, improving water management practice, such as AWD, conjunctive use of saline water and other sources. The area has abundance of water resources to meet irrigation requirement even with increased cropping intensity in future, but requires proper planning to reduce the pressure on groundwater use.

## APPLICATION OF WATER QUALITY INDEX FOR GROUNDWATER QUALITY ASSESSMENT OF NANDED TEHSIL, (M.S.) INDIA

**Vasant Wagh**, Dipak Panaskar, Ranjitsinh Pawar, Aniket Muley and Shrikant Mukate  
(Swami Ramanand Teerth Marathwada University, Dnyanteerth, Vishnupuri, Nanded (MS), India)

**ABSTRACT:** Groundwater is an essential natural resource constituent of our life support system, where, it is used for drinking and irrigation purpose. An attempt has been made to recognize the hydro chemical characteristics of groundwater to develop water quality index model (WQI) in Nanded Tehsil. A total of 50 representative groundwater samples were collected from dug/bore wells during post-monsoon 2012 and analyzed for major cations and anions. The groundwater quality were assessed by different physicochemical parameters such as pH, electrical conductivity (EC), total dissolved solids (TDS), total hardness (TH), calcium ( $\text{Ca}^{2+}$ ), magnesium ( $\text{Mg}^{2+}$ ), sodium ( $\text{Na}^+$ ), potassium ( $\text{K}^+$ ), carbonate ( $\text{CO}_3$ ), bicarbonate ( $\text{HCO}_3$ ), chloride ( $\text{Cl}^-$ ), nitrate ( $\text{NO}_3^-$ ), sulphate ( $\text{SO}_4^-$ ) and phosphate ( $\text{PO}_4^-$ ). The Hydrochemical results were compared with Indian standards (BIS) which illustrate that TDS (16%), TH (22%), Ca (2%), Cl (2%) and Na (12%) samples exceeds the permissible limits. Water quality index (WQI) used to classify water quality as excellent, good, poor, and unsuitable categories. WQI shows that 34% samples are excellent, 60% samples are good and 6% unsuitable for drinking purpose. Through clutching hydro chemical investigation, GIS based IDW technique was used to signify the spatial variation WQI of study area.

**Keywords:** Groundwater, Water Quality Index, GIS, Nanded.  
Email: wagh.vasant@gmail.com

### INTRODUCTION

Groundwater is an important natural resource for drinking water particularly in rural areas of many counties like India. Poor drinking water quality leads to extensive acute and chronic diseases and, in many countries is a major cause of death (USEPA 2007). In the world the quality of water resources is being gradually more degraded as a consequence of its intensified anthropogenic exploitation (Causape et al. 2004). Generally, overexploitation of groundwater leads to quality and quantity is distorted due to human induced activities, agricultural practices, domestic sewage etc. Just the once, the groundwater is polluted, the restoration of such water is still remained a major challenge, therefore, it is crucial to develop the water quality monitoring system for fitness of water for different purposes. Groundwater quality is mainly defined in terms of its physical, chemical and biological characteristics for drinking. Naturally, groundwater quality depends on geological and geochemical composition of rocks, residence time of water, dissolution and precipitation of minerals and oxidation reduction reactions.

The water quality index (WQI) is most important tool to assess the water quality which is extensively helpful to researcher and policy makers for the sustainable management of groundwater. The WQI was first time suggested by Horton (1965). The WQI provides a single numerical digit by integrating water quality parameters with respective regulatory standards, which understand the list of constituents and their concentration present in water (Satmbuk-Giljanovic 1999, Stigter et al 2006). The objectives of the present work are to perform the groundwater quality assessment based on WQI method and generation of WQI map to represent its spatial distribution by using IDW technique for Nanded Tehsil, Maharashtra.

### STUDY AREA

Nanded Tehsil is administrative block of Nanded District located in South Eastern Part of Deccan Volcanic Province of Marathwada region of Maharashtra state. The study area is located between latitudes  $19^{\circ} 3' \text{ N}$  to  $19^{\circ} 17' \text{ N}$  and longitude  $77^{\circ} 10' \text{ E}$  to  $77^{\circ} 25' \text{ E}$  (Fig. 1). The study area comprises with semi arid region and tropical climate. The temperature of study area is ranging from 13 to  $46^{\circ} \text{ C}$ . The average rainfall of the study area is 900 mm, where, 88 % rain receives under the influence of South West Monsoonal winds. Godavari River flows in South West to South East direction having alluvial plain along its coast in the study

area. The thickness of alluvium varies at different places and maximum 20 m encountered in flood plain areas of rivers. The study area is principally irrigated by Godavari and its sub-tributary Asna River and also left bank canal taking off water from Siddheshwar dam of the Purna project, of Parbhani district. The North East part of the study area is the convergence point of Asna and Godavari River. The study area underlain by geological formation mainly Deccan Basalt flows of vesicular, amygdaloidal, weathered, fractured basalt. Black cotton soil and loamy to sandy soil are main soil types covering the study area. The soil has high productivity value for the crops like Cotton, Jawar, Soyabean etc due to rich in plant nutrients.

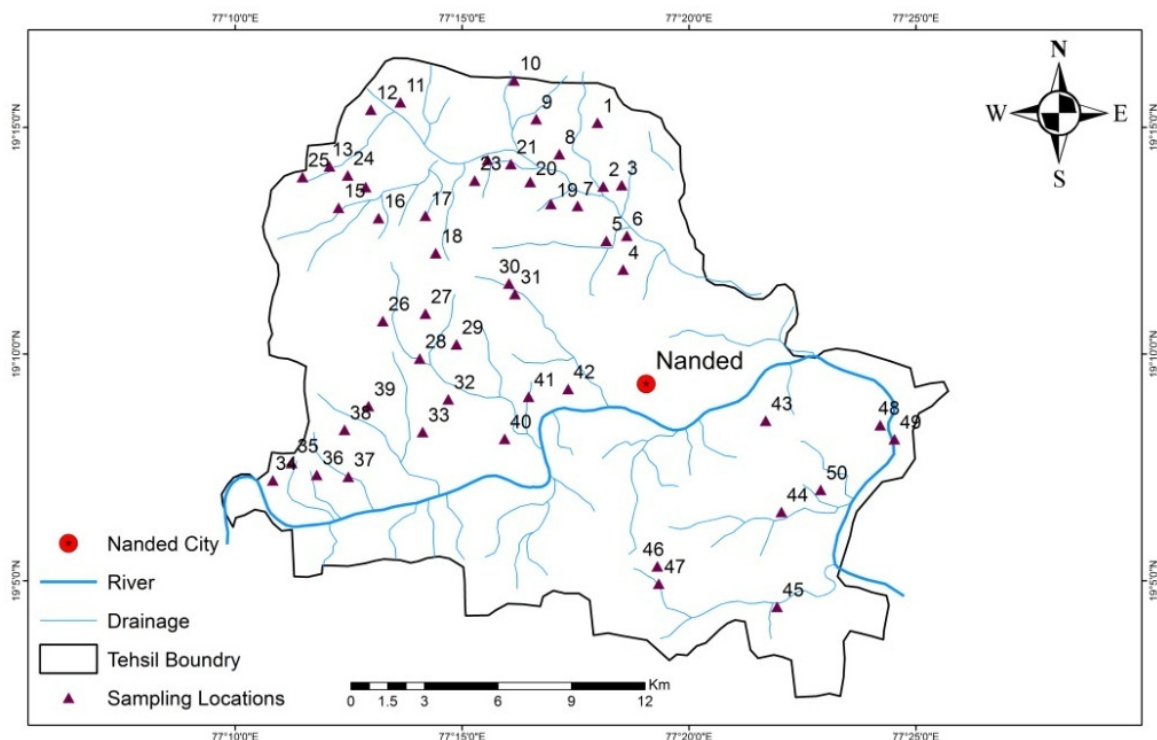


FIGURE 1. Study Area Map with sample locations

## MATERIAL AND METHODOLOGY

A fifty representative groundwater samples were collected from dug wells and bore wells from different locations of Nanded Tehsil for the period of post-monsoon season 2012. Survey of India, Toposheet no's 56 E/5, 56 E/8, 1:50,000 scales were used for the preparation of water quality index map of the study area. The groundwater samples were collected in pre-washed one-litre polyethylene cans after pumping the wells for 5-10 minutes; afterwards these cans were properly sealed, labelled and brought to laboratory for further physicochemical analysis. Location coordinates were recorded by using GPS device. pH and Electrical conductivity measured in the field itself by using portable digital meter. Calcium, magnesium carbonate, bicarbonate and chloride were analyzed in the laboratory by gravimetric analysis following the standard methods of American Public Health Association (APHA 2005). The sodium and potassium ion was determined by using flame photometer (Elico CL 361). The sulphate, phosphate, and nitrate were determined by using spectrophotometer (Shimadzu UV-1800). The Arc GIS 9.3 software was used for the preparation of water quality index maps.

**Water Quality Index Method.** Water Quality Index (WQI) is a technique of rating that provides the composite influence of individual water quality parameters on the overall quality of water for human consumption (Mitra et al 2006). It is computed in three steps (Horton 1965, Yidana 2010). In first step the weight is assigned to each parameter according their relevance to drinking quality of water. The most significant parameter weighted with 5 and least significant with 1. Second step is calculation of relative weight (RWi), computed with the help of eq. No. 1. The third step is quality rating scale (qi) calculation based on dividing the parameter concentration in each water sample by its respective standard (BIS 1998)

multiplied by 100 and its computed with the help of eq. No. 2. The  $W_i$  and  $q_i$  are used to calculate the Sub index  $SI_i$  of each parameter following eq. No. 3. Finally, the water quality index (WQI) is calculated from eq. No. 4.

$$RW_i = AW_i / \sum AW_i \quad (1)$$

Where,  $RW_i$  = Relative weight,  
 $AW_i$  = Assigned Weight  
 $n$  = Number of parameters

The quality rating scale for each parameter is calculated with the following equation

$$q_i = (C_i/S_i) * 100 \quad (2)$$

Where,  $q_i$  = Quality rating for  $i^{th}$  parameter  
 $C_i$  = Concentration of  $i^{th}$  chemical parameter of water sample (mg/l)  
 $S_i$  = permissible standard for  $i^{th}$  parameter set by BIS

Sub index ( $SI_i$ ) for each parameter is determined by equation 3 and final WQI is calculated by following equation 4

$$(SI_i = RW_i * q_i) \quad (3)$$

Where,  $SI_i$  = sub index of  $i^{th}$  parameter  
 $q_i$  = rating based on concentration of  $i^{th}$  parameter

$$WQI = \sum SI_i \quad (4)$$

## RESULTS AND DISCUSSION

**Groundwater Quality Assessment.** The descriptive statistics including minimum, maximum, average and standard deviation of the groundwater samples collected during post-monsoon 2012 are tabulated in Table 1. A total 14 physicochemical parameters were assessed to evaluate the groundwater suitability for drinking purpose. Analytical results for all the physicochemical parameters were compared with BIS (1998) standards, shows that the average pH value in study area is 8.3 which is slightly alkaline in nature where, 6 samples i.e 12% are above the permissible limit. In the study area 16% samples surpass the permissible limit (2000 mg/l) of TDS. Such, high concentration in groundwater is due to leaching of salts from soil and anthropogenic activities, which leads to corrosion of metals. The total hardness ranges from 88.0 to 946.0 mg/l with an average of 233.3 mg/l. It was found that TH value in all groundwater samples are within permissible limit except sample no. 44 (946.0 mg/l). The sample no. 44 is located close to Tuppa industrial area and quality affected due to the percolation untreated effluent or leaching of minerals. Only 2% samples exceed the permissible limit of Calcium which may be due to erosion of parent rock material such as limestone and dolomite. Sodium in groundwater ranges from 17.2 to 630.2 mg/l, where, 12% samples exceed the permissible limit. Generally, the sodium salts occur in groundwater due to rock weathering or dissolution of soil salts stored by the influence of evaporation and it also, indicates its high solubility behavior (Stallard and Edmond 1983). The high chloride concentration was found in sample no. 44 which is far beyond the permissible limit. Consumption of such high chloride content water affects on taste, indigestion, corrosion and palatability, which also leads to heart and kidney related diseases (CPCB 2008). It is observed that the values of Magnesium, Potassium, Carbonate, Bicarbonate, Sulphate and Phosphate are within permissible limit.

**TABLE 1.** Descriptive Statistics of groundwater quality parameters (n = 50)

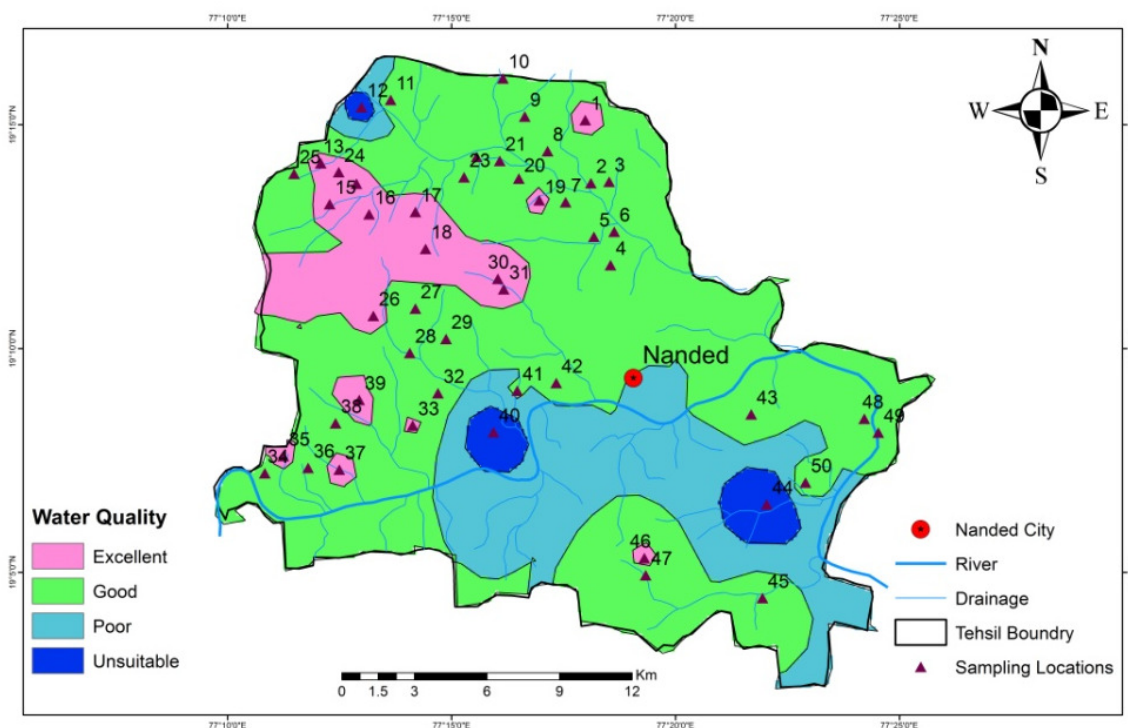
	pH	EC	TDS	TH	Ca	Mg	Na	K	CO <sub>3</sub>	HCO <sub>3</sub>	Cl	NO <sub>3</sub>	SO <sub>4</sub>	PO <sub>4</sub>	WQI
<b>Min.</b>	7.8	816	522.2	88	5.6	8.3	17.2	2	0	80	63.9	0.4	3.9	0	38.1
<b>Max.</b>	8.8	64400	41216	946	352.7	81.4	630.2	8.6	80	460	1043.7	7.2	45.6	0.3	398.7
<b>Avg.</b>	8.3	4792.4	3067.1	233.3	36	34.6	107.4	2.7	25	181.4	175.5	3.3	15.7	0.1	74.7
<b>S.D.</b>	0.2	13120.4	8397	135.1	50.5	16.8	112.8	1.3	16.3	71.5	144.4	1.7	10.2	0.1	71

**TABLE 2.** Relative weight of each water parameter

Parameters	pH	TDS	TH	Ca	Mg	Na	K	CO <sub>3</sub>	HCO <sub>3</sub>	Cl	NO <sub>3</sub>	SO <sub>4</sub>	PO <sub>4</sub>	Total
Weight (Wi)	3	5	3	2	2	3	2	2	2	5	5	3	2	39
Relative weight (RWi)	0.077	0.128	0.077	0.051	0.051	0.077	0.051	0.051	0.051	0.128	0.128	0.077	0.051	1
BIS Standards (1998)	8.5	2000	300	75	30	100	10	--	200	250	45	200	--	

**TABLE 3.** Classification of groundwater samples based on Water Quality Index

Category	Water Type	Number of Samples	% of Samples
0-50.0	Excellent	17	34.0
50.01-100.0	Good	30	60.0
100.01-200.0	Poor	--	--
>200.01	Unsuitable	03	6.0
Total		50	100

**FIGURE 2.** Spatial distribution of Water Quality Index

**Spatial Distribution of Water Quality Index.** The groundwater quality of Nanded tehsil for drinking purpose was evaluated through water quality index method. The water quality index values were interpolated in Arc GIS using IDW technique for preparation of water quality index map of the study area. The different categories in the map was based on the classification shown in Table 3. The water quality index value varies from 38.9 to 398.7 hence it shows large variation of water quality among the groundwater samples. The water quality index were classified into four water types namely Excellent (0-50.0), Good (50.01-100.0), Poor (100.01-200.0) and unsuitable (above 200.01). It is observed that 34% groundwater samples of in the North Western and few patches in N-NE and S-SW part of the study area comes under excellent water type. The good water type represents 60% groundwater samples identified in the study area as shown in Figure 2, hence; 94% samples are fit for drinking purpose. Only 3 samples, located in central part, S-SE near urban area and one patch in North part of the study area are unsuitable for drinking purpose.



## CONCLUSIONS

The present study was carried out to investigate the groundwater quality for drinking purpose in Nanded Tehsil. WQI method has been applied to categorize the different water class and GIS was used to represent its spatial extent in the study area. Analytical results suggests that groundwater in the Tehsil slightly alkaline and moderately hard to very hard in nature. TDS is found higher in 16% of samples, due to the leaching of salts. The concentration of sodium over calcium suggests that cation exchange process in the groundwater at many places. The water quality index of the study area revealed that majority of the samples belongs to excellent to good water type, hence, fit for drinking. Moreover, only 3 samples are unsuitable for drinking. These samples are mainly affected due to high concentration of TDS, TH and Sodium. This study suggests that the possible contamination sources of groundwater such as industrial/domestic waste and fertilizers must be controlled and monitored to protect this precious resource.

## ACKNOWLEDGEMENTS

The author expresses thanks to University Grant Commission for financial assistance to carry out this research work and Director, School of Earth Sciences for providing necessary facilities.

## REFERENCES

- Apha, A. (2005). WEF, 2005. *Standard methods for the examination of water and wastewater*, 21, 258-259.
- Bureau of Indian Standard (BIS), (1998) "Drinking Water—Specification (First Revision) IS-10500." *BIS, New Delhi, India*.
- Causapé, J., Quílez, D., & Aragüés, R. (2004). Assessment of irrigation and environmental quality at the hydrological basin level: II. Salt and nitrate loads in irrigation return flows. *Agricultural Water Management*, 70(3), 211-228.
- CPCB (2008) Guidelines for water quality management. Central Pollution Control Board, Parivesh Bhavan, East Arjun Nagar, New Delhi
- Horton, R. K. (1965). An index number system for rating water quality. *Journal of Water Pollution Control Federation*, 37(3), 300-306.
- Mitra, B. K., Choichi Sasaki, and Enari Keijirou (2006) "Spatial and temporal variation of ground water quality in sand dune area of aomori prefecture in Japan." In *2006 ASAE Annual Meeting*, p. 1. American Society of Agricultural and Biological Engineers
- Scheidt, D. J., & Kalla, P. I. (2007). Everglades ecosystem assessment: water management and quality, eutrophication, mercury contamination, soils and habitat: monitoring for adaptive management: a R-EMAP status report. USEPA Region 4, Athens, GA. *USEPA Region, 4*, 98.
- Stallard, R. F., & Edmond, J. M. (1983). Geochemistry of the Amazon: 2. The influence of geology and weathering environment on the dissolved load. *Journal of Geophysical Research: Oceans*, 88(C14), 9671-9688.
- Štambuk-Giljanović, N. (1999). Water quality evaluation by index in Dalmatia. *Water Research*, 33(16), 3423-3440.
- Stigter, T. Y., Ribeiro, L., & Dill, A. C. (2006). Application of a groundwater quality index as an assessment and communication tool in agro-environmental policies—Two Portuguese case studies. *Journal of Hydrology*, 327(3), 578-591.
- U.S. Environmental Protection Agency (USEPA) (2007) Dallas, TX (2000-05). Chapter 3: Exposure scenario selection. Retrieved Feb 200. RCRA Delisting Technical Support Document. P8
- Yidana, S. M., & Yidana, A. (2010). Assessing water quality using water quality index and multivariate analysis. *Environmental Earth Sciences*, 59(7), 1461-1473.

## **HYDROCHEMICAL CHARACTERIZATION OF GROUNDWATER IN BHOKAR TALUKA OF NANDED DISTRICT, MAHARASHTRA, INDIA**

**Dipak B. Panaskar**, Vasant M. Wagh and Ranjitsinh S. Pawar

(School of Earth Sciences, Swami Ramanand Teerth Marathwada University, Nanded, Maharashtra, India)<sup>17</sup>

**ABSTRACT:** This study is carried out to analyse the Hydrochemical characterisation of Groundwater in Bhokar Taluka, where, fluoride contamination has been recognized as one of the major serious problems. In the study area groundwater is the main source of drinking water, with this context; 89 representative groundwater samples were collected and analysed physicochemical parameters such as pH, EC, TDS, TH, Ca, Mg, Na, K, CO<sub>3</sub>, HCO<sub>3</sub>, TA, Cl, SO<sub>4</sub> and F for pre and post monsoon seasons 2011. It is observed that, pH has remained alkaline in nature in both seasons. Fluoride concentration was recorded in the range 0 to 6.75 mg/l and 0.02 to 6.8 mg/l with an average 0.82 and 0.65 mg/l in pre and post monsoon season; where, the desirable limit is 0.8 to 1.5 mg/l (ISI, 1983; ICMR, 1987). According to Wilcox (1955) classification, EC of the majority of the groundwater samples fall in permissible water class. TDS classification proved that majority of the groundwater samples fall in non-saline and slightly saline class. TH classification shows that majority of the groundwater samples of the study area fall in very hard water class. The Ca, Na, Cl, and SO<sub>4</sub> content of the majority of groundwater samples under the highest desirable limit given by WHO.

**Keywords:** Groundwater, Hydrochemical, Watershed, Fluoride, Bhokar  
Email: dbpanaskar@gmail.com

### **INTRODUCTION**

Groundwater is primary source of water for domestic, agricultural and industrial uses in many countries like India. It is estimated that around one third of world population uses groundwater for drinking purpose (UNEP 1999). The groundwater demand has increased multiple over the years due to population growth, urbanisation, industrialization and agricultural intensification. The groundwater quality is being deteriorated mostly due to overexploitation, increase use of pesticides and fertilizers, improper management of domestic and industrial waste in rural and urban area of many counties. In the developing world, 80 % of all diseases are directly related to poor drinking water and unsanitary conditions (Olajire and Imeokparia, 2001). The chemical composition of groundwater is controlled by many factors that include composition of groundwater from precipitation, geological structure and mineralogy of groundwater from the watersheds and aquifers, and geological processes within the aquifer (Andre et al., 2005).

Bhokar Taluka, the study area is under investigation, where, fluoride contamination in groundwater is reported which remains unexplored so far. Rural dwellers of the study area directly depend on groundwater for drinking and irrigation purpose. Geologically study area is covered by basalt and is underlined by granite from 4 to 20 meter depth and granite is one of the important natural sources of fluoride contamination.

India is one of the 23 nations, which is reported to be endemic to fluorosis disease (UNICEF 1999). In India, nearly 60-65 million people drink fluoride contaminated groundwater leads to 2.5 to 3 million people affected by fluorosis in states like Andhra Pradesh, Bihar, Gujrat, Madhya Pradesh, Punjab, Rajasthan, Assam etc.(Athavale and Das1999; Susheela1999; Rao 2008; Sharma et al.2011). In India the desirable limit of fluoride in drinking water is 0.8 to 1.5 mg/l (ISI, 1983; ICMR, 1987). A higher concentration of fluoride causes dental and skeletal fluorosis and concentration less than 0.8 mg/l cause dental carries.

The objective of the study is Hydrochemical characterization and appraises their suitability for drinking purpose, in addition particularly focusing on fluoride contamination in groundwater of Bhokar Taluka of Nanded District, Maharashtra.

## STUDY AREA

For the present study the Sita Nadi Watershed area of Bhokar Taluka, Nanded District has been selected (Fig. 1). The study area is bounded by longitude  $77^{\circ} 35'$  and  $78^{\circ} 0'$  E and latitude  $19^{\circ} 3'$  and  $19^{\circ} 17'$  N. Geologically, study area is covered by basalt and is underlined by granite from 4 to 20 meter depth and granite is one of the important natural sources of fluoride contamination. Quartz vein is also intruded between Divshi and Kolgaon villages. The width of quartz vein is about 4 meter, and quartz is one of the important sources for fluoride contamination in water.

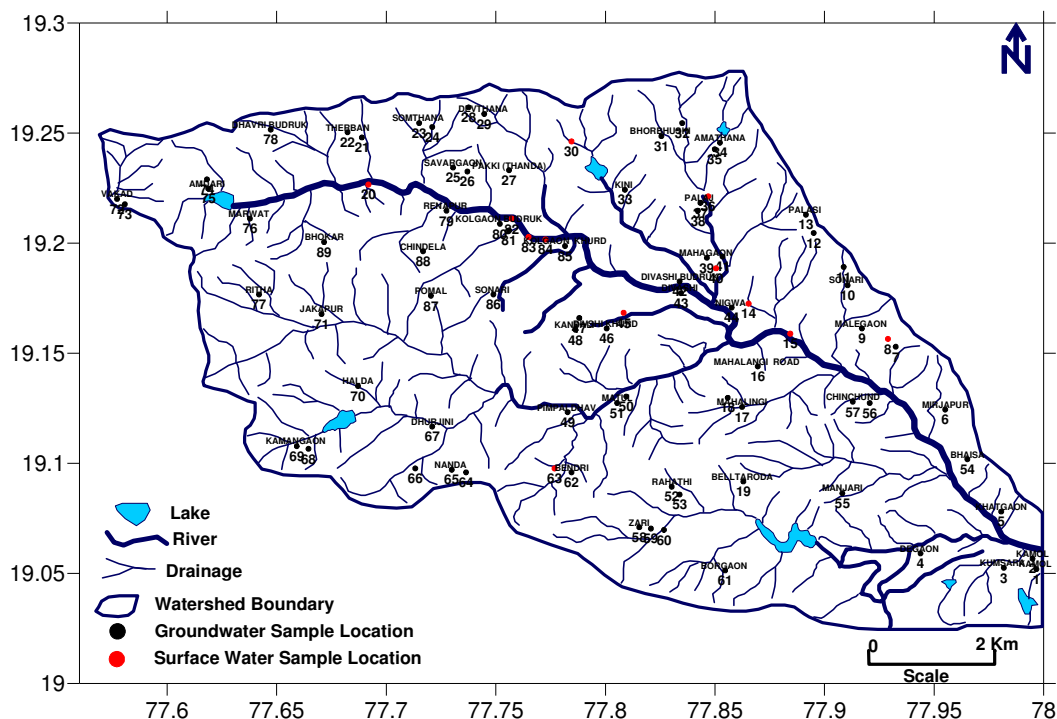


FIGURE 1. Study Area Map with sample locations

## MATERIAL AND METHODOLOGY

Total 89 representative groundwater samples have been collected for pre monsoon and post monsoon season 2011. pH and Electrical conductivity (EC) were measured in the field itself by using portable digital meter. The left over physicochemical parameters such as Ca, Mg,  $\text{CO}_3$ ,  $\text{HCO}_3$  and Cl were analyzed in the laboratory by following the standard methods of American Public Health Association (APHA 2005). The sodium (Na) and potassium (K) ions was determined using flame photometer. The  $\text{SO}_4$ ,  $\text{PO}_4$ ,  $\text{NO}_3$  and F were determined by using spectrophotometer. Surfer 9.0 software was used for the preparation of spatial distribution map of fluoride.

Table 1. Descriptive statistics of Physicochemical Parameters of Pre Monsoon Season 2011

Sr. No.	pH	EC	TDS	TH	Ca	Mg	Na	K	Cl	$\text{HCO}_3$	$\text{CO}_3$	TA	$\text{SO}_4$	F
Min.	7.5	574	367.36	46	3.21	2.92	8.1	5.5	18.46	35	0	45	29	0
Max.	8.9	5740	3673.6	712	193.99	172.5	406.4	266.4	710	440	40	455	132	6.75
Avg.	8.31	1630.5	1043.5	310.29	28.94	56.45	90.72	28.94	147.73	173.71	17.02	190.73	65.67	0.82
Std.	0.28	936.17	599.1	161.38	27.25	42.11	80.33	54.93	118.79	65.75	8.07	67.25	25.08	1.01

## RESULTS AND DISCUSSION

The quality of groundwater is very important because it is the main factor which decides its suitability for domestic, industrial and agricultural purpose. Physicochemical parameters of groundwater samples from Bhokar watershed were determined and assessed in order to understand the variation of the various parameters and their interrelationship of various locations. Data obtained during the course of both field and laboratory analyses of groundwater samples have been discussed as minimum, maximum, average and standard deviation of the parameters, with locations during the pre and post monsoon seasons 2011 have been presented in Table 1 and 2.

**Table 2.** Descriptive statistics of Physicochemical Parameters of Post Monsoon Season 2011

Sr. No.	pH	EC	TDS	TH	Ca	Mg	Na	K	Cl	HCO <sub>3</sub>	CO <sub>3</sub>	TA	SO <sub>4</sub>	F
Min.	7.5	523	334.72	68	9.62	14.5	9.5	5.3	50.6	100	0	100	20	0.02
Max.	8.9	4256	2723.84	642	137.9	329.66	242.1	170.5	412.5	550	20	560	120	6.8
Avg.	8.22	1494.3	956.4	307.4	49.0	122.26	80.72	20.55	192.92	317.87	7.81	325.7	56.73	0.65
StDev.	0.26	744.9	476.7	133.2	24.62	70.13	64.45	33.38	81.21	92.11	5.69	91.83	23.35	0.94

**Table 3.** Classification of EC (Wilcox, 1955), TDS and TH.

Range	Class	Sample Number (%)	
		Pre 11	Post 11
EC (µS/cm)			
< 250	Excellent	00	00
250-750	Good	06(6.8)	13(14.6)
750-2250	Permissible	64(71.9)	64(71.9)
2250-5000	Doubtful	18(20.2)	12(13.5)
> 5000	Unsuitable	01(1.1)	00
TDS (mg/l) (Rabinove et al. 1958)			
< 1000	Non Saline	57 (64.04)	52 (46.28)
1000-3000	Slightly Saline	32 (35.95)	36(32.04)
3000-10000	Moderately Saline	00	1 (0.89)
> 10000	Very Saline	00	00
TH (mg/l) (Sawyer and McCarty, 1967)			
< 75	Soft	02 (3.4)	02 (2.2)
75 - 150	Moderate	16 (18)	06 (6.7)
150 - 300	Hard	27 (30.3)	35 (39.3)
> 300	Verv Hard	43 (48.3)	46 (51.7)

pH of groundwater varies from 7.5 to 8.9 with an average 8.31 for pre and post monsoon season 2011. It can be seen that pH has remained alkaline in both the seasons. pH values of 100 % groundwater samples for both the seasons are above the highest desirable limit, but below maximum permissible limit set by WHO (1998).

Electrical Conductivity (EC) of groundwater samples varies from 574 to 5740  $\mu\text{S/cm}$  and 523 to 4256  $\mu\text{S/cm}$  with an average 1630.45  $\mu\text{S/cm}$  and 1494.34  $\mu\text{S/cm}$  for pre and post monsoon season 2011 respectively. In pre monsoon season high EC is recorded due to ion exchange and solubilization in the aquifer. According to Wilcox (1955) classification of EC (Table 3) the majority of the groundwater samples 71.9 % in the Pre and post monsoon seasons 2011 of the study area falls in permissible water class. Total Dissolved Salts (TDS) of groundwater samples varies wide ranges 367.36 to 3673.6 mg/l and 334.72 to 2723.84 mg/l with an average TDS is 1043.52 mg/l and 956.38 mg/l for pre and post monsoon season 2011 respectively. Generally, the higher concentration of TDS in the groundwater is seen due to the contribution of salts from the soil, weathered parent rock materials and also more residence time in an aquifer body (Darr et al. 2011) According to the classification of TDS (Table 3) the majority of the groundwater samples 64.04 %, 46.28 % and 35.95 %, 32.04 % falls in non saline and slightly saline class in pre and post monsoon

season respectively, however only one sample (sample no. 41) in post monsoon season falls in moderately saline class.

Total Hardness (TH) of groundwater samples varies from wide range of 46 to 712 mg/l and 68 to 642 mg/l with an average 310.25 mg/l and 307.37 mg/l in pre and post monsoon 2011 respectively. Majority of the groundwater samples 48.3 % and 51.7 % in the pre and post monsoon season of 2011 respectively show high TH values than maximum permissible limit given by WHO (1998). According to the classification of TH (Table 3) the majority of the groundwater samples 48.3 % and 51.7 % fall in very hard water class in the pre and post monsoon season. Hardness was slightly increased during post monsoon season; which can be attributed to the leaching content like calcium and magnesium from soil, which is responsible for increase in hardness due to precipitation. Calcium (Ca) of groundwater samples widely varies from 3.21 to 193.99 mg/l and 9.62 to 137.9 mg/l with an average 28.94 mg/l and 49.0 mg/l in the pre and post monsoon season 2011 respectively. Majority of the groundwater samples 94.4 % and 86.5 % in the pre and post monsoon season of 2011 show less Ca values than desirable limit given by WHO (1998) indicating groundwater is good for drinking purposes. Magnesium (Mg) of groundwater samples show wide range from 2.92 to 172.5 mg/l and 14.5 to 329.66 mg/l with an average 56.46 mg/l and 122.26 mg/l in the pre and post monsoon season of 2011 respectively. Majority of the groundwater samples 66.3 % in the pre monsoon season 2011 shows less Mg values than maximum permissible limit and 54 % in the post monsoon season of 2011 show High Mg values than maximum permissible limit given by WHO (1998).

Sodium (Na) of groundwater samples ranges from 8.1 to 406.4 mg/l and 9.5 to 242.1 mg/l with an average 90.72 mg/l and 80.72 mg/l in pre and post monsoon season of 2011 respectively. Majority of the groundwater samples 86.5 % and 91 % in the pre and post monsoon season of 2011 show Less Na content than the highest desirable limit. Potassium (K) of groundwater samples varies from 5.5 to 266.4 mg/l and 5.3 to 170.5 mg/l with an average 28.94 mg/l and 20.55 mg/l in the pre and post monsoon season of 2011 respectively. Chloride (Cl) of groundwater samples varies from 18.46 to 710 mg/l and 50.6 to 412.5 mg/l with an average 147.73 mg/l and 192.92 mg/l in the pre and post monsoon season of 2011 respectively. High chloride content in groundwater may result from natural and anthropogenic sources such as agricultural run-off, use of fertilizers, animal feeds and landfill leachate etc (Taiwo et al. 2011)

Carbonate ( $\text{CO}_3$ ) of groundwater samples varies from 0 to 40 mg/l and 0 to 20 mg/l with an average 17.02 mg/l and 7.81 mg/l in the pre and post monsoon season of 2011 respectively. Bicarbonate ( $\text{HCO}_3$ ) of groundwater samples varies from 35 to 440 mg/l and 100 to 550 mg/l with an average 173.71 mg/l and 317.87 mg/l in the pre and post monsoon season of 2011 respectively. The  $\text{CO}_3$  and  $\text{HCO}_3$  are possibly derived from weathering of silicate rocks, dissolution of  $\text{CO}_3$  precipitates and atmospheric and soil  $\text{CO}_2$  gas (Jeong 2001). Alkalinity (TA) of groundwater samples varies from 45 to 455 mg/l and 100 to 560 mg/l with an average 190.73 mg/l and 325.67 mg/l in the pre and post monsoon season of 2011 respectively. Sulphate ( $\text{SO}_4$ ) of groundwater samples varies from 29 to 132 mg/l and 20 to 120 mg/l with an average 65.67 mg/l and 56.73 mg/l in pre and post monsoon season of 2011 respectively.

Fluoride (F) of groundwater samples in the pre monsoon season of 2011 ranges from 0 to 6.75 mg/l. The maximum Fluoride was recorded from sample No. 11 (1.71 mg/L), 34 (1.91), 37 (1.71), 39 (6.75), 43 (4.02), 48 (1.90), 50 (1.81), 66 (1.81), 75 (1.95), 80 (2.12), 85 (3.98) and 89 (1.83). The spatial distribution of fluoride is as shown in figure 2 (a). The average content of Fluoride in groundwater is 0.82 mg/l which is considerably high, consumption of such water leads to dental and skeletal fluorosis (ICMR 1987). In the post monsoon season 2011, the Fluoride ranges from 0.02 to 6.8 mg/l. The maximum Fluoride was found at sample No. 37 (4.02), 39 (6.8), 42 (2.46), 43 (1.7), 50 (1.72), 85 (3.02). The spatial distribution is as shown in figure 2 (b). The average Fluoride value of the groundwater is 0.65 mg/l, this concentration of fluoride in groundwater may causes dental caries (ICMR 1987). Majority of the groundwater samples 77.5 %, and 87.6 % in the pre and post monsoon season illustrate that less F content than the highest desirable limit.

The desirable limit of fluoride in drinking water is 0.8 to 1.5 mg/l (ISI, 1983; ICMR, 1987). A higher concentration of fluoride causes dental and skeletal fluorosis and concentration less than 0.8 mg/l cause dental carries. The source of fluoride contamination in surface water and groundwater is either natural or anthropogenic or a mixture of both. The higher values of fluoride in groundwater can be attributed to leaching of fluoride from natural sources like granite, mica and other fluoride bearing minerals present in study area and anthropogenic activities like application of phosphate fertilizers because study area has intensive agricultural belt and farmers are using lot of phosphate fertilizers.

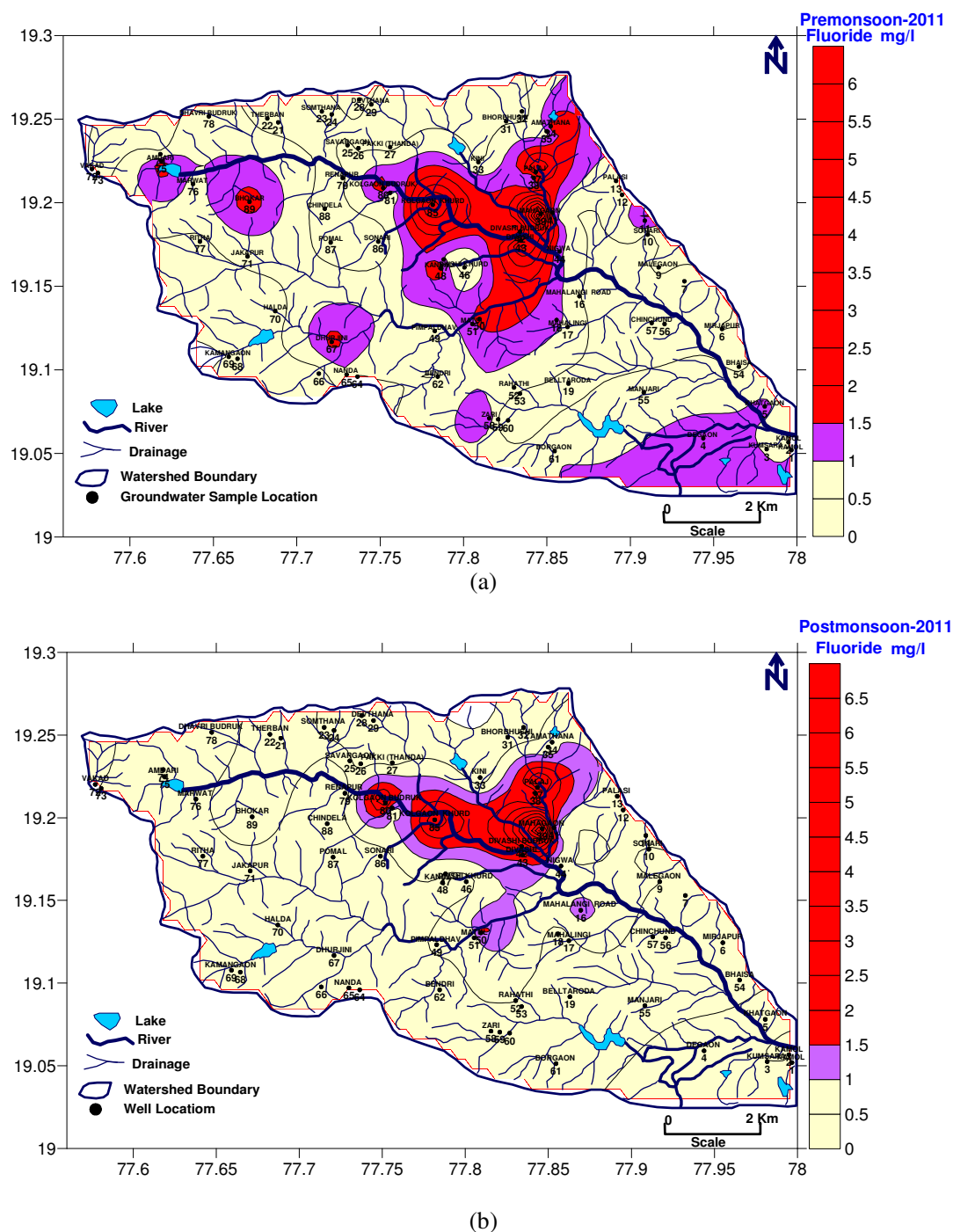


**FIGURE2.** Fluoride Concentration in Study Area (a) Pre-monsoon 2011, (b) post-monsoon 2011

Majority of study area is covered by basalt and is underlined by granite from 4 to 20 meter depth and granite is one of the important natural sources of fluoride contamination. Quartz vein is also intruded between Divshi and Kolgaon villages. The width of quartz vein is about 4 meter, and quartz is one of the important sources for fluoride contamination in water.

The major trend of the lineaments NW- SE and NE- SW. The major lineaments trend in the NW- SE direction while the minor lineaments trend in the NE- SW direction. The one major lineament i.e. Sita

lineament trending in NW- SE direction which follows the Sita River course and passes from Renapur, Kolgaon Budruk, Kolgaon Khurd, Divshi Budruk and Divshi Khurd villages.

## CONCLUSIONS

Hydrochemical characterisation of groundwater of Bhokar Taluka was assessed to determine drinking suitability in pre and post monsoon season of 2011. Physicochemical interpretation confirms that groundwater is alkaline and moderately hard to very hard in nature in both the season of the study area. High EC is recorded in pre monsoon season due to ion exchange and solubilization in the aquifer. The higher concentration of TDS in the groundwater is found due to contribution of salts from the soil and weathered rock materials. Hardness was slightly increased in post monsoon season; it can be attributed to the leaching of calcium and magnesium contents from soil. High chloride content in groundwater resulted from natural and anthropogenic sources. It is confirm that  $\text{CO}_3$ ,  $\text{HCO}_3$  and  $\text{SO}_4$  contents are within permissible limit in both the seasons.

It is interesting to note that the groundwater samples (39, 42 and 43) which are in the vicinity of Sita lineament show higher concentration of fluoride. This can be attributed to the granitic rock as a source of fluoride which is underlined by basalt in this area. Since, the lineament is a weak zone; the fluoride from the granitic rock is getting leached out and contaminates the groundwater in this region. In the pre-monsoon season the fluoride concentration is more and extensively distributed as compared to post-monsoon season in the study area.

For sustainable management of groundwater in study area needs regular monitoring, epidemiological surveillance for dental and skeletal fluorosis check up, installation of fluoride removal plant and conduct fluorosis awareness program through public participation .

## ACKNOWLEDGEMENTS

One of the author, express thanks to Department of Science and Technology (DST), New Delhi, for financial assistance under major research project.

## REFERENCES

- Andre, L., Franceschi, M., Pouchan, P., & Atteia, O. (2005). Using geochemical data and modelling to enhance the understanding of groundwater flow in a regional deep aquifer, Aquitaine Basin, south-west of France. *Journal of Hydrology*, 305(1), 40-62.
- APHA, A. (2005). WEF, 2005. *Standard Methods for the Examination of Water and Wastewater*, 21, 258-259.
- Athavale, R. N., & Das, R. K. (1999). Beware! Fluorosis is zeroing in on you. *Down to Earth*, 8, 24-25.
- Dar, I. A., Sankar, K., Shafi, T., & Dar, M. A. (2011). Investigation of groundwater quality in hardrock terrain using Geoinformation System. *Environmental Monitoring and Assessment*, 176(1-4), 575-595
- ICMR (1987), Indian Council of Medical Research; Manual of Standards of Quality for drinking water Supplies.
- International Nutrition Foundation, & Micronutrient Initiative. (1999). *Preventing Iron Deficiency in Women and Children: Background and Consensus on Key Technical Issues and Resources for Advocacy, Planning, and Implementing National Programmes: UNICEF*. Micronutrient Initiative.
- ISI (1983), (Indian Standard Institute) Indian Standard Specifications for drinking water, IS 10500.
- Jeong, C. H. (2001). Effect of land-use and urbanization on hydrochemistry and contamination of groundwater from Taejon area, Korea. *Journal of Hydrology*, 253, 194-210
- Olajire, A. A., & Imeokparia, F. E. (2001). Water quality assessment of Osun River: Studies on inorganic nutrients. *Environmental Monitoring and Assessment*, 69(1), 17-28.
- Rabinove CJ, Long Ford RH, Brook Hart JW (1958) Saline water sources of north Dakota. US Geological Survey Water Supply Paper 1428, 72.
- Rao, N. S. (2009). Fluoride in groundwater, Varaha River Basin, Visakhapatnam District, Andhra Pradesh, India. *Environmental Monitoring and Assessment*, 152(1-4), 47-60.
- Sawyer, C. N., & McCarty, P. L. (1967). Chemistry for sanitary engineers. In *Chemistry for sanitary engineers*. McGraw-Hill

- Sharma, P., Sarma, H. P., & Mahanta, C. (2012). Evaluation of groundwater quality with emphasis on fluoride concentration in Nalbari district, Assam, Northeast India. *Environmental Earth Sciences*, 65(7), 2147-2159.
- Susheela, A. K. (1999). Fluorosis management programme in India. *Current Science- Bangalore* , 77, 1250-1256.
- Taiwo, A. M., Adeogun, A. O., Olatunde, K. A., & Adegbite, K. I. (2011). Analysis of groundwater quality of hand-dug wells in peri-urban area of Obantoko, Abeokuta, Nigeria for selected physico-chemical parameters. *Pacific J. Sci. & Technol*, 12(1), 527-534.
- UNEP, 1999. *Global Environment Outlook 2000*. Earthscan, London.
- UNICEF (1999) State of the report on the extent of fluoride in drinking water and the resulting endemicity in India. Report by fluorosis and Rural Development Foundation for UNICEF, New Delhi
- Wilcox, L. (1955). Classification and Use Of Irrigation Waters.
- World Health Organization. (1998). *Guidelines for Drinking-Water Quality*. Vol. 2, Health criteria and other supporting information: addendum.



## MODELLING OF ARSENIC REMOVAL FROM GROUNDWATER BY ELECTRODIALYSIS

**Rose Marie O. Mendoza** (Far Eastern University-NRMF, Institute of Medicine, Quezon City, Philippines)

Meng-Wei Wan and Chi-Chuan Kan (Chia Nan University of Pharmacy and Science,

Department of Environmental Engineering and Science, Tainan, Taiwan)

Maria Lourdes P. Dalida (National Graduate School of Engineering, Department of Chemical Engineering, University of the Philippines, Diliman, Quezon City, Philippines)

**ABSTRACT:** A model for Arsenic removal from ground water was evaluated. At varying experimental conditions, the second order homogeneous ordinary differential equation model proposed by Yu and Admassu on ion removal (from pulp and paper mill process stream) was able to predict the concentration, current utilization and removal of As ions from ground water samples efficiently. Two model parameters specifically for arsenic systems was derived: A is a parameter used to describe the characteristics of the solution, while  $\lambda^2/B$  is a parameter that is related to the stack electrical field strength. Post hoc analysis of the model and  $R^2$  values of 0.9899 and above was obtained for all parameters considered which indicate that the model can adequately describe the removal of arsenic from contaminated waters. The model was used to determine the effects of experimental parameters on Arsenic removal from ground water samples in terms of applied potential, feed flow velocity and initial feed concentration. A very satisfactory agreement between model predicted and experimental values of concentration, current utilization and removal efficiencies were obtained.

## INTRODUCTION

Arsenic-related incident covers almost majority of Asia. Bangladesh, Cambodia, China, India, Myanmar, Nepal, Pakistan, Taiwan and Vietnam are countries recently has been identified to use arsenic (As) contaminated ground water for irrigation. This poses serious health hazard to people eating food from the crops irrigated with arsenic contaminated water, in addition to the fact As accumulating in irrigated soils poses a serious threat to sustainable agriculture in affected areas (Brammer and Ravensoft, 2009). Bangladesh's As-contaminated groundwater has been extensively used to irrigate paddy rice, during dry season of 75% of the total area given to rice cultivation with arsenic levels of 4-8  $\mu\text{g/g}$  and reaches to 83  $\mu\text{g/g}$  (Rahman and Hasegawa, 2011). Because of the similar agro-ecological and hydrogeological conditions of these South East Asian regions the threat of arsenic contamination can easily reach neighboring countries. So far, arsenic contamination is widely detected to the alluvial plains of South and South East Asia where rice (paddy) is the main crop irrigated with ground water. According to Ravensoft (2007a,b), the GIS-based-geological-geochemical-hydrological models predict widespread pollution of ground waters in Indonesia, Malaysia and the Philippines – where water supplies were not yet tested for Arsenic.

Mendoza et al. (2014) in their study mentioned the viability of Electrodialysis (ED) as a process to remove inorganic As from contaminated waters. The study also stressed that experiments on arsenic systems should be carefully modelled and optimized to yield higher removal rates, while generating lesser waste by-products which can be more toxic than its source. Galvanin et al. (2015) opined that model-based design of experiment is a satisfactory approach to minimize the number of trials required for actual experimental runs.

To date, there is very less attention focused on model parameters for natural aqueous systems, particularly on arsenic removal and separation using electrodialysis (ED). The Nernst-Planck equation is one of the most utilized and widely-used model for a time-dependent transport and conversion on mass through the motion of charged chemical species in fluid medium (Kirby et al., 2010). Galvanin et al. (2015) utilized the Nernst-Planck approach to model the electrodialytic recovery of multi-valent electrolytes to accomplish desalination using NaCl while Zourmand et al. (2015) combined the Nernst-Planck model with that of Navier-Stokes model to develop a mass transfer model for the prediction of ion transport through electrodialysis (ED) cell using also NaCl solution. Mohammadi et al. (2005) as well as Sadrzadeh and Mohammadi (2007) provided a statistical model of metal ion removal from textile and semiconductor

effluents using electrodialysis and electrodyliasis reversal by a Taguchi L9 OA design. It was only Mendoza et al. (2014) who used the electrodialysis (ED) process in removing arsenic from as-spiked water and come up with an optimum experimental conditions based on maximized As removal or separation. Thus, the burden of treating arsenic contaminated waters that will produce streams of higher arsenic concentration is one of the drawback of the study. The need to initially model arsenic systems to predict its removal from contaminated water will be of great contribution to the environmental sustainability of the said process. Through a model that will mimic the removal of arsenic from aqueous systems and with several related studies, lesser concentrated wastes will be generated which can gear the ED process towards zero-waste technology.

This paper investigates the removal of As from actual groundwater samples through the determination of the concentration and limiting current profile using the Yu and Admassu model (2000) for metal ions removal (from pulp and paper industry) and to come up with an model-generated predictions on arsenic removal at varied experimental conditions. The study also includes the model determination of the effect of experimental parameters such applied potential, feed flow velocity, initial feed concentration and operating time which is then later compared to the actual experimental data.

## MATERIALS AND METHODS

**Materials.** Groundwater samples used in this experiment were obtained from raw water source, well no. 9 and 10 of Taiwan Water Corporation's Water Treatment Plant in Beigang Township, Yunlin, Taiwan. Characteristics of the groundwater used for this study was presented in Table 1. The samples were filtered immediately through a 0.45 $\mu$ m pore size cellulose acetate syringe filter to minimize arsenic III oxidation with air. To further preserve arsenic species in the filtered sample, ethylenediaminetetraacetic acid (EDTA) was added immediately to the filtrate. This preserves the distribution of arsenic species by chelation to metal ions, prevents drastic changes in sample pH and minimizes microbial activity. Filtered samples were stored in PET containers at reduced head space and refrigerated at 4°C (Bednar et al., 2004).

**TABLE 1 Characteristics of the Ground Water Used in This Study**

Cations	Concentration mg/L	Anions	Concentration mg/L
Na <sup>+</sup>	145.50	Cl <sup>-</sup>	130.559
K <sup>+</sup>	34.515	NO <sub>3</sub> <sup>-</sup>	<0.1
Mg <sup>2+</sup>	18.97	SO <sub>4</sub> <sup>2-</sup>	2.285
Ca <sup>2+</sup>	20.75	HCO <sub>3</sub> <sup>-</sup>	119.70
Mn <sup>2+</sup>	0.093	PO <sub>4</sub> <sup>3-</sup>	6.299
Fe <sup>tot</sup>	<0.01	TOC	1.19 mg. C
As <sup>tot</sup>	0.702		

Others:  $E_h = -162.2$  mV; pH = 7.68;  $T = 23^\circ\text{C}$ ; EC = 1388  $\mu\text{S/cm}$

(Obtained from: Taiwan Water Corporation's Water Treatment Plan, Well no. 9 and no. 10, Beigang County, Yunlin, Taiwan)

The ORP and pH of the solutions was monitored using Suntex pH-ORP meter model SP-300. Current and Voltage measurements were performed using a Hao Ling HL 833 digital ammeter and voltmeter, respectively. The total As, As III and As V concentrations and concentrations of cations (Na, Mg, Ca, K, Mn and Fe) of the feed, diluate stream and concentrate stream was determined using a Perkin Elmer 2000 Optima DV Inductively Coupled Plasma - Optical Emission spectrophotometer equipped with a hydride generator (HG-ICP-OES). Anion concentration in the form of nitrates, nitrites, phosphates, sulphates and chlorides, were analyzed using a Dionex DX-120 ion chromatograph (IC) equipped with a Reagent Free Controller (RFC), carbonates were obtained by titrimetric methods and TOC by direct method for drinking

water and wastewaters (Method 10129) using Hach DR 500 UV-VIS Spectrometer. Conductivities of the solution were determined using Suntext EC-410 digital conductivity meter attached to the control panel.

**Methods.** The tailor-made electrodialysis (ED) provided by Shell Kwong Sir Enterprise Co., was used to conduct As removal experiments in the recirculating batch mode. The ED stack is composed of a single hydraulic and single electrical stack with 20 cell pairs situated 0.9 mm apart. Operating temperature for the whole system was set at  $25^{\circ}\text{C} \pm 1^{\circ}\text{C}$ . Maximum parameters for the ED stack as recommended by the manufacturer were indicated in the study of Mendoza et al. (2014). Optimum experimental settings such as applied voltage of 17V, initial feed concentration ( $C_0$ ) of 700 ppb, feed flow rate of 0.033 l/s and a minimum operating time of 92 minutes used by Mendoza et al. (2014) in their study on As-spiked water was considered for model experimental runs. Groundwater samples were pre-treated in the pre-oxidation tank to transform  $\text{As}^{3+}$  to  $\text{As}^{5+}$ , then fed into the feed tank. From the feed tank, contaminated groundwater sample was introduced in the ED stack at an optimum feed flow velocity, and the sample was desalted in 92 minutes using 17V as the applied voltage. As the feed was introduced, the tap water as the electrode flush solution was circulated into the anodic and cathodic compartments. The concentrate stream was dumped into the electrode flush tank and eventually became part of the electrode flush solution.

The samples from the diluate stream were immediately digested with 5% potassium iodide (KI), 5% vitamin C and concentrated HCl. The mixture was set aside for 25 minutes for stabilization and diluted to its marked volume using Ultrapure 18.2 mΩ deionized water. A solid phase extraction membrane, Supelco LC-SAX strong anion resin was used to immediately separate As III from As V at an elution time of 1 minute (Jang et al., 2011). The total As, As III and As V of the sample was analyzed using a Perkin Elmer Inductively Coupled Plasma-Optical Emission Spectrophotometer (HG-ICP-OES) Optima DV2000 at 228.812 nm, using Hydride Generation. A reducing agent in the form of 5% sodium borohydride ( $\text{NaBH}_4$ ) in 0.5% sodium hydroxide (NaOH) was used counter current with the sample to prevent further sample oxidation or metal complexation phenomena. Calibration standards of 1, 5, 10, 50, 100 and 700 ppb are freshly prepared during sample analysis. Two 2 sample replicates, check samples and standards are included to countercheck the accuracy and precision of the determination of the concentrations using HG-ICP-OES.  $R^2$  for each analysis was established at 0.999 or higher. Cations and anion content as well as TOC and bicarbonate were also evaluated.

## RESULTS AND DISCUSSION

In a published paper in 2000 by Z.Yu and W. Admassu, a model for the concentration and current profile was evaluated and used in removing metal ion from pulp and paper mill process stream. The model describes the transport of metal ions in the boundary layers at membrane surfaces and the limiting current density as a function of low velocity and removal efficiency. The general transport equation for the molar flux ( $J$ ) driven by diffusion, migration and convection in the ED channels is governed by the Nernst-Planck equation (Yu and Admassu, 2000):

$$J_{\pm} = -z_{\pm}v_{\pm}FC_{\pm}\nabla\phi - D\nabla C_{\pm} + C_{\pm}u \quad (1)$$

The model was anchored on the following assumptions: (1) the potential is a function of location due to a constant current supply, and the external applied potential is considered constant thus potential gradient will also be considered constant. Thus, equation (1) becomes:

$$\frac{\partial C_{\pm}}{\partial t} + u\nabla C_{\pm} = z_{\pm}v_{\pm}F\nabla \cdot (C_{\pm} + \nabla\phi) + D_{\pm}\nabla^2 C_{\pm} \quad (2)$$

The motion of the charged particles will bring current into the system. The current intensity for the solution is defined as  $i = F\sum zJ$  which gives the equation for the aqueous solution as:

$$i_{\pm} = -F^2\nabla\phi\sum z_{\pm}^2v_{\pm}C_{\pm} - F\sum z_{\pm}D_{\pm}\nabla C_{\pm} + Fu\sum z_{\pm}C_{\pm} \quad (3)$$

To simplify the model equations the following assumptions were made: (1) for a quasi-steady state the time variation of concentration and the diffusion term along the flow direction is negligible compared to convection; and (2) neutrality of charge is satisfied in the whole channel which makes  $z_+C_+ + z_-C_- = 0$

and (3) the influence of the flow profile of fluid is negligible which allowed the system to be considered as a plug flow fluid. The dilute nature of the solution makes its viscosity as that of water which will now flow the schematic flow in Figure 1 (Yu and Admassu, 2000). This follow that:

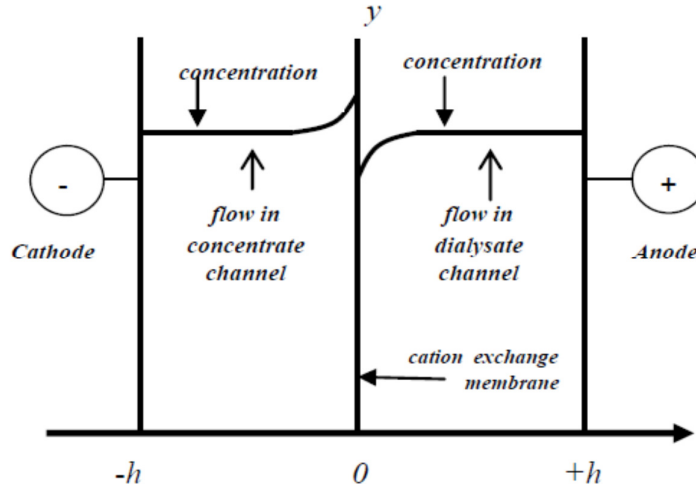


**FIGURE 1.** Flow Scheme of the Solution in the ED Stack

Simplifying equation (3) and inserting it to equation (2) results in:

$$u \frac{\partial C_+}{\partial y} = D_+ \frac{\partial^2 C_+}{\partial x^2} + z_+ v_+ F \frac{d\phi}{dx} \frac{\partial C_+}{\partial x} \quad (4)$$

For the current density and simplification of equation (3) is based on the assumption previously expressed considering a constant potential gradient within the stack. This makes the effect of convection in equation  $u C_+$  negligible. The current in the anionic membrane  $i_- = 0$  since the current density in the cation exchange membrane is the only one being considered in the model. Thus, the current in the cationic membrane is:

$$i_+ = -D_+ F z_+ \frac{dC_+}{dx} - \frac{F^2 z_+^2 D_+ C_+}{RT} \frac{d\phi}{dx} \quad (5)$$

and by principle of electroneutrality and non-ideality on membranes,

$$\frac{dC_+}{dx} = \frac{F z_+ C_+}{RT} \frac{d\phi}{dx} \quad (6)$$

Equation (2) is simplified by setting  $A = u/D_+$  and another parameter as

$$B = z_+ v_+ F / D_+ \cdot d\phi / dx \quad (7)$$

from a deduced dimensionless reduced concentration  $C^* = C_w/C_0$ , equation (2) becomes

$$A \frac{\partial C^*}{\partial y} = \frac{\partial^2 C^*}{\partial x^2} + B \frac{\partial C^*}{\partial x} \quad (8)$$

where  $C_0$  is the initial concentration and  $C_w$  is defined as the wall concentration in the boundary layers near the interface as shown in Figure 3 (Yu and Admassu, 2000). Analyzing Figure 2, the boundary conditions for equation (16) are set as:  $x = 0$ ,  $C^* = C_s$  ( $C^*|_{x=0}$ ),  $x \rightarrow h$  ( $x > x_a$ ),  $C^* = C_h$  ( $C^*|_{x=h}$ ) and  $y = 0$ ,  $C^* = 1$  for  $x > x_a$ .

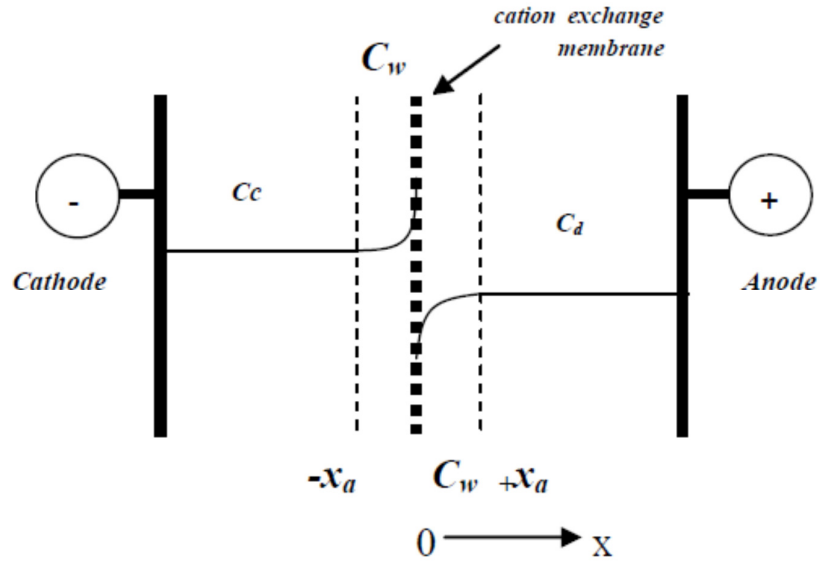


**FIGURE 2.** Boundary layer used in this study for the ED process

The transport of ions in this model assumes that it occurs and only significant along the boundary layers, which is in the region where  $x$  is greater than 0 but less than  $x_a$ . From Figure 3 we can say that  $x_a \ll h$  when  $x > x_a$  and  $x \rightarrow h$ , then  $x \rightarrow \infty$ . This analysis of the boundary layers generates a general solution for equation (8) as:

$$C^*(x, y) = f(y)g(x) \quad (9)$$

which can be written as:

$$\frac{A}{f} \frac{df}{dy} = \frac{1}{g} \left( \frac{d^2g}{dx^2} + B \frac{dg}{dx} \right) \quad (10)$$

In the dialysate channel, the cation transport decreases along the flow direction ( $y$ ). Introducing a constant  $-\lambda^2$  to represent separation constant in the dialysate channel based on the boundary conditions set, equation (10) becomes:

$$\frac{df}{dy} + \frac{\lambda^2}{A} f = 0 \quad (11)$$

which is a second-order homogeneous ordinary differential equation with the form;

$$\frac{d^2g}{dx^2} + B \frac{dg}{dx} + \lambda^2 g = 0 \quad (12)$$

And an auxiliary equation (Kreyzig, 2006):

$$K^2 + BK + \lambda^2 = 0 \quad (13)$$

Equation (13) has two roots:

$$K_{1,2} = -\frac{B}{2} \left\{ 1 \mp \left( 1 - \frac{4\lambda^2}{B^2} \right)^{1/2} \right\} \quad (14)$$

The general solution for Equation (12) (Kreyzig, 2006) is:

$$g(x) = N_1 \exp(K_1 x) + N_2 \exp(K_2 x) \quad (15)$$

Combining equation (11) and equation (13), the reduced concentration in the dialysate channel is:

$$C^*(x, y) = f(y)g(x) = \{m_1 \exp(K_1 x) + m_2 \exp(K_2 x)\} \exp\left(-\frac{\lambda^2}{A} y\right) \quad (16)$$

The integration constants  $m_1$  and  $m_2$  was determined using boundary conditions. For the purpose of simplification of equation (16) the following assumptions were made:  $4\lambda^2/B^2 \ll 1$  and  $\lambda^2/B \ll B$  so that  $K_2 \approx -B$ ; at  $y = 0$ ,  $C^* = 1$  for  $x > x_a$ ,  $x$  becomes large,  $\exp(-Bx) \rightarrow 0$  faster than  $\exp(-\lambda^2/Bx)$  because  $\lambda^2/B \ll B$ . This yields,

$$m_1 = \exp\left(\frac{\lambda^2}{B} h\right) \quad (17)$$

and

$$m_2 = \frac{\exp\left(\frac{\lambda^2}{B} h\right) \left\{ \frac{\left(\frac{d\phi}{dx}\right)_{m,d}}{\frac{d\phi}{dx}} + \left(\frac{RT}{z+F}\right) \left(\frac{\lambda^2}{B}\right) \left(\frac{d\phi}{dx}\right) \right\}}{1 + \left(\frac{d\phi}{dx}\right)_{m,d} / \left(\frac{d\phi}{dx}\right)} \quad (18)$$

and gives the concentration profile at any location in the ED dialysate and concentrate channel, respectively as :

$$\frac{C_w}{C_0} = \left[ 1 - \frac{\left(\frac{d\phi}{dx}\right)_{m,d} / \frac{d\phi}{dx}}{1 + \left(\frac{d\phi}{dx}\right)_{m,d} / \frac{d\phi}{dx}} \exp(-Bx) \right] \exp\left(-\frac{\lambda^2}{A} y\right) \quad (19)$$

For the current density profile equations (5), (6) and (19) yields:

$$i_{w,d} = -2D_+ F z_+ C_0 \left[ B \frac{\left(\frac{d\phi}{dx}\right)_{m,d} / \frac{d\phi}{dx}}{1 + \left(\frac{d\phi}{dx}\right)_{m,d} / \frac{d\phi}{dx}} \exp(-Bx) \exp\left(-\frac{\lambda^2}{A} y\right) \right] \quad (20)$$

Equation (19) and (20) is then simplified by integrating both sides with the boundary condition  $C_s = C_w|_{x=0}$  which results to:

$$C_w - C_s = -\frac{i_+}{2D_+ F z_+} x_a \quad (21)$$

where  $i_+$  is the current flowing in the opposite direction of  $x$ ,  $F$  is the Faraday's constant (96,480 C/mol),  $D_+$  diffusion coefficient ( $\text{cm}^2/\text{s}$ ) of cation in the solution,  $z$  is the charge of ion and  $x_a$  (mm) average thickness of the boundary layer.  $C_w - C_s$  will be greater than 0 which is considered as the concentration of in the diluate compartment when boundary conditions  $C_s = C_w|_{x=0}$  is considered. When  $C_s \rightarrow 0$ ,  $i_+ = i_{lim}$  and :

$$i_{lim} = \frac{2D_+ F z_+}{x_a} C_w|_{x \rightarrow 0} \quad (22)$$

From Kocherginsky (2010), equation (22) has a form:

$$i_{lim} = C_o e^{\frac{-u^*}{u}} \quad (23)$$

where  $u^* = D_+ \lambda^2 y$ . Equation (23) indicates the limiting current density is a function of both initial concentration  $C_0$  and flow velocity  $u$ . The magnitude of the parameter  $\lambda^2$  is a function of initial concentration ( $C_0$ ) removal efficiency (R%) and physical ED stack characteristics.

For equations (19), in the boundary layers, when  $x \approx 0$ , the concentration becomes independent of  $x$  as  $x \rightarrow h$ . This means that the significant removal or separation of ions mainly occurs at the membrane walls/surfaces. As a function of  $y$ , the decrease in the concentrate channel results to an increase in concentration of the concentrate channel. Due to the transport of ions in the boundary layer, the system will tend to polarize when  $y = L$  as  $x \rightarrow 0$ . This makes the field strengths at membrane surface different in the cationic and anionic membrane surfaces. In this model, the field strengths are estimated using the continuity condition of electrical current at specified locations.

From equation (20), the value of current at entrance ( $y=0$ ) is at maximum and decreases continuously as it approaches  $y = L$ . At the membrane surface ( $x=0$ ), the current density also reaches the maximum value. In the boundary layer, the current density decreases as  $x \rightarrow x_a$ , beyond the boundary layer,  $x \rightarrow h$  and  $i \rightarrow 0$ . This strongly suggests that concentration or concentration gradient is one of the factors that can influence current and current density.

From Ohms Law, the intensity of current is directly proportional to the electric field. As such there is a direct variation that can be observed between current density and the surface electrical field ( $d\phi/dx$ )<sub>m,d</sub> which in turn show a direct relationship between ion transport. This resulted in the direct proportionality between current density and initial concentration.

For parameter estimation of the model equations for concentration profile and current density at any location in the ED channel, R% is defined based on as a function of  $\lambda$  is obtained as:

$$S\% = R\% = \frac{C_0 - C}{C_0} \times 100 = \left(1 - \exp\left(-\frac{\lambda^2}{A} L\right)\right) \times 100 \quad (24)$$

Equation (20) is true only when  $0 < (R\%) < 100$ . An evaluation of the concentrate channel, though not so significant in this study must also be performed to facilitate transport equation facilitation. For the concentrate channel, the bulk concentration increases along the flow direction (Yu and Admassu, 2000). To compare the separation of concentrate to that of the dialysate channel, another separation constant in the form of  $\xi$  is defined related to the gain efficiency in the concentrate channel which leads to:

$$R\% = \frac{C_L - C_0}{C_0} \times 100 = \left[\exp\left(\frac{\xi^2}{A} y\right) - 1\right] \times 100 \quad (25)$$

and yields,

$$\xi^2 = \frac{A}{L} \ln\left(1 + \frac{R'\%}{100}\right) \quad (26)$$

**TABLE 2 Typical Values Used For Model Calibration And Model Parameters for the ED Process**

Geometric Sizes	Symbol	Value	Source
Flow distance	L (mm)	360 mm	This study
Flow width	W(mm)	170 mm	This study
Half-channel width	h (mm)	5 mm	This study
Average film thickness	$x_a$	0.45 mm	This study
Number of cell pairs		20	This study
<i>Characteristics of Feed Solution</i>			
Average flow speed	$u$ (c,m/s)	0.0033	This study
Valence (as H <sub>2</sub> AsO <sub>4</sub> )	$z$	1	Clifford and Ghurye, 2005

Initial Concentration	Co (ppb)	700	This study
Diffusion Coefficient	D (cm <sup>2</sup> /s)	0.809x10 <sup>-5</sup>	Leaist (2007)
Density	ρ (g/cm <sup>3</sup> )	1	
Viscosity of water	μ( kg/ m s)	900 x 10 <sup>-6</sup>	Leaist (2007)
<i>Applied Conditions</i>			
Temperature	T (K)	298	This study
Constant electrical field	dθ/dx (vol/m)	100 kg-m/s <sup>2</sup> C	Yu and Admassu (2000)
Removal Efficiency	E%	99.56	This study
<i>Physical Constant</i>			
Faraday Constant	F (C/mol)	96480	
Gas Constant	R (J/K mol)	8.413	

Non-ideality of membrane assumption ensures that there is no retention of cations at the membrane surfaces and in the membrane and indicate that the amount cations removed from the dialysate channel (R%) is equal to the amount of ions gained in the concentrate channel (R'%) which makes the magnitude of  $\lambda^2 > 0$ .

To estimate the magnitude of  $\lambda^2/B$ , model parameters based on typical values in ED process for KCl is used by the paper (Yu and Admassu, 2000), which gives an initial value for Co and an average R% of 50 for batch ED process (Mc Neil and McCoy, 1989). This follows that:

$$\frac{\lambda^2}{B} = \frac{1}{L} \left| \ln \left( 1 - \frac{R\%}{100} \right) \right| \frac{uRT}{z_+ D_+ F (d\phi/dx)} = 0.018/\text{mm}. \quad (27)$$

$$B = \frac{z_+ v_+ F}{D_+} \frac{d\phi}{dx} = \frac{z_+ F}{RT} \frac{d\phi}{dx} = 3.823/\text{mm} \quad (28)$$

$$\frac{\xi^2}{B} = 0.011/\text{mm}. \quad (29)$$

For the model calibration, Table 2 presents the known physical parameters of the ED stack as well as the physical and chemical properties of the solution and the membranes while to facilitate model parameter estimation, typical values for ED process in the table below is used.

The very good agreement between the experimental and model predicted values was dictated by the R<sup>2</sup> values indicated in Table 3 which was found to be greater than 0.98 on all parameters set for the study. Two model parameters were considered for this study; A is a parameter used to describe the characteristics of the solution, while  $\lambda^2/B$  is a parameter that is related to the stack electrical field strength. The increasing values of  $\lambda^2/B$  with respect to increase in initial feed concentration indicate efficient current utilization in the stack and efficient collision of ions during desalination within the stack channel while a constant value of A as the initial concentration increases indicates that ion transport is not limited to solution characteristics, rather it is more dictated by current and potential. Figure 3a shows that the removal of As ions from the feed for both experimental and predicted values are more efficient at applied potentials above 10V.

**Effect of experimental parameters on Arsenic removal from groundwater using ED.** Model predicted values was compared with that of the experimental values in evaluating the effect of experimental parameters on arsenic removal. From Figure 3a model predicted values agrees satisfactorily with that of experimental values, confirming a direct relationship between applied potential %removal at variable



concentration. The %removal was found to increase as the applied potential is increased at high or low initial feed concentrations. The same satisfactory agreement was found between % removal and feed flow velocity at high and low concentrations. However, an inverse relationship was found between %removal and feed flow velocity at varied concentrations as illustrated in Figure 3b. This can be due to the fact that the initial feed flow velocity was complemented by the applied potential resulting in a very fast transit of ions to the boundary layers, which indicates that in an ED system, very low or very high feed flow velocity are both non ideal conditions that may lead to neither increased energy consumption or polarization. Higher removal rate was found to at feed flow velocity of 0.033 l/s.

**TABLE 3 Parameters obtained for Yu and Admassu Model**

<b>Varied Parameters</b>	<b>Correlation Coefficient, R<sup>2</sup></b>	<b><math>\lambda^2/B</math> mm<sup>-1</sup></b>	<b>A cm<sup>-1</sup></b>
<b>Initial Feed Concentration<sup>a</sup></b>			
200 ppb	0.993	0.63690	42.0272
500 ppb	0.966	0.67654	42.0272
700 ppb	0.981	0.73093	42.0272
<b>Feed Flow Velocity<sup>b</sup></b>			
0.0025 m <sup>3</sup> /s	0.994	1.30843	30.9024
0.0033 m <sup>3</sup> /s	0.999	1.30843	42.0272
0.0042 m <sup>3</sup> /s	0.999	1.30843	51.9160
<b>Applied Potential<sup>c</sup></b>			
5V	0.980	0.03133	42.0272
10V	0.993	0.00084	42.0272
17V	0.993	0.00004	42.0272

<sup>a</sup> Applied Potential (E)=3-20V; feed flow rate = 0.0033 m<sup>3</sup>/s; Time = 92 min.

<sup>b</sup> Applied Potential (E)=17V; Initial feed concentration = 700 ppb; Time = 92 min.

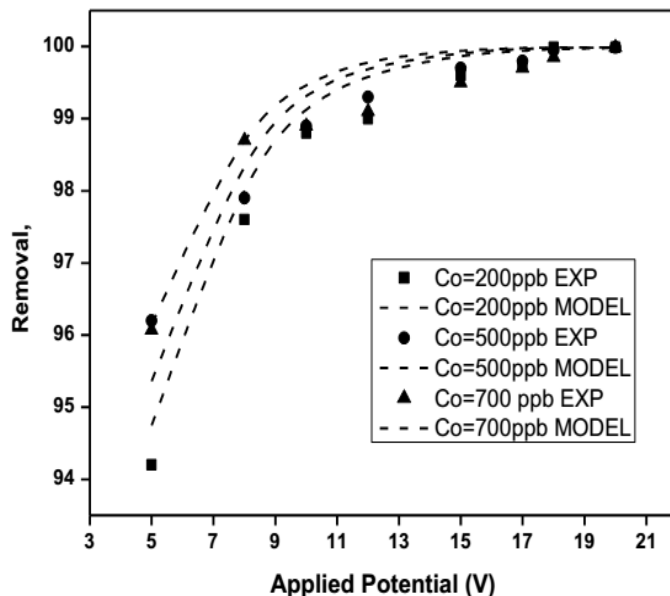
<sup>c</sup> Feed flow rate = 0.0033 m<sup>3</sup>/s; Initial feed concentration = 700 ppb; Time = 92 min.

As observed from Figure 4, an increase in removal rate corresponds to decreases in current utilization. An increase in the electrical field strength parameter as applied potential is increased is a result of stack current utilization. The current in the stack is utilized to transport ions and co-ions across the membrane surfaces. As the ions are transported across, the ions in the diluate stream also decrease which results in the lesser current requirement. As shown in Figure 4, as the removal rates approaches the 90% and above region as current utilization approaches to minimum, and as expected electrical field strength is reduced. The reduction in the electrical field strength in this manner does not necessarily indicate polarization since it can also mark as the end of the desalination process. Both model generated vales and experiment a values accounts for such trend.

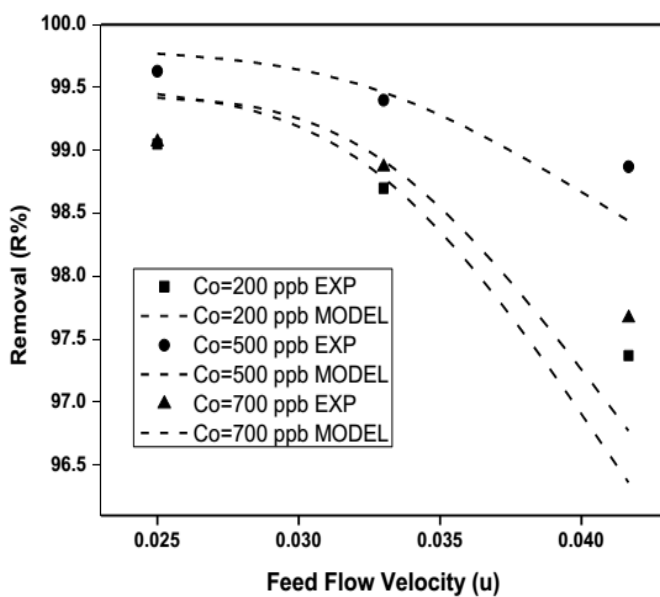
## CONCLUSIONS

The Yu and Admassu model which was initially used to model the concentration and current density profile for the removal of metal ion from pulp and paper mill process stream was evaluated and found to satisfactorily predict removal of arsenic from contaminated water streams and determine the effect of experimental parameters on arsenic removal. Two model parameters was derived: A is a parameter used to describe the characteristics of the solution, while  $\lambda^2/B$  is a parameter that is related to the stack electrical field strength. The increasing values of  $\lambda^2/B$  with respect to increase in initial feed concentration indicate efficient current utilization in the stack and efficient collision of ions during desalination within the stack channel while a constant value of A as the initial concentration increases indicates that ion transport is not limited to solution characteristics, rather it is more dictated by current and potential. Results of this study has been found to support several literature on ED process indicating that removal rate increases as applied voltage and current density increases. In terms of initial feed concentration, the remarkably high removal

rates from 500 – 700 ppb is brought about by the increase in ionic particles that intensifies the current in the stack. Medium feed flow velocity was known to be ideal for arsenic systems. The experimental data generated yielded 2 parameters than can be utilized for arsenic systems.



(a)



(b)

**FIGURE 3.** (a) Experimental and model predicted values on the effect of applied potential on As removal efficiency at variable concentrations; (b). The comparison between experimental values on the effect of feed flow velocity ( $u$ ) to removal efficiency at varied initial feed concentration and constant applied potential of 15V and feed flow velocity of 0.033 l/s (2.0 l/min) and retention time of 92 minutes.

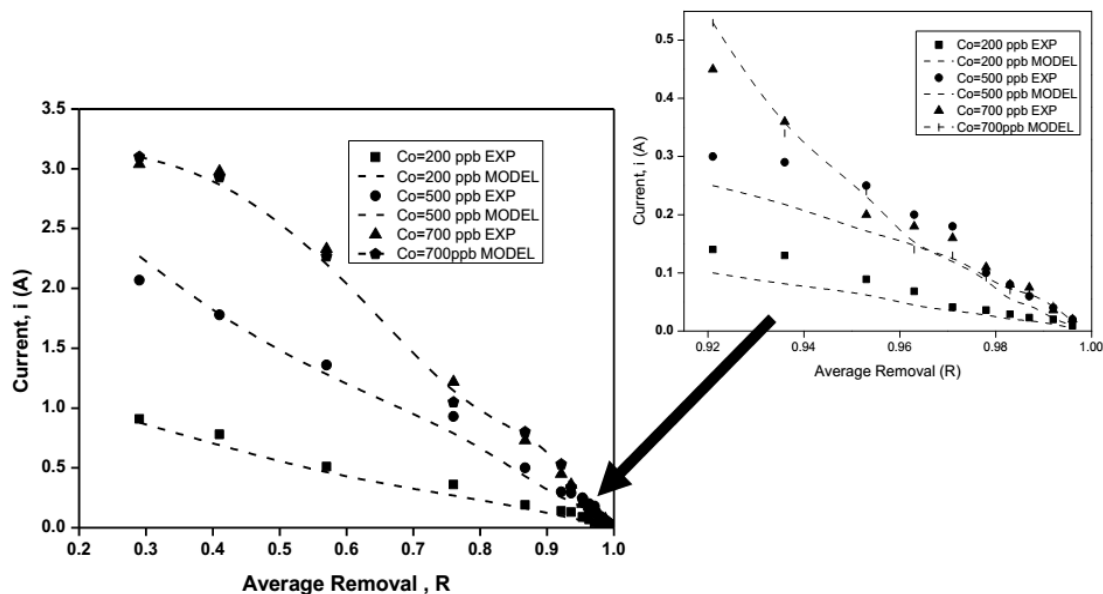


**FIGURE 4.** The experimental and model predicted values of current utilization and removal efficiency at a constant applied potential of 17V and feed flow velocity of 0.033 l/s (2.0 l/min) at variable concentrations.

#### ACKNOWLEDGEMENT

This paper acknowledges the Taiwan National Science Council for financially supporting this research under Contract No. NSC 101-2221-E-041-010-MY3 in collaboration with the Commission on Higher Education-Higher Education Development Program (CHED-HEDP), Republic of the Philippines.

#### REFERENCES

- Bednar, A.J., Gabarino, J.R.,Burkhadt, M.R., Ranville, J.F., Wildeman, T.R. (2004). "Field and laboratory arsenic speciation methods and their application to natural-water analysis". *Water Research* **38**, (2). 355-364.
- Brammer, H. Ravenscroft, P. (2009). "Arsenic in groundwater: A threat to sustainable agriculture in South and South East-Asia." *Environmental International*.**35**, 647-654.
- Chekiaoua, A., Delimi, R. (2015). "Purification of  $H_2SO_4$  by Pickling Bath by Fe (II) ions using Electrodialysis process." *Energy Procedia*. **74**, 1418-1433.
- Galvanin, F., Marchesini, R., Barolo, M., Bezzo, F., Fidaleo, M. (2015). "Optimal design of experiments for parameter identification in electrodialysis models." *Chem. Eng. Res. Design*. **In press, accepted manuscript**, Available on line 12, November 2015.
- Ghurye, G., Clifford, D.,(2004). "As(III) Oxidation using chemical and solid-phase oxidants." *J.AWWA*. **96**(1)84-96.
- Kirby, B.J. (2010). "Micro- and Nanoscale Fluid Mechanics: Transport in Microfluidic Devices: Chapter 11:Species and Charge Transport", <http://www.Kirbyresearch.com/index.cfm/wrap/textbook/microfluidicsnanofluidicsch11.html>, retrieved on line December 22, 2015.
- Mendoza, RM. O., Kan, C-C., Dalida, ML. P., Wan, M-W. (2014). "Feasibility studies on arsenic removal from aqueous solutions by Electrodialysis." *J. Environmental Science and Health, Part A*. **49**, 545-554.
- Mohammadi T., Moheb A., Sadrzadeh M., Rasmi A. (2005). "Modelling of metal ion removal from waste water by electrodialysis." *Separation Purification Technology*, **41**, 73-82.
- Rahman, M.A., Hasegawa, H. (2011). "High levels of inorganic arsenic in rice in areas where arsenic-contaminated water is used for irrigation and cooking." *Science of Total Environment*,**409** (22), 4645-4655.

- Sadrzadeh, M., Rami A., Mohammadi, T., (2007). "Separation of different ions from Waste water at various operating conditions using electrodialysis." *Desalination*. **54**,147-156.
- Zourmand, Z., Faridirad, F., Kasiri, N., Mohammadi, T. (2015). "Mass transfer modelling of desalination through and electrodiaysis cell." *Desalination*. **359**, 41-51.

## PHOSPHATE REMOVAL FROM SYNTHETIC GROUNDWATER BY MIXED ALGAE CULTURE

*Eda Tuna Öztürk*, Güneş Özden and Serdar Göncü  
(Anadolu University, Eskişehir, TURKEY)

**ABSTRACT:** Extremely high levels of phosphate in groundwater can cause health problems. Chemical and physicochemical treatment methods can be applied to reduce phosphate levels in groundwater as well as biological methods. Mixed algae culture was collected from Porsuk Dam, Eskişehir, Turkey and was used in the experiment without any pre-treatment. The growth kinetic of algae culture was investigated in BG-11 medium. The growth kinetic was evaluated by using turbidity and chlorophyll-a measurements. Maximum growth rate was calculated as  $1,6 \text{ day}^{-1}$  by using Monod kinetic equation. During calculations, phosphate was chosen as the substrate. For phosphate removal studies from synthetic groundwater, algae culture in exponential phase was used. Change in the phosphate concentrations by time were measured by SM 4500-P E Ascorbic Acid Method. The initial phosphate concentration was  $8,2 \text{ mg PO}_4^{-3}/\text{L}$  and was reduced to  $0,04 \text{ mg PO}_4^{-3}/\text{L}$  in 9 days. It is shown that mixed algae culture can be used for phosphate removal from groundwater as ex-situ bioremediation processes.

### INTRODUCTION

Natural and anthropogenic sources are the main reasons for phosphate contamination in groundwater. Atmospheric deposition, weathering of soluble inorganic materials, runoff, sedimentation, natural decomposition of rocks and minerals and decaying biomass are the natural sources of phosphate. In addition, fertilizers, animal wastes, detergents, drinking water treatment, synthetic material development surface, wastewater and septic effluent, industrial discharge, phosphate mining and forest fires are the anthropogenic sources for phosphate (Fadiran et al., 2008).

Phosphorus can be removed from water sources by physical, chemical and biological treatment techniques. Physical methods such as electrodialysis and reversed osmosis are expensive and inefficient to remove phosphorus. Chemical techniques, the addition of metal salts, is one of the common method for phosphorus removal. Although, chemical treatment technique is highly effective, remnants of this technique brings additional problems (Clark et al., 1997; Morse et al., 1998). On the other hand, biological treatment methods outstand among the other treatment techniques with its low operational costs, less residue problems and wide range of operational conditions. In-situ and ex-situ methods can be listed as two different approaches for biological groundwater treatment. Recently these two methods are becoming popular for obtaining drinking water from groundwater (Bedient et al., 1997).

Groundwater has become an important water sources. Generally, phosphorus levels are found to be lower in groundwater due to the adsorption processes in the aquifer and vadose zone. Phosphorus contamination in surface water is mostly caused by particulate phosphorus (PP) while dissolved phosphorus (DP) in groundwater. In the vicinity of Eskişehir city, groundwater can be found down to 2 m bgs (below ground surface), causing an increased risk of phosphorus contamination due to the lack of adsorption in aquifer. Moreover, Porsuk Stream, passing through the city, contributes the phosphorus contamination of groundwater with its high phosphorus level up to  $1 \text{ mg PO}_4^{-3}/\text{L}$  (Uğurluoğlu, 2013).

### MATERIALS and METHODS

Mixed algae culture was collected from Porsuk Dam, Eskişehir, Turkey (Figure 1). Porsuk Dam, which is located on Porsuk Stream, has been received intensive amount of pollutants like nitrogen and phosphorus. Because of having high levels of nutrients, it is classified as an eutrophic lake.



**FIGURE 1.** Porsuk Dam, is located northwest of Eskişehir, Turkey.

Algae culture was used in the experiment without any pre-treatment and isolation techniques. Mixed algae culture has been examined morphologically under the microscope and found that *Chlorella* and *Scenedesmus* are the most dominated species in the mixed culture (Figure 2).

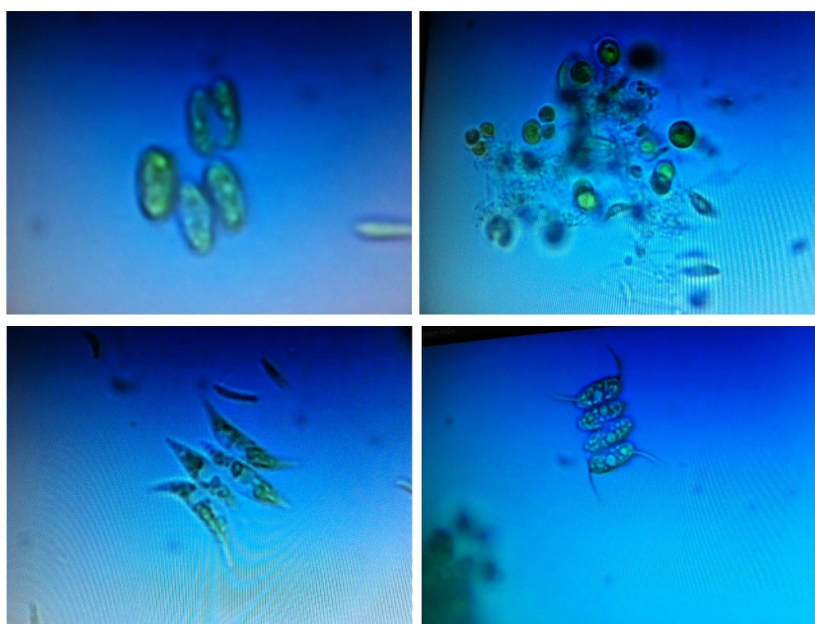


**FIGURE 2.** Mixed algae culture species under microscope.

The growth kinetic of algae culture was investigated in BG-11 medium. Algae : medium ratio was 1:10 in growth kinetic experiment and total volume was chosen 1L. The optimum conditions for algae

culture were chosen as 3000 lux light intensity, room temperature, pH range between 8 – 8.2. Also natural atmospheric CO<sub>2</sub> concentration has been used for aeration of reaction vessel (Cassidy, 2011). The experimental setup is seen in Figure 3. The growth kinetic was investigated by using turbidity and chlorophyll-a measurements. Turbidity was measured by Micro TPW Turbidimeter and chlorophyll-a was measured according to Standard Methods 10200 H. by HACH DR5000 spectrophotometer.

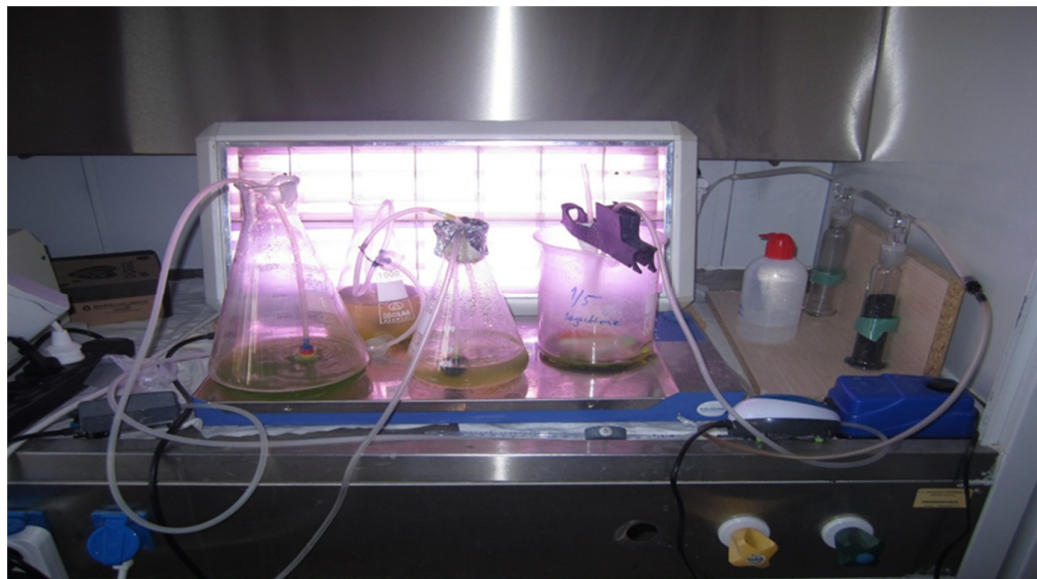


**FIGURE 3.** Experimental setup of mixed algae culture.

For phosphate removal studies from synthetic groundwater, mixed algae culture was used in exponential phase. Change in the phosphate concentrations were determined by SM 4500-P E Ascorbic Acid Method in daily time steps.

## RESULTS AND DISCUSSIONS

As seen in Figure 4, during lag phase which is the first day, algae culture adapted themselves to growth conditions. 1<sup>st</sup> – 3<sup>rd</sup> days are the exponential days, which is a period characterized by cell doubling. After 3<sup>rd</sup> day, due to lack of essential nutrient, growth rate and death rate of the algae concentration were equal.

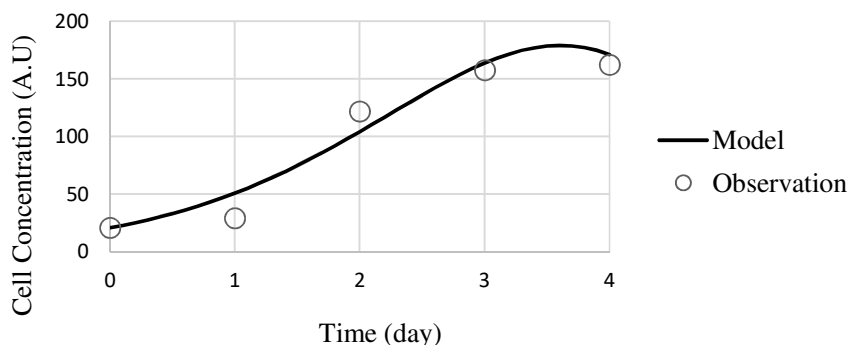


**FIGURE 4.** Mixed algae growth curve.

Monod kinetics parameters have been determined by using Excel solver module with using observation values. It is seen that model results corresponded to observation results (Figure 4 and 5).

Maximum growth rate was calculated as  $1,6 \text{ day}^{-1}$  by using Monod kinetic equation. During calculations, phosphate was chosen as the substrate. Half- velocity constant ( $K_s$ ) was found  $5,5 \text{ mg/L}$  (Figure 5).

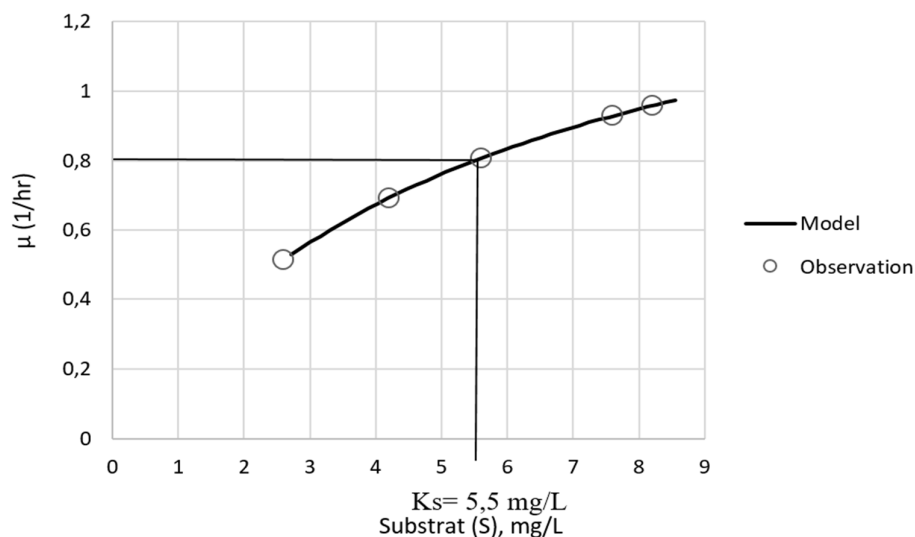


**FIGURE 5.** Growth kinetics of mixed algae culture.

As shown in the Figure 6, phosphate concentration decreased from  $8,2 \text{ mg PO}_4^{-3}/\text{L}$  to  $0,04 \text{ mg PO}_4^{-3}/\text{L}$  in 9 days. The efficiency of phosphate removal was calculated 99.5%. Algae population has increased with using phosphate as a nutrient. Meanwhile, turbidity and pH levels have increased with a reason of algae growth.

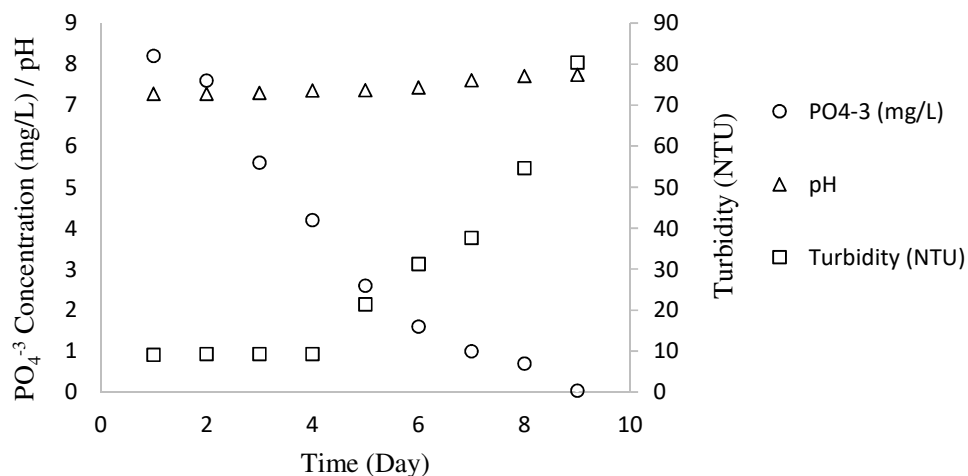


**FIGURE 6.**  $\text{PO}_4^{-3}$ , pH and Turbidity Change in Time.

## CONCLUSION

This study demonstrates that it is possible to calculate specific growth rate and half-specific velocity of mixed algae culture by Monod Equation. Also, phosphate can be removed from synthetic groundwater by mixed algae culture. All the experiments have been done with synthetic groundwater in the laboratory conditions. In reality, groundwater temperature is around  $12^\circ\text{C}$  which is not an optimum temperature for many algae species. To apply this study for real conditions, either different algae culture could be tried or different temperature conditions could be examined.



## **ACKNOWLEDGEMENTS**

The authors thank to Anadolu University, Scientific Research Project Funding (AU BAP) for their financial support [Project number: 1601F023].

## **REFERENCES**

- Bedient, P.B., Rifai, H.S., and Newell C.J. 1997. *Ground Water Contamination Transport and Remediation*. Prentice Hall PTR, Upper Saddle River, NJ.
- Clark, T., Stephenson, T., and Pearce, P.A. 1997. "Phosphorus Removal by Chemical Precipitation in a Biological Aerated Filter." *Water Research* 31(10):2557-2563.
- Fadiran, A.O., Dlamini, S.C., Mavuso, A. 2008. "A Comparative Study of the Phosphate Levels in Some Surface and Ground Water Bodies of Swaziland." *Bull. Chem. Soc. Ethiop.* 22(2):197-206.
- Cassidy, K.O. 2011 *Evaluating Algal Growth at Different Temperatures*. M.S. Thesis, University of Kentucky UKnowledge, Lexington, Kentucky.
- Morse, G.K., Brett, S.W., Guy, J.A., Lester, and J.N. 1998. "Review: Phosphorus Removal and Recovery Technologies". *The Science of the Total Environment* 212(1):69-81.
- Uğurluoğlu, A. 2013. *Seydisuyu Havzası Yeraltı Su Kalitesinin ve Kirlilik Düzeyinin Belirlenmesi*. M.S. Thesis, Anadolu University, Eskişehir, Turkey.

## **GROUNDWATER POLLUTANT LOADING IN URBAN WATERSHEDS ALONG LINED AND UNLINED CHANNELS**

***Barry Hibbs***

(California State University, Los Angeles, USA)

Lined and unlined urban channels and lined storm drains are used worldwide to convey storm runoff away from urban areas. They also convey dry weather flows such as car wash runoff, lawn runoff, and other “nuisance flows” in urban centers. Areas in southern California and elsewhere have shallow water tables where dry weather flows in concrete lined storm drains consist primarily of perennial groundwater baseflows. In these areas, groundwater leaks through cracks, joints, weepholes, and intentional dewatering structures into storm drains, which eventually flows into natural channels, coastal wetlands, and estuaries. The “lined” sections of these channels are hardly impervious; in fact, the lining of the channels often affords excellent opportunities to collect groundwater samples at discrete points that are usually not present along unlined channels where well control is sparse or where technical or legal issues prevent installation of piezometers. Frequently, as much as 95% of the nutrient and trace element loading to urban catchments during dry weather is from seepage of groundwater that is laden with pollutants. Unlined channels mitigate several contaminants more effectively than lined channels due to biologically active hyporheic zone and riparian vegetation. This project presents several examples of our experiences in conducting stream/aquifer studies in lined and unlined channels in Southern California. Sub-projects include evolution of groundwater quality along flowpaths, detection of unwanted recharge mounds in shallow groundwater systems due to leaky water main pipes, and geologic factors in water quantity and water quality fluxes in urban catchments. Tools that are utilized and described include isotopic tracers (O-H-S-N stable isotopes); trace element speciation analysis; and innovative sampling methods.

## **ARSENIC CONTENT IN DRINKING WATER SOURCES AND OCCURENCE OF CANCER IN NALBARI AND KARUP DISTRICT**

***Dipali Das Deka*** and Jogen Chandra Kalita  
(Tihu College and Gauhati University, ASSAM, INDIA)

**ABSTRACT:** At the present time people are aware of about the drinking water contaminants and health risk. Since 1970's, when sampling for contaminants increased, hundreds of manufactured chemicals have been identified in various ground water and other drinking water supplies. Source water contaminants of concern include arsenic, asbestos, radon, agricultural chemicals and hazardous water. Of these, the strongest evidence for cancer risk involves arsenic, which is linked to cancer of the liver, lung, bladder and kidneys. A survey was conducted during 2011 to 2014 in some selected areas of Nalbari and Kamrup district of Assam to know the occurrence of cancer and different types of diets consumed with the help of a prepared questionnaire. Water samples were collected in different regions accordingly during pre and post monsoon period. Spectrophotometric method was used to find out the arsenic in drinking water sources. Our study confirmed a higher level of arsenic content in drinking water sources in all the selected spots. Prevalence of cancer in the study area was also reported high.

### **INTRODUCTION**

Assam is situated in far North East corner of India. The total geographical area of the state is 78, 438 sq kms, which accounts for about 2.4 percent of the country's total geographical area. It has been reported that there is a very high incidence of cancers of all sites in general and tobacco and pesticides related cancers in particular in North East India. Not only Assam but the entire North East region of India has different customs, food habits, life style, and diverse ethnic group. The people of North East India use different types and pattern of tobacco, which is not seen in other parts of the India. There is extensive use of pesticides in tea- gardens in North east, which can lead to widespread occupational and environmental exposures. Epidemiological studies reveal that Assam states have very high incidence of esophageal cancer. The present study area Kamrup and Nalbari district is part of the state of Assam. It has been also reported Kamrup district has highest number of cancer cases (1988) of different types followed by Nagaon Barpeta, Sonitpur, Dhubri and Nalbari (Annual Report: 2013-2014 Dr B Borooah Cancer Institute). The following data will give an idea about the current trends of cancer in Assam (Table 1).

Information on ground water quality of North Eastern India is scanty. Available literature shows that ground water of Assam valleys are highly ferruginous (Aowel 1981). Recent research reveal that the concentration of arsenic in groundwater exceeds the permissible level (50 µg/l based on the water consumption of 2 litre per day WHO in parts of Assam (20 districts out of 24 districts. (Sing 2004). In the State, of the total 56, 180 groundwater samples tested in a three-tier system during the past few years, under a joint plan of action by the State PHED, UNICEF and the IIT Guwahati, 7.95 per cent of the samples were found to be containing over 50 parts per billion (ppb) arsenic and 29.75 per cent were found to be containing over 10 ppb arsenic. The 50 ppb is the Government of India norm, while 10 ppb is the World Health Organisation (WHO) norm for determining safe drinking water in the case of arsenic (Assam Tribune 2014). of 2 litre per day WHO in parts of Assam (20 districts out of 24 districts. (Sing 2004) reveal concentration of arsenic in groundwater exceeds the permissible level (50 µg/l based on the water consumption of 2-litre per day WHO in parts of Assam (20 districts out of 24 districts (Sing 2004).

### **OBJECTIVES**

The main objective of this work was to determine the level of arsenic in drinking water sources in Nalbari and Kamrup district of Assam, India and prevalence of different types of cancer.

**TABLE 1. District -Wise Break –Up of Patients in the State of Assam during 2011- 2012, 2012- 2013, 2013-2014**

SL No.	District	2011-12	2012-13	2013-14
1.	Kokrajhar	73	61	134
2.	Dhubri	239	212	442
3.	Goalpara	145	171	334
4.	Barpeta	333	321	646
5.	Morigaon	181	166	363
6.	Nagaon	483	504	1002
7.	Sonitpur	267	280	643
8.	Lakhimpur	100	144	259
9.	Dhemaji	26	36	90
10.	Tinsukia	65	68	155
11.	Dibrugarh	83	84	159
12.	Sivsagar	110	98	205
13.	Jorhat	191	191	337
14.	Golaghat	125	140	273
15.	Krbi Anglong	75	71	131
16.	Dima Hasao	09	11	17
17.	Cachar	29	19	47
18.	Karimganj	24	20	29
19.	Hailakandi	09	07	15
20.	Bongaingaon	129	131	281
21.	Chirang	55	50	117

SOURCE: Annual report Dr. B.Barooah Cancer Institute (2013-13,2013-2014).

## METHODOLOGY

A survey was conducted during 2011to2014 in some selected areas of Nalbari and Kamrup district of Assam to know the occurrence of cancer and different types of diets consumed with the help of a prepared questionnaire. During the survey, information was also taken for different sources of drinking water. Water samples collected from some selected areas. Spectroscopic method has been applied to find out the concentration of Arsenic in the ground water.

## RESULTS

We have studied 20 different spots of Nalbari and Kamrup (10 from each) where occurrence of different types of cancer also reported. It was observed that in all the selected spots arsenic was present in the drinking water sources. The result is shown in table 2 and table 3.

## CONCLUSIONS

Our study confirmed a higher level of arsenic content in drinking water sources in all the selected spots. Prevalence of cancer in the study area was also reported high. The result indicated that exposure of arsenic in drinking water may be located with occurrence of cancer. However further large scale investigation would certainly throw light behind this higher occurrence of cancer in these area.

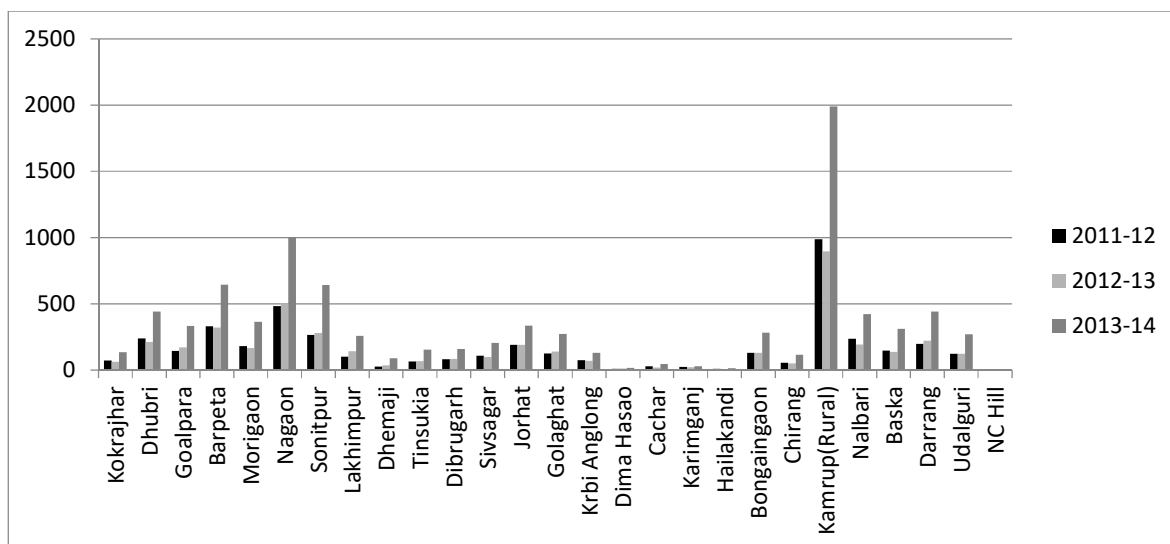


FIGURE 1. Graphical Representation of the Table-1

TABLE 2. Arsenic content in drinking water sources in different places of Nalbari District

SI No	locality	Total population	Cancer patient found	Source of drinking water	Depth (in feet)	Arsenic (µg/L)
1	Haribhanga	4786	07	Tube well	170	510
2	Mugkuchi	2225	10	Tubewell	185	550
3	Bhogpur	1250	11	Tubewell	200	570
4	Bala	1236	12	Tubewell	185	580
5	Kaljar	2616	12	Tubewell	200	590
6	Nizzuliki	2844	12	Tubewell	200	610
7	Mathurapur	3656	15	Tubewell	185	640
8	Ward no3	1335	15	Tubewell	210	710
9	Parmankhoa	504	15	Tubewell	200	720
10	Nannatari	1833	17	Tubewell	200	770

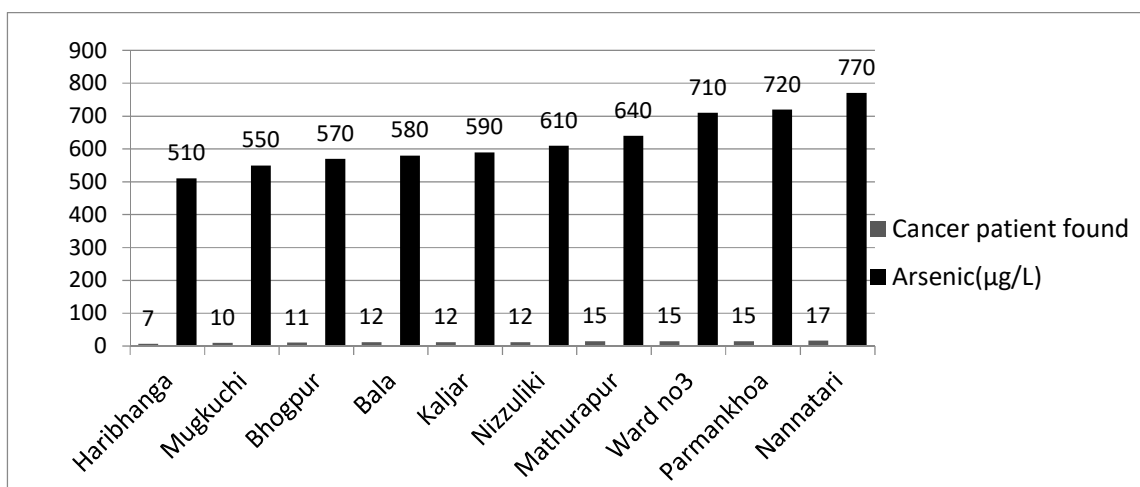
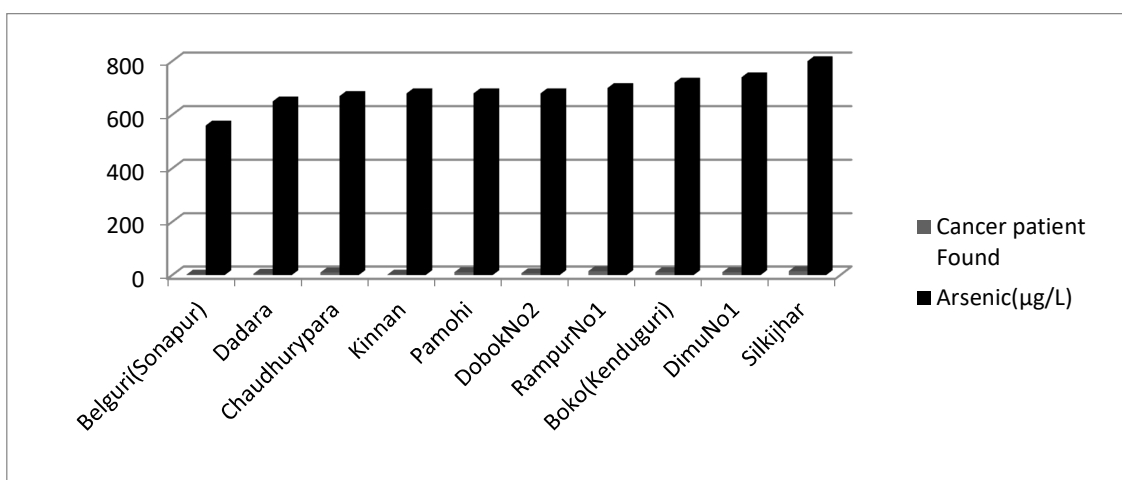


FIGURE 2. Graphical Representation of the Table 2

**TABLE 3.** Arsenic content in drinking water sources in different places of Kamrup district

SINo	Locality	Total Population	Cancer patient Found	Source of drinking water	Depth (in feet)	Arsenic ( $\mu\text{g/L}$ )
1	Belguri(Sonapur)	4917	02	Ring well	85	560
2	Dadara	2000	05	Tubewell	195	650
3	Chaudhurypara	5030	10	Tubewell	180	670
4	Kinnan	100	02	Tubewell	185	680
5	Pamohi	1200	11	Ringwell	80	680
6	DobokNo2	1570	07	Tubewell	200	680
7	RampurNo1	7211	15	Ringwell	180	700
8	Boko(Kenduguri)	5000	11	Ring well	90	720
9	DimuNo1	1045	11	Tubewell	180	740
10	Silkijhar	4086	15	Tubewell	200	800



**FIGURE 3.** Graphical Representation of the Table-3

## ACKNOWLEDGEMENTS

All the family member of the patients including the patients themselves and all the physicians and staff of DR .B. BAROOAH CANCER INSTITUTE is gratefully acknowledged.

## REFERENCES

- Aowal, A.F.S.A. 1981. "Design of an Iron eliminator for hand tube wells." *Journal of IWWA*, .XIII(1):65.
- Chen C.J.andChuangY.C., Lin T.M.andWuHY .1985. "Malignant neoplasm among residents of black foot disease-endemic area in Tiwan: High-Arsenic artesian well water and cancer". *Cancer Res*, 45(11Pt2):5895-5899.
- International Agency for Research on Cancer 1987. IARCmonographs on the evaluation of carcinogenic risks to humans: overall evaluation of carcinogenicity: an updating of IARCmonographs: 1-42, IARC publ. Suppl, 7,100.
- Majumder D.N. 2010. "Effect of chronic intake of arsenic-contaminated water on liver". *Toxicol. Appl. Pharmacol*, 206:169-175.
- Patowary Ajit.2014. "Arsenic Content in state drinking water high".*The AssamTribune*.Sept 6:1

- Sing AK 2004. "Arsenic Contamination in Groundwater of North Eastern India" In: *Proc of Nat . Seminar on Hydrology with focal theme on Water Quality*.
- WHO 2001. Env Health criteria 224: *Arsenic & Arsenic Compounds*. WHO, Geneva
- WHO, 2010. *Arsenic in Drinking Water*. Fact Sheet.
- Zhang A.H., Huang X.X. Jiang X.Y., Luo P., Guo Y.C. and Xue S.Z. 2000. "The progress of study on endemic arsenism due to burning arsenic containing coal in Guizhou province". In: *Metal Ions in Biology and Medicine*. Conteno JA, Collery P, Vernet G, Finkleman RO, Gibb H, Etienne J-Ceds, vol 6, France: John Libbey Eurotext LTD, 53-55.

**SIMULTANEOUS NITRATE AND PHOSPHATE REMOVAL FROM DRINKING WATER  
USING IMMOBILIZED POLYETHYLENEIMINE**

*Enrico T. Nades* and Debora F. Rodrigues  
(University of Houston, Houston, Texas 77008, USA)

A new biosorbent containing polyethylemeine was synthesized for the removal of nitrate and phosphate. The adsorption capacity and optimum conditions for the removal of these contaminants was initially investigated with batch experiments and then by packed bed columns. The batch results demonstrated that the optimum pH for nitrate adsorption was around 4-5 and the adsorption capacity was 100 mg/g and 30 mg/g for nitrate-N and phosphate, respectively. The column experiments aimed to investigate the effect of flow rate, influent concentration and bed height in the removal of the contaminants by the new adsorbent. The adsorption capacity of the new adsorbent was determined to be 120 mg NO<sub>3</sub>-N/g with the Thomas model. The volumetric capacity was determined to be 0.35 eq/L by fitting the results in Adams-Bohart model. Regeneration investigation of the adsorbent demonstrated that the adsorbent regenerates more that 90% of its capacity even after 3 adsorption-desorption cycles with 0.1 M HCl. When real environmental water sample was passed through the column, 97 % of nitrate-N and 70 % of phosphate.



## **SUSPENDED BACTERIA COMMUNITY OF PROCESSING UNITS IN THE TYPICAL DRINKING WATER TREATMENT PLANT OF CHINA**

Weiying Li, **Feng Wang\***, Junpeng Zhang and Wanqi Qi  
(Tongji University, Shanghai, China)

For reducing the amount of organic pollutants in drinking water, advanced water treatment process (AWTP) were adapted on the basis of conventional water treatment process (CWTP) in China, but little attention was paid to suspended bacteria. Focused on a drinking water treatment plant employing AWTP and CWTP simultaneously, this paper aimed at revealing suspended bacteria community structure of different water treatment units by 454-pyrosequencing technique and seeking possible bacteria pivotal for the effects of AWTP. Results showed that conventional water treatment process played little impact on microbial diversity comparing to AWTP. Although complex community composition was beneficial for organics removal, the dominant bacteria varied slightly. Proteobacteria phylum (54.7%~99%) and Betaproteobacteria class (28.6%~86.3%) were dominant during the procedure of drinking water production, while the primary genus was *Limnohabitans* in both the effluent of CWTP (17.4%) and AWTP (25.6%). Furthermore, redundancy analysis implied that the TOC level was positively correlated with the relative abundance of *Limnohabitans*, which was inferred to be one of the crucial contributors for the biodegradable function of activated carbon filtration tank. The paper provided reference for better developing the microbial effects during water treatment procedure in the future.

## **FULL-SCALE STUDIES OF FACTORS RELATED TO BIOLOGICAL STABILITY OF WATER DISTRIBUTION SYSTEM IN SOUTH CHINA**

Weiyang Li, *Junpeng Zhang*, Feng Wang and Wanqi Qi  
(Tongji University, Shanghai, China)

Bacterial regrowth in drinking water, especially opportunistic pathogens growth, leads to the deterioration of water quality and gives risks to the public health. AOC (assimilable organic carbon), BDOC (biodegradable dissolved organic carbon), BRP (bacterial regrowth potential) and HPC (heterotrophic plate count) as biological evaluation methods were examined in a full-scale drinking water distribution system (DWDS) and bench tests. According to the statistical analysis of big data, HPC was significantly correlated with AOC, BRP, BDOC, COD<sub>Mn</sub>, ammonia, free chlorine and temperature. Among these factors, temperature had great effects on bacterial regrowth. When temperature ranged from 25°C to 30°C, HPC numbers were 35.67 times higher than those with water temperature ranging from 5 to 10°C. Organic carbon in DWDS facilitated microbial growth, AOC<sub>P17</sub> was more likely to be utilized by microbes at high temperature and AOC<sub>NOX</sub> increased as temperature rose. Disinfectant affected interaction between nutrients and bacteria. Chlorine imposed greater effects on bacterial regrowth than on chloramine. The bench test using flow cytometry showed that when chlorine was higher than 0.5mg/L or chloramine was more than 0.75mg/L, the HPC level was low and AOC concentration almost unchanged. Conversely, the HPC level increased quickly and declined slightly, with chlorine lower than 0.15mg/L or chloramine less than 0.25mg/L. The biologically stable values with or without different disinfectants were also different after being incubated for 30 days.

## **OPTIONS FOR THE REMOVAL OF ARSENIC FROM DRINKING WATER IN RURAL AREAS OF BIHAR, INDIA**

Astha Kumari<sup>1</sup>, Sudhir Nigam<sup>2</sup> and *Nityanand Singh Maurya*<sup>1</sup>

(<sup>1</sup>Department of Civil Engineering, National Institute of Technology Patna, India; <sup>2</sup>Lakshmi Narain College of Technology and Science, Bhopal 462021, India)

Arsenic is a ubiquitous toxic metalloid of natural origin and ranked as 20<sup>th</sup>, 14<sup>th</sup>, & 12<sup>th</sup> most abundance element in earth crust, seawater and human body respectively. Arsenic is the major constituent of at least 245 different minerals. Though it is a natural origin element, but several anthropogenic activities such as manufacturing of transistors, lasers and semiconductors, as well as in the processing of glass, pigments, textiles, paper, metal adhesives, use of chemical weapons, fertilizer and pesticides, cosmetic industries, combustion of fossil fuels, wood preservation, urban waste management, mining etc are responsible for spreading out it in the environment. It is an essential constituent of human body, but its continuous ingestion may cause several health problems such as palmar hyperkeratosis, hepatic damage, damage to the central neural system, hair loss, chronic headache, skin cancer and cancer of internal organs such lungs, liver, kidney and bladder; colour change on the skin, and hard patches on the palms and soles of the feet. In most cases its adverse effect is not easily detectable because many of its symptoms are also indicative of other illnesses.

Elevated arsenic concentration in groundwater is now well recognized environmental problem and global threat to human health. Approximately 70 countries are currently experiencing high level concentration of arsenic in drinking water. The recent literatures indicate at-least 150 million persons are under high risk of arsenicosis mostly from south-eastern Asian countries such as Bangladesh, India and China. Bihar, the 3<sup>rd</sup> largest populated states of India is also experiencing groundwater contamination due to arsenic. As early as in 2002, arsenic was first detected in village Semaria Ojha Patti of Shahpur block, Bhojpur district. According to Government of Bihar report presently at-least 13 out of 38 districts of Bihar are found to be severely affected by arsenic contamination. Since groundwater is only source of drinking water, thus entire population of approximately 1590 habitations is compulsorily consuming contaminated water. Currently several agencies have installed mini water supply system based on adsorption/ion-exchange process that requires imported/patented media and constant power supply. Majority of the affected population lives in rural areas deprived off from basic infrastructure such as electric power supply and road connectivity. Thus the operation and maintenance of such treatment plants is a big challenge. To make the treatment process sustainable it is necessary to search suitable alternatives which can work in rural areas of Bihar.

Currently various treatment methods such as precipitation/coagulation and filtration, membrane filtration, ion-exchange and adsorption etc are available for the treatment of arsenic contaminated water. But their suitability depends on various characteristics of the water to be treated and socio-economic condition of the consumers. Therefore a treatment method suitable for one place may not solve the problems at other place. These warrant evaluating the available treatment options to search suitable alternatives for rural areas.

The objective of the present study is to evaluate the existing treatment technologies employed for the removal arsenic in rural areas of Bihar. Further various conventional treatment options and recent advancements in arsenic removal processes will be studied and a comparative chart will be prepared on the basis of their removal efficiency, necessity of pre-treatment, electricity, skilled manpower, land and installation as well as operational cost. The outcomes of the study will be helpful in the selection of suitable method for a specific area.

To achieve the above objectives, survey will be conducted to evaluate the existing treatments installed in rural areas of Bihar. Further review of published literature including textbooks, papers presented in reputed conference will be conducted.

On the basis of above studies a comparative chart will be prepared, which will provide ranking of various treatment options for the removal of arsenic from water.

## **POND-WETLAND COMPLEXES AS PROCESSOR OF DRINKING WATER SOURCE**

**Weidong Wang** and Chengqing Yin.

(Research Center for Eco-Environmental Sciences, Chinese Academy of Sciences, Beijing, China)

Shijiuyang Constructed Wetland (110 ha) is a drinking water source treatment wetland with primary structural units of ponds and plant-bed/ditch systems. The wetland can process about 250,000 tonnes of source water in the Xincheng River every day and supplies purified raw water for Shijiuyang Drinking Water Plant. Daily data for 28 months indicated that the major water quality indexes of source water had been improved by one grade. The percentage increase for dissolved oxygen and the removal rates of ammonia nitrogen, iron and manganese were 73.63%, 38.86%, 35.64%, and 22.14% respectively. The treatment performance weight of ponds and plant-bed/ditch systems was roughly equal but they treated different pollutants preferentially. Most water quality indexes had better treatment efficacy with increasing temperature and inlet concentrations. These results revealed that the pond-wetland complexes exhibited strong buffering capacity for source water quality improvement. The treatment cost of Shijiuyang Drinking Water Plant was reduced by about 30.3%. Regional rainfall significantly determined the external river water levels and adversely deteriorated the inlet water quality, thus suggesting that the “hidden” diffuse pollution in the multitudinous stream branches as well as their catchments should be the controlling emphases for river source water protection in the future. The combination of pond and plant-bed/ditch systems provides a successful paradigm for drinking water source pretreatment. Two other larger drinking water source treatment wetlands with ponds and plant-bed/ditch systems are in operation or one in construction in the stream networks of the Yangtze River Delta and more people will be benefited.

## INTERACTION BETWEEN HYDROLYSIS AND FLOCCULATION, AND ITS INFLUENCE ON GENERATION OF DISINFECTION BY-PRODUCTS WITH ALUMINUM

*Hong Shen*, Xin Chen •, Hongbin Chen

(Collaborative Innovation Center for Clean Water, College of Environmental Science and Engineering, Tongji University, Shanghai 200092, P.R. China)

**Introduction.** Aluminum (Al) is commonly found in natural waters, and its salts are often used as coagulants in drinking water treatment. Hence, the effects of Al ions ( $\text{Al}^{3+}$ ) on disinfection and the security of drinking water should not be ignored. In this study, using tannic acid as the model compound of natural organic matters (NOMs), the effects on disinfection by-products (DBPs) and carcinogenic factors (CF) after the addition of  $\text{Al}^{3+}$  with  $\text{Al}^{3+}$ / initial tannic acid molar ratios (MRs) of 0, 1.7, 3.4 and 5.1 (referred to as  $\text{MR}_0$ ,  $\text{MR}_{1.7}$ ,  $\text{MR}_{3.4}$  and  $\text{MR}_{5.1}$ , respectively) during chlorination of synthetic water was investigated.

**Experimental procedures.** The chlorination experiment systems contain a model compound composed of NOMs (tannic acid adjusted to  $2 \pm 0.1$  mg-C/L DOC), different concentrations of metal ions ( $\text{Al}^{3+}$ ), potassium dihydrogen phosphate (1 m mol/L) and sodium hypochlorite (20 mg-Cl/L). The chlorination experiment was conducted under a headspace-free condition in 60-mL amber glass screw-cap vials with PTFE-lined septa, at a stable temperature ( $20 \pm 1^\circ\text{C}$ ) for 7 d of contact time. The aluminum sulfate was added in concentrations of 0, 0.1, 0.2 and 0.3 mg- $\text{Al}^{3+}$ /L (hereafter referred to with the abbreviations  $\text{MR}_0$ ,  $\text{MR}_{1.7}$ ,  $\text{MR}_{3.4}$  and  $\text{MR}_{5.1}$ , respectively) according to the Al/ initial tannic acid molar ratios. The pH was maintained at  $7 \pm 0.02$  by the addition of 1 M  $\text{H}_2\text{SO}_4$  or NaOH. During the 7 d chlorination period, samples were quenched using ammonium chloride before being extracted for DBPs analysis.

**Results and discussion.** The results demonstrated that the presence of  $\text{Al}^{3+}$  in chlorination led to an increase in both DBPs (except for  $\text{MR}_{5.1}$ ) and carcinogenic factors in finished water. These effects arose through a transformation of the distribution ratios of trihalomethanes (THMs) and haloacetic acids (HAAs) in the DBPs after chlorine disinfection. Also, the addition of  $\text{Al}^{3+}$  resulted in inhibition efficiency for THMs, but promotion efficiency for HAAs. With the increase of  $\text{Al}^{3+}$ , the inhibition efficiency for THMs and the promotion efficiency for HAAs were both reduced. According to analyses of the results by ultraviolet spectrophotometer (UV) and size exclusion chromatography (SEC), an equilibrium system can be assumed to exist between hydrolysis and flocculation in tannic acid solution. It could also be inferred that the addition of  $\text{Al}^{3+}$  affected the equilibrium system, which had a direct or indirect influence on the chemical properties of tannic acid, and finally resulted in changing the generation and distribution ratios of the THMs and HAAs of DBPs during chlorination.

## **DEFLUORIDATION POTENTIAL OF VERMICULITE MODIFIED WITH HEXADECYLTRIMETHYLAMMONIUM**

***Tayo Oladipo Ologundudu***, John Ogony Odiyo, Georges-Ivo Ekosse  
(University of Venda, Thohoyandou, Limpopo Province, South Africa)

Vermiculite modified with hexadecyltrimethylammonium, HDTMA, was investigated for its defluoridation potential, as fluorosis is a major health challenge especially in the rural areas across Africa and Asia. 1 M sodium chloride was used to activate the clay mineral before its agitation with 0.2 M HDTMA at 40 °C for 24 hrs. Fluoride removal experiments were carried out using batch adsorption technique coupled with optimisation of experimental parameters such as pH, mass of adsorbent, contact time and temperature. Using 8 mg/L fluoride solution, the results showed a fluoride removal of 51% at pH 4, 2 g, 70 min and 25 °C. The  $pH_{pzc}$ , 6.4, of modified vermiculite enhanced the fluoride removal via electrostatic attraction, while the FTIR analysis revealed that the  $CH_3$  and  $CH_2$  bands introduced to vermiculite by the organic cation, was responsible for defluoridation. The antimicrobial properties of HDTMA, coupled with the defluoridation potential of this adsorbent, showed that vermiculite modified with HDTMA could be developed by further research into a domestic water defluoridation unit. This approach would be effective and economical for practical use especially in non-metropolitan environments.

## **EVALUATION OF WATER QUALITY OF THE ASI (ORONTES) RIVER BETWEEN 1997 AND 2008**

Hasan Göksel Özdilek<sup>1</sup>, Ziya S. Cetiner<sup>2</sup> and Mustafa Kemal Sangün<sup>3</sup>

<sup>1</sup> Çanakkale Onsekiz Mart University, Faculty of Engineering, Terzioğlu Campus 17020 Çanakkale, Turkey. E-mail:hgozdilek@comu.edu.tr

<sup>2</sup> Çanakkale Onsekiz Mart University, Faculty of Engineering, Geological Engineering Department, Terzioğlu Campus 17020 Çanakkale, Turkey

<sup>3</sup> Mustafa Kemal University, Faculty of Science and Letters, Chemistry Department, Tayfur Sokmen Campus 31100 Antakya, Hatay, Turkey

**ABSTRACT:** This paper assesses the changes in water quality of the Orontes (Asi) River, an internationally shared river in the Middle East starting from Lebanon, crossing through Syria and ending in southern Turkey. For this purpose, historical water quality data covering the years between 1997 and 2008 were examined at two water quality monitoring stations, one of which is situated just after the Syrian-Turkish border and the other is located within a large city, Antakya. Results from two comprehensive water quality surveys are also evaluated during October 2005 and February 2006. Since available historical data includes thirteen water quality parameters, which were sampled once a month, our assessment provides comprehensive record of long-term changes in water quality. Water quality index (WQI) developed by the Canadian Minister of the Environment was also used to classify water quality in the river for two additional comprehensive water surveys conducted in October 2006 and February 2007. It was found that wet-weather poses a risk in terms of water quality compared to dry weather conditions. In the lower Orontes River catchment, it was found that a noticeable trend of increasing sodium load, especially in wet years, between the two water quality monitoring stations operated between 1997 and 2008.

**Key Words:** Asi river, water quality index, heavy metals, boron, transboundary waters

## **INTRODUCTION**

In general, water quality is defined by the physical, chemical and biological parameters affecting the well-being of a water body. Water quality is crucially important because of its close linkage with public health and ecological quality. Contamination of water bodies from various sources deprives current and future generations of a birthright and jeopardizes ecological integrity. While point sources of water pollution resulting from independent effluents can be measured directly at the site of concern, nonpoint sources of pollution is a chiefly wet weather driven phenomenon that causes change in pollutant concentrations in a river course.

Changes in water quality can occur for many reasons, such as irrigation schemes, precipitation amounts, extensive use of fertilisers and other types of agricultural aids, mechanization of agricultural activities, exhaust gases, and urban sprawl, all of which can negatively affect natural water quality and sediment transport in river ecosystems (Wei et al. 2009; Tong et al. 2009). Rivers are important since they contribute to pollution control through transport and removal of contaminants and excess nutrients. The factors just aforementioned are all nonpoint sources that may introduce natural nutrients, bacteria, minerals, heavy metals, and toxins into the water bodies.

Recently, many studies related to surface water quality have been conducted in different parts of the globe (Srappier et al. 2000; Wotke et al. 2003; Jarvi et al. 2006; Neal et al. 2010; Bayram et al. 2011; Kumarasamy et al. 2014, Tavakoli et al. 2014, McClain and Maher, 2016), but determination of trends in water quality is a relatively newer issue that requires analysis of reliable and long-term data.

For over a half-century, the Orontes River and many of its tributaries have been used for the discharge of industrial and domestic wastewaters at various locations. Refineries, olive oil production plants, and municipal waste discharges have all contributed to the pollution of the Asi River. This is an international dispute between Syria and Turkey. Similar experiences have been experienced in different parts of the world, because water is an essential part of life (Begon et al. 2006). However, despite the fact that its catchment has the second highest human population density (after the Smaller Meander River situated in western Turkey), the Orontes River is the second richest river (following the Sakarya River in north-western Turkey) in terms of the number of native fish species present (Akbulut et al. 2009). The length of its main branch is 380 km, the total length of the river and its tributaries is nearly 520 km, and its total catchment area is nearly 24,000 km<sup>2</sup>. There are some dams on the river and its tributaries, namely Quattena, Ar-Rastan, Mahardeh, Apamia and Zeyzoun Dams in Syria, and Tahtaköprü (on Karasu branch) and Yarseli Dam (on Beyazcay branch) in Turkey.

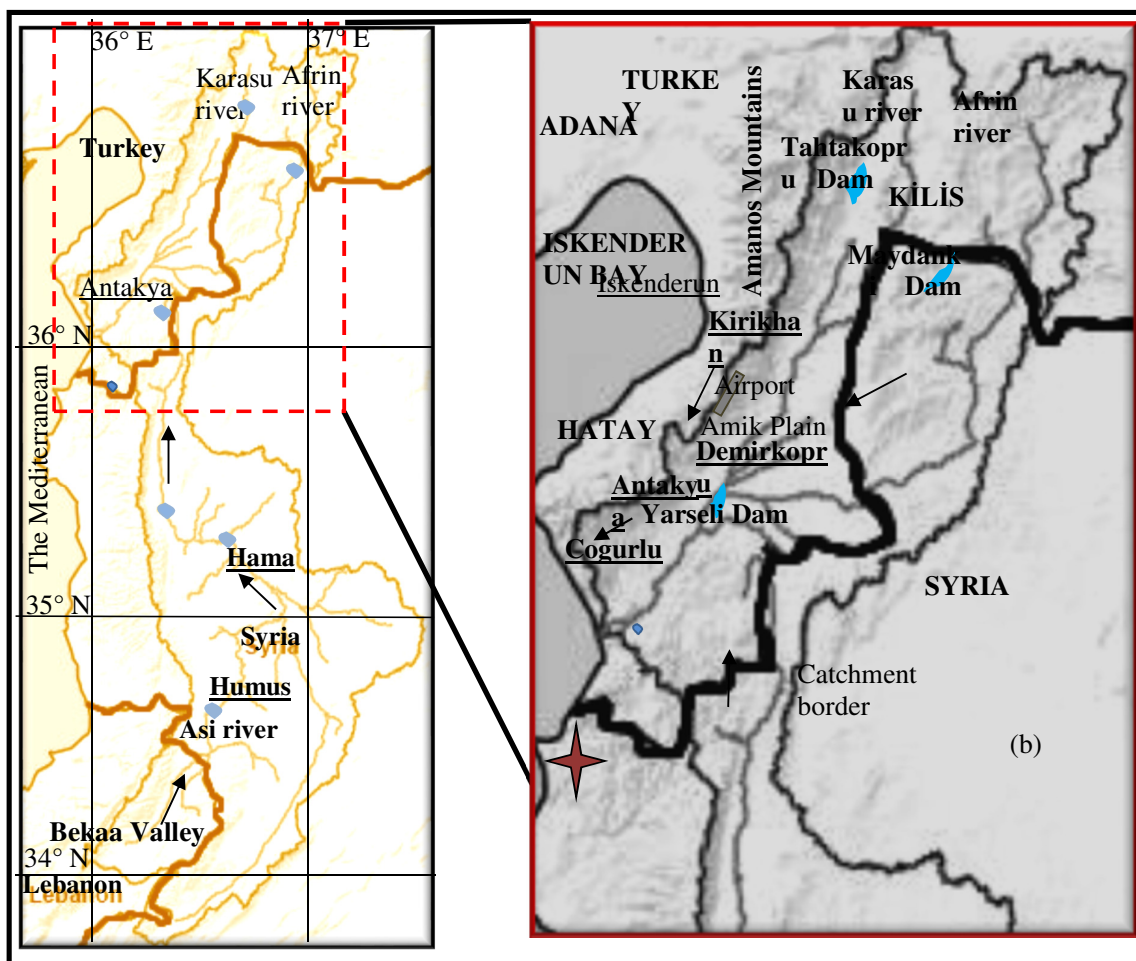


Figure 1. The Asi basin (a) as a whole and (b) its Turkish part in detail

The aim of this paper is to investigate changes in water quality focusing on water quality between 1997 and 2008 in the downstream portion of a transboundary Orontes River (Asi river) situated in a region, where water is crucially scarce. This river is located in the north-eastern Mediterranean. It extends relatively parallel to the eastern Mediterranean coast with a total length of approximately 450 km (Arisoy and Turkoglu, 1998).

The Orontes River originates from a stream located in the Bekaa Valley in the north-eastern tip of the Lebanon and passes through important cities, such as Baalbeck and Hermel (in Lebanon), Humus, Hama, Muhradah, Jisr Ash-Shughur (in Syria), and Antakya (in Turkey), (listed from south to north). The river, defines the border between Syria and Turkey and is fed by Karasu and Afrin (flowing from north to south)



just before Antakya (provincial centre of Hatay), where it flows into the Mediterranean Sea in the district of Samandag.

Kirikhan, located within the middle of the Karasu river, had a population of 70,543 and Reyhanli, close to the Afrin river, had a population of 60,073 in 2000. There are no wastewater treatment plants serving these two areas. Some of the municipalities contributing to effluent discharges that do not have domestic wastewater treatment facilities include Kucukdalyan (population equivalent of 8,095), Narlica (population equivalent of 12,750), Ekinli (population equivalent of 6,459), Guzelburc (population equivalent of 6,281), Kuzeytepe (population equivalent of 6,051), Odabasi (population equivalent of 10,192), Serinyol (population equivalent of 12,517), and Ovakent (population equivalent of 6,288). However, the wastewater discharge of Antakya did not affect the second sampling station situated in the middle of the city. Antakya, the province center of Hatay, has been operating its trickling filter type domestic wastewater treatment plant since 2007 although prior to this year wastewater treatment plant was inactive. The population of Antakya was 186,213 in 2007 and the most recent population is 347,974 (TUIK, 2013).

## **MATERIALS AND METHODS**

First, historical monthly water quality data sampled between 1985 and 2008 was assessed with the parameters taken into account in the model as water acidity (pH), electrical conductivity (EC), sulphate, chlorine, total hardness, and water temperature. The Canadian Water Quality Index was used to detect the trend at Demirkopru water quality monitoring station just after Syrian-Turkish border.

For boron and stream flow, the length of monitoring period and available number of samples are given in Table 2. These samples were taken on monthly basis to evaluate water quality of the river. The aim for this research was to determine the following important points.

(1) Background level of the stream flow water quality of the Orontes River at Demirkopru (just after the Syrian-Turkish border) and

(2) Increase or decrease in water quality in the case of the examined parameters at Antakya city centre

The river samples were analysed for major, minor and trace elements by filtering to 0.45  $\mu\text{m}$  in situ. Boron and sodium samples were determined by inductively coupled plasma mass spectrometer (ICP-MS) on acidified samples. Calibration was conducted using prepared standards, which were cross-checked against internationally certified standards to quality check and correct for potential instrumentation drift. Analysis included three replicates and for every six samples a set of our standards was run. If the standards analyzed differed from their "real values" by more than 5%, the analysis was redone. The lowest detection value was 10  $\mu\text{g L}^{-1}$  for boron and 20  $\mu\text{g L}^{-1}$  for sodium.

Historical stream flow records were received from the Turkish Electrical Power Sources. Corrections have not been made to allow for exact representation of stream flows at water gauges. It is generally assumed that the additional volumetric input of effluents into the Karasu, Afrin (stream flow recorded since 1968), and Asi river between two water gauging stations is relatively insignificant.

In general, two tributaries (Afrin and Karasu) contribute only 14% of the total flow measured downstream of the river, approximately 1 km away from where it flows into the Mediterranean Sea. The only exceptions to this occurred in May, likely due to snowmelt in upper parts in addition to higher surface runoff of the Karasu catchment, and in December when notable precipitation occurs in northern part of the Karasu catchment. According to the official records on meteorological parameters, Kilis, which is the origination point of the Afrin, gets 17% of its total annual precipitation in December.

Finally, two comprehensive water quality surveys were taken into account to examine whether there is a trend in water quality in Turkish part of the river. One survey was performed in the dry period (October 2006), and the other was completed in the wet period (February 2007).

**CWQI 1.0 Model.** The CWQI model presents a mathematical framework for evaluating ambient water quality situations related to water quality objectives set up for different purposes, such as irrigation, domestic water supply, and aquatic life. The model has three measures of difference from important water quality objectives: scope ( $F_1$ ) defined as the number of variables violating water quality limits, frequency ( $F_2$ ), the number of samplings the objectives are not met, and amplitude ( $F_3$ ) the amount by which water quality limits are not met. The index yields a numerical score between 0 (worst water quality) and 100 (the

best attainable water quality). These numbers are divided into five descriptive classes to make the presentation simpler and water quality index (WQI) is computed as

$$F_1 = 100 \times \frac{\text{Number of failed parameters}}{\text{Total number of parameters}} \quad (4)$$

$$F_2 = 100 \times \frac{\text{Number of failed tests}}{\text{Total number of tests}} \quad (5)$$

and  $F_3$  (amplitude) represents the amount by which failed test values violate their objectives.  $F_3$  is computed according to the following three steps.

1<sup>st</sup> Step. The number of times by which an individual level is more than or less than (when the objective is a minimum level) the objective, is expressed an “excursion” and stated as follows. When the test value must not exceed the objective criteria:

$$\text{excursion}_i = \frac{\text{Failed test value } i}{\text{Objective } j} - 1 \quad (6)$$

When the objective is at a minimum level and the parameter must be larger than this minimum.

$$\text{excursion}_i = \frac{\text{Objective } j}{\text{Failed test value } i} - 1 \quad (7)$$

where,

$i$  and  $j = 1, 2, 3, \dots, n$

2<sup>nd</sup> Step. Normalized sum of excursion (NSE), which is defined by the summation the excursion of individual tests from their objective criteria divided by the total number of tests (both those within objective limits and those violating objective limits), is computed as,

$$NSE = \frac{\sum_{i=1}^n \text{excursion } i}{\text{number of tests}} \quad (8)$$

3<sup>rd</sup> Step.  $F_3$  is computed by an asymptotic arithmetical function that scales the NSE to output a score between 0 and 100:

$$F_3 = \frac{NSE}{0.01NSE + 0.01} \quad (9)$$

Finally, the WQI is computed as

$$WQI = 100 - \frac{\sqrt{(F_1^2 + F_2^2 + F_3^2)}}{1.732} \quad (10)$$

If WQI is between 95 and 100, the water is categorized as excellent; whereas, if it falls below 44, the water is classified as poor. This ranking is based on aquatic and irrigation uses of water resources.

## RESULTS AND DISCUSSION

Based on historical data obtained from the General Directorate of Electrical Power Resources Survey and Development Administration of Turkey, water quality index at Demirkopru gauging station (between 1984 and 2007) first dropped to “marginal” status in 1999, while prior to this it was assessed to be in “fair” status. A status ranging from “good” to “marginal” indicates that water quality, is protected generally but is occasionally impaired based on the six available water quality parameters including pH, water temperature, electrical conductivity (EC), sulphate, chlorine, and total hardness constituents (Figure 2). Instead of 1250  $\mu\text{S cm}^{-1}$  limit for EC, a value of 1000  $\mu\text{S cm}^{-1}$  was adopted because the Mann-Kendall trend analysis showed an increasing trend in EC at Demirkopru water quality monitoring station over the past few years. The WQI computed for Demirkopru based on years showed a worsening trend. In 2002, the water quality was evaluated to be at “marginal” status second time in the time series examined (covers the years between 1985 and 2007). One more step was taken to determine whether WQI at Demirkopru water quality monitoring station is increasing or diminishing based on the six parameters listed above. The Mann-Kendall trend analysis was performed for WQI scores computed for yearly data between 1985 and 2007. The outcome of this test showed that the WQI has decreased significantly ( $S=-105$ ;  $SE(S)=37.86$ ;  $u=-2.75$  <  $t=-2.07$ ). It is clear that the water quality at the Demirkopru water quality monitoring station, based only on the six parameters mentioned above, decreased dramatically between 1985 and 2007. This finding indicates that the upstream segments (before Turkish catchment) of the river provide a great deal of contamination. The only marginal state of the WQI was observed in 2002. However, the WQI is close to

64, which is within marginal water quality, after the year 2002. 2002 is the same year that the Zeyzoun Dam collapsed and damaged some parts in the watershed as well as river bed. This might also be related with the sediment contamination. However, further studies are needed to potentially link sediment quality with water quality.

**Dry Weather and Wet Weather Conditions.** Water quality parameters for October 2005 and February 2006 samples were determined at seven different stations. They were also evaluated by the WQI. The water quality parameters examined included: EC (the limit value was chosen to be  $1000 \mu\text{S cm}^{-1}$ ), water temperature (should be less than  $22^\circ\text{C}$ ), pH (should be between 6.5 and 8.5 for potable waters), surface active material (should not be greater than  $0.2 \text{ mg L}^{-1}$ ), chemical oxygen demand (COD should be less than  $30 \text{ mg L}^{-1}$ ), total suspended solids (TSS should be less than  $25 \text{ mg L}^{-1}$ ), nitrate ( $\text{NO}_3\text{-N}$ , which should not exceed  $0.5 \text{ mg L}^{-1}$ ), total phosphorus (TP should be below  $0.65 \text{ mg L}^{-1}$ ), zinc (should be no more than  $3 \mu\text{g L}^{-1}$ ), iron (should be less than  $100 \mu\text{g L}^{-1}$ ), nickel (should be less than  $20 \mu\text{g L}^{-1}$ ), potassium (should be less than  $650 \mu\text{g L}^{-1}$ ), dissolved oxygen (should exceed  $6.5 \text{ mg L}^{-1}$ ), selenium (should be less than  $4.6 \mu\text{g L}^{-1}$ ), boron (should be less than  $1 \text{ mg L}^{-1}$ ), and manganese (should be less than  $0.05 \text{ mg L}^{-1}$ ). The measured values were compared to the toxicity limits of constituents which mainly depend on the water hardness.

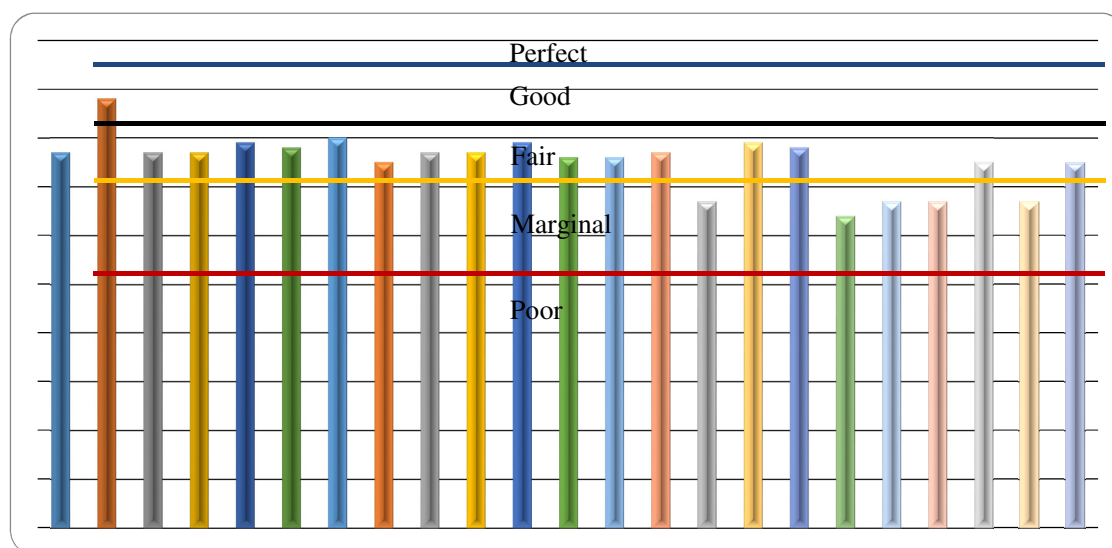


Figure 2. Water quality index with respect to years at Demirkopru water quality monitoring station

Water hardness was determined to range between  $417\text{--}442 \text{ mg L}^{-1} \text{ CaCO}_3$  at seven subsequently located sampling stations in October 2005. At this time, the streamflow was  $13.2 \text{ m}^3 \text{ s}^{-1}$  at Demirkopru, and  $22.9 \text{ m}^3 \text{ s}^{-1}$  at Antakya. In February 2006, the streamflow was  $43.5 \text{ m}^3 \text{ s}^{-1}$  at Demirkopru and  $177.4 \text{ m}^3 \text{ s}^{-1}$  at Antakya (measured by the staff of the General Directorate of Electrical Power Resources Survey and Development Administration of Turkey). With the increase of streamflow, the water hardness of the seven sampling stations ranged from  $187$  to  $195 \text{ mg L}^{-1} \text{ CaCO}_3$  in February 2006.

Copper levels were compared with the fish and aquatic life criteria (Pennsylvania Code, 2009) and were computed to be  $3.5 \mu\text{g L}^{-1}$  for October 2005 (calculations were based on calcium carbonate hardness as  $\text{mg L}^{-1}$  and all measured values as triplicates from seven stations were determined to be on the safe side). On the other hand, all samples from all sampling stations exceeded the limit determined for copper ( $2.8 \mu\text{g L}^{-1}$ ) in February 2006. Especially, after the city centre (Antakya), copper concentrations were determined to be more than  $7 \mu\text{g L}^{-1}$ . For momentary sampling results, neither October 2005 nor February 2006 sampling results exceeded limit values, which were computed as  $52 \mu\text{g L}^{-1}$  for October 2005 and  $24 \mu\text{g L}^{-1}$  for February 2006.

For lead, neither October 2005 nor February 2006 samples were found to exceed their long-term limit values, which were  $12 \mu\text{g L}^{-1}$  for October and  $5 \mu\text{g L}^{-1}$  for February 2006. Furthermore, the momentarily sampling limit values were determined as nearly  $300 \mu\text{g L}^{-1}$  for October 2005 and  $130 \mu\text{g L}^{-1}$  for February 2006.

For selenium, only the first sampling station (just after the Syrian-Turkish border) and the last two stations (close to the river delta) were found to exceed the limit for selenium concentration of  $4.6 \mu\text{g L}^{-1}$  in October 2005. On the other hand, the first two stations were determined to be problematic due to higher selenium compared to the limit value ( $4.6 \mu\text{g L}^{-1}$ ) in February 2006. For nickel all sampling stations and the sampling times were found to violate the limit value (approximately  $5 \mu\text{g L}^{-1}$ ) based on water hardness. The limit value of selenium exists only for continuous concentration for fish and aquatic life.

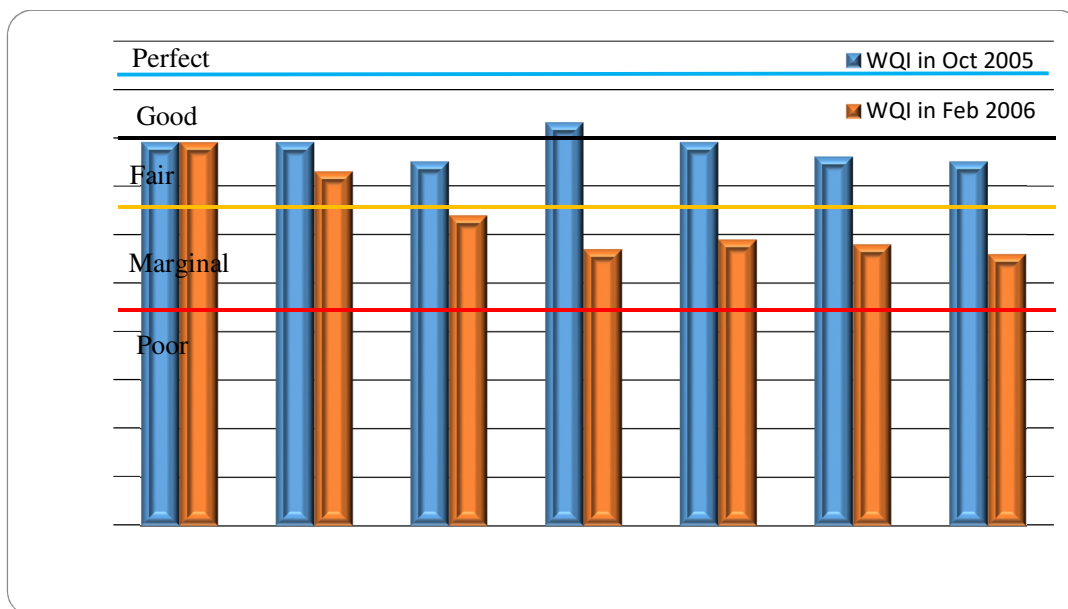


Figure 3. Water quality index result of two different surveys performed on seven stations on the generally within Hatay Province, Turkey

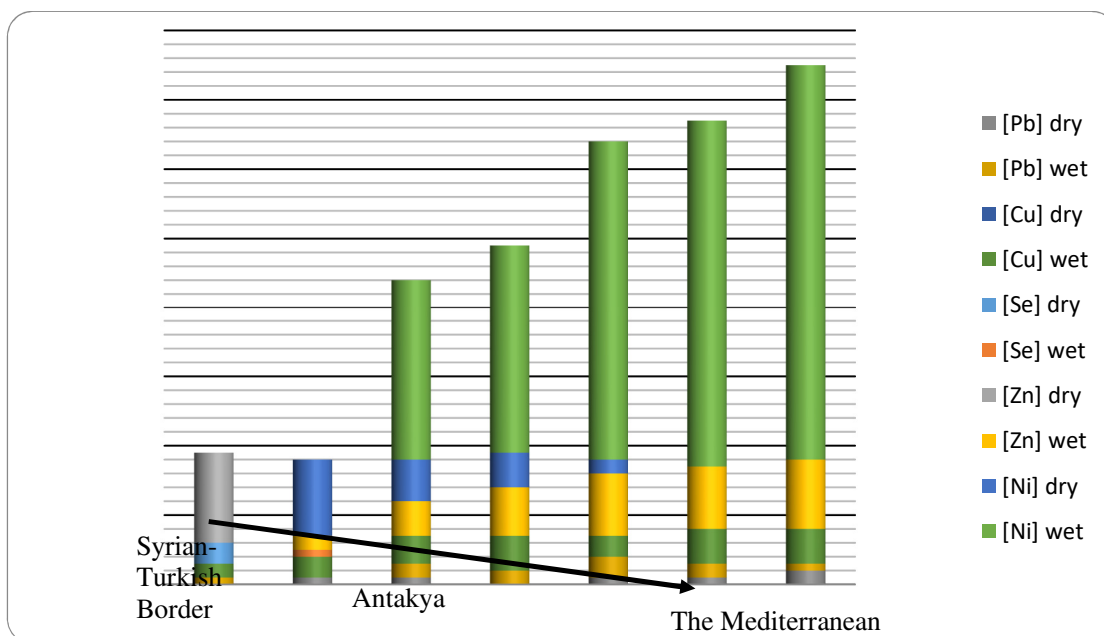


Figure 5. Lead, copper, selenium, zinc and nickel levels ( $\mu\text{g L}^{-1}$ ) for the Orontes River's Turkish part along seven sampling stations in October 2005 (dry period) and February 2006 (wet period)

For zinc, only the first sampling station was found to have a higher concentration compared to the limit value ( $6 \mu\text{g L}^{-1}$ ) in October 2005. Surprisingly, all sampling stations, with the exception of the first

one located just after the Syrian-Turkish border, had an almost three-fold higher zinc concentration than the limit value ( $5.3 \mu\text{g L}^{-1}$ ) in February 2006. Figure 4 represents the measured concentrations of the above mentioned water quality constituents along the seven sampling sites.

Although not illustrated in Figure 4, aluminium concentrations indicated a risk in February 2006 due to the fact that the limit value for momentary sampling is approximately  $750 \mu\text{g L}^{-1}$ ; whereas aluminium concentrations, in October 2005, at sampling stations 3 through 7 were two to three times above the limit value (Pennsylvania Code, 2009).

For chromium, all sampling stations were found to have lower concentrations than the limit value (determined as  $1 \text{ mg L}^{-1}$ ) in February 2006, and the limit value (determined as  $1.9 \text{ mg L}^{-1}$ ) in October 2005. For vanadium, both samplings were found to have lower concentrations than the limit value ( $510 \mu\text{g L}^{-1}$ ) determined for momentary sampling. Similarly, both samplings were not found to exceed the limit value of barium ( $21 \text{ mg L}^{-1}$ ) and of cobalt ( $95 \mu\text{g L}^{-1}$ ).

On one hand, anthropogenic pressures on natural landscapes regulates stream flow more homogenously, but on the other hand, water quality deteriorates due to floods affected by changing basin structure.. In a relatively unoccupied river basin, the River Murray, sodium concentration increased more than thirty fold between Jingellic (2322 km away from the delta) and Tailem Bend (87 km away from the delta) (Mackay et al, 1988).

## CONCLUSION

There has been a noticeable trend of increasing sodium load, especially in wet years, between the two water quality monitoring stations located in the lower Orontes River catchment. Water quality has been improved for a number of reasons, such as wastewater treatment facilities, better waste management plans, and stricter use of chemical aids in agriculture. The increase in some water quality constituents along the river especially during the wet period signifies sediment contamination as well as wash-off of these constituents. However, a comprehensive sediment quality or background analyses need to be completed in the study area.

## REFERENCES

- Akbulut (Emir), N., Bayarı, S., Akbulut, A., Yalçın, Ş., (2009). Rivers of Turkey, in: Tockner, K., Robinson, C. T., and Uehlinger, U. (Eds.) Rivers of Europe. Academic Press, Inc., London, pp. 643-672.
- Arisoy, A.I. and Turkoglu, Y., (1998). Türkiye'nin Sınıraşan ve Sınır Oluşturan Sularının Siyasi Coğrafya Açısından Değerlendirilmesi (in Turkish). Seminar, Gazi University, Ankara.
- Bayram, A., Onsoy, H., Akinci, G, Bulut, V. N., (2011). Variation of total organic carbon content along the Stream Harşit, Eastern Black Sea Basin, Turkey. *Environ. Monit. Assess.* 182 (1-4), 85-95.
- Begon, M., Townsend, C. R., Harper, J.L., (2006). Ecology: From individuals to ecosystems, fourth ed. Blackwell Publishing, Malden, MA.
- Kumarasamy, P., Dahms, H.U., Jeon, H.J., Rajendran, A., James, R.A., (2014). Irrigation water quality assessment-an example from the Tamiraparani river, Southern India. *Arabian J of Geoscience.* 7 (12): 5209-5220.
- Jarvi, H. P., Neal, C., Withers, P. J. A., (2006). Sewage-effluent phosphorus: A greater risk to river eutrophication than agricultural phosphorus? *Sci. Total Environ.* 360 (1-3): 246-253.
- Mackay, N., Hillman, T., Rolls, J., (1988). Water Quality of the River Murray: a review of monitoring 1978-1986. Murray-Darling Basin Commission, Canberra, A. C. T., Water Qual. Rep. No. 1.
- McClain and Maher (2016).
- Neal, C., (2000). The fractionation of the elements in river waters with respect to the continental crust: a UK perspective based on a river enrichment factor approach. *Hydrol. Earth Syst. Sci.* 4: 499-509.
- Neal, C., Williams, R. J., Bowes, M. J., Harrass, M. C., Neal, M., Rowland, P., Wickham, H., Thacker, S., Harman, S., Vincent, C., Jarvie, H. P., (2011). Decreasing boron concentrations in UK rivers: Insights into reductions in detergent formulations since the 1990s and within-catchment storage issues. *Sci. Total Environ.* 408: 1374-1385.

- Pennsylvania Code, (2009). §93.8c. Human Health and aquatic life criteria for toxic substances. Accessed from the internet on December 22, 2011 from: <http://www.pacode.com/secure/data/025/chapter93/s93.8c.html>
- Scheumann, W., Sagsen, I., Tereci, E., (2011). Orontes River Basin: Downstream Challenges and Prospects for Cooperation in Turkey's Water Policy, in: Kibaroglu, A., Scheumann, W., Kramer, A. (Eds.) Springer-Verlag, Berlin Heidelberg, pp. 301-312.
- Tavakoli, A., Kerachian, R., Nikoo, M. R., Soltani, M., & Estalaki, S. M. (2014). Water and waste load allocation in rivers with emphasis on agricultural return flows: application of fractional factorial analysis. *Environmental Monitoring and Assessment*, 186(9), 5935–5949.
- The General Directorate of Electrical Power Resources Survey and Development Administration of Turkey (2010).  
Water Quality Monitoring Stations 1997 and 1998 reports. Unpublished data.
- Tong, S.T.Y., Liu, A. J., Goodrich, J.A., (2009). Assessing the water quality impacts of future land-use changes in an urbanising watershed. *Civil Eng. Environ. Syst.* 26 (1): 3-18.
- TUIK, (2013). Address Based Population Data (in Turkish) 2013. Accessed from the internet on January 20, 2015 from: <http://rapor.tuik.gov.tr>
- Wei, G. L., Yang, Z. F., Cui, B. S., Li, B., Chen, H., Bai, J. H., Dong, S. K., (2009). Impact of Dam construction on Water Quality and Self Purification capacity of the Lancing River, China. *Wat. Res. Man.* 23: 1763-1780.
- Woitke, P., Wellmitz, J., Helm, D., Kube, P., Lepom, P., Lithraty, P., (2003). Analysis and assessment of heavy metal pollution in suspended solids and sediments of the river Danube. *Chemosphere.* 51 (8): 633-642.

## WATER QUALITY ASSESSMENT FOR MELEN WATERSHED IN THE MARMARA REGION, TURKEY

*Ersin Orak<sup>a</sup>*, Atilla Akkoyunlu<sup>b</sup>

a) Çanakkale Onsekiz Mart University Environmental Eng. Department Çanakkale, Turkey

E-Mail : [ersinorak@comu.edu.tr](mailto:ersinorak@comu.edu.tr)

b) Boğaziçi University Department of Civil Engineering 34342 Bebek/İstanbul Turkey

E-mail: [akkoyun@boun.edu.tr](mailto:akkoyun@boun.edu.tr)

**ABSTRACT:** Water quality assessment is necessary for management of water resources. As known environmental processes are very complex. Reflection of this complexity is also seen in water quality models. Therefore finding efficient and sound models in many cases are very difficult. Water quality class assessment for inland water bodies in Turkey, is evaluated for each parameters according to the Water Quality Standards for Inland Waterbodies. This standard is only for a single pollution parameter. In this study authors tried to express the class of water body with the coverage of overall water qualities measured. For this aim, fuzzy syntetic evaluation (FSE), and self-organizing map (SOM) are applied for Melen River and compared with traditional method. FSE and SOM are easy to understand and apply in water quality assessments for watershed water quality management. The Melen River is in the Marmara region of Turkey located in north. This river is used for many application like irrigation of the agricultural lands, drinking water supply and several different industries' process water, It supplies potable water to Istanbul which is most densely populated.mega city in Turkey.

## INTRODUCTION

Water management is now considered among the most important issue for natural resources in any country. Assessment of water quality is very important because it refers to the physical chemical and biological characteristics of water. Many countries have their own management strategies for their water sources protection (Chang, Chen, & Ning, 2001). Water quality assessment is very important for the management applications. Modelling of environmental processes have high complexity, dynamism, and non-linearity. Therefore, finding efficient models in many cases are very difficult (Kalteh, Hjorth, & Berndtsson, 2008). Some new methods are invented to overcome these problems. In this study, two of them are used, namely These are Fuzzy Logic (FL), and Self-Organizing Map (SOM).

Fuzzy logic was introduced by Zadeh (1965) and has become one of the most common approaches in the field of Artificial Intelligence (AI). FL is a multi-valued logic that is an alternative to Aristotelian Logic (Seguí et al., 2013). FL includes fuzzification, application of the fuzzy rule base to data, and finally defuzzification (Icaga, 2007). Fuzzy synthetic evaluation (FSE) is a model, which based on FL, using to assess multiple criteria decision-making (Xu et al., 2010).

Artificial Neural Networks (ANNs) based on supervised and unsupervised learning, are alternative tools for ecological data processing, which become in extensive use over the last decades. Supervised learning is carried out for data estimation (e.g., prediction, revealing the environment–community causality relationships) based on a priori knowledge. Unsupervised learning is useful in extracting information from the data (e.g., ordination, classification) without previous knowledge (T. S. Chon & Park, 2008).

Self-Organizing Maps (SOM) are competitive and unsupervised forms of ANNs pioneered by the Finnish professor, Professor Teuvo Kohonen (1981) (Kohonen, 2001). One of the most widely used ANN algorithms is SOM, which has been used extensively for information extraction without prior knowledge and the efficiency of visualization (T.-S. Chon, 2011).

Water quality class assessment in Turkey, is evaluated for each parameters according to the Water Quality Standards for Inland Waterbodies which are in “Water Pollution Control Regulations of Turkey” (WPCR, 31.12.2004).

## STUDY AREA

The Melen River is in the northern part of Turkey. Its watershed is located in the western Black Sea Region of Turkey (Fig. 1) with a total area of 2,437 km<sup>2</sup>. It has a transitional climate between Western Black Sea, Marmara and Mediterranean regions. It is used mainly for irrigation agriculture, drinking water, and several different industries’ process water. The used water is directly discharged into the Melen River. The other important use of Melen River is that it supplies water to Istanbul City, which is highly populated. The water supplied from Melen River satisfies more than 50% of Istanbul’s water demand due to its high water potential and relatively less degraded water quality (Akiner & Akkoyunlu, 2012), (Koklu, Sengorur, & Topal, 2010), (Erturk et al., 2010), and (Karakaya & Evrendilek, 2010).

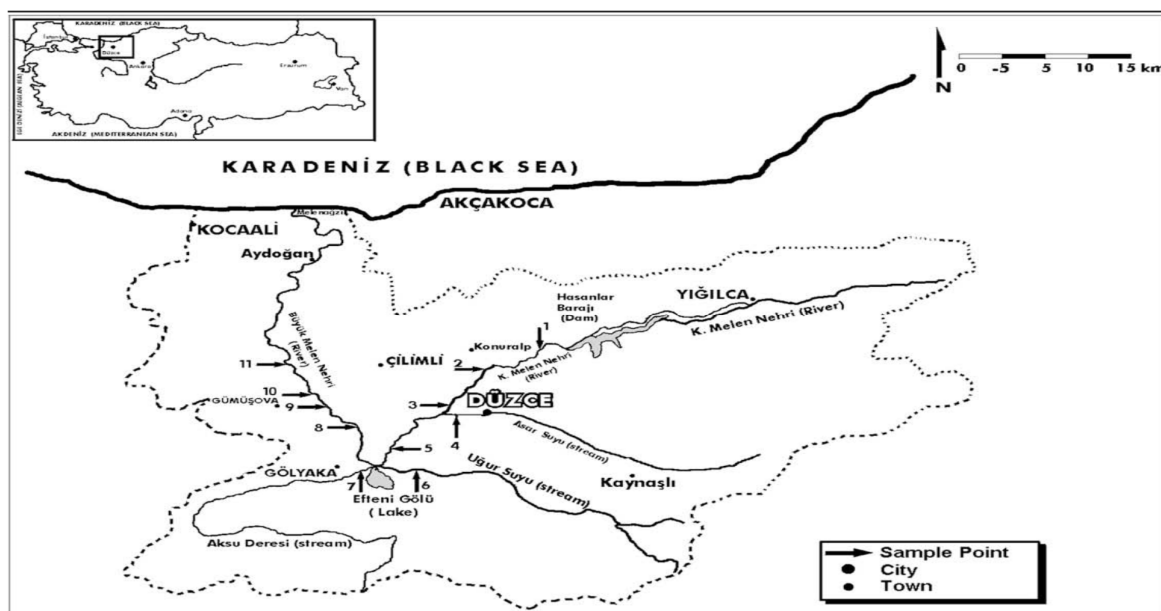


Figure 1 Location map of Melen catchment

In this study, there are twelve observation station, which these are Aksu Creek, Aksu Hasanlar Dam In, Karadere Hasanlar Dam In (quarry), Asar River Before K.Melen River, B.Melen River Bridge Before Pakmaya, B.Melen River Ugurlu Village, K.Melen River Hasanlar Dam In, K.Melen River Hasanlar Dam Bottom Sluice Out, Lahna Stream Before B.Melen, K:Melen River Pasa Konagi, Ugur Creek, and six water quality parameters, namely, dissolved oxygen (DO), ammonium nitrogen (NH<sub>4</sub>-N), nitrite (NO<sub>2</sub>-N), nitrate (NO<sub>3</sub>-N), biological oxygen demand (BOD), and total phosphorous (TP), are measured from 1995 to 2009. Data for this research is provided from the State Hydraulic Works of Turkey (DSI, 2009).

## METHODOLOGY

In the study, water quality classes are given according to the “Water Pollution Control Regulations of Turkey” and two different methodologies, such FL, and SOM are employed for the data treatment and modeling.

**Fuzzy Logic.** The applications of the fuzzy logic are very wide are including process control, management and decision making, operations research etc.

Models based on fuzzy rules are enough to demonstrate uncertainty and inaccuracies in knowledge and data. These models can reflect qualitative sides of knowledge and human outcome processes without a precise quantitative analysis. Thus, they are less certain than traditional numerical models. Nevertheless,



the gains are in simplicity, computational speed and flexibility that result from the use of these models with compensation loss in precision (Lermontov, Yokoyama, Lermontov, & Machado, 2009).

In the beginning of 1990s, classification of river water quality by fuzzy theory has started. Kung et al. (1992) published the application of fuzzy clustering analysis to water quality classification. Fuzzy synthetic evaluation was used by Lu et al. (1999) to investigate and compare the water quality of Fei- Tsui Reservoir in Taiwan. The conclusion of this search showed that most of the water quality records were evaluated as the same trophic state by both the Carlson index and FSE (Lu & Lo, 2002).

Fuzzy evaluation method is applied in three steps. First, the membership functions are identified, which is followed by fuzzy relations matrix (R) and the standard inference mechanisms (Şen, 2010). Finally, the water quality values are obtained through a fuzzy operator.

**Determination of membership function.** In the determination of water quality classes of the different points along the Melen River “Water Quality Standards for Inland Water Bodies” have been employed. This study defines four membership functions ( $\mu$ ), in crisp sets an element may belong the set or not but in fuzzy sets membership degree value between 0 to 1 (Şen & Altunkaynak, 2009). Water quality classes according to the Water Quality Standards for Inland Waterbodies are given below. The standard parameters values related to this study are presented in Table 1 (WPCR, 31.12.2004). A water quality classification in the regulation is as follows:

- Class I: High quality water
- Class II: Slightly polluted water
- Class III: Polluted water
- Class IV: Extremely polluted water

Table 1. The Water Quality of Inland Surface Waters in River, Lakes, and Dam Reservoirs

Parameters	1	2	3	4
Dissolved Oxygen (mg O <sub>2</sub> /L)	8	6	3	< 3
Ammonium Nitrogen (mg NH <sub>4</sub> <sup>+</sup> -N/L)	0.2	1	2	> 2
Nitrite Nitrogen (mg NO <sub>2</sub> <sup>-</sup> -N/L)	0.002	0.01	0.05	> 0.05
Nitrate Nitrogen (mg NO <sub>3</sub> <sup>-</sup> -N/L)	5	10	20	> 20
Total Phosphorus (mg P/L)	0.02	0.16	0.65	> 0.65
Biochemical Oxygen Demand (BOD) (mg/L)	4	8	20	> 20

The calculation of membership functions are as follows:

$$\begin{aligned}
 \mu_1 &= \begin{cases} 1 & \text{if } 0 \leq x \leq D_1 \\ \frac{D_2 - x}{D_2 - D_1} & \text{if } D_1 \leq x \leq D_2 \\ 0 & \text{if } x \geq D_2 \end{cases} & \mu_2 &= \begin{cases} \frac{x - D_1}{D_2 - D_1} & \text{if } D_1 < x < D_2 \\ 1 & \text{if } x = D_2 \\ \frac{D_2 - x}{D_2 - D_1} & \text{if } D_2 < x < D_3 \end{cases} \\
 \mu_3 &= \begin{cases} 0 & \text{if } x \leq D_1 \text{ or } x \geq D_3 \\ \frac{x - D_1}{D_2 - D_1} & \text{if } D_1 < x < D_2 \\ 1 & \text{if } x = D_2 \\ \frac{D_2 - x}{D_2 - D_1} & \text{if } D_2 < x < D_3 \end{cases} & \mu_4 &= \begin{cases} 0 & \text{if } x \leq D_3 \\ \frac{x - D_3}{D_4 - D_3} & \text{if } D_3 \leq x \leq D_4 \\ 1 & \text{if } x \geq D_4 \end{cases}
 \end{aligned} \tag{1}$$

where  $D_i$  ( $i=1, 2, 3, 4$ ) is the value of the water quality class in,  $x$  is the sample water quality value, and  $\mu$  is membership degree value.

Evaluation matrix (R) is set by using the membership values. R is given below, where, i represents DO, NH4-N, NO2-N, NO3-N, TP, BOD; and j is for class I, class II, class III, and class IV water quality.

$$R = \begin{bmatrix} \mu_{11} & \mu_{12} & \mu_{13} & \mu_{14} \\ \mu_{21} & \mu_{22} & \mu_{23} & \mu_{24} \\ \mu_{31} & \mu_{32} & \mu_{33} & \mu_{34} \\ \mu_{41} & \mu_{42} & \mu_{43} & \mu_{44} \\ \mu_{51} & \mu_{52} & \mu_{53} & \mu_{54} \\ \mu_{61} & \mu_{62} & \mu_{63} & \mu_{64} \end{bmatrix} \quad (2)$$

**Determination of weights.** For each pollutant parameter it is necessary to determine a weight, which impacts one another, because each pollutant has its own characteristics. In this study, weights are distributed equally for the main pollutants, which are DO, BOD, TP, and components of nitrogen. The weight matrix is given in the following expression.

$$W = \{W_{DO}(0.25), W_{BOD}(0.25), W_{TP}(0.25), W_{NH4-N} (0.25/3), W_{NO2-N} (0.25/3), W_{NO3-N} (0.25/3)\}$$

**Fuzzy Synthetic Evaluation.** FSE, which has been described earlier, can be calculated as follows:

$$FSE = W \cdot R = \{b1, b2, b3, b4\} \quad (3)$$

The quality class of water body is evaluated depending on the maximum value of the four values (b1, b2, b3, b4).

**Self Organizing Map (SOM).** Ecological data processing is achieved by Artificial Neural Networks (ANNs), which depend on supervised and unsupervised learnings. Although supervised learning is carried out for data estimation (e.g., prediction, showing the environment–community causality relationships) based on a priori knowledge (i.e., templates), unsupervised learning is useful in extracting information from the data (e.g., sorting, classification) without previous knowledge. Self-organizing maps (SOMs), which is a unsupervised learning neural networks based on the Kohonen network, as in Figure 2, are extensively used in the extraction of information from ecological data (Chon and Park).

The term “self-organizing” refers to the ability to learn and organize information without being given the associated-dependent output values for the input pattern (Astel, Tsakovski, Barbieri, & Simeonov, 2007). The self-organizing map describes a mapping from a higher dimensional input space to a lower dimensional map space. The SOM compresses information while preserving the most important topological and/or metric relationships of the primary data elements on the display. It may also be thought to produce some kind of abstractions. These two aspects, visualization and abstraction, can be utilized in a number of ways in complex tasks such as process analysis, machine perception, control, and communication (Kohonen, 2001).

Ecological data are thought to be difficult to analyze due to numerous biological and environmental factors involved in a complex manner in environment organism relationships. The SOM has advantages for information extraction without prior to knowledge and the efficiency of visualization(T.-S. Chon, 2011). The SOM is a fascinating neural network method that has found increasing interest in water resources applications (Kaltch et al., 2008).

The main advantages of the SOM algorithm are its non-linearity and an ability to preserve the topological structure of the data. The typical structure of an SOM consists of two layers; an input layer which contains one neuron for each variable in the data set and a Kohonen or output layer which is connected to every neuron in the input layer through adjustable weights or network parameters(Kaltch et al., 2008).

Since Chon et al. (1996) first applied the SOM to pattern benthic communities in streams, SOMs have been implemented in various aspects of water research, e.g., classifying biological and environmental data and patterning long-term data. The SOM has also proven to be a practical tool in assessing water quality and managing ecosystem (C  r  ghino & Park, 2009).

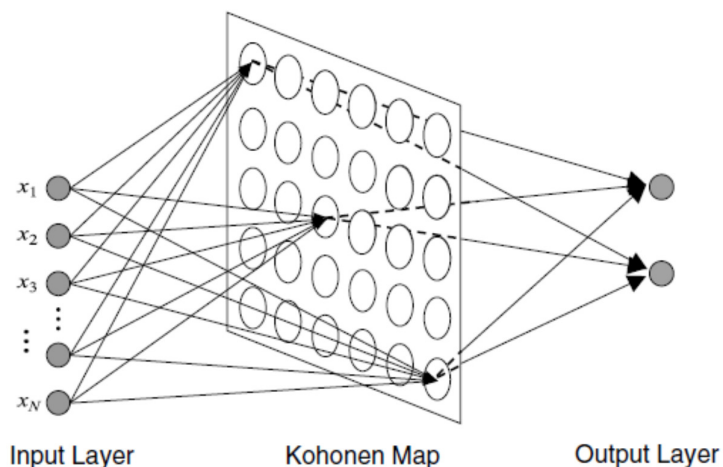


Figure 2. Schematic diagram of SOM.

There are three procedures for applying of SOM as explained in the following three sub-sections: Data gathering and normalization, Training and Extracting information.

**Data gathering and normalization.** Normalizing the pollution parameters is very important, because it transforms the parameters to the range of 0-1, with all parameters having equal importance (Kalteh et al., 2008). In our study, the input data, DO,  $\text{NH}_4\text{-N}$ ,  $\text{NO}_2\text{-N}$ ,  $\text{NO}_3\text{-N}$ , TP, and BOD, are the normalized.

**Training.** It is a iterative procedure and is recommended that the iterations number should be at least 500 times the number of neurons in the output layer (Kalteh et al., 2008). The training strategy is “winner takes all” (Lu & Lo, 2002).

**Extracting information.** After the training of SOM, the results can be post-processed based on visualization, clustering, or local modelling purposes. Figure 3 shows an example of SOM clustering (Kalteh et al., 2008).

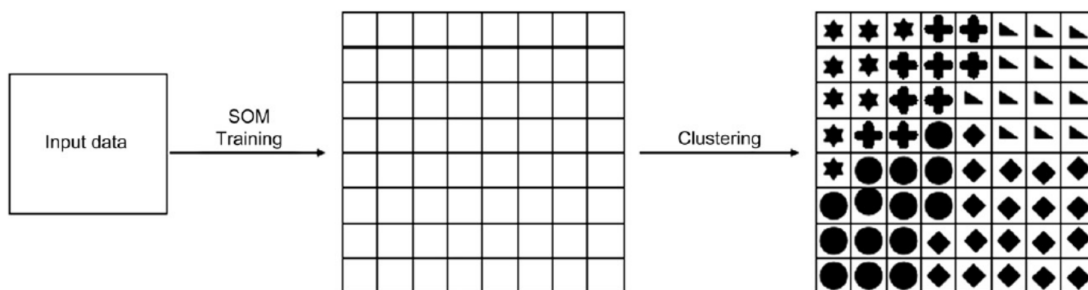


Figure 3. The diagram of a two-level clustering of the SOM. Different symbols represent different clusters

## RESULTS

In this study, there are twelve observation station and dissolved oxygen (DO), ammonium nitrogen ( $\text{NH}_4\text{-N}$ ), nitrite ( $\text{NO}_2\text{-N}$ ), nitrate ( $\text{NO}_3\text{-N}$ ), biological oxygen demand (BOD), and total phosphorous (TP) were measured from 1995 to 2009. The name of observation stations, measurement date, and matching of FSE results and SOM results (%) are given in Table3.

Table 3: The observation stations on the Melen River

Observation Station	Measurement Date	Matching of FSE Results and SOM Results (%)
Aksu Creek	jan.1995 - Oct.2009	98.5
Aksu Hasanlar Dam In	Dec.2006 - Dec.2008	94
Karadere Hasanlar Dam In (quarry)	Dec.2006 - Dec.2008	94
Asar River Before K.Melen River	Dec.2006 - Oct.2009	60
B.Melen River Bridge Before Pakmaya	jan.1995 - Nov.2006	83
B.Melen River after Pakmaya	Dec.2006 - Oct.2009	33.3
B.Melen River Ugurlu Village	jan.1995 - Oct.2009	78
K.Melen River Hasanlar Dam In	Dec.2006 - Dec.2008	94
K.Melen River Hasanlar Dam Bottom Sluice Out	Dec.2006 - Nov.2009	89.3
Lahna Stream Before B. Melen	Dec.2006 - Oct.2009	82.6
K:Melen River PasaKonagi	jan.1995 - Oct.2009	69
Ugur Creek	jan.1995 - Nov.2009	94.7

## CONCLUSION

The Melen River Basin takes place in the north of the Turkey which supports a variety of sectors as irrigation systems in agricultural lands, drinking water and several different industries. In the basin, pollution sources are municipal and industrial wastewater and agricultural run-off. Due to the importance of Melen River for water supply to Istanbul City its water quality assessment is very important.

Ecological data analysis is considered to be difficult because many biological and environmental factors are involved in a complex manner in ecological relationships. In this study, Water Quality Standards for Inland Waterbodies in Turkey are used for showing to water classes for each parameters. Besides, Fuzzy Synthetic Evaluation, and Self-Organizing Map give an overall evaluation which may speed up the management activities in a watershed.. The other advantages of FL and SOM are easy to understand and apply to water quality assessments for watershed quality management.

The results of FSE and SOM are highly similar. According to the results SOM values are getting higher in the case of high pollution. Maybe more polluted regions SOM gives more safely results.

## REFERENCES

- Akiner, M. E., & Akkoyunlu, A. (2012). Modeling and forecasting river flow rate from the Melen Watershed, Turkey. *Journal of Hydrology*, 456-457(0), 121-129. doi:<http://dx.doi.org/10.1016/j.jhydrol.2012.06.031>
- Astel, A., Tsakovski, S., Barbieri, P., & Simeonov, V. (2007). Comparison of self-organizing maps classification approach with cluster and principal components analysis for large environmental data sets. *Water Research*, 41(19), 4566-4578. doi:<http://dx.doi.org/10.1016/j.watres.2007.06.030>
- C  r  ghino, R., & Park, Y. S. (2009). Review of the Self-Organizing Map (SOM) approach in water resources: Commentary. *Environmental Modelling & Software*, 24(8), 945-947. doi:<http://dx.doi.org/10.1016/j.envsoft.2009.01.008>
- Chang, N.-B., Chen, H. W., & Ning, S. K. (2001). Identification of river water quality using the Fuzzy Synthetic Evaluation approach. *Journal of Environmental Management*, 63(3), 293-305. doi:<http://dx.doi.org/10.1006/jema.2001.0483>
- Chon, T.-S. (2011). Self-Organizing Maps applied to ecological sciences. *Ecological Informatics*, 6(1), 50-61. doi:<http://dx.doi.org/10.1016/j.ecoinf.2010.11.002>
- Chon, T. S., & Park, Y. S. (2008). Self-Organizing Map. In S. E. J  rgensen & B. D. Fath (Eds.), *Encyclopedia of Ecology* (pp. 3203-3210). Oxford: Academic Press.

- Erturk, A., Gurel, M., Ekdal, A., Tavsan, C., Ugurluoglu, A., Seker, D. Z., . . . Ozturk, I. (2010). Water quality assessment and meta model development in Melen watershed – Turkey. *Journal of Environmental Management*, 91(7), 1526-1545. doi:<http://dx.doi.org/10.1016/j.jenvman.2010.02.021>
- Icaga, Y. (2007). Fuzzy evaluation of water quality classification. *Ecological Indicators*, 7(3), 710-718. doi:<http://dx.doi.org/10.1016/j.ecolind.2006.08.002>
- Kalteh, A. M., Hjorth, P., & Berndtsson, R. (2008). Review of the self-organizing map (SOM) approach in water resources: Analysis, modelling and application. *Environmental Modelling & Software*, 23(7), 835-845. doi:<http://dx.doi.org/10.1016/j.envsoft.2007.10.001>
- Karakaya, N., & Evrendilek, F. (2010). Water quality time series for Big Melen stream (Turkey): its decomposition analysis and comparison to upstream. *Environmental Monitoring and Assessment*, 165(1-4), 125-136. doi:10.1007/s10661-009-0932-7
- Kohonen, T. (2001). *Self-Organizing Maps*: Springer-Verlag New York, Inc.
- Koklu, R., Sengorur, B., & Topal, B. (2010). Water Quality Assessment Using Multivariate Statistical Methods—A Case Study: Melen River System (Turkey). *Water Resources Management*, 24(5), 959-978. doi:10.1007/s11269-009-9481-7
- Lermontov, A., Yokoyama, L., Lermontov, M., & Machado, M. A. S. (2009). River quality analysis using fuzzy water quality index: Ribeira do Iguape river watershed, Brazil. *Ecological Indicators*, 9(6), 1188-1197. doi:<http://dx.doi.org/10.1016/j.ecolind.2009.02.006>
- Lu, R.-S., & Lo, S.-L. (2002). Diagnosing reservoir water quality using self-organizing maps and fuzzy theory. *Water Research*, 36(9), 2265-2274. doi:[http://dx.doi.org/10.1016/S0043-1354\(01\)00449-3](http://dx.doi.org/10.1016/S0043-1354(01)00449-3)
- Seguí, X., Pujolasus, E., Betrò, S., Àgueda, A., Casal, J., Ocampo-Duque, W., . . . Darbra, R. M. (2013). Fuzzy model for risk assessment of persistent organic pollutants in aquatic ecosystems. *Environmental Pollution*, 178(0), 23-32. doi:<http://dx.doi.org/10.1016/j.envpol.2013.02.014>
- Şen, Z., & Altunkaynak, A. (2009). Fuzzy system modelling of drinking water consumption prediction. *Expert Systems with Applications*, 36(9), 11745-11752. doi:<http://dx.doi.org/10.1016/j.eswa.2009.04.028>
- WPCR. (31.12.2004). Water Pollution Control Regulation. *Resmi Gazete* 25687, 25687.
- Xu, Y., Yeung, J. F. Y., Chan, A. P. C., Chan, D. W. M., Wang, S. Q., & Ke, Y. (2010). Developing a risk assessment model for PPP projects in China — A fuzzy synthetic evaluation approach. *Automation in Construction*, 19(7), 929-943. doi:<http://dx.doi.org/10.1016/j.autcon.2010.06.006>

## ANALYSIS OF ELEVATED CONCENTRATIONS IN TRACE ELEMENTS AND NUTRIENTS IN URBAN CREEK

*Michael Harrison* and Barry Hibbs  
(California State University, Los Angeles, USA)

**ABSTRACT:** Dry weather runoff (imported and recycled water) contributes to perennial flows in the Malibu Creek Watershed located in southern California. Our study investigates an urban creek for selenium, nutrients, and stable water isotopes to further understand inputs and sources. We have found concentrations of 9.9 to 32 ug/L Se and 0.37 to 6.6 mg/L  $\text{NO}_3^-$ -N from groundwater seeps that flow within a storm drain. From the input of a storm drain where dry weather runoff provides perennial flow, concentrations range from 4.1 to 11 ug/L Se and 1.5 to 4.9 mg/L  $\text{NO}_3^-$ -N. Concentrations decrease from 4.1 to 0.74 ug/L Se and 0.12 to 0.59 mg/L  $\text{NO}_3^-$ -N downstream. Moderately high concentrations of nitrate-nitrogen correlating with elevated concentrations of selenium suggest that enriched selenium is oxidized by elevated concentrations of nitrate found in local shallow groundwater and urban runoff. Our results coupled with seasonal analysis of hydrogen and oxygen isotopes further suggest perennial input and mixing of local groundwater throughout the riverine system.

### INTRODUCTION

The Malibu Creek Watershed is located within the Santa Monica Mountains in Los Angeles and Ventura County, California. The upper portion of the watershed exposes the Monterey-Modelo Formation, a Miocene marine deposit. The Monterey-Modelo Formation has been noted for its contribution of high selenium, metals, phosphate, nitrogen, and salinity, content in the Malibu Creek Watershed (LVMWD, 2010).



**FIGURE 1.** Map of residential community north of El Camino Real Creek.



The majority of cities within the upper Malibu Creek Watershed and use recycled water primarily for irrigation. Recent studies in the Malibu Creek Watershed have suggested high concentrations of phosphorus and nitrate may be more of a result of dry weather runoff from urban landscapes (Hibbs, 2014).

To further understand the geologic and anthropogenic controls on nutrient loading we examine El Camino Real Creek. El Camino Real Creek lies amongst Monterey-Modelo Formation strata and fed perennially through a storm drain from a residential community (Figure 1). Studying a creek within the Monterey-Modelo Formation serves as a controlled area that removes the variable that come with larger watershed studies.

## **MATERIALS AND METHODS**

Several stations along El Camino Real Creek were sampled repeatedly to understand the spatial and hydrochemical differences throughout the creek (Figure 2). Samples were collected approximately every 6 weeks for a year period starting October 2014. Each station were measured for temperature, conductivity, and dissolved oxygen were conducted with an YSI 63 YSI 550A meter. Samples were collected filtered and analyzed for nutrients (nitrate and orthophosphate), ions, selenium, and water isotopes.

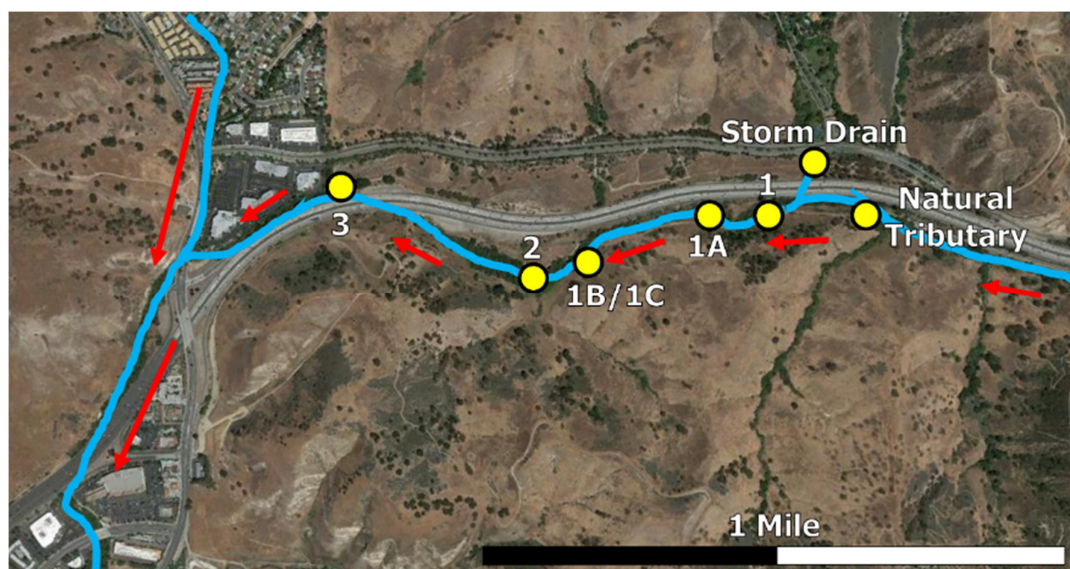


**FIGURE 2.** Map of sampling stations throughout El Camino Real Creek.

## **RESULTS AND DISCUSSION**

Continuous data show concentrations of nitrate and phosphate decreasing downstream from the storm drain (Harrison, 2015). From an initial input at the storm drain where dry weather flows consistently water contains an average of 2.57 mg/L  $\text{NO}_3^- \text{N}$  and an average of 1.60 mg/L  $\text{PO}_4$ . Nutrient values decrease to concentrations averaging 0.22 mg/L  $\text{NO}_3^- \text{N}$  and 0.62 mg/L  $\text{PO}_4$  where El Camino Real Creek converges with Las Virgenes Creek at its most downstream station. The natural tributary source flow developed during the winter season has significantly low concentrations of  $\text{NO}_3^- \text{N}$  that average at 0.31 mg/L and 0.10  $\text{PO}_4$ .

Downstream from the storm drain, El Camino Real Creek has a trend of decreasing  $\text{NO}_3^- \text{N}$  and an initial decrease before stabilization of  $\text{PO}_4$  values (Figure 3). Decreases in nitrate and phosphorus are due to transformative process such as denitrification and vegetation uptake, along with some mixing and dilution with groundwater baseflow that has ambient concentrations of nutrients. Stabilization of phosphorus downstream may be a result of groundwater leaching from phosphatic bearing strata in equilibrium with

vegetation uptake or from accumulation of phosphorus from recycled water sorbing onto soils within the creek.

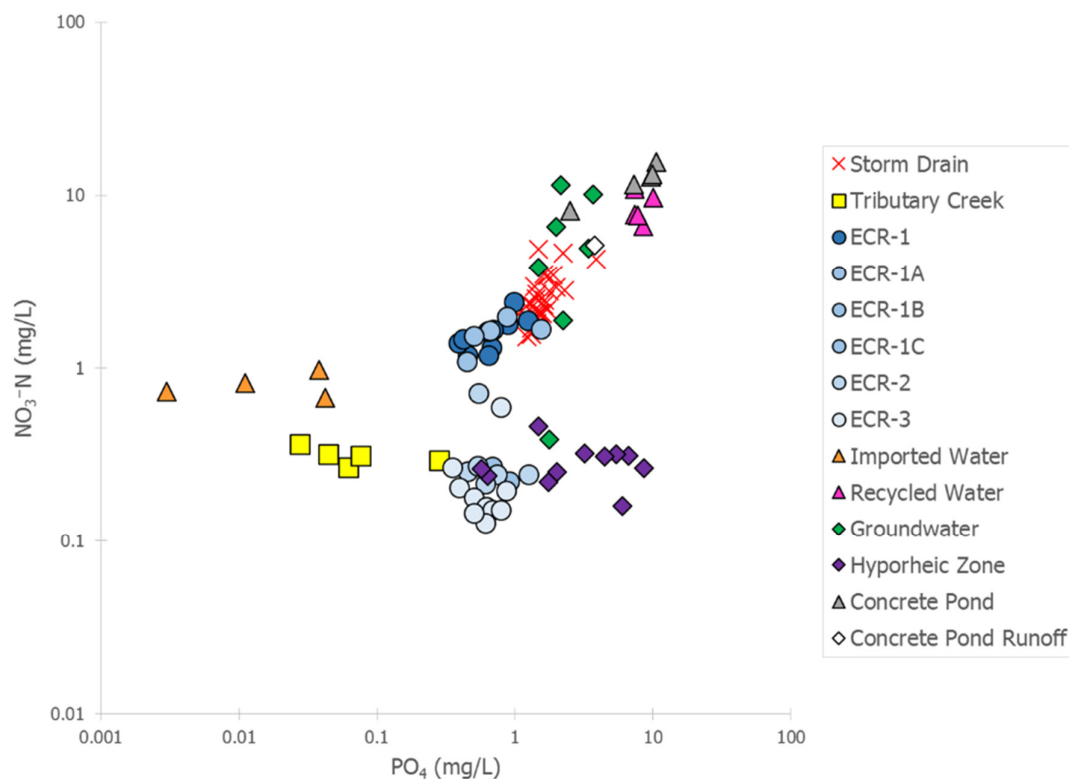


**FIGURE 3.** Concentrations of  $\text{NO}_3\text{-N}$  and  $\text{PO}_4$  throughout El Camino Real Creek and surrounding area.

Local samples of recycled and imported water were established as endmembers for stable water isotope mixing analysis. Imported water includes tap water and recycled wastewater. Both are used for urban water applications in the entire study area. Recycled water and tap water have relatively light isotope values compared to local water derived by precipitation recharge.

The average isotope values for the recycled and imported endmembers are  $-9.3\text{‰}$   $\delta^{18}\text{O}$  and  $-74\text{‰}$   $\delta\text{D}$ . The average isotope values for the samples collected at the storm drain are  $-7.3\text{‰}$   $\delta^{18}\text{O}$  and  $-63\text{‰}$   $\delta\text{D}$ . Samples from the natural tributary have stable isotope values of  $-6\text{‰}$   $\delta^{18}\text{O}$  and  $-41\text{‰}$   $\delta\text{D}$ . The average isotope values for the samples collected along El Camino Real are  $-6.4\text{‰}$   $\delta^{18}\text{O}$  and  $-52\text{‰}$   $\delta\text{D}$ . Samples downstream from the storm drain (Stations 1 through 3) along El Camino Real Creek fit along a mixing line of the plotted stable isotope data with samples collected closest to the storm drain containing the most imported water (Figure 4).

Stable isotopes of hydrogen and oxygen show mixing of recycled water with local groundwater downstream, which demonstrates that nutrients in this creek are not strictly dominated by geologic sources. Isotope data also shows a strong correlation between high concentrations of  $\text{NO}_3\text{-N}$  and  $\text{PO}_4$  with recycled water fractions. Stations that have a percentage of imported and recycled water generally have higher values of  $\text{NO}_3\text{-N}$  and  $\text{PO}_4$ . This correlation strengthens the point that high nutrients from the storm drain are mixing with the natural tributary and groundwater downstream.

We have found Se concentrations of from groundwater seeps that flow within an urban storm drain. From the input of a storm drain concentrations of Se range from 4.1 to 11  $\mu\text{g/L}$ . Concentrations of Se



decrease from 4.1 to 0.74 ug/L downstream, where El Camino Real Creek converges with Las Virgenes Creek. Within the hyporheic zone at Station 1A Se concentrations range from 0.48 to 1.3 ug/L.

Groundwater samples range from 0.37 to 6.6 mg/L  $\text{NO}_3^-$  N while surface water samples range from 1.5 to 4.9 mg/L  $\text{NO}_3^-$  N upstream near the storm drain. Further downstream, after the creek flows move through a riparian area, nitrate concentrations in surface water decrease to 0.12 to 0.59 mg/L  $\text{NO}_3^-$  N. Hyporheic samples range from 0.16 to 0.38 mg/L  $\text{NO}_3^-$  N.

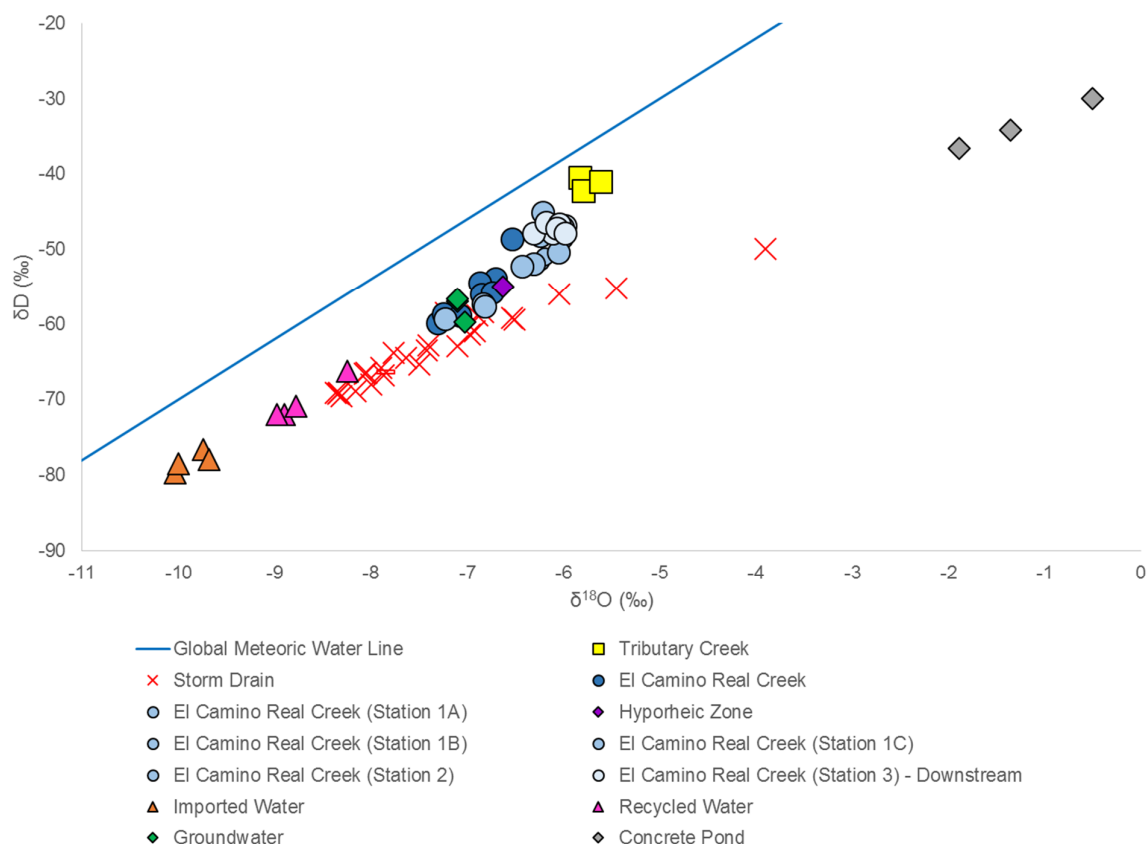


**FIGURE 4.** Stable water isotope data from samples collected at El Camino Real Creek along with endmembers.

Moderately high concentrations of nitrate-nitrogen are correlated with elevated concentrations of selenium in surface water and groundwater near the creek. Elevated concentrations of nitrate in surface water are associated with recycled water used for urban irrigation, and/or legacy nitrate sources from groundwater baseflow. Seasonal analysis of hydrogen and oxygen isotopes suggest perennial input and mixing of local groundwater throughout the riverine system.

## CONCLUSIONS

This investigation suggest that enriched selenium found in local groundwater is oxidized by elevated concentrations of nitrate found in groundwater and dry weather urban runoff (imported and recycled water) that penetrates the hyporheic zone. Being able to identify source flows and the seasonal hydrochemical changes has helped understanding of the water rock interaction of recycled water with Monterey-Modelo Formation.

Many streams within the Malibu Creek Watershed contain pollutants that have not met water quality standards by regulatory agencies. By understanding the geologic and anthropogenic controls of nutrients, trace metals, and source flows further regulatory action can be made in urbanized watersheds.

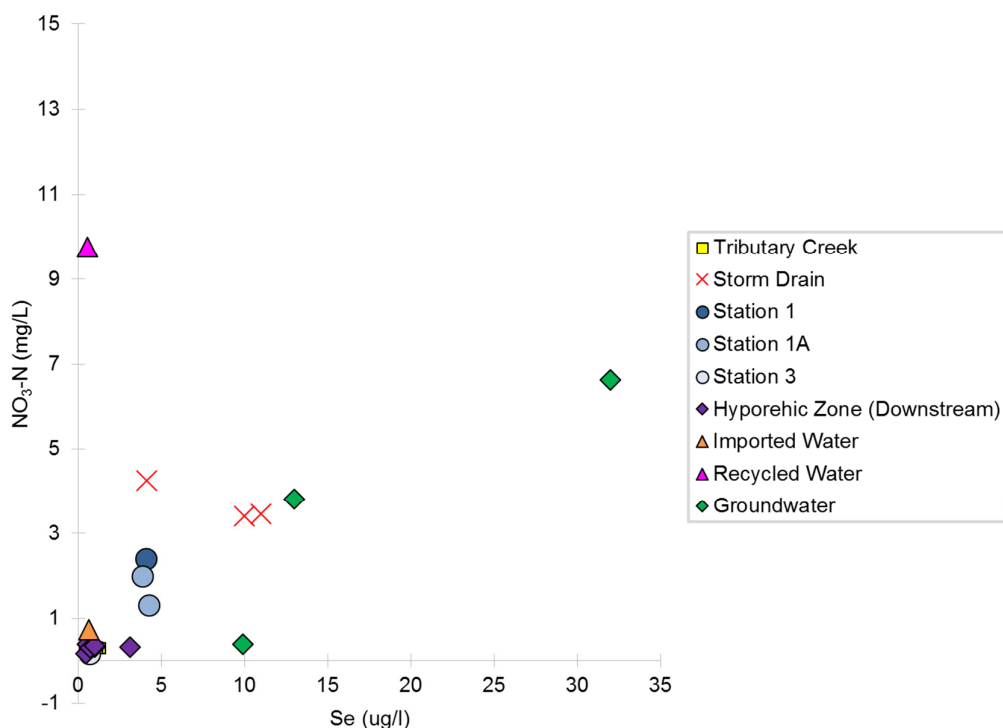


**FIGURE 5.** Selenium verses nitrate-nitrogen graph of samples collected at El Camino Real Creek along with endmembers.

## ACKNOWLEDGEMENTS

Funding for this project is provided by the National Science Foundation under Grant # HRD-1363399.

## REFERENCES

- Harrison, M., Hibbs, B., 2015, Isotopic and hydrochemical identification of source waters and pollutants in Malibu Creek Watershed, CA: in *Water is Not for Gambling, Utilizing Science to Reduce Uncertainty: Proceedings of 2015 Joint Conference of University Council on Water Resources (UCOWR), and The National Institute for Water Research (NIWR)*: 123 – 128.
- Hibbs, B. 2014. *New models for origin of salinity in upper Malibu Creek watershed and nearby watersheds*. Presented at California State University, Los Angeles, CA. August 19, 2014.
- Las Virgenes Municipal Water District. n.d. Section 3: *Natural Source Assessment - The Monterey / Modelo Formation*. Available at <http://www.lvmwd.com/Home/ShowDocument?id=2273>. Accessed April 12, 2016.

## **INFLUENCE OF POLLUTANT PROCESS UNCERTAINTY ON THE PREDICTION OF STORMWATER QUALITY IN URBAN CATCHMENTS**

**Buddhi Wijesiri**, Prasanna Egodawatta, James McGree, Ashantha Goonetilleke  
(Queensland University of Technology (QUT), Brisbane, Queensland, Australia)

**ABSTRACT:** Stormwater quality in urban catchments is influenced by the variability in pollutant build-up and wash-off processes. The process variability results in uncertainty which influences stormwater quality modelling outcomes. This highlights the need for quantitative assessment of process uncertainty prior to utilising modelling outcomes for decision making. However, poor characterisation of process variability limits the quantitative assessment of process uncertainty. It was hypothesised that the temporal variations in the particle load <150µm and >150µm during pollutant build-up and wash-off are the primary factors that characterise process variability. Accordingly, the incorporation of the characteristics of build-up and wash-off process variability into mathematical models enables accounting of process uncertainty as part of the modelling outcomes. Compared to the case where process uncertainty is not considered, it was found that the upper limit of uncertainty associated with stormwater quality predictions changes when process uncertainty is accounted for in the uncertainty assessment. Furthermore, the uncertainty assessment revealed that the impact of build-up process uncertainty on predicted stormwater quality is greater than that of wash-off process uncertainty. This confirmed that build-up process variability contributes significantly to the uncertainty associated with the prediction of stormwater quality.

### **INTRODUCTION**

Stormwater pollution is a major concern in the context of urban water management, as stormwater runoff transports a range of pollutants such as particulate solids and particle-bound heavy metals into urban receiving waters (Brown and Peake, 2006; Zhao and Li, 2013). Therefore, it is necessary to improve stormwater quality through effective pollution mitigation. The designing of pollution mitigation strategies requires information on catchment stormwater quality, which are commonly generated using stormwater quality models. However, two types of uncertainty: uncertainty in modelling of pollutant processes (build-up and wash-off) and uncertainty inherent to these processes primarily influence the interpretation of modelling outcomes (Loucks et al., 2005).

Process modelling uncertainty arises from several sources such as model structure, model parameters and input and calibration data (Dotto et al., 2012). On the other hand, uncertainty inherent to pollutant build-up and wash-off stems from the variability associated with these processes (Zoppou, 2001). The behaviour of particles that transport pollutants such as heavy metals and hydrocarbons during build-up and wash-off generates process variability. The temporal variations in load and composition of particle-bound pollutants also contribute to variability in build-up and wash-off processes. In this context, particles <150µm and >150µm play a significant role due to differences in particle behaviour and pollutant affinity for the different particle size fractions (Hvitved-Jacobsen et al., 2010; Wijesiri et al., 2015a, b). Although modelling uncertainty is generally understood, only limited research studies have investigated process uncertainty (Sun et al., 2012; Wijesiri et al., 2016). Accurate accounting of process uncertainty is necessary for informed decision making for effective stormwater pollution mitigation.

The research study was undertaken to investigate the impact of process uncertainty on the prediction of stormwater quality in urban catchments. It was hypothesised that the temporal variations in the particle load <150µm and >150µm during build-up and wash-off primarily influence process variability. Accordingly, prediction of stormwater quality and assessment of associated uncertainty were based on the mathematical models of pollutant build-up and wash-off, in which process variability is accurately accounted. The methodology described by Wijesiri et al. (2015a) was adopted for incorporating process variability into these mathematical models.

### **MATERIALS AND METHODS**

A 105ha urban residential catchment, namely, Highland Park (Figure 1), located in Gold Coast, Australia was selected for the investigation. Build-up and wash-off sampling were undertaken on asphalt paved road sites within the catchment. Particulate build-up samples were collected for different antecedent dry periods using a portable wet vacuum system. A rainfall simulator was used to simulate storm events with different intensities and durations for wash-off sample collection. Further details of the sampling procedures can be found in Egodawatta et al. (2007) and Hengren et al. (2006). The samples were analysed for particle size distribution and particulate solids load (after wet sieving into particle size fractions <150µm and >150µm) using standard test methods.



**FIGURE 1. Aerial view of catchment and road sites (Map Data: Google, DigitalGlobe.**

For the selected catchment, a runoff model was developed using the Mike URBAN – SWMM module, which is a physically based hydrologic modelling software (MikeUrban, 2014). The catchment-specific hydrologic parameters were determined using field data. As such, model calibration was not required for this investigation. Boundary conditions for the runoff model were set using rainfall data selected from a ten year period (2004-2014) of rainfall records for the study area. Runoff was then simulated for sixty-five selected storm events which occurred in two representative years, 2005 and 2008.

Prediction of catchment stormwater quality and quantification of uncertainty were undertaken based on two scenarios: (1) using the primary build-up and wash-off models (Equations 1 and 2) which were proposed by Ball et al. (1998) and Sartor and Boyd (1972), respectively, where process variability is poorly characterised. The detailed discussions on the application of these models in relation to stormwater quality modelling can be found in Obropta and Kardos (2007) and Zoppou (2001); and (2) using modified build-up and wash-off models (Equations 3 and 4), proposed by Wijesiri et al. (2015a) which were derived incorporating process variability.

$$B_{\text{primary}} = \alpha t^{\beta} \quad (1)$$

$$W_{\text{primary}} = W_0 (1 - \exp(-kIt)) \quad (2)$$

$$B_{\text{revised}} = [B_{(<150)} = \alpha_{(<150)} t^{\beta_{(<150)}}] + [B_{(>150)} = \alpha_{(>150)} t^{\beta_{(>150)}}] \quad (3)$$

$$W_{\text{revised}} = B_{(<150)} (1 - \exp(-k_{(<150)}It)) + B_{(>150)} (1 - \exp(-k_{(>150)}It)) \quad (4)$$

Where: B – build-up load; W – amount of material washed-off;  $W_0$  – amount of material available at the beginning of storm event; t – antecedent dry period/storm event duration; I – storm event intensity;  $\alpha$ ,  $\beta$ , k – build-up and wash-off coefficients (subscripts indicate corresponding particle size fraction).

Given the catchment area, particulate build-up and wash-off could be predicted using the primary and revised models. The model parameters were estimated employing the ‘non-linear least squares

regression' technique using MATLAB in-built function 'nlinfit' (MathWorks, 2013). The proportional error model defined as  $y = f + \theta f \varepsilon$  was assumed as the form of the error term using the variable  $\varepsilon \sim N(0, 1)$  with the function value  $f$  and the error parameter  $\theta$  (initial estimate of  $\theta$  set to be the default value =1). In order to quantify the uncertainty associated with model predictions, a large number of mathematical simulations (10,000) of build-up and wash-off were performed. These simulations were performed by primarily accounting for residual errors and parameter uncertainty. This enabled the determination of specific upper and lower uncertainty limits for each prediction. In this investigation, upper and lower uncertainty limits were set to account for 95% uncertainty interval.

## RESULTS AND DISCUSSION

**Accounting for Build-Up and Wash-Off Process Uncertainty.** The uncertainty associated with catchment stormwater quality predicted as Event Mean Concentration (EMC) was compared between primary and revised models. As evident from Figure 2, the uncertainty bandwidth (difference between upper and lower uncertainty limits) corresponding to the EMCs predicted with the revised models shows an increase. However, it was found that the predicted EMCs of primary and revised models were slightly different. Therefore, the relative uncertainty bandwidth (RUB), which is the ratio between uncertainty bandwidth and predicted EMC, was also analysed. Figure 3 confirms the increase in uncertainty associated with EMCs predicted using the revised model. This increase in uncertainty can be related to the revised mathematical form of the primary models, which in fact result from the incorporation of process variability. Moreover, it is important to note that this change in uncertainty should not be considered as a consequence of common reasons such as adoption of complex model structures which results in the increase in uncertainty.

Accordingly, it is possible to conclude that accurate characterisation of process variability enables the accounting of process uncertainty as a part of the uncertainty associated with model predictions. This means that typical uncertainty assessment techniques, which primarily focus on modelling uncertainty, can also be employed together with the approach derived in this investigation in order to assess the overall uncertainty that influences the interpretation of stormwater quality predictions. However, it is also important to note that the current uncertainty assessment techniques need to be improved as they have drawbacks such as relying on subjective criteria, effect of prior knowledge and accounting only for a few uncertainty sources (Dotto et al., 2012). For example, commonly adopted GLUE method is influenced by user defined likelihood measures (Freni et al., 2009). Further, uncertainty analyses, which adopt the classical Bayesian approach, are prevented from being objective due to the influence of prior knowledge on Bayesian updating (Freni and Mannina, 2010).

Moreover, when applying the approach derived for assessing process uncertainty, practical approaches would be required to assist stormwater management personnel for understanding and quantifying process uncertainty. This is due to inadequate knowledge of how the assessment of process uncertainty can be utilised for informed decision making in the context of stormwater pollution mitigation. For example, the knowledge created in the current research study can be effectively utilised by the academic researchers, industry practitioners, and technology developers for creating stormwater quality modelling software which are embedded with tools to assess both process and modelling uncertainty. Such modelling tools will help stormwater water management personnel to accurately interpret the information relating to stormwater quality, leading to enhanced stormwater pollution mitigation.

**Characterisation of the Influence of Process Uncertainty.** It is evident from Figure 2 that the change in uncertainty is predominantly influenced by the increase in the upper uncertainty limit. This change in upper uncertainty limit is consistently greater than that of the lower uncertainty limit. This shows the changes in the range in which stormwater quality predictions vary, and on the other hand reflects the influence of process variability on pollutant loads entrained in stormwater runoff. As such, in a case where process uncertainty is not accounted for, the predicted catchment stormwater quality may not be appropriately interpreted, leading to ineffective decision making in relation to the designing of stormwater pollution mitigation strategies.

Moreover, in relation to the revised models, the variation in RUBs over different build-up events is greater than the variation in RUBs over different wash-off events (Fig. 3). This implies that compared to

the pollutant wash-off process variability, the pollutant build-up process variability plays a more important role in influencing catchment stormwater quality. Therefore, stormwater pollution mitigation strategies need to specifically account for temporal variations in particle-bound pollutant load and composition during build-up.

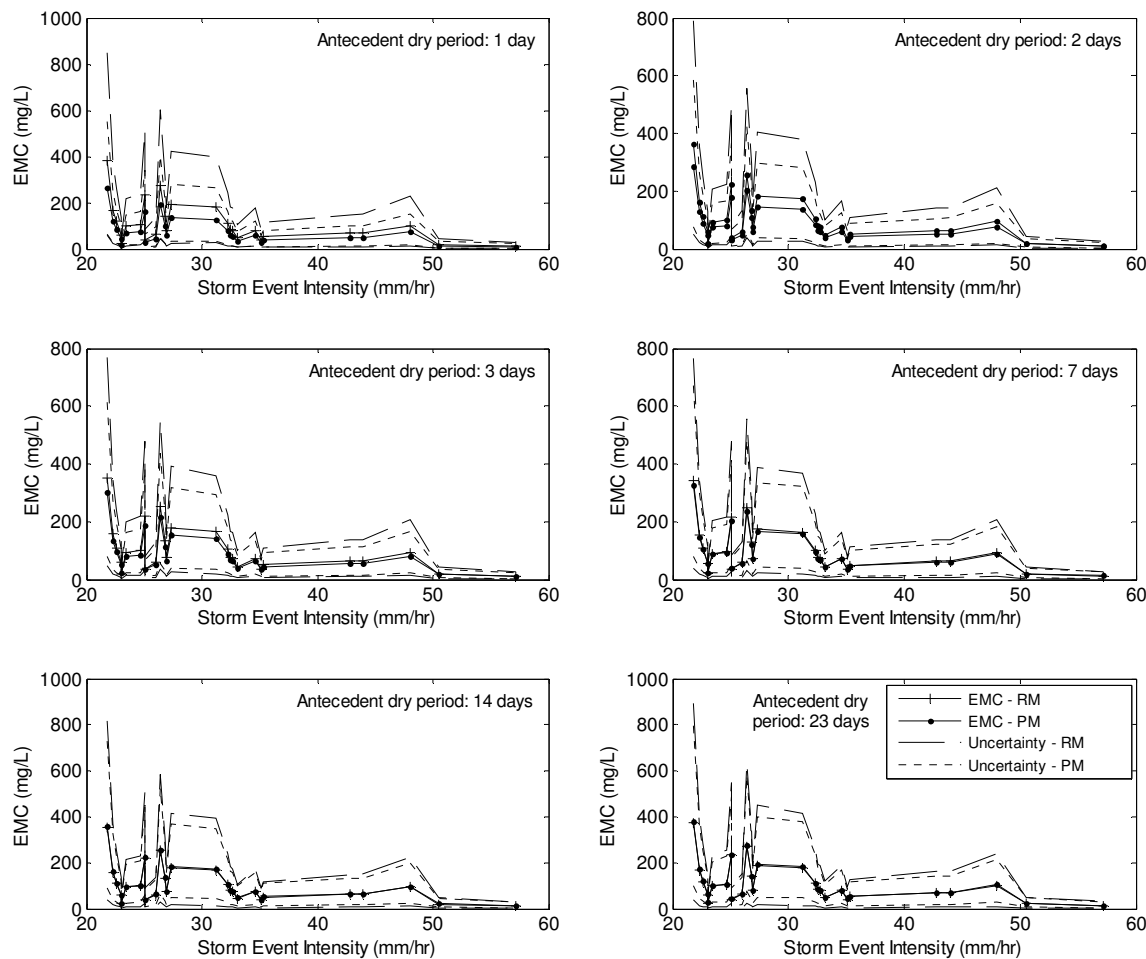


**FIGURE 2. Comparison of uncertainty limits between primary and revised models – year 2005 storm events; note: PM – primary models, and RM – revised models.**

## CONCLUSIONS

The investigation discussed in this paper derived an approach to quantitatively assess the uncertainty inherent to pollutant build-up and wash-off processes. The approach enables the accounting of process uncertainty as an integral part of the uncertainty associated with stormwater quality predictions. Accounting of process uncertainty significantly changes the upper limit of the uncertainty associated with predicted EMCs of particulate solids. The change in uncertainty limits relates to the limits within which stormwater quality predictions vary. This highlights the influence of process variability on the variations in pollutant loads released into stormwater runoff. Further, the influence of build-up process uncertainty on predicted stormwater quality was found to be significant compared to that of wash-off process uncertainty.

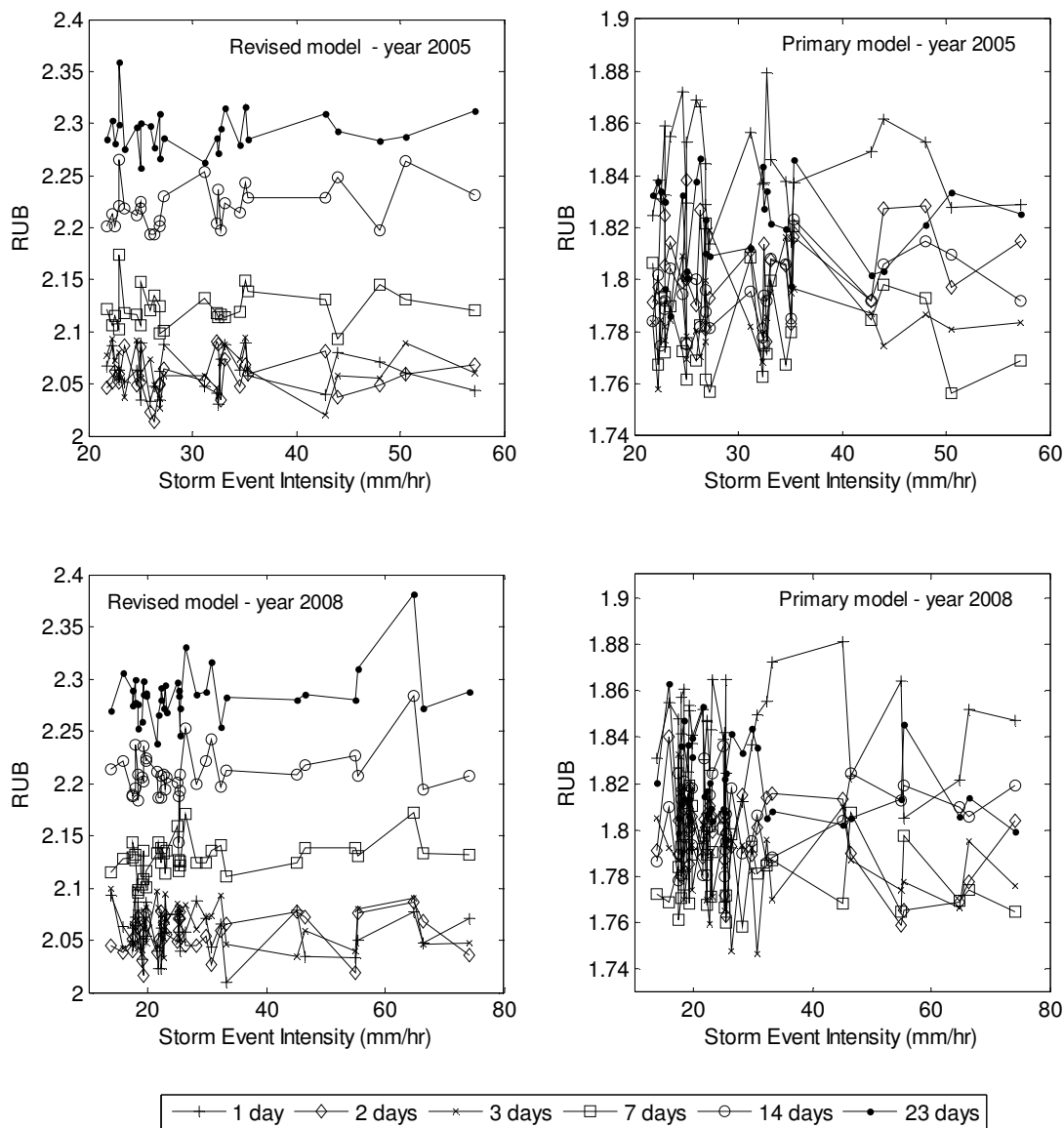


**FIGURE 3. Comparison of relative uncertainty bandwidth (RUB) between primary and revised models.**

#### ACKNOWLEDGEMENTS

The authors would like to acknowledge Queensland University of Technology (QUT) for the scholarship provided to the first author for undertaking doctoral studies.

#### REFERENCES

- Ball, J. E., Jenks, R., Aubourg, D. (1998). An Assessment of the Availability of Pollutant Constituents on Road Surfaces. *Science of the Total Environment*, 209(2–3), 243-254.
- Brown, J. N., Peake, B. M. (2006). Sources of Heavy Metals and Polycyclic Aromatic Hydrocarbons in Urban Stormwater Runoff *Science of the Total Environment*, 359, 145-155.

- Dotto, C. B. S., Mannina, G., Kleidorfer, M., Vezzaro, L., Henrichs, M., McCarthy, D. T., Freni, G., Rauch, W., Deletic, A. (2012). Comparison of Different Uncertainty Techniques in Urban Stormwater Quantity and Quality Modelling. *Water Research*, 46(8), 2545-2558.
- Egodawatta, P., Thomas, E., Goonetilleke, A. (2007). Mathematical Interpretation of Pollutant Wash-off from Urban Road Surfaces Using Simulated Rainfall. *Water Research*, 41(13), 3025-3031.
- Freni, G., Mannina, G. (2010). Uncertainty in Water Quality Modelling: The Applicability of Variance Decomposition Approach. *Journal of hydrology*, 394(3-4), 324-333.
- Freni, G., Mannina, G., Viviani, G. (2009). Uncertainty in Urban Stormwater Quality Modelling: The Influence of Likelihood Measure Formulation in the GLUE Methodology. *Science of the Total Environment*, 408(1), 138-145.
- Herngren, L., Goonetilleke, A., Ayoko, G. A. (2006). Analysis of Heavy Metals in Road-deposited Sediments. *Analytica Chimica Acta*, 571(2), 270-278.
- Hvitved-Jacobsen, T., Vollertsen, J., Nielsen, A. H. (2010). *Urban and Highway Stormwater Pollution: Concepts and Engineering*: CRC Press, Taylor and Francis Group.
- Loucks, D. P., Van Beek, E., Stedinger, J. R., Dijkman, J. P., Villars, M. T. (2005). *Water Resources Systems Planning and Management: An Introduction to Methods, Models and Applications*: Paris: UNESCO.
- MathWorks. (2013). MATLAB & Simulink (Version R2013a): MathWorks Inc. Massachusetts, USA.
- MikeUrban. (2014). *Mike Urban Collection System - User Guide*. Danish Hydraulic Institute.
- Obropta, C. C., Kardos, J. S. (2007). Review of Urban Stormwater Quality Models: Deterministic, Stochastic, and Hybrid Approaches. *Journal of the American Water Resources Association*, 43(6), 1508-1523.
- Sartor, J. D., Boyd, G. B. (1972). *Water Pollution Aspects of street Surface Contaminants* EPA-R2-72-081. U.S. Environmental Protection Agency, Washington, D.C.
- Sun, S., Fu, G., Djordjević, S., Khu, S.-T. (2012). Separating Aleatory and Epistemic Uncertainties: Probabilistic Sewer Flooding Evaluation Using Probability Box. *Journal of hydrology*, 420-421(0), 360-372.
- Wijesiri, B., Egodawatta, P., McGree, J., Goonetilleke, A. (2015a). Incorporating Process Variability into Stormwater Quality Modelling. *Science of the Total Environment*, 533(0), 454-461.
- Wijesiri, B., Egodawatta, P., McGree, J., Goonetilleke, A. (2015b). Influence of Pollutant Build-up on Variability in Wash-off from Urban Road Surfaces. *Science of the Total Environment*, 527-528(0), 344-350.
- Wijesiri, B., Egodawatta, P., McGree, J., Goonetilleke, A. (2015c). Process Variability of Pollutant Build-up on Urban Road Surfaces. *Science of the Total Environment*, 518-519(0), 434-440.
- Wijesiri, B., Egodawatta, P., McGree, J., Goonetilleke, A. (2016). Assessing Uncertainty in Pollutant Build-up and Wash-off Processes. *Environmental Pollution*, 212, 48-56.
- Zhao, H., Li, X. (2013). Risk Assessment of Metals in Road-deposited Sediment along an Urban-rural Gradient. *Environmental Pollution*, 174(0), 297-304.
- Zoppou, C. (2001). Review of Urban Storm Water Models. *Environmental Modelling & Software*, 16(3), 195-231.



## CONTAMINANT REDUCTION BY PERVIOUS CONCRETE PAVEMENT AND BAMBOO BIORETENTION BASIN

**Vincent Hwang** (Southeastern Educational Society, Mayagüez, Puerto Rico 00680)

Amber Masters (University of Puerto Rico, Mayagüez, PR, 00680)

Evelyn Montalvo (Southeastern Educational Society, Mayagüez, Puerto Rico 00680)

Sangchul Hwang\* (University of Puerto Rico, Mayagüez, PR, 00680)

Pervious concrete pavement (PCP) and bamboo bioretention basin (BBB) were combined for urban stormwater runoff volume control and water quality enhancement. A nanogeopolymer pervious concrete pavement (GPCP) was produced with the optimized mix design of water-to-binder at 36.0%, coal fly ash-to-binder at 29.5% and nano-iron oxide-to-binder at 0.78%. A regular pervious concrete pavement (RPCP) was produced an optimum mix design of water-to-binder at 36.7% and coal fly ash-to-binder at 21.4%. For both GPCP and RPCP, gravels in size of 4.75-12.5 mm were used at a mass ratio of gravel-to-binder at 4:1. A miniature bamboo species (*Dracaena sanderiana*) was used to accommodate the lab-scale experiment. GPCP or RPCP was served as a pre-treatment for urban stormwater runoff capture and infiltration as well as reduction of phosphate and fecal coliform, whereas BBB was a post-treatment for further pollution abatement especially for nitrate reduction. For comparison purposes, a typical impervious concrete pavement (IMCP) (i.e., control) was also run in parallel. Results showed that both PCPs excelled phosphate and fecal coliform reduction by >90% and >80%, respectively, but were poor in nitrate reduction. However, BBB reduced nitrate by >60%. Either GPCP+BBB or RPCP+BBB outperformed IMCP+BBB in stormwater runoff control and water quality enhancement. An enhanced growth of *D. sanderiana*, judged by the Chlorophyll a on the leaf and the body mass, was also observed during the experiment. Therefore, it is concluded that a treatment train of PCP and BBB would effectively control urban storm water in terms of runoff volume and water quality enhancement.

## TOXICOLOGY OF AZO DYES WITH RESPECT TO THEIR METABOLICALLY PRODUCED AND CHEMICALLY RELATED AROMATIC AMINES

King-Thom Chung

(The University of Memphis, Memphis, TN, USA)

Azo dyes are synthetic organic dyes and are widely used in various industries. The public health concern of azo dyes can be traced to the discovery of the medical use of Prontosil, which is the first chemotherapeutical drug studied by Gerhardt Domagk, *et al.* in the 1930s. The active component of Prontosil a reductively cleaved (azo reduction) product, *p*-aminophenyl- sulfonamide that contains sulfur. Thus, the significance of azo reduction is revealed in the production of the biological active compounds, mainly aromatic amines. Many aromatic amines can be metabolically produced by human intestinal microflora and to a lesser extent by liver azo-reductase.

Some azo dyes such as 4-aminoazobenzene, *o*-aminoazotoluene, Methyl Yellow, Methyl, Yellow derivatives, Sudan azo dyes, Para Red, Trypan Blue, and others with structures containing free amine groups can be carcinogenic when the azo linkage is not being cleaved. However, the carcinogenicity of many other azo dyes is due to their cleaved component aromatic amines such as benzidine, benzidine congeners, *p*-phenylenediamine. etc.. Other structurally related compounds such as 4-aminobiphenyl, *o*-toluidine, aniline, *p*-nitroaniline, and some monocyclic aromatic amines such as 2, 4-diaminotoluene, 2-nitro-*p*-phenylenediamine, 2-amino-4-nitrophenol, 4-nitro-*o*-phenylenediamine, *m*-phenylenediamine, and *o*-phenylenediamine are also reported to be carcinogenic.

*p*-Phenylenediamine (*p*-PDA) is usually mixed with H<sub>2</sub>O<sub>2</sub> for hair dyeing. Oxidized *p*-PDA becomes a diaminophenazine or Bandrowski base, which is extremely mutagenic. Commercial hair dye *p*-PDA was reported to be contaminated with carcinogenic 4-aminobiphenyl. *p*-PDA is also a contact allergen that can induce throat irritation in the pharynx and larynx, and cause dermatitis and bronchial asthma. Allergenic aromatic amines also include *o*-phenylenediamine, *m*-phenylene-diamine, *p*-toluidine, *p*-sulfanilic acid, *p*-aminobenzoic acid, 2-amino-*p*-cresol, *p*-nitroaniline, 2-*l*-amino-naphthol-sulfonic acid, etc.

Azo dyes such as Disperse Blue 106, Disperse Blue 124, Methyl Yellow, 4-aminoazobenzene and *o*-aminoazotoluene were reported to be allergenic. Azo dye Trypan Blue has also been shown to be carcinogenic and teratogenic. Food certified azo dyes Tartrazine and Sunset Yellow were also reported to be allergenic to humans. Sulfonamide drugs, some of which may not be azo dyes cleaved products, have also been reported to induced human maladies such as allergy, urinary tract disorders, haemopoietic disorders, porphyria, hypersensitive reactions, etc. Various human disorders caused by many other aromatic amines were also reported. Azo dyes and their metabolites, primarily aromatic amines, are therefore significant chemicals affecting human health and damaging our environments.

## **SIGNIFICANCE AND APPLICATION OF THE GLOBAL DRINKING WATER QUALITY INDEX: LEBANON CASE STUDY**

**Mey Jurdi\***, Sami Ramia (American University of Beirut, Beirut Lebanon)

Samira Korfali (Lebanese American University, Beirut, Lebanon)

Nabil Amacha (Lebanese University)

Joumana Nasr, Rola Ajib and Sara Chehab (American University of Beirut)

The management of the quality of potable piped water supplies remains a major challenge in developing countries in the absence of sufficient technical and financial resources. Proper water quality monitoring is an essential component of risk assessment based on which proper quality management could be recommended. As such, it is important to enhance the quality of monitoring activities under the prevailing deficient and bureaucratic systems.

Hence, the objectives of the research work were to examine the significance and application of the Global Drinking Water Quality Index in monitoring the quality and the safety of piped water supplies in Lebanon. As such, a drinking water quality index was adapted to reflect on acceptability, health and safety of potable water supplies. The quality indicators were chosen to reflect on the major characteristics of the water supply in Lebanon. The water quality assessment included parameters relating to water desirability (turbidity, color, hardness etc.), acceptability (pH, ammonia, chlorides, sulfates etc.), safety (nitrates, copper, cadmium, fecal coliform, etc.) and conditions of distribution network (iron, copper, zinc etc.). Fluoride and mercury levels were not included in the computation of the index as levels are relatively minimal in water supplies, as documented by earlier studies. On the other hand, the total hardness was included as mostly ground water sources feed distribution networks. Moreover, the sensitivity of the developed index to reflect on water quality changes and to identify and flag problematic distribution areas was also examined.

Results showed that the development and use of such a quality index can help identify changes in the quality of the water supply in a way that summarizes complex scientific data into a simpler form of risk assessment and reporting and risk communication. Moreover, it can be adopted and used as a screening tool for further evaluation; this is important given the deficient water quality monitoring systems that require more extensive resources.

## **COLIFORM COUNTS AND PLANKTON SPECIES IN LAWAYE RIVER, BATANGAS AS INDICATORS OF POLLUTION**

**Natividad F. Lacdan**, Jose Rafael L.Lopez, and Renz Michael F.Pasilan  
(University of the Philippines Manila, Manila, Philippines)

Lawaye River in San Juan, Batangas, Philippines is an important source of water for local residents. It finally drains into the waters of the Verde Island Passage Corridor. However, there has been insufficient researches regarding the water quality of the river. This study was conducted to determine the water quality of Lawaye River, using coliform counts and plankton species composition. Four sampling sites were set up along the river: boundary between Rosario and San Juan towns, upstream, midstream and downstream. Fecal coliform count was quantified using the multiple tube fermentation method while detection of the coliform, *Escherichia coli* involved the Presumptive, Confirmatory and Completed tests along with the IMVic profiles. Plankton analysis involved the identification of various plankton genera found in the river. Nygaard's and Palmer's indices were then used to determine the river's trophic state and pollution status. The coliform concentration in all sites was found to be well beyond the normal range. Plankton analysis showed that sampling areas in Lawaye River were found to have different levels of organic pollution. The Palmer's and Nygaard's Indices demonstrated that the downstream and midstream sites registered the highest probability of having organic pollution, while the sites found on the upstream and boundary were comparatively normal and oligotrophic. Factors, such as improper waste disposal, effluents from drainage and agricultural runoffs could have contributed to the observed results.

## EFFECTS OF SUPER-SATURATION CONTROL STRATEGIES ON HYDROXYAPATITE (HAP) CRYSTALLIZATION PROCESS FOR PHOSPHORUS RECOVERY FROM WASTEWATER

Hongliang Dai<sup>a,b</sup>, Xiwu Lu<sup>a,b\*</sup>

<sup>a</sup>School of Energy and Environment, Southeast University, No. 2 Sipailou Road, Nanjing 210096, China.

E-mail: [daihongliang103@163.com](mailto:daihongliang103@163.com);

<sup>b</sup>ERC Taihu Lake Water Environment (Wuxi), No. 99 Linghu Road, Wuxi 214135, China.

E-mail: [230149342@seu.edu.cn](mailto:230149342@seu.edu.cn); [xiwulu@seu.edu.cn](mailto:xiwulu@seu.edu.cn)

**ABSTRACT:** The HAP crystallization process for phosphorus removal from wastewater contributes to an environmental friendly production due to the fact that it helps reduce or eliminate the water eutrophication as well as increases the recovery of mineral resources. However, the generated microcrystalline with poor settle-ability in high levels of super-saturation solution has a negative effect on the phosphorus recovery efficiency. In order to overcome the drawback, multiple reagent feed ports (four feed ports) and different recirculation ratio (1.0, 1.5, 2.0, 2.5, 3.0) were investigated to control the levels of super-saturation in an air-agitated reactor with calcite as seeds. The results showed that the approach of multiple reagent feed ports could improve the conversion ratio of orthophosphate, but it had a limited effect (~3% improvement) on phosphorus recovery efficiency (deposition on the seeds). With the increase in the recirculation ratio, the recovery efficiency was increased gradually and reached an optimal value of 85.63% under the recirculation ratio of 2.5 and four feed ports. This is because of that the adopted strategies could reduce the level of super-saturation by diluting the concentration of the reagents and inhibit large numbers of microcrystalline coinstantaneous occurrence. Meanwhile, the crystallized products were detected and analyzed by scanning electron microscope (SEM) with X-ray spectroscopy (EDS) and X-ray diffraction (XRD), which were proved to be HAP with a lofty purity. Collectively, these results demonstrated that super-saturation control using conventional approaches had a limited improvement in the phosphorus recovery efficiency in the form of HAP and the new control strategies for super-saturation dispersion should be developed in the further study.

**Key Words:** Phosphorus recovery; Super-saturation control; Hydroxyapatite; Induced crystallization; Air-agitated reactor.

## INTRODUCTION

Phosphorus is a limited and non-renewable mineral resource, making a significant contribution to the development of agriculture and industry <sup>[1-2]</sup>. World phosphorus reserves will run out in between 50 to 100 years <sup>[3]</sup>. Meanwhile, excessive phosphorus content in wastewater will result in a serious eutrophication <sup>[4]</sup>. For these reasons, phosphorus recovery from wastewater can prevent the loss of nutrient resources and alleviate the environmental impacts of excess phosphorus on receiving waters. Municipal wastewater as hidden treasure of phosphorus resource satisfies the world's phosphorus demand of 15~20% by its recovery and recycling <sup>[5-6]</sup>. Many wastewater treatment plants built on the enhanced biological phosphorus removal (EBPR) process provide a phosphate-rich stream (anaerobic supernatant, ~20 mg/L) to make phosphorus recovery and reuse feasible <sup>[5, 18]</sup>.

Induced crystallization for phosphorus recovery in the form of hydroxyapatite (HAP) from the wastewater is an economical and efficient approach, possessing the characteristics of effective phosphorus recovery and high-quality crystallization products <sup>[7-9]</sup>. The mechanism of HAP crystallization follows three chemical stages: the formation of super-saturation, nucleation (crystal birth) and crystal growth <sup>[10]</sup>. According to the classical nucleation theory, primary homogenous nucleation will form small particles (microcrystalline) in the high-level super-saturation solution <sup>[11]</sup>. The generated tiny particles called microcrystalline with poor settleability have a negative effect on the solid-liquid separation and subsequent recovery of crystallized products <sup>[12-13]</sup>. Karapinar et al. <sup>[10]</sup> showed that the increase of super-saturation

levels in solution would lead to a decrease in phosphorus efficiency (precipitation on seeds), though the total precipitation efficiency was increased. Generally, the levels of super-saturation can be reduced by using the lower reagent concentrations. However, high levels of super-saturation ( $SI > 0$ ) are produced even at low reagent concentration during HAP crystallization process due to the smaller solubility products ( $2.35 \times 10^{-59}$  mol/L,  $25^\circ\text{C}$ ) [14].

Conventional approaches to control the levels of super-saturation are the multiple reagents feed points and reaction liquid reflux for studying the sparingly soluble compounds' recovery *via* crystallization reaction [12-13]. Seckler et al. [15] studied the calcium phosphate precipitation in FBR and showed that microcrystalline aggregation process could be improved by distributing the super-saturation more evenly throughout the reactor with a recirculation stream. Taty Costodes and Lewis [13] studied nickel hydroxycarbonate precipitation using the approach of multiple reagents feed points, and the results showed that the amount of fines produced inside the reactor was significantly reduced using multiple reagent feed points. This was attributed to effective control of the high levels of super-saturation produced near the reagent inlet point. Mokone et al. [12] studied the effect of control strategies used to manage super-saturation during the precipitation reactions of copper and zinc sulphide in FBR, and the results showed that extremely high super-saturation prevalent during metal sulphide precipitation was difficult to control using conventional approaches and suggested that the seeded FBR was unsuitable for this application. This is because FBR can't achieve perfect mixing with an even distribution of super-saturation [13, 19]. Meanwhile, the reaction of HAP crystallization merely occurs in alkaline conditions and needs a completely mixed state. Increasing the pH of wastewater by adding alkali (sodium hydroxide) requires complicated and expensive equipment to add chemical with a pH sensor. The air-agitated reactor is more popular due to stripping of  $\text{CO}_2$  to increase the pH by aeration and providing a perfectly mixed system [16-17].

In the present study, conventional super-saturation control strategies (multiple reagent feed points and recirculation flow) were taken to investigate the effects on process efficiency and particle characteristics for HAP crystallization process in an air-agitated reactor. The performance of the phosphorus recovery was investigated by measuring the orthophosphate content and the saturation index (SI) of solution under different operation conditions. Meanwhile, the precipitate's characteristics were analyzed by scanning electron microscopy (SEM) with energy dispersive X-ray analysis (EDS), and X-ray diffraction (XRD). The results are expected to solve the problem of low phosphorus recovery efficiency due to the homogeneous nucleation in the HAP crystallization process

## MATERIALS AND METHODS

**Experimental Apparatus and Procedures.** The experimental setup (**Fig. 1**) consisted of a continuously air-agitated crystallization column of 2.5 L working volume with an overall height of 1300 mm. The reactor consists of precipitation area, buffer area and reaction area, with four sampling points and four feed ports. The stock solutions for HAP formation were continuously pumped into the reactor using peristaltic pumps. Experiments were carried out at laboratory temperature ( $25 \pm 2^\circ\text{C}$ ). In order to prevent the loss of seeds, the outlets of reactor were coated with a 120 ASTM mesh sieve (0.12 mm). As the removal efficiency depends on the active specific surface area of the seeds, the size of calcite seeds was 0.15~0.21 mm, and the seeds dosage were 30 g/L. The seeds inside the reactor can promote heterogeneous primary nucleation and/or secondary nucleation.

**Table 1. Process conditions in the air-agitated crystallization column**

Parameter	Value
Inlet P concentration	~23 mg/L
Inlet Ca/P ratio	2.5
Inlet P flow rate	80 ml/min
Inlet Ca flow rate	8 ml/min
Re-circulation flow ratio	1.0, 1.5, 2.0, 2.5, 3.0
Reagent feed ports	4
Working volume	2.5 L

Other conditions given in Table 1 were carried out at constant Ca/P ratio (2.5) and aeration rate rates (300 L/h). Precipitation is induced by addition of a precipitating reagent into the reactor. When investigating the performance of the system, the reactor must be run continuously for at least 2 days with the “saturated” solution of HAP so as to allow a first layer of HAP to cover the seeds.

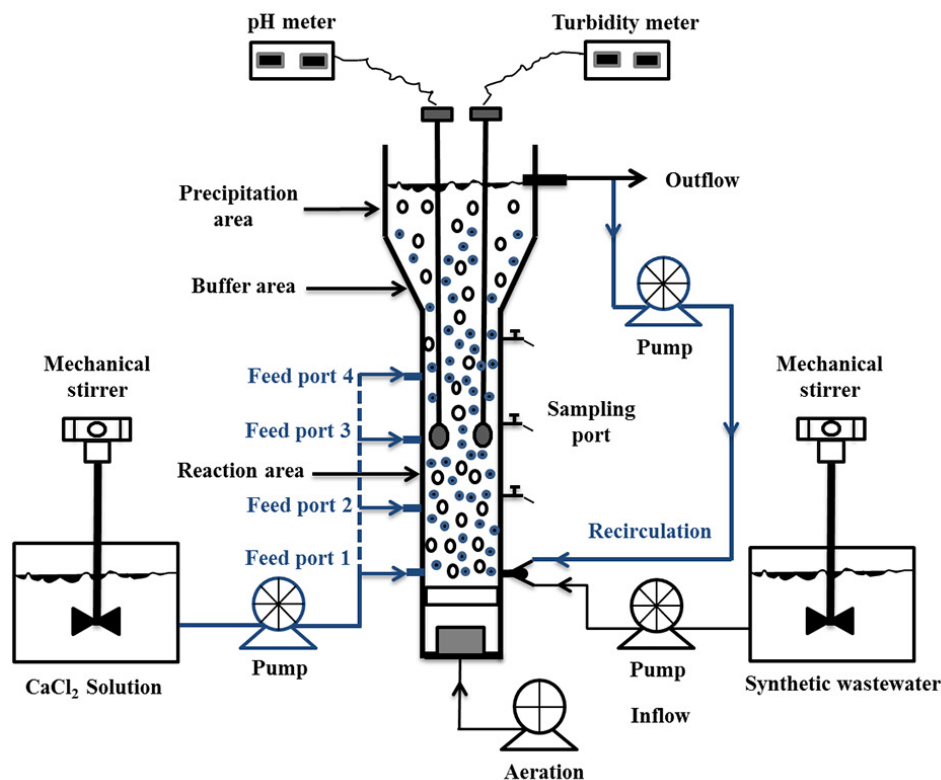


**Fig.1. Schematic diagram of a continuously air-agitated crystallization column for phosphorus recovery**

**Solution Preparation.** The anaerobic supernatant was taken from an EBPR process (anaerobic-anoxic/nitrifying two sludge process) established by our group<sup>[18]</sup>, and the concentrations of constituents were given in table 2. An air stripping for alkalinity reduction and pH increase was used to pretreat the anaerobic supernatant. In order to investigate the proposed process on recovering phosphorus in form of HAP, two stock solutions ( $\text{CaCl}_2$  and anaerobic supernatant) were continuously pumped into the reactor with the volume ratio equal to 0.1, and the final molar ratio of  $\text{Ca}^{2+}$  and  $\text{PO}_4^{3-}$  was 2.5 by adjusting the concentration of  $\text{CaCl}_2$  solution. All the reagents used throughout this investigation were analytical grade and originated from Aladdin (China).

**Table 2. Characteristics of anaerobic supernatant of EBPR process used in experiments.**

Parameters	$\text{PO}_4^{3-}\text{-P}$ (mg/L)	$\text{NH}_4^+\text{-N}$ (mg/L)	COD (mg/L)	$\text{Mg}^{2+}$ (mg/L)	pH	Turbidity (NTU)	Alkalinity (mg/L)
Anaerobic supernatant	$23.1 \pm 2.5$	$36.4 \pm 4.3$	$75.7 \pm 8.6$	$2.5 \pm 1.1$	$7.6 \pm 0.3$	$30.5 \pm 2.1$	$302.7 \pm 22.6$

#### Calculation Methods of Several Evaluation Parameters

**Process parameters.** The generated microcrystalline of homogeneous nucleation in the liquid phase and abrasion of the grains in the air-agitated reactor lead to small particle products, which leave the reactor

with the effluent, together with the remaining phosphorus in solution, the fraction of the phosphorus is not possible to recover.

For the interpretation of the crystallization process, the following parameters were taken into account: the amount of the recovered phosphorus ( $X_R$ : Recovery efficiency), the amount of orthophosphate transformation ( $X_T$ : Transformation ratio), and the amount of microcrystalline with poor settleability in solution ( $X_M$ : Microcrystalline ratio). Three evaluation parameters  $X_R$ ,  $X_M$ ,  $X_T$  were calculated according to equations (1), (2), (3) and (4), respectively.

$$X_R = (C_{in} - C_{out}) / C_{in} \times 100 \% \quad (1)$$

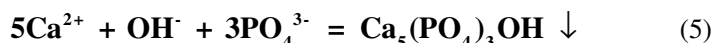
$$X_M = (C_{out} - C_{out-d}) / C_{in} \times 100 \% \quad (2)$$

$$X_T = (C_{in} - C_{out-d}) / C_{in} \times 100 \% \quad (3)$$

$$X_T = X_R + X_M \quad (4)$$

Where  $C_{in}$  is the phosphorus concentration of influent (mg/L);  $C_{out}$  is the total phosphorus concentration of effluent from crystallization reactor (mg/L);  $C_{out-d}$  is the phosphorus concentration of effluent which is rapidly filtrated by 0.45  $\mu$ m membranes (Millipore HAWP01300, USA) after sampling.

**Saturation index calculations.** Hydroxyapatite (HAP,  $\text{Ca}_5(\text{PO}_4)_3\text{OH}$ ) is a sparingly soluble salt ( $K_{sp}=2.35 \times 10^{-59}$  mol/L, 25 °C) [14]. Theoretically, the principal chemical reaction of HAP formation is based on the reaction shown in equations (5).



Thermodynamic properties of HAP crystallization can be well reflected by the saturation index (SI). In this study, SI calculations for HAP in the effluent were performed with the aid of Visual MINTEQ (Version 3.0). The calculation of SI was defined as follows:

$$SI = \log (IAP/K_{sp}) \quad (6)$$

Where,  $IAP$  is the ion activity product, and  $K_{sp}$  represents the thermodynamic solubility product of the precipitate phase. The solution is deemed to be unsaturated when  $SI$  is below zero, and no precipitation occurs. The solution is supersaturated when  $SI$  is above zero, and precipitation occurs spontaneously.

**Analysis and Characterization.** Water samples of 10 ml were taken from the effluent of the reactor at different times, then acidified with 2 M hydrochloric acid and stored in PE plastic containers at 4 °C until analysis. Water samples were filtrated rapidly with 0.45  $\mu$ m membranes (Millipore HAWP01300, USA) before acidification for investigating the concentration of dissolvable phosphorus. The chemical oxygen demand (COD), total phosphorus, ammonia and alkalinity were carried out in accordance with Standard Methods [20]. Calcium and magnesium were analyzed by an atomic absorption spectrometer (PerkinElmer AAS, USA). Turbidity and pH measurements were conducted with a turbidity meter (HACH SOLITAX-1720E) and pH meter (YSI Pro Plus, USA), respectively.

The settling rate of the fine particles (microcrystalline) which remained in suspension was measured after operating the process 30 d (without the seed material) into an Imhoff settling cone and then measuring the change in the height of the suspension as a function of time for 2 h. The settling results are represented as the ratio between the suspension height ( $H$ ) at a specific time and the initial suspension height ( $H_0$ ) [12].

The pellets removed from the bottom of the reactor were dried in an oven at 60 °C for 24 h and then used for microstructural analysis. Crystallized products used for morphological and micro-structural analysis were obtained from the reactor at the end of experiment (i.e. after 30 d). Morphology of phosphorus-coated seeds and microcrystalline were determined using scanning electron micrography (SEM) with energy dispersive spectrometry (EDS) techniques (Hitach S-4800, Japan). X-ray diffraction analysis (XRD) for the products structure was carried out utilizing a D8 ADVANCE diffractometer (Bruker AXS, Japan).

## RESULTS AND DISCUSSION

**The performance of Air-Agitated Crystallization Column on Phosphorus Recovery.** The generated small particles (i.e. microcrystalline) with poor settleability during the crystallization process have a



negative effect on the phosphorus recovery from wastewater. The completely air-agitated crystallization reactor coupled with two-sludge process could successfully recover P from the anaerobic supernatant in by our previous study [18]. In this section, an experiment was performed to evaluate the phosphorus recovery efficiencies from anaerobic supernatant in a continuously single air-agitated reactor, and the effects of different sampling ports for conversion efficiency ( $X_T$ ) and microcrystalline ratio ( $X_M$ ) were also investigated in the process.

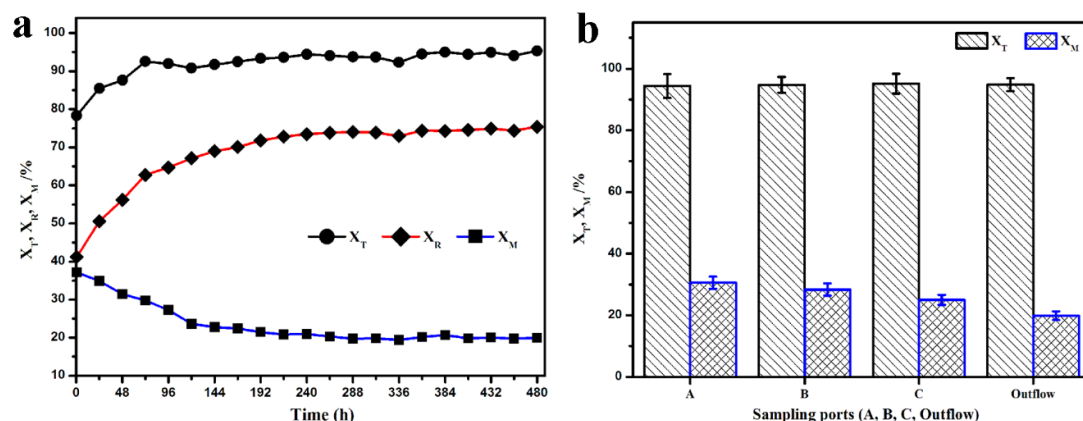


**Fig. 2. The performance of air-agitated crystallization column on phosphorus recovery (a: the variation of  $X_T$ ,  $X_R$ , and  $X_M$  as a function of time; b: the variation of  $X_T$  and  $X_M$  in different sampling ports).**

Fig. 2 showed how the performance of air-agitated crystallization column on phosphorus recovery during 480 h operations. At the beginning of the process operation, the white precipitations were produced and the turbidity of the solution was increased. This demonstrated that homogeneous nucleation happened in the high super-saturation solution and a large number of microcrystalline were produced [10]. As illustrated in Fig. 2a,  $X_R$  was approximately 42 %, but the  $X_T$  and  $X_M$  were 78.34 % and 37.13 %, respectively, in the beginning of the process operation. With the operation of the system, the  $X_R$  was continually improved. After 120 h, the  $X_R$  was reached to 70.08 % and  $X_M$  was down to 22.39 %, then the stable recovery efficiency was maintained throughout the following operational period: the average was 72.38 % of  $X_R$  and the range was 19.47~23.78 % of  $X_M$ , indicating that phosphorus had been successfully transferred from the solid phase to the liquid phase and induced crystallization with seed crystal had a starting period before products completely covered [7, 21]. At beginning of the experiment, different surface structure and constituent between newly formed crystals and seed crystals hampered the microcrystalline from depositing upon the surface of the seed. As the seed crystals were gradually covered by the crystallization products, the crystals could better growth on the surface of the seed crystals and effectively improve the phosphorus recovery in the process [21-22]. Aldaco et al. [19] showed that the similar variation tendency of  $X_R$  when studying the calcium fluoride recovery from fluoride wastewater in a fluidized bed reactor.

The results of  $X_T$  and  $X_M$  in different sampling ports (A, B, C and Outflow) are presented in Fig. 2b. The  $X_M$  was decreased with the increase of the sampling ports' height, whereas the  $X_T$  was almost constant. In the air-agitated reactor for HAP crystallization, the rising velocity slowed down due to the presence of precipitation area and buffer area, which lead to settling behavior of partial microcrystalline. Therefore, the value of  $X_M$  in the outflow port was lower than the sampling ports of the reaction area, but the  $X_T$  had not been affected by the position of the sampling ports. The higher microcrystalline ratio in the reaction system indicated that the solution was in a high super-saturation state and occurring homogeneous crystallization immediately. Because of the fine size and poor settleability of microcrystalline, it is difficultly to adhere to the surface of the seed crystal and easy to flow out from the reactor, resulting in the low phosphorus recovery efficiency [10, 15]. Therefore, super-saturation control and microcrystalline capture are necessary to avoid the homogeneous nucleation and consequently to achieve a high phosphorus recovery in further investigations.

**Effects of the Number of Feed Points (FP) on Process Efficiency.** When the two solutions ( $\text{CaCl}_2$  and phosphorus-containing wastewater) were continuously fed into the reactor with a certain proportion and the incoming mixed stream creates super-saturation, homogeneous nucleation occurs immediately. An increase in recovery efficiency is obtained if the level of super-saturation produced near the inlet point is controlled below that required for homogeneous nucleation<sup>[12-13]</sup>. Multiple reagents feed points as a conventional approach was utilized to control the levels of super-saturation when studying the sparingly soluble compounds recovery *via* crystallization reaction<sup>[12-13]</sup>. In order to primarily understand the effects of the number of feed points on process efficiency, different numbers (1, 2, 3, and 4) of feed points were used in the study. All data presented as a function of the number of feed points was obtained after operating the process of 30 d. Fig. 3 shows that the approach of multiple reagent feed ports could improve the conversion ratio (~5% improvement) of orthophosphate, but it had a limited effect (~3 % improvement) on the phosphorus recovery efficiency (deposition on the seeds). The SI and pH of the solution, on the other hand, was slightly lower than the one feed port was employed. The amount of microcrystalline produced was substantial (~21%) when the one feed port configuration was used and slightly increased using four FP (~23%). In spite of multiple reagents feed ports could reduce super-saturation at the reagent inlet points, the SI was always above zero due to the smaller solubility products of HAP ( $2.35 \times 10^{-59}$  mol/L, 25 °C)<sup>[14]</sup>. Therefore, increasing the number of feed ports could not decrease the microcrystalline ratio and improve the phosphorus recovery efficiency during the HAP crystallization process.

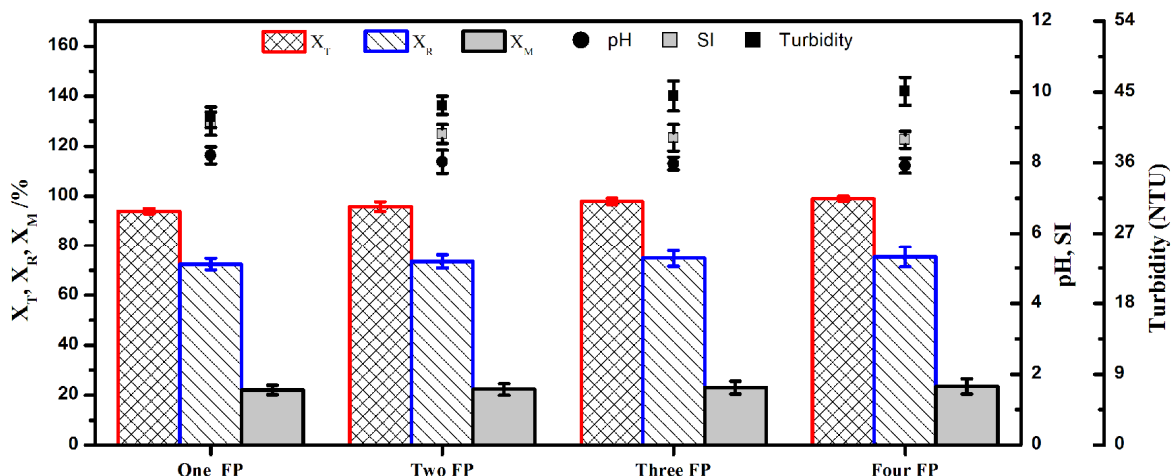


Fig. 3. The variation of process efficiency, pH, SI and turbidity as a function of the number of feed points (without recirculation flow).

**Effects of Recirculation Flow Rate on Process Efficiency.** Process efficiency, pH, SI and turbidity as a function of the different recirculation flow ratios were shown in Fig. 4. The conversion ratio did not be affected by the change of the recirculation flow ratio. However, the amount of microcrystalline recovered from suspension and the SI, pH and turbidity of the solution appeared to be affected. With the increase of the recirculation ratio, the recovery efficiency was increased gradually and reached an optimal value of 85.63 % under the recirculation ratio of 2.5. Because it can reduce the level of super-saturation by diluting the concentration of the reagents and inhibiting the large number of microcrystalline occurred simultaneously and also provide a perfectly mixed state of the reaction system and amounts of microcrystalline as seeds for heterogeneous nucleation. The results agreed with the obtained by Seckler et al.<sup>[15]</sup> studying the phosphorus recovery in the form of HAP in FBR.

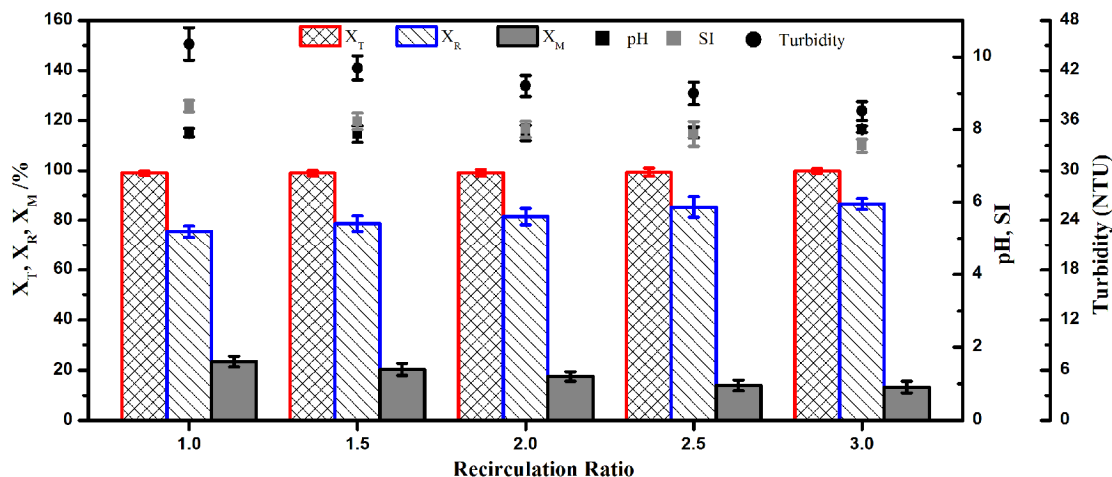


Fig. 4. The variation of process efficiency, pH, SI and turbidity as a function of the different recirculation flow ratios (four feed ports).

**Long-term Performance of the Air-Agitated Crystallization Column for Phosphorus Recovery.** In order to evaluate the phosphorus recovery efficiencies and the stability of the air-agitated crystallization column operated with four feed ports and recirculation ratio of 2.5, a long term continuous flow (30 d) experiment was carried out. As shown in Fig. 5, a stable and high phosphorus recovery efficiency and low microcrystalline ratio were maintained throughout the operational period: the average was 86.82 % and 13.14 %, varied in the ranges of 83.45~87.39 % and 12.48~14.83 %, respectively, which were increased by 19.95 % and reduced by 39.14 % compared with the initial operation condition. The results indicated that conventional approaches using multiple reagents feed points and recirculation flow had a limited effect on the inhibition of homogeneous nucleation and the improvement of phosphorus recovery efficiency.

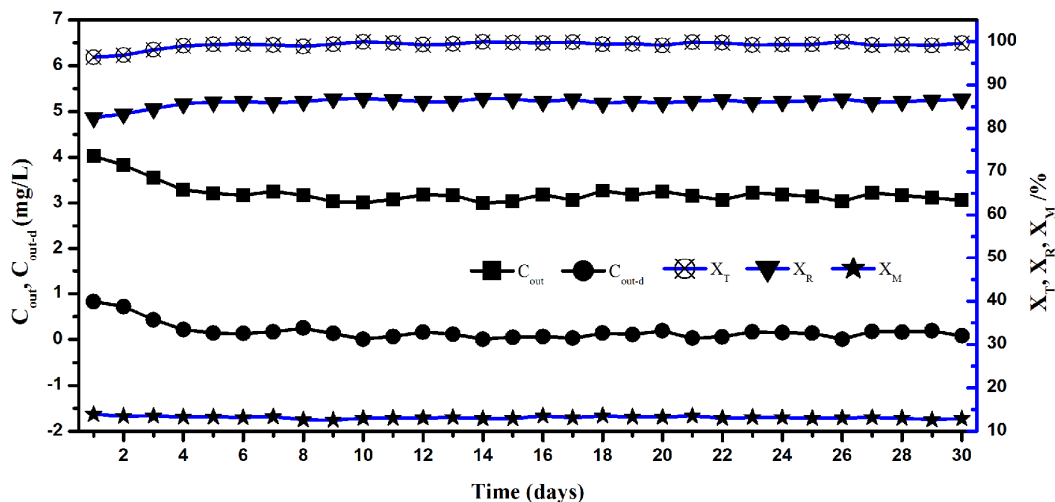
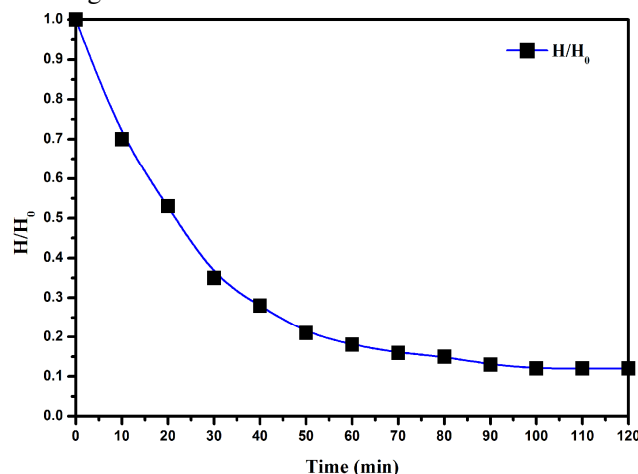


Fig. 5. The performance of air-agitated crystallization column as a function of time (30 d, four feed ports and recirculation flow ratio of 2.5).

**Characteristics of Crystallization Products.** Settling characteristics of microcrystalline particles was studied by a static settling experiment, and the charge on the surface of the microcrystalline using zeta potential measurements. Morphologies and structures of crystallized products were characterized by means of scanning electron micrograph (SEM) with energy dispersive spectrometry (EDS), and X-ray diffraction (XRD).

**Setting characteristics and zeta potential of microcrystalline.** In order to overcome the drawbacks of microcrystalline with poor settleability on the phosphorus recovery efficiency, the settling characteristics of microcrystalline was measured over a period of 2 h. Fig. 6 shows the results for the settling behavior of the microcrystalline particles which could not be recovered from suspension. The results showed that the microcrystalline particles of HAP had relatively long time (90 min) to completely precipitate under quiescent conditions. The electrostatic forces of microcrystalline particles had a negative effect on their aggregation and precipitation. Therefore, the charge on the surface of the microcrystalline using zeta potential measurement was investigated. The results show that the zeta potential of the microcrystalline was ~20 mV (data not shown). Thus, the poor settling behavior of the HAP microcrystalline can be ascribed to the highly negative surface charge.



**Fig. 6. Settling characteristics of microcrystalline particles obtained from the air-agitated crystallization column after operating 30 d.**

**Morphologies and structures of crystallized products.** Morphology features of the seeds and microcrystalline were examined by SEM. Fig. 7 (S1-S2) showed SEM micrographs of seed particles before and after HAP crystallization in the air-agitated crystallization column. Comparison of these micrographs showed that crystals formation caused a rougher surface of the seed crystal. The micrograph in Fig. 7 (S2) revealed that the amorphously distributed crystalline substance covered all the calcite seeds, which were assumed to be HAP [7, 21, 22]. The micrographs of microcrystalline (Fig.7 (S3)) showed a looser crystal structure compared with coated seeds.

Fig.7 (E1-E3) presented the quantitatively analyzed elemental composition of the seeds and crystal products by EDS. The prominent elements in the seed surface and microcrystalline were calcium and phosphorus, with traces of magnesium and chlorine. As shown in Fig.7 (E2-E3), the mole ratio (Ca/P) of the coated seeds was 2.48 and microcrystalline was 1.69. Compared with the theoretical Ca/P of HAP (1.67) and its precursors (1.33~1.59) [21, 23], the higher Ca/P of crystal products on the seed surface due to the main component of seed crystal was calcium carbonate. The ratio of the microcrystalline (1.69) was similar to the theoretical ratio of HAP (1.67) [25]. The presence of magnesium (Fig.7 (E2-E3)) indicated that the co-precipitation of calcium phosphate with magnesium ammonium phosphate had happened [24].

XRD analysis was carried out to investigate the structure of crystallized products in the air-agitated crystallization column. The XRD spectrograms of the seed crystal and microcrystalline were presented in Fig. 7 (X1-X3). The results illustrated that all the products had matched well with the standard peaks of HAP from ICDD (International Centre for Diffraction Data, PDF 73-0293). HAP formation was noted as being poorly crystalline from XRD, which can be ascribed to its small crystallite size and generated amorphous phase of calcium phosphate (ACP, OCP, and DCPD) [26]. These similar phenomena were found in the experiments for production of HAP powder performed by several researchers [6, 7, 18, 22]. Meanwhile, the presence of XRD spectrograms of calcite revealed that the co-precipitation of phosphorus with carbonate [27]. There were no the XRD spectrograms of MAP and dolomite due to the trace amounts of magnesium in wastewater.

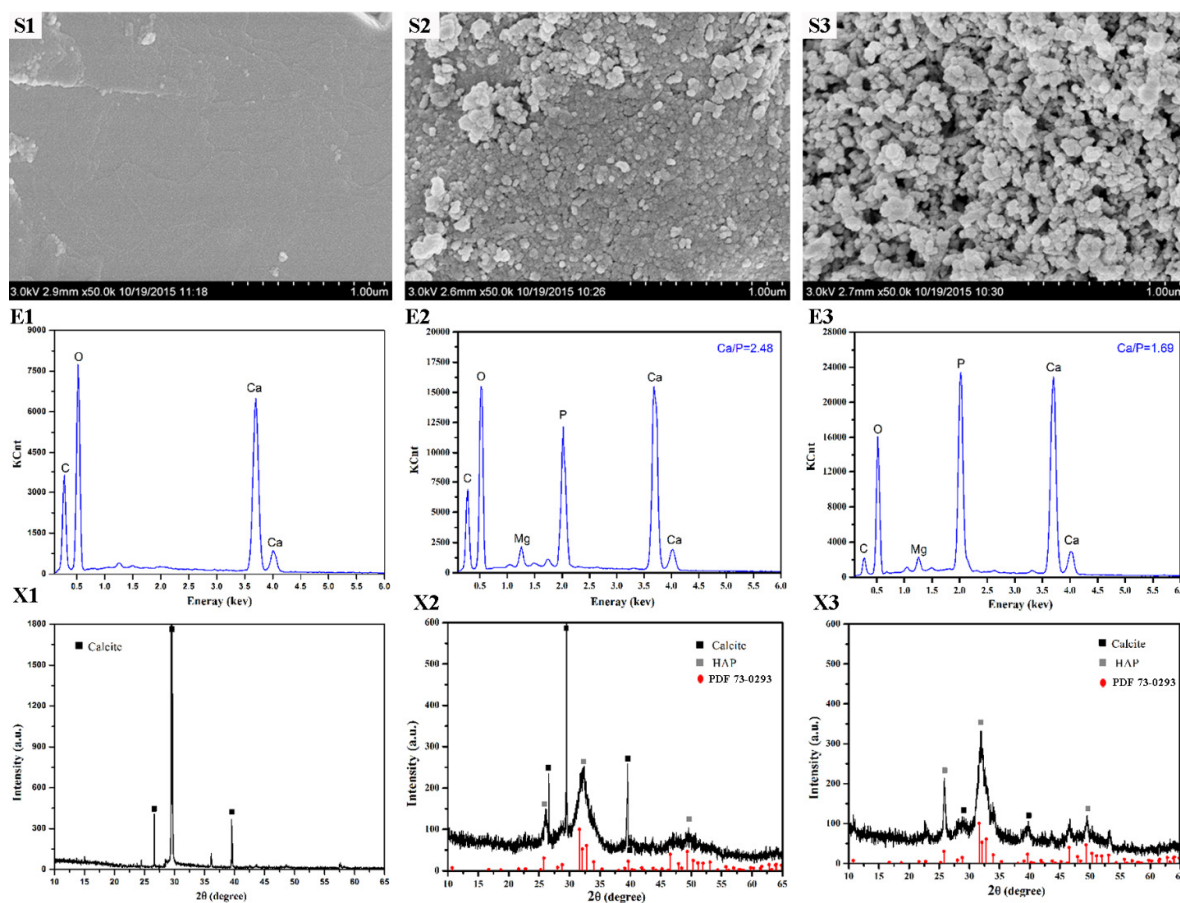


**Fig. 7.** SEM micrographs, EDS analysis graph and X-Ray diffraction diagrams of seeds and microcrystalline in the air-agitated crystallization column (after 30 d, SEM micrographs (S1-S3), EDS analysis graph (E1-E3) and X-Ray diffraction diagrams (X1-X3) of initial seeds, coated seeds and microcrystalline, respectively).

## CONCLUSIONS

After 30 d operation under a condition of multiple reagent feed points (four FP) and recirculation ratio (2.5), the phosphorus recovery efficiency ( $X_R$ ) and microcrystalline ratio ( $X_M$ ) were maintained at the average of 86.82 % and 13.14 %, respectively, which were only increased by 19.95 % and reduced by 39.14 % compared with the initial operation condition. The microcrystalline particles had a relatively long time (90 min) to completely precipitate under quiescent conditions due to the highly negative surface charge ( $\sim 20$  mV) of microcrystalline particles inhibited their aggregation and precipitation. SEM micrographs showed that the surfaces of the calcite seeds were coated with a large amount of amorphously distributed crystalline substance, which was speculated to be HAP and its precursors (ACP, OCP and DOCP). The results of EDS and XRD analysis were all verify the speculation. EDS mapping also showed the Ca/P (1.69) of microcrystalline was similar to the theoretical ratio of HAP (1.67). The results presented in this study showed a limited improvement on the phosphorus recovery in the form of HAP, associated with the conventional techniques of taking the measures of multiple reagent feed points and recirculation stream. New control strategies for super-saturation dispersion should be developed in the further study.

## ACKNOWLEDGEMENTS

This research has been supported by the National Twelfth Five-year Major Projects (2012ZX07101\_005), the National Natural Science Foundation of China (51078074) and the Fundamental



Research Funds for the Central Universities: the Research Innovation Program for College Graduates of Jiangsu Province (KYLX15\_0073). We thank the anonymous reviewers for their constructive comments that improved the manuscript.

## REFERENCES

- [1] Guan, W., Ji, F.Y., Chen, Q.K., Yan, P., Zhang, Q., 2013. Preparation and phosphorus recovery performance of porous calcium-silicate-hydrate, *Ceram. Int.* 39(2), 1385-1391.
- [2] Rahman, M.M., Salleh, M.A.M., Rashid, U., Ahsan, A., Hossain, M.M., Ra, C.S., 2014. Production of slow release crystal fertilizer from wastewaters through struvite crystallization- A review, *Arab. J. Chem.* 7(1), 139-155.
- [3] Cordell, D., Drangert, J. O., White, S., 2009. The story of phosphorus: global food security and food for thought. *Global Environ. Chang.* 19(2), 292-305.
- [4] Le Corre, K.S., Valsami-Jones, E., Hobbs, P., Parsons, S.A., 2009. Phosphorus Recovery from Wastewater by Struvite Crystallization: A Review, *Crit. Rev. Env. Sci. Tec.* 39(6), 433-477.
- [5] Yuan, Z., Pratt, S., Batstone, D.J., 2012. Phosphorus recovery from wastewater through microbial processes. *Curr. Opin. Biotech.* 23 (6), 878-883.
- [6] Qiu, G., Law, Y.M., Das, S., TING, Y.P., 2015. Direct and complete phosphorus recovery from municipal wastewater using a hybrid microfiltration-forward osmosis membrane bioreactor process with seawater brine as draw solution. *Environ. Sci. Technol.* 49(10), 6156-6163.
- [7] Song, Y.H., Weidler, P.G., Berg, U., Nüesch, R., Donnert, D., 2006. Calcite-seeded crystallization of calcium phosphate for phosphorus recovery. *Chemosphere*, 63 (2), 236-243.
- [8] Hosni, K., Moussa, S.B., Chachi, A., Amor, M.B., 2008. The removal of  $\text{PO}_4^{3-}$  by calcium hydroxide from synthetic wastewater: optimization of the operating conditions. *Desalination* 223 (1), 337-343.
- [9] Okano, K., Uemoto, M., Kagami, J., Miura, K., Aketo, T., Toda, M., Honda K., Ohtake, H., 2013. Novel technique for phosphorus recovery from aqueous solutions using amorphous calcium silicate hydrates (A-CSHs). *Water Res.* 47 (7), 2251-2259.
- [10] Karapinar, N., Hoffmann, E., Hahn, H.H., 2006. P-recovery by secondary nucleation and growth of calcium phosphates on magnetite mineral. *Water Res.* 40 (6), 1210-1216.
- [11] Nývlt, J., Sohnel, O., Matuchova, M., Broul, M., 1985. In: *The Kinetics of Industrial Crystallization*, Academia, Prague.
- [12] Mokone, T.P., Van Hille, R.P., Lewis, A.E., 2012. Metal sulphides from wastewater: Assessing the impact of super-saturation control strategies. *Water Res.* 46 (7), 2088-2100.
- [13] Costodes, V.T., Lewis, A.E., 2006. Reactive crystallization of nickel hydroxy-carbonate in fluidized-bed reactor: fines production and column design. *Chem. Eng. Sci.* 61 (5), 1377-1385.
- [14] Kumar, R., Prakash, K.H., Cheang, P., Khor, K.A., 2004. Temperature driven morphological changes of chemically precipitated hydroxyapatite nanoparticles. *Langmuir* 20 (13), 5196-5200.
- [15] Seckler, M.M., Bruinsma, O.S.L., Van Rosmalen, G.M., 1996. Phosphate removal in a fluidized bed-I. Identification of physical processes. *Water Res.* 30 (7), 1585-1588.
- [16] Battistoni, P., Fava, G., Pavan, P., Musacco, A., Cecchi, F., 1997. Phosphate removal in anaerobic liquors by struvite crystallization without addition of chemicals: preliminary results. *Water Res.* 31 (11), 2925-2929.
- [17] Suzuki, K., Tanaka, Y., Osada, T., Waki, M., 2002. Removal of phosphate, magnesium and calcium from swine wastewater through crystallization enhanced by aeration. *Water Res.* 36 (12), 2991-2998.
- [18] Shi, J., Lu, X.W., Yu, R., Zhu, W.T., 2012. Nutrient removal and phosphorus recovery performances of a novel anaerobic-anoxic/nitrifying/induced crystallization process. *Bioresour. Technol.* 121(2), 183-189.
- [19] Aldaco, R., Garea, A., Irabien, A., 2007. Calcium fluoride recovery from fluoride wastewater in a fluidized bed reactor. *Water Res.* 41(4), 810-818.
- [20] APHA, 2005. *Standard Methods for the Examination of Water & Wastewater*, twenty-first ed. American Public Health Association, American Water Works Association and Water Environment Federation, Washington, DC, U.S.A.

- [21] Kim, E.H., Lee, D.W., Hwang, H.K., Yim, S., 2006. Recovery of phosphates from wastewater using converter slag: Kinetics analysis of a completely mixed phosphorus crystallization process. *Chemosphere* 63 (2), 192-201.
- [22] Chen, X., Kong, H., Wu, D., Wang, X., Lin, Y., 2009. Phosphate removal and recovery through crystallization of hydroxyapatite using xonotlite as seed viron. *Sci.* 21 (5), 575-80.
- [23] Wang, L., Nancollas, G.H., 2008. Calcium orthophosphates: crystallization and dissolution. *Chem. Rev.* 108 (11), 4628-4669.
- [24] Ohlinger, K.N., Young, T.M., Schroeder, E.D., 1998. Predicting struvite formation in digestion. *Water Res.* 32 (12), 3607-3614.
- [25] Tervahauta, T., van der Weijden, R.D., Flemming, R.L., Leal, L.H., Zeeman, G., Buisman, C.J., 2014. Calcium phosphate granulation in anaerobic treatment of black water: a new approach to phosphorus recovery. *Water Res.* 48(1), 632-642.
- [26] Combes, C., Rey, C., 2010. Amorphous calcium phosphates: synthesis, properties and uses in biomaterials. *Acta Biomater.* 6 (9), 3362-3378.
- [27] Song, Y.H., Hahn, H.H., Hoffmann, E., 2002. Effects of solution conditions on the precipitation of phosphate for recovery: A thermodynamic evaluation. *Chemosphere* 48 (10), 1029-1034.

## **PHYTOREMEDIATION OF NUTRIENT-RICH WASTEWATERS USING DUCKWEED**

***Summer Lentini*** and ***Emily Smith*** (Wilkes University, Wilkes-Barre, PA, USA)

David Petrik (T&M Associates, Bethlehem, PA, USA)

Sara Arana (IES Engineers, Blue Bell, PA, USA)

Release of treated municipal wastewaters after biological treatment and containing nutrients such as nitrates and phosphates and their effects on surface waters has been well documented for many decades. Traditional treatment methods of reducing nutrient loads on receiving water bodies involve biological and/or chemical methods many of which are energy-intense and relatively expensive in the long run. Preliminary studies have shown that phytoremediation, which is a technology that uses plants to remove contaminants, can be used for effective removal of nitrates and phosphates. This study focuses on the potential of an aquatic macrophyte, *Lemna minor* (duckweed), to remove phosphates and nitrates from wastewater. Tests conducted with varying duckweed areal densities, water depths, and initial nutrient concentrations indicate nitrates and phosphates removal consistently at 95% and above levels.



## **EFFECTS OF ANAEROBIC DIGESTION ON THE COMBUSTION OF SEWAGE SLUDGE**

**Emrehan Berkay Çelebi**, Aysegül Aksoy and F. Dilek Sanin  
(Middle East Technical University, Ankara, Turkey)

**ABSTRACT:** Around the world, especially in the developing countries, sludge management is a topic gaining increasing importance, as the number of treatment plants and the people connected to these plants are on the rise. Old approaches seeing sludge as a waste, including landfilling, leave its place for new applications where sludge acts as an energy source or a resource as fertilizer. Combustion or co-combustion of sludge exploits its energy potential while providing stabilization and reduction in volume. Besides combustion, anaerobic digestion has been in use for a long time, serving to both stabilize the sludge and provide energy in terms of biogas. Anaerobic digestion is known to reduce the organic content of sludge, in turn, reducing its calorific value. The effects of anaerobic digestion enhanced by ultrasound pretreatment, on the combustion properties of sludge are demonstrated experimentally. 2.5 L anaerobic batch reactors were used to quantify how the calorific value of the sludge changes with digestion time. On the average, over 71 days, methane production from the sonicated reactors was 8.6 L, 32% more than the control. Observed removals were 49% for VS and 38% for COD. Calorific values of the samples were reduced by 30% on the average. The ash content remained relatively the same.

### **INTRODUCTION**

Sludge is produced in abundance all around the world as the byproduct of wastewater treatment. Its quantity is expected to increase along with increased wastewater production and new treatment plants (Kelessidis and Stasinakis, 2012). In many countries, landfilling the sludge after dewatering had been the most popular method of disposal. However, due to stricter regulations (Landfill Directive in EU), this will no longer be applicable. It is likely that revenue generating disposal methods like land application and co-combustion will gain more popularity (Kelessidis and Stasinakis 2012).

The three major benefits of co-combustion include firstly the utilization of sludge's heating value, instead of direct disposal. Thus, sludge is transformed into an energy source. Secondly, sludge replaces some part of the original fuel, leading to the conservation of that fuel source. Finally, remainder of the sludge after co-combustion, ash, is significantly easier to dispose of than sludge itself (Onaka 2000). Also as studied by Wzorek (2012), sludge itself can be used as an energy source during cement production furthermore, its ash can be incorporated into cement without having adverse effects.

The important parameters for combustion of sludge include water content, lower heating value, and the amount of ash produced (Werther and Ogada 1999). The water in the sludge that would be used as a fuel results in negative effects on the overall combustion process such as lowering of the combustion temperature. These effects need to be mitigated by drying the sludge up to or over 90% dry solids (Werther and Ogada 1999). Calorific value or the lower heating value indicates the amount of energy that will be released during combustion. Sewage sludge that has not been subjected to any stabilization procedure is expected to have a calorific value around 17 kJ/g, whereas, digestion processes will reduce this value to about 10 kJ/g (Werther and Ogada 1999). When compared to the calorific values of high quality coal (33 kJ/g) and lignite (6 kJ/g), it is seen that sludge can provide as much energy as medium quality coal.

Biogas resulting from anaerobic digestion provides another opportunity to use the energy potential of sludge. While conventional digesters are used all around the world for decades, new practices aim to increase organic loading rates, biogas yield and its production rate (Pérez-Elvira et al. 2006; Braguglia et al. 2012a). For the purpose of the latter, pretreatment studies are commonly conducted. Xu et al. (2011) observed an increase in VS reduction and biogas production when ultrasound pretreatment was applied. Braguglia et al. (2012b) compared ultrasound and ozone pretreatment methods and demonstrated 20% increase in biogas production. Another study showed that during anaerobic digestion in the form of a BMP

assay, sonication provided a higher increase in biogas yield at lower food to microorganism (F/M) ratios (Braguglia et al. 2012a).

Although both combustion and anaerobic digestion of sewage sludge are investigated separately in the literature, effects of digestion on fuel properties of sludge have not been studied extensively. Within the scope of this study, sludge samples taken from a municipal wastewater treatment plant were subjected to ultrasound pretreatment and then anaerobic digestion in the form of large batch reactors. Calorific values were measured during digestion to quantify the change in the total amount of energy that can be harvested.

## **MATERIALS AND METHODS**

**Sludge Samples.** Ankara Central Wastewater Treatment Plant was the source for both the waste activated sludge (WAS) that was digested, and the anaerobic seed sludge. The plant is designed to treat 760,000 m<sup>3</sup> of wastewater daily, using a conventional activated sludge treatment system for the wastewater line. The plant includes anaerobic digesters with a solids retention time (SRT) of 14 days, where mixed primary and secondary sludge are digested together (Official Website of Ankara Metropolitan Municipality, General Directorate of Water and Sewage Administration, 2014). The WAS samples were taken from the return activated sludge line and the seed samples were taken from the digesters. Samples were left to settle for a day at 4 °C following sampling to obtain concentrated sludge.

**Ultrasound Pretreatment and Setup.** WAS samples were sonicated for different time periods after settling using a laboratory scale sonicator, Sartorius Labsonic P. Sonication frequency was set as 24 kHz and the amplitude was 100%. Probe diameter was selected as 22 mm. The frequency of the device was 1, which resulted in the maximum power of 255 W. The volume of the samples sonicated were 350 mL, yielding a constant sonication density of 0.73 W/mL. Sonication duration was set to be 10 minutes while the F/M ratio was 1 (g VS/ g VSS) following the prior studies of Apul and Sanin (2010) and K ksoy and Sanin (2010). Temperature control was applied during sonication. Beakers holding 350 mL sludge sample each were placed in an ice bath for the whole duration to keep the samples at 25 to 30 °C. The seed sludge taken from the digester (ADS) was not sonicated to preserve the microorganisms required for anaerobic digestion.

**Analytical Methods.** For the calorific value analysis, samples were dried at 105 °C to constant weights. Then they were sieved through a 60 mesh size sieve prior to combustion in the calorimeter (LECO AC500). Elemental compositions of the samples were also determined using an analyzer (LECO TruSpec CHN) after drying. For TS and VS measurements, Standard Methods 2540B and 2540E; for VS and VSS measurements, Standard Methods 2540D and 2540E were used, respectively (APHA, AWWA, and WEF, 2005). Ash content was determined according to ASTM Standard Method D3174-12 (ASTM, 2012). COD analyses were conducted using Hach COD kits and Hach DR 3900 spectrophotometer in accordance with the USEPA approved dichromate method (Jirka and Carter, 1975). The amount of biogas produced were measured using a gas collection column filled with a brine solution consisting of 10% NaCl (w/v) and 2% H<sub>2</sub>SO<sub>4</sub> (v/v) to prevent the dissolution of the produced biogas. Composition of the biogas was determined by a gas chromatograph (GC) equipped with a thermal conductivity detector (TCD) (Agilent Technologies, 6890N). The carrier gas in the system had a velocity of 29 cm/s and the HP-Plot Q capillary column had the dimensions of 30.0 m × 530 µm × 40.0 µm. Temperature program set the temperature at 45 °C for the first minute, and then increased to 65 °C at a rate of 10 °C/min.

## **RESULTS**

Reactors were operated for 71 days until the biogas production was negligible. Monitored parameters include TS, VS, COD, calorific value, ash content, elemental composition and biogas volume and composition.

Shown in Figure 1 are the methane productions from the reactors. First of the non-sonicated reactors (U0A) showed a cumulative production of 6.71 L, while the second of the non-sonicated reactors (U0B) had 6.31 L. Sonicated reactors had more methane production, from first of the sonicated reactors (U10A) 8.81 L was observed, while the second sonicated reactor (U10B) produced 8.43 L. On the whole, a 32.1% increase was documented. This increase is higher than the increase in biogas production which was

calculated to be 15.2%, indicating that more of the produced biogas is methane when sonicated sludge is digested.

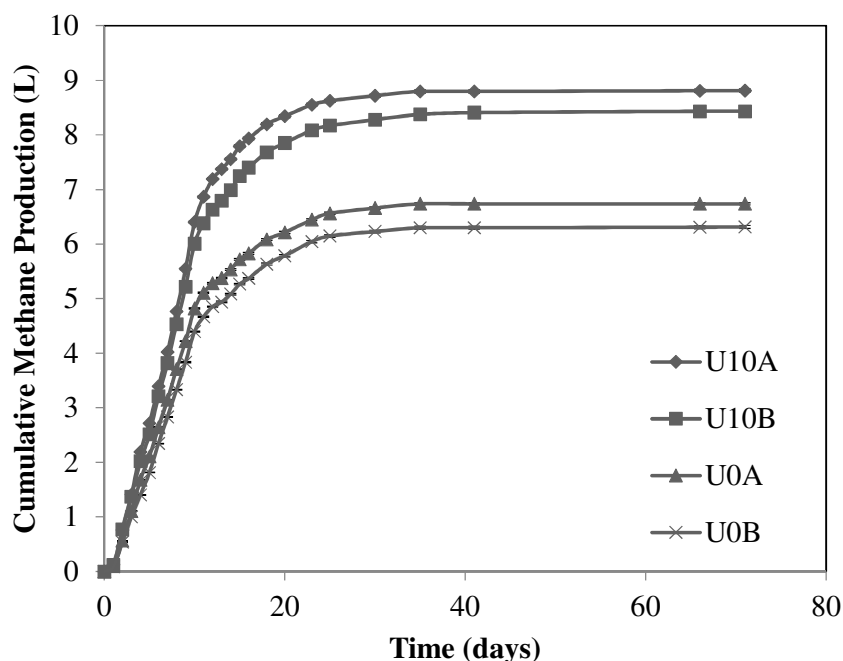


**FIGURE 1.** Cumulative methane productions of sonicated and non-sonicated reactors

When VS removal is considered, all four reactors showed a similar pattern, with sonicated reactors being one or two days ahead of the non-pretreated reactors, in terms of the progression of digestion, especially during the first two weeks (Figure 2). U10A had a VS concentration of 21583 mg/L which is reduced to 10817 mg/L, showing a 49.9% removal. U10B had 21267 mg/L initially and 10717 mg/L after the digestion, totaling to 49.6% removal in VS. U0A started with a VS concentration of 21717 mg/L and it was reduced to 11150 mg/L, displaying a removal rate of 48.7%. Finally, U0B had its VS concentration reduced from 21633 mg/L to 11100 mg/L, a 48.7% reduction overall. COD concentrations of the samples were also measured during digestion. U10A had its COD reduced from 42025 mg/L to 25950 mg/L, with a 38.3% reduction. The other sonicated reactor, U10B, showed a 39.0% decrease from 41800 mg/L to 25000 mg/L. As expected, sonicated samples exhibited more COD removal. Control groups of U0A and U0B showed 37.9% (from 43275 mg/L to 26875 mg/L) and 37.5% (from 43650 mg/L to 27300 mg/L) reductions, respectively.

As displayed in Figure 3, calorific values of sludge from each of the reactors were measured during anaerobic digestion to show how it changes with respect to time. Prior to digestion, the first of the sonicated reactors, U10A, had 14730 J/g, while the second one, U10B, had 14680 J/g. Control reactor U0A had 15552 J/g and the second control reactor U0B had 15550 J/g. On the very first day, the initial calorific values were reduced by about 10%. From this point forward, the decrease showed a declining pattern up to day 30. During this time, sonicated reactors displayed a lower calorific value, as more of the carbon was converted to biogas (and methane). After the 30-day mark, calorific values were stabilized and final values were 9845 J/g for U10A (33.1% decrease), 9950 J/g for U10B (32.2% decrease), 10183 J/g for U0A (30.0% decrease) and finally 10108 J/g for U0B (30.4% decrease). Following the same pattern for biogas and methane productions, and VS and COD removal, sonication reduced the calorific value further compared to the case with no pretreatment. It should be noted that while the reduction in calorific value is significant by itself, it gets magnified when the reduction in TS concentration is also considered.

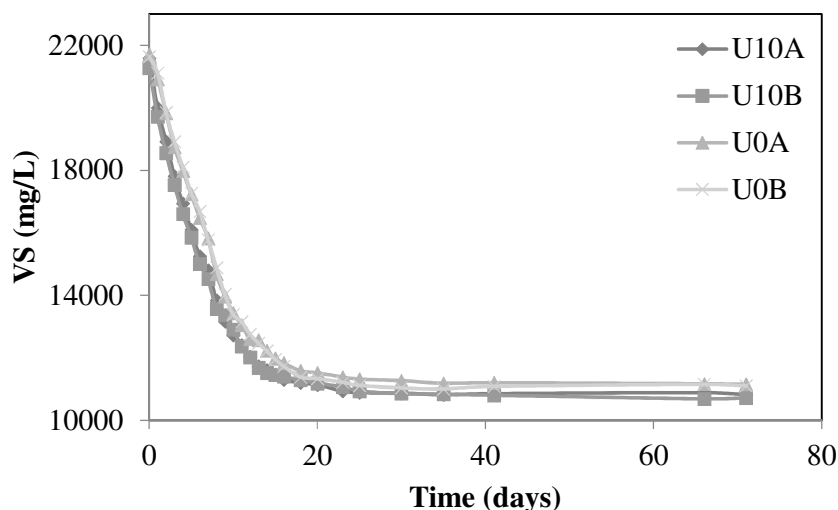


**FIGURE 2.** Changes in the VS concentrations with respect to time

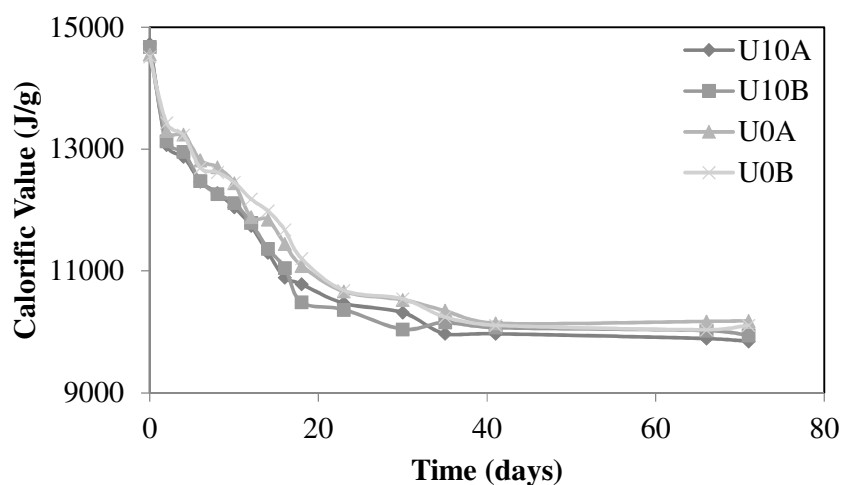


**FIGURE 3.** Changes in the calorific values with respect to time

Ash concentrations of the reactors were tracked in both mg/L and percent of dry solids. The concentrations fluctuate between 13000 mg/L and 14000 mg/L for the sonicated reactors and 12500 mg/L and 13000 mg/L for the non-sonicated reactors. On the other hand, the relative amount of ash within the sludge was found to increase as the total solids amount decreased. The initial ash contents which were 36.5% of U10A, 37.6% of U10B, 34.2% of U0A and 34.3% of U0B were found to increase to 52.3% for U10A, 52.2% for U10B, 49.0% for U0A and 49.0% for U0B. In other words, at the end of digestion, about half the sludge consisted of incombustible and inert ash for both sonicated and non-pretreated sludge.

Elemental analysis was done throughout the digestion duration to quantify the changes in carbon, hydrogen and nitrogen contents of the sludge. On the average, sludge from all four reactors started with 31.9% carbon and the non-sonicated reactors ended up both with 24.7%. Sonication reduced this further to 22.7% for U10A and 23.5% for U10B. Reason for this additional loss can be attributed to the increase in biogas production due to sonication. Hydrogen levels decreased as digestion progressed, as it took part in methane yielding reactions during digestion. Initially, samples contained 4.7% hydrogen, and this value decreased while showing some fluctuations, towards 3.4% finally. Nitrogen content remained between 1.8% and 2.7% throughout digestion, without showing any significant changes.

## CONCLUSION

The overview of the results indicates that ultrasound pretreatment has indeed improved VS and COD removals and methane yield. Overall methane productions were 8.6 L for sonicated reactors and 6.5 L for control reactors. VS removals were 49% on the average while the COD removal rates were 38%. Ash content of the samples started with about 35% and they increased to 51% on the average. As for the calorific value of the sludge, overall, 30% reduction was observed throughout the samples, magnified further by the reduction of the amount of combustible solids.

While ultrasound pretreatment is shown to enhance anaerobic digestion significantly, energy calculations should be done to include the complete system before judging ultrasound pretreatment coupled with anaerobic digestion as worthy or not. Also, while calorific values were indeed reduced by anaerobic digestion, overall situation may demand the sludge to be digested before combustion to negate some of the associated costs of transportation and handling. To sum up, results should be evaluated on a case-by-case basis in order to enhance the energy yield from the whole sludge treatment scheme.

## REFERENCES

- APHA, AWWA, & WEF. (2005). *Standard Methods for the Examination of Water and Wastewater* (21st ed.). Washington, DC.: American Public Health Association, American Water Works Association, Water Environment Federation.
- Apul, O. G., & Sanin, F. D. (2010). Ultrasonic pretreatment and subsequent anaerobic digestion under different operational conditions. *Bioresource Technology*, 101(23), 8984–8992.
- ASTM. (2012). *D3174-12, Standard Test Method for Ash in the Analysis Sample of Coal and Coke from Coal*. West Conshohocken, PA: ASTM International.
- Braguglia, C. M., Gagliano, M. C., & Rossetti, S. (2012a). High frequency ultrasound pretreatment for sludge anaerobic digestion: Effect on floc structure and microbial population. *Bioresource Technology*, 110, 43–49.
- Braguglia, C. M., Gianico, A., & Mininni, G. (2012b). Comparison between ozone and ultrasound disintegration on sludge anaerobic digestion. *Journal of Environmental Management*, 95(SUPPL.).
- Jirka, A. M., & Carter, M. J. (1975). Micro semi-automated analysis of surface and wastewaters for chemical oxygen demand. *Analytical Chemistry*, 47(8), 1397–1402.
- Kelessidis, A., & Stasinakis, A. S. (2012). Comparative study of the methods used for treatment and final disposal of sewage sludge in European countries. *Waste Management*, 32(6), 1186–1195.
- Köksoy, G. T., & Sanin, F. D. (2010). Effect of digester F/M ratio on gas production and sludge minimization of ultrasonically treated sludge. *Water Science and Technology*, 62(7), 1510–1517.
- Official Website of Ankara Metropolitan Municipality, General Directorate of Water and Sewage Administration. (2014). Retrieved March 23, 2015, from <https://www.aski.gov.tr/en/>
- Onaka, T. (2000). Sewage can make Portland cement: a new technology for ultimate reuse of sewage sludge. *Water Science and Technology*, 41(8), 93–98.
- Pérez-Elvira, S. I., Nieto Diez, P., & Fdz-Polanco, F. (2006). Sludge minimisation technologies. *Reviews in Environmental Science and Biotechnology*, 5(4), 375–398.
- Werther, J., & Ogada, T. (1999). Sewage sludge combustion. *Progress in Energy and Combustion Science*, 25(1), 55–116.
- Wzorek, M. (2012). Characterisation of the properties of alternative fuels containing sewage sludge. *Fuel Processing Technology*, 104, 80–89.
- Xu, H., He, P., Yu, G., & Shao, L. (2011). Effect of ultrasonic pretreatment on anaerobic digestion and its sludge dewaterability. *Journal of Environmental Sciences*, 23(9), 1472–1478.

## **CHANGE OF pH AND ORP WITH APPLIED DC ON LEACHATE ACTIVATED SLUDGE**

***Gülizar Kurtoğlu Akkaya\****, Elif Sekman, Selin Top, Senem Yazici Guvenc, Ece Sagir, Mahir Ince and Mehmet Sinan Bilgili (Yildiz Technical University, Istanbul, TURKEY)

Leachate from landfill is a very high polluted wastewater having a complex structure. Few reasearchers was made for leachate treatment by SMEBR (submerged electro membrane bioreactor) system. First of all, leachate activated sludge taken from the aeration tank of a leachate treatment facility (Istanbul Odayeri Sanitary Landfill) is consistently ventilated until the run is performed. DC (direct current) is given to 500 ml activated sludge samples at different currents and exposure durations. After each run, samples taken from near of anode and cathode, pH and ORP are transiently measured. Afterwards, obtained results are commented according to current and exposure durations.

## **COMBUSTION CHARACTERISTICS AND KINETICS OF THE PULPING EFFLUENT SLUDGE USING THERMOGRAVIMETRIC ANALYSIS**

***Kanhaiya Lal*** and Anurag Garg  
(Indian Institute of Technology Bombay, Mumbai, INDIA)

Examining the performance of carbon products of various activation levels sometimes play important role, especially to determine the operating conditions of large scale activated carbon manufacturing plants. This study compares the removal performance of phenol from water using biochar and two physically (steam) activated carbons (having two different activation levels) produced from the same biomass, Albizia, an invasive plant. First, biochar was produced from Albizia by pyrolysis process at 850 °F. This biochar was then physically activated at 1500 °F with two different activation times (residence times of 20 minutes and 35 minutes). The iodine numbers (IN) of each of these three products, biochar and two activated carbons were determined to be 132 mg/g, 835 mg/g and 1103 mg/g respectively. Batch kinetic experiments and isotherm studies were performed to compare the effect of activation levels of activated carbons (IN of 1103 mg/g and 835 mg/g) with biochar (used as baseline with IN of 132 mg/g) on phenol adsorption. Batch kinetic studies (with 1 mg/L of phenol concentration and 2 h mixing time) showed that phenol removal can be increased more than 1.5 times with a target dosage range 200 mg/L to 400 mg/L if activated carbons are used rather than biochar. The equilibrium data were found well represented by Freundlich isotherm model.

## **REDUCED SLUDGE GROWTH AT HIGH BULK LIQUOR DO INDUCED BY INCREASED MAINTENANCE**

**Anwar Khursheed** (AMU, Aligarh-202002, India)

A. A. Kazmi & Meena Sharma (Indian Institute of Technology Roorkee, Roorkee-247667, India)

Rubia Z. Gaur (Agriculture Research Organisation Volcani Centre, Israel 50250)

Abid Ali Khan (Jamia Millia Islamia, New Delhi-110055, India)

Vinay Kumar Tyagi (TERI University, New Delhi 110070, India)

Sludge handling is a matter of great concern being largest in volume out of the constituents removed during wastewater treatment. Sludge reduction by physico-chemical methods results in buildup of chemicals, which may require further treatment. Owing these reasons various biologically sustainable methods of sludge reduction including application of high oxygenation have been successfully tested.

Experiments on actual sewage in two lab scale SBRs were conducted under normal (1.5-2.5 mgDO/L and high DO (HDO: 3-6.5 mgDO/L) regimes. it was observed that microorganism allocated substrate between maintenance and growth in the form of maintenance coefficient. This could be induced by endogenous respiration owing to high SRT, predation on bacteria, chemical toxicity, adverse environment, viral attack on bacteria. Every treatment plant may experience one or more maintenance causing factors nevertheless high SRT and prevailing environmental conditions are imminent and therefore considered as primary maintenance ( $m_p$ ), while remaining is classified as secondary ( $m_s$ ).

Average yield coefficient reduction at HDO was 32.7% and 28.2% compared to stoichiometric and at normal DO respectively (Figure). The observed primary and secondary maintenance was 0.11gCOD/gVSS.d ( $\pm 0.01$ ) at an SRT of 25.2d ( $\pm 2.0$ ) and 0.096gCOD/gVSS.d ( $\pm 0.045$ ) at an SRT of 24.2d ( $\pm 3.6$ d) respectively.



## EFFECT OF THERMAL-ALKALINE PRETREATMENT ON MICROBIAL COMMUNITIES IN AN ANAEROBIC DIGESTION OF HIGH-SOLID SLUDGE

**Wang Tao**, Gao Peng and Dai Xiaohu  
(Tongji University, Shanghai, China)

In order to obtain more methane, most studies in literatures were centered on enhancing the hydrolysis of sludge anaerobic digestion which was proved as un-efficient. In this paper, a thermal-alkaline pretreatment method, i.e., pretreating sludge at 100°C for 60 min and then adjusting the initial pH 9.0 was proposed to significantly enhance methane production from an anaerobic digestion of high-solid sludge. During the fermentation time of 60-80d, the optimal condition increased the biogas production to 1.20-fold of the control. In this study, the underlying mechanisms for the improved methane production under the optimal conditions were investigated by using 454 pyrosequencing and fluorescent in situ hybridization (FISH) to analyze the microbial communities shift in the anaerobic digestion reactors of high-solid sludge. It was found that thermal-alkaline pretreatment increased the abundances of *Bacteroidetes sp.* and *Firmicutes sp.*, which was able to enhance the degradation of macromolecular organic material, indicated that more volatile fatty acids were produced after thermal-alkaline pretreatment. Meanwhile, the abundance of methane-producing archaea (such as *Methanosaeta sp.* and *Methanosarcina sp.*) in the reactor of pretreated high-solid sludge was also higher than that of the control, which benefited the methanogenesis of volatile fatty acids. Therefore, thermal-alkaline pretreatment of high-solid sludge increased the abundances of bacteria and archaea involved in an anaerobic digestion system, which resulted in the efficient production of methane.

## **EFFICIENT ANAEROBIC PRODUCTION OF VOLATILE FATTY ACIDS FROM SEWAGE SLUDGE BY ALKYL POLYGLUCOSE**

**Jingyang Luo**, Leiyu Feng, Yinglong Su, Yinguang, Chen  
(Tongji University, Shanghai, P.R.China)<sup>44</sup>

Volatile fatty acids (VFAs), the preferred carbon sources for biological nutrients removal, can be produced from sewage sludge (SS) during anaerobic digestion, by which both sludge reduction and recovery of carbon resources are accomplished. The addition of alkyl polyglucose (APG) remarkably stimulated the VFAs production, especially the propionic acid, in the anaerobic digestion system via simultaneously accelerating solubilization and hydrolysis, enhancing acidification, inhibiting methanogenesis and balancing carbon to nitrogen (C/N) ratio of SS. Also the feasible operation time for maximum VFAs accumulation was shortened in the presence of APG. The VFAs accumulation reached  $2988 \pm 60$  mg COD/L at 0.3 g APG/g total suspended solids (TSS) within 4 d, while it was only 578.1 mg COD/L in the control within 6 d. The corresponding yield of propionic acid was  $1312 \pm 25$  mg COD/L, 7.9-fold of the control. Mechanism investigations have found that both the solubilization and hydrolysis of SS were accelerated by reducing the surface tension and increasing the zeta potential of fermentation liquid, and the acidification was enhanced, while the methanogenesis was inhibited in the presence of APG. Further exploration revealed that the activities of key enzymes responsible for organic compounds hydrolysis and VFAs production were all greatly promoted due to the adjustment of C/N ratio of substrates by APG. Moreover, the microbial community in the APG reactors was shifted to be beneficial for the VFA production via 454 high-throughput pyrosequencing analysis.

## PRETREATMENT PERFORMANCE OF A NOVEL AWFR FOR DECENTRALIZED DOMESTIC WASTEWATER

Juanhong Li and Xiwu Lu

(Southeast University, Nanjing, Jiangsu, China)

**ABSTRACT:** Anaerobic reactor is of great interest for domestic wastewater treatment due to the reduced-carbon footprint concept. In this work, a novel wool-felt filter reactor (AWFR) was designed and applied to treat real decentralized domestic wastewater. A lab-scale AWFR (with HRT of 3 day) was operated for 90 days in winter (temperature 8-15°C). The pollutant removal of lab-scale AWFR and the archaeal communities were investigated. Results demonstrated that the removal efficiency of COD, TN and TP were  $49.5\pm5.7\%$ ,  $13.8\pm4.0\%$  and  $18.6\pm6.7\%$ , respectively. The average methane yield was 115L/kg·COD<sub>removal</sub>. In addition, the acetate and propionate were slightly accumulated in effluent due to lower temperature in winter. Based on the phylogenetic analysis of High-throughput MiSeq sequencing, *Methanobacterium* and *Methanolinea* were the predominant genera in the AWFR performance, indicating that hydrogenotrophic methanogenesis pathway played a critical role for methane production of the AWFR system in winter. Overall, the AWFR with a stable performance is a promising cost-efficient pretreatment in decentralized domestic wastewater treatment.

## INTRODUCTION

Recent years, more attention has been focused on anaerobic techniques in treating decentralized domestic wastewater, particularly in the rural areas of China. Anaerobic treatment has proven to be an eco-friendly technology due to less sludge production, higher efficiency and higher energy methane recovery (Bandara et al., 2012; Gao et al., 2014a; Lew et al., 2011; Smith et al., 2013). A number of full-scale anaerobic treatment processes have recently been built and applied in tropical regions (Aiyuk et al., 2006). Nevertheless, without of heating systems, low operation temperature has been cite as a barrier to affecting the performance of anaerobic process and shift of microbial communities. Therefore, various anaerobic reactors have been properly designed to investigate the temperature effect on the performance of anaerobic treatment process (Bandara et al., 2012; Feng et al., 2008; Lew et al., 2011; Smith et al., 2013; Sumino et al., 2012). As a modern high-rate reactor, the anaerobic filter (AF) is widespread application in wastewater treatment. Carriers in the AF play a crucial role in anaerobic performance due to the large surface for microorganism attach on. In fact, many types of carriers are developed for application in wastewater treatment, such as PVC, glass, elastic fiber, nonwoven, and so on (Loupasaki & Diamadopoulos, 2013; Van Haandel et al., 2006; Wu et al., 2013). Wool felt is a natural porous and low-cost carrier. Nonetheless, to our knowledge, wool-felt carrier has not been used in anaerobic wastewater treatment.

In order to enhance performance of anaerobic process in treating decentralized domestic wastewater at low temperature, a novel anaerobic wool-felt filter reactor was designed as an alternative biotechnology for pre-treatment. Archaeal communities play an important role in organic matter removal. Molecular technologies including FISH, PCR-DGGE, and T-RFLP are effective to evaluate the major archaeal communities, but are inadequate to gain in-depth knowledge of archaeal communities (Ariesyady., 2007; Bandara., 2012; Lew., 2009). Unlike these molecular technologies, high-throughput MiSeq sequencing deeply reveals the structure of archaeal communities and the archaeal mechanism during the anaerobic operation.

The main objective of this study was to evaluate the performance of the anaerobic wool-felt filter reactor (AWFR) treating decentralized domestic wastewater in winter. Moreover, high-throughput MiSeq sequencing as a next generation sequencing tool was first conducted to investigate the archaeal communities in the AWFR system in winter.

## MATERIALS AND METHODS

**The AWFR System Configuration.** The AWFR consisted of Polyvinyl chloride polymer column with 50 L effective working volume packed with vertical wool felt carriers. The reactor was continuously fed with decentralized domestic wastewater via a peristaltic pump. The AWFR was operated in winter at an HRT of 3 days for 91 days. The temperature of the reactor ranged from 8 °C to 15 °C. The characteristic of the decentralized domestic wastewater was as follows: COD  $229 \pm 35$  mg/L, TP  $2.6 \pm 0.7$  mg/L, TN  $26.8 \pm 4.4$  mg/L, pH  $6.9 \pm 0.2$ . Seed anaerobic sludge was obtained from a municipal wastewater treatment plant in Wuxi, China. The concentration of total suspended solids (TSS) and volatile suspended solids (VSS) were 29.5 g/L and 16.8 g/L, respectively.

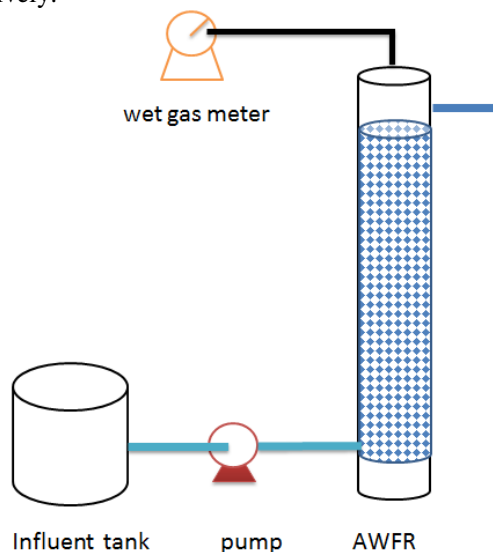


**FIGURE 1.** Schematic diagram of the experimental AWFR

**Chemical Analysis and Microbial Analysis.** Chemical oxygen demand (COD), total nitrogen (TN), total phosphorus (TP), total suspended solids (TSS) and volatile suspended solids (VSS) were measured according to the Standard Methods (APHA, 1998). Biogas production was measured using a wet gas meter. The volatile fatty acids were analyzed using gas chromatography GC3900 (Teng Hai, Shandong, China) equipped with a flame ionization detector. The pH was measured with a portable YSI-pH100 meter. Attached biofilm samples were collected from AWFR on day 10 and day 90. The V3-V4 region of archaeal 16S rRNA genes was amplified using primers 349F and 806R. The PCR products were cloned and sequenced by Illumina MiSeq System.

## RESULTS AND DISCUSSION

**Performance of the AWFR System.** The removal efficiency of COD, TN and TP are presented in Fig2a, b and c. Generally, the results indicated that the AWFR had a stable performance on organic matter degradation in winter with temperature ranged from 8 to 15 °C. Despite that the influent COD concentration ranged from 176 mg/L to 312 mg/L, the average effluent COD concentration was  $113 \pm 13$  mg/L, with a removal efficiency of  $49.5 \pm 5.7\%$  in winter. Compared to the previous study (Wu et al., 2013), the COD removal efficiency was greater, probably due to the higher activity of microorganism and the configuration of carrier in AWFR. These results were subject to confirmation by sequencing analysis. In addition, the influent concentration of TN and TP fluctuated from 20.4 mg/L to 35.7 mg/L, and 1.3 mg/L to 4.0 mg/L, respectively. The effluent TN concentration was slightly lower than influent, the average TN removal efficiency was  $13.8 \pm 4.0\%$ . The TN removal might be mainly attributed to microbial assimilation. Meanwhile, average TP removal efficiency was 18.6–6.7% throughout the whole operation. These findings were similar to previous study (Feng et al., 2008). Different with TN removal pathway, the mechanism of

TP removal might be related to biofilm adsorption and microbial assimilation. Obviously, the concentration of TN and TP effluent could not comply with discharge standards. Hence, future studies should focus on the post-treatment performance of the AWFR.

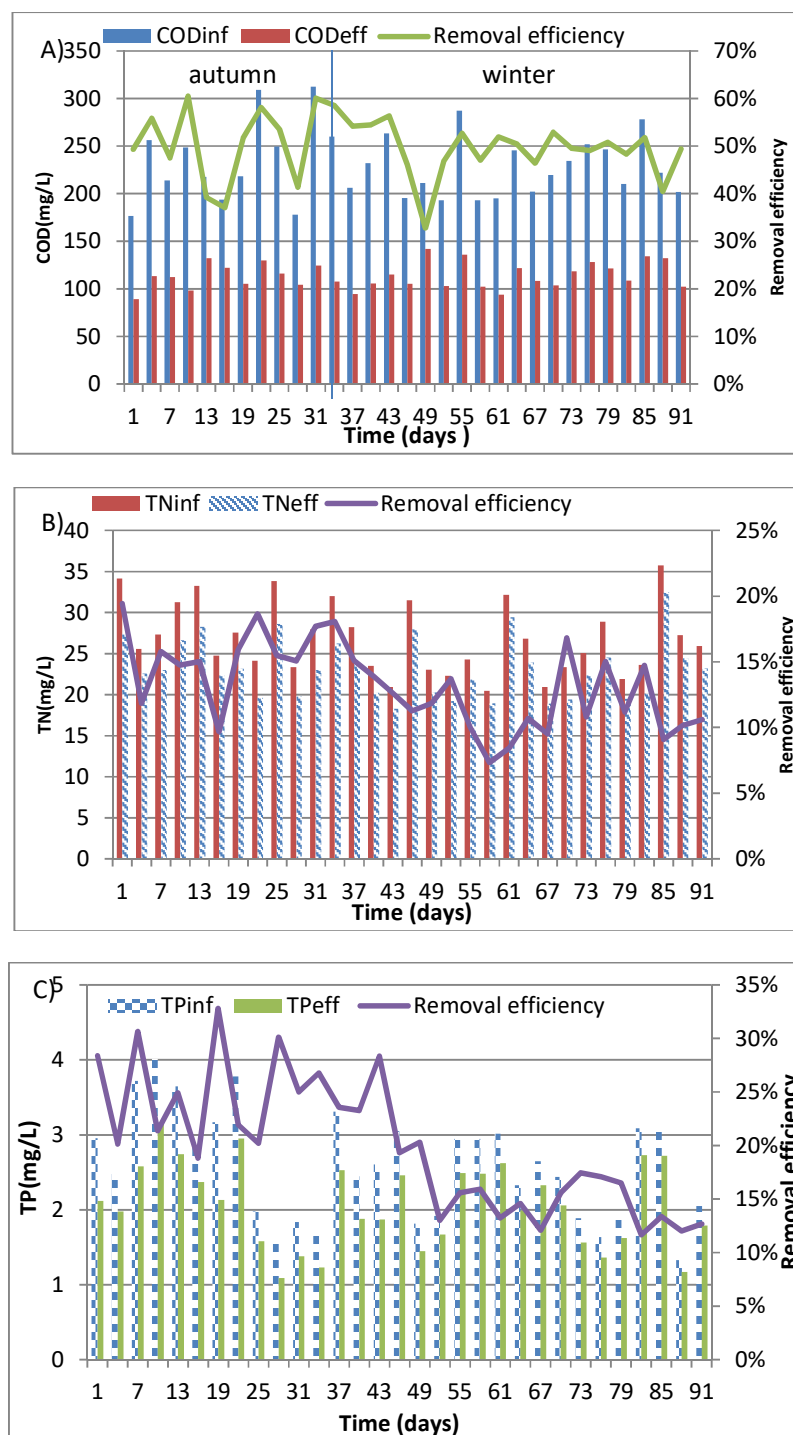


**FIGURE 2.** Variation of (A) COD, (B) TN, (C) TP and removal efficiencies

**VFAs and Biogas Production.** To evaluate the performance of AWFR in winter, VFAs and daily biogas production were to measure. As shown in Fig. 3a, acetate and propionate were the main components of the

effluent VFAs. It was observed that acetate and propionate increased from autumn to winter in response to a decreased in COD removal efficiency. Acetate and propionate accumulation results were also observed in previous study (Gao et al., 2014a). Meanwhile, the daily CH<sub>4</sub> production decreased from autumn to winter. This result was consistent with an increase in VFAs effluent. However, the average CH<sub>4</sub> production in winter was still  $876 \pm 418$  mL/d, whereas the average methane yield was 115 L/kg·CODremoval. Considering these findings, we postulated that low temperature might be responsible for the microbial activity and the production of biogas.

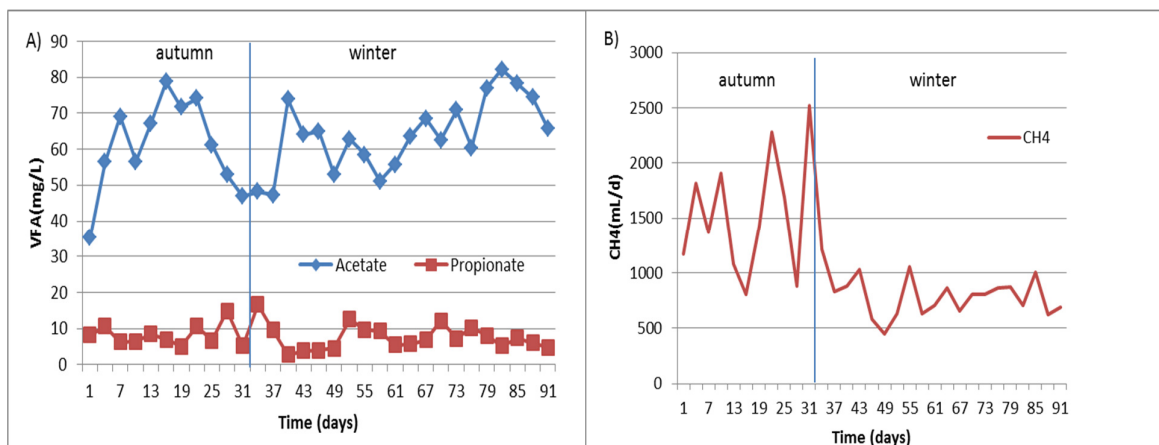


FIGURE 3. VFAs production (A) and daily CH<sub>4</sub> production (B) throughout the whole operation

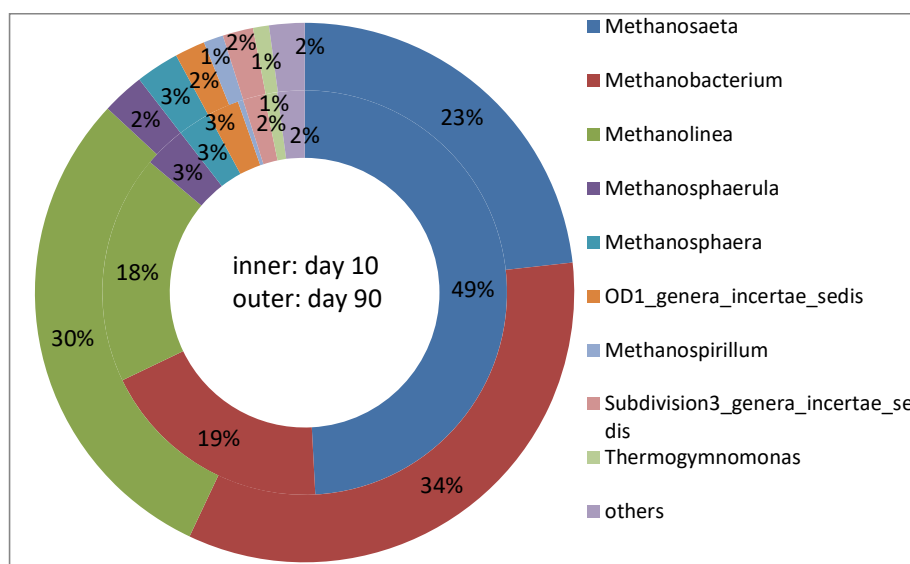


FIGURE 4. Archaeal community structures and compositions at genus level

**Diversity of Microbial Community in the AWFR System.** Microbial communities in the system are crucial for organic matter degradation. In order to get deep insight into the information of archaeal community structure, 16S rRNA gene PCR products were used for sequencing by Illumina MiSeq System (Fig. 4). The taxonomic classification of the samples was compared at order and genus levels. According to the RDP Classifier, the sequencing results showed that archaeal community had a lower diversity affiliated with three major orders (*Methanosarcinales*, *Methanobacteriales* and *Methanomicrobiales*). These findings are in agreement with previous studies (Bandara et al., 2012; Gomec et al., 2008). At genus

level, it was remarkably observed that the genus *Methanosaeta* (49%) played a crucial role in autumn. It was well-known that *Methanosaeta* affiliated with *Methanosarcinales* was a type of acetoclastic methanogene (Fey & Conrad, 2000). Unlike in autumn, the hydrogenotrophic *Methanobacterium* was the most dominated genus in winter (day 90), whereas *Methanolinea* affiliated with the order *Methanomicrobiales*, as a type of hydrogenotrophic methanogen, was the subdominant genus. These genera were also detected by previous studies (Bandara et al., 2012; Gomec et al., 2008). Difference with traditional PCR-DGGE technique, the genera *Methanosphaerula*, *Methanosphaera* and *Methanospirillum* were detected at low relative abundance. These findings indicated that hydrogenotrophic methanogenesis pathway play a key role for methane production in winter.

## CONCLUSIONS

The AWFR was achieved good performance in treating decentralized domestic wastewater with an HRT of 3 days. The results showed that removal efficiencies of COD, TN and TP  $49.5 \pm 5.7\%$ ,  $13.8 \pm 4.0\%$  and  $18.6 \pm 6.7\%$  were achieved, respectively. And the daily  $\text{CH}_4$  production was stable in winter. The hydrogenotrophic genera *Methanobacterium*, and *Methanolinea* had crucial functions in the conversion of organic matter to methane in winter. In addition, post-treatment is required to remove nutrients (N, P). Based on the study, AWFR has proved to be a sustainable option for pre-treatment decentralized domestic wastewater.

## ACKNOWLEDGEMENTS

This research was supported by China National Water Pollution Control and Management Technology Major Projects (2012ZX07101-005).

## REFERENCES

- Aiyuk, S., Forrez, I., van Haandel, A., Verstraete, W. 2006. "Anaerobic and complementary treatment of domestic sewage in regions with hot climates—A review". *Bioresour. Technol.* **97**(17), 2225-2241.
- APHA. 1998. Standard methods for the examination of water and wastewater. *Washington, DC*.
- Ariesyady, H.D., Ito, T., Okabe, S. 2007. "Functional bacterial and archaeal community structures of major trophic groups in a full-scale anaerobic sludge digester". *Water. Res.* **41**(7), 1554-1568.
- Bandara, W.M., Kindaichi, T., Satoh, H., Sasakawa, M., Nakahara, Y., Takahashi, M., Okabe, S. 2012. "Anaerobic treatment of municipal wastewater at ambient temperature: Analysis of archaeal community structure and recovery of dissolved methane". *Water. Res.* **46**(17), 5756-5764.
- Feng, H., Hu, L., Mahmood, Q., Qiu, C., Fang, C., Shen, D. 2008. "Anaerobic domestic wastewater treatment with bamboo carrier anaerobic baffled reactor". *Int. Biodeter. Biodegr.* **62**(3), 232-238.
- Fey, A., Conrad, R. 2000. "Effect of temperature on carbon and electron flow and on the archaeal community in methanogenic rice field soil". *Appl. Environ. Microbiol.* **66**(11), 4790-4797.
- Gao, D.-W., Hu, Q., Yao, C., Ren, N.-Q. 2014a. "ATreatment of domestic wastewater by an integrated anaerobic fluidized-bed membrane bioreactor under moderate to low temperature conditions". *Bioresour. Technol.* **159**, 193-198.
- Gomec, C.Y., Letsiou, I., Ozturk, I., Eroglu, V., Wilderer, P.A. 2008. "Identification of Archaeal population in the granular sludge of an UASB reactor treating sewage at low temperatures". *J. Environ. Sci. Health Part A.* **43**(13), 1504-1510.
- Lew, B., Lustig, I., Beliaevski, M., Tarre, S., Green, M. 2011. "An integrated UASB-sludge digester system for raw domestic wastewater treatment in temperate climates". *Bioresour. Technol.* **102**(7), 4921-4924.
- Lew, B., Tarre, S., Beliaevski, M., Green, M. 2009. "Anaerobic degradation pathway and kinetics of domestic wastewater at low temperatures". *Bioresour. Technol.* **100**(24), 6155-6162.
- Loupasaki, E., Diamadopoulos, E. 2013. "Attached growth systems for wastewater treatment in small and rural communities: a review". *J. Chem. Technol. Bio.* **88**(2), 190-204.
- Smith, A.L., Skerlos, S.J., Raskin, L. 2013. "Psychrophilic anaerobic membrane bioreactor treatment of domestic wastewater". *Water. Res.* **47**(4), 1655-1665.
- Sumino, H., Murota, R., Miyashita, A., Imachi, H., Ohashi, A., Harada, H., Syutsubo, K. 2012. "Treatment of low-strength wastewater in an anaerobic down-flow hanging sponge (AnDHS) reactor at low temperature". *J. Environ. Sci. Health Part A.* **47**(12), 1803-1808.

- Van Haandel, A., Kato, M.T., Cavalcanti, P.F., Florencio, L. 2006. "Anaerobic reactor design concepts for the treatment of domestic wastewater". *Rev. Environ. Sci. Biotechnol.***5**(1), 21-38.
- Wu, Y., Zhu, W., Lu, X. 2013. "Identifying key parameters in a novel multistep bio-ecological wastewater treatment process for rural areas". *Ecol. Eng.* **61**, 166-173.



## **A COMPARATIVE STUDY ON LIGHT GREY WATER FROM BUILDINGS WITH DIFFERENT FUNCTIONS**

Giresunlu, E., *Belér-Baykal, B.* and Afacan, E.  
(Istanbul Technical University, Istanbul, TURKEY)

**ABSTRACT:** Grey water is one of the streams generated upon segregation of domestic wastewater, originating mainly from various washing functions in the household and excludes toilet wastewater. It constitutes about three fourths of conventional domestic wastewater by volume, and may be returned to almost any point in the water cycle upon proper treatment. The need for characterization of this stream will become more obvious/critical, as grey water reuse becomes widespread. This work aims to contribute to grey water reuse by characterizing grey water collected from buildings with different functions but from similar sources/points of origin, i.e. wash basins, showers/bath tubs. Raw grey water characteristics in all three buildings were comparable to weak domestic wastewater or had better quality for physicochemical parameters. There were however differences in terms of quality when the three sources were compared. The highest pollution level was observed in the student residence hall (SRH) followed by the five-star hotel (FSH) and the university building (UB). The results of microbiological analyses revealed that grey water contains appreciable amounts of microbiological indicators. SRH had the highest pollution potential in terms of microbiological indicators, with comparable quality to weak domestic wastewater for total coliforms and to strong domestic wastewater for fecal coliforms.

### **INTRODUCTION**

Several domestic wastewater management approaches are being proposed for reusing domestic wastewater as a source rather than discarding it as a waste. One of those approaches is stream segregation, which is based on the separation of different domestic wastewater streams at their sources of generation. Grey water is one of the streams generated upon such segregation, originating mainly from various washing functions in the household. Actually it is the entire domestic wastewater with the exception of that which comes from toilets. It constitutes about three fourths of wastewater volume, with a lower pollution potential as compared to conventional domestic wastewater (Belér-Baykal, 2015). Grey water may further be categorized as light and dark grey water (Birks and Hills, 2007) based on the pollution potential of each sub-stream. Of those, light grey water is that part which comes from wash basins, showers and bath tubs.

Characterization of grey water is an important issue for its management and it will become more significant as grey water reuse becomes widespread. Depending on the function of the building from which grey water is collected and the specific source in the household it originates from, its characteristics may change considerably. Table 1 lists several pieces of work from literature focusing upon characteristics of light grey water originating from different types of buildings. A survey of the table reveals that the quality of grey water is variable even if it originates from exactly the same origin in the same type of buildings. As grey water contains about 40% of organic matter in domestic wastewater (Belér-Baykal, 2015), it is the pollutant studied the most in the literature. Moreover, due to their relatively low concentrations, nitrogen and phosphorus are not considered as problematic pollutants.

A survey of Table 1 reveals that more than half of the articles did not report microbiological indicators in untreated grey water. This is probably because the infection risk is generally attributed to fecal contamination, and grey water is segregated at the source without coming in contact with feces (Winblad et al., 2004). However, concentrations of the microbiological indicators reported in Table 1 show that grey water may contain those indicators at high levels, therefore they need to be controlled carefully when grey water reuse is intended.

As a considerable amount of organic matter is contained in grey water, the first consideration in treatment is to remove organics. Therefore, treatment systems with a biological treatment unit are generally preferred. Although after proper treatment grey water may be returned to almost any point in the water cycle, reclaimed grey water is most frequently used for toilet flushing and irrigation, in

**TABLE 1.** Characteristics of light grey water.

Source	Grey water fraction	Parameter	Concentration	Unit	Reference
Hotel	Bath/shower and wash basin	COD	171	mg/L	March et al. (2005)
		TSS	44	mg/L	
		TN	11.4	mg/L	
		Turbidity	20	NTU	
Hotel	Bath/shower and wash basin	COD	72.7±50	mg/L	Gual et al. (2008)
		TSS	32.2±7	mg/L	
		TN	4.1±2	mg/L	
		Turbidity	38.8±20	NTU	
Student residence hall	Bath/shower and wash basin	BOD	46.4±26.6	mg/L	Birks & Hills (2007)
		sBOD	31.2	mg/L	
		COD	96.3±52.6	mg/L	
		TSS	36.8±29.4	mg/L	
		TP	0.86±0.82	mg/L	
		TKN	4.6±2.8	mg/L	
		Turbidity	26.5±21	NTU	
		Total coliform	7.34	log <sub>10</sub> cfu/100 mL	
		E. coli	5.59	log <sub>10</sub> cfu/100 mL	
Student residence hall	Bath/shower and wash basin	Enterococci	3.40	log <sub>10</sub> cfu/100 mL	Friedler et al. (2008)
		BOD	95	mg/L	
		COD	270	mg/L	
		TSS	147	mg/L	
		TKN	11	mg/L	
Student residence hall	Bath/shower and wash basin	BOD	20	mg/L	Winward et al. (2008)
		COD	86	mg/L	
		TSS	29	mg/L	
		Total coliform	5.4±0.8	log <sub>10</sub> cfu/100 mL	
		E. coli	2.8±0.8	log <sub>10</sub> cfu/100 mL	
		Enterococci	2.8±0.9	log <sub>10</sub> cfu/100 mL	
Student residence hall	Bath/shower and wash basin	BOD	43.9±10.6	mg/L	Kadewa et al (2010)
		COD	151±88	mg/L	
		Turbidity	57.6±14.7	NTU	
University building	Wash basins	COD	248	mg/L	Sarioglu (2011)
		TSS	<10	mg/L	
		NH <sub>4</sub> -N	0.45	mg/L	
		Turbidity	12	NTU	

addition to uses such as car washing, groundwater recharge, fire extinguishing, etc. where the water does not need to be at the quality of drinking water.

This work aims to contribute to grey water reuse by characterizing grey water collected from buildings with different functions but from similar sources/points of origin, i.e light grey water. Within the context of this work, a five-star hotel (FSH) and a student residence hall (SRH) both collecting grey water from bathtubs, showers and wash-basins, and a university building (UB) collecting from wash-basins of restrooms were investigated. Characterization was made taking both physicochemical parameters (Chemical Oxygen Demand (COD), soluble COD, Biochemical Oxygen Demand (BOD), Total Suspended Solids (TSS), Volatile Suspended Solids (VSS), Ammonical-N (NH<sub>3</sub>-N), Total Kjeldahl Nitrogen (TKN), Orthophosphate (PO<sub>4</sub>-P) and Total Phosphorous (TP)) and microbiological indicators (Total Coliforms (TC), Fecal Coliforms (FC), E. coli (EC) and enterococci (ENT)) into account.

## MATERIALS AND METHODS

The five-star hotel and the student (girls) residence hall investigated collect their grey water from washbasins and showers/bathtubs. After proper treatment, treated grey water is reused for toilet flushing

and irrigation in the hotel, while it is reused for toilet flushing only in the student residence hall. The main treatment unit employed in both buildings is membrane bioreactors (MBR). Grey water samples were taken from the equalization tank, which are located before the MBRs, to characterize raw grey water quality.

On the other hand, in the university building, the grey water collection system is for research purposes only and the grey water is not reclaimed. Water generated at the lavatories' washbasins are collected in a tank, which also serves the purpose of equalization.

Sampling in the five-star hotel was done every-week throughout one year, while the student residence hall and the university building grey water were sampled every month, covering a complete academic year. Samples were taken as grab samples.

In terms of physicochemical parameters, samples were analyzed for organic matter through COD, sCOD and BOD and solid matter concentrations were determined using TSS and VSS.  $\text{NH}_3\text{-N}$ , TKN,  $\text{PO}_4\text{-P}$  and TP were the parameters analyzed for assessing the occurrence of nutrients. All physicochemical analyses were carried out according to APHA Standard Methods (Rice et al., 2012) except for COD and sCOD, as ISO 6060 method was used for these analyses.

Microbiological quality was analyzed in terms of total coliforms and fecal coliforms, as these indicator groups have been used conventionally over the past years. Additionally, *E. coli* and enterococci were also monitored since they were identified as indicators which had a better correlation to occurrence of diseases (USEPA, 1986; WHO, 1999). ISO 8199 was the method used for all microbiological analyses. All analyses were carried out with three different dilutions and in triplicate.

## RESULTS AND DISCUSSION

The results obtained in this work for physicochemical parameters are summarized in Figure 1 and Table 2, and for microbiological indicators in Figure 2.

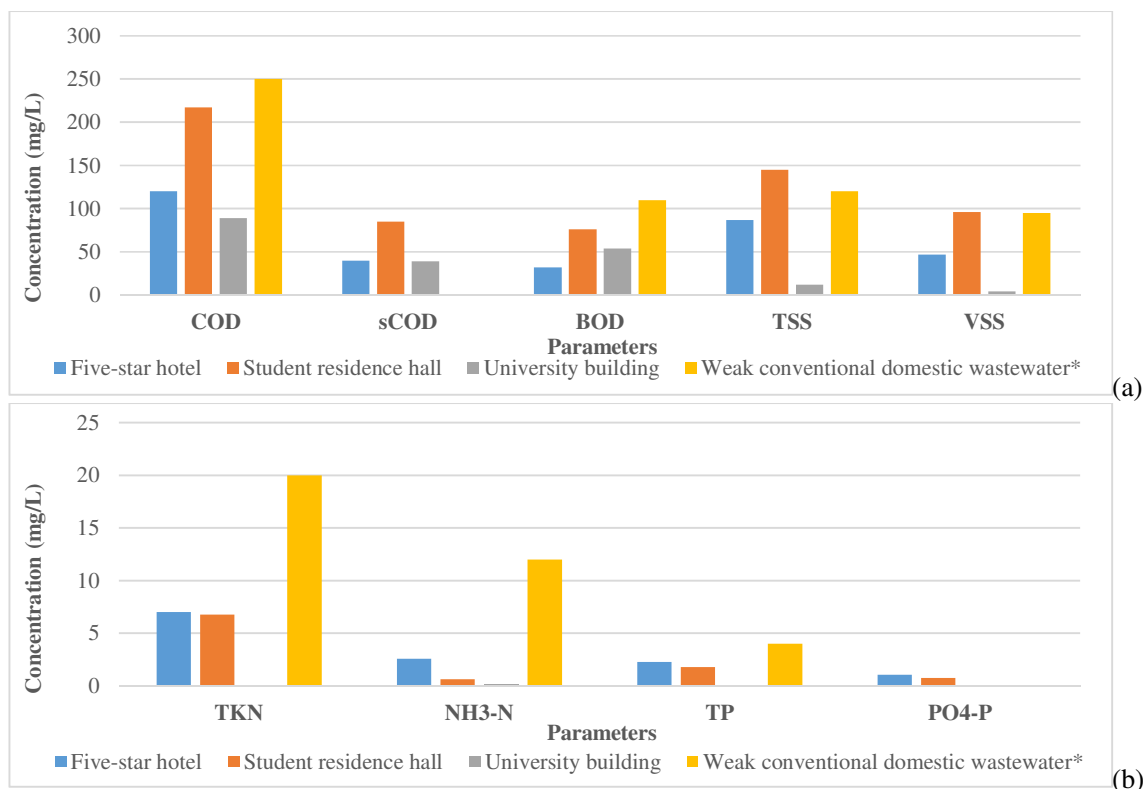
The average concentrations of organic matter and solid matter are shown in Figure 1-a, together with their counterparts for weak conventional domestic wastewater quality as given by Metcalf & Eddy (2003). Average BOD was less than 110 mg/l in all cases indicating that all three buildings showed lower pollution potential in terms of organic matter as compared to weak conventional domestic wastewater, with only one value exceeding this concentration. The lowest pollution potential in terms of solid matter was observed for the university building and it was followed by the five-star hotel, both lower as compared to the typical values for weak conventional domestic wastewater. However, the student residence hall showed somewhat lower quality in terms of solids as compared to weak conventional domestic wastewater.

Figure 1-b, showing the average nutrient concentrations in grey water samples in terms of TKN,  $\text{NH}_3\text{-N}$ , TP and  $\text{PO}_4\text{-P}$ , reveals that nutrients in all of the grey water samples were at a level much lower than weak conventional domestic wastewater. As observed from both Table 2 and Figure 1-b, the highest TKN and TP average concentrations were calculated for the hotel grey water, as 6.99 and 2.29 mg/L.

All in all, analysis of the results of physicochemical parameters has revealed that raw grey water characteristics in all three buildings were comparable to weak domestic wastewater or had better quality as can be observed from Figure 1. Moreover, priority components in this group were organic matter and solids. Specifically, solid concentration for grey water treatment is important as one of the most used systems for grey water reclamation employs membranes, as in the case of two of the buildings studied, which tend to be clogged very fast if the suspended solid concentrations are high.

There were however differences in terms of quality when the three sources were compared, as summarized in Table 2. The highest concentrations in terms of the parameters representing the priority components organic matter and solids was observed in the student residence hall followed by the five-star hotel and the university building. Organic matter concentrations were the highest in the student residence hall with averages as 217 mg/l COD, 76 mg/l BOD, followed by the five-star hotel with 120 mg/l COD, 32 mg/l BOD, which was about half of that of student residence hall, although both buildings collected from the same sources. The university building had lower values, 89 mg/l COD, 54 mg/l BOD, which was expected, because the source of grey water was wash-basins only.

The analyses showed that the highest TSS and VSS concentrations were observed in the student residence hall with 145 and 96 mg/L, respectively, similar to the organic matter.



**FIGURE 5.** Average concentrations in terms of (a) organic matter and solid concentrations and (b) nutrients, as compared to typical concentrations of weak conventional domestic wastewater.  
\*Metcalf & Eddy, 2003

concentrations. The five-star hotel was the second most polluted grey water source in terms of TSS and VSS concentrations as 87 and 47 mg/L, respectively. Solid concentrations in university building were very low, as shown in Table 2.

The highest pollution potential regarding organic matter and solids were thus observed in the student residence hall. This could be attributed to occasional food washes and dish-washing practiced in wash-basins together with concentrated personal care products use/activities in the girls' residence hall.

A survey of the BOD/COD ratios showing the tendency towards biodegradation and sCOD/COD ratios as an indicator of particulate fraction reveals that the organic matter in grey water was mostly non-biodegradable or slowly biodegradable and in particulate form in the five-star hotel (35%, 39%) and in the student residence hall (26%, 33%). Based on these results, the option of membrane filtration could also be evaluated in favor of leaving out the biological step, with low values of BOD and particulate organics predominating solid matter, especially in the five-star hotel.

Data regarding microbiological quality were limited in comparison to physicochemical parameters, nevertheless they are plotted in Figure 2. Microbiological analyses were carried out using three samples for five-star hotel, four samples for student residence hall and three samples for university building, all worked in sets of triplicates. The results however were supported by another project undertaken in the same hotel (Beler-Baykal, 2014).

The results of the microbiological analyses showed that grey water collected from the student residence hall had the highest pollution potential with mean concentrations of 7.18 log<sub>10</sub> cfu/100 mL of total coliform, 6.95 log<sub>10</sub> cfu/100 mL of fecal coliform, 6.92 log<sub>10</sub> cfu/100 mL of *E. coli* and 4.16 log<sub>10</sub> cfu/100 mL of enterococci. Five-star hotel grey water had lower pollution potential as compared to student residence hall. Grey water from the university building showed the lowest pollution potential in terms of all microbiological indicators. The only source free of enterococci was the five-star hotel. The characteristic microbiological indicator concentrations for conventional domestic wastewater are given in Table 2. A comparison with these values reveals that the average concentrations of total coliforms in the five-star hotel and the university building were comparable to weak domestic wastewater characteristics. On the other

hand, university building samples showed lower concentrations as compared to weak domestic wastewater. In terms of fecal coliforms, the five-star hotel and the student residence hall grey water were comparable to strong conventional domestic wastewater. In this case, the university building grey water was comparable to weak domestic wastewater.

**TABLE 2.** Results of physicochemical analyses (n: sample number)

Location	Five-star hotel				Student residence hall				University building			
Parameters (mg/L)	min	max	avg	n	min	max	avg	n	min	max	avg	n
COD	30	710	<b>120</b>	41	99	598	<b>217</b>	8	38	121	<b>89</b>	7
sCOD	30	125	<b>40</b>	37	59	94	<b>85</b>	5	30	57	<b>39</b>	7
BOD	8	82	<b>32</b>	35	54	124	<b>76</b>	7	19	78	<b>54</b>	5
TSS	16	838	<b>87</b>	41	44	328	<b>145</b>	8	4	18	<b>12</b>	7
VSS	9	376	<b>47</b>	40	4	216	<b>96</b>	8	0	7	<b>4</b>	7
TKN	2.11	35.65	<b>6.99</b>	36	4.05	16.89	<b>6.76</b>	8	-	-	<b>-</b>	0
NH <sub>3</sub> -N	0.58	5.55	<b>2.58</b>	36	0	0.86	<b>0.62</b>	8	0.04	0.21	<b>0.14</b>	7
TP	0.73	8.35	<b>2.29</b>	36	1.35	2.17	<b>1.78</b>	8	-	-	<b>-</b>	0
PO <sub>4</sub> -P	0	4.01	<b>1.05</b>	36	0.27	1.19	<b>0.75</b>	8	0	0.01	<b>0</b>	7

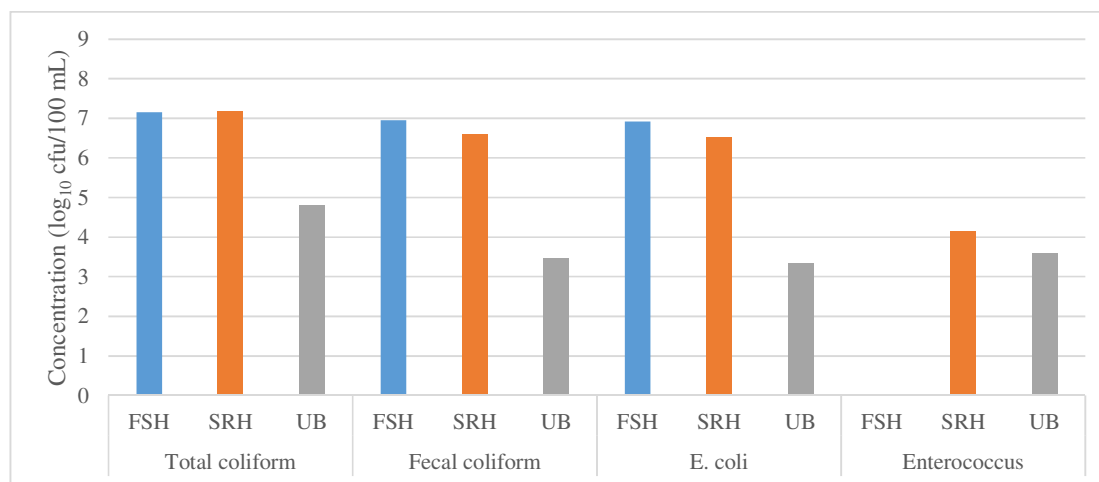


**FIGURE 6.** Average concentrations of microbiological indicators.

A comparison with the literature values listed in Table 1 reveals that, COD and TN values in the hotel grey water in this work falls within the range of values reported, whereas the average concentration of TSS in this study is almost twice as high as the ones listed. Student residence hall grey water falls within the range reported in the literature in terms of organics and nitrogen, while TSS concentration is comparable and TP concentration is higher in this study as compared to those reported. University building grey water showed lower or comparable concentrations as compared to its counterpart given in the table. Microbiological indicators were investigated in only two pieces of work reported in Table 1, and both of them concentrated on student residence hall grey water. Values obtained in this work for the student residence hall were higher as compared to the literature data. Moreover, hotel grey water showed lower quality in terms of all indicators tested. The university building grey water showed higher concentrations in terms of total coliforms, while showing better quality in terms of E. coli and enterococcus. These differences show that even if the function of the buildings where grey water is collected from and the source of grey water are the same with those in the literature, the quality of grey water may change significantly.

The data obtained in this work has revealed that light grey water quality tends to show variations according to the function of the building where it is collected, even if the sources of collection are the same. Characterization of the specific grey water to be reclaimed may play a major role in the selection of grey water reclamation schemes.

**TABLE 2.** Microbiological indicator concentrations in domestic wastewater (Metcalf & Eddy, 2003)

	Weak	Intermediate	Strong
Total coliform (log <sub>10</sub> cfu/100 mL)	6-8	7-9	8-10
Fecal coliform (log <sub>10</sub> cfu/100 mL)	3-5	4-6	5-8

## CONCLUSION

Raw grey water in all three buildings showed characteristics comparable to weak domestic wastewater or had better quality in terms of physicochemical parameters. Organic matter concentrations were lower than typical values for weak domestic wastewater, while solids were comparable or better. All sources showed similar characteristics in terms of nutrients, which were considerably lower as compared to weak domestic wastewater.

On the other hand, although all are light grey water, the three sources showed different quality when compared to each other. Student residence hall has shown the highest pollution potential in terms of organic matter and solids and it was followed by the five-star hotel and the university building respectively.

The results of the analyses showed that the larger fraction of organic matter was in particulate form, and the average BOD concentrations were low, which raises the question whether a biological unit should be employed or not.

Even though the physicochemical parameters showed low pollution potential, the amount of microbiological indicators were appreciable. Total coliform concentrations were comparable to the typical values of weak domestic wastewater, while the fecal coliform concentrations could go as high as strong domestic wastewater. Therefore, microbiological indicators should not be overlooked while reusing grey water, to sustain public health.

In summary, the results of this work have revealed that even if the origins of the grey water are the same in terms of the source where they are collected, the quality of grey water may change significantly depending upon the function of the buildings. Characterization of the specific grey water to be processed is crucial in determining the reclamation scheme.

## REFERENCES

- Beler-Baykal, B. 2014. Atiksularin akimlarina ayrilmasi ve gri su geri kazanimi (Stream segregation and grey water reclamation) in Turkish, online at <http://www.csb.gov.tr/db/tay/webmenu/webmenu13378.pdf>
- Beler-Baykal, B. 2015. "Stream segregation in household use: A review of grey water as an alternative source of water and yellow water as an alternative source of fertilizers", *Water Quality Exposure and Health*, 7(1), 27-37.
- Birks, R. and Hills, S. 2007. "Characterization of indicator organisms and pathogens in domestic greywater for recycling." *Environmental Monitoring and Assessment*, 126, 61-69.
- Friedler, E. and Alfiya, Y. 2010. "Physicochemical treatment of office and public buildings greywater." *Water Science and Technology*, 62(10), 2357-2363.
- Gual, M., Moia, A. and March, J.G. 2008. "Monitoring of an indoor plant for osmosis rejection and greywater reuse to flush toilets in a hotel." *Desalination*, 219(2008), 81-88.
- ISO 6060:1989 "Water quality – Determination of the chemical oxygen demand"
- ISO 8199:005 "Water quality -- General guidance on numeration of microorganisms by culture with membrane filtration"
- Kadewa, W.W., Le Corre, K., Pidou, M., Jeffrey, P.J. and Jefferson, B. 2010. "Comparison of grey water treatment performance by a cascading sand filter and a constructed wetland." *Water Science and Technology*, 62(7), 1471-1478.
- March, J.G., Gual, M. and Ramonell, J. 2005. "A kinetic model for chlorine composition in grey water." *Desalination*, 181(2005), 267-273.
- Metcalf & Eddy. 2003. *Wastewater engineering treatment and reuse* 4th ed., McGraw Hill, New York, NY, USA.
- Rice, E. W., Bridgewater, L., Water Environment Federation, American Water Works Association, and American Public Health Association. 2012. *Standard methods for the examination of water and wastewater* (22nd 2012 ed.). Washington, D.C: American Public Health Association.

- Sarioglu, S. 2011. *Low load greywater and municipal wastewater treatment by membrane bioreactor*. M.S. Thesis, Institute of Environmental Sciences, Bogazici University.
- USEPA. 1986. *Ambient Water Quality Criteria for Bacteria*.
- Winblad, U., Simpson-Hérbert, M., Calvert, P. & Stockholm Environment Institute. 2004. *Ecological sanitation*, 2., rev. and enlarg ed, Stockholm Environment Institute Stockholm, Stockholm.
- WHO. 1999. *Health-based monitoring of recreational water: The feasibility of a new approach* (The Annapolis Protocol). Geneva, Switzerland.
- Winward, G.P., Avery, L.M., Frazer-Williams, R., Pidou, M., Jeffrey, P., Stephenson, T. and Jefferson, B. 2008. "A study of the microbial quality of grey water and an evaluation of treatment technologies for reuse." *Ecological Engineering*, 32, 187-197.

## A PILOT-SCALE STUDY OF A MODIFIED WASTEWATER TREATMENT WITH SLUDGE REDUCTION EFFECT

Chenyi Shi, Yushan Wang, Xiang Wei, Wuzhen Guo, Meishan Lin, Jinxin Tan, and Lianpeng Sun.  
(Sun Yat-Sen University, Guangzhou 510275, Guangdong, China)

**ABSTRACT:** The MOSA (Modified Oxidic-Settling-Anaerobic) process generates less excess sludge during the process of wastewater treatment, but many studies on the MOSA process are undertaken at the laboratory scale or based on synthetic wastewater, which are not sufficient for practical application or to achieve ideal sludge reduction. A 10-m<sup>3</sup>/d pilot-scale system was established to treat municipal sewage. The A/O process and the A/O-MOSA process were performed in sequence to study the sludge reduction efficiency of the MOSA process by comparing the effluent quality and the sludge yield of the two processes. The study indicated that, compared with the separate A/O process, the A/O-MOSA process achieved a 35% sludge reduction without any influence on the effluence properties, but resulted in a small increase in the total phosphorus (TP) concentration. After adding Al<sub>2</sub>(SO<sub>4</sub>)<sub>3</sub> into the aerobic basin, the TP concentration in the effluent can be kept under 1.0mg/L while simultaneously achieving a 33% sludge reduction. The results indicate the good stability and sludge reduction efficiency of the MOSA process.

### INTRODUCTION

The Oxidic-Settling-Anaerobic (OSA) process inserts an anaerobic reactor between the aeration basin and secondary settling basin, exhibits excellent performance in sludge reduction. Subsequently, many researchers have further studied the OSA process and have obtained good results in reducing excess sludge (Chen et al., 2003; Novak et al., 2007; Wu et al., 2013; Sun et al., 2015), highlighting the representative mechanisms of excess sludge reduction, such as energy uncoupling and sludge decay (Chen et al., 2003), extracellular polymeric substances and metal complex degradation (Novak et al., 2007). Tan and Sun established a modified Oxidic-Settling-Anaerobic (MOSA) process by changing the sludge interchange rate and mode (Tan, 2014). Many studies on MOSA have been undertaken at the laboratory scale and not sufficient for practical application or to achieve ideal sludge reduction. Therefore, this study was undertaken at the pilot scale using municipal sewage and aimed at evaluating the performance of sludge reduction and the effluent properties of the MOSA process to lay a foundation for applying the MOSA process at full scale.

### MATERIALS AND METHODS

Based on the A/O process in the municipal wastewater treatment plant (WWTP) in Zhenan, Foshan, China, which treats 100000 m<sup>3</sup> of wastewater every day, this A/O-MOSA pilot-scale system was operated in the same manner as the A/O process in the plant. For this system, the hydraulic retention time (HRT) of the anaerobic and aerobic basins was 1.35h and 5.05h, respectively, while the sludge concentration was in the range of 2000 to 3500 mg/L and the dissolved oxygen (DO) was between 2.0-4.0 mg/L. Figure 1 schematizes the 10-m<sup>3</sup>/d pilot system based on the MOSA process, with a sludge retention time (SRT) of 5d and an interchange

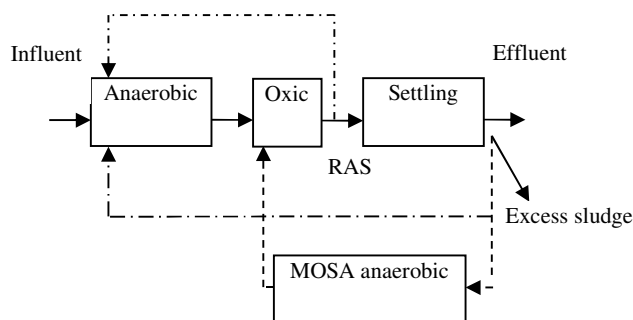


FIGURE 1. Schematic diagram of the A/O-MOSA process



rate (IR) of 10%. The system was operated at 4 cycles. The sludge was pumped into the MOSA reactor from the secondary settling tank of the A/O process and then flowed into an oxic tank. The amount of wasted sludge was calculated according to the growth of the sludge in the oxic tank. This system has been steadily operated for 212 days (A/O process was applied for the first 60 days, the A/O-MOSA process was applied for the next 130 days, and the last 22 days were used for the chemical phosphorus removal experiment under the A/O-MOSA system.) After a 2-week sludge cultivation under anaerobic conditions, the MOSA reactor was started and inserted into the A/O process, which formed the complete A/O-MOSA system. The data were collected in periods from the 61th to 90th, 156th to 190th, and 191th to 212th day, which were denoted as A/O-MOSA I, A/O-MOSA II, and A/O-MOSA III, respectively. For the 91th ~115th day, the influent properties fluctuated because of equipment failure in the pilot-scale system and maintenance of the WWTP. The temperature for the A/O and A/O-MOSA I period was 26-33°C, while that for the A/O and A/O-MOSA I periods was 14-20°C. All of the quality parameters were measured according to the Standard Methods (State Environmental Protection Administration of China, 2002).

## RESULTS AND DISCUSSION

Before and after starting the MOSA reactor, the removal effects of COD and SS are shown in Figure 2 and Figure 3. We can observe that the system had a high efficiency for the removal of COD and SS. During the operation of the A/O process, the average removal rates of COD was 79.1%. And 82.6% in A/O-MOSA I, 77.1% in A/O-MOSA II. There was no significant difference in the removal rate of organic matter in various stages. Switching in the MOSA anaerobic tank had no adverse effects on the A/O process; the MOSA anaerobic still retained a higher removal rate for organic matter.

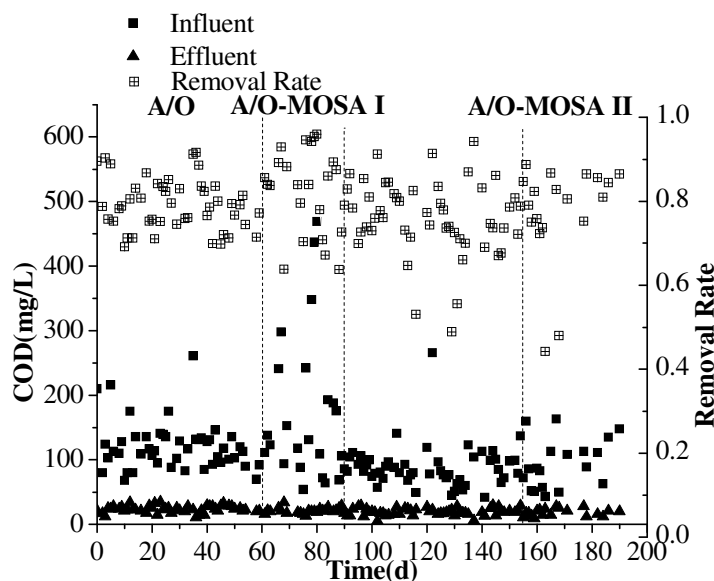


FIGURE2. COD removal rate over the entire operational period

From Figure 3, the removal rate of SS was found to be elementarily unanimous, the SS of the effluent remained at 13~17 mg/L. The average removal rate of SS was 75.1%; and 78.3% and 82.8% in the A/O-MOSA I and A/O-MOSA II system, respectively. In this research, the insertion of the MOSA anaerobic reactor improved the treatment efficiency of the effluent SS.

The removal of  $\text{NH}_4\text{-N}$  and TN in the system is shown in Figure 4 and Figure 5. From Figure 4, starting the MOSA reactor did not negatively impact the removal of  $\text{NH}_4\text{-N}$ . In the entire experimental stage, the concentration of  $\text{NH}_4\text{-N}$  in the effluent was under 0.6 mg/L, and the removal rate reached 97.8%. The system had a good removal efficiency for  $\text{NH}_4\text{-N}$ .

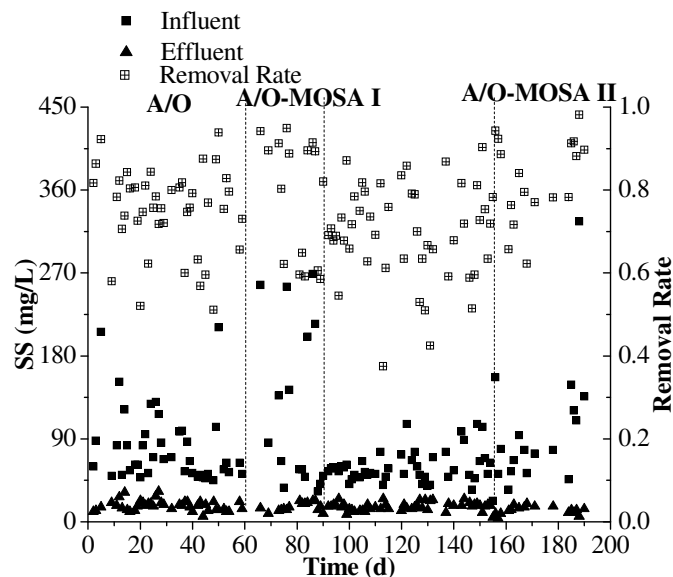


FIGURE 3. SS removal rate over the entire operation period

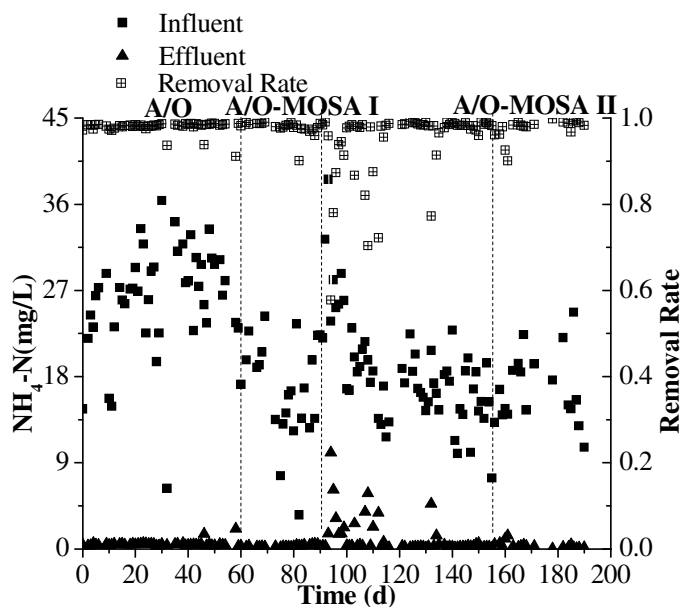


FIGURE 4.  $\text{NH}_4\text{-N}$  removal rate over the entire operational period

From Figure 5, we can see that the average removal rates of TN in A/O, A/O-MOSA I and A/O-MOSA II were 33.4%, 38.2% and 30.4%, respectively. Compared to A/O, after inserting the MOSA reactor, the removal efficiency of TN exhibited a trend from increasing to decreasing. The main reasons for this behavior were as follows: (1) In the A/O process, C/N is required to be as high as 8.0 (Rasool et al., 2014). In this study, C/N in A/O, A/O-MOSA I, and A/O-MOSA II was 3.0, 7.5, and 4.0. In A/O MOSA I, the greatest carbon source was found, contributing to the best denitrification effect. (2) The optimum temperature of denitrification is 20~35°C (Ma, et al., 2008). During the period of operation of the A/O and A/O-MOSA I systems, the temperature was 26~33°C, which is in the range of the most suitable temperature for denitrification. In the A/O-MOSA II operation period, the temperature was 14~22°C, which affected the

denitrification rate, resulting in the decrease of the TN removal efficiency. The removal of phosphorus in this system is shown in Figure 6. During the effective operation of the system, the effluent TP removal rate was only 26.7%. Both the A/O and A/O-MOSA processes had an undesirable TP removal effect, and inserting the MOSA anaerobic reactor resulted in a further decrease of the TP removal efficiency. The primary reasons for the observed behavior were as follows: (1) The SS concentration in the effluent was high and the average concentration was 17mg/L, directly leading to the poor dephosphorization effect. (2)Lack of carbon source. Wentzel et al. (1991) believed that to remove 1.0 mg of phosphorus requires 7.5~10.7 mg of COD of VFAs. During the operational period, the average concentrations of influent of COD were 130mg/L (3)In the course of system operation, the average concentration of  $\text{NO}_3^-$  in the returned sludge reached 7.4mg/L, the PAOs could not become the dominant bacteria; as a result, the biological phosphorus removal process was restricted. (4) The sludge that entered into the MOSA anaerobic reactor released plenty of phosphorus in the anaerobic condition, and the soluble TP in the exchanged sludge was as high as 70 mg/L, which increased the TP load in the process and impacted the process. In addition, the A/O-MOSA system had a lower sludge yield, which reduced the discharge of excess sludge, indirectly leading to the extension of SRT. Consequently, the phosphorus in the system could not be discharged in time.

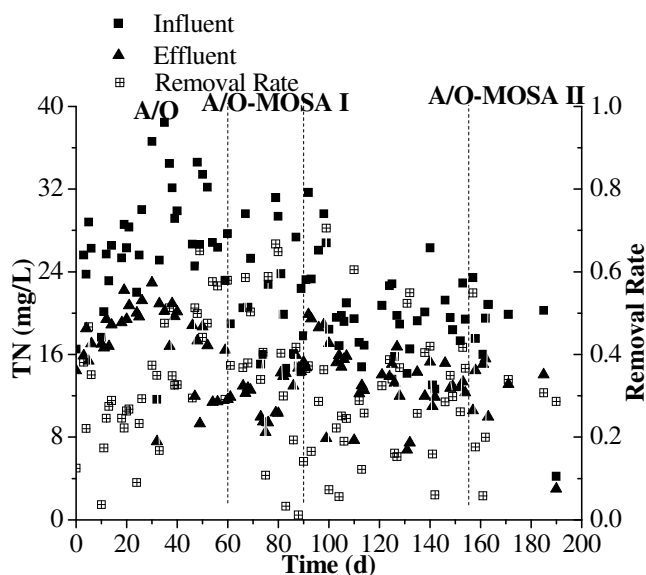


FIGURE 5. TN removal rate over the entire operational period

To improve the TP removal effect in the effluent for the A/O-MOSA system, this experiment added chemical agents to intensify phosphorus removal. From the 36th day in the A/O-MOSA II operation (A/O-MOSA III stage), we added an  $\text{Al}_2(\text{SO}_4)_3$  solution to the tail end of the aerobic tank and the continuous run for 22 days.. The TP changes in A/O-MOSA III operational period is shown in Figure 7. Figure 7 shows that in the A/O-MOSA III stage, the average concentration of the influent TP was 1.90mg/L, while the effluent TP was 0.57mg/L, with an average removal rate of 61.0%.

The apparent sludge yield is calculated by the type 1 equation(Tan, 2014):

$$Y_{\text{obs}} = \frac{(MLSS_2 - MLSS_1) \times V_a + W}{\sum_{i=1}^n (COD_1 - COD_2) \times Q} \quad (1)$$

The  $Y_{\text{obs}}$  of A/O, A/O-MOSA I, A/O-MOSA II and A/O-MOSA III were 0.244, 0.152, 0.167 and 0.165 kg-MLSS/kg-COD, respectively. Therefore, the sludge reduction effect of A/O-MOSA I, A/O-MOSA II and A/O-MOSA III was 38%, 32% and 33%, respectively. The average sludge reduction effect was 35%. The sludge reduction effect of A/O-MOSA II was relatively lower, and the primary cause was the impact from the temperature reduction. Zhang et al.(2006) found that improving the temperature was beneficial to the sludge reduction effect in the OSA process. Before and after using the chemical phosphorus

removal method, the sludge reduction effects exhibited no significant differences. Chemical phosphorus removal had no adverse effects on the sludge reduction effect in the A/O-MOSA process.

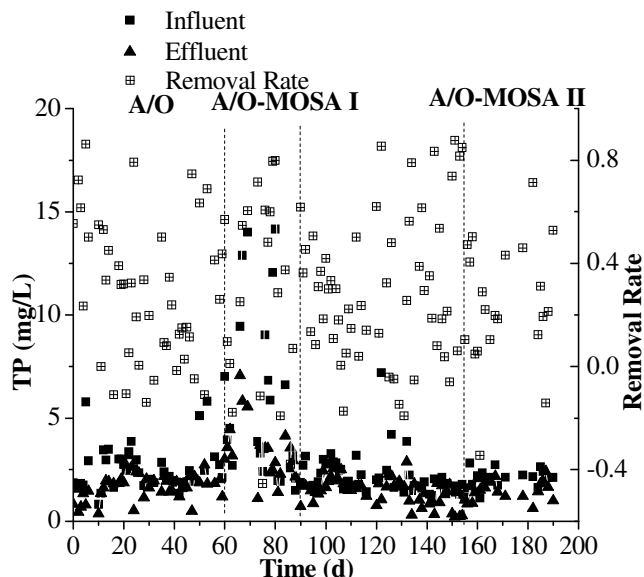


FIGURE6. TP removal rate over the entire operational period

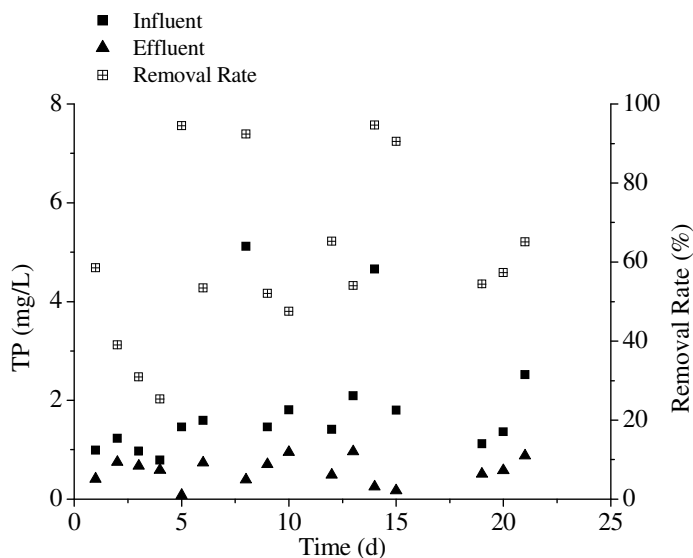


FIGURE7. TP removal rate using the chemical phosphorus removal method

## CONCLUSIONS

This research is based on a practical system and established a 10-m<sup>3</sup>/d A/O-MOSA pilot-scale model using actual sewage and involves a multi-stage comparison study. The experimental conclusions were as follows:

(1) In the experimental process, no significant changes for each indicator in the effluent were found, except for TP. The insertion of the MOSA anaerobic reactor did not cause an obviously negative impact on the original technology.

(2) Chemical phosphorus removal through the addition of  $Al_2(SO_4)_3$  solved the problem of the MOSA process: a poor removal efficiency for TP, which could reduce the level of TP in the effluent to

below 1.0mg/L. Compared with the A/O process, the A/O-MOSA process provided a favorable sludge reduction effect, with a sludge reduction rate of 35%. Meanwhile, adding a chemical phosphorus removal step did not negatively influence the sludge reduction, with the sludge reduction rate remaining high at 33%.

#### ACKNOWLEDGEMENTS

This work is supported by the Science & Research Program of Guangdong (Contract No. 2012A032300005), the Science & Research Development Program of Foshan (2012AA100091)

#### REFERENCES

- Chen, G. H., An, K. J., Saby, S., et al., 2003. Possible cause of excess sludge reduction in an oxic-settling-anaerobic activated sludge process (OSA process). *Water Res.* 37(16), 3855-3866.
- Ma, J., Peng, Y. Z., Wang, L., Wang, et al., 2008. Effect of temperature on denitrification and profiles of pH during the process. *China Environ. Sci.* 28 (11), 1004-1008. (in Chinese).
- Novak, J. T., Chon, D. H., Curtis, B. A., et al., 2007. Biological solids reduction using the Cannibal process. *Water Environ. Res.* 79(12), 2380-2386.
- State Environmental Protection Administration of China. 2002. Standard Methods for the Examination of Water and Waste Water (Fourth Version), *Environmental Science publication* in China, Beijing. (in Chinese).
- Sun, L. P., Chen, J. F., Guo, W. Z., et al., 2015. Study of the sludge reduction in an oxic-settling-anaerobic activated sludge process based on UNITANK. *Water Sci. Technol.* 71 (1), 111-116.
- Tan, J. X. *A pilot-scale study of sludge reduction in a modified Oxic-Settling-Anaerobic (MOSA) process based on A/O*. 2014. Master Dissertation, Sun Yat-sen University, Guangzhou, China. (in Chinese).
- Wang, L. K., Zeng, G. M., Yang, Z. H., et al., 2014. Operation of partial nitrification to nitrite of landfill leachate and its performance with respect to different oxygen conditions. *Biochem. Eng. J.* 87,62-68.
- Wentzel, M. C., Lotter, L. H., Ekama, G. A., et al., 1991. Evaluation of biochemical models for biological excess phosphorus removal. *Water Sci. Technol.* 23(4-6), 567-576.
- Wu, K., Li, S. Y., Jiang, F., Wang, G. J., et al., 2013. A new oxic-settling-anaerobic (NOSA®) activated sludge process for minimizing excess sludge in secondary biological treatment plants: a pilot-scale evaluation of the absorption-biodegradation process. *Water Sci. Technol.* 68(3), 530-536.
- Zhang, B., Ji, F. Y., Guan C., et al., 2006. Research on municipal wastewater sludge reduction in OSA process and its influencing factors. *Journal of Chongqing Jianzhu University.* (01), 92-95. (in Chinese).

**DISSOLVED METHANE RECOVERY FROM ANAEROBIC ATTACHED GROWTH  
REACTOR TREATING SYNTHETIC DOMESTIC WASTEWATER**

**Brian Crone** and George Sorial (University of Cincinnati, Cincinnati, OH, USA)  
Jay Garland (United States Environmental Protection Agency, Cincinnati, OH, USA)

Anaerobic treatment processes have the potential to be energy neutral or energy producing when treating Domestic Wastewater. To date the largest barrier to this accomplishment has been the loss of between 10-100% of the potential energy in the form of dissolved methane in the effluent. The magnitude of potential energy loss is dependent on process temperature and configuration. For this study a novel reactor design that combines anaerobic attached growth processes and non-porous hollow fiber degassing membranes for treatment synthetic domestic waste water and simultaneous recovery of dissolved methane will be evaluated. Biomass will be cultured directly on membrane fibers which have been functionalized to improve bacterial and archaeal adhesion and which will be evacuated using a vacuum pump. Direct culturing on the degassing membrane will allow for removal of biogas constituents into the lumen of the hollow fibers as constituents are produced and before they can diffuse into the bulk solution. Removal of dissolved carbon dioxide will decrease carbonic acid concentrations and the need for additional alkalinity. This will improve process stability and reduce operating costs. Biogas recovery will also provide thermodynamically favorable conditions for Chemical Oxygen Demand (COD) removal by maintaining low hydrogen and methane partial pressures. It is postulated that the combination of the anaerobic biological treatment and physical degassing into a single reactor will reduce capital and operating costs while achieving efficient treatment efficiencies and high potential energy recovery.

## **A NOVEL AND COST-EFFECTIVE SEWAGE TREATMENT PROCESS WITH ENERGY RECOVERY AND AUTOTROPHIC NITROGEN REMOVAL**

**Dawen Gao**

(Northeast Forestry University, Harbin 150040, China)

A system combined an upflow anaerobic fixed bed (UAFB) and an expanded granular sludge bed (EGSB) was designed and verified as a success for treating real sewage with simultaneous energy recovery and autotrophic nitrogen removal. The effects of the temperature and HRT on the combined system were investigated. The impact of temperature (stepwise decreased from 30°C to 20°C and 10°C) was a primary focus, aiming to reveal the response of the anaerobic digestion (AD) and anammox efficiency to the temperature variation. As the temperature decreases, the sCOD removal rate was 90.6%, 90.0% and 84.7% respectively; TN removal was 69.4%, 48.8 %, 38.4% respectively;  $\text{NH}_4^+\text{-N}$  removal was 91.3%, 74.9%, 65.1% respectively. Methanogenic activity of UAFB was significantly influenced by low temperatures, while the unavoidable growth of heterotrophic organisms in EGSB also contributed to the sCOD removal by utilizing a certain amount of VFAs, even at 10°C. Lower working temperature (10/20°C) limited the growth and activity of AOB and anammox bacteria, but improved the NOB activity. Shorting HRT reduced the COD removal, but the effluent COD was still less than 50 mg/L. When decreasing HRT from 4 h to 2 h, the ammonia removal changed from 88.7% to 66.2%, but the reactor recovered and run stably with increasing HRT to 4 h. Compared with  $\text{A}^2\text{/O}$  wastewater treatment process, the integrated sewage treatment process could decrease the construction investment cost by 52.1%, cut down the floor space by more than 90% and save the running expense by 14.9% annually. At the same time, the economic value created by using methane into electric power generation and sewage recycling was about 20.5% running cost.

## ENRICHMENT OF DENITRIFYING METHANOTROPHIC BACTERIA OF THE NC10 PHYLUM FROM ACTIVATED SLUDGE

**Shubham Singh** and Jih-Gaw Lin  
(National Chiao Tung University, Taiwan)

Anaerobic treatment processes in wastewater treatment industries discharge methane in gaseous as well as in aqueous form. Methane is considered a powerful greenhouse gas that has a global warming potential 25 times greater than carbon dioxide over a 100-year period. While methane in the gaseous phase can be easily collected and purified, dissolved methane is difficult to recover. Therefore, a post-treatment process is needed in anaerobic systems to oxidize dissolved methane, thereby reducing greenhouse gas emissions and making anaerobic wastewater treatment a more eco-friendly technology. Nitrite dependent denitrifying anaerobic methane oxidation (N-Damo) is a novel process for simultaneous carbon and nitrogen removal. This process is assigned to a methanotroph that has been identified as a member of the phylum NC 10 and named “*Candidatus Methyloirabilis oxyfera (M. oxyfera)*”. This bacterium utilizes methane as electron donor as well as carbon source and nitrite as electron acceptor to oxidize methane into carbon dioxide. In this study, we are enriching the denitrifying methanotrophic bacteria of the NC10 Phylum (*M. oxyfera*) by using activated sludge from Xin-Feng wastewater treatment plant, Taiwan as inoculum. A 3 L bioreactor (working volume 2.5 L) was setup and has been in operation in sequencing batch mode for better biomass retention with a hydraulic retention time (HRT) of 10 days. For the first 34 days, the reactor was operated at ambient temperature (19-26°C) and after day 35 temperature was controlled at 30°C. The pH is also controlled between 7-7.5 manually by adding 1 M HCl. Temperature, pH, alkalinity, oxidation-reduction potential (ORP) and dissolved oxygen (DO) are continuously monitored. Nitrite loading rate (NiLR), nitrate loading rate (NaLR) and total nitrogen loading rate are 2.1 mg NO<sub>2</sub><sup>-</sup> -N L<sup>-1</sup> d<sup>-1</sup>, 2 mg NO<sub>3</sub><sup>-</sup> -N L<sup>-1</sup> d<sup>-1</sup>, and 4.1 mg N L<sup>-1</sup> d<sup>-1</sup> respectively. From day 7 onwards, both nitrite and nitrate are completely removed in the effluent. Since day 34, reactor temperature was changed to 30°C and agitation was reduced to 50 RPM from 100 RPM. There was a sudden drop in ORP after adjusting temperature and agitation speed, and nitrate removal efficiency was also decreased from 100% to 75%. It took another 5 days to reach nitrate removal efficiency to its original value. After day 39, total nitrogen removal was 4.1 mg N L<sup>-1</sup> d<sup>-1</sup>. From day 65, improved medium was provided, which also caused some turbulence in removal efficiency but recovered to stable state by day 76. So far by our knowledge, this is the fastest cultivated and acclimated n-damo of the NC10 Phylum. In the future we plan to increase the total nitrogen rate exponentially and will monitor the subsequent removal efficiency.



## SURFACE ENGINEERED GREEN POLYMER FOR ENHANCED WATER DECONTAMINATION

Gurpreet Kaur Khaira and **Moushumi Ghosh\***

(Department of Biotechnology, Thapar University, Patiala-147004, Punjab, India)

\*Email: mghosh@thapar.edu

**ABSTRACT:** We report the microbicidal activity of an exopolymer produced by *Klebsiella terrigena* and attributes for disinfection of water. The exopolymer possessed an intrinsic ability to rapidly bind waterborne pathogens due to surface structure through quaternization. The latter could significantly ( $p < 0.05$ ) bind and inactivate key water borne pathogens-*Salmonella typhimurium*, *Shigella flexneri* 2a, *Aeromonas hydrophila*, *Yersinia enterocolitica*, *Listeria monocytogenes* and *Escherichia coli* O157:H7 ATCC to an order of 4 log at ambient temperature over a period of 30 minutes. Physical and chemical analysis revealed that the quaternized biopolymer possessed total sugar and total protein content of 66.8% and 2.45% (w/w), uronic acid (2.83%) and pyruvic acid (7.4%) attributable to acidic polysaccharide. The 'surface engineered' or quaternized biopolymer or green polymer exhibited high polydispersity index, stability over wide pH (5-9) and temperature range (25-45°C) as well as low dosage requirement and safety demonstrable from animal studies. These results suggest a potential of this biomaterial for affording water hygiene through water disinfection and a future scope for development of the biopolymer based sensors for determining the extent of decontamination achieved.

**Keywords:** biofloculants, cell membrane, water borne pathogens, *K. terrigena*, quaternization, water borne pathogens

### 1. INTRODUCTION

The quality of water has been strongly recognized as an indicator of socio-economic development. This is because the quality of water, whether used for drinking or domestic purposes, food production or recreational purposes has an important impact on health. Water of poor quality can cause disease outbreaks and can contribute to background rates of disease manifesting themselves on different time scales. Waterborne pathogens present a formidable threat to water; these pathogens include various types of bacteria, protozoan parasites, viruses and other microorganisms (Cabral 2010). Surface and groundwater, both are contaminated by bacteria and viruses, whereas parasitic protozoa appear predominantly in surface water. Their entry into drinking water occurs upon contamination of the water source by sewage and animal waste, or when wells are not properly sealed or constructed.

Waterborne pathogenic bacteria are extremely adept in acquiring resistance to conventionally used synthetic disinfectants for rendering water potable. Disinfectants derived from natural molecules are currently envisioned as promising futuristic options for water treatment since they do not induce resistance and are completely non-toxic to human. Surface modification of non-toxic, biodegradable, and environment friendly microbial extracellular polymers containing amino groups can lead to an effective and safe substitute to chemical biocides as the cationic biopolymers containing quaternary ammonium groups have gained wide attention in the recent years (Kurane et al., 1986; Siedenbiedel and Tiller, 2012, Tan et al., 2013). The role and subsequent importance of quaternary ammonium compounds (QACs) as membrane-active agents with a target site, predominantly at the cytoplasmic (inner) membrane in bacteria or the plasma membrane (Tan et al., 2013) is well established.

Chitosan have been modified through various techniques, the intensive methylation of chitosan generates the N,N,N-trimethyl derivative, characterized by possessing positive charges in chains as a consequence of the quaternization of the amino groups in the C-2 position of the chitosan structure (Sieval et al., 1998). Quaternized chitosan is a water-soluble polyelectrolyte with enhanced antibacterial activity

used in various biomedical applications. The activity in these polymers is described as the result of ionic interaction between chitosan positive charges and the negatively charged cell surface of bacteria. Polysaccharide microbial polymers with similar structures to chitosan can be chemically modified in order to enhance or impart specific properties. The biopolymeric derivatives can be synthesized by either covalent addition of a substituent containing a quaternary ammonium group, or by quaternization of the amino groups of the parent polymer (Britto et al., 2011). It is the latter method which has received most attention with alkylation agents such as alkyl halide which is usually employed.

The biopolymer produced by *Klebsiella terrigena* has been reported in previous studies to be effective in removal of *Cryptosporidium* oocysts and *Salmonella* (Ghosh et al., 2009a,b) by flocculation. In an attempt to endow antibacterial functions we chemically altered the surface properties of a biopolymeric flocculant produced by *K. terrigena* and chitosan for the sake of comparison. Alteration were brought about in the native biopolymers through quaternization, and the trimethyl biopolymeric derivatives (N,N,N trimethyl biopolymer and N,N,N trimethyl chitosan, abbreviated as TMB and TMC, respectively) were investigated for their antibacterial activity against the major water borne pathogens. Fourier transform infrared (FT-IR) absorbance spectroscopy (in the mid-IR range, usually defined as 4000-400cm<sup>-1</sup> or 2500-25000nm) has sufficient resolution to distinguish intact microbial cells at the strain level. The resulting spectra for microbial cells represent the “total” biochemical composition of those cells. FTIR spectroscopy measures vibrations of functional groups and highly polar bonds. Therefore spectral features of many important biochemical constituents create a “fingerprint” for a bacterial strain. The importance of FT-IR spectroscopy as a physicochemical method to determine the global chemical features of cells suggests its adequacy to study the molecular changes after treatment with antibacterial agents (Ashtiani et al., 2009). The present study reports the development of biopolymeric flocculant with antibacterial activity with a view to enhance the scope of applicability of the bioflocculant as a natural antibacterial agent for water treatment.

## MATERIALS AND METHODS

All chemicals were purchased from Sigma chemicals company (Sigma, Mo, USA). All other reagents were of the highest grade available commercially.

### Biopolymer Producing Strain and Indicator Strains

**Biopolymer producing strain.** An industrial wastewater isolate, *Klebsiella terrigena* (Accession number EU082029), was used in this study (Ghosh et al., 2009a,b). The amino rich biopolymer producing strain was preserved in glycerol stock solutions at -80°C. The strain was revived in LB agar plate and incubated overnight at 37°C and a single colony was picked and transferred in FIB broth and was grown to mid log phase at 37°C.

**Indicator strains.** For testing the antibacterial activity of antibacterial polymer(s), selected bacterial strains, *Salmonella typhimurium* ATCC 25315, *Shigella flexneri* Type 2a, *Aeromonas hydrophila* ATCC 35654, *Yersinia enterocolitica* ATCC 9610, *Listeria monocytogenes* ATCC19111 and *Escherichia Coli* O157:H7 ATCC 32150 were maintained in Tryptone Soy Broth (TSB) with 2% glycerol and stored at 4°C. The cultures were revived in Brain Heart Infusion (BHI) agar plate and incubated overnight at 37°C. Prior to the experiments, single colonies were picked and transferred in BHI broth which was incubated for 18-24h at 37°C.

**Biopolymer Production.** Cells were removed from the culture medium by centrifugation and the biopolymer was separated by the addition of two volumes of ethanol (99.5%) to 500mL of concentrated supernatant, and allowed to precipitate at 40°C for 24hr. The precipitated polymer was collected by filtration (Whatman GF Filter) and dialyzed extensively using dialysis tubing (Cellulose, MWCO 12000 Da), against deionized water. Crude biopolymer was purified by addition of a 10% solution of cetylpyridinium chloride. The precipitated polymer complex was collected by centrifugation at 10,000rpm for 20min at 4°C and redissolved in 10% NaCl solution. Three volumes of ethanol were added to recover the purified biopolymer, which was further dialyzed and lyophilized to powder and stored until further use (Ghosh et al., 2009a,b).

**Synthesis and Characterization of N, N, N Trimethyl Biopolymeric Derivative (TMB).** Purified biopolymer (150mg) was dissolved in dimethylsulfate (2.4mL) and deionized water (0.6mL). The solution was then filtered to eliminate the impurities. Sodium hydroxide (0.18mg) and sodium chloride (0.132mg)

were added to the resulting suspension, followed by stirring the solution at ambient temperature for six hours. The product was precipitated using acetone, filtered and vacuum dried. White precipitates obtained were redissolved in deionized water (20mL) and subjected to dialysis using a dialysis membrane for one day. Dialyzed solution was then lyophilized to get white fluffy powder (4.5mg) (Belalia et al., 2008).

NMR analysis is as follows that  $^1\text{H}$  NMR spectra of biopolymer and N, N, N-trimethyl derivative (TMB) was recorded using Bruker Avance II (400 MHz) spectrometer. For this analysis, samples were dissolved in  $\text{D}_2\text{O}$ .

**Evaluation of Flocculating Activity.** TMB was evaluated for its ability to flocculate suspended solids of varied size; the native biopolymer was used as a comparison. A standard solution of suspended solids of 2000 NTU was made by suspending active carbon, silica, magnesium hydroxide, cellulose and yeast in 100mL water. A bacterial suspension of 2000 NTU was also used for this study. A suspension of desired turbidity was prepared by diluting the suspension from stock to desired turbidity with a turbidimeter (Cyber Scan TBDIR1000 Meter, Eutech, Netherlands). An assay was performed by adding 10mL  $\text{CaCl}_2$  (5mM), 0.5mL biopolymer (2mg/l) and 9.5mL of distilled water to 80mL of these solutions. The pH was adjusted to  $7 \pm 0.2$  and the solutions were allowed to stand at room temperature for 5min. 20mL of aliquots were withdrawn from the upper phase and its turbidity was measured. Its flocculating activity was calculated by recording its optical density with a spectrophotometer at 550nm. Flocculating activity of purified biopolymer and TMB in water was measured against distilled water as control according to method of Kurane et al., (1986). Activity (%) was defined and calculated as  $(B-A)/B \times 100$ . The activity was expressed as the mean value from duplicate determinations.

**Determination of Antibacterial Activity.** The antibacterial activity of biopolymeric derivative was determined against the six selected pathogenic cultures. Prior to experiments, the respective cultures were revived in BHI broth by incubating at  $37^\circ\text{C}$  for 18hr. For a preliminary screening uniform sized discs prepared from whatman filter paper were soaked in sterile solution of  $100\mu\text{g/ml}$  of each native biopolymer and TMB, placed on the assay plate containing  $100\mu\text{l}$  of culture on BHI broth. All plates were incubated at  $37^\circ\text{C}$  for 12 hr, after which the diameters of inhibition zones were observed. The experiments were performed in triplicates.

**Killing kinetics:** Antibacterial activity of TMB was assayed by microdilution method, using a sterile 96 well-microtiter plate (Raafat et al., 2008). Briefly, serial twofold dilutions of TMB solutions were prepared in the appropriate culture medium in sterile 96-well round bottom polystyrene microtiter plates (Bioscreen C, Thermolab systems, Helsinki, Finland). Final TMB concentrations used were  $1-100\mu\text{g/ml}$ . Minimal inhibitory concentration (MIC) was determined by microtiter broth dilution method (Andrews 2001). The indicator bacterial pathogenic cultures were grown in the respective broth at  $37^\circ\text{C}$  to an optical density of 1 at 600nm and subsequently diluted in the same medium to about  $10^7\text{CFU/ml}$ . The solution of biopolymer and TMB were added, and their inhibitory effect was observed. Each well of the microtiter plate then received  $100\mu\text{L}$  of the inoculated medium, and the plates were incubated at  $37^\circ\text{C}$  for up to 24hr. MIC was defined as the lowest concentration of compound required to completely inhibit microbial growth after incubation. The MIC determinations were carried out in triplicates, with two independent experiments performed. The surviving  $\log_{10}\text{CFU/ml}$  was recorded against time for each of the different quaternized biopolymer concentrations.

## Leakage Assays

**Preparation of washed cell suspensions.** Pregrown bacterial cells were separated by centrifugation at  $11,000 \times g$  for 10min from the culture medium (BHI). Cell pellets were washed in 10mM PBS (pH 7.0) and diluted with the same buffer to approximately  $10^7\text{CFU/ml}$  at an absorbance (OD 600nm) of 1.

**Leakage of glucose, lactate dehydrogenase (LDH) and protein from treated bacterial cells.** To examine the effect of quaternized derivative on cell leakage and the viability of the indicator strain, inoculum of the test organism (1ml) was inoculated into sterile deionized water (10ml) with or without quaternized derivative in a culture tube. The mixture, containing water-soluble biopolymeric derivative (TMB) and indicator cultures were incubated at  $37^\circ\text{C}$  with shaking (120rpm) for 12h. At regular interval of 1h, aliquots were withdrawn for determination of protein and glucose contents and lactate dehydrogenase (LDH) activity. The cell suspension was centrifuged at  $8,000 \times g$  for 15min, and the supernatant was

measured for LDH activity, protein and glucose contents. The glucose content was analyzed by a glucose assay kit (DiaSys Diagnostic Systems GmbH, Holzheim, Germany). A sample or glucose standard (0.0–3.0mg/dl, 200µl) was added to reagent (1ml) containing glucose dehydrogenase. After incubation at 25°C for 15min, the absorbance at 334 nm was recorded. The LDH activity was analyzed by an LDH assay kit (Clontech, USA). A 200µl sample was added to 1ml reagent containing NADH and incubated at 25°C. LDH activity was then determined by measuring the rate of decrease of the NADH concentration which was monitored by recording the change of absorbance at 334nm. The protein concentration was measured by absorbance at 280nm.

**Extraction and FT-IR Analysis of Lipopolysaccharides (LPS) of Target Pathogen.** Lipopolysaccharide from the pathogen treated with quaternized derivatives and control cells was extracted by hot phenol-water method as described by Westphal and Jann, (1965) with some modifications. In brief, bacterial suspensions ( $10^8$  CFU/ml) were centrifuged at  $10,000 \times g$  for 5min. The pellets were washed twice in PBS (pH=7.2) (0.15M) containing 0.15mM  $\text{CaCl}_2$  and 0.5mM  $\text{MgCl}_2$ . Pellets were then re-suspended in 10ml PBS and sonicated for 10min on ice. In order to eliminate contaminating protein and nucleic acids, treatment with proteinase K, DNase and RNase was performed prior to extraction step. For this purpose, proteinase K (100µg/ml) (Roche, Mannheim, Germany) was added to the cell mixture and the tubes were kept at 65°C for an additional hour. Mixture was subsequently treated with RNase (40µg/ml) (Roche, Mannheim, Germany) and DNase (20µg/ml) (Roche, Mannheim, Germany) in the presence of 1µl/ml 20%  $\text{MgSO}_4$  and 4µl/ml chloroform and incubation was continued at 37°C overnight. At the next step, an equal volume of hot (65–70°C) 90% phenol was added to the mixtures followed by vigorous shaking at 65–70°C for 15min. Suspensions were then cooled on ice, transferred to 1.5ml polypropylene tubes and centrifuged at  $8500 \times g$  for 15min. Supernatants were transferred to 15ml conical centrifuge tubes and phenol phases were re-extracted by 300µl distilled water. Sodium acetate at 0.5M final concentration and 10 volumes of 95% ethanol were added to the extracts and samples were stored at –20°C overnight in order to precipitate LPS. Tubes were then centrifuged at  $2000 \times g$ , 4°C for 10min and the pellets were re-suspended in 1ml distilled water. Extensive dialysis against double distilled water at 4°C was carried out at the next step until the residual phenol in the aqueous phases was totally eliminated. Final purified LPS product was lyophilized and stored at 4°C.

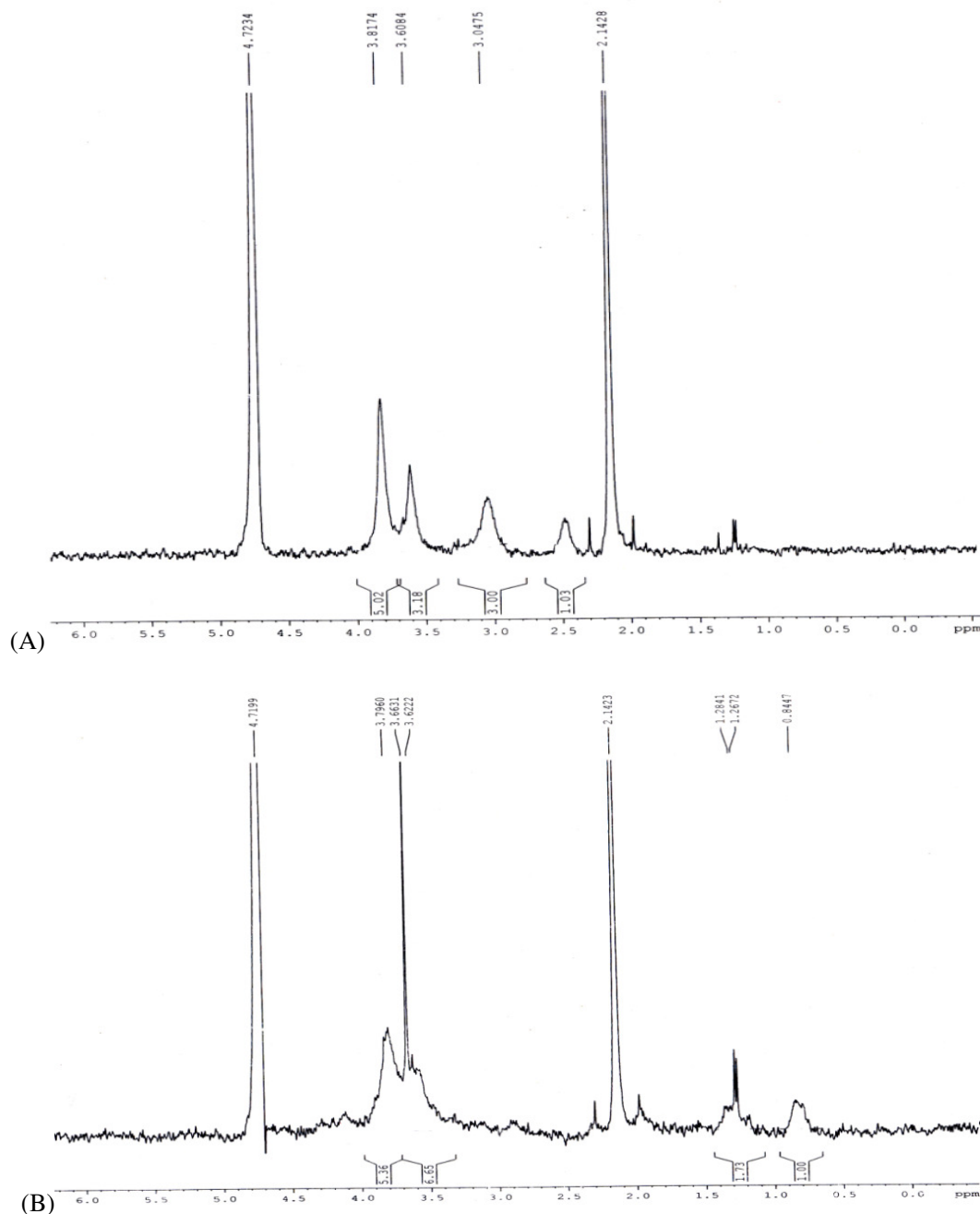
LPS were analyzed by Nicolet magma, FTIR spectrometer equipped with a Maillard-I-Alanine doped deuterated triglycine sulphate (DLA TGS) detector using KBr pellets. To prevent absorption from ambient, the system was purged with dry nitrogen. For each spectrum, 64 scans were co-added at spectral resolution of  $4\text{cm}^{-1}$ . The spectra covered the wave number ranging from  $4000\text{--}400\text{cm}^{-1}$  frequencies for all sharp bands were determined accurately from the original baseline corrected spectra of corresponding group using a software OPUS (version 6.5). The different FT-IR spectra graphs were drawn by origin software (version 6.0).

**Electron Microscopy.** Indicator pathogenic cells treated with TMB as described above were used to visualize structural damage, following 20, 40 and 60 minutes of incubation; the cells were washed twice with phosphate buffer saline (PBS) and fixed in a fixative (2% glutaraldehyde, 2% paraformaldehyde, and 0.5%  $\text{CaCl}_2$  in 0.1M cacodylate buffer). Samples were post fixed in 1.33% osmium tetroxide, dehydrated in graded ethanol and infiltrated with a 1:1 mixture of propylene oxide. For SEM, cells were sputtered with a 300Å thick layer of gold using an ion coater and examined in a scanning electron microscope (JSM-7100F, JEOL, Japan).

## RESULTS AND DISCUSSION

**Synthesis and Characterization of Quaternized Biopolymeric Derivative(s).** Amino group present in the polysaccharide backbone of the bioflocculant were transformed into quaternary ammonium compounds synthetically so that the polymer that could effectively bind, would also be able to inactivate the water borne pathogen simultaneously. Methylation is an effective approach in quaternization of polymers. Synthesis of trimethyl biopolymeric derivatives leads to methylation of the amino groups in the C-2 position of biopolymer to form quaternary amino groups with fixed positive charges on the repeating units of the quaternized polymer chain. Also the advantage of introducing methyl groups at different levels on the

polymeric backbone can be controlled externally with ease. Quaternization process using either dimethyl sulphate have been well documented for obtaining quaternary ammonium compounds of chitosan (de Britto et al., 2007; Belalia et al., 2008; Tan et al., 2013). Thus, the suitability and applicability of the same was attempted in case of the selected biopolymeric flocculant in the present study.



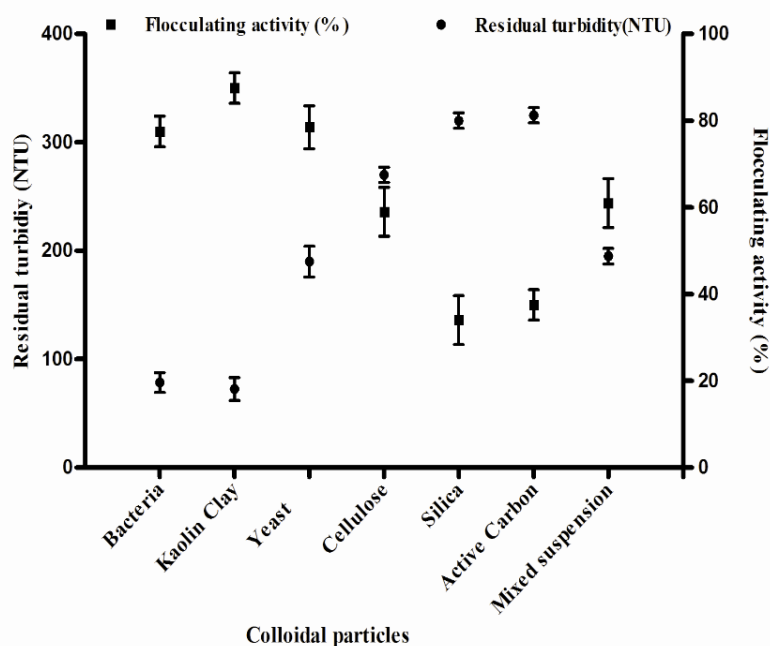
**Fig. 1.**  $^1\text{H}$  NMR spectrum of biopolymer (A) and TMB (B) dissolved in  $\text{D}_2\text{O}$ .

Fig. 1 depicts the  $^1\text{H}$ -NMR spectra of the biopolymer and quaternized biopolymer (TMB), respectively. The spectra revealed an intense signal at 3.66 ppm corresponding to the trimethylammonium group. Sieval et al. (1998) indicated the peak at 3.6 ppm is assigned to the trimethyl amino group, the peak at 3.1 ppm is assigned to dimethyl amino groups and the peaks between 4.7 and 5.7 ppm are assigned to  $^1\text{H}$

protons. As evident from the enlargement of the peak at 3.6 ppm, a longer reaction time resulted in an increase in the degree of quaternization of the polymer.

**Flocculating Efficiency of the Quaternized Biopolymer.** Results revealed that TMB aggregated a wide range of colloidal particles, over concentrations of 2-10ppm. As illustrated in Fig. 2, the most effective flocculation was achieved in suspensions comprising very low and low sized particles at even low concentration of the biopolymer. Whereas the efficacy of flocculation of suspension of medium sized particles ranged from 30-40% that too at relatively higher concentration of 8-10ppm of the biopolymer. The suspensions of large sized particles showed 50-65% flocculant activity at the same concentration range that flocculated in the range of 70-90% in case of low and very low sized particle suspension. This might be due to non-uniform distribution of pore size on the biopolymer surface; also the number of sites available for binding low and very low sized particles might be more than that of binding medium and large sized particles. However, large variations in the degree of flocculation were observed, where the kaolin particles (size $\sim$ 2 $\mu$ ) showed highest flocculating activity (90%). The quaternized biopolymer was found to have good flocculating activity against bacteria ( $\sim$ 0.5-0.8 $\mu$ m) similar to its native counterpart.

This phenomenon might be due to the increase of polymer and particle complexes that start to form and the maximum removal of turbidity is at the dosage value when almost all polymer sites are occupied by the particles. Beyond that optimum dosage value, the turbidity removal decreases probably due to lack of polymer sites for interaction with the colloidal particles. The flocculant dosage leading to the maximum flocculation efficiency value is considered as optimal dosage value. The mechanism of the flocculation with TMB may be explained by a combination of charge neutralization and polymer bridging.



**Fig. 2.** Efficiency of removal of varied size colloidal particles in solution applied with different doses of TMB and native biopolymer ranging from 2ppm-10ppm. The corresponding size of the particles are following [ $\sim$ 0.5-0.8 $\mu$ m (bacterial cell suspension),  $\sim$ 4-7 $\mu$ m (Kaolin, yeast cell suspension, cellulose),  $\sim$ 15-20 $\mu$ m (silica),  $\sim$ 100 $\mu$ m (Active carbon)]

**Biocidal Activity of Quaternized Biopolymeric Flocculant Against Pathogens.** The antibacterial activity of biopolymer and TMB was assessed thereafter against the respective pathogens by observing the zone of inhibitions and determining MICs. Results obtained by the agar disc diffusion assay of the quaternized biopolymer indicated a strong inhibition by TMB, the native biopolymer failed to inhibit (data not shown). The orders of zone of inhibition with TMB were found to be *Salmonella* > *Shigella* > *Aeromonas* > *Yersinia* > *E.coli* 0157:H7 > *Listeria*. The gram-positive *Listeria* was inhibited the least by both the quaternized derivatives. TMB significantly ( $p < 0.05$ ) inhibited the growth of the pathogens in 60 to 90 minutes at

concentrations ranging from 50 to 100µg/ml. The effect of TMB on the pathogens is shown in Table 1(a) where a reduction of 4 log CFU/ml was evident after 60-70min of treatment and the respective MIC values are depicted in Table 1(b). The higher antibacterial activity of quaternized biopolymeric derivative could be due to the permanent positive charges on the quaternized biopolymeric flocculant chain, as a consequence of the quaternization of the amino groups. The activity resulted from the interaction between the positively charged amino groups of the biopolymer and negatively charged cell surface of gram negative bacteria and also due to the flocculant activity of the biopolymer.

**Table. 1(a)** Killing kinetics for BF (Bioflocculant), N,N,N- trimethyl biopolymer, (TMB), chitosan and N,N,N-trimethyl chitosan, (TMC) against indicator waterborne pathogens. Each value is expressed as mean  $\pm$  SD (n = 3)

	BF		Chitosan		TMB			TMC		
	25	100	25	100	25	75	100	25	75	100
<b><i>Salmonella typhimurium</i> ATCC 23564</b>	NZ	14 $\pm$ 0.6	NZ	10 $\pm$ 0.4	14 $\pm$ 0.5	22 $\pm$ 0.4	25 $\pm$ 0.5	NZ	12 $\pm$ 0.4	15 $\pm$ 0.7
<b><i>Shigella flexneri</i> 2a</b>	NZ	12 $\pm$ 0.2	NZ	8 $\pm$ 0.6	15 $\pm$ 0.3	24 $\pm$ 0.6	25 $\pm$ 0.9	NZ	10 $\pm$ 0.3	12 $\pm$ 0.6
<b><i>Aeromonas hydrophila</i> ATCC 35654</b>	NZ	13 $\pm$ 0.7	NZ	11 $\pm$ 0.3	13 $\pm$ 0.1	20 $\pm$ 0.3	23 $\pm$ 0.5	9 $\pm$ 0.3	14 $\pm$ 0.7	18 $\pm$ 0.4
<b><i>Yersinia enterocolitica</i> ATCC 9610</b>	NZ	13 $\pm$ 0.5	NZ	12 $\pm$ 0.2	10 $\pm$ 0.6	19 $\pm$ 0.6	21 $\pm$ 0.3	10 $\pm$ 0.4	17 $\pm$ 0.9	19 $\pm$ 0.5
<b><i>Escherichia coli</i> O157:H7 ATCC 32150</b>	NZ	14 $\pm$ 0.2	NZ	11 $\pm$ 0.8	10 $\pm$ 0.7	16 $\pm$ 0.8	16 $\pm$ 0.5	9 $\pm$ 0.1	16 $\pm$ 0.4	18 $\pm$ 0.6
<b><i>Listeria monocytogenes</i> ATCC 19111</b>	NZ	13 $\pm$ 0.1	NZ	9 $\pm$ 0.7	NZ	14 $\pm$ 0.5	16 $\pm$ 0.2	8 $\pm$ 0.2	11 $\pm$ 0.4	11 $\pm$ 0.5

ND: Not determined; NZ: No zone observed; Diameters includes the diameter of disc (6 mm)

Table 1(b): Minimum inhibitory concentration (MIC, µg/mL) of Chitosan and quaternized bioflocculant derivatives- TMC and TMB against six bacterial pathogens (in BHI media)

Bacteria	TMC	TMB
<b><i>S. typhimurium</i></b>	74	60
<b><i>A. hydrophilla</i></b>	71	62
<b><i>Y. enterocolitica</i></b>	67	65
<b><i>E. coli</i> O157:H7</b>	70	68
<b><i>L. monocytogenes</i></b>	80	72
<b><i>S. flexneri</i> 2a</b>	78	62

**Biochemical Responses of Water Borne Pathogens.** Insights on mode of action of antibacterial agents are crucial both for structure refinement/design modification of antibacterial agents and fate of target pathogens. In order to elucidate the possible mechanism of the inhibitory action of TMB against target pathogen was further assessed for its membrane potential, permeability intactness through measurement of glucose,

protein leakage and lactate dehydrogenase activity. Cellular damage and death was also studied by electron microscopy and FT-IR spectroscopy.

Table 2 summarizes the effect of TMB and TMC on leakage of protein from target pathogen in the extracellular media. Treatment of pathogens with a concentration of 76 $\mu$ g/ml of TMB led to rapid leakage of protein from the bacterial cells within a period of 3h. The amount of protein detected in post treatment increased gradually over time for all organisms. In order to elucidate the possible mechanism of the bactericidal action of quaternized biopolymers, leakage of glucose and Lactate dehydrogenase (LDH) enzyme from treated pathogens were studied. In the present study, treatment of pathogen with a concentration of 76 $\mu$ g/ml of TMB led to rapid leakage of glucose and LDH within a period of 3h (Table 2), though a minor increase in glucose and LDH levels in the extracellular media was observed after 6h, no further increase in the levels of glucose, protein or LDH occurred thereafter.

**Table 2.** Effect of biopolymeric derivative (TMB) (75  $\mu$ gml<sup>-1</sup>) on leakage of glucose concentration, lactate dehydrogenase and protein level in the extracellular media of bacterial pathogen cultured at 37 °C for up to 3 h. Control is bacterial cells in distilled water without TMB treatment. Each value is expressed as mean  $\pm$  SD (n = 3).

Bacterial strain	LDH activity (U/L)		Glucose (mg/dl)		Protein absorbance (280 nm)	
	0 h	3 h	0 h	3 h	0 h	3 h
	0	17.44 $\pm$ 0.08	0	0.42 $\pm$ 0.06	0	0.616 $\pm$ 0.04
<b>Control</b>	0	0.02 $\pm$ 0.001	0	0.03 $\pm$ 0.001	0	0.018 $\pm$ 0.004

Several authors have proposed that the antimicrobial action of chitosan could be explained by a more direct disturbance of membrane functions. The reactive amino groups in chitosan could interact with a multitude of anionic groups on the surface of the cell to alter its permeability. This causes the leakage of intracellular components such as glucose and LDH, resulting in a destabilized cell membrane beyond repair and subsequent cell death.

**Analysis of Lipopolysaccharides (LPS) Isolated from Treated Pathogens.** The LPS of inactivated pathogenic strains following biopolymer, chitosan, TMB and TMC treatment was examined by mid-infrared spectroscopy (4000-400cm<sup>-1</sup>) (Fig. 4). Treatment with biopolymer, chitosan and TMC resulted in no changes on the LPS region of the gram negative pathogens, whereas the structure of amide, polysaccharide and fingerprint region was completely altered on treatment with TMB. Hence, results reveal significant effect of TMB on the structure of LPS region of target pathogens. The results obtained in this study are similar to those reported in most instances Rafaat et al(2005)suggesting membrane damage by TMB to be the principal mechanism for inactivation.

In order to correlate spectroscopic data with ultra-structural changes caused by biopolymer treatment, scanning electron micrograph data was collected for treated bacterial cells at various time intervals. The intracellular changes were observed in TMB treated pathogens when compared to the non-treated cells including cytoplasmic membrane disruption and blebbing. Besides, remarkable modifications of cell membrane and disruption of cell membranes occurred after only a short period of exposure (Fig. 5).

Overall, the observations of our study indicated the efficacy of TMB in inactivating water borne pathogens by directly damaging their membranes; whether flocculation of the target pathogens is followed by inactivation, remains to be examined. Based on the results of this study, a potential application of the TMB for enhanced water safety is implicated.



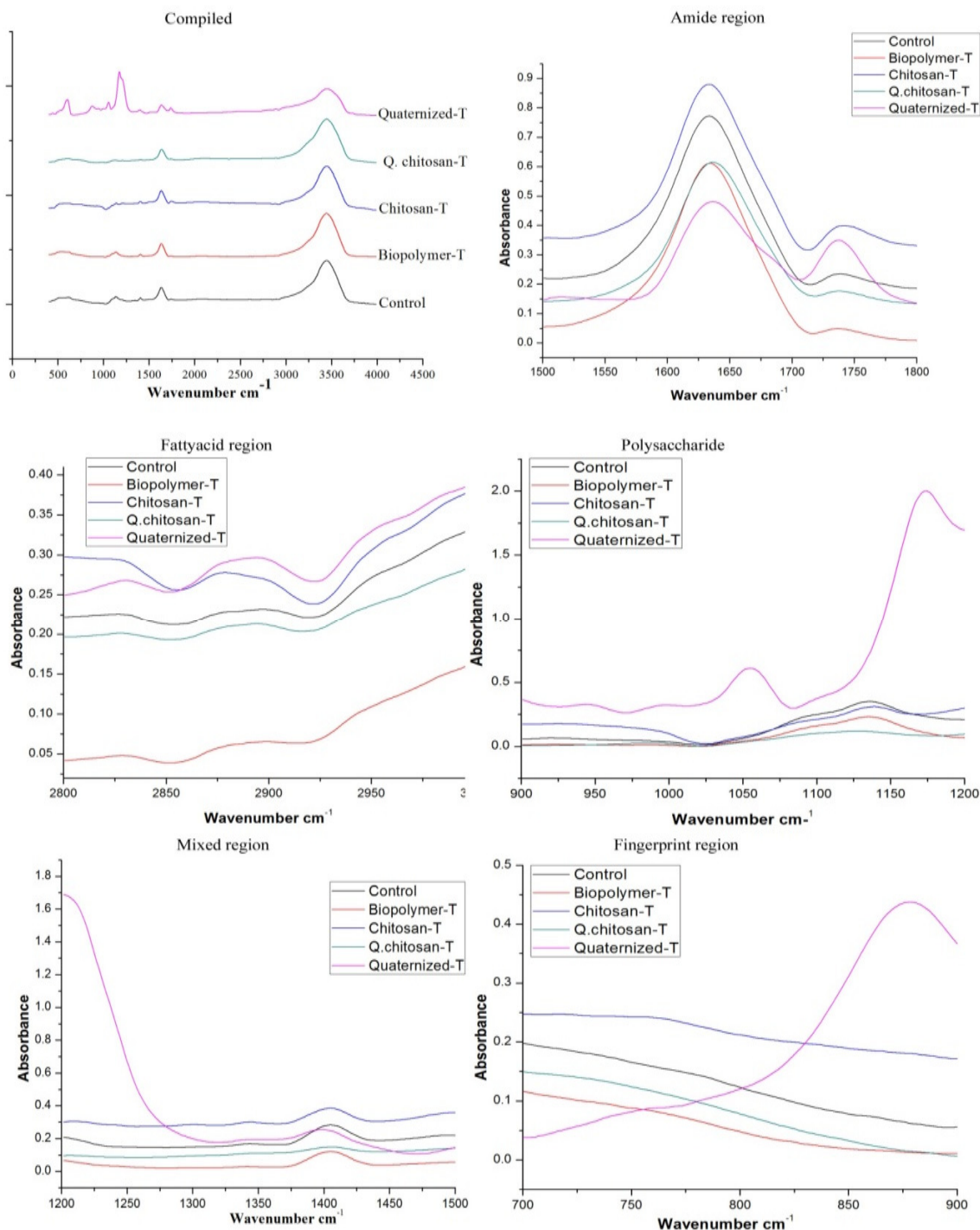


**Fig. 4.** Representative FT-IR spectra of LPS isolated from the pathogens (control), biopolymer treated bacterial cells (Biopolymer-T) and quaternized biopolymer treated bacterial cells (Quaternized-T).

## CONCLUSION

This study reported the biocidal effects of a polymeric flocculant produced by *K. terrigena*. Quarternization was effective in rendering biocidal properties to the native biopolymer, the quaternized biopolymeric flocculant led to rapid inactivation of water borne bacterial pathogenic strains. Cell death occurred presumably by a rapid release of cytoplasmic enzymes, changes in electrical conductivity and

FTIR spectra. Gross morphological changes on cell membranes of bacteria were observed from electron micrographs of exposed cells. The newly developed biocidal biopolymeric flocculant may have significant applications in both removing and inactivating bacterial pathogens transmitted through water.

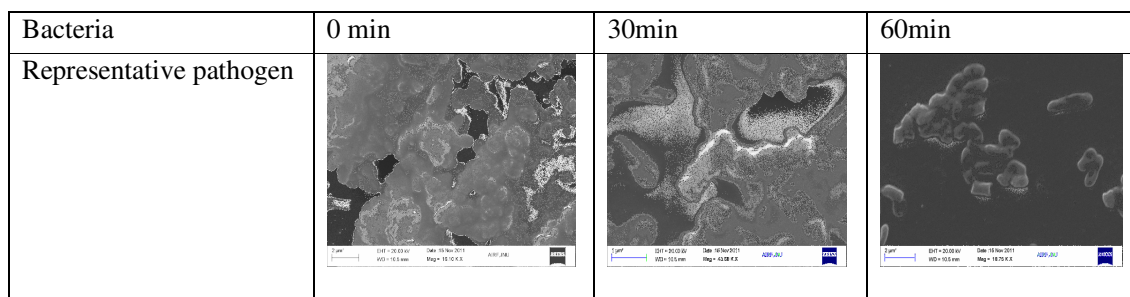


**Fig. 5.** Scanning electron micrographs of indicator bacteria treated with TMB in mid-logarithmic growth at  $10^7$ CFU/ml at various time intervals.

## ACKNOWLEDGEMENT

The authors would like to acknowledge DST UKEIRI for financial assistance in carrying out this work.

## REFERENCES

- Ahmed, A.M., Shimamoto, T., 2014. Isolation and molecular characterization of *Salmonella enterica*, *Escherichia coli* O157: H7 and *Shigella* spp. from meat and dairy products in Egypt. *Int. J. Food Microbiol.* 168, 57-62.
- Ashtiani, M.T. H., Monajemzadeh, M., Kashi, L. 2009. Trends in antimicrobial resistance of fecal *Shigella* and *Salmonella* isolates in Tehran, Iran. *Indian J. Pathol. Microbiol.* 52, 52-55
- Belalia, R., Grelier, S., Benaissa, M., Coma, V. 2008. New bioactive biomaterials based on quaternized chitosan. *J. Agric. Food Chem.* 56, 1582–1588.
- Britto, D., Assis, B.G. 2007. A novel method for obtaining a quaternary salt of chitosan. *Carbohydr. Polym.* 69, 305–310.
- CDC 2009 Health, United States, 2009 with Special Feature on Medical Technology. Centers for Disease control and Prevention, United States.
- de Britto, D., Celi Goy, R., Campana Filho, S.P., Assis, O.B. 2011. Quaternary salts of chitosan: history, antimicrobial features, and prospects. *Int. J. Carbohydr. Chem.* 2011, 1-12.
- Ghosh, M., Pathak, S., Ganguli, A. 2009a. Effective removal of *Cryptosporidium* by a novel bioflocculant. *Water Environ. Res.* 81, 160–164.
- Ghosh, M., Pathak, S., Ganguli, A. 2009b. Application of a novel biopolymer for removal of *Salmonella* from poultry wastewater. *Environ. Technol.* 30, 337–344.
- Kotloff, K.L., Winickoff, J.P., Ivanoff, B., Clemens, J.D., Swerdlow, D.L., Sansonetti, P.J., Adak, G.K., Levine, M.M., 1999. Global burden of *Shigella* infections: implications for vaccine development and implementation of control strategies. *Bull. World Health Organ.* 77, 651-666.
- Kurane, R., Takeda, K., Suzuki, T. 1986. Screening for and characteristics of microbial flocculants. *Agric. Biol. Chem.* 50, 2301-2307.
- Raafat, D., Barga, K., Haas, A., Sahl, H. 2008. Insights into the mode of action of chitosan as an antibacterial compound. *Appl. Environ. Microbiol.* 74, 3764–3773.
- Rolfo, F., Marin, G. H., Silberman, M., Pattin, J., Giugnio, S., Gatti, B., Bettiol, M., Rigoni, A., 2011. Epidemiological study of shigellosis in an urban area of Argentina. *J. Infect. Dev. Ctries.* 6, 324-328.
- Siedenbiedel, F., Tiller, J. C. 2012. Antimicrobial polymers in solution and on surfaces: overview and functional principles. *Polymers.* 4, 46-71.

- Sieval, A.B., Thanou, M., Kotze, A.F., Verhoef, J.C., Brussee, J., Junginger, H.E. 1998. Preparation and NMR characterization of highly substituted N-trimethyl chitosan chloride. *Carbohydr. Polym.* 36, 157-165.
- Tan, H., Ma, R., Lin, C., Liu, Z. Tang, T. 2013. Quaternized chitosan as an antimicrobial agent: antimicrobial activity, mechanism of action and biomedical applications in orthopaedics. *Int. J. Mol. Sci.* 14, 1854–1869.
- Westphal, O. 1965. Bacterial lipopolysaccharide-extraction with phenol water and further application of procedure. *Methods carbohydr. chem.* 1, 83-91.
- WHO 2005 Guidelines for the control of shigellosis, including epidemics due to *Shigella dysenteriae* type 1. World Health Organization, Geneva.
- Woodward, D.L., Rodgers, F.G., 2000. Surveillance of antimicrobial resistance in *Salmonella*, *Shigella* and *Vibrio cholerae* in Latin America and the Caribbean: A collaborative project. *Can. J. Infect. Dis.* 11, 181.

## VOLATILE FATTY ACID PRODUCTION DURING ACIDIFICATION OF OLIVE MILL WASTEWATER

Havva BAG<sup>1</sup>, Secil ERDEM<sup>1</sup>, *Canan CAN YARIMTEPE*<sup>1\*</sup>, Orhan Ince<sup>2</sup> and Nilgün AYMAN OZ<sup>1</sup>

<sup>1</sup>Canakkale Onsekiz Mart University, Canakkale, Turkey

<sup>2</sup>Istanbul Technical University, İstanbul, Turkey

**ABSTRACT:** This study aims to investigate acidification potential of oil mill wastewater (OMW) via acidification reactors. During the study, tVFA production was determined; pH, sCOD, TSS, Total Volatile Fatty Acid concentration and composition were monitored. Acidification reactors were performed for 60 days and according to datas for first 60 days; tVFA concentration ( in terms of Acetic Acid), gradually increased from 450 mg/l to 5278 mg/l. During the process, changes in Volatile Fatty Acid composition have been observed. While each VFA concentration were increased, also other VFA compounds, not detected in influent, were determined in the effluent. During acidification process, changes in sCOD concentration were monitored daily. No major changes were observed in organic matter concentration during process. Therefore, loss of organic matter was not mentioned. Although there is no change in organic matter concentration but there is increase in tVFA concentration. Therefore it is indicated that organic matter change from thus acidification process was performed successfully.

## INTRODUCTION

Marmara and Aegean region including Canakkale is main part for olive oil production in Türkiye. Olive mill wastewater (OMW), has high amount of organic matter and also toxic and inhibitor materials such as lipids and phenolic compounds. Therefore it is not easy to treat such strong wastewater with conventional treatment processes. In literature several treatment methods have been tested for OMW such as physico chemical treatment, advance treatment and biological treatment. As physico chemical treatment ;centrifuge (Turano et al., 2002), physicochemical treatment (Ginos et al., 2006), membrane filtration (Boari ve ark., 1984; Bradley 1980) have been examined. In addition as advance treatment; ozone (Amat et al., 2003), fenton oxidation (Rivas et al., 2001), combination of ozone and fentone (Filipakopoulou ve ark., 1999) have been tested. However due to high operation cost and sludge production of chemical treatment technologies, new alternative treatment process are required. In literature there are also some studies about biological treatment of OMW such as aerobic treatment (Bertin et al., 2001) and anerobic treatment (El-Gohary et al., 2009; Azbar et al., (2008). However, anaerobic treatment of OMW is limited due to high polyphenol and lipid concentrations.

Because of its complex composition, a sufficient treatment solution have not been addressed for OMW management, so far. However, it is possible to produce clean energy such as methane and hydrogen and recover resource metarials such VFAs (Volatile Fatty Acids) and phenolic compounds from olive mill wastewater. With this study, environmental pollution originating from olive mill wastewater can be reduced in terms of color and turbidity, at the same time energy production and resource recovery in a form of VFA can be provided.

In literature there is limited studies about VFA production from OMW. Scoma et al. (2013) have studied the effects of HRT on acidification from pretreated OMW (according to phenolic compounds). They have tested 1, 3, 5 and 7 day of HRT and have selected optimum HRT as 1 day. In optimum conditions, it is reported that while initial VFA concentrations are at very low levels, final VFA concentrations are measured as 10 gr/l. In addition acetic acid, butyric acid and propionic acid were found the dominant VFAs.

Recently, acidification phase receives considerable attention and relevant studies covered a wide range of operational parameters. Since acidogenic reactor plays a crucial role in the conversion of complex organic substrates to VFA (intermediate fermentation product), the initial aim of this study is to optimise the acidogenic reactor to provide feed with high amount of VFA to second stage treatment.

Therefore, the aim of this study is investigation of acidification potential of OMW via anaerobic sequencing batch reactors.

## MATERIALS AND METHODS

The raw OMW was collected from an Olive Oil Production Factory in Canakkale, Turkiye in December, 2014. OMW composition is given in Tablo 1.

**Table 1. OMW Composition**

Parameters	Unit	OMW
pH		4,991
Conductivity	µs/cm2	13950
Turbidity	NTU	16100
Color	ptCO	38200
TS	mg/L	48544
TVS	mg/L	41272
TSS	mg/L	20900
COD	mg/L	87716
TOC	mg/l	23883
SCOD	mg/L	40306
Total Phenol	mg/L	6560

Acidification process were performed with 1 liter anaerobic reactors consisting separate gas and sample ports which were submerged in a water bath with a temperature control and magnetic stirrer units. Seed sludge which is used in acidification reactors was obtained from a yeast factory's acidification reactors, in Izmir. Table 2. shows sludge sludge properties.

**Table 2. Seed sludge properties**

Parameter	Unit	Value
Total Solid Matter	mg/l	163382
Total Volatile Solid	mg/l	60612
Total Suspended Solid	mg/l	88305
Total Volatile Suspended Solid	mg/l	35092

With aim of determination optimal conditions for acidification; organic loading rate was increased gradually as 5000 mg COD/l, 10000 mg COD/l and 20000 mg COD/l while microorganism concentration was stable at 5000 mg TVS/l in reactors. In this case; study was started with 1 gr COD/ gr TVS as S/X ratio and increased gradually to 2 gr COD/ gr TVS and 4 gr COD/ gr TVS for testing. Acidification reactors were performed for 2 days hydraulic retention time at pH 5-5,5. During the study; pH, sCOD and TSS were determined according to standard methods (APHA, 1998). After acidification process; in olive mill wastewater samples, volatile fatty acid concentration especially acetic acid concentration was monitored with GC. Acidification efficiencies were determined as acidification rate and calculated by following equation:

$$\text{Acidification rate, \%} = \text{VFA}_{\text{COD}} / \text{Total COD}$$

## RESULTS AND DISCUSSIONS

With the aim of acidification potential investment of OMW, anaerobic sequencing batch reactors were performed as acidification reactor. The study was started with 1 g COD/ g TVS as S/X ratio and increased gradually to 2 g COD/ g TVS, 4 g COD/ g TVS and 8 g COD/ g TVS for testing at pH 5-5,5. Acidification performed for 2 days hydraulic retention time. The best acidification rate was achieved at 4 g COD/ g VSS as S/X ratio, 2 days as HRT and  $5,5 \pm 0,1$ . Therefore, acidification reactors have been performed in optimum conditions with raw OMW. Acidification reactors were performed for 60 days and according to data for first 60 days; tVFA concentration (in terms of Acetic Acid), was gradually increased from 450 mg/l to 5278 mg/l. Total VFA concentrations in acidification reactor operated for 60 days at optimal conditions are shown in Figure 1.

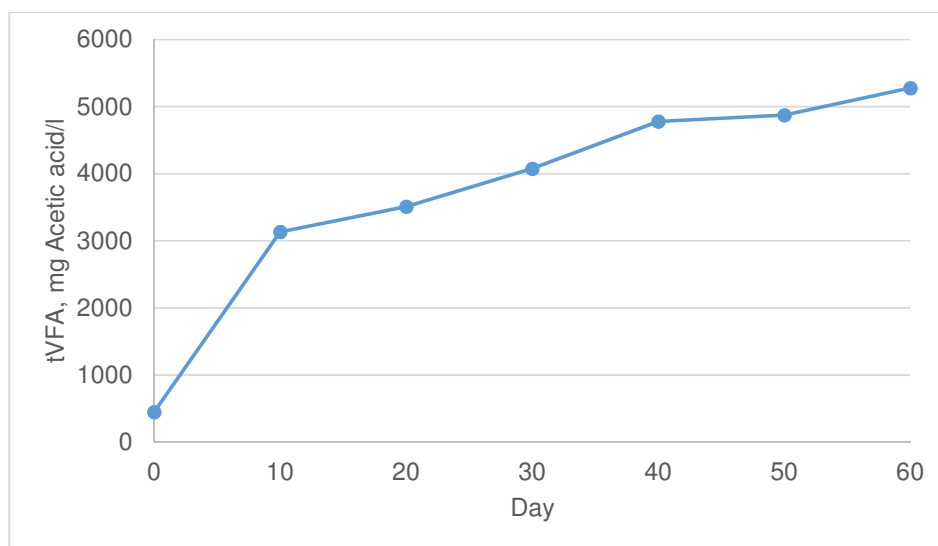


**Figure 1. Total VFA concentrations in acidification reactor**

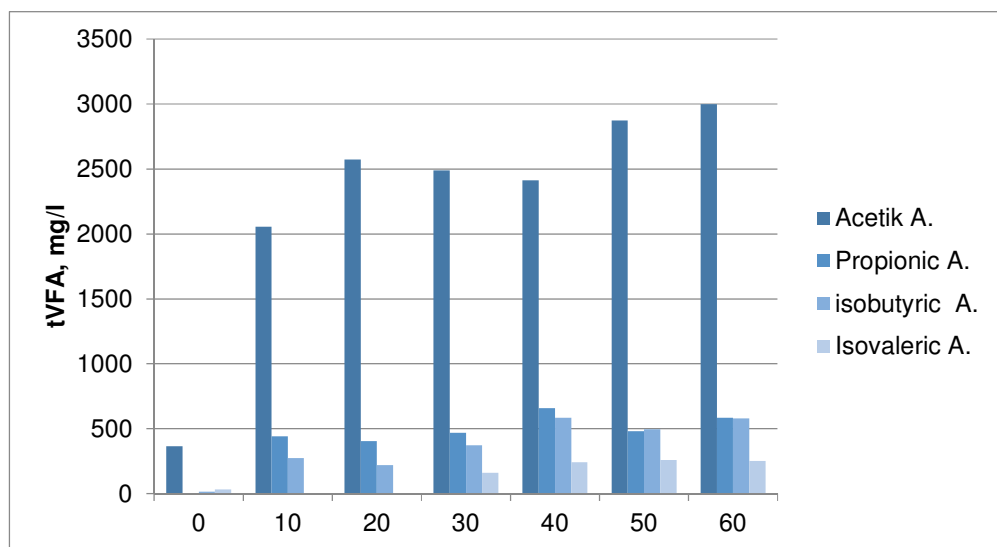


**Figure 2. Total volatile fatty acid composition in acidification reactor**

During the process, Volatile Fatty Acid composition was also monitored. After acidification process, changes in Volatile Fatty Acid composition have observed. Figure 2 shows influent and effluent Total volatile fatty acid composition in acidification reactor operated for 60 days.

While each VFA concentration were increased, also other VFA compounds, not detected in

influent, were determined in effluent. During acidification process, changes in sCOD concentration were monitored daily. Figure 3. shows the changes in sCOD concentration during acidification.

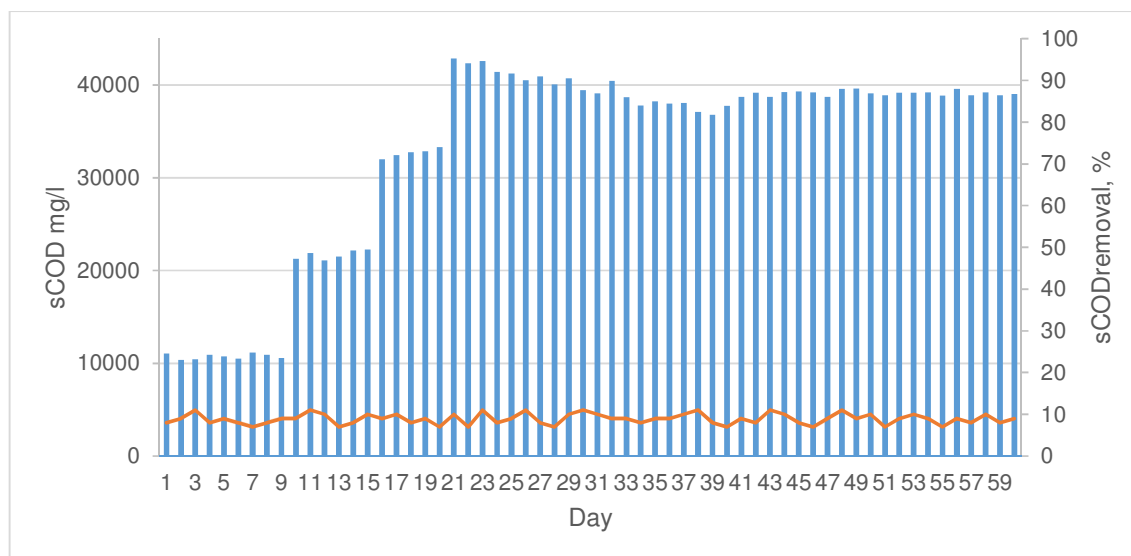


**Figure 3. changes in sCOD concentration during acidification**

No major changes were observed in organic matter concentration during process. Therefore loss of organic matter was not mentioned. Although there is no change in organic matter concentration but there is an increase in tVFA concentration. Therefore it indicates that acidification process has been performed successfully.

## CONCLUSIONS

In biological systems; efficiency is directly related to the amount of organic matter which can be converted into VFA. Therefore, it is important to convert organic matter in wastewater to VFA by a process such as acidification prior to biological processes. The results obtained from acidification can be enhanced by combination of the advance processes. At this point, acidogenic fermentation can be used to produce mainly organic acids (e.g. VFA) with several advantages. It is strategically important to test alternative technologies in the area of wastewater treatment especially for complex wastewater such as OMW. The operation of acidification reactors may offer two main benefits: sustainable clean energy production and the potential for pollution reduction. With the tVFA concentration increase, more efficient results can be obtained from next treatment processes for energy and resource recovery.

## ACKNOWLEDGEMENT

Financial support by The Scientific and Technological Research Council of Turkey (TUBITAK) was gratefully acknowledged (Project No.: 114Y179).

## REFERENCES

- AMAT A.M., Arques A., Beneyto H., Garcí'a A., Miranda M.A., Seguí S., Ozonisation coupled with biological degradation for treatment of phenolic pollutants: a mechanistically based study, *Chemosphere* , 53, 79– 86, (2003).
- APHA, AWWA, WPCF, *Standard Methods for the Examination of Water and Wastewater*, 20th., American Public Health Association, Washington, DC, (1998).
- AZBAR, N. Ursillo, P. and Speece, R., Effect of process configuration and substrate complexity on the performance of anaerobic processes, *Water Research*, 35 (3), 817-829, (2000).
- BERTIN, L., Majone, M., Di Gioi, D., Fav, F., An aerobic fixed-phase biofilm reactor system for the degradation of the low-molecular weight aromatic compounds occurring in the effluents of anaerobic digestors treating olive mill wastewaters, *Journal of Biotechnology* , 87, 161–177, (2001).

- BOARI, G., Brunetti, A., Passino, R., and Rozzi, A. Anaerobic digestion of olive oil mill wastewaters. *Agricultural wastes*, 10(3), 161-175, (1984).
- BRADLEY R.M. and Baruchello L. *Primary wastes in the olive oil industry Effluent Water Treatment Journal*, 20, 176–177, (1980).
- GINOS, A., Manios, T., Mantzavinos, D., Treatment of olive mill effluents by coagulation–flocculation–hydrogen peroxide oxidation and effect on phytotoxicity, *Journal of Hazardous Materials*, 133, 135–142, (2006).
- RIVAS F.J., Beltrán F.J., Gimeno O., Frades J., Treatment of olive oil mill wastewater by Fenton’s reagent. *J Agric Food Chem* 49, 1873– 80, (2001).
- TURANO, E., Curcio, S., De Paola, M. G., Calabrò, V., & Iorio, G., An integrated centrifugation–ultrafiltration system in the treatment of olive mill wastewater. *Journal of Membrane Science*, 209(2), 519-531, (2002).



## DECOLORIZATION OF ANAEROBICALLY DIGESTED MOLASSES SPENTWASH BY FUNGAL STRAIN: ISOLATION AND SCREENING OF STRAINS

**Mrityunjay Singh Chauhan** (Maulana Azad National Institute of Technology, Bhopal, INDIA)  
Anil K. Dikshit (Indian Institute of Technology Bombay, Mumbai, INDIA)

India is among the top five sugar producing countries in the world with an annual production of 17.6 million tons of sugar. Molasses is the mother liquor left-over after crystallization of sugar from concentrated cane juice. Almost all of the Indian distilleries use molasses as raw material for alcohol production. For production of one litre of alcohol, about 4-10 kg of molasses is required and about 15 litres of wastewater (commonly known as spent wash) is generated. Spent wash is characterized by its high organic and inorganic loading coupled with dark brown or black colour. Looking to its pollution potential, distillery industry is categorized among top 15 polluting industries in India.

This study was carried out with the objective of isolating fungal species suitable for decolorizing anaerobically digested molasses spentwash (ADMS). A total of eight fungal species were isolated from the sludge of anaerobic digester or the lagoon. The ADMS was pretreated with 15 g/L poly aluminum chloride. Fungal isolates were grown in 10% ADMS amended with nutrients over 15 days, where V-1, V-7 and V-8 showed significant growth. The secondary screening was carried out for the above three strains in 50% ADMS enriched with nutrients, only V-7 and V-8 showed growth with V8 showing profuse growth. The growths of V-7 and V-8 along with decolorization were monitored over 15 days. About 70% decolorization of ADMS could be achieved by V-8 isolate with subsequent reduction in COD within the three days of inoculation. Fungal Isolate was named as V-8(IITB) and identified as *Aspergillus niger*.

Results of isolation, screening, growth pattern, identification and feasibility of treating ADMS are discussed in this paper.

## IMPROVEMENT OF BACTERIAL BIODEMULSIFIER BIOSYNTHESIS IN PERMEABILIZING AGENT-ENHANCED UTILIZATION OF RAPE OIL

Yuyan Zhang, Kaiming Peng, Yansong Wei, and Xiangfeng Huang  
(Tongji University, Shanghai, China)

Biodemulsifiers have obtained growing interest in the applications for separation of the oil and water phases from emulsions in petroleum oil recovery and oily wastewater treatment, owing to their superiorities of wide applicability and environmental compatibility over traditional chemical demulsifiers. Biodemulsifier-producing strains prefer hydrophobic organic compound (HOC) as a carbon source, in which transmembrane transport of HOC is generally the rate-limiting step. Permeabilizing agent-enhanced HOC bioavailability is a promising strategy to increase the yields of biodemulsifiers.

In this study, twenty-four kinds of permeabilizing agents with different concentrations, as medium additives, were separately used for improving rape oil utilization to enhance the biosynthesis of bacterial demulsifier *Alcaligenes* sp. S-XJ-1, including surfactants (Tweens, Spans, Triton X-100, CHAPS, CTAB, SDS, rhamnolipid, and saponin), organic solvents (glycerol, DMSO, toluene, alcohol, hexane, and 1-dodecanol), and others (EDTA, biotin, lysozyme, glycine, and proline). The demulsification capability was evaluated by bottle test and Turbiscan Lab Expert. Cell membrane permeability was characterized by transmission electron microscopy (TEM) and fluorescein diacetate (FDA) assay.

Results showed that saponin, Span60, CHAPS, 1-dodecanol, DMSO, biotin, glycine, or proline could simultaneously promote the yields and demulsification capability of the S-XJ-1. Among them, 0.05% of saponin was optimal to enhance the yields, demulsification ratio, and demulsification speed, which increased by 2.4 times, 18%, and 4.0 times, respectively. For cells cultivated with 0.05% saponin, the TEM images showed that their cell membranes became incomplete and the average thickness of their cell walls decreased about 4 nm, and FDA assay indicated that their fluorescence intensities increased by 5.9 times. We also found that oil solubilization and stimulated cellular metabolism contributed to the increased yields, and that the demulsification boost was related to responses of cell-surface properties and composition. Thus, saponin addition overcame the permeability barrier of the cell envelope and accelerated the transport of rape oil into cells, providing benefits for demulsifier biosynthesis. This study provides a simple, yet effective strategy to enhance biodemulsifier production.

## **SURFACTANT REMOVAL BY METAL OXIDES AND ADSOLUBILIZATION OF ORGANICS IN EXHAUSTED MATERIAL**

Suman Koner (Jalpaiguri Govt. Engineering College, Jalpaiguri, India)

Anjali Pal (Indian Institute of Technology, Kharagpur, India)

**Asok Adak** (Indian Institute of Engineering Science and Technology, Shibpur, Howrah, India. Email: asok@civil.iiests.ac.in)

**ABSTRACT:** The present study deals with the removal of ionic surfactants using oppositely charged metal oxides and use of exhausted metal oxides for removal of other organic pollutants like crystal violet (CV) dye and 2,4-dichlorophenoxyacetic acid (2,4-D) through adsolubilization process. Sodium dodecyl sulfate (SDS), a representative of anionic surfactant was removed from its highly concentrated wastewater by neutral alumina and exhausted adsorbent called surfactant modified alumina (SMA) was used to treat CV bearing wastewater. In similar fashion cetyltrimethylammonium bromide (CTAB), a representative of cationic surfactant was removed by silica gel waste (SGW) collected from a local factory at Kolkata, India. The surfactant modified silica gel waste (SMSGW) was utilized as an adsorbing media for removal of 2,4-D from agricultural wastewater.

**Keywords:** Adsorption, Adsolubilization, Surfactant, Dye, Herbicide.

### **INTRODUCTION**

The agricultural, industrial and domestic activities result in the generation of large amounts of wastewater containing a number of ‘pollutants’ which are potentially hazardous to human health, terrestrial and aquatic ecosystem. Among them, surfactants, dyes and pesticides are widely used. Surfactants are harmful to human beings, fishes and vegetation. They are responsible for causing foams in rivers and effluent treatment plants to reduce the quality of water. Surfactants cause short term as well as long-term changes in ecosystem. The main environmental concern with dyes is their absorption and reflection of sunlight entering the water and thus causing reduction in photosynthesis and DO level in river (Donia et al., 2009). Most of the pesticides including 2,4-D are potentially carcinogenic and poor biodegradability of these compounds make these environmentally stable (Carter 2000; Chao et al., 2008).

The conventional methods for surfactant removal from the water environment involve processes such as chemical oxidation, reverse osmosis, chemical precipitation, adsorption, various biological methods etc. Use of metal oxides for treatment of surfactant bearing wastewater has drawn much attention in recent years. The ionic surfactants are adsorbed on the surface of metal oxide due to (1) electrical attraction between charged surface and ionic head groups of surfactant and (2) interaction between the long hydrocarbon chains of surfactant molecules through formation of monolayer, partial bilayer or bilayer structure depending on surfactant concentration (Somasundaran and Fuerstenau, 1966). These surfactant layers formed on solid surface have the ability to solubilize different organics within their structure. This phenomenon is known as adsolubilization (Kitiyanan et al., 1996). Thus, the metal oxides serve dual purposes – firstly they remove the ionic surfactant and then remove different other organics commonly present in the wastewater.

Thus the present study aims at removal of two ionic surfactant viz. SDS and CTAB by using alumina and SGW respectively from highly concentrated solution and then at reuse of surface modified metal oxides such as SMA and SMSGW for the removal of CV dye and 2,4-D herbicide respectively from water environment.

### **MATERIALS AND METHODS**

**Reagents.** SDS (BDH, India), CTAB (Hi-Media, India), CV dye (BDH, India) and 2,4-D (Merck, India) were used as received. All other chemicals used in this study were of high purity and used without further purification. All the chemicals were of Analytical Reagent Grade.

**Adsorbent.** Alumina was supplied by SRL, India and used as such without further grinding and sieving. The granulation of neutral alumina was 70 – 290 mesh ASTM, molecular weight was 101.96 and zero point charge ( $Z_{pc}$ ) was 9.15.

SGW was prepared from solid waste generated from a local silica gel factory located at Kolkata, India. After collection, the material was thoroughly washed with tap water followed by distilled water, dried at 100°C and then sieved. About 70% of the total material lies in the particle size between 150 - 300 microns and that was used for the study. The zero point charge of SGW was found to be 2.0.

For preparation of SMA, alumina (200 g) was shaken for 24 hours with 2 L of SDS solution having 20000 mg/L concentration. The NaCl dose was 2500 mg/L and the pH 4.4±0.1. After shaking, the supernatant was discarded and the alumina was washed thoroughly initially with tap water and finally with distilled water. Then the material was dried at 60°C for 24 hours. The alumina thus obtained is SMA and was used as an adsorbent for CV dye removal from water environment.

In similar fashion, 180 g SGW (at a dose of 30 g/L) was shaken with 6 L of CTAB solution having concentration of 7500 mg/L for 2 h. After shaking, the supernatant was discarded and the SGW was washed thoroughly initially with tap water and finally with distilled water and then dried at 60 °C for 24 h. The SGW was thus converted to SMSGW and was used as an adsorbent for 2,4-D removal from wastewater.

**Analytical Method.** Spectrophotometric method was used for the determination of SDS (Adak et al., 2005), CS (Few and Ottewill, 1956) and 2,4-D (Kundu et al., 2005). The CV dye was also measured by spectrophotometric method at its  $\lambda_{max}$  of 591 nm.

**Experimental Studies.** The batch experiments were carried out using synthetic samples of SDS and CTAB separately in distilled water at 25±2°C in a mechanical shaker at an agitation speed of 150 rpm. The sorption equilibrium time was studied using initial surfactant concentrations of 2000 mg/L and adsorbent dose of 100 g/L for alumina and 30 g/L for SGW. The pH for both the solution was 6.8±0.1 and the shaking time was varied from 0 to 120 minutes. The experiments were also carried out to check the effectiveness of both metal oxides (alumina & SGW) for treatment of real wastewater. The real wastewater containing AS was collected from small scale laundry and the same containing CS was collected from a textile industry. The major water chemistry parameter for both the wastewater is reported in Table No 1.

The efficiency of the exhausted metal oxides such as SMA and SMSGW were tested. A sample similar to real wastewater was prepared following the composition given by Sapari (Sapari, 1996) containing CV concentration 200 mg/L in the laboratory and was used to check the efficacy of SMA by conducting batch kinetic study and optimum dose calculation. For kinetic study the SMA dose was fixed at 6 g/L and the shaking time was varied from 0 to 105 minutes where for optimum dose calculation SMA quantity was varied from 0 to 8 g/L with a contact period of 60 minutes.

Efficacy of SMSGW was tested in similar fashion described above with the real wastewater containing 2,4-D concentration 32.90 mg/L (2,4-D sodium salt). The 2,4-D sodium salt (Commercially known as Salix salt) are applied to control broad leaf weed in the tea garden. After application of salix salt there was a heavy storm and the wastewater was collected from the surface runoff of a local tea garden situated in Jalpaiguri district of the state West Bengal, India.

Table 1. Quality Parameter for Laundry and Textile Wastewater

Parameter	Laundry Wastewater	Textile Wastewater
pH	9.1	9.2
TDS	2154 mg/L	720 mg/L
Surfactant	8068 mg/L as AS	362 mg/L as CS

## RESULTS AND DISCUSSION

**Surfactant Removal by Metal Oxide.** Kinetic study was carried out in order to find out the equilibrium contact time for SDS or CTAB uptake by alumina and SGW respectively. In case of SDS removal the equilibrium time was found to be 90 minutes (Figure 1a). However, for CTAB adsorption it was only 30 minutes (Figure 1a). The adsorption capacity at equilibrium was 12.4 mg/g for SDS. This value was quite high in case of CTAB adsorption by SGW and it was 42.72 mg/g. In general the lower value of equilibrium contact time compared to activated carbon adsorption would be advantageous, since it would facilitate to reduce the reactor volume in case of continuous mode of operation in the field.

In order to investigate the mechanism of solute adsorption onto the adsorbent, four kinetic models viz., first order reaction model (Benfield Randall, 1980), pseudo-first order equation of Lagergren (1898), second order reaction model and pseudo-second order reaction model of Ho and McKay (1999) were analyzed and it was found that the reaction followed the pseudo-second order reaction model best (Figure 1b) for both the cases. This indicated that the rate limiting step for both the cases was chemical adsorption or chemisorption (Ho and McKay, 1999).

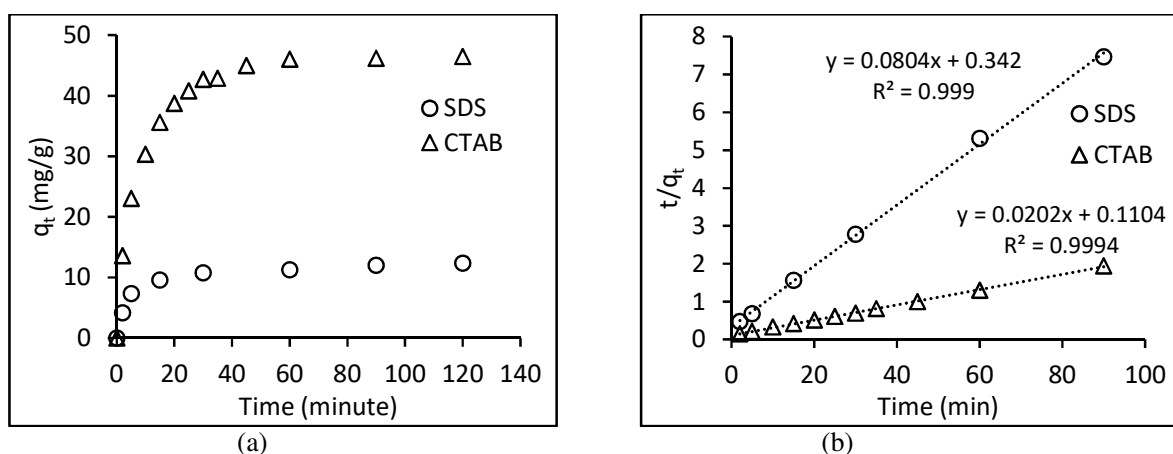


**Figure 1.** Kinetic study of SDS and CTAB removal by metal oxide - (a) adsorption capacity variation with time and (b) linearized plot of pseudo-second order reaction model.

The experiments were carried out to check the effectiveness of both the metal oxides for treatment of real wastewater. The source and quality of the wastewater has been reported above. A series of 100 mL samples of AS bearing wastewater were shaken for 45 minutes with adsorbents at varying doses (0 to 180 g/L). It was found that the removal of AS increases with the increase of alumina dose and the removal remained almost constant (Figure 2a) beyond the adsorbent dose of 120 g/L. The removal of AS at this stage was found to be 94%. Hence 120 g/L was selected as the optimum adsorbent dose. However, the removal of SDS under similar experimental condition using distilled water spiked sample was only 55%. This might be due to presence of high amount of total dissolved solids (anions and cations) in wastewater which increased the removal efficiency. The presence of various anions and cations generally decrease the lateral repulsive force between the head groups of the ionic surfactants causing increased adsorption capacity (Luciani et al., 2001). The kinetics study was conducted with optimum adsorbent dose of 120 g/l at varying time and shown in Figure 2b. The rate of adsorption was very rapid initially. It was noticed that ~ 87% removal of AS took place within half an hour and then gradually increased upto 94% and 96% in 45 and 60 minutes respectively. The equilibrium time for wastewater was found to be less than SDS-spiked in distilled water. The presence of salts in wastewater made the reaction faster than in the case of distilled water.

Experiments were also carried out to find out the effectiveness of SGW for removal of CS from actual wastewater samples under the experimental conditions used for this study. A series of 100 mL portions of CS bearing wastewater were shaken for 30 minutes with varying SGW doses (0 to 20 g/l). It was noticed that the removal was found to be almost constant after a dose of 10 g/l (Figure 2a). At this stage 87% removal was achieved. The adsorption capacity of SGW was found to vary from 13.32 to 73.85 mg of

CS /g of SGW. It was very interesting to observe that the removal efficiency in distilled water spiked sample was 76%. In this case the adsorption capacity of SGW was found to vary from 12.44 to 58.91 mg of CS /g of SGW. Like SDS removal, presence of high amount of total dissolved solids (TDS) in wastewater and also higher pH value which increased the adsorption capacity. Moreover, the adsolubilization of other organics present in the real wastewater e.g. dyestuff was found to take place along with the removal of CS from wastewater. The kinetic study revealed that a contact time of 30 minutes would be sufficient to attain the equilibrium (Figure 2b).

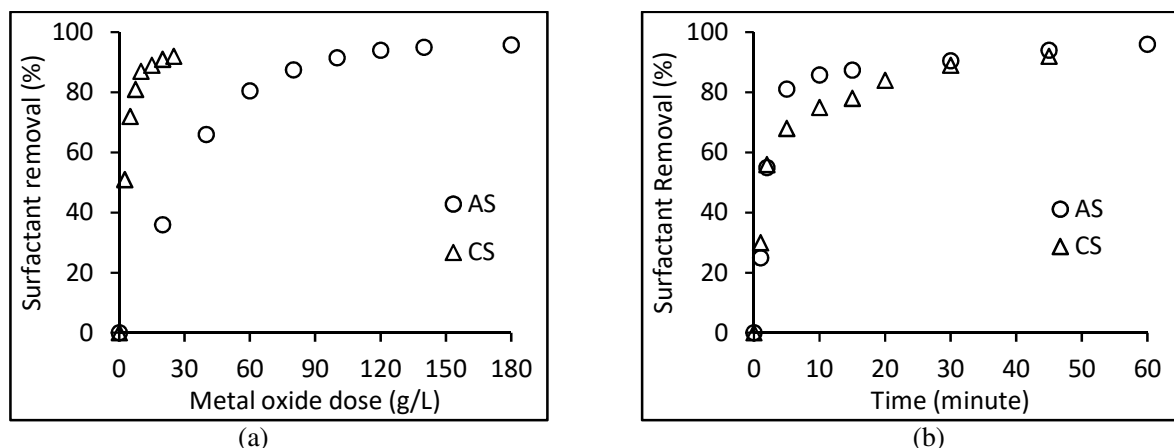


**Figure 2.** Removal of AS and CS from real wastewater by alumina and SGW respectively – (a) adsorbent dose study and (b) kinetic study

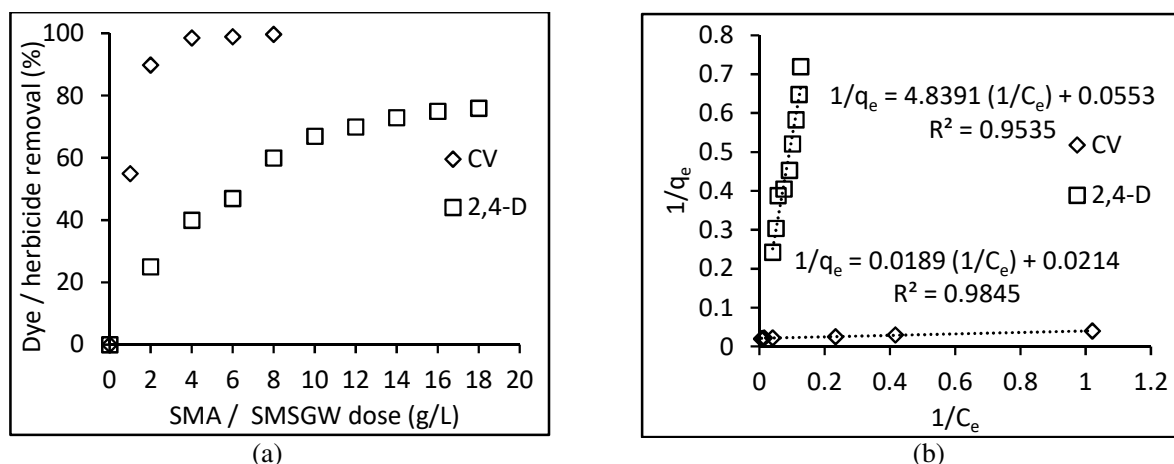


**Figure 3.** Removal of dye and herbicide from real wastewater by SMA and SMSGW respectively – (a) adsorbent dose study and (b) linearized plot of Langmuir isotherm model

**CV Dye and 2,-4 D Removal By Exhausted Sludge.** Experiments were carried out to find out the effectiveness of SMA for removal of CV from prepared synthetic wastewater following the composition given by Sapari (Sapari, 1996) and the same for SMSGW for 2,4-D removal from a real wastewater collected from a tea garden as mentioned earlier. The crystal violet concentration in wastewater was 200 mg/L. The pH was  $10.9 \pm 0.1$ , total dissolved solid (TDS) was 3030 mg/L and the turbidity was 120 NTU. Since the pH of the raw wastewater was  $10.9 \pm 0.1$ , it was brought down to  $7.0 \pm 0.1$  by adding acid before being treated with SMA. The effect of adsorbent dose was studied using 0 to 8 g/l of adsorbent. The shaking time was 60 minutes and the temperature was  $25 \pm 2^\circ\text{C}$ . The optimum adsorbent dose was found to be 6 g/L and corresponding removal of CV was 99 % (Figure 3a). Kinetics studies were carried out with adsorbent dose of 6 g/l. The shaking time was varied from 0 to 105 minutes. The equilibrium time was found to be 30

min only. The adsorption followed Langmuir isotherm model and the maximum adsorption capacity of CV by SMA was found to be 46.72 mg/g at 30 °C (Figure 3b). The adsorption capacity for distilled water spiked CV sample was found to be similar as above.

The performance of SMSGW was also evaluated by applying it for the treatment of real wastewater containing 2,4-D sodium salt concentration of 32.90 mg/L as mentioned earlier. After collection, the wastewater was filtered to remove suspended solids. Figure 3a shows the effect of adsorbent dose. The dose of SMSGW was varied from 0 to 18 g/l and the shaking time was 20 min. It was noticed from the figure that the optimum adsorbent dose was 16 g/l and the capacity as found from Langmuir isotherm was 18.03 mg/g at 30 °C (Figure 3b). However, the adsorption capacity for distilled water spiked 2,4-D sample was found to be 33.9 mg/g. Such lower value of adsorption capacity was due to the presence of dissolved salts in the wastewater. Moreover, higher solubility of 2,4-D sodium salt (45000 mg/l) than 2,4-D acid (900 mg/l) produced lower affinity towards adsorption.

## CONCLUSION

The ionic surfactants could effectively be removed using oppositely charged metal oxides as adsorbent. The equilibrium contact time was very short compared to time requirement for activated carbon adsorbent. The reaction for both cases followed pseudo-second order reaction model. The removal of AS or CS by alumina or SGW respectively was found to be more in actual wastewater compared to distilled water spiked samples due to presence of high TDS in wastewater. The real wastewaters contained 8068 mg/L of AS and 362 mg/L of CS. Dose study revealed that 10 g/L of SGW dose could remove ~87% of CS within 30 minutes. The regeneration of exhausted metal oxide could be done by acid or alkali. Furthermore, the waste adsorbent having surfactant coating on its surface could be used for removal of different organic pollutants from wastewater through adsolubilization process. SMA and SMSGW were used for removal of CV dye and 2,4-D herbicide from real wastewater. The uptake capacity of CV and 2,4-D were found to be 46.72 and 18.03 mg/g respectively. Thus, alumina and SGW were evaluated as adsorbents for efficient removal of surfactants and other organic pollutants like dye and herbicide from wastewater.

## REFERENCES

- Adak, A., Bandyopadhyay, M. and Pal, A. 2005. "Spectrophotometric determination of anionic surfactants in wastewater using acridine orange". *Indian Journal of Chemical Technology*, 12(2): 145-148.
- Benefield, L.D. and Randall, C.W. 1980. "Biological process design for wastewater treatment". 1<sup>st</sup> Ed., Prentice-Hall, Inc., USA.
- Carter, A.D. 2000. "Herbicide movement in soils: principles, pathways and processes". *Weed Research*, 40: 13-122.
- Chao, Y.-F., Chen, P.-C., Wang, S.-L. 2008. "Adsorption of 2,4-D on Mg/Al-NO<sub>3</sub> layered double hydroxides with varying layer charge density". *Applied Clay Science*, 40: 193-200.
- Donia, M.M., Atia, A.A., Al-amrani, W.A. and El-Nahas A.M. 2009. "Effect of structural properties of acid dyes on their adsorption behaviour from aqueous solutions by amine modified silica". *Journal of Hazardous Material*, 161: 1544-1550.
- Few, A.V. and Ottewill, R.H. 1956. "A spectrophotometric method for the determination of cationic detergents", *Journal of Colloid Science*, 11: 34-38.
- Ho, Y.S. and McKay, G. 1999. "Pseudo second order model for sorption process". *Process Biochemistry*, 34: 451-465.
- Kitiyanan, B., O'Haver, J. H., Harwell, J. H. and Osuwan, S. 1996. "Adsolubilization of styrene and isoprene in cetyltrimethylammoniumbromide admicelle on precipitated silica". *Langmuir*, 12: 2162-2168.
- Kundu, S., Pal, A. and Dikshit, A.K. 2005. "UV induced degradation of 2,4-D: kinetics, mechanism and effect of various conditions on the degradation", *Separation and Purification Technology*, 44: 121-129.
- Lagergren, S. 1898. "Zurtheorie der sogenannten adsorption gelösterstoffe", Bil. K. Svenska
- Luciani, L., Denoyel, R. and Rouquerol, J. 2001. "Poly (ethoxy) anionic surfactants: micellization and adsorption at the solid/liquid interface". *Colloids and Surfaces A: Physicochemical and Engineering Aspects*, 178: 297-312.
- Sapari, N. 1996. "Treatment and reuse of textile wastewater by overland flow". *Desalination*, 106: 179-182.

- Somasundaran, P. and Fuerstenau, D.W. 1966. "Mechanism of alkyl sulfonate adsorption at the alumina-water interface". *J. Phys. Chem.*, 70(1): 90-96.
- Venteskapsakad, Handl. 24; as cited by Wasay et al. 1996. *Water Research*, 30(5): 1143-1148.



## **A COMPARATIVE STUDY ON PRODUCTION OF ACTIVATED CARBON FROM HARDWOOD CHIPS AND PELLETS**

**Hafiz Ahmad\*** and Brandon Madden (Florida State University, Panama City, FL, USA)  
Jordan Mayers (AECOM, Tallahassee, FL, USA)

**ABSTRACT:** Selection of feed-stock from same biomass but different forms sometimes plays an important role in decision-making, especially for building large scale manufacturing plants. Hardwoods in the form of chips and pellets are available in the market and they can be used for commercial production of activated carbon. But the production yields, adsorptive capacity/quality from each form are not known. In this study, first, biochar was produced from hardwood chips and pellets by the pyrolysis process at 850 °F. The biochar was then physically activated (by steam activation) at 1500 °F with various activation (residence) times and different categories of activated carbons were produced. Systematic laboratory tests were performed to determine the yield and iodine number (an indicator of adsorptive capacity, adsorbent quality and surface area) of each product. Models were developed to relate adsorptive capacity (iodine number) and production yield for the activated carbon produced from each type of feed-stock. The study confirmed that chips would be significantly easier to steam activate than pellets and it will give higher yield result than pellets to achieve iodine number of 700 mg/g or more. About 13% more dry wood (by weight) would be required to produce activated carbon with a desirable iodine number of 800 mg/g if hardwood pellets are used rather than chips.

### **INTRODUCTION**

Activated carbon is the highly porous form of solid carbon. They are commonly produced from carbonaceous raw materials using physical and chemical activation methods (Wang, et al., 2013). These carbon products have highly developed internal surface area and porosity which make them eligible for versatile applications. Activated carbon is used in water treatment, gas purification, metal extraction, air filters, medical purposes, energy storage, soil remediation etc. (Kumar, et al., 2006). This pore structure and pore size distribution of activated carbon significantly depends on the nature of the starting material (Gergova et al., 1993, 1994).

In this study, the feedstocks of interest are hardwood chips and pellets. Hardwood chips are medium-sized solid material made by cutting or chipping larger pieces of wood and are commercially done with wood-chipper. On the other hand, hardwood pellets are compressed biomass made by the hammer milling of dried sawdust. In recent years, the rapid increase in pellet production and its easy and large scale commercial availability has made it a good candidate for activated carbon production like hardwood chips. This leads to an opportunity, which was given to us to evaluate these two feed stocks (hardwood chips and pellets) to produce various grade activated carbons and compare their qualities and yields.

In physical activation, biochar is produced during the first step, by pyrolysis of the precursor. This step removes the non-carbon species and produces char with high percentage of carbon (Dalai and Azargohar, 2007). This char has undeveloped porous structure, which makes its usage limited for many practical applications and requires enhancing its porous structures by the activation process (Marsh et al., 1997, Derbyshire, et al., 1995). The second step of physical activation is high temperature gasification (activation) using oxidizing agents such as steam or carbon dioxide, which produces activated carbon with high porosity. This pore development is due to the penetration of the oxidizing agent into the internal structure of the biochar, opening up the blockage of pores by removing the tar and widening the pores (Dalai and Azargohar, 2007). For a certain temperature, the porosity of the activated carbon usually increases with the increase of activation time. However, the yield of the product decreases with the increase of activation time due to its burn-off. Therefore, there is an immense need for finding a balance between porosity, yield and activation time to evaluate a feed stock for its commercial application to produce activated carbon. In this study, two feed stocks (hardwood chips and pellets) are evaluated and compared for production of

activated carbon by finding the relationship between production yield and its porosity derived from different activation times.

# MATERIALS AND METHOD

Biochar and activated carbon from a biomass was prepared by the procedure described in detail elsewhere (Mayers, 2014). A total of 6 tests were performed. Out of these six tests, three were performed for hardwood chips and the other three were for hardwood pellets. Table 1 shows the details of these tests. Initially, the hardwood chips and pellets were cleaned with brushes, all foreign materials were removed and then oven dried. For each test, the dried material was then pyrolysed at 850 °F using a pyrolysis apparatus schematic diagram of which is shown in Figure 1.

**TABLE1: Test conditions for various grade activated carbon production**

Tests	Hardwood Sample	Preparation Conditions		
		Pyrolysis Temperature (°F)	Activation Temperature (°F)	Activation / residence time (minute)
Test-1	chips	850	1500	6
Test-2				12
Test-3				20
Test-4	pellets	850	1500	6
Test-5				12
Test-6				20

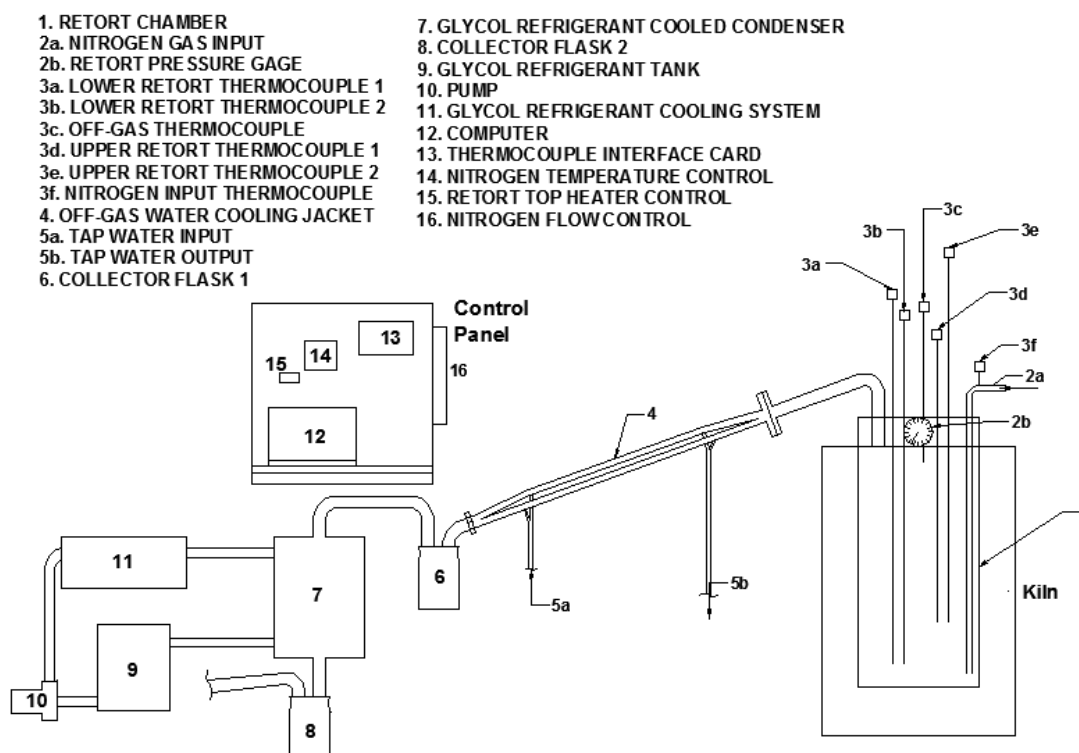


**FIGURE 1.** Schematic diagram of pyrolysis apparatus

The biochar produced from hardwood chips and pellets after pyrolysis (in retort chamber (#1)) was physically activated (steam activation) at 1500 °F for three activation (residence) times (20 minutes, 12 minutes and 6 minutes) and three different grades of activated carbons were produced from each feed stock.

Similar/identical experimental conditions were applied for carbonization and activation process of the two feed stocks. The yield of activated carbon was calculated as follows (Eq. (1)):

$$Y\% = M/M_0 \times 100 \quad (1)$$

Where, M is the mass of activated carbon and  $M_0$  is the mass of air dried feed stock (hardwood chips and pellets).

The iodine numbers (mg of iodine adsorbed/g of activated carbon) of each of these six activated carbon products were determined according to ASTM 4607-86 (1994). This number (i.e. mg of iodine adsorbed per g of activated carbon) is referred as iodine numbers throughout this paper. Besides iodine number, another parameter calculated was modified iodine number (mg of iodine adsorbed/g of wood) and it is expressed as follows:

$$\begin{aligned} \text{Modified iodine number} &= \text{mg I / g of wood} \\ &= (\text{mg I/g of activated carbon}) \times (\text{g of activated carbon/g of wood}) \\ &= \text{iodine number} \times \text{yield} \end{aligned}$$

## RESULTS AND ANALYSIS

**Comparison of Yields and Iodine Numbers.** Figure 2(a) shows activated carbon yields at various activation/residence time. As seen in this Figure, yield decreases with the increase of activation time. This is due to the fact that burn-off of carbon increases with the increase of activation time. Activated carbon yield from hardwood chips at 6 minute residence time was 17.18%, and it is 15.29% when residence time is 12 minute and it went down to 12.77% when residence time was increased to 20 minutes. Similar pattern was also observed for hardwood pellets. Activated carbon yields from pellets were 17.17%, 14.58%, 10.67% for 6, 12 and 20 minute residence times respectively.

Comparing the yields of hardwood chips and pellets at each activation time, it was found that yield of activated carbon from hardwood chips is higher than that of pellets in all cases (Figure 2(a)). As for example, activated carbon yield from chips for the 20 minute residence time is 12.77% while it is 10.67% for pellets for the same residence time. This indicates, activated carbon production from hardwood chips could be more favorable than pellets.

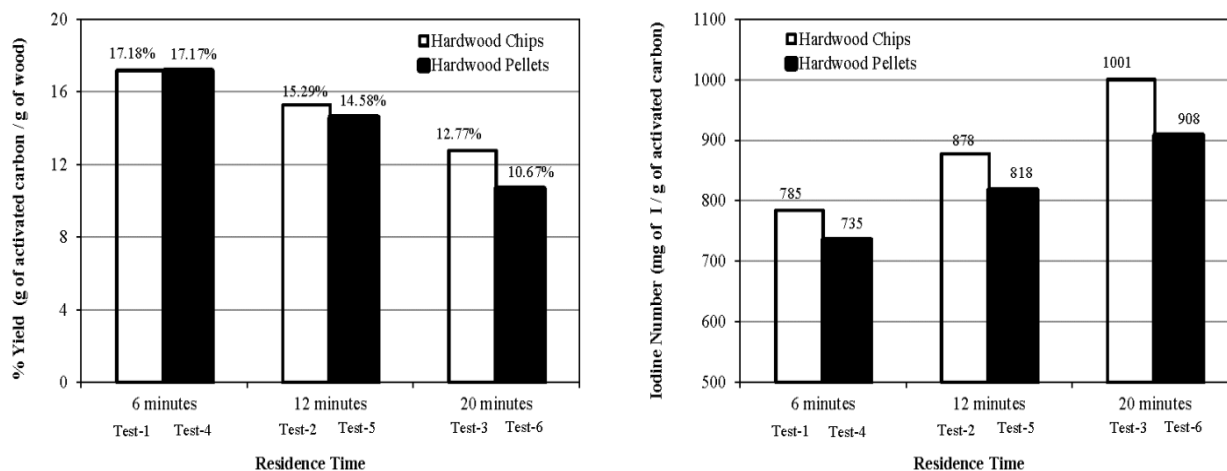


**FIGURE 2.** (a) Activated carbon yield at various activation times, (b) Iodine numbers of activated carbon produced at various activation times.

Though increase of residence time reduces the yield of activated carbons, the opposite phenomena occur for the quality of the carbon product. In other words, with the increase of temperature, the iodine number increases (Figure 2(b)) indicating more porous, more surface area and more adsorptive capacity of the products. Iodine number for the activated carbon produced from hardwood chips was 785 mg/g for the 6 minute residence time. This iodine number increases to 878 mg/g and 1001 mg/g for the residence time of 12 minutes and 20 minutes respectively. Similar pattern observed for hardwood pellets. Iodine numbers

determined for hardwood pellets were 735 mg/g, 818 mg/g, 908 mg/g for the residence time of 6 minutes, 12 minutes and 20 minutes respectively.

Comparing the iodine numbers of hardwood chips and pellets (Figure 2(b)), it is seen that the iodine number of activated carbon from hardwood chips is higher than that of pellets in all cases. Iodine number of activated carbon from hardwood chips is 785 mg/g while it is 735 mg/g for pellets for the same residence time (6 minutes). For 12 minutes residence time, iodine numbers of chips and pellet are 878 and 818 mg/g respectively. For the 20 minute residence time the iodine number for chips is 1001 mg/g while it is 908 mg/g for pellet for the same residence time. This again indicates that activated carbon production from hardwood chips could provide better quality product than that of pellets.

**Model Development.** As mentioned above and seen in Figure 2(b), the increase in residence time increases the iodine number (i.e. quality of the product). However, this increase in iodine number was achieved at the expense of the yield of activated carbon (Figure 2(a)). So, it is imperative to find a relationship between iodine number and yield of activated carbon derived from each feed stock (hardwood chips and hardwood pellets) and compare them. Iodine numbers vs. yield of activated carbon from feed stocks are plotted and presented in Figure 3. These plots within the range tested exhibit a linear correlation (the correlation coefficients of plots,  $R^2$ , are greater than 0.99 in both cases). Considering linear relationship (within the test range) of iodine number and product yield for hardwood chips and pellets, following relationships were determined (Figure 3).

$$\text{Hardwood chips:} \quad Y = -4896.9 X + 1625.9 \quad (2)$$

$$\text{Hardwood pellets:} \quad Y = -2631.2 X + 1192.3 \quad (3)$$

Where, Y and X are iodine number (mg I/g of activated carbon) and yield (g of activated carbon/g of wood) respectively.

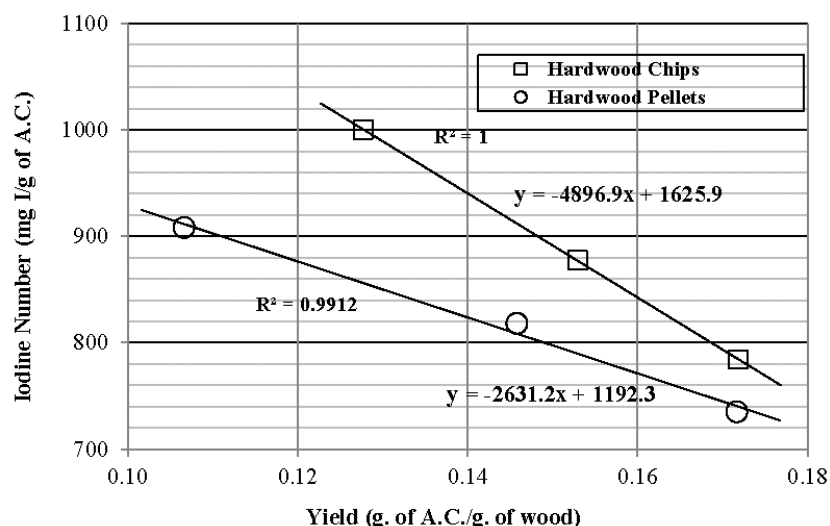


**FIGURE 3.** Iodine number vs. activated carbon yield from woods

Comparing the hardwood pellets with chips, Figure 3 shows that the yield of activated carbon from hardwood chips is significantly higher than pellets at the higher iodine numbers (700 mg/g). In other words, to achieve a certain yield, higher iodine number can be produced from hardwood chips than that from hardwood pellets. As for example, from Figure 3, it is seen that to achieve a 14% yield (wood basis), approximate iodine number from hardwood pellet is 820 mg/g. On the other hand, from same 14% yield (wood basis), approximate iodine number from hardwood chips is 940 mg/g.

In industry, it is more conventional to express the porosity characteristics per unit mass of raw material instead of the product (Dalai and Azargohar, 2007). So, to further investigate, plots of modified iodine number (mg. I/g of dry wood) vs. iodine number (mg I/g of activated carbon) are plotted for hardwood chips and pellets and shown in Figure 4. These curves are generated by using the models

((equation (2) for hardwood chips and equation (3) for hardwood pellets). For different iodine numbers the corresponding yield was calculated from the equation. Then, the modified iodine number was determined by taking the product of iodine number and corresponding yield (which was detailed earlier).

It can be seen that from Figure 4 that dry wood basis porosity (i.e. modified iodine number) exhibits a maximum value when it reaches to a certain porosity of activated carbon (i.e. iodine number). To achieve the iodine number 800 mg/g, modified iodine numbers were found 120 mg/g for hardwood pellet and 138 mg/g hardwood chips (Figure 4). These infer that, 1 mg of iodine can be adsorbed in 8.33 mg of wood pellets while same 1 mg of iodine can be adsorbed in 7.25 mg of wood chips indicating about 13% more wood is needed to achieve the same porosity if hardwood pellets are used rather than chips.

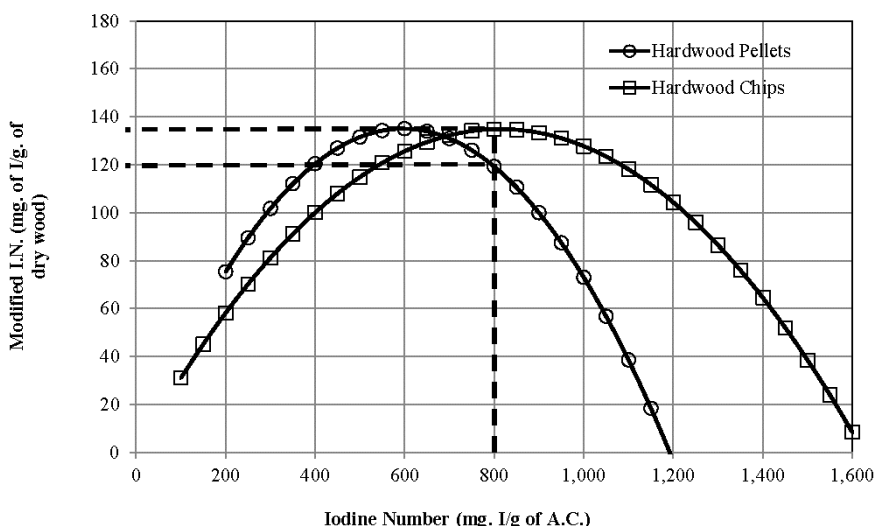


**FIGURE 4.** Modified iodine number vs. iodine number

## CONCLUSIONS

Various grades of activated carbons were produced from hardwood chips and hardwood pellets by the method of physical activation. The effect of activation times (for 1500°F temperature) on adsorption capacity, production yields was studied. The study demonstrates that by increasing temperature, the adsorptive capacity of the activated carbon can be increased but this will result in decrease of the product yield. Models were developed to relate adsorptive capacity (iodine number) and production yield for the products produced from each type of feed-stock (i.e. hardwood chips and pellets). The study confirmed that chips would give higher yield result than pellets to achieve iodine number of 700 mg/g or more. Additionally, 13% more dry wood would be required to produce activated carbon with a desirable iodine number of 800 mg/g if hardwood pellets are used rather than chips.

## ACKNOWLEDGEMENT

The authors gratefully acknowledge the financial support provided by the Pyrolysis Tech. LLC., Gladwyne, Pennsylvania.

## REFERENCES

- Dalai, A.K. and R. Azargohar. 2007. "Production of Activated Carbon from Biochar Using Chemical and Physical Activation: Mechanism and Modeling", *In Materials, Chemical, and Energy from Forest Biomass*; Argyropoulos, D.; ACS Symposium Series; American Chemical Society: Washington D.C.
- Derbyshire, F., M. Jagtoyen and M. Thwaites, "Porosity in Carbons: Characterization and Applications" In W. Patrick Jr. (Ed.), Edward Arnold, London, 1995, Chapter 9.
- Gergova, K., N. Petrov and S. Eser. 1994. "Adsorption Properties and Microstructure of Activated Carbons Produced from Agricultural Byproducts by Steam Pyrolysis" *Carbon* 32, 693–702.

- Gergova, K., N. Petrov, V. Minkova. 1993. "A Comparison of Adsorption Characteristics of Various Activated Carbon" *J. Chem. Tech. Biotechnol.* 56, 77–82.
- Kumar, B.G.P., K. Shivakamy, L.R. Miranda and M. Velan. 2006. "Preparation of Steam Activated Carbon from Rubberwood Sawdust (*Hevea brasiliensis*) and its Adsorption Kinetics" *J. Hazard Mater.* 136: 922–929.
- Marsh, H., E.A. Heintz and F. Rodriguez-Reinoso. 1997. "Introduction to Carbon Technologies", First ed., Universidad de Alicante, Secretariado de Publicaciones, Chapter 2.
- Mayers, J. 2014. *Pyrolysis and Activation of an Invasive Species*. M.S. Thesis, Florida State University, Tallahassee, FL.
- Wang, X., D. Li, W. Li, J. Peng, H. Xia, L., Zhang, S. Guo and G. Chen. 2013. "Optimization of Mesoporous Activated Aarbon from Coconut Shells by Chemical Activation with Phosphoric Acid" *BioResources*, 8(4): 6184-6195.

## MOLECULAR SIMULATION AND VALIDATION STUDIES OF RESORCINOL ADSORPTION ON ORDERED MESOPOROUS CARBON

Bing Chao, *Zaki Uddin Ahmad* and Daniel Dianchen Gang\*  
(University of Louisiana at Lafayette, Lafayette, LA70504, USA)

**ABSTRACT:** Ordered Mesoporous Carbons (OMCs) with well-controlled pore structure and narrow pore size distribution demonstrated great potential as highly functional adsorbents. The pore size and surface chemistry of OMCs were considered as two most important factors that affect the adsorption capacity of organic compounds. The objective of this study was to optimize the structure of OMCs for resorcinol adsorption by changing the pore size and oxygen content using computational approach. New rhombic OMC models with varied pore size and oxygen content were constructed using Materials Visualizer module. The specific surface area, total pore volume and resorcinol adsorption capacity results were calculated by Forcite and sorption module in Materials Studio package. The simulation results were validated by the experimental data. Experimentally, the OMCs were synthesized using sucrose as carbon precursor by hard-template method. The tunable pore size (4 nm to 15 nm) and oxygen content of the OMCs are obtained by adjusting the amount of boric acid as a pore-expanding reagent. The experimental results such as BET surface area, pore size distribution and adsorption capacity of resorcinol were compared with the simulation results.

### INTRODUCTION

Ordered Mesoporous Carbons (OMCs) with well-controlled pore structure and narrow pore-size distribution demonstrate great promise for their adsorption of inorganic and organic contaminants. Several methods (Yuan et al., 2007; Kim et al., 2005; Peng et al., 2008) have been proposed and studied experimentally to prepare OMCs and investigate the relationship between OMCs' characterizations and adsorption capacity. Based on their studies, the pore size and surface chemistry of OMC are identified as two important factors that affected the adsorption capacity for organic compounds. Even though extensive experimental studies have been carried out on adsorption process over OMCs, the interactions between OMCs and adsorbates are not fully understood. As a complementary technique, molecular simulation method has been introduced. Zhou et al. (2008) constructed a hexagonal model of MCM-41 and studied CO<sub>2</sub> adsorption on MCM-41 by the Grand Canonical ensemble Monte Carlo (GCMC) simulation. Chen et al. (2009) constructed a MCM-41 model using Materials Visualizer module and investigated the toluene adsorption. In all these works, it was generally assumed that rectangular structure is the repetitive unit. However, OMC prepared by SBA-15 as the hard template possessed two-dimensional hexagonal (p6mm) pore structure (Fig.1). The rectangular model subjected to several limitations such as difficulties on controlling the pore size and forming the hexagonal structure. So in this study, a new rhombic template was proposed as the repetitive unit of OMC models.

Herein, we present a study of OMCs with different pore sizes and oxygen contents using Materials Studio to investigate the structural information and adsorption behaviour and find out the optimal pore size and oxygen content for resorcinol adsorption. In the experimental phase, the OMCs with varied pore sizes and oxygen contents were synthesized using boric acid as the pore-expanding reagent following the work of Dai et al. (2010).

### MATERIALS AND METHODS

**Construction of OMC models.** In this study, a new OMC model using rhombus shaped repetitive cell and ZSM-5 (Fig. 2(a)) as the unit cell was proposed. ZSM-5 is an aluminosilicate zeolite abundant in micropores. The unit cell was modified by changing all the other atoms to carbon atoms. The obtained structures were

optimized by Forcite module. The lattice parameter of angle was set to  $\alpha = 90^\circ$ ,  $\beta = 90^\circ$  and  $\gamma = 120^\circ$  in order to build a hexagonal array structure.

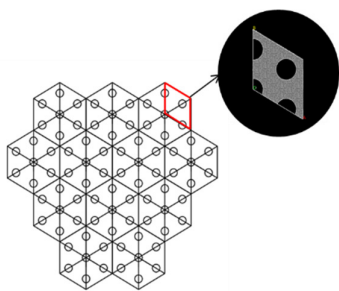


**FIGURE 1.** Repetitive unit for OMC model

The OMC models with different pore sizes (from 4 nm to 12 nm) can be obtained by changing the radius of the carving cylindrical channel. OMCs model with varied oxygen content was modelled by adding O atoms on the unsaturated C atom sites. The final models generated were geometrically optimized by Forcite module in Materials Studio packages via COMPASS force field.

**Fabrication of OMCs.** The synthesis of SBA-15 followed the method reported by Zhao et al. (1998) with modification on the reaction temperature and period. The mixture of silica source (Tetraethyl Orthosilicate, TEOS) and surfactant Pluronic P123 (PEO-PPO-PEO, BASF) was placed in a water bath for 4h at 40°C, followed by aging for 24h at 90°C. The SBA-15 was obtained after calcination in air at 550°C

for 8h. Different amount of boric acid were added to obtain different pore size expansion. The carbon replicas were denoted as OMC-x. The x value indicated the molar ratio of boric acid to carbon precursor, which is varied from 0 to 12. In a typical synthesis of OMC-1, 0.27 g of boric acid (99.8 wt%), 1.5 g of sucrose and 4 drops of concentrated  $\text{H}_2\text{SO}_4$  were dissolved in 5.0 ml distilled water. After adding 2 g of SBA-15, the mixture was heated at 100°C for 6 h and subsequently at 160°C for another 6 h. The resulted composite was impregnated again with an aqueous solution of 0.09 g of boric acid, 0.51 g of sucrose and 15 drops of concentrated  $\text{H}_2\text{SO}_4$ . The dried composite was carbonized at 700°C for 8 h under the nitrogen atmosphere. Finally, the OMC-1 was obtained by the removal of SBA-15 using 48% HF solution at room temperature.

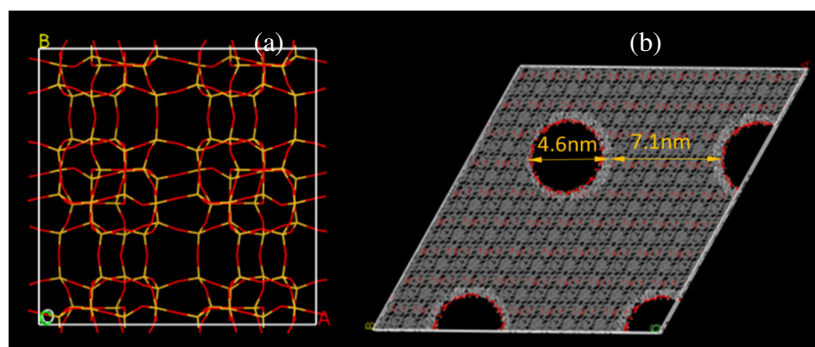


**FIGURE 2.** The model of (a) ZSM-5 repetitive unit (b) OMC

## RESULT AND DISCUSSION

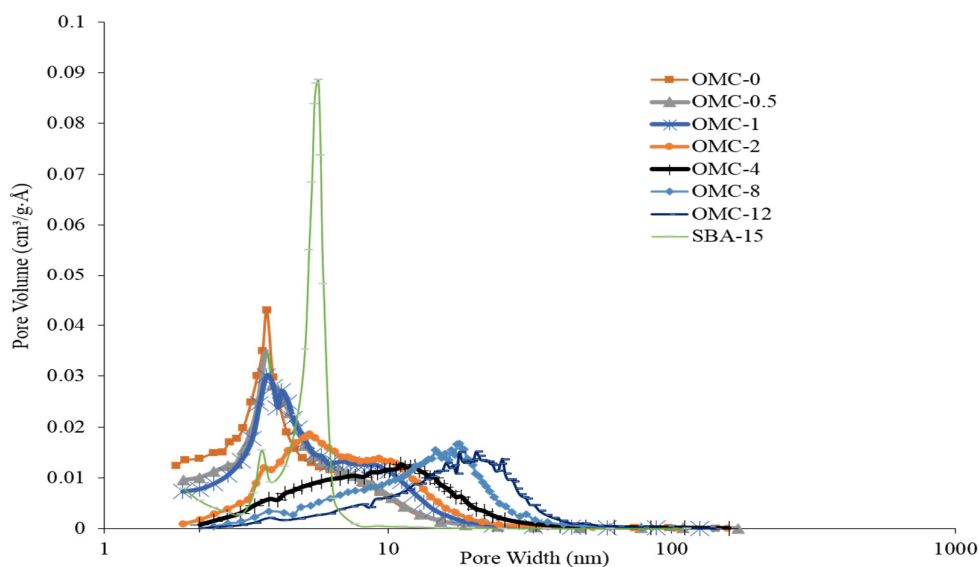
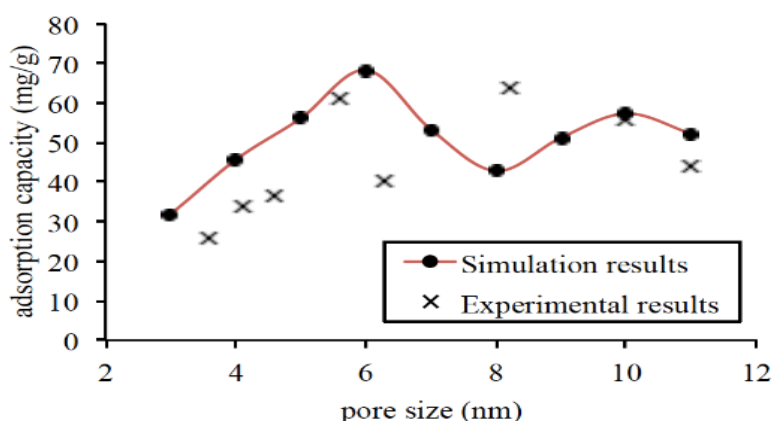
**Verification of the OMC model.** A reliable model of OMC materials is the basic criteria for simulating the adsorption process. The optimized OMC with the same unit cell parameter of OMC-0 is shown in Fig. 2(b). The radius of the pore is 4.6 nm and wall thickness is 7.1 nm, respectively. The optimized structure parameter and element contents of the OMC model and OMC-0 sample made by sucrose were listed in Table 1. The decrease in surface area and pore volume was caused by the ideally ordered structure assumed for the OMC model. Similar results were obtained in the MCM-41 model built by Chen et al. (2009). However, such difference has no significant effect on describing pore structure of the experimentally produced OMCs, while other parameters match the real experimental results.

The adsorption process was simulated by Soption module which was based on GCMC theory. The loading of resorcinol in equilibrium was 157 adsorbed resorcinol per cell. After calculating, the simulated adsorption capacity of OMC model was 41 mg/g, which approached the experimental data of 36.5 mg/g. Therefore, the OMC model is a reliable model for adsorption simulation.



**TABLE 1.** Lattice parameters and element contents of OMC model and OMC-0 sample

Name	Pore size (nm)	Wall thickness (nm)	Oxygen content (%)	Carbon content (%)	Density (g/cm <sup>3</sup> )	Pore volume V(cm <sup>3</sup> /g)	SSA (m <sup>2</sup> /g)
OMC model	4.6	7.1	11.2	85.3	1.13	1.36	969.3
OMC-0 sample	4.6	7.1	13.3	83.7	1.12	1.58	1404.2

**FIGURE 3.** Pore size distributions for SBA-15 and OMCs**FIGURE 4.** Comparison of the simulation results and experimental results: adsorption capacity vs. pore size**Resorcinol****Adsorption on OMC.**

**Effect of pore size.** The increase in the pore size with the increase in boron content was confirmed by pore size distributions (Fig. 3). The pore size distributions were determined by the desorption branches of the isotherms. The OMC-4, OMC-8 and OMC-12 give flatter peaks, which indicated wider ranges of

pore size and less ordered structure. The largest pore size (11.3 nm) was obtained by OMC-12, which was extremely close to the unit cell length. For these three samples, the wall thickness was too thin to support the rigid carbon structure and therefore, less ordered carbon structure was obtained. The same observation was obtained by Ryoo et al. (2001). In general, the OMCs made with different ratio of boric acid to sucrose have tailored pore sizes ranging from 4.6 nm to 11.3 nm. In order to investigate the effect of pore size on the adsorption performance, a series of OMC models with different pore sizes (from 3 nm to 11 nm) were built using Materials Studio. The unit cell parameter was maintained at 11.7 nm, which was the same as the experimental OMCs. The simulation results are shown in Table 2. The relationships between the pore sizes with adsorption capacities were plotted and compared with the experimental data as shown in Fig. 4. The simulation results and experimental data showed a similar trend with average relative error of 0.1938. That means the simulation results well fitted the experimental results. The highest adsorption capacity could be obtained at the diameter of 6 nm, which also yielded a larger surface area. The larger pore size did not promise a better adsorption capacity. From simulation results, it was observed that the specific surface area was the main factor affecting the adsorption capacity, which satisfied the conclusion drawn by You et al. (2009).

**TABLE 2.** Structural parameter and adsorption capacity of the OMC model

Pore size (nm)	Density (g/cm <sup>3</sup> )	Specific surface area (m <sup>2</sup> /g)	Wall thickness (nm)	Adsorption capacity (mg/g)
3	1.06	808.53	8.7	31.5
4	0.955	973.2	7.7	45.6
5	0.857	1132.2	6.7	56.1
6	0.77	1347.6	5.7	68.3
7	0.73	1148.5	4.7	53.3
8	0.666	954.3	3.7	42.8
9	0.613	963.2	2.7	51.2
10	0.579	986.7	1.7	57.3
11	0.543	990.3	0.7	52.2

**Effect of oxygen content.** The effects of oxygen content on the surface of the OMC model were evaluated by constructing the OMC model doped with different amount of oxygen atoms and pore size of 4.6 nm as the basic structure. Oxygen content was the only variable in this iteration of simulation. The oxygen atoms existed in the form of hydroxyl groups and carboxyl groups and distributed on the surface of the pore structure. The simulation results are shown in Table 3.

**TABLE 3.** Adsorption simulation results for OMC model with different oxygen contents

Pore size (nm)	Oxygen content (%)	Density (g/cm <sup>3</sup> )	SSA (m <sup>2</sup> /g)	Adsorption capacity (mg/g)
4.6	0	0.87	1028.3	41.3
4.6	2.9	0.92	1030.5	43.6
4.6	4.4	1.03	1031.4	45.1
4.6	6.2	1.28	1033.5	45.8
4.6	9.6	1.49	1035.7	46.7
4.6	12.3	1.69	1036.8	47.2

It was observed from Fig. 5 that the adsorption capacity of resorcinol increased with additional oxygen atoms distributed on the pore surface. Comparing with the influence of specific surface area with the influence of oxygen-containing functional groups, the specific surface area increased the adsorption capacity up to approximate 116% while the influence of oxygen-containing functional group for the adsorption of resorcinol was nearly negligible confirming that the adsorption process was more of a physical process rather than a chemical process.

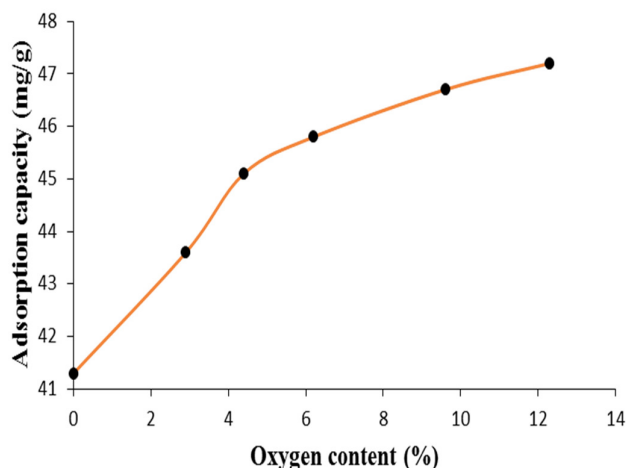


**Figure 5.** The plot of adsorption capacity vs. oxygen content

## CONCLUSION

synthesized

precursor and boric acid as the pore expanding reagent via hard template method. The experimentally obtained results were used for validating the results of computational simulation on the adsorption of resorcinol. In the simulation, OMC models with different pore sizes and oxygen contents were constructed to evaluate the adsorption performance of OMC materials for resorcinol removal. The GCMC simulation on resorcinol adsorption suggested that (a) the optimal pore sizes were found to be around 6 nm and the corresponding adsorption capacity of 68.3 mg/g; (b) with the increase in oxygen content, the adsorption capacity increased with growth rate of 14%. The improvement of adsorption capacity was not significant comparing with the influence of specific surface area, since the adsorption process was more of a physical process rather than chemical process.

OMC materials were using sucrose as the carbon

## ACKNOWLEDGEMENTS

This work was supported by the Louisiana Board of Regents under BORSF (2010-2015)-LaSpace and by NASA under award NNX10AI40H.

## REFERENCES

- Chen, H., H. Xi, X. Cai and Y. Qian. 2009. "Experimental and molecular simulation studies of a ZSM-5-MCM-41 micro-mesoporous molecular sieve." *Microporous and Mesoporous Materials*. 118(1-3):396-402.
- Dai, W., M. Zheng, Y. Zhao, S. Liao, G. Ji and J. Cao. 2010. "Template synthesis of three-dimensional cubic ordered mesoporous carbon with tunable pore sizes." *Nanoscale Res. Lett.* 5(1): 103-107.
- Guo, R., J. Guo, F. Yu, D. D. Gang. 2013. "Synthesis and surface functional group modifications of ordered mesoporous carbons for resorcinol removal." *Microporous and Mesoporous Materials*. 175: 141-146.
- Kim, D. J., H. I. Lei, J. E. Yie, S. Kim and J. M. Kim. 2005. "Ordered mesoporous carbons: implication of surface chemistry, pore structure and adsorption of methyl mercaptan." *Carbon*. 43(9): 1868-1873.
- Lee, H. I., J. H. Kim, D. J. You, J. E. Lee, J. M. Kim, W. S. Ahn, C. Pak, S. H. Joo, H. Chang and D. Seung. 2008. "Rational synthesis pathway for ordered mesoporous carbon with controllable 30 to 100-angstrom pores." *Advanced Material*. 20(4): 757-762.
- Peng, X. D., D. Cao and W. Wang. 2008. "Heterogeneity characterization of ordered mesoporous carbon adsorbent CMK-1 for methane and hydrogen storage: GCMC simulation and comparison with experiment." *Journal of Physical Chemistry*. 112(33): 13024-13036.

- Ren, H., W. Shou, C. Ren and D. Gang. 2016. "Preparation and post-treatments of ordered mesoporous carbons (OMC) for resorcinol removal." *International Journal of Environmental Science and Technology*. 13(6): 1505-1514.
- Ryoo, R., S. H. Joo, S. Jun, T. Tsubakiyama and O. Terasaki. 2001. "Ordered mesoporous carbon molecular sieves by template synthesis: the structural varieties." *Studies in Surface Science and Catalysis*. 135: 150.
- Shou, W., B. Chao, Z. U. Ahmad and D. Gang. 2016. "Ordered mesoporous carbon preparation by the in situ radical polymerization of acrylamide and its application for resorcinol removal." *Journal of Applied Polymer Science*. 133(19): 43426.
- You, C., Y. Xu, Y. Wang, S. Zhang, J. Kong, D. Zhao and B. Liu. 2009. "Electrocatalytic oxidation of NADH based on bicontinuous gyroidal mesoporous carbon with low overpotential." *Electrochemistry Communication*. 11(1): 227-230.
- Yuan, X., S. Zhou, W. Xing, H. Cui, X. Dai, X. Liu and Z. Yan. 2007. "Aqueous dye adsorption on ordered mesoporous carbons." *Journal of Colloid and Interface Science*. 310:83-89.
- Zhao, D., S. Sun, Q. Li, J. Feng and G. D. Stucky. 2000. "Morphological control of highly ordered mesoporous silica SBA-15." *Chemistry of Materials*. 12(2): 275-279.
- Zhao, J. 2014. *Simulation on the self-assembly behavior of ordered mesoporous carbons and their performance in adsorption*. M.S. Thesis, South China University of Technology, China.
- Zhou, S., Y. Huang, J. Hu, H. Liu and J. Jiang. 2008. "Computer simulation of adsorption of CO<sub>2</sub>, N<sub>2</sub> and flue gas in a mimetic MCM-41." *Journal of Physical Chemistry C*. 112:11295-11300.

## **PHENOL REMOVAL FROM WATER USING BIOCHAR AND ACTIVATED CARBON FROM ALBIZIA: AN INVASIVE PLANT EVALUATION**

*Hafiz Ahmad*, Korhan Adalier, Brandon Madden and  
Douglas Brown (Florida State University, Panama City, FL, USA)

**ABSTRACT:** Examining the performance of carbon products of various activation levels sometimes play important role, especially to determine the operating conditions of large scale activated carbon manufacturing plants. This study compares the removal performance of phenol from water using biochar and two physically (steam) activated carbons (having two different activation levels) produced from the same biomass, Albizia, an invasive plant. First, biochar was produced from Albizia by pyrolysis process at 850 °F. This biochar was then physically activated at 1500 °F with two different activation times (20 minutes and 35 minutes). The iodine number (an indicator of adsorbent quality, surface area and porosity) of each of these three products, biochar and two activated carbons were determined to be 132 mg/g, 835 mg/g and 1103 mg/g respectively. Batch kinetic experiments and isotherm studies were performed to compare the effect of activation levels of activated carbons (iodine number of 1103 mg/g and 835 mg/g) with biochar (used as base-line with iodine number of 132 mg/g) on phenol adsorption. Batch kinetic studies showed that phenol removal can be increased more than 1.5 times with a target dosage range 200 mg/L to 400 mg/L if activated carbons are used rather than biochar. The equilibrium data represented by Freundlich isotherm model also supported the above results showing the enhanced performance of activated carbon compared to biochar on phenol removal.

### **INTRODUCTION**

Phenols are toxic organic pollutants, common in industrial effluent such as oil refineries, coal tar, disinfectants, pharmaceutical and steel industries (Lin and Juang, 2009). Besides these industrial sources, phenolic derivatives exist in pesticides, insecticides, domestic wastewater. The US Environmental Protection Agency (EPA) regulations call for lowering phenol content in the wastewater to less than 1 mg/L (Banat, et al., 2000). Removal of the phenolic pollutant from wastewater is very difficult by conventional biological treatment process as they are resistant to microbial degradation. Besides biodegradation, other common phenol removal methods that are in practice include stripping, solvent extraction, oxidation, ion exchange and adsorption methods. Among them, the carbon adsorption method has become a popular method in recent years because of its large adsorption capacities, fast adsorption kinetics and relative ease of regeneration (Subramanyam and Das, 2009).

The adsorption of phenol depends on various factors such as surface areas, micro-pore volumes, adsorption capacities of the carbon. These characteristics are controlled by the operating conditions (e.g. temperature, heating rate, residence time etc.) during their production/activation. This operating condition is controlled to achieve the desired activation level (i.e. quality) of the product for its end-use. As for example, for the targeted application of carbon to remove phenol from aqueous solution, various qualities of carbon products can be produced by controlling two major operating conditions (temperature and residence time) during pyrolysis and activation process. However, the prediction of optimum activation level for most efficient removal of phenol from aqueous solution is quite difficult without laboratory tests and/or model study. Therefore, it is essential to test the effectiveness especially for the products which are derived from low-cost, less-known invasive plants like Albizia.

In our recent research (Mayers, 2014), biochar and various grades of activated carbons were produced from Albizia, an invasive fast-growing plant of tropical regions. The biochar was produced by pyrolysis method and this biochar was further physically activated to produce activated carbon of two activation levels by controlling the activation residence times. Activation level and porosity of these carbon products from this low-cost feedstock were assessed by iodine numbers, a popular parameter used to estimate relative surface area, adsorptive capacity (Wang et al., 2013). To evaluate the performance of phenol removal from water, in this paper, bio-char (iodine number 132 mg/g) is used as a base-line. Then,

two different activated carbons (iodine numbers 835 mg/g and 1103 mg/g) were used to compare their effectiveness with the base-line (i.e. biochar).

## MATERIALS AND METHOD

**Adsorbent Preparation.** Biochar and activated carbon from Albizia plant was prepared by the procedure described in detail elsewhere (Mayers, 2014). Initially, the Albizia chips were cleaned with brushes, all foreign materials were removed and then oven dried. The dried material was then pyrolysed at 850 °F using a pyrolysis apparatus schematic diagram of which is shown in Figure 1.

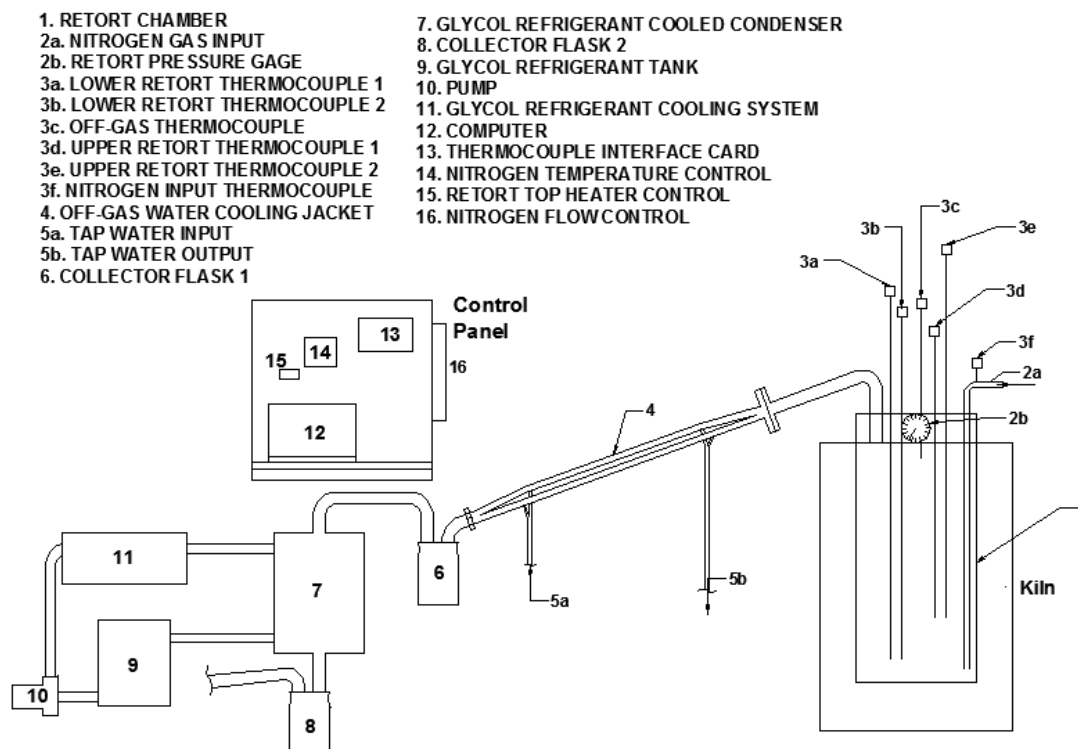


FIGURE 1. Schematic diagram of pyrolysis apparatus

TABLE 1: Iodine number, surface area and major preparation conditions of adsorbents

Absorbent	Preparation Conditions			Adsorbent Quality	
	Pyrolysis Temperature (°F)	Activation Temperature (°F)	Activation time (minute)	Iodine Number (mg/g)	Surface Area (m <sup>2</sup> /g)
Biochar (referred BC#132 afterwards)	850	-	-	132	130
Activated Carbon (referred AC#835 afterwards)	850	1500	20	835	823
Activated Carbon (referred AC#1103 afterwards)	850	1500	35	1103	1009

The biochar produced after pyrolysis (in retort chamber #1) is then physically activated (steam activation) at 1500 °F for two residence times (20 minutes and 35 minutes) and two different grades of

activated carbons were produced. The iodine numbers (IN) of each of these three products were determined. The surface areas of the same products were estimated using the model proposed by Mianowski et al. 2007. The values of iodine number (IN), surface area of each product and their production operating conditions are shown in Table 1.

**Adsorption Procedure.** All the three carbon products (BC#132, AC#835, AC#1103) were first ground using a standard mortar and pestle then passed through a #250 sieve. The samples were then dried at 320 °F for a period of 24 hours. Different amount of adsorbents (dose ranging from 20 mg/L to 400 mg/L) were then added to each 1000 mL flask containing 1.0 mg/L (i.e. 1000 µg/L) phenol solutions. All these 1000 mL flasks were sealed and installed in a water shaker (120 rpm) with a constant temperature of 77 °F and the adsorption experiments were run at a batch mode. After equilibrium (2 hour), the mixing was stopped, and the mixed solution was filtered with filter paper (Whatman No. 42) and analyzed for the residual phenol concentration, which was determined by measuring its absorbance at 510 nm using a Perkin Elmer Lambda XLS spectrophotometer (Method 420.1, EPA). Phenol removal percentage (R%) was calculated as follows (Eq. (1)):

$$R\% = [(C_0 - C_e)/C_i] \times 100 \quad (1)$$

The amount of adsorption at equilibrium,  $q_e$  (mg/g), was calculated by (Eq. (2)):

$$q_e = [(C_0 - C_e)V]/M \quad (4)$$

Where,  $C_0$  and  $C_e$  (mg/L) are the liquid-phase concentrations of phenol at initial and equilibrium, respectively.  $V$  (L) is the volume of the solution, and  $M$  (g) is the mass of dry adsorbent used.

## RESULTS AND ANALYSIS

**Comparison of Phenol Removal.** Figure 2 shows the phenol removal using various doses of BC#132, AC#835 and AC#1103 from the solution of pH 6.2. Carbon dosage was varied from 24 mg/L to 400 mg/L. The results show that the activated carbons (AC#835 and AC#1103) are more effective than biochar (BS#132) for the quantitative removal of 1 mg/L (i.e. 1000 µg/L) of phenol in 1000 ml. The phenol removal can be increased more than 1.5 times with a target dosage range 200 mg/L to 400 mg/L if activated carbons

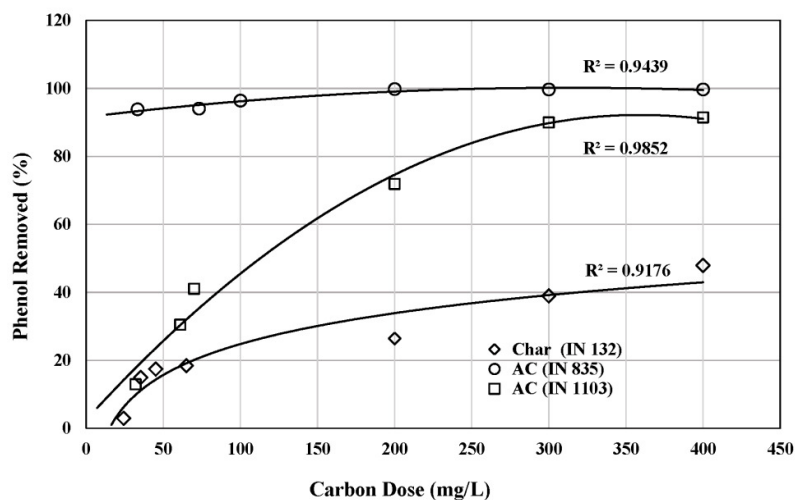


**FIGURE 2.** Effect of carbon dose on removal of phenol

are used rather than biochar. For example, for biochar (base-line), 39% phenol removal is achieved with a dose of 300 mg/L but at that same dose, AC#1103 achieves a removal of 90% while AC#835 achieves 99.7%.

The removal of phenol using BS#132 and AC#1103 significantly improves up to the doses of 200 mg/L. Beyond this dose (200 mg/L), the change of removal efficiency is relatively small for these two products. However, for AC#835, a low carbon dosage of 100 mg/L can achieve significant (96%) removal of phenol. Beyond this dosage, the change of removal efficiency of AC#835 is minor. It is evident from the results that among these three products, the best phenol removal can be achieved by the activated carbon with IN of 832 mg/g (AC#835).

**Phenol Adsorption on the Adsorbents.** Phenol adsorption onto three different adsorbents were calculated and shown in Figure 3 (a). Comparing the capacity of phenol adsorption at 2 hour time, it is clear that activated carbons (AC#835 and AC#1103) are much better performer than biochar (BC#132, base-line) for phenol removal. Maximum phenol adsorption achieved was 5 mg/g using AC#835 while lowest adsorption was 1.2 mg/g on BC#132 (Figure 3(a)) with a 200 mg/L of dose. High phenol adsorption was also achieved by using AC#1103 (3.6 mg/g) with the same dose. This reveals that activation is needed to enhance quality of biochar. However, optimum activation condition to capture maximum phenol is approximately 1500 °F temperature and 20 minute residence time (that resulted AC#835).

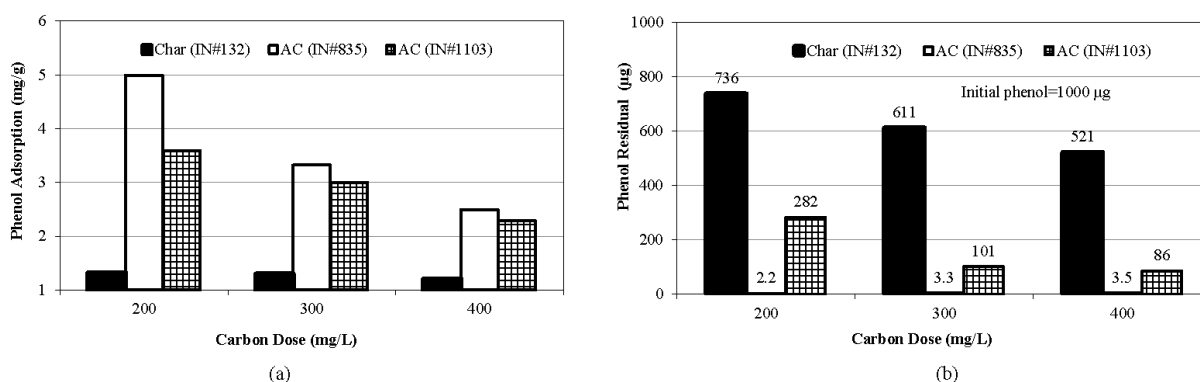


**FIGURE 3.** (a) Phenol Adsorption by carbon products, (b) Phenol residual at equilibrium.

For AC#835, phenol removal due to addition of this product beyond the dose of 200 mg/L is relatively small (Figure 2). At this dose, 99.8% phenol is removed using this AC#835. Also, Figure 3 (a) shows that the dose of 200 mg/L exhibits better phenol adsorption rate (5 mg/g) for this product compared to the other doses (i.e. 300 mg/L, 400 mg/L). This suggests that the 200 mg/L of AC#835 dose could be used for high performance phenol treatment process.

**Phenol Residual in Water.** Figure 3(b) shows the results of residual phenol in the solution at equilibrium (2 hour). As seen in this Figure, the maximum phenol residual in the solution was 736 µg when BC#132 is used while residual was lowest (2.2 µg) when AC#835 is used. In other words, maximum phenol was removed when AC#835 was used. Low residual of phenol was also found when AC#1103 was used. This again shows that biochar activation significantly improves the adsorption capacity of the adsorbent and thereby improves the phenol removal efficiency. This also implies that by enhancing the surface area and porosity to an optimum level, the biochar can be converted to a high-performing product (like AC#835).

**Adsorption Isotherm.** Adsorption isotherm plays a vital role for the analysis and design of adsorption systems as well as model prediction (Mukherjee et al., 2007). It describes how solutes interact with adsorbents, and is critical in optimizing the use of adsorbents (Hameed and Rahman, 2008). The Freundlich isotherm models were commonly used to describe the relationship between the amount of phenol adsorbed and its equilibrium concentration in solutions. The Freundlich isotherm is given by (Eq. (3)):

$$q_e = K_F C_e^{1/n} \quad (3)$$

where  $q_e$  (mg/g) amount of adsorption at equilibrium,  $C_e$  (mg/L) is the liquid-phase concentrations of phenol at equilibrium.  $K_F$  and  $n$  are Freundlich constants. The linear form of the above Equation is (Eq. (4)):

$$\log q_e = \log K_F + (1/n) \log C_e \quad (4)$$



which will have a straight line with a slope of  $1/n$  and an intercept of  $\log(K_F)$  when  $\log(q_e)$  is plotted against  $\log(C_e)$ .  $K_F ((\text{mg/g})(\text{L/mg})^{1/n})$  is an indicator of the adsorption capacity. The larger  $K_F$  value indicates that the adsorbent has a larger adsorption capacity and a favorable adsorbent (Mukherjee et. al., 2007). On the other hand,  $1/n$  value ranging between 0 and 1 is a measure of adsorption intensity. The value of  $1/n$  less than 1 represents a favorable adsorption condition (McKay, et al., 1982).

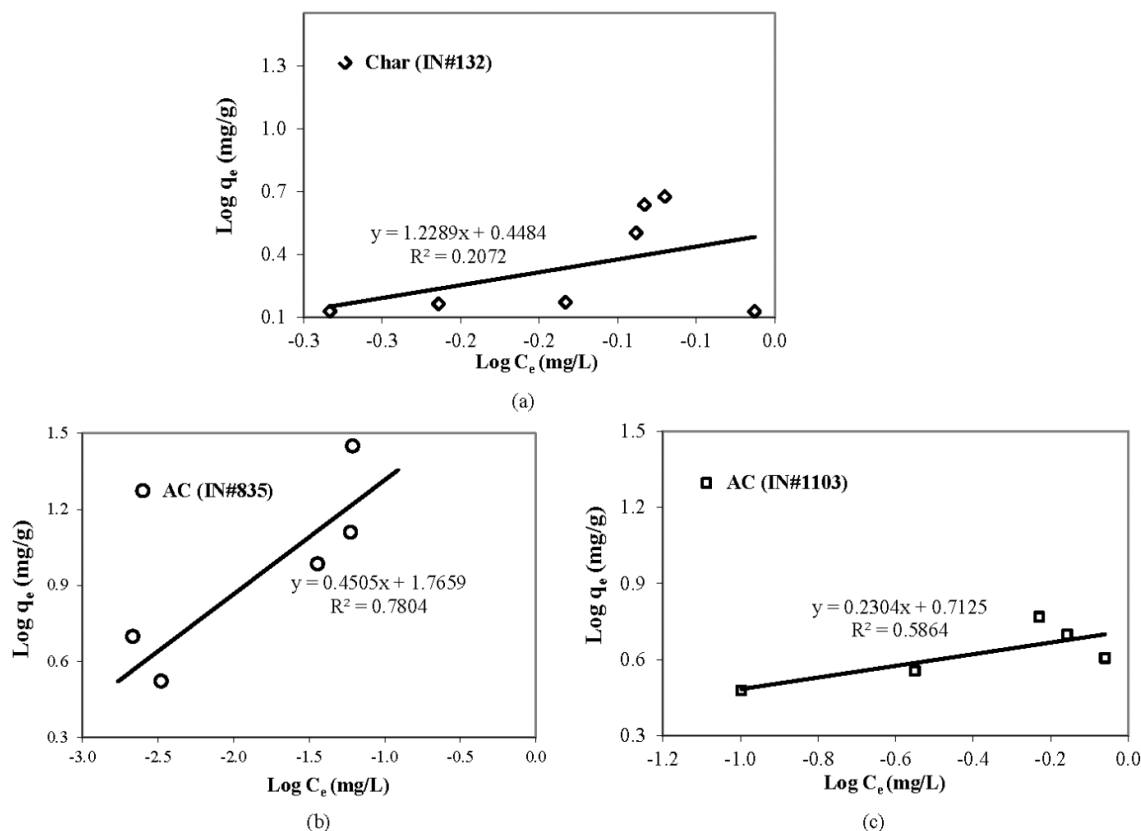


**FIGURE 4.** Freundlich adsorption isotherm of phenol onto (a) BC#132, (b) AC#837 and (c) AC#1103.

The data obtained in this study were used to plot  $\log q_e$  vs.  $\log C_e$  and presented in Figure 4. The values of constants  $K_F$  and  $1/n$  are also calculated and shown in Table 2. A comparison of the values of  $K_F$  reveals that AC#835 has the highest  $K_F$  value (58.33) indicating it has the largest adsorption capacity and most favorable adsorbent among the three products. The lowest  $K_F$  value of 2.81 obtained for BC#132 suggests that it has the lowest adsorption capacity. Furthermore, comparing the value of  $1/n$  for the three products, it is found that  $1/n$  for AC#835 and AC#1103 are less than 1 while the  $1/n$  for BC#132 is more than 1. These values again indicate the easy adsorption by AC#835 and AC#1103 compared to BC#132. For AC#835 adsorbent ( $R^2=0.7804$ ), the Freundlich isotherm model gave a slightly better fit than the AC#1103 ( $R^2=0.5864$ ). However, BC#132 results show poor fit of the Freundlich isotherm model. This model study also suggests that biochar activation to an optimum level enhances the performance of the adsorbent.

**TABLE 2. Freundlich isotherm coefficients**

Absorbent	$K_F ((\text{mg/g})(\text{L/mg})^{1/n})$	$1/n$	$R^2$
Biochar (BC#132)	2.81	1.2289	0.2072
Activated Carbon (AC#835)	58.33	0.4505	0.7804
Activated Carbon (AC#1103)	5.16	0.2304	0.5864

## CONCLUSIONS

The phenol adsorption performance by various grades carbon products from Albizia was investigated using batch tests. The study demonstrates that it is possible to remove phenol from aqueous solution in a safe manner using biochar and activated carbon produced from Albizia, an invasive plant. However, preparation method of these carbon products has significant effect on phenol adsorption capacity. Comparing the adsorption performance, the study suggests that phenol removal can be enhanced significantly when biochar is activated and converted to activated carbon. Activated carbon produced with a 20 minute residence time (i.e. AC#835) at temperature 1500 °F proved to be most effective for phenol removal. The removal efficiency of this carbon product is 1.5 times more than that of biochar with a target dosage range 200 mg/L to 400 mg/L. Even a small dose of 100 mg/L of AC#835 can achieve more than 96% removal efficiency.

## REFERENCES

- Banat, F.A., B. Al-Bashir, S. Al-Asheh and O. Hayajneh. 2000. "Adsorption of phenol by bentonite", *Environ. Pollut.* 107: 391-398.
- Hameed, B.H., A.A. Rahman, 2008 "Removal of phenol from aqueous solutions by adsorption onto activated carbon prepared from biomass material", *J. Hazard. Mater.* 160: 576–581.
- Lin, S-H. and R-S. Juang. 2009. "Adsorption of phenol and its derivatives from water using synthetic resins and low-cost natural adsorbents: a review". *J Environ. Manag.* 90(3): 1336–1349.
- Mayers, J. 2014. *Pyrolysis and Activation of an Invasive Species*. M.S. Thesis, Florida State University, Tallahassee, FL.
- McKay, G., H.S. Blair, J.R. Gardner. 1982. "Adsorption of dyes on chitin-1: equilibrium studies", *J. Appl. Polym. Sci.* (27): 3043–3057.
- Mianowski, A., M. Owczarek, and A. Marecka. 2007. "Surface Area of Activated Carbon Determined by the Iodine Adsorption Number." *Energy Sources, Part A*, 29.9, pp 839-850. Taylor & Francis, LLC, Abingdon, UK.
- Mukherjee, S., S. Kumar, A. K. Misra, M. Fan. 2007. "Removal of phenol from water environment by activated carbon, bagasse ash and wood charcoal", *Chem. Eng. J.* 129: 133-142.
- Subramanyam, B. and A. Das. 2009. "Study of the adsorption of phenol by two soils based on kinetic and isotherm modeling analyses", *Desalination* 249(3): 914–921.
- Wang X., D. Li, W. Li, J. Peng, H. Xia, L., Zhang, S. Guo and G. Chen. 2013. "Optimization of mesoporous activated carbon from coconut shells by chemical activation with phosphoric acid" *BioResources*, 8(4): 6184-6195.

## EXPERIMENTAL STUDY OF CONGO RED AND DIRECT RED 80 ADSORPTION FROM WATER ONTO CARBON NANOTUBES

**Madhu Agarwal\*** & Priti Kumari (Department of Chemical Engineering, Malaviya National Institute of Technology Jaipur, India)

**ABSTRACT:** This study investigated the potential use of carbon nanotubes as an adsorbent for the removal of Congo red & Direct red 80 dyes from aqueous solution. Batch adsorption study was carried out for removal of both the dyes from aqueous solution in the presence of carbon nanotubes. The effect of various operating conditions such as adsorbent dose, initial dye concentration, and pH, temperature & contact time on dye adsorption on carbon nanotubes was studied. It was found that for both the dyes maximum removal was achieved at pH 2. The removal of dyes increases with adsorbent dosage but decreases with initial dye concentration. Langmuir isotherm gave a better fit to the adsorption compare to the Freundlich for both dyes. Adsorption kinetics followed the pseudo second order kinetic. The adsorption efficiency of carbon nano-tubes was estimated to 125 mg/g for Congo red & 79.325mg/g for direct red 80 at adsorbent dose of 0.010g/50 ml of 10ppm dye solution at equilibrium time of 80 min. and 105 min. respectively and at optimum dose of 0.015 the capacity becomes 100 mg/g for Congo red & 66 mg/g for direct red 80.

## INTRODUCTION

Dyes are widely used in industries such as textiles, paper, paints, leather, rubber, plastics, cosmetics, food and drug etc. to color their products. Textiles industries consumed more than 60 % dyes of the total world production. It is estimated that 10-20% of dye was lost during the dying process and release as effluent (Zhiqiao et al.,2007). Due to their chemical structures, dyes are resistant to fading on exposure to light, water and many chemicals and, therefore, are difficult to be decolorized once released into the aquatic environment (Sharma and. Janveja,2008). Many of the organic dyes are hazardous and may affect aquatic life and even the food chain. Therefore, it is very important to develop new systems that can be used for removing dyes from waters. Research is being carried out for removal dyes using physicochemical, chemical and biological treatment technologies, such as chemical coagulation–flocculation (Pavan et al., 2008) different type of oxidation processes (Neelmegani et al., 2004), membrane filtration and adsorption (Purkait et al., 2007) for the removal of coloured dye from wastewater. Among these advanced treatments, at this moment, adsorption is considered more effective and less expensive than other technologies. Activated carbon is the most used material owing to its adsorption capacity, but it is very expensive and its regeneration is difficult (Sharma and. Janveja,2008). Since adsorption was best suitable and reasonable method for removal of dyes hence many authors were used different adsorbents for dye removal. Nagarethinam and Mariappan, 2002, used the bamboo dust carbon for adsorption of CR dye and they achieved a maximum adsorption capacity of 101.9mg/g for removal of CR dye. Recently cylindrical graphene- CNT hybrid was developed by Lunhong and Jing, 2012 and they used it for adsorption of Methylene blue (MB) dye and achieved a maximum adsorption capacity of 81.97 mg/g for the removal of MB from aqueous solution. The removal efficiency reached 97% for low concentration (10mg/l initial) of MB. In recent times carbon Nano tube has got greater attention in field of scientific development. It has shown a great prospect in developing the future Nano structure with novel properties. The high strength and stiffness property of CNTs have made it a potential reinforcing material. In the present research multiwall carbon nanotube (MWCNT) in the range of 8-15nm subsequently applied for the dyes removal. The effect of factor such as initial pH, adsorbent dose (mg/ml) and contact time (t) on Congo red (CR) and direct red 80(DR 80) removal percentage was investigated and optimized. Isotherm of adsorption was examined by fitting the experimental data to various isotherm equations, and it was found that Langmuir is the best model with high correlation coefficient for both dyes. The kinetics of adsorption using pseudo first order and second order were tested with experimental data for their validation.

## MATERIAL AND METHODS

**Batch Experimental Studies.** Batch experiments were conducted to investigate the effect of parameters like pH, contact time and adsorbent dose, on the adsorptive removal of CR & DR 80. For each experimental run, 50ml of 10mg/L of CR & DR 80 solution at various pH in the range of 1-8 was mixed with 10mg/50ml to 25mg/50ml of adsorbent. This mixture was agitated in incubator shaker with constant speed of 200 rpm till equilibrium reached. Thereafter, all the samples were centrifuged at 4000rpm for 20min to settle down suspended particles. After centrifugation clear supernatant samples were obtained and the supernatant solution was estimated accurately by UV spectrophotometer for remaining dye in the solution. The kinetics of adsorption was determined by analyzing adsorptive uptake of the dye from the aqueous solution at different time interval. For adsorption isotherms, different concentration of dye solution was agitated with known amount of adsorbent till the equilibrium.

The amount of dye adsorbed was calculated from the following equation:

$$q = \frac{(C_0 - C_e)V}{m} \quad (1)$$

Where  $q$  is the amount of dye adsorbed per unit weight of adsorbent (mg/g);  $C_0$  the initial concentration (mg/l);  $C_e$  the concentration of CR or DR 80 in solution at equilibrium time (mg/l);  $V$  the solution volume (l);  $m$  is the adsorbent dosage (mg/ml).

## RESULT AND DISCUSSION

**SEM analysis of commercial CNT.** The CNTS is characterized by SEM to observe very fine structures of samples. Fig 1 shows a SEM image of CNTs. The noodle shapes in the figure are CNTs having average diameter 12 nm. CNTs formed in cluster and very thin, many roots of carbon not properly converted into carbon nanotubes due to presence of some impurities.

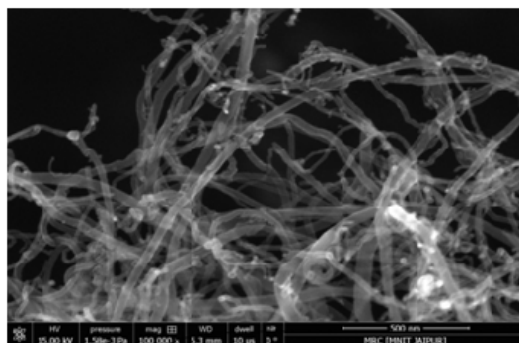
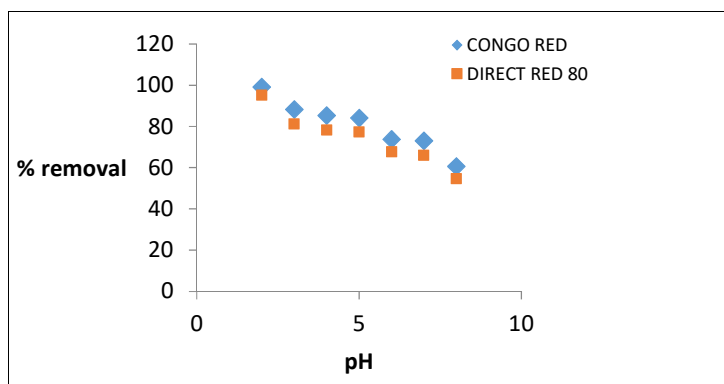


FIGURE 1: SEM Images of CNT

**Effect of pH.** The medium pH is a critical parameter in adsorption process as it strongly affects the structural stability and color intensity of CR and DR 80 dye. After adjusting the pH value (1-8), solution was kept in incubator. After equilibrium time (150 min) the dye solution was withdrawn and centrifuged. The supernatant was checked for presence of dye in UV spectrophotometer. Fig 2 Shows that at pH 2-5 more than 90% dye has been removed thereafter removal of dye decreases as pH increases. The maximum removal (99.1%) was obtained at pH 2. That's why further experiment is conducted at pH 2.

**Effect of Adsorbent Dosage and Initial Concentration.** The effect of adsorbent dosage on CR adsorption was conducted by varying adsorbent dosage from 10mg/50ml to 25mg/50ml at dye concentration of 10 ppm. With increase in adsorbent dosages (CNT) the percent removal of dye also increases for both CR and DR 80, due to the increase in adsorbent surface area hence, increase in total number of exchange sites. As depicted in fig 3(a) and 3(b) when adsorbent dosage change from 15 mg/ml to 20 mg/ml, there is slight change in percent removal, therefore, it was considered that 15 mg can be taken as optimum dose for both the dyes.



**FIGURE 2.** Effect of pH on adsorption of CR & DR 80 (10ppm) onto CNT (15mg/ml) at 303K, agitation speed 200rpm for the equilibrium time

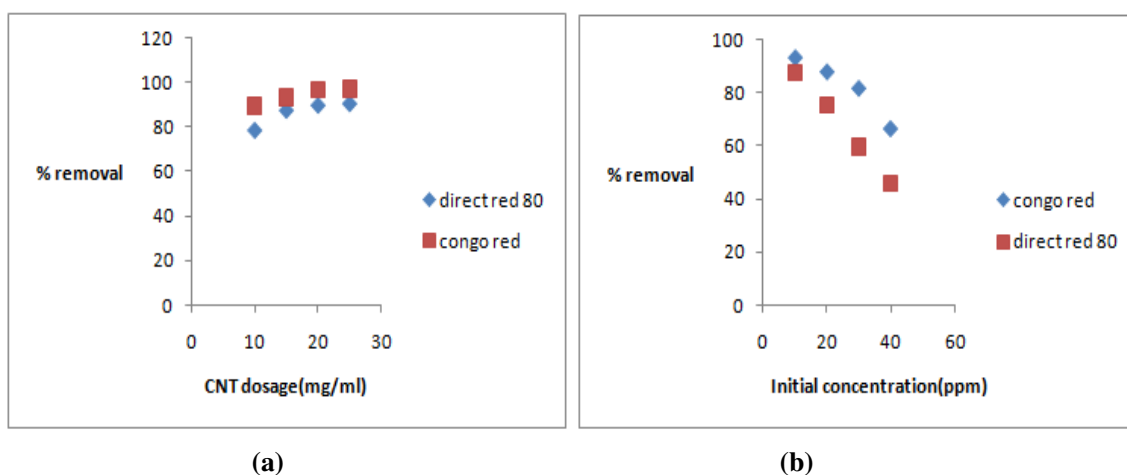


**FIGURE 3.** Effect of (a) Adsorbent Dosage (10, 15, 20, 25 Mg) at Dye Concentration 10ppm (b) Initial Concentration (10, 20, 30, 40ppm) at Adsorbent Dosage 15mg, Contact Time 80 min for CR and 105 min for DR 80, Temperature (303K) & Agitation Speed 200 Rpm for Congo Red & Direct Red 80

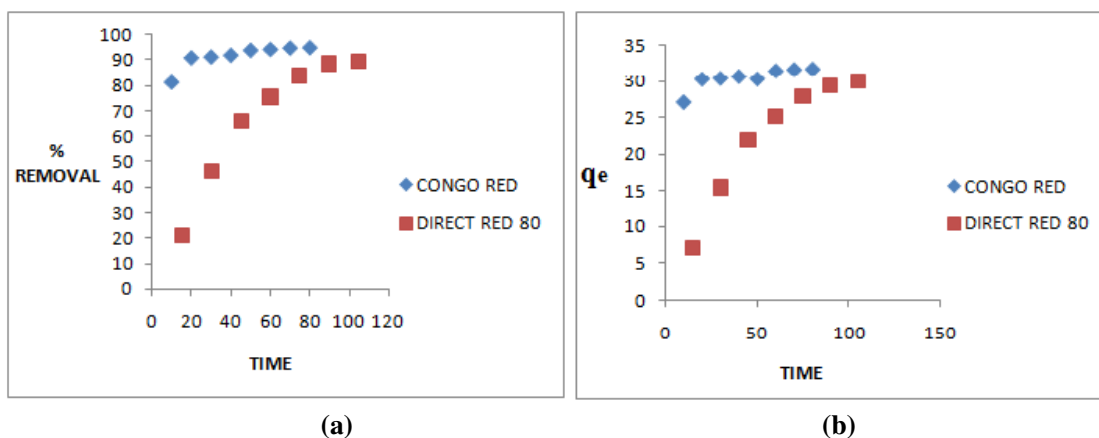


**FIGURE 4.** Effect of Contact Time on (a) Percent Removal (b) Amount Adsorbed per unit mass of adsorbent at 10 ppm dye concentrations, 303 K temp., and adsorbent dose 15mg /50ml dye solution

The effect of initial dye concentration on adsorption of the CR and DR 80 was investigated in the concentration range 10-40 ppm. The results are shown in fig 3(a, b). When concentration was 10ppm percent removal was maximum as compare to 20, 30, 40 ppm, hence further study is carried out at 10 ppm.

The decrease in percent removal with increase in initial dye concentration was more for DR 80 than CR; this may be due to less affinity of DR 80 with CNT compared to CR.

**Effect of Contact Time and Concentration of Dye on Adsorption.** The Fig 4(a, b) shows percent removal and the amount of dye adsorbed per unit mass of adsorbent with respect to time. Both percent removal and  $q_e$  (mg/g) increases with increase in contact time. The percent removal of dye increases sharply within initial 15min. after that it increases slowly and at 80min it become constant for CR. For DR 80 the increase in percent removal was slow from beginning and become constant at 105 min. More than 90% removal was achieved for both the dyes at equilibrium time. The amount of dye adsorbed per unit mass of adsorbent was very high for CR at beginning but same was very low for DR 80. Close to equilibrium time both dyes adsorbed efficiently on adsorbent under consideration (fig 4(b)).

**Adsorption Kinetics.** In order to investigate the adsorption process of CR and DR 80 on the adsorbent (CNT), pseudo first-order and pseudo second-order kinetics models were fitted to experimental data. The pseudo-first-order equation used is given below;

$$\log(q_e - q_t) = \log q_e - \frac{k_1}{2.303} t \quad (2)$$

Where  $q_e$  and  $q_t$  are the amount of CR and DR 80 adsorbed at equilibrium and at a time  $t$ ,  $k_1$  is the first order rate constant (min). The slope and intercept of plot  $\log(q_e - q_t)$  v/s  $t$  were used to determine the pseudo first order rate constant  $k_1$  and  $q_e$ . Pseudo second order model is;

$$\frac{t}{q_t} = \frac{1}{k_2 q_e^2} + \frac{1}{q_e} t, \quad (3)$$

Where  $k_2$  (g/mg min) is the rate constant, slope and intercept of plots  $t/q_t$  v/s  $t$  are used to calculate  $q_e$  and  $K_2$ . The results obtained for constants were summarized in Table 1. The fig. 5 (a,b) shows that pseudo second order kinetics model better fits to the experimental data obtained for both dyes.

**TABLE 1.** Kinetic Parameters for CR and DR 80 Removal using 15 mg/ml Adsorbent Dose over Dye Concentration of 10 ppm

Type Of Dye	Pseudo First Order Model			Pseudo Second Order Model		
	$K_1$	$q_{ecal}$	$R^2$	$K_2 * 10$	$q_{ecal}$	$R^2$
Congo Red	0.02533	1.7576	0.648	0.155	33.33	0.999
Direct Red 80	0.0368	4.75882	0.939	0.00162	62.5	0.944

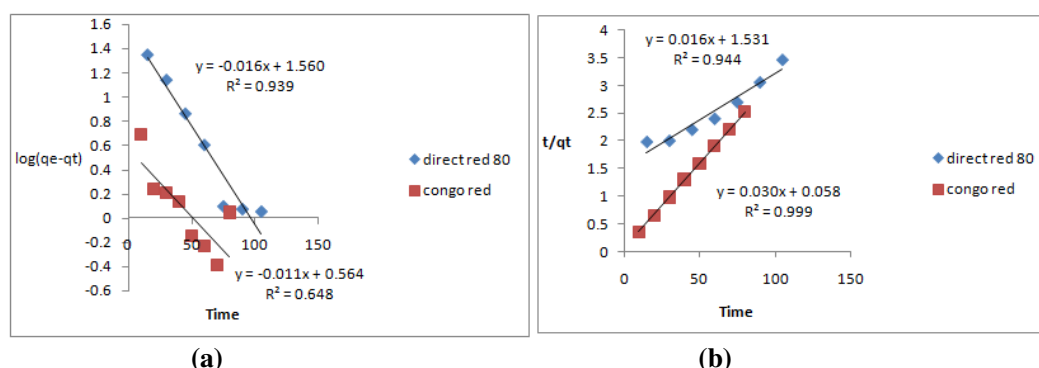


**FIGURE 5.** Plots for Different Kinetics Model (a) Pseudo 1<sup>st</sup> Order and (b) Pseudo Second Order for Removal of CR And DR 80 At 10ppm Concentration, 303 K, Adsorbent Dose 15g/50ml & Equilibrium Time 80 min

Correlation coefficient for pseudo second order is closer to unity compare to pseudo first order kinetics. Therefore sorption can be approximated more appropriately by the pseudo-second-order kinetic model than the first-order kinetic model for the adsorption of CR and DR 80 as depicted in table 1.

**Adsorption Isotherm.** The dyes adsorption equilibrium data were fitted for Langmuir; Freundlich and Temkin Isotherms (fig. 6). The optimization of an adsorption process requires an understanding of the driving forces that govern the interaction between adsorbent and adsorbate. The  $R^2$  value in case of Langmuir isotherm for CR is 0.996 and for DR 80 is 0.9997. The isotherm results indicate that the adsorption of CR and DR 80 onto adsorbent (CNT) is consistent with Langmuir isotherm model as shown in fig. 6(a). This value is greater than those  $R^2$  values calculated for the Freundlich & Temkin isotherm, listed in table 2. Langmuir isotherm represented by,

$$\frac{C_e}{q_e} = \frac{C_e}{q_{\max}} + \frac{1}{q_{\max} K_L}$$

(4)

$$R_L = 1 / (1 + K_a C_0)$$

(5)

Where  $R_L$  is equilibrium parameter express as essential characteristics of Langmuir isotherm;  $C_e$  is the concentration of dye (ppm) at equilibrium. The constant  $Q_m$  is the adsorption capacity (mg/g) and  $K_L$  is related to energy of adsorption (l/mg). Value of  $Q_m$  and  $K_L$  calculated from the slope and intercept of the linear equation of isotherm.

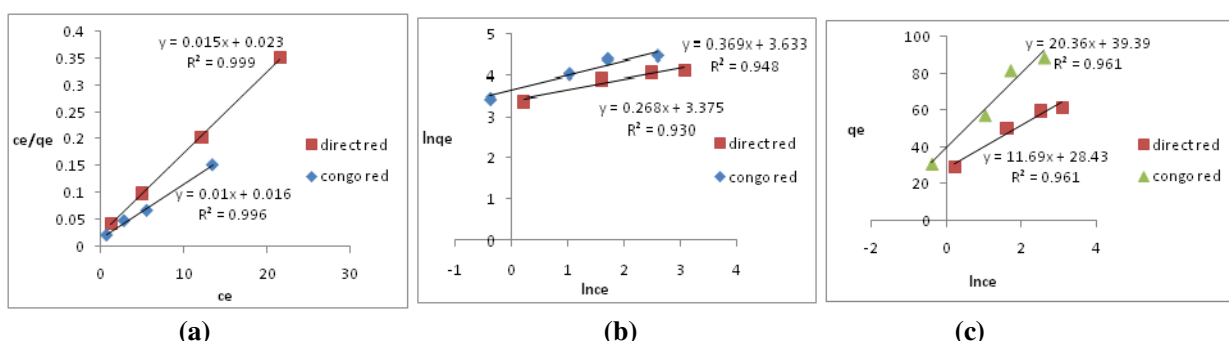


**FIGURE 6.** Isotherm of Adsorption for Removal of Congo Red And Direct Red 80 Dyes by Commercial CNTs (a)Langmuir (b) Freundlich (c) Temkin

**TABLE 2.** Isotherm Constants of CR and DR 80 onto Multiwall CNT

Type of Dye	Temkin			Langmuir						
	1/n	$K_f$	$R^2$	$B_1$	$K_T$	$R^2$	$Q_m$	$K_a$	$R^2$	$R_L$
Congo Red	.37	37.84	0.947	20.35	6.92	0.96	100	0.616	0.996	0.0392-.14
Direct Red 80	0.26	29.25	0.93	11.7	11.36	0.96	65.789	0.661	0.9997	.0692-.17

**TABLE 3.** Comparison of adsorption capacity of various adsorbents for adsorption of CR and DR 80

Adsorbent	Dye	Adsorption Capacity(mg/g)	References
CNT	Direct Red 80	66.00	Present Work
Mixture Almond Shells	Direct Red 80	22.42	Doulati et al., 2008
Orange Peel	Direct Red 80	21.05	Arami et al., 2005
CNT	Congo Red	100.0	Present Work
Magnetically Modified Fodder Yeast Cell	Congo Red	49.7	Safarik et al., 2007
Palm Kernel Seed Coat	Congo Red	66.23	Yuzhu and Viraghavan 2002
Fungus Aspergillus Niger	Congo Red	14.72	Oladoja and Akinladi 2009
Carbonized Coir Pith	Congo Red	6.7	Yuzhu and Viraghavan 2002
Banana Peel	Congo Red	18.2	Annadurai et al., 2002]

## CONCLUSION

The study presented revealed that MWCNT can be used as a good and low cost adsorbent with high efficiency as reported in table 3. With high adsorption capacity of 100 mg/g for CR in equilibrium time 80 min & for DR 80 adsorption capacity of 66.0 mg/g in equilibrium time 105 min. At pH 2 and at adsorbent dose of 0.015g percent removal was more than 95% for both the dyes. Langmuir isotherm gave a better fit

to the adsorption isotherm compared to the Freundlich and Temkin adsorption isotherm for both dyes. A theoretical adsorption capacity of 125 mg/g for Congo red & 79.325mg/g for direct red 80 was obtained at lower adsorption dose (0.010g). Adsorption Kinetics followed the second order kinetics model.

## REFERENCES

- Annadurai, G., R.S. Juang, and D.J. Lee. 2002. "Use of cellulose-based wastes for adsorption of dyes from aqueous solutions". *J. Hazard. Mater.* B92: 263–274.
- Arami, M., N. Yousefi Limaee, N.M. Mahmoodi, and N. Salman Tabrizi. 2005. "Removal of dyes from colored textile wastewater by orange peel adsorbent: equilibrium and kinetic studies". *J. Colloid Interf. Sci.* 288: 371–376.
- Doulati Ardejani, F., Kh. Badii, N. Yousefi Limaee, S.Z. Shafaei, and A.R. Mirhabibi. 2008. "Adsorption of direct red 80 dye from aqueous solution onto almond shells: effect of pH, initial concentration and shell type". *Journal of Hazardous Materials.* 151: 730–737.
- Lunhong, Ai and J. Jing. 2012. "Removal of methylene blue from aqueous solution with self-assembled cylindrical graphene–carbon nanotube hybrid". *Chemical Engineerin Journal.* 192:156-163.
- Nagarethinam, K., and M. Mariappan. 2002. "Adsorption of congo red on various activated carbons, a comparative study". *Water Air Soil Pollut.* 138: 289–305.
- Neelmegani, R., V. Baskaran, R. Dhancekar, and T. Viruthgiri. 2004. "Decolorisation of synthetic dyes using rice straw attached pleurotus oslereths". *Indian J. Chem. Techo.* 11: 622-625.
- Oladoja and Akinlabi. 2009. "Congo red biosorption on palm kernel seed coat". *Ind. Eng. Chem. Res.* 48: 6188–6196.
- Pavan, F. A., S. L.P. Dias, E. C. Lima, and E.V. Benvenutti. 2008. "Removal of Congo red from aqueous solution by anilinepropylsilica xerogel". *Dyes and Pigments.* 76: 64-69.
- Purkait, M.K., A Maiti, Das Gupta, and S. De. 2007. "Removal of congo red using activated carbon and its regeneration". *J. Hazard. Mater.* 145: 287–295.
- Safarik, I., L.F.T. Rego, M. Borovska, E. Mosiniewicz-Szablewska, F. Weyda, and M. Safarikova. 2007. "New magnetically responsive yeast-based biosorbent for the efficient removal of water-soluble dyes". *Enzyme Microb. Technol.* 40:1551–1556.
- Sharma, J., and B. Janveja. 2008. "A study on removal of congo red dye from the effluents of textile industry using rice husk carbon activated by steam". *Rasayan J. Chem.* 1(4): 936-942.
- Yuzhu, F., and T. Viraraghavan. 2002. "Removal of Congo red from an aqueous solution by fungus *Aspergillus Niger*". *Adv. Environ. Res.* 7: 239–247.
- Zhiqiao, H., S. Shuang, Z. Huamin, Y. Haiping, and C. Jianmeng. 2007. "C.I. Reactive Black 5 decolorization by combined sonolysis and ozonation". *Ultrasonics Sonochem.* 14 (3):298-304.



## COPPER(II) BIOSORPTION CHARACTERISTICS OF A NOVEL BIOSORBENT COMBINATION: FUNGUS AND AGRICULTURAL WASTE

Jingyao Wang and Chongwei Cui\* (Harbin Institute of Technology, Harbin, China)

**ABSTRACT:** All previous attempts have examined fungus and agricultural waste separately. The present work is therefore novel as it uses a combination of fungus and agricultural waste for removal of copper(II) from aqueous solutions. The biosorbent was corn stalk fermented by *Aspergillus niger* (fermented corn stalk). Results show that the content of O in fermented corn stalk, compared with that of in raw corn stalk, declined as the C, N, P, and K increased, and that the zeta potential was lower. Fermented corn stalk exhibited a short biosorption equilibrium time (60 min), high biosorption capacity (11.2 mg/g), and high removal efficiency at pH 3. The fact that the biosorption capacity of fermented corn stalk was better than that of raw corn stalk under identical conditions can be attributed to the sprawl of *Aspergillus niger* (biosorption capacity was better than raw corn stalk) and the enzyme system secreted by *Aspergillus niger* which changed the surface properties of raw corn stalk. The biosorption mechanism was involved in chelation with functional groups such as N-H, C=O, C-O, and C=C, and the biosorption data obtained were well described by the pseudo-second order and the Freundlich isotherm model.

### INTRODUCTION

Recently, low cost adsorbent materials from the forestry, fishing, and agriculture industries have attracted the attention of several researchers thanks to their high volume, low value, and underutilized biomaterials, and because they contain high levels of cellulose, hemicellulose, and lignin (Abdolali et al., 2014). Corn is one of the most widely produced crops in the world and it can be used as an alternative raw material for the preparation of various functional polymers. However, due to the intermolecular hydrogen bonds involving cellulose hydroxyl groups in corn stalk, its biosorption capacity is generally low. Zheng used acrylonitrile to modify corn stalk to biosorb Cd(II) so that its biosorption capacity was triple that of raw corn stalk (Zheng et al., 2010a). The corn stalk was also treated to be corn stalk graft copolymers as a kind of biosorbent to biosorb heavy metal (Zheng et al., 2010b). Although these chemical modifications can improve biosorption capacity, we must still consider other aspects, such as secondary pollution of chemical modification and cost. Therefore, microbiological modification may be a processing technology. *Aspergillus niger*, as one kind of mycelium fungus, was commonly used in the fermentation industry, because it has abundant enzymes (including amylase, pectinase, and cellulase) and is non-toxic and inexpensive (Odetallah et al., 2005). For the past two decades, researchers have been conducting biosorption studies with *Aspergillus niger*, since it is easy to acquire and to separate from the liquid medium (Amini et al., 2009). The Cr(III) from tanning effluents was removed by *Aspergillus niger* and isolated from the tanning environment (Sepehr et al., 2012). Malihe Amini studied the biosorption of nickel(II) from aqueous solutions by *Aspergillus niger* with response surface methodology methods (Amini et al., 2009). Baik separated the components of *Aspergillus niger* mycelium and used them to biosorb heavy metal and found that chitosan contributed most to the biosorptive capacity (Baik et al., 2002). To the best of our knowledge, there are no reports on the application of a combination of fungus and agricultural waste in the removal of heavy metals. However, this combination of biosorbents has two advantages: first one was some enzymes secreted by the fungus can modify agricultural waste and change the properties of cell surfaces, and second was the propagation of fungi, which have a higher biosorption capacity than agricultural waste, can lead to the improvement of biosorption capacity. Hence, we decided to use *Aspergillus niger* to ferment corn stalk and called the combination of biosorbents “fermented corn stalk.” The aim of this study was to testify to the effectiveness of this combination of biosorbents by comparing the biosorption capacities of fermented corn stalk and raw corn stalk under various dosages, deciding on the best pH for fermented corn stalk, and characterizing the biosorbents with SEM-EDX and Fourier infrared (FTIR) spectroscopy. Subsequently, the fermented corn stalk was systematically studied using a combination of kinetics and isothermal modeling.

## MATERIALS AND METHODS

**Microorganism.** *Aspergillus niger* 98003, purchased from CMCC; Spore suspension: washed the aerial mycelium with water and adjusted the concentration to  $10^6$ . The spore concentration of the final suspension was determined by counting in a hemocytometer.

**The preparation of corn stalk biosorbent.** Corn stalk washed with distilled water, crushed with grinder (FW100, Tianjin Theis brand), sieved with a standard sieve to obtain powder with a particle diameter of 0.3 mm. The powder was dried in an electrically heated blast dry box to a constant weight.

**The preparation of fermented corn stalk.** Spore suspension was added to the corn stalk powder at a ratio of 1:1. Seven days later, when the aerial mycelia of *Aspergillus niger* covered the entire medium, they were collected and placed in a dry box at 60° C to ensure constant weight.

**Comparison of raw corn stalk and fermented rice straw.** Specific dosages (0.1, 0.3, 0.5, 0.7, 1.0 g) of raw corn stalk and fermented corn stalk were each placed in 100 mL of  $\text{CuSO}_4 \cdot 5\text{H}_2\text{O}$  solution, with an initial  $\text{Cu}^{2+}$  concentration of 30 mg/L (since the concentration of most industrial wastewater is under 50mg/L) and shaken at 30° C and 100 rpm for two hours.

**The effect of different initial acidity on fermented corn stalk.** Fermented corn stalks were placed in 100 mL of  $\text{CuSO}_4 \cdot 5\text{H}_2\text{O}$  solution with an initial  $\text{Cu}^{2+}$  concentration of 30 mg/L and initial pH values of 2.0, 3.0, 4.0, 5.0, and 5.3 (the natural pH) achieved by addition of  $\text{H}_2\text{SO}_4$ . The flasks were shaken at 30° C and 100 rpm for two hours to ensure the best pH value.

**Experiment of fermented corn stalk on biosorption kinetics.** Ten 0.1 g samples of fermented corn stalk were placed in 100 mL of  $\text{CuSO}_4$  solution with an initial  $\text{Cu}^{2+}$  concentration of 30 mg/L and were shaken at 30° C and 100 rpm for 1, 3, 5, 10, 15, 30, 60, 90, 120, and 150 minutes.

**Experiment of fermented corn stalk on biosorption equilibrium.** Nine 0.1 g samples of fermented corn stalk were placed in 100 mL of  $\text{CuSO}_4$  solution with initial  $\text{Cu}^{2+}$  concentrations of 10, 30, 60, 90, 120, 150, 200, 250, and 300 mg/L and were shaken at 30° C and 100 rpm for two hours.

**Data processing.** The  $\text{Cu}^+$  solution was filtered through a membrane with a pore diameter of 0.45  $\mu\text{m}$  and analyzed by Inductively Coupled Plasma Mass Spectrometry to determine the concentrations of the  $\text{Cu}^{2+}$  before and after biosorption (Göksungur et al., 2005).

**FTIR and SEM-EDX analysis of fermented rice straw and raw rice straw.** The raw rice straw and fermented rice straw samples were screened before and after biosorption by Fourier Transform Infrared Spectroscopy (FTIR 1730 model, Perkin-Elmer Corporation) using the KBr tablet method (Lodeiro et al., 2006). SEM in combination with EDX can provide information about the morphology and elemental component of the two kinds of biosorbents (Chen et al., 2014).

## RESULTS AND DISCUSSION

**Comparison of raw corn stalk and fermented corn stalk with different dosages.** The high sorption capacity was the key factor of a biosorbent (Won et al., 2014). Fig. 1 shows that the biosorption value for fermented corn stalk was 3.4 mg/g. By contrast, the biosorption value for raw corn stalk was only 1.8 mg/g when the dosage was 0.1g. Furthermore, the biosorption values for fermented corn stalk were higher than those for raw corn stalk for all other dosages. Which can be ascribed to two points: the sprawl aerial mycelia of *Aspergillus niger* accounted for part of the biosorbents, thus affecting the proportion of corn stalk, and cellulase and protease may have enzymolysized the components of corn stalk during the fermentation process, thus causing the biosorption properties to change.

**Effect of pH and zeta potential analysis.** Another parameter which can influence heavy metal removal is pH value. It can affect the characterization and availability of metal ions and change the surface functional group chemistry of biosorbents (Abdolali et al., 2014). Since the pH of the 30mg/L  $\text{Cu}^{2+}$  solution was 5.3, we decided the range of pH should be from 1 to 5.3. Fig. 2 shows that biosorption of  $\text{Cu}^{2+}$  by fermented corn stalk increased sharply as the pH increased (from 1 to 3) and attained maximum biosorption at pH 3. After that, the biosorption efficiency decreased as the pH increased. Which ascribed to the  $\text{Cu}^{2+}$  ions had to compete with  $\text{H}_3\text{O}^+$  ions for biosorption sites and functional groups of fermented corn stalk were more protonated when pH was lower. As the pH increased to 3, the  $\text{Cu}^{2+}$  biosorption capacity also increased to its peak. This can be attributed to the increase in negative charge on the biosorbent surface and the reduction of  $\text{H}^+$  ions (Hu et al., 2015). The Zeta potential stands for the charge of the sample surface. The Zeta potential of raw corn stalk and fermented corn stalk was -19.6 (biosorption capacity = 1.8 mg/g) and -23.67 (biosorption capacity = 3.4 mg/g), respectively, which indicates that the biosorption process was

related to electrostatic attraction. In addition, fermented corn stalk was more negative than raw corn stalk, which means the former can attract more positive ions( better biosorption capacity).

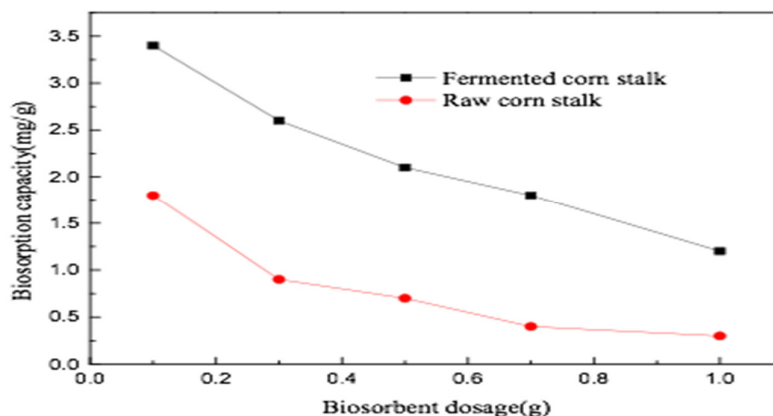


FIGURE 1. Biosorption Value

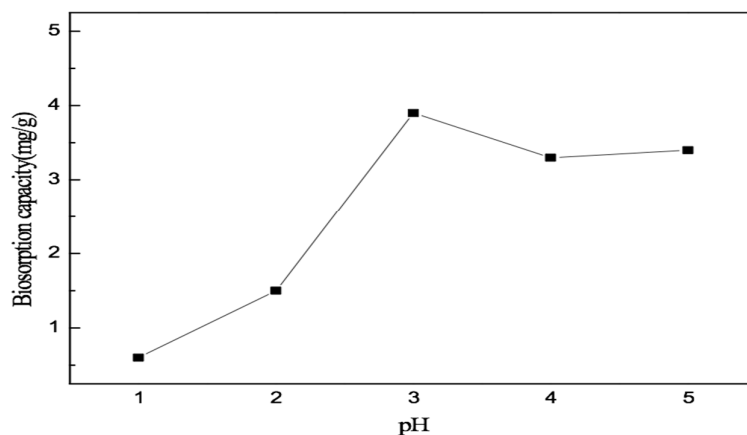


FIGURE 2. Biosorption of Cu<sup>2+</sup>

**FTIR of raw corn stalk and fermented corn stalk.** Fig.3 shows that the bands observed at 1722–1740cm<sup>-1</sup> were assigned to a C=O stretching of carboxylic acid or pectin ester (Jacques et al., 2007). The bands observed at 2920 cm<sup>-1</sup> indicated the presence of C–H group (Chen et al., 2011a). The peak at 1420 cm<sup>-1</sup> corresponds to the C=C stretching in the aromatic ring. In addition, the CH<sub>3</sub> deformation and –OH bending could have occurred at 1376cm (Petrović et al., 2016). The bands at 1605 cm<sup>-1</sup> corresponded to the N–H amine stretching band of the amino groups (Chen et al., 2011b) and some bonds, such as 834 and 665 in the fingerprint region, stand for out-of-plane vibration of N-H belonging to amine. Two additional bonds after fermentation. The strong peak at 1635 cm<sup>-1</sup> is C=O stretching vibration of carboxylic acid that exists in the intermolecular hydrogen bond (Jacques et al., 2007) The main components of *Aspergillus niger* were chitosan and lipids, the reproduction of which contributed to the increase of C=O. Another peak at 1106 cm<sup>-1</sup> is assigned to C–O stretching vibration (Subbaiah et al., 2011), which may be caused by cellulose hydrolyzation, because when cellulase was secreted glucose was generated. After biosorption, the wavenumber of peaks such as at 1605, 1425, 1731, and 665 cm<sup>-1</sup> shifted, indicating the involvement of N–H, C=O, C=C, and C–O in adsorption. Although all of the above-mentioned groups were involved in the Cu<sup>2+</sup> biosorption on the corn stalk, carbonyl was the main functional group that involved in this biosorption. The FTIR analysis confirmed that the complexation process could occur in the biosorption of Cu<sup>2+</sup> on the corn stalk.

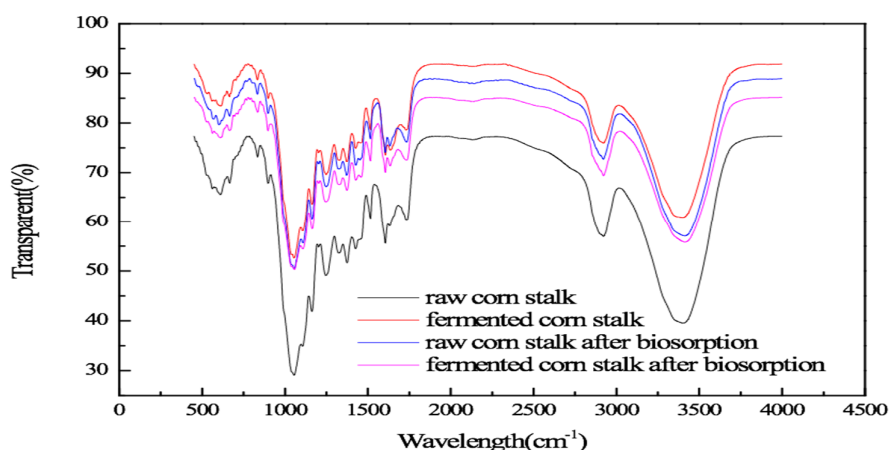


FIGURE.3. FTIR of raw corn stalk and fermented corn stalk before and after biosorption

**SEM-EDX of raw corn stalk and fermented corn stalk.** Fig. 4a shows that raw corn stalk has irregular fragments and pores on the otherwise smooth surface, which can be caused by cellulose and lignin which have rigid structures, whereas corn cobs have loose structures. After fermentation using *Aspergillus niger*, the structure became more rough and some *Aspergillus niger* spores emerged (Fig. 4b.), because the enzymatic hydrolysis of cellulose on the surface of the fiber modified the surface characteristics either by removing or masking the functional groups or by exposing more binding sites (Pehlivan et al., 2012). That give rise to the change in corn stalk surface properties, together with the appearance of *Aspergillus niger*, and led to the improvement of biosorption capacity. In addition, EDX results shown some differences (at%) between raw corn stalk and fermented corn stalk. After fermentation, the content of O for fermented corn stalk declined when compared to that for raw corn stalk as the C, N, P, and K increased. The reasons can be concluded as follows: The main component of corn stalk is cellulose. When it was degraded by the *Aspergillus niger*, polysaccharide glucose molecules were released and the glucose was primarily composed of C and O, which led to a decrease of C and O on the fermented corn stalk. However, during this time, in the later stage of aerial mycelia growth, a type of reproductive organ (spores) can be produced. The spores primarily consisted of C (67.63%) according to my previous analysis of XPS. Thus, compared with raw corn stalk, the content of C increased after fermentation. In addition, with the extent of the *Aspergillus niger* mycelium, chitin, and protein, the main content of *Aspergillus niger* cells increased, which led to an increase in N, P, and K.

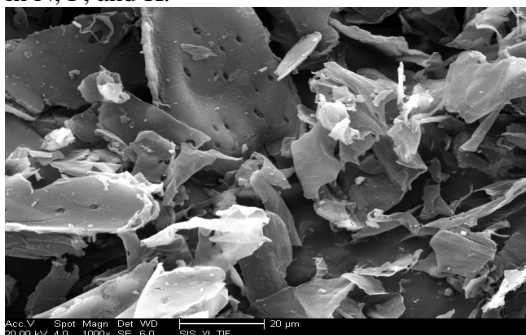


FIGURE.4a. SEM image of raw corn stalk

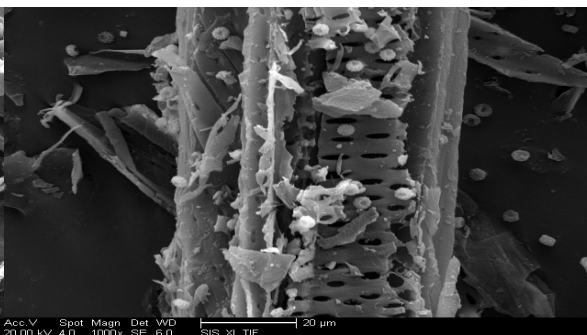


FIGURE 4b. SEM image of fermented corn stalk

**Biosorption kinetics of  $\text{Cu}^{2+}$  by fermented corn stalk.** The sorption kinetics reflect the relationship between sorption rate and sorption time (Ding et al., 2012). Lagergren's first-order kinetic equation (Fig. 5a) and a pseudo-second-order kinetic equation (Fig. 5b) were adopted to simulate the relationship between  $\text{Cu}^{2+}$  biosorption capacity and biosorption time. The pseudo-second order equation was better ( $R^2 = 0.995$ ) than Lagergren's first-order equation ( $R^2 = 0.958$ ) to simulate the dynamic  $\text{Cu}^{2+}$  sorption process by fermented

corn stalk. The data which fit in the pseudo-second-order equation (Fig. 5) meant that a chemical process such as ion exchange took place, little physical adsorption was involved in the chemical reaction as the data fit in Lagergren's first-order models as well ( $R^2 > 0.90$ ). This result was similar to the study by Zheng, whose biosorbents were corn stalk xanthates (XMCS) with alkali treatment, and the process fit in the pseudo-second-order model (Zheng & Meng, 2016).

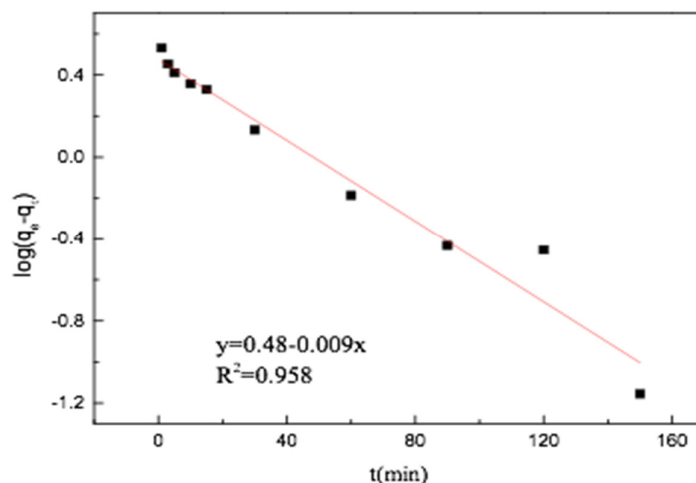


FIGURE 5a. Biosorption kinetics of  $\text{Cu}^{2+}$  (Lagergren's first-order kinetic)

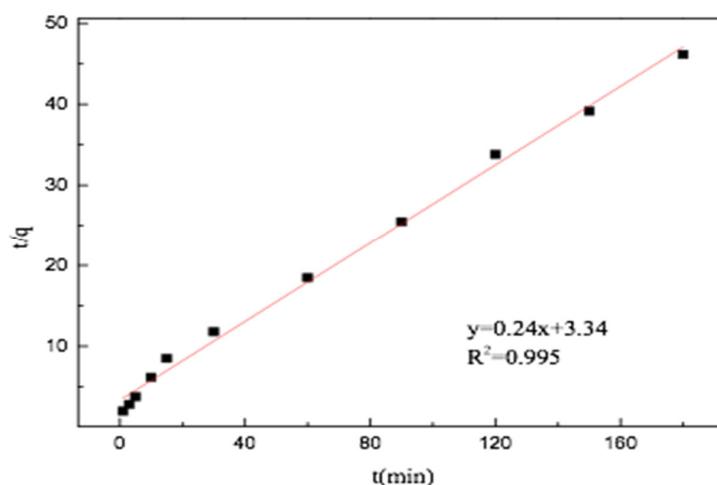


FIGURE 5b. Biosorption kinetics of  $\text{Cu}^{2+}$  (pseudo-second-order kinetic)

**Isotherm biosorption of fermented corn stalk.** The sorption isotherm model describes the relationship between sorption capacity and equilibrium concentration (Fig.6). The theoretical maximum uptake from the Langmuir isotherm (Fig. 6a) was 28.49 mg/g and the efficiency of sorption was 0.843. The results were clearly better in the Freundlich model ( $R^2 = 0.997$ ) (Fig. 6b). The obtained values of  $1/n$  ( $0.1 < 1/n < 1$ ) indicated a higher adsorbent ability of  $\text{Cu}^{2+}$  in this study (Chen et al., 2011b). Since the Freundlich model assumes that the surface is heterogeneous and the adsorption process is multilayer in nature, we conclude that there was a heterogeneous distribution of the available active sites onto the fermented corn stalk surface (Yu & Luo, 2014). The Freundlich relationship is an empirical equation and stands for a heterogeneous process of biosorption. Similar results were acquired by Buasri, who modified

corn cobs with phosphoric acid (PA) to remove  $Zn^{2+}$  from aqueous solution (Buasri et al., 2012). However, unmodified rice straw acted in accordance with the Langmuir model in Ding's study, and his degree of fitting was 100% (Ding et al., 2012). Thus, this phenomenon indicates that the microbial treatment affected the biosorbent materials, changed the functional groups and binding sites on the surface, and led to the properties of biosorption. This result was similar to the study by Ebrahimi, whose biosorbents were *Alhagi maurorum* seeds, and the process fit very well in the Freundlich model (Ebrahimi et al., 2015).

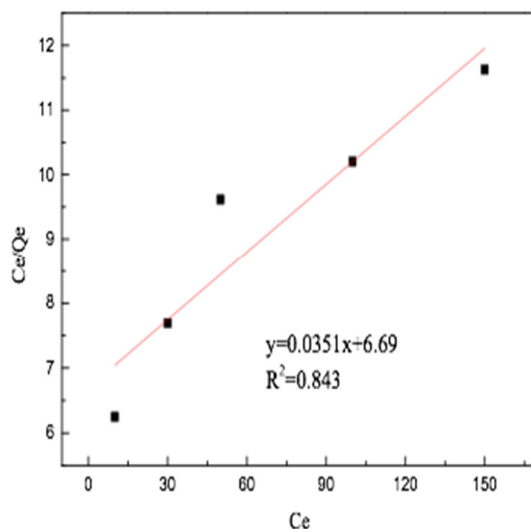


FIGURE 6a. Isotherm biosorption of fermented corn stalk (Langmuir isotherm)

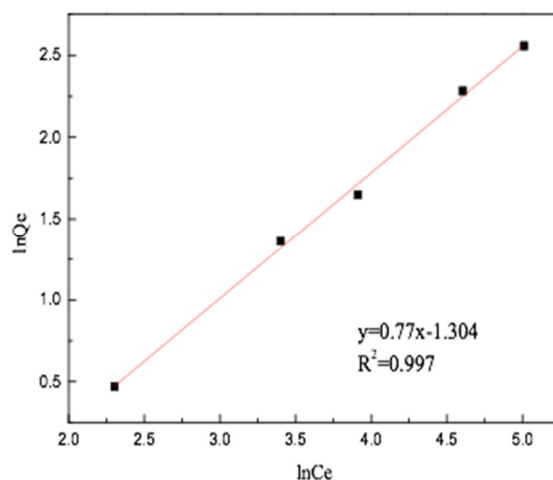


FIGURE 6c. Isotherm biosorption of fermented corn stalk (Freundlich model)

## CONCLUSIONS

- (1) Fermented corn stalk exhibited a short biosorption equilibrium time (60 min), high biosorption capacity (11.2 mg/g), and high removal efficiency at pH 3. The content of O in fermented corn stalk, compared with that of in raw corn stalk, declined as the C, N, P, and K increased, and that the zeta potential was lower. The biosorption data obtained were well described by the pseudo-second order and the Freundlich isotherm model.

- (2) The biosorption mechanism was involved in electrostatic attraction and chelation with functional groups such as N-H, C=O, C-O, and C=C, and The fact that the biosorption capacity of fermented corn stalk was better than that of raw corn stalk under identical conditions can be attributed to the sprawl of *Aspergillus niger* (biosorption capacity was better than raw corn stalk) and the enzyme system secreted by *Aspergillus niger* which changed the surface properties of raw corn stalk.
- (3) Although the process of biosorption is environmentally-friendly, and biosorption capacity of fermented corn stalk was higher than that of raw corn stalk, the capacity of the combination always be the focus of our attention. In further study, the fungi can be mutant by UV or modified by genetic engineering, to improve the performance of this combination biosorbent.

## ACKNOWLEDGEMENTS

This study was financially supported by heavy metal wastewater treatment technology received from Heilongjiang Academy of Sciences (GC13C3042) and the heavy metal pollution emergency control of the National Environmental Protection Public Welfare Projects (201209048).

## REFERENCES

- Abdolali, A., Guo, W.S., Ngo, H.H., Chen, S.S., Nguyen, N.C., Tung, K.L. 2014. Typical lignocellulosic wastes and by-products for biosorption process in water and wastewater treatment: A critical review. *Bioresource Technology*, **160**, 57-66.
- Amini, M., Younesi, H., Bahramifar, N. 2009. Biosorption of nickel(II) from aqueous solution by *Aspergillus niger*: Response surface methodology and isotherm study. *Chemosphere*, **75**(11), 1483-1491.
- Baik, W.Y., Bae, J.H., Cho, K.M., Hartmeier, W. 2002. Biosorption of heavy metals using whole mold mycelia and parts thereof. *Bioresource Technology*, **81**(3), 167-170.
- Buasri, A., Chaiyut, N., Tapang, K., Jaroensin, S., Panphrom, S. 2012. Equilibrium and Kinetic Studies of Biosorption of Zn(II) Ions from Wastewater Using Modified Corn Cob. *APCBEE Procedia*, **3**, 60-64.
- Chen, C., Wen, D., Wang, J. 2014. Cellular surface characteristics of *Saccharomyces cerevisiae* before and after Ag(I) biosorption. *Bioresource Technology*, **156**, 380-383.
- Chen, S., Yue, Q., Gao, B., Li, Q., Xu, X. 2011a. Preparation and characteristics of anion exchanger from corn stalks. *Desalination*, **274**(1-3), 113-119.
- Chen, S., Yue, Q., Gao, B., Li, Q., Xu, X. 2011b. Removal of Cr(VI) from aqueous solution using modified corn stalks: Characteristic, equilibrium, kinetic and thermodynamic study. *Chemical Engineering Journal*, **168**(2), 909-917.
- Ding, Y., Jing, D., Gong, H., Zhou, L., Yang, X. 2012. Biosorption of aquatic cadmium(II) by unmodified rice straw. *Bioresource Technology*, **114**, 20-25.
- Ebrahimi, A., Ehteshami, M., Dahrazma, B. 2015. Isotherm and kinetic studies for the biosorption of cadmium from aqueous solution by *Alhaji maurorum* seed. *Process Safety and Environmental Protection*, **98**, 374-382.
- Göksungur, Y., Üren, S., Güvenç, U. 2005. Biosorption of cadmium and lead ions by ethanol treated waste baker's yeast biomass. *Bioresource Technology*, **96**(1), 103-109.
- Hu, H., Zhang, J., Lu, K., Tian, Y. 2015. Characterization of *Acidosasa edulis* shoot shell and its biosorption of copper ions from aqueous solution. *Journal of Environmental Chemical Engineering*, **3**(1), 357-364.
- Jacques, R.A., Lima, E.C., Dias, S.L.P., Mazzocato, A.C., Pavan, F.A. 2007. Yellow passion-fruit shell as biosorbent to remove Cr(III) and Pb(II) from aqueous solution. *Separation and Purification Technology*, **57**(1), 193-198.
- Lodeiro, P., Barriada, J.L., Herrero, R., Sastre de Vicente, M.E. 2006. The marine macroalga *Cystoseira baccata* as biosorbent for cadmium(II) and lead(II) removal: Kinetic and equilibrium studies. *Environmental Pollution*, **142**(2), 264-273.
- Monser, L., Adhoum, N. 2002. Modified activated carbon for the removal of copper, zinc, chromium and cyanide from wastewater. *Separation and Purification Technology*, **26**(2-3), 137-146.
- Odetallah, N.H., Wang, J.J., Garlich, J.D., Shih, J.C.H. 2005. Versazyme supplementation of broiler diets improves market growth performance. *Poultry Science*, **84**(6), 858-864.

- Pehlivan, E., Altun, T., Parlayici, Ş. 2012. Modified barley straw as a potential biosorbent for removal of copper ions from aqueous solution. *Food Chemistry*, **135**(4), 2229-2234.
- Petrović, M., Šoštarić, T., Stojanović, M., Milojković, J., Mihajlović, M., Stanojević, M., Stanković, S. 2016. Removal of Pb<sup>2+</sup> ions by raw corn silk (*Zea mays* L.) as a novel biosorbent. *Journal of the Taiwan Institute of Chemical Engineers*, **58**, 407-416.
- Sepehr, M.N., Nasser, S., Zarrabi, M., Samarghandi, M.R., Amrane, A. 2012. Removal of Cr (III) from tanning effluent by *Aspergillus niger* in airlift bioreactor. *Separation and Purification Technology*, **96**, 256-262.
- Subbaiah, M.V., Vijaya, Y., Reddy, A.S., Yuvaraja, G., Krishnaiah, A. 2011. Equilibrium, kinetic and thermodynamic studies on the biosorption of Cu(II) onto *Trametes versicolor* biomass. *Desalination*, **276**(1-3), 310-316.
- Won, S.W., Kotte, P., Wei, W., Lim, A., Yun, Y.-S. 2014. Biosorbents for recovery of precious metals. *Bioresource Technology*, **160**, 203-212.
- Yu, L., Luo, Y.-m. 2014. The adsorption mechanism of anionic and cationic dyes by Jerusalem artichoke stalk-based mesoporous activated carbon. *Journal of Environmental Chemical Engineering*, **2**(1), 220-229.
- Zheng, L., Dang, Z., Yi, X., Zhang, H. 2010a. Equilibrium and kinetic studies of adsorption of Cd(II) from aqueous solution using modified corn stalk. *Journal of Hazardous Materials*, **176**(1-3), 650-656.
- Zheng, L., Dang, Z., Zhu, C., Yi, X., Zhang, H., Liu, C. 2010b. Removal of cadmium(II) from aqueous solution by corn stalk graft copolymers. *Bioresource Technology*, **101**(15), 5820-5826.
- Zheng, L., Meng, P. 2016. Preparation, characterization of corn stalk xanthates and its feasibility for Cd (II) removal from aqueous solution. *Journal of the Taiwan Institute of Chemical Engineers*, **58**, 391-400.



## SUN-CORAL POWDER AS ADSORBENT FOR PHOSPHORUS REMOVAL IN WASTEWATER

M.T.G Vianna and Marcia Marques  
(Rio de Janeiro State University, Rio de Janeiro, Brazil)

**ABSTRACT:** Searching for low-cost and efficient strategies for phosphorus (P) removal is justified, once its discharge throughout untreated wastewater is related to eutrophication of water bodies. In Brazil, two exotic species known as sun-coral introduced during the 80's are currently spread along 2,000 km of the Brazilian coast representing a serious threat to the Brazilian marine biodiversity. Since they have exoskeletons with high concentration of calcium carbonate, the present investigation focused on the removal of phosphorus from wastewater, using exoskeleton's powder in three forms: raw (RSC); physically modified (SCA) and chemically modified (SCC). A Central Composite Design was applied to the assays along to studies of kinetics, thermodynamics and equilibrium, besides sorbent's characterization by XRD and SEM-EDX techniques. The maximum P removal capacities of RSC, SCA and SCC were 6826, 7062 and 9597 mg P kg<sup>-1</sup>, respectively. In all cases, the adsorption followed the pseudo-second-order kinetic model being the process thermodynamically appropriate. For Real wastewater samples, RSC and SCA adsorbents removed around 80% and the SCC material removed 100% of the P contained in the wastewater. Based on these results, exoskeleton powder proved to be an attractive option for wastewater treatment and may contribute to the control of sun-coral population.

### INTRODUCTION

The excessive release of phosphorus (P), nitrogen (N) and the organic load, by discharge of domestic and industrial effluents associated to other suitable environmental conditions causes eutrophication of water bodies. This well-known phenomenon is responsible for aquatic ecosystems degradation; damage to reservoirs; offensive odour and bad taste in treated water (Su et al., 2013). Thus, removal of phosphorus from effluents is an important strategy aiming the preservation of aquatic systems (Karageorgiou et al., 2007). The form in which orthophosphate is found in water ( $\text{PO}_4^{3-}$ ,  $\text{HPO}_4^{2-}$ ,  $\text{H}_2\text{PO}_4^-$  or  $\text{H}_3\text{PO}_4$ ) depends on the pH. In a typical wastewater, the predominant form is  $\text{HPO}_4^{2-}$  (Mangwandi et al., 2014). Orthophosphate is considered to be the only type of P directly assimilated by most plants and algae (Loganathan et al., 2014).

The method most commonly used for phosphorus removal from wastewater is chemical precipitation, although is relatively expensive and demands proper sludge disposal. Alternative methods for phosphorus removal include biological treatment, electro-dialysis, reverse osmosis, ultrafiltration and adsorption. Among them, adsorption seems to be an effective treatment option because of simplicity of operation, design and economic point of view (Karageorgiou et al., 2007).

Natural materials such as apatite, bauxite, limestone, sand, shells, among others, have been used as adsorbents for removal of phosphates from water (Vohla et al., 2011). In common, these materials have high concentration of calcium (Ca), iron (Fe) and aluminium (Al) in their structures with high yield for phosphorus removal, through adsorption processes.

The introduction of exotic species in aquatic environments has long been considered an environmental problem that affects the integrity of natural communities, mechanisms such as competition, predation and parasitism, and alters food webs and nutrient cycles (Bax et al., 2003). Some of these invasive species have high concentrations of calcium in their exoskeleton composition, potentially useful in water treatment, particularly for phosphorus removal.

**The sun coral problem in the Brazilian coast.** Sun coral (Fig. 1) refers to two species (*Tubastraea coccinea* and *Tubastraea tagusensis*, Scleractinia order, Dendrophylliidae family) native from Asia and very abundant in the Indian and Pacific oceans. However, the sun corals are invasive species that rapidly colonizes large areas, in recent decades, its range distribution has increased, and today, the species is considered pantropical, being observed in Caribbean Sea (Puerto Rico and Curaçao), Gulf of Mexico

(including the Flower Garden Banks Marine Sanctuary and Florida Keys) and Western Atlantic (Brazilian Coast) (Sammarco et al., 2013). In Brazilian Coast, Sun coral was first observed the 1980s, in an oil and gas platforms in Northern of Rio de Janeiro state. Currently, the sun coral's occupation extends over 2000 km of the Brazilian coast (Fig. 1). These corals are opportunistic species with high production of oocytes, early childbearing age, short time incubation embryo and hermaphroditism (Creed and De Paula, 2007). Sun coral produces substances with anti-fouling and anti-predatory properties and releases allelopathic substances that cause necrosis to Brazilian endemic species posing serious threat to the Brazilian marine biodiversity and affect species economically important.



**FIGURE 7.** Sun coral (Photo taken by Joel Creed/Projeto Coral-Sol/BrBio) and its occupation along the Brazilian coastline (modified map from Google Earth).

During recent years, the Public Prosecutor's Office has moved civil actions in different Brazilian states, requesting an injunction to protect the marine environment and control sun coral expansion. Currently, attempts to control the expansion of coral sun infestation includes manual and mechanical removal and inoculation by specific bacteria and viruses. One strategy to promote the removal of these species would be to assign use to the extracted material, making the extraction economically attractive. This study aims to investigate the capacity of exoskeleton (in powder form) of sun coral in removing P from synthetic and real wastewaters.

## **MATERIALS AND METHODS**

**Materials.** All chemicals were purchased from Sigma-Aldrich and all solution were prepared using deionized Milli-Q water (Millipore TM – resistivity of  $\geq 18.2 \text{ M}\Omega \text{ cm}^{-2}$ ). All P solutions were prepared by dissolving the primary standard potassium dihydrogen phosphate ( $\text{KH}_2\text{PO}_4$ ) in Milli-Q water. For pH adjustment, solutions of 0.1N sodium hydroxide (NaOH) and 0.1N hydrochloric acid (HCl) and a multiparameter 5 Star Orion (Method: 4500 H + B) were used (Eaton et al., 2005).

**Preparing Sun Coral Powder.** The sun coral was obtained from Ilha Grande Bay, Rio de Janeiro, Brazil. The material collected was dehydrated in an oven at  $60^\circ \text{C}$  during 72 h. The sun coral exoskeleton was then, washed at room temperature to remove the remaining impurities. Subsequently, the exoskeleton was submerged in vessels containing sodium hypochlorite 10% ( $\text{NaClO}$ -10% w/v). The exoskeleton was washed with hot Milli-Q water ( $90^\circ \text{C}$ ) and then, crushed and sieved with a 200-mesh sieve ( $75 \mu\text{m}$ ). The washed exoskeleton was divided into three portions: The first portion was used with no further modification (RSC);

the second portion was kept in a muffle furnace at 700 °C for 2 h (SCA) before use; the third portion was kept in a muffle furnace at 900 °C for 2 h (SCC).

**Characterization of Sun Coral Powders.** The XRD patterns were recorded on a Brucker-AXS D4 Endeavour powder X-ray diffractometer using  $\text{CoK}\alpha$  radiation (40 kV, 40 mA). The measurements were performed in a  $\theta$  scanning range of 4–80° with a 0.020 step size and 91s of measurement time for each step at ambient temperature and pressure. Scanning electron microscopy with energy dispersive X-ray analysis (SEM-EDX), model FEI Quanta 400 FEG, was used to examine the morphology and chemical composition of the sun coral powder before and after adsorption experiments.

**Phosphorus Analysis.** The determination of total phosphorus in water followed the 4500-P E ascorbic acid Method described by APHA in 4500-P E method (Eaton et al., 2005). The amount of phosphorous removed by adsorption in relation to the mass of adsorbent was determined according to Equation 1:

$$\frac{P_{\text{removed}}(\text{mg})}{\text{ads}_{\text{mass}}(\text{Kg})} = \frac{[P_i - P_f] \cdot V_{\text{Psolution}}}{\text{ads}_{\text{mass}}} \quad (1)$$

Where  $P_i$  and  $P_f$  are the initial and final concentration of P, respectively;  $V_{\text{Psolution}}$  (L) is the volume of phosphorus solution utilized in the experiment;  $\text{ads}_{\text{mass}}$  (Kg) is the amount of exoskeleton powder utilized (RSC, SCA or SCC) in each batch. The result is expressed in milligrams of phosphorus removed per kilograms of adsorbent.

**Experimental Setup: Factorial Design.** Three independent variables were selected as the most important ones for the process of phosphorus removal by the adsorbents RSC, SCA and SCC: (i) pH, (ii) adsorbate/adsorbent ratio and (iii) temperature. In order to assess the best interactions between variables with the purpose of optimizing the phosphorus removal, a central composite design (CCD) was used (Rodrigues and Iemma, 2014). The variables and levels (Table 1) were chosen based on the ranges observed in studies with domestic wastewater available in literature.

**TABLE 3.** Coded levels (5) for independent variables (3) selected to be used in study for assays of phosphorus removal from water by RSC, SCA and SCC powder as sorbent.

Variables	Levels				
	-1.68	-1	0	+1	+1.68
pH	5.32	6.0	7.0	8.0	8.68
Adsorbate/adsorbent ratio	0.4	1.25	2.5	3.75	4.6
Temperature °C	23.6	27	32	37	40.4

The experiments were performed in batch mode as predicted by the experimental design. The study was conducted on an orbital shaker (150 rpm) in 250 ml Erlenmeyer flasks containing 100 ml of water with dissolved phosphorous in amounts to fit to a mass of 400 mg adsorbent respecting the adsorbate/adsorbent ratio predicted by experimental design.

In total, 18 runs (including the central points of CCD) were performed in random sequence. This planning allows obtaining mathematical models with linear and quadratic parameters (multiple regressions) of the studied variables. By combining the different levels presented in the experimental design, it was possible to examine the independent effects of each variable in response to removal, as well as the effect due to the interaction between them.

**Kinetic, Equilibrium and Thermodynamic Studies.** The assay with better P removal is repeated. During the batch experiment, aliquots of 2 ml were removed from the solution to measure the P concentration. Aliquots were taken at intervals of 2 min 30 sec and after 30 min the experiment was stopped. The results were applied to the following kinetic models: pseudo-first-order and pseudo-second-order; For equilibrium studies, all variables were fixed, excepting for the initial P concentration. The concentration range varied from 5 to 100 mg l<sup>-1</sup> by placing the P solutions in contact with 400 mg of each material used as adsorbent. After the equilibrium period, the P concentration was analysed to obtain the constants of Langmuir and

Freudlich models; Thermodynamics was evaluated using five temperatures (25, 30, 35, 40 and 45 °C), in the equilibrium time. Free energy, enthalpy and entropy of process, were obtained using Van't Hoff and Free Gibbs Energy equations.

**P Removal from Real Wastewater.** Experiments were carried out with a real effluent obtained after biological treatment in a municipal wastewater treatment plant located in Niteroi city, Rio de Janeiro, Brazil. The P concentration of the real effluent was measured before and after adsorption treatment. Batch studies were conducted in triplicates, using an orbital shaker and 250 ml Erlenmeyer flasks containing 100 ml of real wastewater. The temperature and the pH of the effluent were not changed due to practical reasons and to avoid additional costs in a future full-scale plant. The results obtained in the experiment was compared with the predicted by the theoretical model.

## RESULTS AND DISCUSSION

**Phosphorus removal studies.** The range of P removal, in the applied range of parameters, using RSC varied from 287.6 to 3685.5 mg P kg<sup>-1</sup>; for CSA varied from 315.0 to 3712.5 mg P kg<sup>-1</sup>; and for SCC varied from 355.0 to 4567.5 mg P kg<sup>-1</sup>. In all materials, the maximum removal occurred in run 12 with pH 7.0, adsorbate/adsorbent ratio of 4.6 (P concentration of 18.4 mg l<sup>-1</sup>) and temperature of 32 °C. Using the experimental results, the regression model for P removal in each material were obtained:

$$P \text{ removal } \left( \frac{\text{mg P}}{\text{kg RSC}} \right) = 1892.50 + 37.49 (pH) + 1005.9 (Adb/ads \text{ ratio}) + 38.18 (Adb/ads \text{ ratio})^2 - 12.03 (Temp) \quad R^2=0,99 \quad (2)$$

$$P \text{ removal } \left( \frac{\text{mg P}}{\text{kg SCA}} \right) = 1926.76 + 38.42 (pH) + 1005.35 (Adb/ads \text{ ratio}) + 33.75 (Adb/ads \text{ ratio})^2 - 8.78 (Temp) \quad R^2=0,99 \quad (3)$$

$$P \text{ removal } \left( \frac{\text{mg P}}{\text{kg CSQ}} \right) = 2455.06 + 1250.07 (Adb/ads \text{ ratio}) \quad R^2=0,99 \quad (4)$$

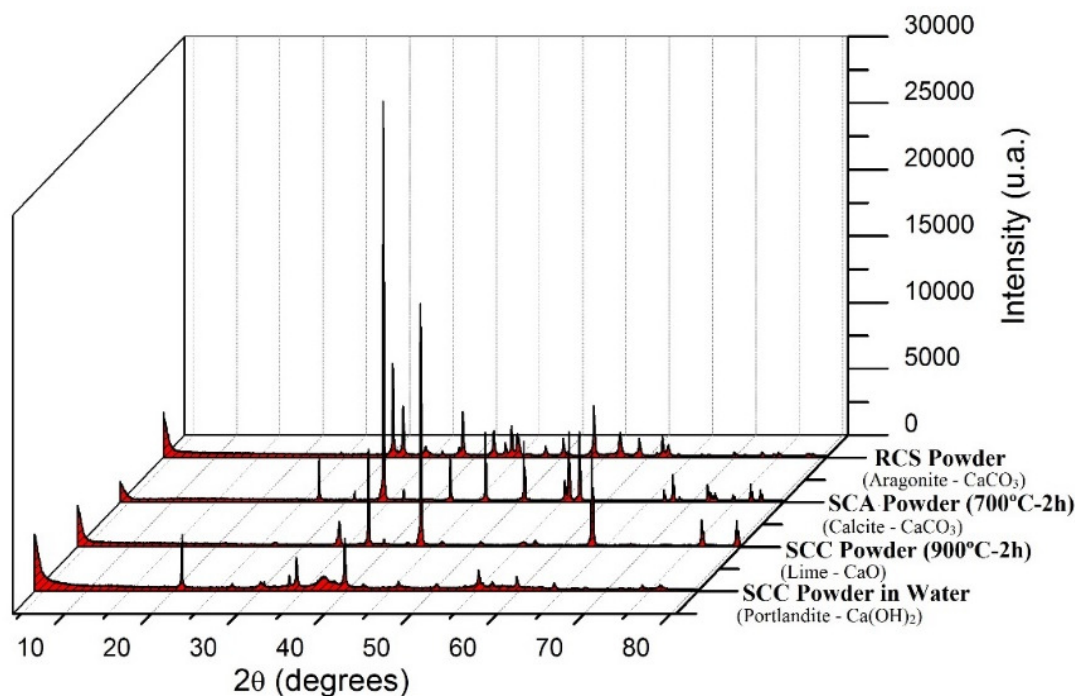
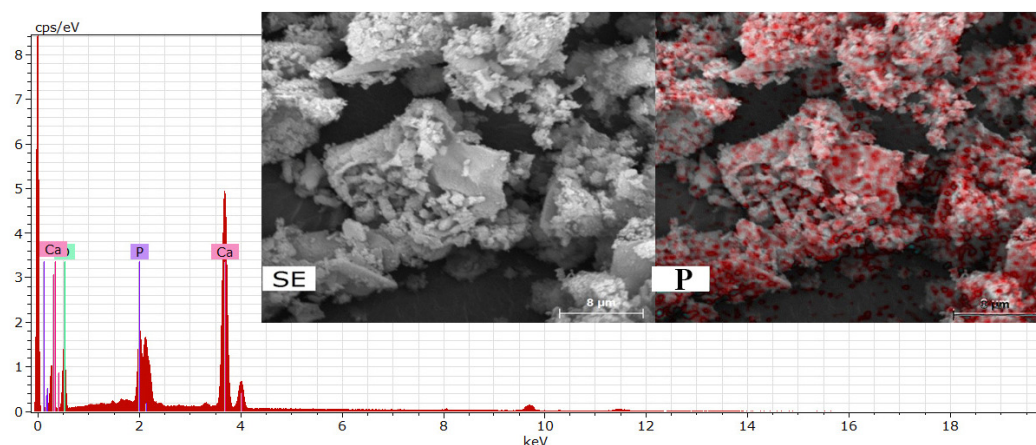


FIGURE 2. XRD patterns – Processes overview

**Characterization of sun coral powders.** The XRD patterns (Fig. 2) reveals that the RSC is composed by orthorhombic calcium carbonate, namely Aragonite; the crystalline structure of RSC changes when exposed to heat at 700 °C, forming a rhombohedral crystal of calcium carbonate, called calcite (SCA). When exposed to 900 °C, the material changed chemically by decomposition of calcium carbonate forming calcium oxide, the calcium oxide obtained exhibits a cubic crystalline form called lime (SCC). After adsorption processes the crystalline structure of RSC and SCA materials remained unchanged, however, the SCC reacted with water producing calcium hydroxide with cubic crystalline structure, called Portlandite. The Portlandite material remained unchanged after adsorption processes. Figure 3 shows the SEM images of SCC after phosphorus adsorption processes. The EDX analysis was used to determine the composition and content on the material surface. The EDX spectra confirmed the existence of P adsorbed to the surface of the sun coral powder. The EDX technique applied together with SEM image revealed where the P uptake occurred in the surface material.



**FIGURE 3.** SEM-EDX images for SCC material, before and after adsorption.

**TABLE 4.** Best results obtained in Kinetic, Equilibrium and Thermodynamic Studies

Kinetic Model		R <sup>2</sup>	k <sub>2</sub> (g mg P <sup>-1</sup> min <sup>-1</sup> )	
RSC	Pseudo-second-order	0.9944	0.1952	
SCA	Pseudo-second-order	0.9981	0.3431	
CSS	Pseudo-second-order	0.9993	0.1843	
Equilibrium Model		R <sup>2</sup>	Q <sub>max</sub> (mg g <sup>-1</sup> )	K <sub>L</sub> (l mg <sup>-1</sup> )
RSC	Langmuir	0.9979	6.826	0.7157
SCA	Langmuir	0.9989	7.062	10.351
CSS	Langmuir	0.9979	9.597	41.513
Thermodynamic		ΔS (J K <sup>-1</sup> mol <sup>-1</sup> )	ΔH (KJ mol <sup>-1</sup> )	ΔG* (KJ mol <sup>-1</sup> )
RSC	Spontaneous and Exothermic	10.59	-22.20	-25.35
SCA	Spontaneous and Exothermic	13.71	-22.19	-26.27
CSS	Spontaneous and Exothermic	44.99	-16.24	-29.65

\* Temperature of 25° C

**Kinetic, Equilibrium and Thermodynamic studies.** According to kinetic results, the best-fit model was the pseudo-second order model (R<sup>2</sup> close to 1.0) and all processes reached the equilibrium around 20 min; For Equilibrium, the results revealed that Langmuir model is the one that best describes the P adsorption by sun coral-based adsorbents, which indicates that the adsorption sites are distributed homogeneously on the



surface of the adsorbent. The highest capacity for P removal from water achieved by sun coral-based adsorbents RSC, SCA, SCC under the studied conditions were 6826, 7062 and 9597 mg P kg<sup>-1</sup>, respectively; The negative value of change in enthalpy ( $\Delta H$ ) shows that the adsorption is exothermic. Negative values of free energy ( $\Delta G$ ) indicated the feasibility and spontaneity of adsorption.

**P removal from real wastewater.** The levels applied for different independent variables were encoded and included in the P removal model obtained by CCD (Table 3). The mass of adsorbent used in all experiments were 37 mg to fit the +1.68 coded value of adsorbate/adsorbent ratio. To minimize the influence of P consumption by microbiological routes, taking into account the kinetic parameters, the assays were performed within 20 min. Table 3 shows high levels of P removal. The initial concentration of P in wastewater (1.71 mg l<sup>-1</sup>) reduced to 0.37, 0.36 and 0.02 mg P l<sup>-1</sup> when the wastewater was treated with RSC, SCA and SCC, representing reductions of 78.17, 79.14 and 98.6% respectively. These results show that the powder obtained with exoskeleton of sun coral is a promising material for using in filters aiming P removal. The model obtained with spiked water showed good fit when used in real wastewater; in all cases, the difference between predicted and real values was below 2%.

**TABLE 3.** P removal by sun coral powders in real wastewater.

	Variables	CCD uncoded	CCD code	P removal predicted	Amount of P removed	SD	P removal (%)
RSC	pH	6.58	-0.42				
	Temperature	27.4 °C	-0.92	0.136	0.1337	0.0004	78.17
	P total	1.71 mg l <sup>-1</sup>	1.68	mg P in 37 mg <sup>-1</sup>	mg P in 37 mg <sup>-1</sup>		
SCA	pH	6.58	-0.42				
	Temperature	27.4 °C	-0.92	0.137	0.1353	0.0044	79.14
	P total	1.71 mg l <sup>-1</sup>	1.68	mg P in 37 mg <sup>-1</sup>	mg P in 37 mg <sup>-1</sup>		
SCC	pH	6.58	-0.42				
	Temperature	27.4 °C	-0.92	0.169	0.1687	0.0044	98.64
	P total	1.71 mg l <sup>-1</sup>	1.68	mg P in 37 mg <sup>-1</sup>	mg P in 37 mg <sup>-1</sup>		

## CONCLUSIONS

The highest capacity for P removal from water achieved by sun coral-based adsorbents RSC, SCA, SCC under the studied conditions were 6826, 7062 and 9597 mg P kg<sup>-1</sup> respectively. In all cases, the adsorption process followed the Langmuir model, the pseudo-second-order kinetic model and was thermodynamically appropriate. According to the results, sun coral-based adsorbents proved to be a good option for wastewater treatment, particularly when associated to the mandatory removal of these invasive species from the coastal areas. Next steps of this research involves the use of the obtained parameters to project lab-scale and real-scale filters aiming P removal. The real-scale filter will be installed in an Engineered Ecosystem located in Ilha Grande, Rio de Janeiro, Brazil.

## ACKNOWLEDGMENTS

The authors acknowledge the financial support to the project provided by the Research Support Foundation of Rio de Janeiro (FAPERJ) and the scholarship provided to the first author by the Coordination for the Improvement of Higher Education Personnel (CAPES).

## REFERENCES

- Bax, N., Williamson, A., Aguero, M., Gonzalez, E., Geeves, W., 2003. Marine invasive alien species: a threat to global biodiversity. *Mar. policy* 27, 313–323.
- Creed, J.C., De Paula, A.F., 2007. Substratum preference during recruitment of two invasive alien corals onto shallow-subtidal tropical rocky shores. *Mar. Ecol. Prog. Ser.* 330, 101–111.
- Eaton, A.D., Clesceri, L.S., Greenberg, A.E., 2005. *Standard methods for the examination of water and wastewater* American Public Health Association. Washington, DC 20001–23710.
- Karageorgiou, K., Paschalis, M., Anastassakis, G.N., 2007. Removal of phosphate species from solution by adsorption onto calcite used as natural adsorbent. *J. Hazard. Mater.* 139, 447–52.

- Loganathan, P., Vigneswaran, S., Kandasamy, J., Bolan, N.S., 2014. Removal and recovery of phosphate from water using sorption. *Crit. Rev. Environ. Sci. Technol.* 44, 847–907.
- Mangwandi, C., Albadarin, A.B., Glocheux, Y., Walker, G.M., 2014. Removal of ortho-phosphate from aqueous solution by adsorption onto dolomite. *J. Environ. Chem. Eng.* 2, 1123–1130.
- Rodrigues, M.I., Iemma, A.F., 2014. *Experimental Design and Process Optimization*, Ilustred. ed. CRC press, Boca Raton, FL.
- Sammarco, P.W., Porter, S. a, Sinclair, J., Genazzio, M., 2013. Depth distribution of a new invasive coral (Gulf of Mexico)—*Tubastraea micranthus*, comparisons with *T. coccinea*, and implications for control. *Manag. Biol. Invasions* 4, 291–303.
- Su, Y., Cui, H., Li, Q., Gao, S., Shang, J.K., 2013. Strong adsorption of phosphate by amorphous zirconium oxide nanoparticles. *Water Res.* 47, 5018–26.
- Vohla, C., Kõiv, M., Bavor, H.J., Chazarenc, F., Mander, Ü., 2011. Filter materials for phosphorus removal from wastewater in treatment wetlands—A review. *Ecol. Eng.* 37, 70–89.

## **COMPARATIVE STUDY OF ADSORPTION OF DYES ONTO ACTIVATED CARBON AND CHITOSAN IMPREGNATED ACTIVATED CARBON**

***Pratyusha Reddy Reddy\****, George A. Sorial  
(University of Cincinnati, Cincinnati, OH, USA)

Dyes are organic compounds that impart color when applied to a substrate. The presence of dyes in wastewater makes it aesthetically unacceptable and are known to pose problems to the aquatic environment. It is important to treat the dye containing wastewater before its discharge into water bodies. Among the wastewater treatment methods available, adsorption is commonly used for the removal of dyes from wastewater. Activated carbon is a popular adsorbent used for treating organic compounds present in water and wastewater. Activated carbon is expensive, hence, other low-cost alternatives are being investigated. One such low-cost option could be the modification of commercial activated carbon with chitosan, a polymer present in the hard shells of crustaceans which could lead to higher adsorption capacities.

In this work, three different types of dyes adsorption behavior are evaluated by two adsorbents- commercial activated carbon (Filtrisorb F400) and commercial activated carbon impregnated with chitosan. The dyes used are acid blue 113 (AB113), basic blue 3 (BB3) and direct blue 71 (DB71). Single solute and multi solute adsorption studies are carried for each of the adsorbents. The single solute adsorption isotherms are modelled against the two well-known isotherm equations Freundlich and Langmuir isotherm equations. The multi solute are evaluated against predictions by the Ideal Adsorbed Solution Model.



## **NATURAL IRON-BASED MATERIAL AS A COST-EFFECTIVE SOLUTION FOR THE TREATMENT OF ARSENIC CONTAMINATED WATERS FROM GOLD MINE**

***Małgorzata Szlachta*** and Patryk Wójtowicz  
(Wrocław University of Technology, Wrocław, Poland)

Arsenic is a chemical element widely known for its high toxicity to humans and aquatic organisms. It may occur naturally in the aquatic environment or may be released into the water through industrial sources. In some areas, excessive quantities of arsenic found in natural waters often originate from the mining activities. The impact of mining operations on the natural environment depends on the amount of arsenic bearing minerals in the exploited rock. The gold mines are a potential source of arsenic due to arsenopyrite, which is usually present in the sulphide ores associated with sediment-hosted gold deposits. To prevent contamination of rivers, lakes and groundwater, the arsenic species should be captured and effectively removed from gold mine effluents. The adsorption/ion exchange process due to its technical applicability for the treatment of large volumes of water may offer a good solution for the robust and cost-effective treatment of mine process waters and effluents.

The main objective of this work was to evaluate the efficiency of natural iron-based material in the treatment of arsenic contaminated mine waters. The material used in the study was crushed iron ore composed of hematite, maghemite and limonite originating from Romania. To investigate the performance of tested material, the batch adsorption technique was applied. The adsorption experiments were carried out in the laboratory scale and included adsorption kinetics and multi-load tests as well as experiments with various material dose and solution pH. In the first phase of the research, the model solutions spiked with arsenic(III) and (V) were used for the tests. Furthermore, with the aim of practical application, the performance of natural iron-based material was verified with the use of real arsenic contaminated waters from the gold mines in Finland.

It was confirmed that arsenic has a strong affinity for iron rich surfaces, therefore the application of natural material investigated in the study may provide suitable and cost-effective treatment of arsenic-rich mine waters. It was also found that the efficiency of the process depends on operating parameters, including contact time, material dose and solution pH. However, it was observed that arsenite was more difficult to remove from water compared to the arsenate. Therefore, when considering the treatment of mine process waters and effluents by adsorption using studied natural material the peroxidation step to convert trivalent arsenic to pentavalent is recommended.

The problem presented in this work is currently being addressed in the international SUSMIN project “Tools for sustainable gold mining in the EU”.

## **CONVERSION OF BLACK LIQUOR INTO ACTIVATED CARBON FOR CIPROFLOXACIN REMOVAL FROM WASTEWATER**

**Anirudh Gupta** and Anurag Garg  
(Indian Institute of Technology Bombay, Mumbai, INDIA)

Black liquor is a major by-product generated from a pulp and paper mill. It can be considered as a precursor for activated carbon (AC) preparation due to high carbon content. In the present study, the effectiveness of black liquor derived AC was investigated for the treatment of synthetic wastewater contaminated by ciprofloxacin (CPX), a pharmaceutically active compound toxic to aquatic organisms. The black liquor was transformed into an adsorbent using chemical activation process mediated by  $\text{ZnCl}_2$ . The Brunauer-Emmet-Teller (BET) surface area and total pore volume of the adsorbent were found to be  $600 \text{ m}^2/\text{g}$  and  $0.324 \text{ cm}^3/\text{g}$ , respectively. The  $\text{pH}_{\text{PZC}}$  (i.e. point of zero charge) of the adsorbent was slightly below the neutral pH (= 6.6). The batch adsorption runs were conducted in an orbital shaker with 50 ml of synthetic wastewater (initial CPX concentration = 20 – 100 mg/l) with an adsorbent dosage of 2 g/l. The CPX concentration was measured at 278 nm using UV-visible spectrophotometer. The equilibrium time for the CPX adsorption was found to be 12 h. The adsorption capacity of the waste derived adsorbent was ranged between 8 – 32 mg/g at an optimum pH of 7.0. The equilibrium data was found fit to Freundlich and Langmuir isotherm models. The CPX adsorption on AC was found to be spontaneous and favourable. The adsorption kinetic data could fit well in pseudo first order equation and intra-particle diffusion model.

**MULTIWALLED CARBON NANOTUBES AS A NOVEL SOLID-PHASE EXTRACTION ADSORBENT FOR TPH DETERMINATION IN CONTAMINATED WATER**

***Akinpelu A Adeola<sup>a</sup>, Ilyas Muhammad <sup>a</sup>, Ahsan M Shemsi <sup>a</sup>***

(<sup>a</sup>Center of Environment and Water King Fahd University of Petroleum and Minerals, Dhahran Saudi Arabia)

The application of Multiwalled carbon nanotubes (MWCNTs) as a novel adsorbent of solid-phase extraction (SPE) for the determination of total petroleum hydrocarbon (TPH) was investigated using gas chromatography (GC) coupled with flame ionization detector (FID). Parameters influencing the optimum extraction of TPH such as, elution solvent, solvent volume, elution flow rate and sample loading flow rate, were examined. Elution with hexane and so also Isopropanol followed by Hexane/Dichloromethane at 3ml/min elution flow rate were observed to be the optimum conditions for efficient extraction of TPH from contaminated water. The calibration curves for 22 TPH standards were linear in the range of 100-5000n/L, with correlation coefficients ( $r^2$ ) between 0.9981 and 0.9991. There was a good precision as seen in (RSD) which is 1.42%-7.04%. It was concluded that MWCNTs packed cartridge coupled with FID is an excellent option for the determination of TPH in contaminated water.

## **AMMONIA NITROGEN ADSORPTION BY ZEOLITE AND WETLAND SOILS UNDER DIFFERENT TEMPERATURES**

**Wei Huang** and Weidong Wang

(Research Center for Eco-Environmental Sciences, Chinese Academy of Sciences, Beijing, China)

Adsorption characteristics of ammonia nitrogen on zeolite and soils from natural and constructed wetlands were investigated by batch experiments under different temperatures. The effects of relevant parameters including contact time, temperature, and initial ammonia concentration were examined, respectively. The results showed that although it would need at least one hour to reach exchange equilibrium, ammonia adsorption by zeolite occurred rapidly within the initial fifteen minutes of contact time, and the ammonia adsorption capacity of zeolite increased with temperature (from 4 to 35 Celsius degree). However, the adsorption capacity of soils decreased with the increase of temperature, which was contrary to zeolite. The adsorption capacity of zeolite was 5 to 15 times those of reed-bed rhizospheric soils from constructed wetlands in the Yangtze River delta and from natural wetlands in Baiyangdian Lake of north China plain under the same condition. Ammonia adsorbed by zeolite during the cold seasons were desorbed, and then nitrified in warm seasons, which resulted in a bio-regeneration of zeolite. This could relieve the seasonal fluctuation in ammonia nitrogen removal.

**HETEROGENEOUS CATALYTIC DEGRADATION OF ACETAMINOPHEN AND  
SIMULTANEOUS OXIDATION/ADSORPTION OF ARSENITE BY Cu-Zn-Fe-LDH**

**Hongtao Lu**, Zhiliang Zhu, Jianyao Zhu  
(Tongji University, Shanghai, CHINA)

A three metal layered double hydroxide Cu-Zn-Fe-LDH was synthesized and used as a heterogeneous Fenton-like oxidation catalyst and adsorbent to simultaneously remove acetaminophen (Paracetamol) and arsenic. The degradation of acetaminophen and oxidation/adsorption of arsenite were studied in aqueous solution under natural water pH range. Degradation of Paracetamol was accelerated with decrease of pH or increase in  $\text{H}_2\text{O}_2$  concentration and catalyst dosage. When the catalyst dosage was  $0.5 \text{ g}\cdot\text{L}^{-1}$  and  $\text{H}_2\text{O}_2$  dosage of  $30 \text{ mmol}\cdot\text{L}^{-1}$ , the acetaminophen was totally degraded within 24h. The synthesized Cu-Zn-Fe-LDH was also a possible efficient adsorbent for arsenate removal from aqueous solutions, the maximum adsorption capacity was  $126.13 \text{ mg}\cdot\text{g}^{-1}$ . In the presence of hydrogen peroxide, the arsenite was gradually oxidized into arsenate and adsorbed at the same time by Cu-Zn-Fe-LDH. The simulate water sample with coexistence of arsenic and Paracetamol had been treated by the Cu-Zn-Fe-LDH material. The residual arsenic concentration was below  $10 \mu\text{g}\cdot\text{L}^{-1}$  and the Paracetamol were not detected in the solution by UPLC. This material can be used for simultaneous removal of acetaminophen and arsenic (As(III) and As(V)).

**ELECTROSPRAYING *SACCHAROMYCES CEREVISIAE* IMMOBILIZED ONTO  
COMPOSITE NANOFIBROUS MATS FOR HEAVY METALS ADSORPTION**

**Hongbing Deng**, Xiaodan Qiu, Zhaoyang Zeng  
(Wuhan University, Wuhan, China)

*Saccharomyces cerevisiae* (SCV) immobilized electrospun polymer-layered silicate nanofibrous mats were fabricated via electrospraying method. These organic-inorganic composite nanofibrous mats, including cellulose acetate/rectorite (CA/REC) and polycaprolactone/chitosan/REC (PCL/CS/REC) nanofibrous mats, have three-dimensional nanofibrous structure, ultrafine fiber diameter and big specific surface area. SCV colonies distribute on the surface of polymer-layered silicate nanofibrous mats with fiber diameter range from 52 to 292 nm. With SCV, the composite nanofibrous mats get obvious adsorption capacity, especially for heavy metals such as  $\text{Cr}^{6+}$ ,  $\text{Pb}^{2+}$  and  $\text{Cu}^{2+}$ . The surface areas of composite nanofibrous mats increase with the addition of REC, a kind of layered silicate with super large surface area and interlayer distance. Within a certain range, the more REC is added, the higher adsorption capacities are obtained. And CS, also an adsorption agent, could remarkably improve the adsorption effect of the nanofibrous mats. SCV-PCL/CS/REC composite nanofibrous mats have an adsorption capacity of  $215.1 \pm 19.8$  mg/g toward  $\text{Pb}^{2+}$ . SCV immobilized electrospun polymer-layered silicate nanofibrous mats can serve as a bio-polymer-layered silicate composite thin film for the adsorption of heavy metals in water.

## SYNERGISTIC ADSORPTION AND DEGRADATION OF AQUEOUS CONTAMINANTS USING MAGNETIC MESOPOROUS ADSORBENT

Yaocheng Deng, *Lin Tang*, Jingjing Wang  
(Hunan University, Changsha, China)

Magnetic mesoporous materials, due to their high surface areas, large pore volumes, excellent physical-chemical properties and convenience for recovery, have been widely investigated as promising candidates for the treatment of aqueous contaminants. And meanwhile, the large surface areas make mesoporous materials not only good adsorbent, but also excellent support for some other oxidant or reductant, which will greatly enhance the removal efficiency for environmental contaminants. Considering the excellent characteristics of magnetic mesoporous materials mentioned above, we have conducted a series of studies based on them for environment remediation.

Hexavalent chromium (Cr(VI)) is a highly toxic pollutant, which is able to cause carcinogenesis, mutation to humans and animals. Therefore, developing effective methods to remove Cr(VI) from the environment is of great significance to human health and ecological system. To effectively remove Cr(VI) in aqueous solution, we have prepared some adsorbents based on magnetic mesoporous materials. First of all, we considered mesoporous silica (SBA-15). We synthesized polyaniline grafted magnetic mesoporous silica composite (PANI-Fe/SBA-15) for the adsorption and reduction of Cr(VI). The results showed that the prepared PANI-Fe/SBA-15 presented great removal efficiency for Cr(VI) due to the efficient adsorption and synergistic reduction by PANI, and the maximum adsorption capacity reached to 193.85 mg g<sup>-1</sup>, which presented great potential for realistic application. Mesoporous carbon is also a good adsorbent with better bioavailability, so we also incorporated ordered mesoporous carbon with polyaniline and iron nanoparticles, to prepare a new adsorbent (PANI-Fe/OMC). The adsorption capacity of the functionalized material was 2- and 10-fold compared with pristine SBA-15 and the magnetic mesoporous carbon (Fe/OMC), and the adsorption process of Cr(VI) was demonstrated to be the chemisorption. Besides, carbon nanorods (CMK-3) with hexagonally ordered uniform mesoporous structure have shown good performance as adsorptive media due to its unique physical and chemical proprieties. To improve the adsorption capacity and obtain reusability of the mesoporous material, we doped iron inside CMK-3 for magnetic property (Fe/CMK-3). We found its synergistic effect on adsorption and reduction of Cr(VI). Under the optimal conditions, Fe/CMK-3 showed the maximal removal capacity of 256.85 mg g<sup>-1</sup>, which was larger than that of pure CMK-3 as 182.03 mg g<sup>-1</sup>. The excellent performance of Fe/CMK-3 could be contributed to the following two aspects. On one hand, the large specific surface area presented great adsorption capacity for Cr(VI); on the other hand, due to the existence of Fe<sup>0</sup>, Cr(VI) could be reduced to Cr(III) with lower toxicity. Besides, the synthesized Fe/CMK-3 can be regenerated and showed high removal efficiency even after seven cycles.

Additionally, we have also prepared some mesoporous materials for the removal of organic pollutant in aqueous solution. For example, we prepared nanoscale zero-valent iron particles immobilized on mesoporous silica for the reductive degradation of aqueous p-nitrophenol, and phosphorus-doped ordered mesoporous carbons embedded with Pd/Fe bimetal nanoparticles for the dechlorination of 2,4-dichlorophenol.

Briefly, magnetic mesoporous adsorbent based composites can efficiently remove heavy metal or organic pollutants with combined adsorption and degradation process, and present great potential for wastewater treatment.

## PERSULFATE ACTIVATION IN THE PRESENCE OF FORMIC ACID FOR CARBON TETRACHLORIDE AND CHROMIUM (VI) REMOVAL

Xiaogang Gu and Shuguang Lu (East China University of Science and Technology, Shanghai, China)

**ABSTRACT:** In this study, carbon tetrachloride (CT) and Cr(VI) removal performance was investigated by means of the thermal activation of persulfate, in the presence of formic acid to turn the oxidizing capacity of the reaction mixture into a reductive one by the generation of carbon dioxide anion free radicals ( $\text{CO}_2^{\cdot-}$ ). The Effects of the initial concentrations of persulfate, formic acid, and contaminants on CT and Cr(VI) removal performance were evaluated, respectively. The results indicated that CT and Cr(VI) could be effectively removed in the thermally activated PS system in the presence of FA. CT and Cr(VI) removal performance was found to increase with increasing PS and formic concentrations. And Cr(VI) removal decreased with increasing the initial Cr(VI) concentration, while no obvious influence of the initial CT concentration was observed.

### INTRODUCTION

Carbon tetrachloride (CT, a kind of chlorinated aliphatic hydrocarbon) and hexavalent chromium Cr (VI) have been frequently detected in the groundwater of the National Priority List (NPL) sites in USA (Choi et al., 2009). In-situ chemical oxidation (ISCO) is becoming an effective method for in-situ soil and groundwater remediation, which is capable of breaking down many contaminants in solid or aqueous phases. Among the ISCO oxidants, persulfate (PS) is a promising new oxidant. ISCO using PS has been documented to treat aquifers contaminated groundwater (Tsitonaki et al., 2010).

Thermally activated PS system has been carried out to effectively degrade the toxic organic contaminants (Gu et al., 2011). And the addition of formate to the thermally activated PS system has been successfully applied to degrade trichloroacetic acid (Mora et al., 2009). To our best knowledge, the performance of perchlorinated hydrocarbons and Cr(VI) reduction in the thermally activated PS system in the presence of formic acid (FA) has never been studied, and it is expected that thermally activated PS system in the presence of FA may generate more reductive radicals that can remove CT and Cr(VI) in groundwater efficiently. Therefore, the objective of this study was to investigate the performance of CT and Cr(VI) removal in the thermally activated PS system in the presence of FA.

### EXPERIMENTAL

**Materials.** Sodium persulfate (98.0%), formic acid (99.0%), and potassium iodide (99.0%) were purchased from Shanghai Jingchun Reagent Co. Ltd. (Shanghai, China). Carbon tetrachloride (CT, 99.5%) and n-Hexane (97%) were purchased from Shanghai Lingfeng Chemical Reagent Co. Ltd. Methyl viologen dichloride (MV2+) was purchased from Aladdin Reagent Ltd Co. (Shanghai, China). Ultrapure water from a Milli-Q water process (Classic DI, ELGA, Marlow, U.K.) was used for preparing aqueous solutions.

**Experimental Procedures.** All reactions were conducted in a series of 24 mL borosilicate vials capped with polytetrafluoroethylene (PTFE) lined septa under controlled temperature (20~50 °C). CT, Cr(VI), and PS solutions were prepared by dissolving reagents at room temperature into Milli-Q water to make stock solutions. Each stock solution and desired volume of FA were added to the volumetric flask at desired concentration, then a series of reaction vials were fully filled. The reaction vials were sacrificed at different intervals for immediate analyses. The initial pH in all experiments was unadjusted except in the test for investigating the influence solution pH.

**Analytical Methods.** The concentration of CT was quantified after extraction with hexane by a gas chromatograph (GC, Agilent 7890A, Palo Alto, CA) equipped with an autosampler (Agilent 7693). The

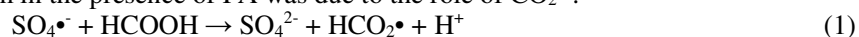


Cr(VI) concentration was determined using the 1,5-diphenylcarbazide method on a 722N visible spectrophotometer (Hach DR 6000, Loveland, CO).

## RESULTS AND DISCUSSION

**Enhanced CT and Cr(VI) removal with the presence of FA in PS system.** FIGURE 1 shows the CT and Cr(VI) removal performance in the thermally activated PS system in the presence of FA and in different control groups. 2.3% and 3.4% CT lost in the CT alone group and in CT solution with the presence of FA at 50 °C within 180 min reaction time, respectively. The loss of the component was likely due to the thermolysis and volatilization of CT in solution. However, the degradation of CT was significantly increased when FA was added to CT solution. Complete CT degradation was achieved for reactions carried out at PS concentration of 20 mM and FA concentration of 30 mM over 180 min. According to Cr(VI), the results of control tests showed that there was no observable Cr(VI) removal when PS or FA was applied solely in the thermal systems. However, Cr(VI) removal did occur when PS and FA were applied together at 50 °C (FIGURE 1b).

In the presence of FA,  $\text{SO}_4^{\bullet-}$  and  $\text{HO}^{\bullet}$  generated in the chain reaction were scavenged to yield  $\text{HCO}_2^{\bullet}$  via Eqs. 1-2. Carbon dioxide radical anion ( $\text{CO}_2^{\bullet-}$ ) formed from the propagation reactions as shown in Eq. 3 (Lin et al., 2008).  $\text{CO}_2^{\bullet-}$  is a strongly reducing species, with a redox potential of -2.0 V vs. NHE (normal hydrogen electrode). The addition of FA to the solution can turn the oxidizing capacity of the reaction mixture into a reductive one, since  $\text{CO}_2^{\bullet-}$  can transfer an electron rapidly to quinones, nitro and nitroso compounds, pyridinium and viologen ions, porphyrins, oxygen, and many other organic and inorganic compounds (Neta et al, 1998). Therefore, it is deduced that the removal of CT and Cr(VI) in the thermally activated PS system in the presence of FA was due to the role of  $\text{CO}_2^{\bullet-}$ .



**Effects of initial PS, FA and CT concentrations on CT degradation.** To study the effect of PS concentration on CT degradation in the thermally activated PS system in the presence of FA, different PS concentrations were used in the reaction (FIGURE 2). When the PS concentration was more than 20 mM, complete CT degradation was achieved in 180 min, and in contrast CT degraded 40.0% and 9.8% with the PS concentrations of 10 and 5 mM, respectively (FIGURE 2a). The results showed that the rate of CT degradation increased as the initial PS concentration increased. With the increase of PS concentration, the amount of  $\text{SO}_4^{\bullet-}$  and  $\text{HO}^{\bullet}$  were elevated and more  $\text{CO}_2^{\bullet-}$  generated through Eqs. 1-3. Liang et al. found that when PS concentration was more than 6.75 mM in the degradation of trichloroethylene in the ferrous activated PS system, increase in PS concentration only resulted in smaller increases in trichloroethylene removal (Liang et al., 2004). Similarly, excess amount of  $\text{CO}_2^{\bullet-}$  would lead to radical-radical recombination as shown in Eq. 4, which might stop the increase of CT degradation rate (Cooper et al., 2009).



Different concentrations of FA were applied to evaluate the effect of FA concentration on CT degradation performance and the results are displayed in FIGURE 2(b). It could be seen that CT removal efficiency increased with the increase of FA concentration from 5 to 100 mM. Complete CT degradation could be achieved in 180 min when the FA concentration was over 30 mM, while CT degraded 80.6%, 56.7% and 46.3% with the FA concentrations of 20, 10 and 5 mM, respectively. The increased concentration of FA induced the reactions as shown in Eqs. 1-2 reactions, therefore more  $\text{CO}_2^{\bullet-}$  were generated in the system.

The variation of CT degradation efficiency in the thermally activated system in the presence of FA under different initial CT concentrations, ranging from 0.01 mM to 1 mM, was also investigated and the results are shown in FIGURE 2(c). CT degradation rate followed zero order rate kinetics as shown in FIGURE 2(c). When the initial CT concentration increased, the slopes of these lines were almost the same and the CT degradation rates were nearly constant.

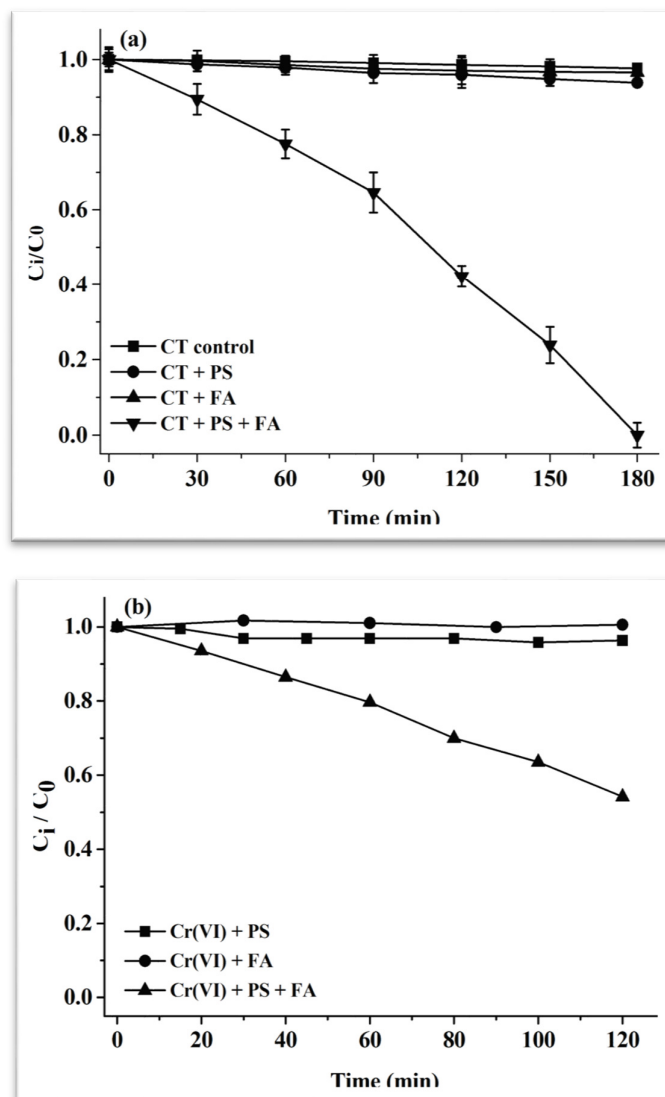


FIGURE 1. CT (a) and Cr(VI) (b) removal in the thermally activated PS system in the presence of FA (50°C,  $[CT]_0 = 10 \mu\text{M}$ ,  $[Cr(VI)]_0 = 0.2 \text{ mM}$ ,  $[PS] = 20 \text{ mM}$ ,  $[FA] = 30 \text{ mM}$ )

**Effects of initial PS, FA and Cr(VI) concentrations on Cr(VI) removal.** The effect of initial PS concentration at 50 °C was investigated by varying the initial PS concentration in the range of 20~100 mM, while keeping the initial FA concentration constant at 100 mM (FIGURE 3a). It can be seen that, with the increase of the initial PS concentration, the removal efficiency increased. When the initial concentrations of persulfate, formic acid, and Cr(VI) were 100 mM, 100 mM, and 0.2 mM, respectively, Cr(VI) could be almost completely removed at 2 h.

Moreover, the influence of initial FA concentrations of 20 mM to 200 mM was investigated at a temperature of 50 °C, and the results are shown in FIGURE 3b. Complete removal of Cr(VI) was achieved in 2 h at the experimental conditions, and the removal efficiency increased with the increase of FA concentration. The results of FIGURE 3a and 3b strongly suggested that the removal of Cr(VI) proceeded more rapidly with increasing PS and FA concentrations, and PS played a much more important role than the initial FA concentration. The influence of PS and FA concentrations on Cr(VI) removal were consistent with the results of CT degradation.

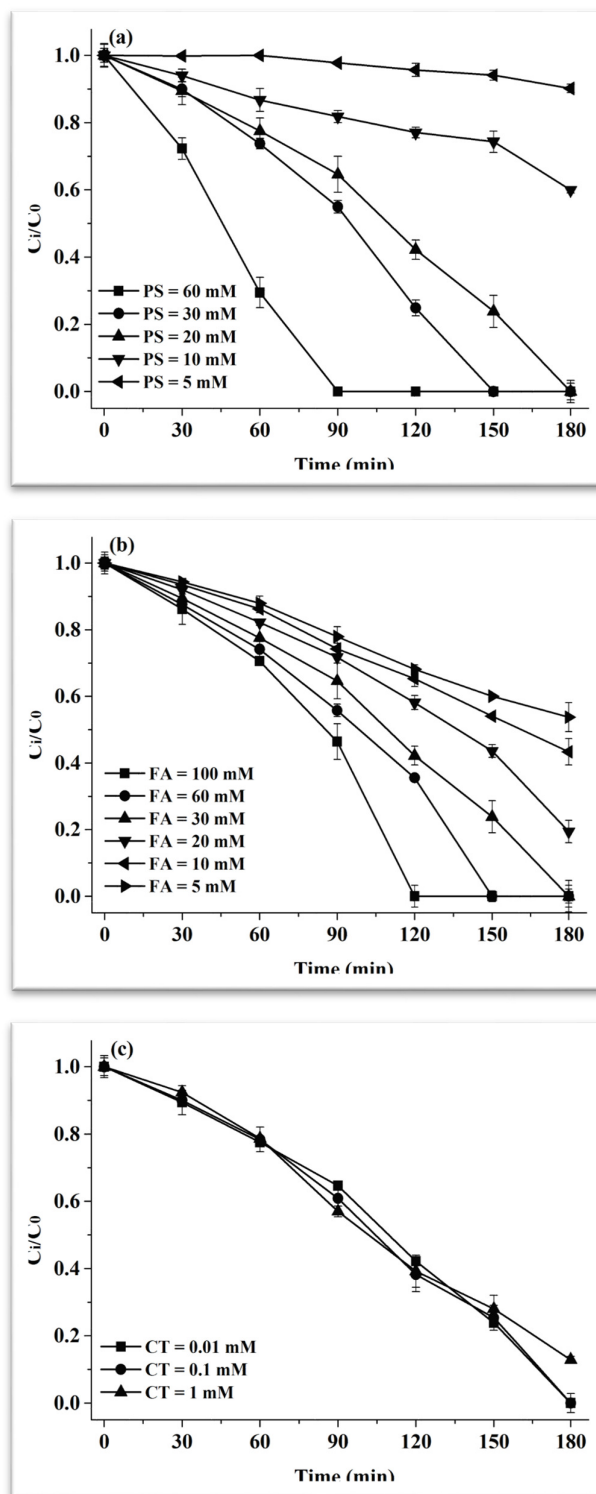
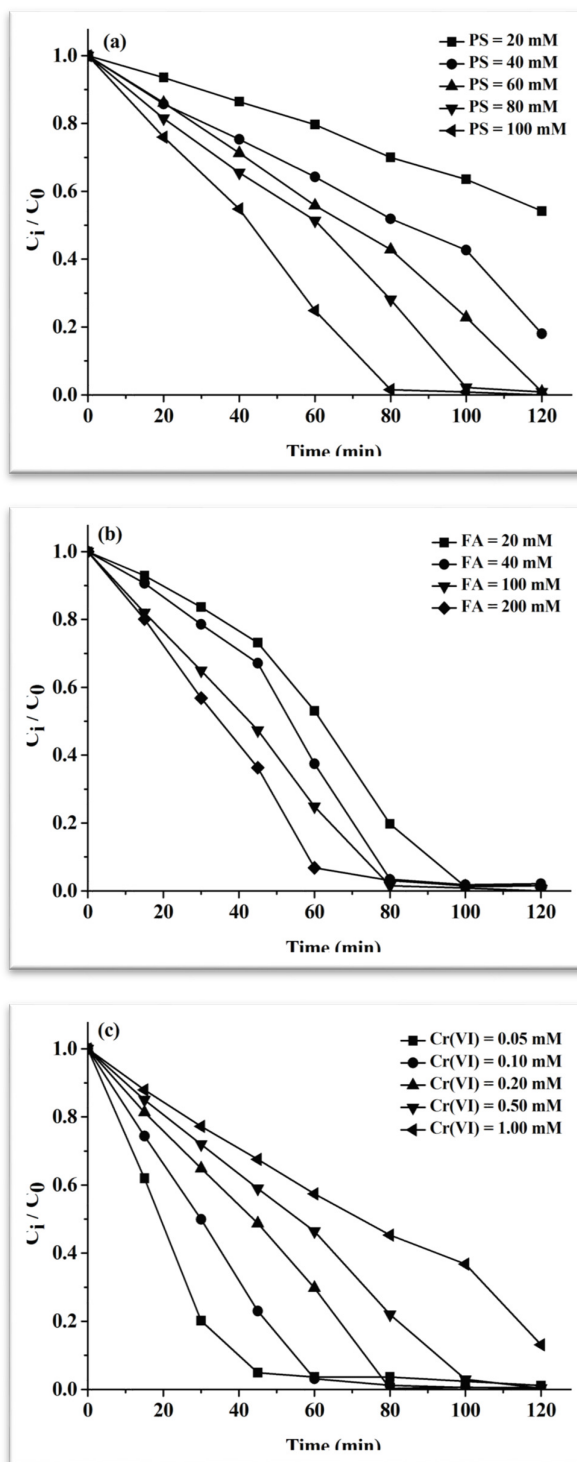


FIGURE 2. Effect of initial concentration on CT degradation. (a) PS (50 °C,  $[CT]_0 = 10 \mu M$ ,  $[FA] = 30 mM$ ); (b) FA (50 °C,  $[CT]_0 = 10 \mu M$ ,  $[PS] = 20 mM$ ); (c) CT (50 °C,  $[PS] = 20 mM$ ,  $[FA] = 30 mM$ ).



**FIGURE 3.** Effect of initial concentration on Cr(VI) removal. (a) PS (50 °C,  $[Cr(VI)_0] = 0.2$  mM,  $[FA] = 100$  mM); (b) FA (50 °C,  $[Cr(VI)_0] = 0.2$  mM,  $[PS] = 100$  mM); (c) CT (50 °C,  $[PS] = 100$  mM,  $[FA] = 100$  mM).

As shown in FIGURE 3c, concentration, various Cr(VI) concentrations (0.05 mM~1.00 mM) were conducted to investigated the effect on Cr(VI) removal. Unlike CT tests, the removal efficiency of Cr(VI) decreased with the increase of initial Cr(VI) concentration, and the slopes of Cr(VI) removal were different. However, the removal rates of Cr(VI) were nearly constant.

## CONCLUSIONS

This study confirmed that CT and Cr (VI) could be effectively removed in the thermally activated PS system in the presence of FA at 50 °C, and contaminants removal followed a model. CT degradation rate increased with increasing PS or FA dosage, and no obvious effect of the initial CT on CT degradation rate was observed. Cr (VI) removal was found to increase with increasing PS and formic concentrations, and decrease with increasing the initial Cr(VI) concentration. In conclusion, this study demonstrated that thermally activated PS system in the presence of FA is a promising technique in ISCO remediation for CT and Cr(VI)-contaminated sites.

## ACKNOWLEDGEMENT

This study was financially supported by the grant from the National Natural Science Foundation of China (No.41373094) and China Postdoctoral Science Foundation (2015M570341).

## REFERENCES

- Choi, J. Y., K. H. Choi, W. J. Lee. 2009. "Effects of transition metal and sulfide on the reductive dechlorination of carbon tetrachloride and 1,1,1-trichloroethane by FeS". *J. Hazard. Mater.* 162: 1151-1158.
- Cooper W. J., C. J. Cramer, N. H. Martin, S. P. Mezyk, K. E. O'Shea, C. Sonntag. 2009. "Free radical mechanisms for the treatment of methyl tert-butyl ether (MTBE) via advanced oxidation/reductive processes in aqueous solutions." *Chem. Rev.* 109: 1302-1345.
- Gu, X. G., S. G. Lu, L. Li, Z. F. Qiu, Q. Sui, K. F. Lin, Q. S. Luo. 2010. "Oxidation of 1,1,1-trichloroethane stimulated by thermally activated persulfate". *Ind. Eng. Chem. Res.* 50(19): 11029-11036.
- Lin, M. Z., Y. Katsumura, Y. Muroya, H. He, T. Miyazaki, D. Hiroishi. 2008. "Pulse radiolysis of sodium formate aqueous solution up to 400°C: absorption spectra, kinetics and yield of carboxyl radical CO<sub>2</sub>'". *Radiat. Phys. Chem.* 77: 1208-1212.
- Liang, C. J., C. J. Bruell, M. C. Marley. 2004. "Persulfate oxidation for in situ remediation of TCE. I. activated by ferrous ion with and without a persulfate-thiosulfate redox couple." *Chemosphere* 55: 1213-1223.
- Mora, V. C., J. A. Rosso, G. C. Roux, D. O. Martire, M. C. Gonzalez. 2009. "Thermally activated peroxydisulfate in the presence of additives: A clean method for the degradation of pollutants". *Chemosphere*, 75: 1405-1409.
- Neta P., R. E. Huie, A. B. Ross. 1998. "Rate constants for reactions of inorganic radicals in aqueous solution." *J. Phys. Chem. Ref. Data.* 17: 1027-1284.
- Tsitonaki, A., B. Petri, M. Crimi, H. Mosbaek, R. L. Siegrist, P. L. Bjerg. 2010. "In situ chemical oxidation of contaminated soil and groundwater using persulfate: A review". *Crit. Rev. Env. Sci. Tec.* 40(1): 55-91.

## ENHANCED SETTLING OF SUSPENDED SOLIDS IN OLIVE MILL WASTEWATER BY APPLICATION OF HIGH FREQUENCY ULTRASOUND

Alev Cagla Uzun, *Canan Can Yarımtepe*, Nilgün Ayman Öz  
(Canakkale Onsekiz Mart University, Canakkale, Turkey)

**ABSTRACT:** The aim of the study is to investigate effect of high frequency ultrasound on biogas and methane production from olive mill wastewater (OMW) in anaerobic batch reactors. OMW was sonicated at 582 kHz for different durations. Optimum time was selected as 10 minutes based on total chemical oxygen demand (COD) and suspended solids. Then, anaerobic batch reactors were fed with ultrasound pretreated and raw OMW to determine impact of the process on biogas and methane production. Sonication of OMW before anaerobic batch tests increased both biogas production and methane yield in anaerobic reactors by 8% and 37%, respectively. The results showed that high frequency ultrasound before anaerobic processes has a positive effect especially on methane production rate. Another outcome of the study, it has been observed that high frequency ultrasound caused enhanced settling of suspended solids of OMW samples. After 60 minutes of high frequency ultrasound, OMW sample was left for two hours and suspended solids settled quickly. After settling, 54% decrease in SS concentration at supernatant was recorded.

### INTRODUCTION

Anaerobic treatment is a sustainable option for olive mill effluents, which contain very high organic matter concentration. Olive mill wastewaters also contain high particulate matter, which cannot be efficiently removed during settling process. The character of the wastewater limits the performances of anaerobic reactors according to COD removal and biogas production. Low frequency ultrasound before anaerobic treatment has been proposed for facilitating hydrolysis step and increasing biodegradation rate. In recently, there is also an interest in high frequency ultrasound, which is an oxidative process, for wastewaters containing complex compounds. So far, several studies have been reported in literature on application of high frequency ultrasound on different wastewaters and waste activated sludge whereas combination of the process with anaerobic batch process for OMW has not been reported so far. Therefore, the aim of this study is investigation of effect of high frequency ultrasonic pretreatment on settling of suspended solids, biogas and methane production in anaerobic batch processes.

### MATERIALS AND METHODS

The OMW was collected from a factory which produced olive oil with three phase process, in Canakkale, Turkey at November 12, 2012. The composition of the OMW sample is summarized in Table 1.

Complete analysis were carried out according to the Standard Methods (APHA, 1998). Meinhardt Ultrasound multifrequency at 582 kHz was used during ultrasound experiments. Sonication was performed during 60 min on 500 mL of OMW. During sonication process, changes in tCOD, turbidity and suspended solids were monitored. After ultrasound, untreated and ultrasound pretreated samples were fed to anaerobic batch reactors. Glass reactors with 900 ml active volume were used in the anaerobic batch reactors. Anaerobic seed sludge was taken from a brewery factory's EGSB reactor.

Untreated and ultrasound pretreated OMW samples were added to reactors with seed sludge and dilution water and F/M ratio was set to 0,5 in reactors. Biogas production was monitored with milli gas counter. Biogas composition was determined by Gas Chromatography.

### RESULTS AND DISCUSSIONS

In this study, effect of high frequency ultrasound on biogas and methane production of OMW was investigated. Ultrasound was applied to OMW during 60 min. However, after 10 minutes there was not a

change in tCOD concentration. Therefore, optimum time for application of ultrasound was chosen as 10 minutes. Fig. 1. shows variation in total COD concentration and Fig. 2. Shows total COD removal efficiencies during ultrasound at 582 kHz.

Table 1. OMW Composition

Parameter	Unit	Value
pH	-	5,142
Turbidity	NTU	11688±1060
Total Chemical Oxygen Demand (TCOD)	mg/L	68543±3337
Soluble Chemical Oxygen Demand (SCOD)	mg/L	40506±1719
Biochemical Oxygen Demand (BOD)	mg/L	17119
Conductivity	µs/cm	9190
Total Nitrogen (TN)	mg/L	219
Total Organic Carbon (TOC)	mg/L	14835
Suspended Solids (SS)	mg/L	12598±1032
Total Solid (TS)	mg/L	49143
Phenol	mg/L	5056
Color	pt	29807±8887
Soluble Color	pt	11035±4410

After 10 min sonication, tCOD concentration was decreased about 16% compared with the raw OMW sample. High frequency ultrasound has been previously reported as effective in breaking down organic matter in sludge samples (Braguglia et. al., 2012). Fig. 3. shows variation in turbidity and suspended solids concentration and Fig. 4. shows turbidity and suspended solids removal efficiencies in during ultrasound at 582 kHz.

22% decrease in SS concentration has been recorded after 10 min sonication. These results showed pretreatment have a significant impact on disrupting organic matter. After 10 minutes ultrasound pretreatment, the OMW sample was fed to anaerobic batch reactor at F/M ratio of 0.5. Another anaerobic batch reactor was fed with raw OMW under the same operating conditions as a control reactor.

During the batch anaerobic tests, biogas production and methane content were monitored for raw and pretreated OMW. Fig. 5. shows cumulative biogas production and Fig. 6. shows methane production in raw and ultrasound pretreated anaerobic batch reactors.

The comparison between batch anaerobic tests carried out with untreated and sonicated OMW showed an increase in both biogas production by 8% and methane production by 37%. In the literature, there is no reported study for high frequency ultrasound assisted anaerobic treatment of OMW. Ultrasound

assisted anaerobic treatment can be used for complex wastewaters such as OMW to obtain a better efficiencies in anaerobic processes such as COD removal and methane production. However, the research area needs further investigations.

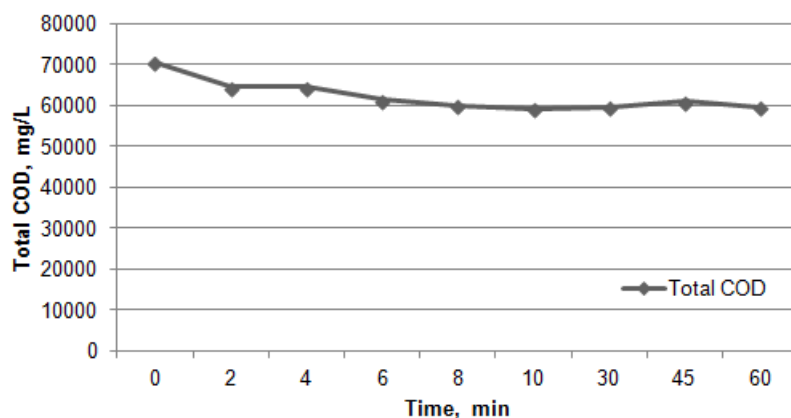


Figure 1. Variation in total COD concentration during ultrasound at 582 kHz

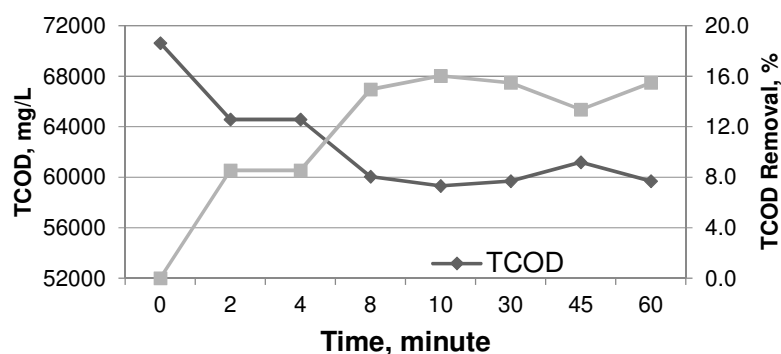


Figure 2. Total COD removal efficiencies during ultrasound at 582 kHz

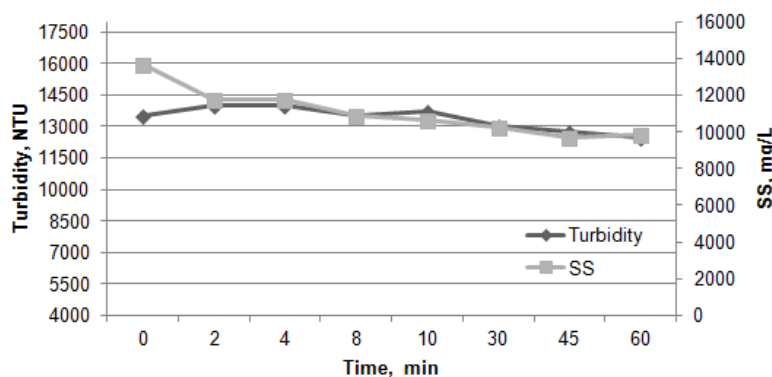


Figure 3. Variation in turbidity and suspended solids during ultrasound at 582 kHz

Another outcome of the study, after high frequency ultrasound was applied to OMW samples, enhanced settling of suspended solids of OMW was recorded. After application of 60 minutes of high frequency ultrasound, OMW sample was left for two hours and then suspended solids settled quickly.



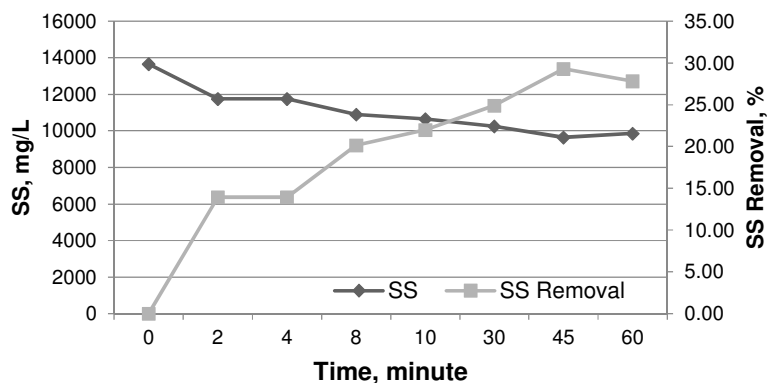


Figure 4. turbidity and suspended solids removal efficiencies in during ultrasound at 582 kHz

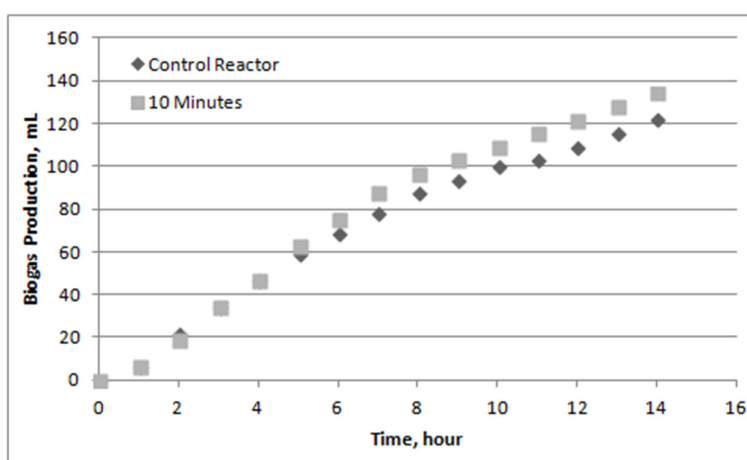


Figure 5. Cumulative biogas production in raw and ultrasound pretreated anaerobic batch reactors

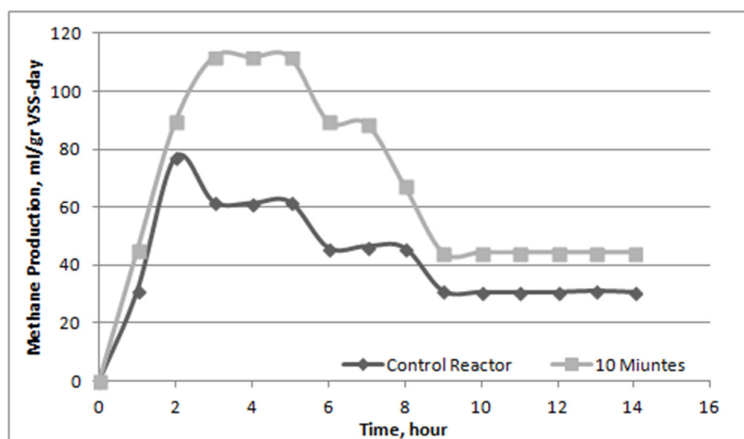


Figure 6. Methane production in raw and ultrasound pretreated anaerobic batch reactors

After settling, 54% decrease in SS concentration at supernatant was recorded. It should also be mentioned that raw OMW could not settle with gravity even after 1 day. High frequency ultrasound has been previously reported as effective in settling of microorganisms in water samples (Bosma et. al., 2003) and sludge (Guangming et. al., 2006). But there is no report on enhancement of settling for wastewater samples.

## **CONCLUSIONS**

As a result, application of ultrasound to complex industrial wastewaters such as OMW showed promising results. Especially, as a pretreatment prior to the anaerobic system, it can enhance both pollutant removal efficiencies and biogas production. However, there is a need for a further investigation.

## **ACKNOWLEDGEMENT**

Financial support by The Scientific and Technological Research Council of Turkey (TUBITAK) was gratefully acknowledged (Project No.: 111Y112).

## **REFERENCES**

- APHA, AWWA, WPCF, Standard Methods for the Examination of Water and Wastewater, 20th ed., American Public Health Association, Washington, DC, 1998.
- Bosma R., Spronsen, W.A., Tramper J. and Wijffels H. R. (2003) Ultrasound, a new separation technique to harvest microalgae, *Journal of Applied Phycology* 15: 143–153.
- Zhang, Guangming, Panyue Zhang, and Yanming Chen. (2006) Ultrasonic enhancement of industrial sludge settling ability and dewatering ability, *Tsinghua Science & Technology* 11.3: 374-378.

## **STUDY OF A FLUIDIZED BED REACTOR FOR PHENOL PHOTOCATALYSIS**

***Guillermo Rincon\**** and Enrique La Motta  
(University of New Orleans, New Orleans, Louisiana, USA)

A bench-scale tubular reactor with recirculation was built in order to study the efficiency of the photocatalytic oxidation of phenol on fluidized titanium oxide-coated silica gel beads. A UV-C lamp was used as source of photons. A bed of silica gel beads was fluidized by means of fluid recirculation and forced to follow upward helical flow around the lamp. Anatase was successfully synthesized on silica gel particles with average diameters 224, 357 and 461 microns, as confirmed by scanning electron micrographs, through a sol-gel technique using a titanium tetraisopropoxide / hydrochloric acid / ethanol precursor.

Experimental results confirmed that the efficiency of phenol photocatalytic degradation decreases with increasing pollutant concentration. Also, the highest removal was achieved at initial pH 3, and it decreased with increasing pH. When NaCl was added to the solution, COD removal increased with increasing salinity. Additionally, it was found that dissolved oxygen is indispensable for photocatalysis to proceed, and saturation of the treated mixture with oxygen was achieved by keeping the liquid in contact with pure oxygen at 1 atm.

Finally, a statistical model based on the exponential decay fit of phenol-derived COD vs irradiation time data in the experimental reactor was proposed (minimum  $R^2 = 0.9840$ ) to allow for the accurate estimation of the reactor efficiency for any given initial COD.

## DEVELOPMENT OF BiVO<sub>4</sub> PHOTOANODE FOR DEGRADING POLLUTANTS

**Oin Shi** and Hui Wang\* (Beijing Forestry University, Beijing, China)  
Zhaoyong Bian (Beijing Normal University, Beijing, China)

Chlorinated phenols (CPs) are detrimental environmental pollutants due to their hazardous impact. The efficient photoelectrochemical degradation of CPs has attracted much attention by using various photo-anodes. Bismuth vanadate (BiVO<sub>4</sub>) has been identified as one of the most promising photoanode materials. However, the typical efficiencies of unmodified BiVO<sub>4</sub> photoanodes for degradation of pollutants were not impressive as they suffer from excessive electron-hole recombination and poor charge transport properties. In this work, a FeOOH/BiP<sub>0.02</sub>V<sub>0.98</sub>O<sub>4</sub> modified graphene composite photoelectrocatalyst was prepared by using three strategies to alleviate these limitations, including P-doping, pairing with oxygen evolution catalysts and construction of composite structures. The composite photoelectrocatalyst was characterized by X-ray diffraction (XRD), scanning electron microscopy (SEM), transmission electron microscopy (TEM), atomic force microscopy (AFM), X-ray photoelectron spectroscopy (XPS). Its photoelectrocatalytic performance was investigated via electrochemical measurements (LAS and EIS) in a three-electrode system in a solution containing 0.1 M NaSO<sub>4</sub> and 1 mM 2,4-dichlorophenol, to highlight its potential application in photoelectrocatalytic electrooxidation of CPs. The characterization results showed that BiVO<sub>4</sub> and BiP<sub>0.02</sub>V<sub>0.98</sub>O<sub>4</sub> have a uniform scheelite-monoclinic structure at a size of 100-200 nm. A thin FeOOH layer was photo-deposited on the BiP<sub>0.02</sub>V<sub>0.98</sub>O<sub>4</sub> surface as an OEC layer successfully. Graphene nanosheets could be found wrapping the FeOOH/BiP<sub>0.02</sub>V<sub>0.98</sub>O<sub>4</sub> particles in the FeOOH/BiP<sub>0.02</sub>V<sub>0.98</sub>O<sub>4</sub>-graphene composite. The photocurrent densities had an elevation with the increase in this order: BiVO<sub>4</sub>, BiP<sub>0.02</sub>V<sub>0.98</sub>O<sub>4</sub>, FeOOH/BiP<sub>0.02</sub>V<sub>0.98</sub>O<sub>4</sub>, FeOOH/BiP<sub>0.02</sub>V<sub>0.98</sub>O<sub>4</sub>-graphene. It meant that the FeOOH/BiP<sub>0.02</sub>V<sub>0.98</sub>O<sub>4</sub>-graphene photoelectrocatalyst posed the highest catalytic activity for photoelectrochemical oxidation of 2,4-dichlorophenol. The EIS analyses were performed to understand the phenomenon. The fitted values of R<sub>t</sub> are 37964, 7351, 3655, and 1236 Ω for pristine BiVO<sub>4</sub>, BiP<sub>0.02</sub>V<sub>0.98</sub>O<sub>4</sub>, FeOOH/BiP<sub>0.02</sub>V<sub>0.98</sub>O<sub>4</sub>, FeOOH/BiP<sub>0.02</sub>V<sub>0.98</sub>O<sub>4</sub>-graphene electrodes, respectively. The FeOOH/BiP<sub>0.02</sub>V<sub>0.98</sub>O<sub>4</sub>-graphene electrode showed the fastest interfacial electron transfer which is in accordance with its enhanced photoelectroactivity.

## OPTIMIZATION OF OPERATING PARAMETERS ON REACTIVE BLACK 5 DYE REMOVAL BY ELECTROCOAGULATION PROCESS AND ENERGY CONSUMPTION

Mook Wei Tze and Mohamed Kheireddine Aroua (University of Malaya, Kuala Lumpur, Malaysia);  
*Małgorzata Szlachta* (Wrocław University of Technology, Wrocław, Poland)

The textile industry is one the major sector responsible for severe water pollution as it discards large amount of colour wastewater. Reactive dye comprises 20 to 30% of the total dye market as their vivid colours and easily attach to fibre polymer. However, reactive dye is high stability and resistant to biological degradation. Hence, reactive dye wastewater treatment becomes a greater challenge for researchers. Electrocoagulation (EC) is one of the effective and economical method to treat dye wastewater. The simplicity of operation, low energy consumption, low sludge generation and high efficiency made EC become a favourable treatment technique. In EC process, no chemicals are added to form coagulant. Instead, it is generated in situ through electrolytic oxidation of anode material.

In this work, Response Surface Methodology (RSM) and Central Composite Design (CCD) were proposed to optimize the operating parameters on the energy consumption and removal efficiency of Reactive Black 5 dye (RB5) through electrocoagulation process. The RSM is a valuable tool to build an equation model, reduce number of experiments, observe interaction between parameters and obtain optimum conditions for desirable responses.

The effects of initial pH and current density on RB5 removal efficiency and energy consumption were investigated. It was found that with increasing pH more RB5 were removed. At a lower pH, the  $H^+$  reduced to hydrogen gas ( $H_2$ ) at the cathode, which reduced the amount of hydroxide ions generated. However, the removal of dye was observed to decrease at a pH beyond 6.5. This could be because the  $Fe(OH)_3$  dissolves to form  $Fe(OH)_4^-$  and migrates to the anode surface to undergo oxidation; hence anodic generation of  $Fe^{2+}$  was negatively affected.

It was also found that the low current density failed to have a sufficient impact upon the RB5 removal process. According to Faraday's law, higher current density enhances coagulant generated to react with RB5 and increases the removal rate. Moreover, the bubble generation rate is directly proportional to the current density, which is beneficial for pollutant removed by  $H_2$  flotation. The highest RB5 removal was found at neutral pH and higher current density.

The current density is directly proportional to the electrical energy consumption (EEC) because current plays a major part in EEC calculation. While pH had a least effect as the EEC trend insignificant changed. In order to achieve high RB5 removal and low EEC, the optimum conditions suggested by RSM which were current density of  $2.13 \text{ mA/cm}^2$  and pH of 6.6. The predicted result was 80.1% and 30.7 kWh/kg dye, which the percentage error between experimental and predicted results was only 3-5%.

## **QUARTZ SAND FILTER MEDIUM FOR OILY WASTEWATER BY HYDROPHOBIC MODIFICATION**

***Wei Bigui***

(Lanzhou Jiaotong University, Lanzhou 730070, Gansu, China)

The quartz sand was surface dry process modified using Titanate coupling agent DN101 to improve the lipophilic-hydrophobic property of filter medium. The effect of reaction time, the dosage of Titanate coupling agent DN101 and reaction temperature were studied by single factor experiment, Results show that when the reaction time was 70 min, DN101 dosage was 1.2% and reaction temperature was 60 °C, the effect of DN101 dry process modified quartz sand was the best. Lipophilic Hydrophilic Ratio(LHR) could be increased from 1.25 to 11.1, The adsorption capacity of modified quartz sand was greatly improved from  $0.17 \text{ mg} \cdot \text{g}^{-1}$  to  $0.25 \text{ mg} \cdot \text{g}^{-1}$  for  $15.61 \text{ mg} \cdot \text{L}^{-1}$  oily wastewater; The filter removal rate of modified quartz sand was improved from 72.6% to 97.8% for  $17.3 \text{ mg} \cdot \text{L}^{-1}$  oily wastewater. SEM, XPS and FTIR shown that DN101 combined with quartz sand surface functional groups in the form of chemical bonds, formed a uniform and stable cladding layer on the surface of quartz sand.

## **CONSTRUCTION OF Fe-TAML ACTIVATOR SYSTEMS TO DEGRADE SULFUR-CONTAINING CONTAMINANTS IN WATERS**

*Qingquan Liu* and Xiyun Cai

(Dalian University of Technology, Dalian, China)

Sulfur-containing compounds commonly undergo *in vivo* sulfoxidation (transformation of thioethers to sulfoxides or sulfoxides to sulfones), which in turn alter reactivity, translocation, and thus toxicity of the parents. Similarly, sulfur-containing compounds were degraded in soils and waters to form sulfoxide and sulfone. These metabolites are often recalcitrant, compared to the parent, and often detected in high frequency and at high levels in waters, thereby being similar or more toxic than the parent itself. Iron-tetraamidomacrocyclic ligand (Fe-TAML) activators are small molecule mimics of short-circuited P450 enzymes through formation of Iron (V/IV)-oxo-TAML intermediates under the activation of H<sub>2</sub>O<sub>2</sub>. In this study, attempts to degrade sulfur-containing compounds (i.e., pesticides and pharmaceuticals) in waters were conducted using Fe-TAML/H<sub>2</sub>O<sub>2</sub>. Fe-TAML activators exhibited degradation efficiencies of 10%-99% toward 14 sulfur-containing contaminants in water at a catalyst:substrate ratio of 1:500 within 60 min. The degradation processes of sulfur-containing compounds were investigated with fenamiphos as a model compound. Results show that fenamiphos via successive oxidation at the sulphur atom and oxidative hydrolysis at the P-O group, and ultimately all metabolites can be mineralized. These two processes were pH-dependent, both of which accelerated rapidly with increasing pH. For example, fenamiphos was completely oxidized to fenamiphos sulfoxide (FSO) in approximately stoichiometry within 10 min at pH 12 and at a catalyst:substrate ratio of 1:500, and this intermediate proceeded further sulfoxidation to form fenamiphos sulfone (FSO<sub>2</sub>) at rather low yields (nearly 5%). These two intermediates underwent rapid oxidative hydrolysis to form phenol intermediates (i.e., FSO-OH and FSO<sub>2</sub>-OH). All phenol compounds were totally mineralized within 5 min. The presence of typical natural water constituents (e.g., DOC, Mg<sup>2+</sup> and Ca<sup>2+</sup>) did not diminish the catalysis efficiency of Fe-TAML activators. A strongly basic anion exchange resin was combined to the Fe-TAML catalytic system for eliminating sulfur-containing contaminants in wastewater without adjusting its pH. Therefore, Fe-TAML activators may be a choice for the removal of sulfur-containing contaminants in waters.

## p-AgI ANCHORED ON n-Bi<sub>2</sub>O<sub>2</sub>CO<sub>3</sub> SHEETS BY Co-CRYSTALLIZATION WITH EXCELLENT PHOTOCATALYTIC PERFORMANCES UNDER VISIBLE LIGHT

Lili Zhang and Chun Hu

(Chinese Academy of Sciences, Beijing, China)

**Introduction.** The development of efficient and stable visible-light photocatalysts has become one of the most important topics in water purification and hydrogen generation. It is known that the photocatalytic activity of semiconductors depends strongly on the specific surface area, particle size, the band match and crystal facets. Considering these important factors, we prepared a p-n heterojunction photocatalyst, p-AgI/n-Bi<sub>2</sub>O<sub>2</sub>CO<sub>3</sub>, by a one-step co-crystallization method for the first time. We found that a strong interaction existed between AgI and Bi<sub>2</sub>O<sub>2</sub>CO<sub>3</sub>. The in-situ combination of AgI and Bi<sub>2</sub>O<sub>2</sub>CO<sub>3</sub> led to the transformation of the morphology, the increase of the BET surface area, the reduction of particle size and the change of exposed lattice facets. Importantly, the visible-light photocatalytic activity of p-AgI/n-Bi<sub>2</sub>O<sub>2</sub>CO<sub>3</sub> significantly increased compared to the single AgI and Bi<sub>2</sub>O<sub>2</sub>CO<sub>3</sub>. A possible photocatalytic mechanism was discussed in detail.

**Objectives.** The main objective of this study was to verify the strong interaction of p-AgI and n-Bi<sub>2</sub>O<sub>2</sub>CO<sub>3</sub>, the enhanced visible light photocatalytic activity of p-AgI/n-Bi<sub>2</sub>O<sub>2</sub>CO<sub>3</sub> and clarify the photocatalytic mechanism.

**Methods.** A novel visible-light-responsive photocatalyst, monodispersed AgI nanoparticles anchored on the surface of Bi<sub>2</sub>O<sub>2</sub>CO<sub>3</sub> sheets (AgI/BOC), was prepared by a one-step co-crystallization method. The characterization of the catalysts were studied via SEM, TEM, XRD, XPS, FT-IR, UV-Vis DRS, N<sub>2</sub> adsorption-desorption and Electrochemical measurements. The analysis methods included HPLC, TOC, ICP-OES and ESR.

**Results and Conclusions.** The single BOC mainly exposed the {001} facets, while BOC in AgI/BOC exposed more (110) facets. In comparison with the pristine BOC and AgI, the positive shift in the binding energy of Bi 4f, O 1s and C 1s for carbonate and the negative shift in the binding energy of Ag 3d and I 3d in AgI/BOC revealed that the alternation of the distribution of the electric charge in the composite. The variation of FTIR spectra indicated the significant change of chemical environments of CO<sub>3</sub><sup>2-</sup> after in-situ combining BOC with AgI. Therefore, a strong interaction existed between AgI and Bi<sub>2</sub>O<sub>2</sub>CO<sub>3</sub>. Moreover, the migration and separation of photogenerated carriers have been improved significantly evidenced by electrochemical impedance spectroscopy, transient current measurement, and photo-luminescence spectra. The formation of p-n junction was also confirmed by electrochemical measurements. In this case, AgI/BOC exhibited an exceptional performance in contaminant degradation. The 2-chlorophenol (10 ppm) could be completely degraded within 60 min, and around 60.5% of TOC was degraded within 60 min in the suspension of AgI/BOC under visible light, which is much higher than the 7.5% and 2.7% of 2-chlorophenol degradation in the single AgI and BOC suspension under similar conditions, respectively, indicating the excellent activity of AgI/BOC under visible light. After the reaction, no Ag and Bi were detected in the solutions. The activity of AgI/BOC did not decrease after seven successive cycles of degradation testing, which suggested that AgI/BOC was a stable catalyst for visible-light photocatalytic reactions.



## **COST ANALYSIS OF ELECTRO DIALYSIS CELL FOR DESALINATING BRACKISH WATER**

Naglaa M. Eid

(Faculty of Engineering, UAE University, Al Ain, United Arab Emirates)

Freshwater resources are becoming increasingly limited due to current uses and growing demands. The use and development of non-conventional water resources such as brackish water could be a possible solution to overcome the imminent shortages of freshwater

In this paper, Electro dialysis, the technique based on the transport of ions through selective membranes under the influence of an electrical field, was utilized to desalinate highly concentrated Al Ain brackish groundwater. The design and optimization of an electro dialysis cell for desalinating brackish groundwater was studied.

A number of laboratory experiments were conducted to test the effect of different design parameters on the configured cell and evaluate different operational schemes as well. The tested parameters were the ED applied voltage, initial salt concentration, the hydraulic flow velocity and the ratios of the volume of the solution in the concentrate compartment to the volume of the solution in the dilute compartment. The operating energy of the tested schemes was also evaluated to help in selecting the optimum operation system achieving the highest desired efficiency with the lowest possible energy. Cost analysis for running and maintaining the obtained optimum operation system was performed and the cost was then compared to the corresponding cost of other desalination membrane techniques.

**MIXED METAL OXIDES DERIVED FROM Ce-DOPED Zn-Al LAYERED DOUBLE HYDROXIDE: SYNTHESIS, CHARACTERIZATION AND PHOTOCATALYTIC ACTIVITY**

**Jianyao Zhu**, Zhiliang Zhu, and Hongtao Lu  
(Tongji University, Shanghai, China)

In this work, a series of Zn-Al-Ce mixed metal oxide (ZnAlCe-MMO) photocatalysts with different Ce doping content were prepared by calcination of Ce-doped Zn-Al layered double hydroxide (ZnAlCe-LDH) precursors at various temperatures in air atmosphere. The materials were characterized by X-ray diffraction (XRD), scanning electron microscopy (SEM), transmission electron microscopy (TEM), Fourier transform infrared (FTIR) spectroscopy, UV-vis diffuse reflectance spectroscopy (DRS), Brunauer-Emmett-Teller (BET) surface area measurements, thermogravimetric analysis (TGA) and X-ray photoelectron spectroscopy (XPS) analysis. The photocatalytic activities of the samples were evaluated by the photodegradation of rhodamine B (RhB) dye in aqueous solution under simulated solar light irradiation. The results show that the ZnAlCe-MMO samples exhibit much higher photocatalytic activities than ZnAl-MMO, and the optimal Ce doping content is 5 mol% ( $n_{\text{Ce}}/(n_{\text{Zn}}+n_{\text{Al}}+n_{\text{Ce}})$ ). The enhanced photocatalytic activity of the ZnAlCe-MMO is mainly attributed to the increasing in the separation efficiency of electrons and holes. The effect of the calcination temperature was also investigated and the optimal calcination temperature is 750°C. The enhanced photocatalytic performance of LDH calcined at 750°C can be attributed to the formation of well-crystallized mixed metal oxides during calcination. Under optimal conditions, 97.8% degradation efficiency of RhB was achieved after 240 min reaction. The active species trapping experiments suggest that hole ( $h^+$ ) plays the most important role while superoxide radical ( $\bullet\text{O}_2^-$ ) and hydroxyl radical ( $\bullet\text{OH}$ ) are the other two active species during the photocatalytic process. Moreover, the photocatalyst was demonstrated to have good stability and reusability.

**A NOVEL PROCESS BY A SMALL MOLECULE ENHANCED EFFECTIVE DEGRADATION FOR METHYL ORANGE DYE IN AQUEOUS SOLUTIONS UNDER UV-VIS IRRADIATION**

Jingjing Wang, *Renbi Bai*

(National University of Singapore, 117576 Singapore)

The development of effective technologies to treat recalcitrant organic dye wastewater has long been of great research and practical interest. In this study, a small molecule, formic acid (FA), was employed as a process enhancer in the degradation of methyl orange (MO) dye in aqueous solutions under the condition of UV-Vis light irradiation with air aeration at the ambient temperature. It was found that decolouration of the dye solution was rapidly achieved, reducing the time from more than 10 h without FA to less than 2 h with the presence of FA. Mineralization rate of MO dye reached as high as about 82% in 1.5 h for MO dye at the initial concentration of  $25 \text{ mg}\cdot\text{L}^{-1}$ , in contrast to nearly no mineralization for a similar system without the FA added. The study revealed that the generation of  $\text{H}_2\text{O}_2$  species in the system was enhanced and the produced  $\text{OH}\cdot$  radicals contributed to the effective degradation of the MO dye. The variation of the initial concentration of MO dye, FA dosage and solution pH was all found to have some impact on the degradation efficiency under the same strength of UV-Vis light irradiation and air aeration. The MO dye degradation performance was found to follow a first-order reaction rate to the MO dye concentration in most cases and there existed a positive correlation between the reaction rate constant and the FA dosage used. Compared to the traditional  $\text{H}_2\text{O}_2$ /UV-Vis oxidation system, the use of a small molecule, such as FA, as a process-enhancing species, has the advantages of low cost, easy availability, and safe to use, and so on. The study demonstrates a promising approach to use a readily available small molecule to enhance the degradation of recalcitrant organic pollutants, such as MO dye, especially in their pre-treatment before a biological process may be applied.

**PHYSICO-CHEMICAL QUALITIES OF THE TREATED FINAL EFFLUENT DISCHARGES  
OF SOME WASTEWATER TREATMENT PLANTS IN BUFFALO CITY MUNICIPALITY,  
EASTERN CAPE, SOUTH AFRICA**

T Kulati, OO Okoh and AI Okoh

(Department of Chemistry, University of Fort Hare, Alice 5700, South Africa)

It is well known that successive stages of treatment at a sewage plant reduce the quantity of suspended solids, the organic matter content, the nutrient constituent, the microbial load and the biochemical oxygen demand of sewage, so that the polluting strength of the final effluent becomes a small fraction of that of the sewage received at the plant. Therefore, the efficiency of four wastewater treatment plants that serve the Buffalo City Municipality area in the Eastern Cape Province of South Africa was investigated with regards to nutrient removal and physicochemical characteristics that might lead to the pollution of receiving waterbodies. The study was conducted from September 2012 to August 2013 and standard physicochemical methods were used. The quality of the effluents were acceptable with respect to the temperature (21.3-21.9 °C), pH (7.2-7.4), electrical conductivity (351-410  $\mu\text{S}/\text{cm}$ ), total dissolved solids (221-260), dissolved oxygen (6.38-7.71 mg/l), biological oxygen demand (2.93-4.52 mg/l), residual chlorine (0.13-0.26), nitrate (6.89-9.20 mg/l); nitrite (0.34-1.92 mg/l). However, the concentrations of chemical oxygen demand (234-260 mg/l), orthophosphate (2.67-5.95 mg/l) and turbidity (4.96-8.59 NTU) were severally outside the compliance levels of the South African Guidelines for the protection of aquatic ecosystems.

## **APPLICATION OF ELECTROHYDROLYSIS PROCESS FOR VINEGAR WASTEWATER AND MUNICIPAL WASTEWATER MIXTURE**

Faruk Hakan CANBAZ, Canan Can YARIMTEPE, Rabia ERARSLAN, Elif ERDOGAN and Nilgun Ayman OZ

(Çanakkale Onsekiz Mart University, Department of Environmental Engineering, Çanakkale/Turkey)

In this study, mixture of vinegar wastewater and municipal wastewater was subjected to different DC voltages (4-8 V) for hydrogen gas production and COD removal by using two different type of electrodes (aluminium and copper) . Effects of applied DC voltage and type of electrodes on hydrogen gas production and COD, sCOD, turbidity, Total Suspended Solids and Color removals were investigated. Vinegar fermentation wastewater was obtained from a Fermentation Company in Izmir and municipal wastewater was obtained from Kepez WWTP in Turkey. Electrohydrolysis process was carried out in a lab-scale 1 L glass reactor with consists a cover supporting two parallel aluminum or copper electrodes. A direct current with different voltages including 4, 5, 6, 7 and 8 voltages were tested by using a power supply. For electrodes comparison, applied DC voltage was constant at 4 V. The highest cumulative hydrogen production (200 ml) for 75 min and hydrogen content of gas (88%) was obtained with the aluminium electrode. The highest cumulative hydrogen production (470 ml) for 75 min and hydrogen content of gas (90%) were obtained with 8 V DC voltage. Net energy production efficiency (consumed energy/produces energy) also reached the highest level (54%) with 8 V DC voltage application. COD removal from wastewater mix with 8 DC voltage application was the most effective voltage with 36%. In the most effective conditions; sCOD, Turbidity, TSS and Color removal efficiencies was determined as 32%, 82%, 44% and 92%, respectively. The results indicated that Hydrogen gas production from electrohydrolysis of vinegar wastewater/municipal wastewater mixture was found to be a fast and effective method with high energy production and pollutant removal efficiencies in terms of turbidity and color.

Financial support by The Scientific and Technological Research Council of Turkey (TUBITAK) was gratefully acknowledged (Project No.: A-2209 (2014-1)).

## REMOVAL AND DEGRADATION PATHWAY OF SULFAMETHOXAZOLE FROM MUNICIPAL WASTEWATER BY ANAEROBIC MEMBRANE BIOREACTOR

*Chun-Hai Wei*, Claudia Sanchez Huerta and TorOve Leiknes

(King Abdullah University of Science and Technology, Thuwal 23955-6900, Saudi Arabia)

**ABSTRACT:** A widely used antibiotic sulfonamide, Sulfamethoxazole (SMX) with chemical abstracts service (CAS) number of 723-46-6 has been detected in the influent and effluent of municipal wastewater treatment plant and thus in the discharging water bodies, resulting in the potential harmful effects on public health and aquatic ecosystems. Removal and degradation pathway of SMX from synthetic municipal wastewater treatment via a lab-scale mesophilic anaerobic membrane bioreactor (AnMBR) were systematically investigated in this study. During the whole operation of around 100 d under different feed SMX concentrations (10-1000  $\mu\text{g/L}$ ) and bulk organics concentrations (chemical oxygen demand 800-2000  $\text{mg/L}$ ) and the same hydraulic retention time (1 d), both SMX and bulk organics removal were over 96%. SMX degradation followed first order reaction kinetics with rate constant of  $0.147\text{ h}^{-1}$  and half-life of 4.7 h based on removal independent on feed concentrations. 5 degradation products were detected: N-Butylbenzenesulfonamide (CAS 3622-84-2) detected under all feed SMX concentrations; Sulfanilamide (CAS 63-74-1) detected under feed SMX concentrations of 100 and 1000  $\mu\text{g/L}$ ; Sulfisomidine (CAS 515-64-0), 4-Aminothiophenol (CAS 1193-02-8) and Aniline (CAS 62-53-3) detected under feed SMX concentration of 1000  $\mu\text{g/L}$  only. Thus, a degradation pathway of SMX from municipal wastewater treatment via AnMBR was firstly proposed.

## INTRODUCTION

Organic micro-pollutants (OMPs) in water environment including pharmaceutically active compounds, personal care products, household chemicals, pesticides and etc., have received increasing attention in recent years due to their potential harmful effects on public health and aquatic ecosystems. Among them, antibiotics are incurred more concerns due to their direct toxicity to aquatic creatures as well as potential development of antibiotic resistance genes and species. As a widely used antibiotic sulfonamide, Sulfamethoxazole (SMX) with chemical abstracts service (CAS) number of 723-46-6 has been frequently detected in raw wastewater and effluent of municipal wastewater treatment plant (WWTP) and even in surface water (Boreen et al., 2004; Abegglen et al., 2009; Dirany et al., 2010; Alidina et al., 2014). Eliminating SMX in WWTP is an important solution to control its discharge that may impact ecosystems and potentially follow the water cycle back to drinking water sources.

As a hybrid process of anaerobic digestion and membrane separation for municipal wastewater treatment, anaerobic membrane bioreactor (AnMBR) can achieve high biomass (thus high methane recovery) and good permeate quality due to the complete rejection of suspended solids by microfiltration (MF) or ultrafiltration (UF) membrane (Wei et al., 2014). Previous AnMBR studies on OMPs removal (Monsalvo et al., 2014; Wijekoon et al., 2015; Wei et al., 2016) also showed good SMX removal (over 95%) mainly through biodegradation due to its negatively charged nature at  $\text{pH} > 5.7$  and low sorption capacity (Boreen et al., 2004). However, there is no information available on SMX's degradation products and pathway in AnMBR so far. Considering the relatively complex molecular structure of SMX, it would be expected the occurrence of some degradation products rather than complete mineralization in AnMBR. Thus, the objective of this study was to investigate the removal and degradation pathway of SMX from synthetic municipal wastewater treatment by AnMBR.

## MATERIALS AND METHODS

**AnMBR Set-Up.** A lab-scale AnMBR set-up consisted of a completely mixed anaerobic activated sludge bioreactor (volume 2 L, temperature  $35^\circ\text{C}$ , pH 7, stirrer speed 200 rpm, hydraulic retention time 1 d) and a side-stream crossflow hollow fibre UF membrane module (polyvinylidene fluoride, nominal pore size 30

nm, filtration area 310 cm<sup>2</sup>). Synthetic municipal wastewater with chemical oxygen demand (COD) of 800 mg/L spiked SMX at different concentrations (10, 100, 1000 µg/L, in the range of real SMX concentration detected in raw municipal wastewater) using concentrated SMX stock solution in methanol (1 g/L) was used as the feed of AnMBR. The details of AnMBR set-up and synthetic municipal wastewater recipe can be found in our previous publication (Wei et al., 2014). Before starting experiment, the AnMBR had been assimilated to the synthetic municipal wastewater spiked low concentration (10 µg/L) SMX (Wei et al., 2016). The whole experiments were classified as 7 phases depending on feed SMX concentration: Phase 1 (1-20 d) feed SMX 10 µg/L, Phase 2 (21-33 d) feed SMX 100 µg/L, Phase 3 (34-54 d) feed SMX 1000 µg/L, Phase 4 (55-61 d) no SMX spiking to wash out residual SMX in AnMBR, Phase 5 (62-88 d), feed SMX 10 µg/L, Phase 6 (89-98) feed SMX 100 µg/L, and Phase 7 (99-113 d) feed SMX 1000 µg/L. SMX removal was intensively investigated in Phase 1-3, where the detection methods of SMX degradation products were also explored. In Phase 5-7, SMX degradation products were intensively investigated while SMX removal was confirmed again. No sludge was wasted except sampling for biomass measurement during the whole operation.

**Analytical Methods.** For SMX quantification, liquid samples (100-1000 ml) spiked the isotope (SMX-d4) to control SMX recovery were firstly pre-concentrated into 10 ml via Dionex Autotrace 280 solid-phase extraction (SPE) instrument (Thermo Scientific) using Oasis HLB SPE cartridges (Waters) and the elution solvents of methanol followed by 10% methanol in methyl tert-butyl ether (MTBE), and further concentrated into the final volume of 1 ml via evaporation under 40°C and nitrogen stripping. Then the concentrated samples were quantified via Agilent Technology 1260 Infinity Liquid Chromatography (LC) with a Phenomenex Luna 5u C18 column using mobile phase of water and methanol containing 0.1% formic acid followed by Applied Biosystems SCIEX QTRAP 5500 Mass Spectrometry (MS) with positive electrospray ionization mode. For degradation products qualification, liquid samples (1-12 L) were firstly pre-concentrated via the above-mentioned SPE using different solvents (dichloromethane, ethyl acetate, acetone, methanol, MTBE, methanol followed by 10% methanol in MTBE) and the above-mentioned evaporation to final volume of 0.1-0.5 ml. Then the final concentrated samples were measured via Agilent Technology 7890A Gas Chromatography (GC) with Agilent J&W HP-5ms column (helium as carrier gas) followed by Agilent Technology 5975C Mass Spectrometry. The GC oven program started at an initial temperature of 60°C for 3 min, and ramped until 320°C with a heating rate of 20°C/min and remained at 320°C for 5 min. The main peaks from total ion chromatography of samples were finally identified via comparing the mass spectra of samples to standard compounds in the NIST mass spectral library. Only compounds with matching probability over 70% and repetitively detected under different extraction solvents could be identified as SMX degradation products. Commercial COD kits (TNT series, Hach Company) were used to measure the COD of influent and permeate based on the method of rapid digestion (150°C, 2 h) followed by colorimetric measurement. Biogas composition and volume (reported under temperature of 25°C and pressure of 1 atm) were measured according to the gas bag method (Ambler and Logan, 2011) based on gas chromatography (SRI 310C). Biomass concentration in terms of mixed liquor (volatile) suspended solids (ML(V)SS) was measured according to the standard method of glass fiber filtration followed by sequential drying at 105°C and 550°C.

## RESULTS AND DISCUSSION

**Bulk Organics Removal.** During the whole operation, MLVSS was in the range of 2.5-4.3 g/L with MLVSS/MLSS ratio of 0.8-0.85, indicating roughly stable biomass characteristics. Summarized results on bulk COD and SMX removal were shown in TABLE 1. The feed COD increased from 800 to 2000 mg/L with feed SMX concentration from 10 to 1000 µg/L due to methanol contribution (1 ml methanol in 1 L feed equivalent to COD of 1200 mg/L) from concentrated SMX (dissolved in pure methanol) spiking. Despite feed COD increase with feed SMX concentration, permeate COD was mostly below 50 mg/L and thus COD removal was always over 96%, indicating the good biological performance as well as no inhibition effects of SMX on bulk organics removal. There was a relative stable biogas composition with methane (80-95%), carbon dioxide (<10%) and nitrogen (<10%). With feed COD increase from 800 to 2000 mg/L, methane production also increased from 80 to 230 ml/gCOD<sub>removed</sub>. These results were similar to our previous study (Wei et al., 2014).

TABLE 1 Bulk COD and SMX removal in AnMBR (n=5)

Phase	COD			SMX		
	Feed (mg/L)	Permeate (mg/L)	Removal (%)	Feed (µg/L)	Permeate (µg/L)	Removal (%)
Phase 1 (1-20 d)	810	25.2±5.0	96.9±0.6	10	0.32±0.09	96.8±0.9
Phase 2 (21-33 d)	920	27.3±2.9	97.0±0.3	100	2.9±0.8	97.1±0.8
Phase 3 (34-54 d)	2000	39.3±9.8	98.0±0.5	1000	25.4±3.3	97.5±0.3
Phase 5 (62-88 d)	810	30.0±5.5	96.3±0.7	10	0.33±0.16	96.7±1.6
Phase 6 (89-98 d)	920	31.9±3.8	96.5±0.4	100	3.0±0.2	97.0±0.2
Phase 7 (99-113 d)	2000	48.6±6.3	97.6±0.3	1000	27.7±3.5	97.2±0.4

**SMX Removal.** From TABLE 1, during all phases with a large range of feed concentration (10 to 1000 µg/L), SMX removal were over 96%, indicating the very good degradation capacity of AnMBR. A good reproducibility for SMX removal was also confirmed via comparing phases with the same feed SMX concentration (Phase 1 and 5, Phase 2 and 6, Phase 3 and 7). In addition, SMX removal under different feed concentrations (10, 100, and 1000 µg/L) and the same hydraulic retention time (1 d) was fallen into a narrow range of around 97%, indicating its independence on feed concentration. This could deduce that SMX degradation would follow first order reaction kinetics (shown in Equation 1 and 2, where  $C$  was SMX concentration at time  $t$ ,  $C_0$  was feed SMX concentration,  $k$  was rate constant,  $t$  was reaction time,  $t_{1/2}$  was half-life.) with rate constant of  $0.147 \text{ h}^{-1}$  and half-life of 4.7 h.

$$C = C_0 e^{-kt} \quad (1)$$

$$t_{1/2} = \ln(2) / k \quad (2)$$

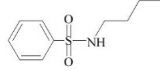
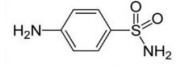
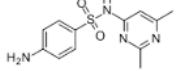
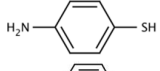
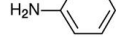
**SMX Degradation Products.** 5 degradation products (shown in TABLE 2) were identified via GC-MS analysis of permeate samples extracted by different SPE solvents (dichloromethane, ethyl acetate, acetone, methanol, MTBE, methanol followed by 10% methanol in MTBE). Under feed SMX concentration of 10 µg/L (i.e., the maximum value in normal raw municipal wastewater without receiving untreated hospital and pharmaceuticals wastewater containing high-concentration SMX) in Phase 1 and 5, only N-Butylbenzenesulfonamide (CAS number 3622-84-2) was detected under all tested SPE solvents and a large range of SPE-evaporation concentrating factor from 1k to 120k (i.e., 1/12 L permeate sample concentrating to 1/0.1 ml via SPE followed by evaporation). Compared with parent compound of SMX (CAS number 723-46-6), N-Butylbenzenesulfonamide as a degradation product does not contain antibiotic sulfonamide group. This indicated that even AnMBR treatment did not achieve complete mineralization of SMX but still produced permeate free of antibiotic functions. In addition, further degradation of N-Butylbenzenesulfonamide was also overserved in Phase 2, where its peak area (i.e., concentration) in 1k concentrated permeate samples using methanol followed by 10% methanol in MTBE as SPE solvents decreased significantly with operation time.

In Phase 2 and 6 with feed SMX concentration of 100 µg/L, Sulfanilamide (CAS number 63-74-1) being an antibiotic sulfonamide was detected besides N-Butylbenzenesulfonamide. In Phase 3 and 7 with feed SMX concentration of 1000 µg/L, Sulfisomidine (CAS number 515-64-0) being an antibiotic sulfonamide, 4-Aminothiophenol (CAS number 1193-02-8) and Aniline (CAS number 62-53-3) without antibiotic functions were detected besides N-Butylbenzenesulfonamide and Sulfanilamide. The reasons behind the sequential occurrence of N-Butylbenzenesulfonamide, Sulfanilamide, and Sulfisomidine, 4-Aminothiophenol, Aniline in Phase 1-3 and 5-7 with increasing feed SMX of 10, 100 and 1000 µg/L might be as follows: 1) All 5 products could be formed under all tested conditions but at different concentrations, resulting in their sequential detection due to the concentrating factor limitation of SPE-evaporation. However, it was unlikely happened because the concentrating factor had been reached to a very high level of 20k (even 120k in Phase 5) in this study. 2) All 5 products could be formed under all tested conditions but degraded further at different rates, resulting in their sequential detection due to their different degradation rates. N-Butylbenzenesulfonamide, Sulfanilamide, and 4-Aminothiophenol, Aniline might follow this rule based on the decreasing sequence of their molecular structural complexity (i.e., generally reverse sequence of degradability). However, Sulfisomidine could not follow this rule due to its similar structure to SMX. 3) Product formation could depend on SMX loading rate to biomass in terms of µg SMX per g MLVSS per day, which was roughly proportional to feed SMX concentration based on the roughly



stable biomass concentration in this study. With the sequential increase of feed SMX concentration from 10 to 100 to 1000 µg/L, N-Butylbenzenesulfonamide, Sulfanilamide and Sulfisomidine might be formed sequentially based on the metabolic response of anaerobic microorganism to increasing SMX loading rate.

**TABLE 2 Degradation Products of SMX in AnMBR Identified by GC-MS**

No.	Compound name	CAS number	Molecular formula	Molecular weight (Dalton)	Molecular structure	GC elution time (min)	Detection under feed SMX concentrations (µg/L)
1	Benzenesulfonamide, N-Butyl-	3622-84-2	C <sub>10</sub> H <sub>15</sub> NO <sub>2</sub> S	213		11.1-11.2	10, 100, 1000
2	Sulfanilamide	63-74-1	C <sub>6</sub> H <sub>8</sub> N <sub>2</sub> O <sub>2</sub> S	172		12.2 -12.5	100, 1000
3	Sulfisomidine	515-64-0	C <sub>12</sub> H <sub>14</sub> N <sub>4</sub> O <sub>2</sub> S	278		14.5 -15.5	1000
4	4-Aminothiophenol	1193-02-8	C <sub>6</sub> H <sub>7</sub> NS	125		8.1-8.2	1000
5	Aniline	62-53-3	C <sub>6</sub> H <sub>7</sub> N	93		5.1-5.5	1000

To the best of our knowledge, no degradation products of SMX in AnMBR have been reported so far in the literature. Among the detected degradation products of SMX in this study, Sulfanilamide, 4-Aminothiophenol and Aniline have been detected in batch tests using an aerobic cold-adapted bacterium *Pseudomonas psychrophila* HA-4 (Jiang et al., 2014) and using electrochemical degradation at boron-doped diamond electrode (de Amorim et al., 2013) for SMX degradation. N-Butylbenzenesulfonamide and Sulfisomidine are firstly reported as SMX degradation products from this study. Interestingly, 3-Amino-5-methylisoxazole (CAS number 1072-67-9) as a hydrolysis product of SMX has been reported in a few studies for SMX degradation using an aerobic bacterium *Microbacterium sp.* strain BR1 (Ricken et al., 2013), an aerobic cold-adapted bacterium *Pseudomonas psychrophila* HA-4 (Jiang et al., 2014) and an anodic chamber of microbial fuel cell (Wang et al., 2015). However, the 5-methylisoxazole group of SMX was not hydrolyzed but directly accepted protons to form butane (shown in FIGURE 1) in this study. This could be due to the anaerobic bacteria used in this study different with the above-mentioned studies.

**SMX Degradation Pathway.** Based on the identified degradation products, the proposed degradation pathway of SMX via AnMBR treatment was firstly shown in FIGURE 1, which was divided into 3 routes. The first route was that the amine and 5-methylisoxazole group of SMX accepted protons to form N-Butylbenzenesulfonamide, which could be further degraded. The first route was activated under the lowest feed SMX concentration of 10 µg/L in this study. The second route was that the sulfonamide group of SMX accepted a proton to form Sulfanilamide, which was further degraded to Aniline via deamination and desulfurization simultaneously and/or deamination to 4-Aminothiophenol followed by desulfurization. Aniline might be finally mineralized based on its simple molecular structure (Jiang et al., 2014) and the fact of no detection under feed SMX concentration of 100 µg/L, indicating its possible complete degradation. The second route was activated under feed SMX concentration of 100 µg/L in this study. The third route was that the 5-methylisoxazole group of SMX was substituted by 4-Amino-2,6-dimethylpyrimidine to form Sulfisomidine, which might be degraded further based on its similar molecular structure to SMX. The third route might only be activated under feed SMX concentration of 1000 µg/L in this study. In addition, it could be deducted based on the formation pathway of main degradation products that in AnMBR, the amine group of SMX was transformed to ammonia; 5-methylisoxazole group of SMX was transformed to butane (would be easily degraded further by anaerobic microorganism due to its simple chain structure), ammonia and water; sulfonamide group of SMX was transformed to hydrogen sulfide, ammonia and water.

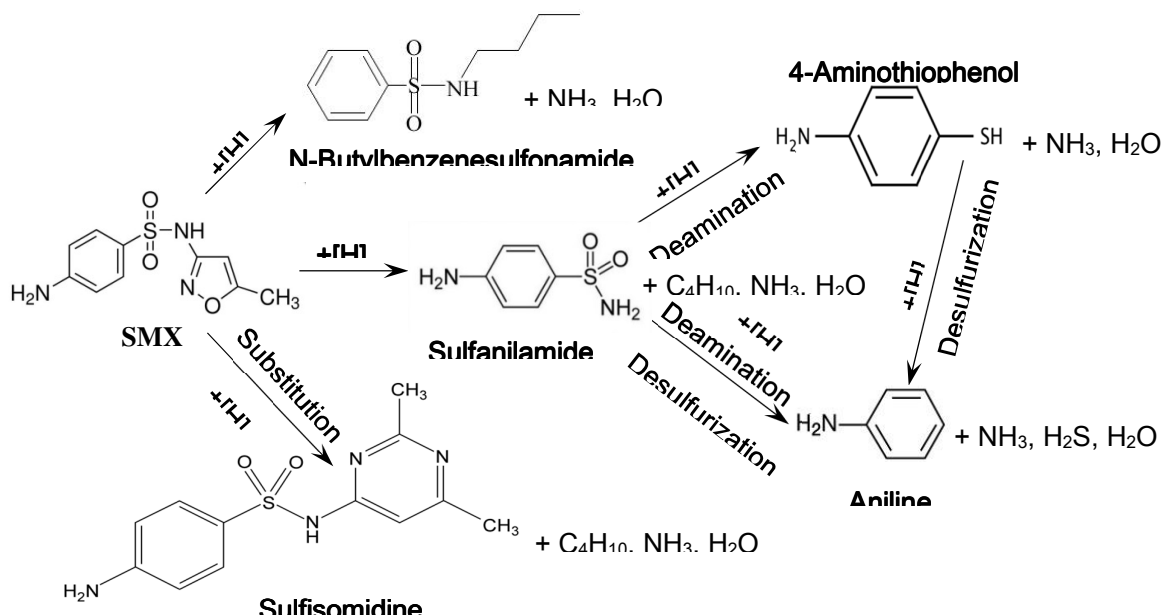


FIGURE 1 Proposed Degradation Pathway of SMX in AnMBR

## CONCLUSIONS

In this study, the lab-scale mesophilic AnMBR process for synthetic municipal wastewater (spiked SMX) treatment showed very good removal performance (over 96%) for both bulk organics and SMX in a large range of feed COD (800-2000 mg/L) and SMX (10-1000  $\mu\text{g/L}$ ) concentration under the same hydraulic retention time (1 d) and roughly stable biomass characteristics (MLVSS of 2.5-4.3 g/L, MLVSS/MLSS ratio of 0.8-0.85). Methane production increased from 80 to 230 ml/gCOD<sub>removed</sub> with feed COD increase from 800 to 2000 mg/L. Based on the removal independent on feed concentration, SMX degradation was deduced to follow first order reaction kinetics with rate constant of 0.147 h<sup>-1</sup> and half-life of 4.7 h. 5 degradation products were identified via GC-MS analysis of concentrated permeate samples via SPE using multiple solvents (dichloromethane, ethyl acetate, acetone, methanol, MTBE, methanol followed by 10% methanol in MTBE) followed by evaporation. N-Butylbenzenesulfonamide (CAS number 3622-84-2) without antibiotic functions was firstly detected as SMX's degradation product under all feed SMX concentrations and especially the sole degradation product under feed SMX concentration of 10  $\mu\text{g/L}$  (i.e., the maximum SMX concentration occurred in normal raw municipal wastewater) in this study. Sulfanilamide (CAS number 63-74-1) still being an antibiotic sulfonamide was detected under feed SMX concentrations of 100 and 1000  $\mu\text{g/L}$ . Sulfisomidine (CAS number 515-64-0) still being an antibiotic sulfonamide, 4-Aminothiophenol (CAS number 1193-02-8) and Aniline (CAS number 62-53-3) without antibiotic functions were detected under feed SMX concentration of 1000  $\mu\text{g/L}$  only. Based on the identified degradation products, a degradation pathway of SMX from municipal wastewater treatment via AnMBR was firstly proposed, which consisted of 3 degradation routes for the formation of N-Butylbenzenesulfonamide, Sulfanilamide (then degraded further to 4-Aminothiophenol and Aniline), and Sulfisomidine, respectively.

## ACKNOWLEDGEMENTS

This work has been financed by KAUST Center Competitive Funding Project on Anaerobic Membrane Bioreactor. Dr. Tao Zhang and Ms. Tong Zhan were greatly appreciated for their kind technical supports on LC-MS and GC-MS.

## REFERENCES

- Abegglen, C., A. Joss, C. S. McArdell, G. Fink, M. P. Schlüsener, T. A. Ternes and H. Siegrist. 2009. "The Fate of Selected Micropollutants in a Single-house MBR." *Water Res.* 43: 2036-2046.

- Alidina, M., C. Hoppe-Jones, M. Yoon, A. F. Hamadeh, D. Li and J. E. Drewes. 2014. "The Occurrence of Emerging Trace Organic Chemicals in Wastewater Effluents in Saudi Arabia." *Sci. Total Environ.* 478: 152-162.
- Ambler, J. R. and B. E. Logan. 2011. "Evaluation of Stainless Steel Cathodes and a Bicarbonate Buffer for Hydrogen Production in Microbial Electrolysis Cells using a New Method for Measuring Gas Production." *Int. J. Hydrogen Energ.* 36(1): 160-166.
- Boreen, A. L., W. A. Arnold and K. McNeill. 2004. "Photochemical Fate of Sulfa Drugs in the Aquatic Environment: Sulfa Drugs Containing Five-membered Heterocyclic Groups." *Environ. Sci. & Technol.* 38(14): 3933-3940.
- de Amorim, K. P., L. L. Romualdo and L. S. Andrade. 2013. "Electrochemical Degradation of Sulfamethoxazole and Trimethoprim at Boron-Doped Diamond Electrode: Performance, Kinetics and Reaction Pathway." *Sep. Purif. Technol.* 120: 319-327.
- Dirany, A., I. Sirés, N. Oturan and M. A. Oturan. 2010. "Electrochemical Abatement of the Antibiotic Sulfamethoxazole from Water." *Chemosphere* 81(5): 594-602.
- Jiang, B., A. Li, D. Cui, R. Cai, F. Ma and Y. Wang. 2014. "Biodegradation and Metabolic Pathway of Sulfamethoxazole by *Pseudomonas psychrophila* HA-4, a Newly Isolated Cold-Adapted Sulfamethoxazole-Degrading Bacterium." *Appl. Microbiol. Biotechnol.* 98: 4671-4681.
- Monsalvo, V. M., J. A. McDonald, S. J. Khan and P. Le-Clech. 2014. "Removal of Trace Organics by Anaerobic Membrane Bioreactors." *Water Res.* 49: 103-112.
- Ricken, B., P. F. X. Corvini, D. Cichocka, M. Parisi, M. Lenz, D. Wyss, P. M. Martínez-Lavanchy, J. A. Müller, P. Shahgaldian, L. G. Tulli, H. P. E. Kohler and B. A. Kolvenbach. 2013. "*ipso*-Hydroxylation and Subsequent Fragmentation: a Novel Microbial Strategy to Eliminate Sulfonamide Antibiotics." *Appl. Environ. Microbiol.* 79(18): 5550-5558.
- Wang, L., Y. Wu, Y. Zheng, L. Liu and F. Zhao. 2015. "Efficient Degradation of Sulfamethoxazole and the Response of Microbial Communities in Microbial Fuel Cells." *RSC Adv.* 5: 56430-56437.
- Wei, C. H., C. Hoppe-Jones, G. Amy and T. Leiknes. 2016. "Organic Micro-Pollutants' Removal via Anaerobic Membrane Bioreactor with Ultrafiltration and Nanofiltration." *J. Water Reuse Desal.* in press, DOI: 10.2166/wrd.2015.138.
- Wei, C. H., M. Harb, G. Amy, P. Y. Hong and T. Leiknes. 2014. "Sustainable Organic Loading Rate and Energy Recovery Potential of Mesophilic Anaerobic Membrane Bioreactor for Municipal Wastewater Treatment." *Bioresource Technol.* 166: 326-334.
- Wijekoon, K. C., J. A. McDonald, S. J. Khan, F. I. Hai, W. E. Price and L. D. Nghiem. 2015. "Development of a Predictive Framework to Assess the Removal of Trace Organic Chemicals by Anaerobic Membrane Bioreactor." *Bioresource Technol.* 189: 391-398.

## OH RADICAL FORMATIONS IN PHYTO-FENTON PROCESS: DETECTION AND APPLICATION

Shigeki Nara, Yoshihiko Inagaki, and Yutaka Sakakibara

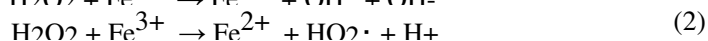
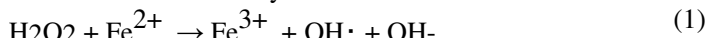
(Department of Civil and Environmental Engineering, Waseda University, Tokyo, Japan)

**ABSTRACT:** Phyto-Fenton process utilizing endogenous H<sub>2</sub>O<sub>2</sub> in aquatic plants and iron catalyst has a potential to be a low cost and high performance phytoremediation technology. In this study, OH radical formations and reaction sites in this process were analyzed using an OH radical probe, 3'-(p-aminophenyl) fluorescein (APF) and a confocal laser scanning microscopy. Strong fluorescence was observed at whole parts inside a root, when ferrous sulfate was used as iron catalyst. On the other hand, fluorescence was observed from peripheral parts when using ferrihydrite colloids and/or ferric-ion zeolite. Reaction sites of OH radical formations could be observed in vertical and horizontal sections of aquatic plants. These results indicated Fenton and Fenton like reactions occur simultaneously and the OH radical formation sites could be controlled by the selection of iron compounds. Furthermore, pentachlorophenol (PCP) could be removed by the present Phyto-Fenton process. In addition, tetrachlorohydroquinone (TCHQ) was detected as one of intermediate byproducts in treated water; while no intermediate detected in the absence of iron compounds. A further study will be needed to optimize the OH radical formations as well as decompositions of refractory pollutants.

### INTRODUCTION

Recently, as water consumption in the world is increasing with increasing world population and economic growth, water problem becomes more serious. Especially, in developing countries implementations of modern sewage treatment systems are not always feasible because of high initial and operation costs. We proposed a low cost/high performance water and wastewater treatment process, Phyto-Fenton process (A. R. Reis et al, 2011; Y. Inagaki et al, 2016), where OH radicals can be produced through Fenton and Fenton like reaction utilizing endogenous H<sub>2</sub>O<sub>2</sub> in aquatic plants.

Fenton reaction and Fenton-like reaction are shown in Reactions (1) and (2), respectively. Hydrogen peroxide is converted to OH radicals which can decomposes almost every organic pollutant. This process has a potential to be a low cost and high performance phytoremediation technology. This research was conducted to analyze the mechanism of Phyto-Fenton reaction and reaction sites generating OH radicals in the presence of different iron catalysts.



### MATERIAL AND METHODS

**Observation with Confocal Laser Scanning Microscopy.** In order to identify the OH radical generation and its reaction sites in plants, a fluorescence reagent, 3'-(p-aminophenyl) fluorescein (APF) was used and fluorescence was observed with a confocal laser scanning microscopy (FV-1000D, Olympus). Slight fluorescence was observed in the absence of iron catalyst. However, strong fluorescence could be observed if OH radical reacted with APF (Setsukinai et al., 2003). The mechanism of fluorescence emission from APF is shown in FIGURE 1. A confocal scanning microscopy is enables to observe the emission in three-dimensional structures and thereby to collect a series of images at different depths.

In experiments, plants (0.20 g F.W.) were cultivated for one day in a test tube containing phosphate buffer with 20 mg-Fe/L iron compounds and 5 mmol/L APF. Three types of iron compounds: ferrous sulfate, ferric ion zeolite and ferrihydrite colloids, were used as iron catalyst. After cultivation, fluorescence was observed with the microscopy.

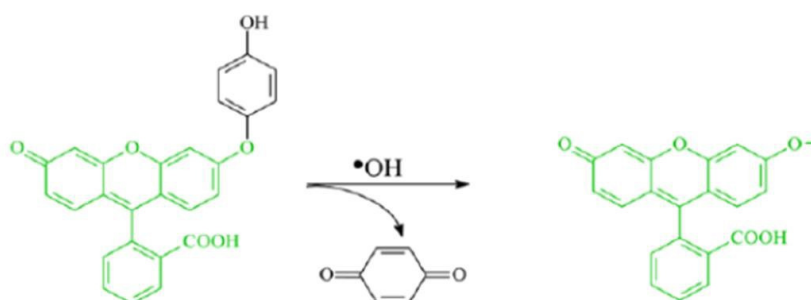


FIGURE 1. illustration of fluorescence probe reaction with OH radicals.

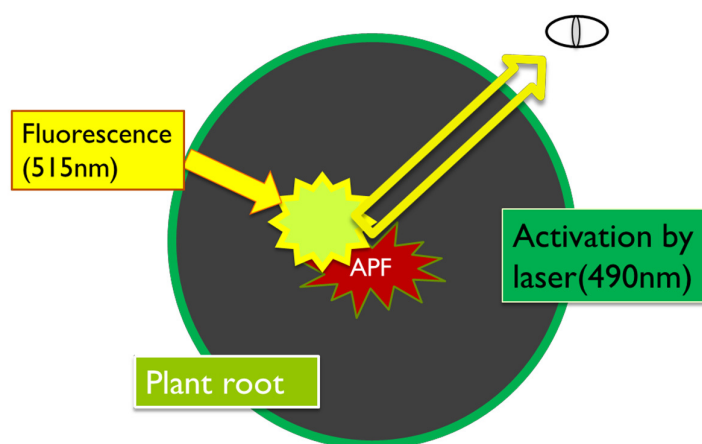


FIGURE 2. Conceptual diagram of confocal laser scanning microscopy in detecting OH radical generation sites in phyto-Fenton process.

### Treatment of Pentachlorophenol(PCP)

**Measurement of PCP concentration.** Experiments were conducted to confirm removal and decomposition of PCP. Plants were cultivated for one week in test tubes containing PCP with and without iron catalyst. Details of experimental condition are shown in TABLE 1. Procedures in preparation of samples are shown in FIGURE 3. PCP concentration was measured with GC-ECD (6890, Agilent).

TABLE 1. Experimental conditions for Batch treatment of PCP.

Resctor No.	R1	R2	R3	R4
PCP Conc. (mg/L)	10.6	10.6	10.6	10.6
Fe Conc. (mg/L)	0	20	0	20
Plant (g F.W.)	0	0	0.20	0/2
Type of iron	Ferrous sulfate( $\text{FeSO}_4$ )			
pH	Around 4.5			

**Identification of PCP by-products.** Batch treatments of PCP were conducted for one week to detect intermediate products from PCP. Plants were cultivated in test tubes, containing PCP with and without iron catalyst. 20mg/L ferrous sulfate was used as iron catalyst. After treatment, solution was analyzed with LCMS (Xevo G2-XS Qtof, Waters).

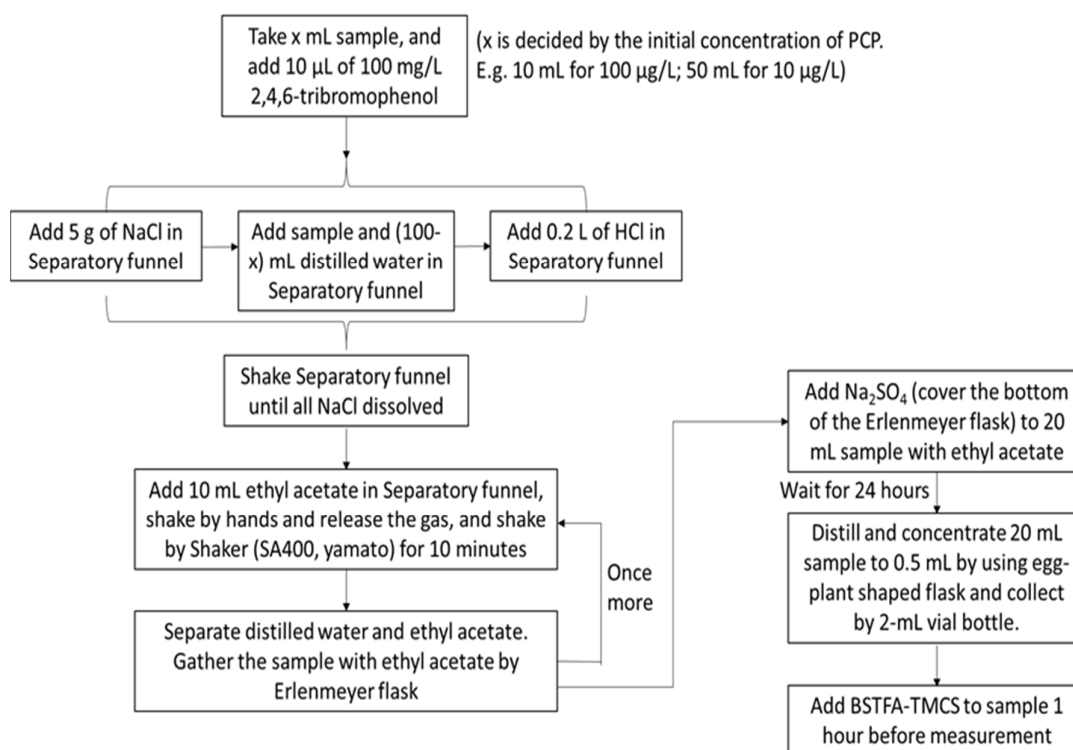


FIGURE 3. Pre-preparation of PCP samples

## RESULTS AND DISCUSSION

**Observation with Confocal Laser Scanning Microscopy.** Fluorescence from plants is shown in FIGURE 4. In each image, central area indicates X-Y plane, bottom side X-Z plane and right side Y-Z plane, respectively. As shown in (A), strong fluorescence was observed from root at every plane, when ferrous sulfate was used as iron catalyst. On the other hand, when ferric ion zeolite and ferrihydrite colloids were used as iron catalyst, strong fluorescence was observed from the surface of plant's root. It is supposed that the difference of results was attributable to difference in size of iron catalyst.

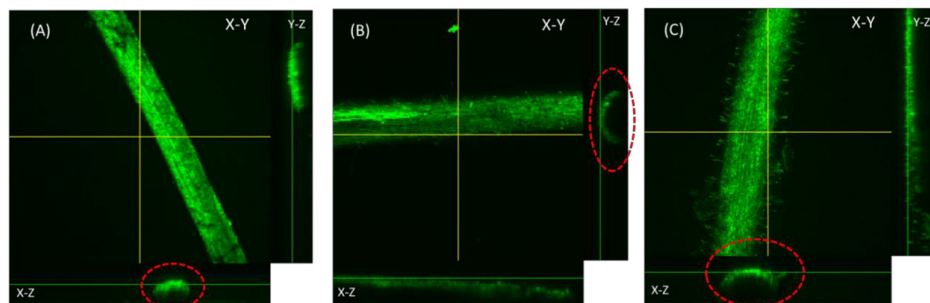


FIGURE 4. Fluorescence from plants in the presence of (A) ferrous sulfate, (B) ferric-ion zeolite, and (C) ferrihydrite colloids.

**Treatment of Pentachlorophenol(PCP) Measurement of PCP Concentration.** PCP concentrations after treatment are compared in FIGURE 5. From the comparisons, it was found that PCP concentration was the



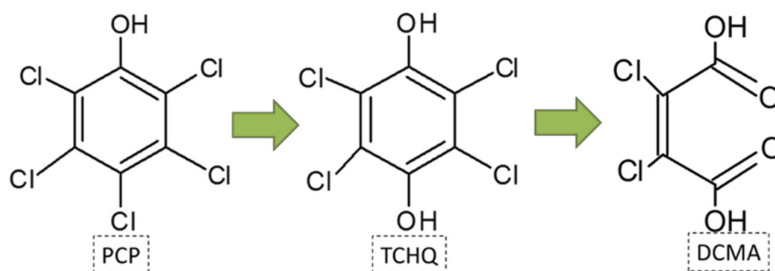


FIGURE 7. PCP degradation pathway by Fenton reaction (Zimbron and Reardon, 2009).

## CONCLUSIONS

We confirmed phyto-Fenton reaction occurs in plants. Moreover, it was found reaction sites of OH radical generations were affected by a type of iron catalyst. In batch treatment, PCP was decomposed to TCHQ by Phyto-Fenton reaction. Furthermore, it was demonstrated a confocal laser microscopy is a useful tool to identify the OH radical generations. A further study will be needed to optimize the process.

## ACKNOWLEDGEMENTS

A part of this work was supported by a Grant-in-Aid for Scientific Research (B) (15H02846), the Japanese Ministry of Education, Culture, Sports, Science and Technology (MEXT).

## REFERENCES

- Inagaki Y., Cong V. H., Sakakibara Y. 2016. "Identification and application of Phyto-Fenton Reactions." *Chemosphere*, **144**, 1443-1450
- Reis, A.R. and Sakakibara, Y. 2011. "Continuous treatment of endocrine disrupting chemicals by aquatic plants and biological Fenton Reaction.", *JSCE, Ser. G (Environmental Research)*, **67**(7), 725-734.
- Setsukunai, K., Urano, Y., Kakinuma, K., Majima, H. J. and Nagano, T. 2003. "Development of Novel Fluorescence Probes That Can Reliably Detect Reactive Oxygen Species and Distinguish Specific Species", *The Journal of biological chemistry*, **278**(5), 3170-3185
- Zimbron, J. A. and Reardon, K. F. 2009. "Fenton's oxidation of pentachlorophenol", *Water Research*, **43**(7), 1831-1840



## CONTINUOUS TREATMENT OF WASTEWATERS CONTAINING PPCPS BY AN ELECTROCHEMICAL ADVANCED OXIDATION PROCESS

**Junya Suzuki**, Eiji Kawada, Taiki Maehata and Yutaka Sakakibara (Department of Civil and Environmental Engineering, Waseda University, Tokyo, Japan)

**ABSTRACT:** A novel electrochemical advanced oxidation process (AOP) was proposed and continuous treatments of a synthetic wastewater and tertiary effluent from a municipal WWTP were conducted under different operating conditions. The electrochemical AOP consists of SnO<sub>2</sub> anode for O<sub>3</sub> production and multiple cathode compartments packed with either granular Pt/Ti electrodes or granular activated carbons (GACs) for OH radical formation through the reduction of produced O<sub>3</sub>. The synthetic wastewater was prepared by dissolving antibiotics such as tetracycline, erythromycin and sulfamethoxazole. From experiments using the synthetic wastewater, it was found that all PPCPs were decomposed completely. Moreover, decrease in TOC was not observed for Pt/Ti granular cathodes, while significant decrease observed for GAC cathodes. Main intermediate products from PPCPs were identified, which were similar to those in AOPs reported in former studies. Furthermore, experimental results for tertiary effluent demonstrated that superior TOC removals could be achieved for GAC cathodes. These results suggest that PPCPs and other organic pollutants were firstly absorbed on GAC and then decomposed by OH radicals. Energy consumptions were in the range of 0.3-4 kWh/m<sup>3</sup>. From these results, we concluded that the proposed electrochemical AOP would be a feasible alternative to former AOPs because of simpler operation and structure.

### INTRODUCTION

In public water bodies, PPCPs such as antibiotics, antipyretics, and analgesics have been detected and have attracted attention as emerging pollutants. Especially, antibiotics have been deeply concerned, because micro-organisms exposed to antibiotics may acquire antibiotic resistances. As conventional wastewater and water treatment processes are not able to remove antibiotics completely, developments of innovative technology are needed (Yunlong et al., 2014; Bendz et al., 2005).

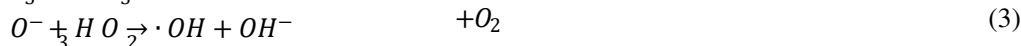
In advanced oxidation processes (AOPs), sufficient quantity of OH radicals can be produced. As OH radicals are a strong which can decompose almost every organic pollutant, it is considered AOPs are one of the technology applicable to antibiotics removal. There are different types of AOPs such as UV irradiation with injection of ozone and/or H<sub>2</sub>O<sub>2</sub>, supersonic treatment, and electrolysis; however most are complicated in operation and reactor configurations (Glaze et al., 1989; Hoare, 1985). In this study, we proposed a novel electrochemical AOP and investigated treatment performances.

Mechanisms of the proposed electrochemical AOP are represented by Reactions (1) to (3).

Anode:



Cathode:



By an application of electric current, ozone is produced from anode in Reaction (1), and is reduced to OH radicals via ozonide ion in Reactions (2) and (3). Highly concentrated electrolyte is required to increase the yield for Reaction (1). In this respect, we used a solid polymer electrolyte membrane. On the other hand, it was reported that a rate limiting step is the mass transfer of ozone from bulk liquid to

cathode surface; therefor granular electrodes were used to enhance overall removal performances (Kishimoto et al., 2005; Seader et al., 1952).

## MATERIALS AND METHODS

**Electrode and Experimental Apparatus.** In this study,  $\text{SnO}_2$  electrode was used for the generation of ozone. It was prepared referring to former studies (Cui et al., 2009; Parsa et al., 2012), where Ti expanded substrate was coated with solution containing  $\text{SnO}_2$  precursors, dried and heated at  $390^\circ\text{C}$ . Some electrodes were prepared at different coating times (5-20). Surface area is  $2.3\text{ cm}^2$ . SPE membrane (Nafion N-117, USA) was sandwiched by  $\text{SnO}_2$  and stainless mesh.

**FIGURE 1.** shows the schematic diagram of experimental apparatus. Main body was built using stainless and fluorocarbon resin sheet. The anode with SPE membrane was equipped in the reactor. Four cathodic compartments were installed downstream from the anode and granular electrodes (Pt/Ti or activated carbon) were packed inside. Cathode surface area and effective volume were about  $1500\text{ cm}^2$  and  $35\text{ mL}$ , respectively.

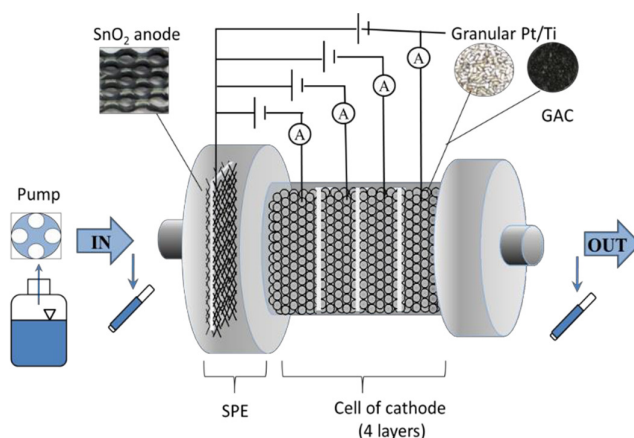


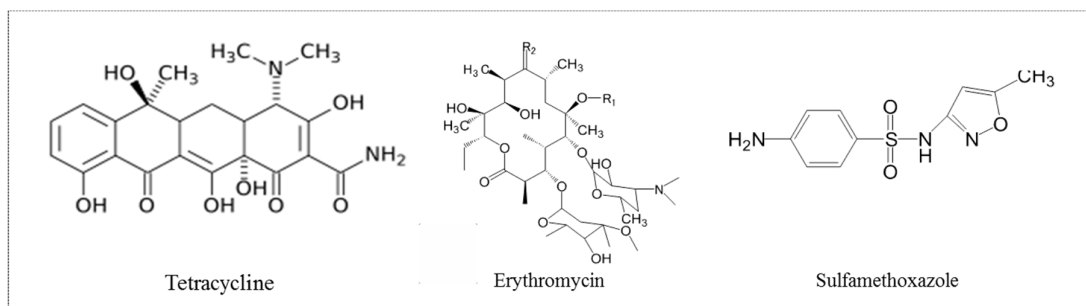
**FIGURE 1.** A main part of experimental apparatus (Electrolytic cell).

**Continuous Antibiotics Removal Experiments.** Electrolytic cell (FIGURE 1.) was used in continuous treatments of antibiotics. Synthetic wastewater was fed continuously and influent and effluent concentrations of antibiotics were measured under different operating conditions (i.e. applied currents, HRT and pH). In this study, electric current passing SPE membrane is defined as “ozone oxidation current”, and one passing every cathode as “ozone reduction current”. The same electric current was applied to each cathode compartment. Details of experimental procedures were shown in TABLE 1.

Synthetic wastewater containing  $1\text{ mg/L}$  each tetracycline (TC), sulfamethoxazole (SMX) or erythromycin with  $1\text{ mM}$   $\text{Na}_2\text{SO}_4$  was prepared using de-ionized water. Structures of antibiotics were shown in **FIGURE 2**. pH of synthetic wastewater was adjusted using HCl or NaOH solution. Antibiotics and their intermediate products were measured with GC/MS (HP-1100, Agilent Technologies, Germany) and LC/MS/MS (UPLC-QToF, Waters, USA).

**TABLE 1.** Experimental conditions.

Experiment	Solution	Cathode cell	O <sub>3</sub> oxidation current (mA)	O <sub>3</sub> reduction current (mA)	HRT (min)	pH
Continuous treatment of PPCPs	1mg/L antibiotics, 1mM Na <sub>2</sub> SO <sub>4</sub>	Pt/Ti or GAC	0-75	1.5	2.5, 5, 10	3.5, 5.5, 7.5, 9.5

**FIGURE 2.** Antibiotics used in this study.

## RESULTS AND DISCUSSION

**Treatment of PPCPs (Tetracycline).** In continuous experiments, effluent concentrations of antibiotics approached to steady-state values. **FIGURE 2.** shows normalized effluent concentrations of tetracycline against oxidation currents under different HRTs and pH conditions. As shown in Figure, effluent tetracycline concentrations decreased with increasing current. Satisfactory removal was achieved at pH 5.5 and 7.5. Longer the HRT, lower the effluent concentrations. Comparing results for Pt/Ti and GAC electrodes, more tetracycline was removed. This was attributable to adsorption by GAC. In experiments of sulfamethoxazole and erythromycin treatments, similar results were observed (data not shown) and the effectiveness of the proposed process was demonstrated.

**Decrease in Bactericidal Effect.** **FIGURE 4.** shows the results of bactericidal effect to coliform. The bar indicated by (a) was 10-fold diluted secondary effluent, where number of colonies was about 60 in 100mL sample. The bars (b) and (d) were mixtures of influent 20-fold diluted TC and 35-fold diluted SMX solutions with the 10- fold diluted secondary effluent, respectively. In contrast, the bars (c) and (d) indicate results for effluent samples prepared in the same manner to (b) and (d), respectively. As shown, the numbers of colonies for (b) and (d) were smaller in (b) and (d) than (a), due to bactericidal effects by TC and SMX. However, the numbers of colonies in (a), (c) and (e) were almost identical, demonstrating that bactericidal effects were removed by the present process.

**By-products of Tetracycline.** **FIGURE 5.** shows intermediate products (marked by red color dotted lines) identified in the effluent in TCA treatments. In comparison, reaction pathways of Tetracycline in AOP in the literature (Joonseon et al., 2010) were shown. Reaction path was comprised of multi-steps reactions. A further study will be needed to quantitative distributions of the intermediates.

**Comparison of Energy Consumption.** **FIGURE 5.** shows energy consumptions in this study with those for other AOPs under 90% removal efficiency. The energy consumption in this study was about 0.3-

$4kWh/m^3$ . Although target pollutants and their concentrations are different, the energy consumptions was similar to or smaller than former AOPs.

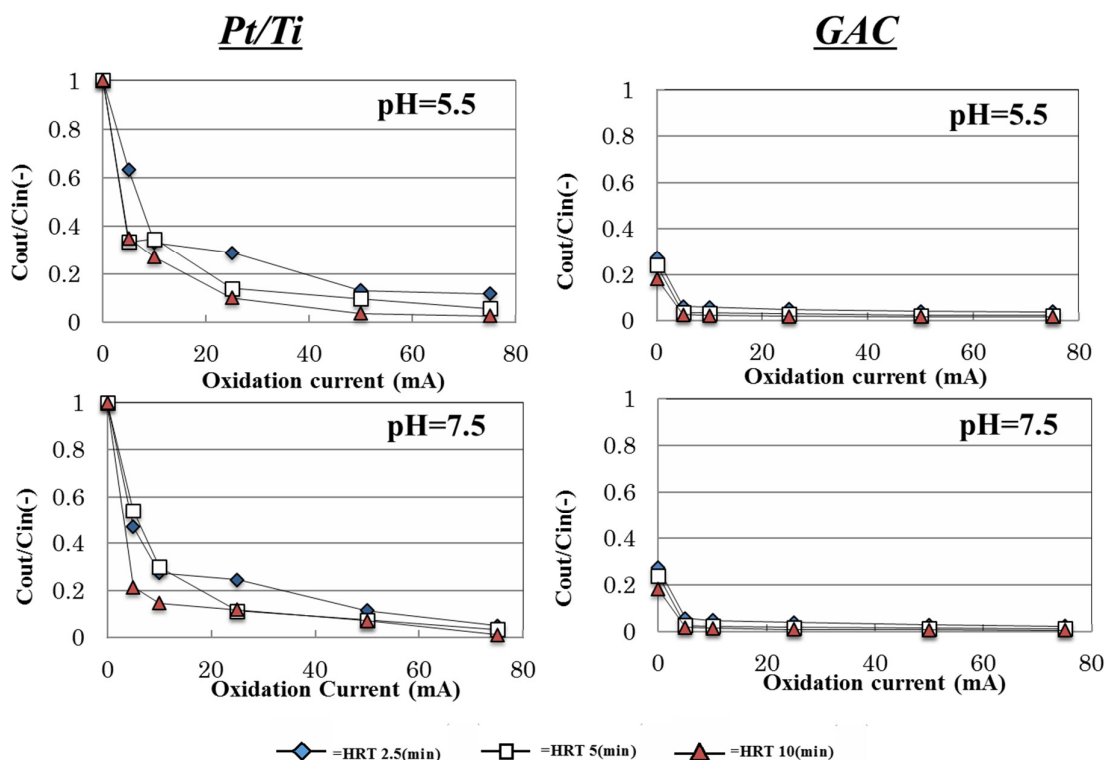


FIGURE 3. Continuous treatment experiment (Tetracycline)

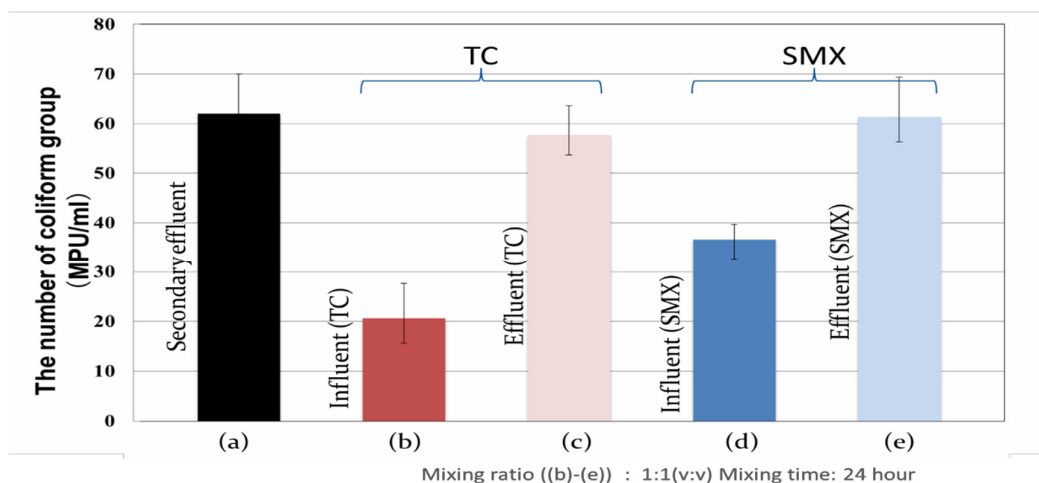


FIGURE 4. Decrease in bactericidal effect to coliform

## CONCLUSIONS

From continuous experiments for tetracycline, sulfamethoxazole and erythromycin, the following conclusions were drawn;

- The proposed electrochemical AOP could remove and decompose PPCPs.

- Reduction in bactericidal effect of coliform bacteria was achieved by the process.
- Energy consumption was  $0.3\text{-}4\text{ kWh/m}^3$ , which was similar to or less than former AOPs.
- The present process is very simple in operation and control; and is considered as a feasible alternative to former AOPs.

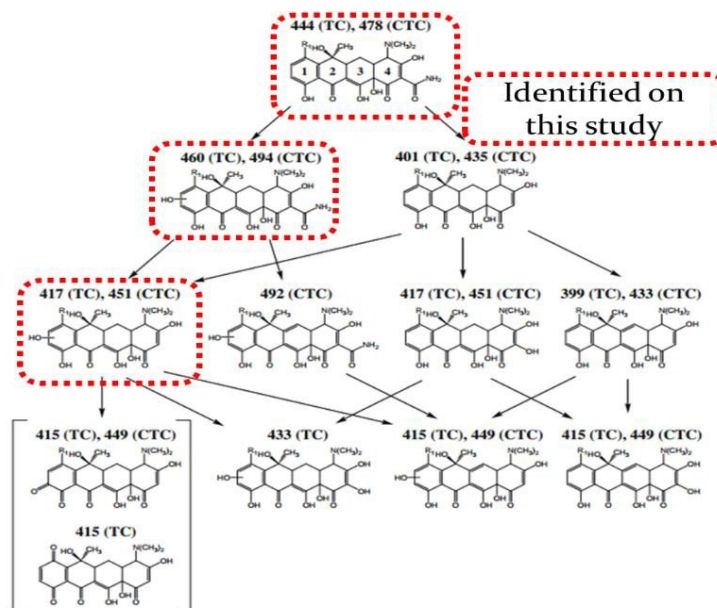


**FIGURE 5.** Reaction pathways of Tetracycline on AOPs (Joonseon et al., 2010) and intermediate products identified in this study.

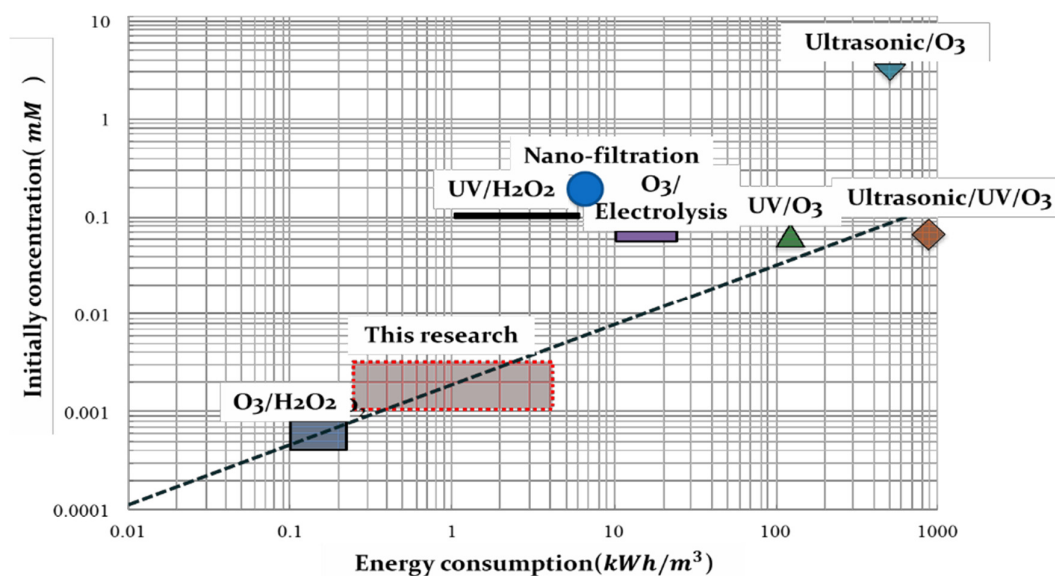


**FIGURE 6.** Comparison of energy consumption under 90% removal efficiency.

## ACKNOWLEDGEMENT

This study was supported in part by Grant-in-Aid for Scientific Research (B) (No. 24360219), the Ministry of Education Culture, Sports, Science and Technology (MEXT) Japan.

## REFERENCES

- Bendz D. Paxéus N. A., Ginn T. R. and Loge F. J. 2005. "Occurrence and fate of pharmaceutically active compounds in the environment, a case study: Høje River in Sweden". *Journal of Hazardous Materials*, 122(3): 195-204
- Cui Y., Wang Y., Wang B., Zhou H., Chan K. Y., and Li X. Y. 2009. "Electrochemical generation of ozone in a membrane electrode assembly cell with convective flow". *Journal of The Electrochemical Society*, 156(4): E75-E80
- Glaze W. H. and Kang J. 1989. "Advanced Oxidation Process. Description of a kinetic model for the oxidation of hazardous materials in aqueous media with ozone and hydrogen peroxide in a semibatch reactor". *Industrial and Engineering Chemistry Research*, 28: 1573-1580
- Hoare J. P. 1985. "Standard potentials in aqueous solution". *Marcel Dekker*, New York, 49-66
- Joonseon J., Weihua S., William J. C., Jinyoung J., John G. 2010. "Degradation of tetracycline antibiotics: Mechanisms and kinetic studies for advanced oxidation/reduction processes". *Chemosphere*, 78: 533-540
- Kishimoto N., Morita Y., Tsuno H., Oomura T. and Mizutani H. 2005. "Advanced Oxidation effect of ozonation combined with electrolysis". *Water Research*, 39:4661-4672
- Parsa J. B., Abbasi M. and Cornell A. 2012. "Improvement of current efficiency of the Ti/Sn-Sb-Ni oxide electrode via carbon nanotubes for ozone generation". *Journal of The Electrochemical Society*, 159(5): D265-D269
- Seader J.D. and Tobias C. W. 1952. "Ozone by electrolysis of sulfuric acid". *Industrial and Engineering Chemistry*, 44(9): 2207-2211
- Yunlong L., Wenshan G. and Huu H. N. 2014. "A review on the occurrence of micropollutants in the aquatic environment and their fate and removal during wastewater treatment". *Science of the Total Environment*, 474: 619-641

## **ACUTE TOXICITY OF GRAPHENE NANOPATELET TO BACTERIAL COMMUNITIES IN ACTIVATED SLUDGE**

***Hang Ngoc Nguyen*** and Debora Frigi Rodrigues

(Civil and Environmental Engineering, University of Houston, Houston, TX)

Carbon based nanomaterials are used extensively in many applications in different fields. Graphene is the building block of graphitic materials such as flullerenes, carbon nano-tube and graphite. Graphene consists of monolayer of carbon atoms arranged in a two-dimensional hexagonal lattice. Graphene is stronger than steel, has high electrical conductivity and has antimicrobial properties. Graphene has been increasingly used in research and in industrial applications such as in energy, automotive, aerospace, electronics and biomedical devices. With all these emerging applications, the question we have to ask “Where will all the graphene go after use and disposal?”. Wastewater is one of the most common discharges that all the waste including graphene will finally end up. Leaking and bleaching from graphene based devices will introduce graphene in the wastewater. Graphene has been shown to exhibit antimicrobial properties, so its impact to the biological treatment process in wastewater treatment plant needs to be investigated. This study aims to understand how graphene interacts with activated sludge in biological treatment process at the acute toxicity level. We study the acute toxicity of graphene nanoplatelet suspension to the performance of activated sludge in lab scale reactors. The activated sludge was collected directly from a wastewater treatment plant, and then cultivated in the lab for 44 hours with synthetic wastewater before running the reactors with different concentrations of graphene suspension from 0 to 300 mg/L. The performance of the reactors in removal of nutrient, ammonia, phosphate, nitrate and chemical oxygen demand were determined. Genes of interest were quantified using real time PCR with standard curve. Metagenomics of 16S rRNA was also performed to investigate the changes in the population of microbes in activated sludge in the presence of graphene. Initial results show that graphene reduces the nutrient removal in the treatment and has the potential to affect microbial community in the activated sludge.

## **ISOLATION OF BACTERIA FROM LAKE WATERS ASSOCIATED WITH WASTEWATER EFFLUENTS CAPABLE OF DEGRADING VARIOUS PHARMACEUTICALS**

*Noreen Gallagher* and Dr. Jeff Lodge

(Thomas H Gosnell School of Life Sciences, Rochester Institute of Technology, Rochester, NY, USA)

Many wastewater treatment plants are not properly equipped for the removal of non-steroidal anti-inflammatory drugs such as ibuprofen and naproxen and analgesics such as acetaminophen. These compounds are continually discharged into surface waters and, although in a very low concentration, their presence is becoming an emerging issue. NSAIDs, analgesics, and their metabolites are biologically active in surface waters and, as a result, possess potentially harmful effects to the environment as well as public health through the consumption of water and food containing residues of these compounds.

One objective of this project is to isolate and characterize heterotrophic bacteria that are capable of degrading NSAIDs (ibuprofen and naproxen) and analgesics (acetaminophen) from several areas in Western NY associated with wastewater effluent outfalls. From the various isolates the best degraders will be chosen to further study their degradation rates, % degradation, and the environmental parameters that are important in enhancing degradation rates. Another objective is to show that these organisms may be important in controlling pharmaceutical levels in surface waters.

Water and sediment samples from three wastewater effluent outfall areas along Lake Ontario in the Rochester area and one outfall area in Onondaga Lake (Syracuse area) were used in various enrichment techniques to isolate potential bacteria capable of degrading ibuprofen, naproxen, and acetaminophen. Potential isolates are then grown on the pharmaceutical of choice as the sole carbon source as a second selection. Organisms shown to grow at high rates on various pharmaceuticals are then further studied to determine degradation rates, % degradation, and environmental parameters important in enhancing degradation rates in lake waters.

Preliminary results from various enrichment experiments have led to the isolation of various heterotrophic bacteria capable of growing on ibuprofen, naproxen, or acetaminophen as their sole carbon source. One isolate from Onondaga Lake (Syracuse) degraded 80% of the acetaminophen in 5 days. One isolate from Charlotte Beach (Rochester) and one from Payne Beach (Rochester) were also able to degrade 80% of acetaminophen in 5 days. Two isolates from Durand Eastman Beach significantly degraded ibuprofen while an isolate from Payne Beach degrades 80% of naproxen. These isolates are being studied further as well as some new recent isolates that were found.

Utilizing various enrichment techniques our lab has been able to isolate various heterotrophic bacteria from Lake Ontario and Onondaga Lake that can degrade ibuprofen, naproxen, and acetaminophen. This data shows that there are endogenous heterotrophs located near wastewater outfalls that can degrade various pharmaceuticals and may be applied to a commercial process to try and reduce the amount of pharmaceuticals entering surface waters.



## **CHARACTERIZATION AND QUANTIFICATION OF DOM IN WASTEWATER AND ITS INTERACTION WITH PHARMACEUTICALS**

**Sanjeeb Mohapatra\***, Neha Sharma and Suparna Mukherji  
(Indian Institute of Technology Bombay, Mumbai, India)  
Lokesh P. Padhye  
(The University of Auckland, Auckland, New Zealand)

Dissolved organic matter (DOM) plays a vital role on contaminant transport in both natural waters and wastewater. It may potentially alter the fate of pharmaceuticals in aqueous systems by forming complexes. The seasonal variation in DOM concentration over three seasons in two major WWTPs in Mumbai, India was determined based on total organic carbon (TOC) measurements. Initial DOM characterization using specific UV absorbance (SUVA) was followed by characterization using fluorescence spectroscopy and parallel factor (PARAFAC) analysis. PARAFAC analysis was performed using the three-dimensional excitation–emission matrix (3-D EEM) representing the three major DOM components. In the samples collected during the summer season, protein-like fluorescence peak representative of tryptophan analogues was found at excitation and emission wavelength of 280 and 340 nm, respectively. Tyrosine analogue peaks were also observed at both the WWTPs for samples collected in the monsoon season. Comparatively higher intensity of tryptophan like fluorescence was observed in the samples collected in the winter season.

In-situ measurements were also carried out to assess interactions between four common pharmaceuticals and two distinct DOM sources, i.e., DOM in untreated wastewater and Suwannee River DOM. The pharmaceuticals selected for this study were atenolol, atorvastatin, sulfamethoxazole, and ranitidine. Pharmaceuticals were spiked in aqueous DOM solution to achieve concentration over the range 100 to 1000 mg/L and quenching of DOM fluorophores due to interaction with the pharmaceuticals was determined. The concentration of pharmaceuticals in solution was quantified using high resolution liquid chromatography tandem mass spectrometry (HR LC-MS/MS). At varying concentrations of pharmaceuticals, and DOM the interaction of pharmaceuticals with different components of DOM was quantified through PARAFAC analysis to reveal the interaction of pharmaceuticals with DOM. The results indicate significant interaction between pharmaceuticals and DOM that may potentially affect the fate and transport of pharmaceuticals in the environment. Such interactions may also be responsible for poor recovery of pharmaceuticals from wastewater.

**DEEP INSIGHTS INTO THE MECHANISM OF 2,4-DI-TERT-BUTYLPHENOL(2,4-D)  
DEGRADATION BY USING UV/PERSULFATE WITH A NEW MODEL**

**Qiongfang Wang**, Yisheng Shao, Naiyun Gao and Xiang Shen (Tongji University, Shanghai, China )  
Yisheng Shao (China Academy of Urban Planning & Design, Beijing, China)

In this research, it was the first time to assessed the degradation of 2,4-Di-tert-butylphenol (2,4-D) using a ultraviolet/persulfate (UV/PS) process. The results showed that 2,4-D could be degraded effectively using this process. The process was modeled based on a steady-state assumption that both hydroxyl and sulfate radicals reacted with 2,4-D. The second order rate constants for 2,4-D reacting with  $\text{SO}_4^{\cdot -}$  and  $\text{OH}^{\cdot}$  were estimated to be  $(3.07 \pm 0.03) \times 10^9$  and  $(1.62 \pm 0.13) \times 10^{10} \text{ M}^{-1}\text{s}^{-1}$  at pH 7, respectively. The pseudo-first order rate constants ( $k_o$ ) of 2,4-D increased with increasing dosage of PS. The pH did not affect the degradation of 2,4-D directly in acidic condition, while the degradation reduced a little from pH 7 to 10 but was strongly inhibited at pH 11. Dihydrogen phosphate and lower nitrate concentrations had no effect on the degradation of 2,4-D, whereas 50mM nitrate concentration suppressed the degradation. Bicarbonate, hydrogen phosphate and natural organic matter (NOM) inhibited the degradation of 2,4-D dramatically through consuming  $\text{SO}_4^{\cdot -}$  and  $\text{OH}^{\cdot}$ , which were likely to be the main radical scavengers in natural waters when using UV/PS process to control 2,4-D. The degradation of 2,4-D was much enhanced by adding different dosages of  $\text{Cl}^-$ . The degradation pathways were proposed by Liquid Chromatography-Mass/Mass Spectroscopy (LC-MS/MS) analysis.

## REMOVAL OF ESTRIOL IN WATER USING SEQUENTIALLY COUPLED MEMBRANE FILTRATION/TiO<sub>2</sub> PHOTOCATALYTIC PROCESSES

Irwing M. Ramírez-Sánchez<sup>1</sup>, Ashantha Goonetilleke<sup>2</sup>, Erick R. Bandala<sup>3,4\*</sup>

1. Universidad de las Americas, Puebla. Sta. Catarina Martir, Cholula 72810 Puebla. Mexico.
2. Queensland University of Technology. GPO Box 2434, Brisbane, Queensland 4001, Australia.
3. Desert Research Institute (DRI). 755 E. Flamingo Road. Las Vegas, 89119-7363 Nevada, USA.  
E-mail: erick.bandala@dri.edu
4. Graduate Program Hydrologic Sciences. University of Nevada, Reno. Reno, NV 89557, USA

**ABSTRACT:** A coupling system of membrane separation and photocatalytic oxidation was evaluated for the removal of estriol (E3) in water. An aqueous solution containing estriol was fed to the membrane unit, which generated a permeate flow with a pollutant concentration that was below the method detection limit and a reject flux with an increased estrogen concentration. Subsequently, the reject stream was treated using a photocatalytic processes. Membrane technology was used in addition to the photocatalytic processes and an NF90 membrane was selected based on the proposed E3 concentration. The results demonstrated that

### INTRODUCTION

Emerging contaminants (ECs) are recognized as significant water pollutants (Czech and Rubinowska, 2013). Many ECs affect human and wildlife endocrine systems once they are released into the environment and are considered endocrine disrupting compounds (EDCs). Natural and synthetic estrogens are among the most important EDCs that occur as pollutants in drinking water and wastewater. The natural estrogens found in water include estrone (E1), 17 $\beta$ -estradiol (E2), and estriol (E3) and the synthetic steroid estrogens found in water include ethinyl estradiol (EE2), mestranol and quinestrol. Removing estrogens from aquatic environments after they have been released is complicated because of their low concentrations, but because of their biological activity, even significantly low amounts of estrogens have been shown to be detrimental (Carvalho et al., 2015).

Several removal methodologies have been proposed for treating estrogens in water. Among them, membrane filtration has been shown to be useful for removing estrogens from drinking water and wastewater (Bodzek and Dudziak, 2006). The capability of nanofiltration (NF), a membrane filtration technique that shares properties with ultrafiltration and reverse osmosis, to remove natural and synthetic estrogens from the water matrix has been studied. Reports show that NF efficiently removes estrogen from water. For example, Schafer et al. (2003) reported 80%-99% E1 retention using diverse membrane types. The authors suggested that retention efficiencies depend on the adsorptive effects, which are driven by hydrogen bonding between E1 and the membranes. Other authors have found a decreasing rejection of E1 after 24 hours of filtration (Hu et al., 2007) and some studies on estradiol desorption have reported negative rejection (McCallum et al., 2008).

The main drawback of using NF to remove estrogens is that it generates reject effluent. Because it is a phase-change process, NF generates a permeate flow that has a lower concentration of the contaminant and a reject flow in which the mass balance of the process increases the contaminant concentration. The concentration of estrogens in the reject solution after NF depends on several factors, including the feed water chemistry, membrane type, and solute properties. Studies have shown that the main mechanisms for estrogens rejection are related with adsorption (Yoon et al., 2004); desorption (McCallum et al., 2008); the octanol/water partition coefficient (Bodzek and Dudziak, 2006); pH, pKa, and the membrane's surface charge (Hu et al., 2007); the presence of natural organic matter; and the initial concentration (Jin et al., 2010).

McCallum et al. (2008) found that when the maximal initial adsorption is reached, steady-state rejection is achieved and size exclusion phenomena govern the rejection. When membrane processes are developed, concentrated rejected effluents could increase health hazards and potential toxicity because of the increased concentration of pollutants. To reduce the effects of concentrated effluent during NF processes,

coupled systems to remove and degrade estrogens over sequential stages or coupled hybrid systems have been proposed (Grzechulska-Damszel et al., 2010), such as coagulation–NF or NF advanced oxidation processes (AOPs), to achieve significant (e.g., 95.4%–99.9%) removal efficiencies (Berberidou et al., 2009; Ganiyu et al., 2015). Recently, coupling an NF90 membrane with UV/TiO<sub>2</sub> was shown to concentrate and degraded pharmaceuticals (Martínez et al., 2013). Currently, there are very few studies on coupled NF and postconcentrate photocatalytic treatment (Ganiyu et al., 2015) for reducing E3, and therefore more research is needed to expand our understanding of the rates of estrogen concentration and degradation. Coupling AOPs with membrane filtration has been studied as a pretreatment for the membrane feed stream, a posttreatment of nonrejected pollutants in permeate (Pereira et al., 2012), and a treatment for highly concentrated organic compounds in a concentrate stream (Martínez et al., 2013). In all of these cases, separation and degradation were simultaneously achieved in the hybrid processes (Ganiyu et al., 2015). This study analyzed NF using suspended photoactivated TiO<sub>2</sub> as a posttreatment process for the concentrate stream before discharge. This report shows that coupling NF with a TiO<sub>2</sub>-based photocatalytic process effectively concentrates and further degrades estrogen.

## MATERIALS AND METHODS

**Chemicals and Membranes.** All the chemicals used were of analytical grade. Estriol was obtained from Sigma-Aldrich (USA). Estriol pK<sub>a</sub> is above 10.54. A stock solution of E3 (10 μM) was prepared by adding 0.0028 g of E3 to 1 L of deionized water. The solution was then stored in an amber flask. An NF90 membrane sheet from Dow Chemical was selected and supplied by Sterlitech (USA). The properties of the polyamide layer of NF90 (Zhang et al., 2016) are as follows: MWCo, 200–400 Da; max temperature, 45°C; pH range, 3–10; salt rejection, 85%–95% (NaCl), >97% (CaCl<sub>2</sub>); and top layer composition, thin-film composite polyamide. Aeroxide® TiO<sub>2</sub> P25 (previously known as Degussa P25, 50±15 m<sup>2</sup> g<sup>−1</sup> specific surface area, 21 nm average primary particle size, 80:20 anatase/rutile ratio, according to the manufacturer) was obtained from Evonik Industries and used as the photocatalyst.

**First stage: Nanofiltration Processes.** All membrane filtration experiments were carried out in a cross-flow cell as described in Figure 1A. The flow cell was constructed in the lab using Nylamid®, a polyamide engineered plastic. The membrane support was made of sintered stainless steel filter plate (filter rating: 10 μm; maximum pore diameter: 30 μm; permeability: 160 m<sup>3</sup> h<sup>−1</sup> m<sup>−2</sup> kPa<sup>−1</sup>, according to the manufacturer specification) supplied by Baoji Qixin Titanium Co., Ltd. The water pressure pump used was a DC 24V electric diaphragm pump, which is capable of providing a maximum discharge pressure of 10 bar and a maximum flow rate of 16 L min<sup>−1</sup>. The membrane was set up on two concentric O-rings® to prevent filtration outside the cell. The effective membrane surface area was calculated as 48 cm<sup>2</sup> (8 cm x 6 cm). A new membrane was used for each experiment. The operating pressure on the membrane was adjusted using a bypass valve. The working pressure was 6 kg cm<sup>−2</sup> (588.4 kPa) and a 1 L reservoir was used to store the feed solution and collect the concentrate effluent. The membrane was compacted for 4 hours at 6 kg cm<sup>−2</sup> using deionized water. The temperature of the feed solution was kept at 22 ± 2 °C using a cylindrical, water-cooled, jacketed, glass vessel with a thermostatic bath (Polystat®, Cole-Palmer). After the membrane was compacted, the concentrate and permeate reservoirs were emptied and filled with a test solution. A test solution of 300 mL was placed in the concentrate reservoir and the filtration process was conducted at 6 kg cm<sup>−2</sup> using the NF90 membrane. The retinate stream was continuously recirculated to the feed tank. Samples were taken from the concentrate reservoir and filtrate reservoir every 30 minutes during a period of 300 minutes.

**Post-treatment: Photocatalytic Degradation of E3 of Concentrate Solution.** As a post-treatment for the concentrated solution, an aliquot of 100 mL of the NF's concentrate stage was taken for photocatalytic degradation of E3. The lamps were positioned in the center and horizontally above the photoreactor (Figure 1B). The solution was irradiated with two 15 W blacklight lamps (GE, F15T8 BLB) that emitted radiation mainly in the 350–400 nm ( $\lambda_{\text{max}} = 360$  nm) wavelength interval. The horizontal and vertical position of the photoreactor was kept constant for the experiment. The temperature was controlled using a thermostatic bath (Polystat, Cole-Palmer). The overall system was placed in a closed box to avoid the effects of sunlight or any other artificial radiation source. Initially a study for photocatalytic degradation of E3 was performed

to determine the effect of catalyst loading using 20, 40, 80 and 160 mg L<sup>-1</sup> of TiO<sub>2</sub>, from this study the TiO<sub>2</sub> photocatalyst load selected was 20 mg L<sup>-1</sup> to be used in the post-treatment processes. In all the photocatalytic experiments a dark period (no radiation) was allowed for 20 minutes, during which time E3 and the photocatalyst were stirred without any radiation source to ensure adsorption equilibrium in the solution.

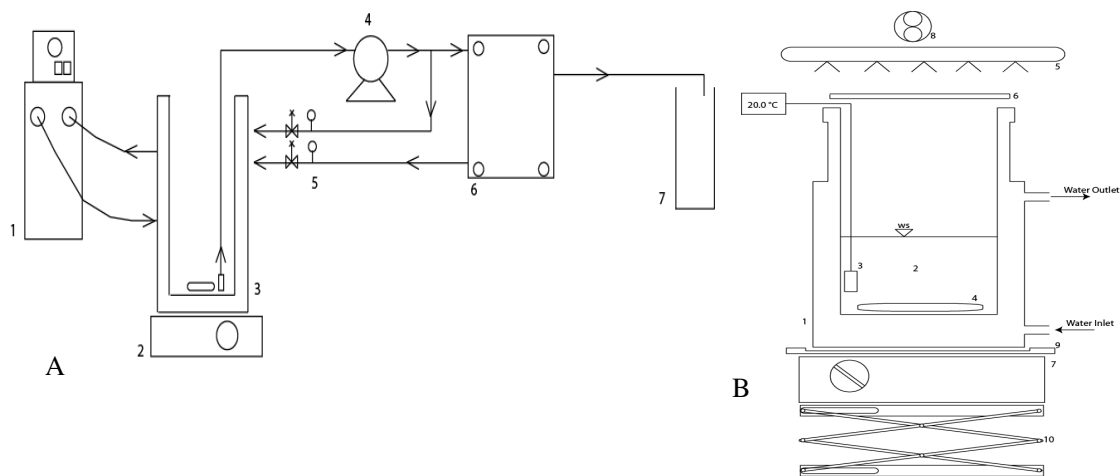


**FIGURE 1 A).** Cross-flow nanofiltration system setup: 1) temperature-controlled water bath, 2) stirring plate, 3) concentrate reservoir, 4) diaphragm pump, 5) pressure gauge, 6) cross-flow filtration cell, and 7) filtrate reservoir. **B).** Photocatalytic reactor setup: 1) glass reactor, 2) testing solution, 3) temperature probe, 4) spin bar, 5) backlight lamp, 6) optical filter (if needed), 7) stirring plate, 8) cooling fan, 9) horizontal position setup, and 10) lab jack lifting platform

**Analytical Methods.** Estriol was monitored using an HPLC system (Waters 1515) equipped with a UV detector (Waters 2787) with an injection volume of 20  $\mu$ L. Estriol determinations were performed at isocratic analytical mode using a 150 mm  $\times$  4.6 mm with Inertsil<sup>®</sup> ODS-3, 5  $\mu$ m column thermostated at 25  $^{\circ}$ C. The UV detection was set at  $\lambda$ = 280 nm and the mobile phase used was methanol (49%) and ultrapure water (51%) at a flow rate of 1 mL min<sup>-1</sup>. The retention time was 10 minutes and the method detection limit was determined to be 0.1  $\mu$ M.

## RESULTS AND DISCUSSION

**Concentration of Estriol by Nanofiltration Processes.** The experiment was divided into two phases: the first was nanofiltration, which started with a 1  $\mu$ M E3 solution, and the second was the photocatalytic degradation of concentrate using TiO<sub>2</sub> activated with UV radiation. The nanofiltration process was run for 180 minutes (Figure 2A). The flux throughout the membrane that was obtained during nanofiltration was 17 L m<sup>-2</sup> h<sup>-1</sup>. Flux evolution was constant and no decline was observed during the experiment. The initial volume of the feed solution was 500 mL and the final volume after nanofiltration was 150 mL. The estriol concentration in permeate was below the method detection limit for the entire experiment. The concentration of E3 in the rejected flow increased continuously, as shown in Figure 2A. The steric hindrance because of the molecular weight of E3 (280 g mol<sup>-1</sup>) and the MWCo of NF90 membranes (200-400 Da) was the main factor that determined the retention capacity. The adsorption/desorption dynamic phenomenon was also an important mechanism that was taken into account for estrogen rejection (Yoon et al., 2004; Hu et al., 2007). Based on this information, it can be assumed that the cross flow tangential velocity on the membrane was sufficiently high to avoid building up a polarization layer with high concentration of E3. This reduced polarization layer kept E3 rejection rate for equal E3 concentration in bulk solution than boundary layer of the membrane. Charge rejection phenomena could be less important because at pH = 7.0, all E3 molecules are not dissociated due to their pK<sub>a</sub> value (10.54) and the zeta potential of the NF90 membrane (-55 mV) at that pH (Wang et al., 2016).

**3.2 Photocatalytic Degradation of Estriol.** Figure 2B shows the photocatalytic degradation of E3 using different  $\text{TiO}_2$  catalyst loads. As shown, an increase in the catalyst load generated an increase in the reaction rate, with a load of  $160 \text{ mg L}^{-1}$  having the highest removal efficiency. These results are in agreement with previous reports that found the same trend. It was also found that further increases in the catalyst load led to a decrease in the efficiency of the process, which was also previously reported (data not shown).

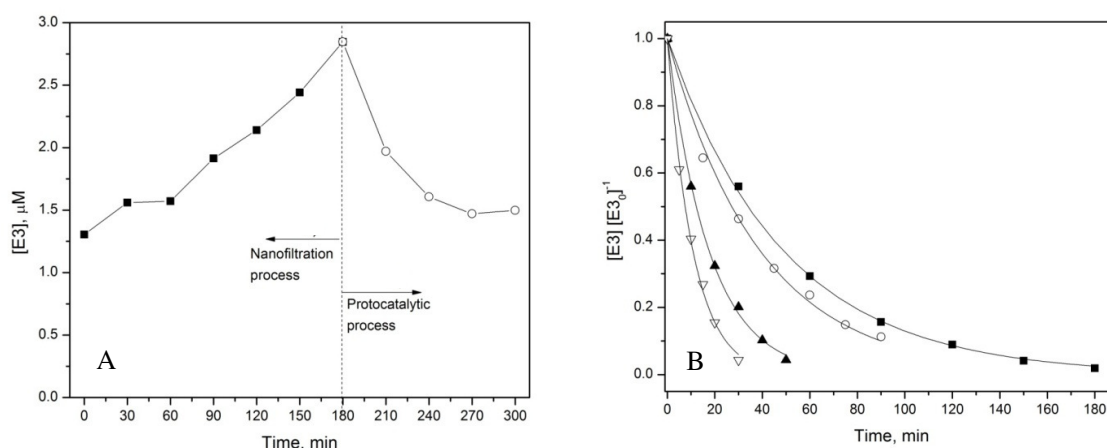


**FIGURE 2 A).** Coupled membrane filtration and  $\text{TiO}_2$  photocatalytic processes for concentration-degradation of estriol: —■— = concentrate solution; —○— = concentrate solution under photocatalytic process. **B).** Catalyst load effect on degradation of E3 under backlight lamp (GE F15T8 BLB); experimental data: ■ =  $20 \text{ mg L}^{-1}$ , ○ =  $40 \text{ mg L}^{-1}$ , ▲ =  $80 \text{ mg L}^{-1}$ , ▽ =  $160 \text{ mg L}^{-1}$  and (—) = first-order kinetic model.

The kinetic analysis of the experimental data depicted in Figure 2B fit a pseudo-first-order kinetic model. The kinetic model fitted the experimental data fairly well, which is also shown in Figure 2B (solid lines). For all the catalyst loads tested, approximately the same removal efficiency (i.e., 95%) was achieved and the only difference in the experimental runs was the time of irradiation required. Approximately 180 minutes of photocatalytic treatment were needed to achieve 95% degradation of E3 using  $20 \text{ mg L}^{-1}$  of the photocatalyst load, whereas the same removal was obtained after only 30 minutes (one sixth of the reaction time) using  $160 \text{ mg L}^{-1}$  (eight times more load). These results agree with previous reports that have demonstrated that higher concentrations of the photocatalyst overdoses the system, which leads to a decrease in degradation efficiency because of radiation scattering, reduced penetration, and  $\text{TiO}_2$  agglomeration (Colina-Márquez et al., 2015). Considering that the increase in the catalyst load did not generate the expected improvement in E3 degradation, further experiments were performed using the lowest catalyst load to favor the efficiency of the overall process. After 180 minutes of concentration by the NF processes, an aliquot 100 mL of concentrate solution was taken and submitted to photocatalytic degradation using  $\text{TiO}_2$ . As stated previously,  $\text{TiO}_2$  was dispersed in a concentrate solution to get  $20 \text{ mg L}^{-1}$ .

The degradation of E3 in the concentrate (Figure 2A) for time periods of 180 minutes and up to 300 minutes showed that it also follows a pseudo-first-order kinetics, which was previously observed for the experiments with variable photocatalyst loads. It is well known that the phenol moiety of E3 is responsible for absorption at 280 nm. For this reason, any change in its structure will produce changes in molar absorption at this wavelength. When the E3 solution was degraded using  $\text{TiO}_2$  and UV radiation, it was observed that the initial adsorption of the solution decreased as a function of time following a first-order reaction.

## CONCLUSIONS

Further studies of E3 adsorption on the membrane should be conducted to obtain a mass balance. It was confirmed that NF90 membrane can effectively reject estriol and it is feasible concentrating by recalculating the reject stream of the NF process. It has been demonstrated, using the load tested, that UV/ $\text{TiO}_2$  degradation of estriol can be a feasible coupled process for E3 degradation when E3 found in

rejected effluents of a nanofiltration process. Further studies should compare the effects of pH and salt concentration on the rejection and degradation of estriol in water. This work highlights an advanced, coupled NF system and heterogeneous UV/TiO<sub>2</sub> photocatalysis to reduce the discharge volume that should be treated when estrogen compounds are removed from the permeate effluents of NF systems.

## ACKNOWLEDGMENTS

The Aerioxide® P25 Evonik catalyst used for this work was provided by Intertrade S.A. de C.V., the supplier of Evonik Industries in Mexico. The research was partially supported by CONACYT under Project CB-2011/168285. The authors thank Dr. M.A. Quiroz Alfaro for his excellent technical help and allowing the use of materials and equipment at the UDLAP's electrochemical lab.

## REFERENCES

- Berberidou, C., S. Avlonitis, and I. Poullos. 2009. "Dyestuff Effluent Treatment by Integrated Sequential Photocatalytic Oxidation and Membrane Filtration." *Desalination* 249 (3): 1099–1106.
- Bodzek, M., and M. Dudziak. 2006. "Removal of Natural Estrogens and Synthetic Compounds Considered to Be Endocrine Disrupting Substances (EDs) by Coagulation and Nanofiltration." *Pol. J. Environ. Stud.* 15 (1): 35–40.
- Carvalho, A. R M, V. V. Cardoso, A. Rodrigues, E. Ferreira, M. J. Benoliel, and E. A. Duarte. 2015. "Occurrence and Analysis of Endocrine-Disrupting Compounds in a Water Supply System." *Environ. Monit. Assess.* 187 (3): 139.
- Colina-Márquez, J., F. Machuca-Martínez, and G. Li Puma. 2015. "Modeling the Photocatalytic Mineralization in Water of Commercial Formulation of Estrogens 17-  $\beta$  Estradiol (E2) and Nomegestrol Acetate in Contraceptive Pills in a Solar Powered Compound Parabolic Collector." *Molecules*, 13354–13373.
- Czech, B., and K. Rubinowska. 2013. "TiO<sub>2</sub>-Assisted Photocatalytic Degradation of Diclofenac, Metoprolol, Estrone and Chloramphenicol as Endocrine Disruptors in Water." *Adsorption* 19 (2): 619–630.
- Ganiyu, S.O., E. D. Van Hullebusch, M. Cretin, G. Esposito, and M. A. Oturan. 2015. "Coupling of Membrane Filtration and Advanced Oxidation Processes for Removal of Pharmaceutical Residues: A Critical Review." *Sep. Purif. Technol.* 156: 891-914
- Grzechulska-Damszel, J., S. Mozia, and A.W. Morawski. 2010. "Integration of Photocatalysis with Membrane Processes for Purification of Water Contaminated with Organic Dyes." *Catal. Today* 156 (3-4): 295–300.
- Hu, J. Y., X. Jin, and S. L. Ong. 2007. "Rejection of Estrone by Nanofiltration: Influence of Solution Chemistry." *J. Membr. Sci.* 302 (1-2): 188–96.
- Jin, X., J. Hu, and S. L. Ong. 2010. "Removal of Natural Hormone Estrone from Secondary Effluents Using Nanofiltration and Reverse Osmosis." *Water Res.* 44 (2): 638–48.
- Martínez, F., M. J. López-Muñoz, J. Aguado, J. A. Melero, J. Arsuaga, A. Sotto, R. Molina, et al. 2013. "Coupling Membrane Separation and Photocatalytic Oxidation Processes for the Degradation of Pharmaceutical Pollutants." *Water Res.* 47 (15): 5647–5658.
- McCallum, E. A., H. Hyung, T. Anh Do, C. H. Huang, and J. Hong Kim. 2008. "Adsorption, Desorption, and Steady-State Removal of 17 $\beta$ -Estradiol by Nanofiltration Membranes." *J. Membr. Sci.* 319 (1-2): 38–43.
- Pereira, V. J., J. Galinha, M. T. B. Crespo, C. T. Matos, and J. G. Crespo. 2012. "Integration of Nanofiltration, UV Photolysis, and Advanced Oxidation Processes for the Removal of Hormones from Surface Water Sources." *Sep. Purif. Technol.* 95: 89–96.
- Schafer, A. I., L. D. Nghiem, and T. D. Waite. 2003. "Removal of the Natural Hormone Estrone from Aqueous Solutions Using Nanofiltration and Reverse Osmosis." *Environ. Sci. Technol.* 37 (1): 182–188.
- Wang, J., Z. Wang, Y. Liu, J. Wang, and S. Wang. 2016. "Surface Modification of NF Membrane with Zwitterionic Polymer to Improve Anti-Biofouling Property." *J. Membr. Sci.* 514 (September): 407–417.
- Yoon, Y., P. Westerhoff, J. Yoon, and S. A. Snyder. 2004. "Removal of 17 $\beta$  Estradiol and Fluoranthene by Nanofiltration and Ultrafiltration." *J. Environ. Eng.* 130 (12): 1460–1467.

Zhang, R., S.Yu, W. Shi, J.Tian, L. Jin, B. Zhang, L. Li, and Z. Zhang. 2016. "Optimization of a Membrane Cleaning Strategy for Advanced Treatment of Polymer Flooding Produced Water by Nanofiltration." *RSC Adv.* 6 (34): 28844–2853.



## STUDY ON THE INFLUENCE OF ADDITION OF ACIDS ON PARTICLE SIZE AND SURFACE AREA OF TITANIUM DIOXIDE PHOTOCATALYST

Padmini Ellappan<sup>a</sup> and *Lima Rose Miranda*<sup>a\*</sup>

<sup>a</sup> (Carbon Research and Engineering Laboratory, Department of Chemical Engineering, A.C.Tech, Anna University, Chennai, India 600 025. \*Email: limamiranda2007@gmail.com)

**ABSTRACT:** An investigation was carried out on the synthesis of titanium dioxide nano powders via the sol gel method, examining the influence of addition of different acids during preparation of the catalyst. The resulting powders were characterized by X-ray diffraction and surface area. The X-ray diffraction revealed that there was formation of a pure crystalline phase, consisting only of anatase for catalyst prepared by the addition of glacial acetic acid. The catalyst prepared using glacial acetic acid yielded a particle size of 7.1 nm and specific surface area of 175.72 m<sup>2</sup>gm<sup>-1</sup>. The effect of the particle size on the degradation of Acid Red 88, 3, 4- Dichloroaniline and Nitrobenzene was studied and the studies revealed the importance of particle size in degradation effects.

**Keywords:** solgel; acids; particle size; characterization; acid red 88; nitrobenzene; photocatalysis

### INTRODUCTION

Generally any photocatalytic process considers Titania as the best choice as it fits other desirable criteria, despite the low solar absorbance property. Properties of TiO<sub>2</sub> that makes it more advantageous are it is cheap, nontoxic, photolytically and chemically stable, and reusable with a high turnover rate. Modification of the chemical and physical characteristics of TiO<sub>2</sub>, including absorption range and particle size are rather simple and are considered the most important means of modification of titania's oxidation capabilities.

Different methods have been employed for the synthesis of titanium dioxide, such as chemical precipitation (Pedraza and Vasquez, 1999; Scolan and Sanchez, 1998), the sol-gel method (Gartner et al., 2004; Su et al., 2006), hydrothermal (Wu et al., 2002) and solvothermal processes (Kim et al., 2003; Yin et al., 2003), combustion method (Nagaveni et al., 2003), a microemulsion-mediated process (Hong et al., 2003), electrochemical synthesis (Karuppuchamy et al., 2006), fungus-mediated synthesis (Jha et al., 2009) and chemical vapour deposition (CVD) (Jones and Chalker 2003). Venkatachalam et al. (2007) reported the preparation of titanium dioxide nanoparticles via the sol-gel method with different reaction parameters, such as different hydrolyzing agents, molar ratio, aging time and calcinations temperature. They obtained nanocrystals of titanium dioxide with high surface area and different ratios of anatase /rutile.

Sol-gel synthesis has become one of the most promising and important methods employed in nanomaterial production and nanotechnology (Pavasupree et al., 2008). It is a simple route process with moderate conditions such as low temperature and short reaction times producing highly crystalline oxides. This method due to its characteristics mostly used to produce ceramic materials, allowing the control of the particle size, morphology and phase composition (Su et al, 2006; Wang, 2007).

The optimal particle size (and thus surface area) of titania has been studied by many groups over the years and the particle size affects both the amount of pollutants that can adsorb to the surface and the amount of charge carrier recombination that can occur, since recombination is a surface process (Serpone et al 1995, Calza et al 2007, Zhang et al 1998). In general, nanoscale titanium dioxide (1-100 nm) is considered the most active in the degradation of organic compounds, although nano scale catalysts are available and moderately effective (Tahiri et al 1996). The differences in the photocatalytic activity are likely to be related to the differences in the BET surface, impurities, lattice mismatches or density of hydroxyl groups on the catalyst's surface, since these factors could affect the adsorption behavior of a pollutant or intermediate molecule and the life time and recombination rate of electron-hole pairs (Tahiri et al 1996).

The aim of this study was to investigate the effects of addition of different acids during the preparation of the catalyst by solgel method on the TiO<sub>2</sub> physical properties such as particle size and surface area.

## MATERIALS AND METHOD

**Chemicals Used.** The chemicals used for the preparation of catalyst were Titanium isopropoxide and glacial Acetic acid supplied by Sigma Aldrich. The other chemicals used were Ethanol, Citric acid, Nitric acid, Sulfuric acid, Ammonia supplied by Central drug house, Mumbai. Water used for preparation of solution was distilled water. . All the chemical reagents were of analytical grade. The model compound chosen for degradation was Acid Red 88, 3, 4- dichloroaniline and Nitrobenzene.

**Preparation of Catalyst.** The following catalysts were prepared (Table 1) using different acids. Titanium dioxide sol was prepared using Titanium isopropoxide as precursor. 8 mL of Titanium isopropoxide was mixed with 42 mL of ethanol and stirred well. To this 100 mL of 50% ethanol was added slowly and continuously stirred for 30 min at a temperature of 80°C for the hydrolysis reaction to take place. To this mixture 10 mL of glacial acetic acid / citric acid/ nitric acid/ sulphuric acid was added. The solution was left for 48 hrs to age. The gel obtained was dried at 110°C for 24 hrs. The dried gel was ground and calcined at 500°C for 4 hours. This catalyst is referred to as TiO<sub>2</sub> (sol) [Carp et al 2004].

**Table 1:** Different catalyst prepared

Acid used	Referred in text as
Acetic Acid	Ti-A
Citric acid	Ti-C
Nitric acid	Ti-N
Sulphuric acid	Ti-S

**Catalyst Characterization.** The crystalline phase was obtained by a Philips Pw 1830 X-ray diffractometer (XRD) operated at 40 kV and 35 mA and a Philips X' Pert X-ray diffractometer operated at 40 kV and 30 mA, both of which used Cu K $\alpha$  radiation source at  $\lambda$  of 1.54 Å. XRD data were collected from 2 $\theta$  of 20-60 degree. Each of the crushed samples was either coated on the inverse side of cello tape and made its surface smooth by pressing with a spatula or spread on a small piece of glass and pressed with another smooth-surfaced glass.

Scherrer's equation was used to calculate the crystallite size as given in equation 1 (Patterson et al., 1939).

$$D = \frac{k\lambda}{\beta \cos \theta} \quad (1)$$

where d is the crystallite size (nm)

k is the constant whose value is approximately 0.9

$\lambda$  is the wavelength of the X-ray radiation source (0.154 nm for Cu K $\alpha$ )

$\beta$  is the full width at half maximum intensity (FWHM) (radians)

$\theta_B$  is the Bragg angle at the position of the peak maximum

The anatase content was also calculated applying Spurr-Myers equation as given in equation 2 (Spurr et al., 1957).

$$w_A = \frac{1}{1+1.26I_R/I_A} \quad (2)$$

where  $w_A$  is the weight fraction of anatase in the mixture

$I_R$  is the intensity of the diffraction peak of rutile

$I_A$  is the intensity of the diffraction peak of anatase

The specific surface area of the catalysts was determined by nitrogen adsorption at 77 K by BET Quanta chrome instrument. All the samples received a preliminary heat treatment at 100 – 120 °C under 10<sup>-2</sup>

<sup>2</sup> Torr vacuum for 4 hours to eliminate the trace amount of water present in the samples. The specific surface area was calculated using the BET method.

The particle size was also calculated using the surface area calculated from BET isotherms determined using BET Quanta chrome instrument as given in equation 3.

$$\text{Particle diameter } D = \frac{6000}{S_{\text{BET}} \cdot \rho} \quad (3)$$

where  $S_{\text{BET}}$  is the surface area ( $\text{m}^2\text{g}^{-1}$ ) and  $\rho$  is the density of the catalyst which is approximately  $4.2 \text{ gcm}^{-3}$  for Titania based particles.

**Photocatalytic Degradation Studies.** The photocatalytic degradation using the prepared catalyst was studied in an annular photoreactor of capacity of 1000 mL. The visible light of intensity 500 W was chosen for irradiating the solution. The catalyst quantity in all the cases were  $0.1 \text{ gL}^{-1}$  and irradiation time of 120 min was maintained. Knowing the initial and final concentration of the solution i.e. before and after irradiation, the % degradation (%PCD) was calculated. In the case of AR 88 and NB, initial solution concentration of  $50 \text{ mgL}^{-1}$  was used while for DCA  $10 \text{ mgL}^{-1}$  of concentration was used.

## RESULTS AND DISCUSSION

Figure 1 show a series of XRD patterns of the prepared  $\text{TiO}_2$  samples following the addition of different acids during catalyst preparation. All diffraction peaks show the complete formation of the crystalline anatase phase and were indexed according to the JCPDS card No. 89-4921. The peaks at  $2\theta=27^\circ$ ,  $36^\circ$  and  $54.3^\circ$  indicate the presence of the  $\text{TiO}_2$  in the rutile phase while peaks at  $2\theta=25.5^\circ$ ,  $37.2^\circ$ ,  $48^\circ$ , and  $62.6^\circ$  indicate the presence of the anatase phase. No peaks related to brookite phases were observed in the XRD patterns of Ti-A, Ti-C, Ti-N and Ti-S, whereas rutile phases were observed in all the catalyst prepared except Ti-A. The XRD pattern of the Ti-A was compared with data files and all the sharp peaks observed in the XRD pattern belong to anatase phase of  $\text{TiO}_2$ . The other crystalline forms of  $\text{TiO}_2$ , rutile and brookite, have not been detected. The sol-gel synthesis route using glacial acetic acid presents the advantage of obtaining phase-pure  $\text{TiO}_2$  nanoparticles.

From the diffractogram, the widths of the bases of the peaks and their intensity characterize the size of the nanocrystals, because small crystals may promote a more intense spreading due to internal reflections that occur in the system. Considering the diffractograms shown in Fig. 1, it can be observed that the samples obtained using acetic acid present sharp peaks, revealing that the nanocrystals obtained have a smaller size. This fact is evidenced by the calculation of the average crystallite size using the Scherrer equation, as shown in Table 2. The average crystallite size of the nano- $\text{TiO}_2$  applying Scherer equation was found to be 7.1 nm.

Comparing the samples synthesized using different acid based on the specific surface area as shown in Table 1, higher specific surface area were observed in Ti-A sample as compared to other catalysts. In addition, in Table 2, it is observed that the average crystallite size calculated using XRD and BET analysis was almost the same. The pore volume and the pore radius of Ti-A was the maximum as compared to other catalyst.

Photocatalysis, using semiconductor particles under sufficient irradiation energy for the simultaneous reduction and oxidation of different redox systems, has been intensively studied for Acid Red 88 (AR88), Nitrobenzene (NB) and 3,4-dichloraniline (DCA) using the prepared nanocrystalline catalyst. Photocatalytic degradation of AR88, DCA and NB in the presence of Visible light are shown in Figures 2, 3 and 4 respectively.

It could be seen for all the three model compounds chosen, the degradation was higher with Ti-A as compared to other catalyst. Ti-A performed better due to small particle size and larger specific area. More active sites are available on the surface of Ti-A hence there is better electron formation leading to better degradation. The differences in the photocatalytic activity of catalysts are likely to be due to differences in the BET-surface, impurities, lattice mismatches or density of hydroxyl groups present on the catalysts surface. Since they will affect the adsorption behaviour of a pollutant or intermediate molecule and the lifetime and recombination rate of electron-hole pairs, there is a difference in the performance of the catalysts prepared.

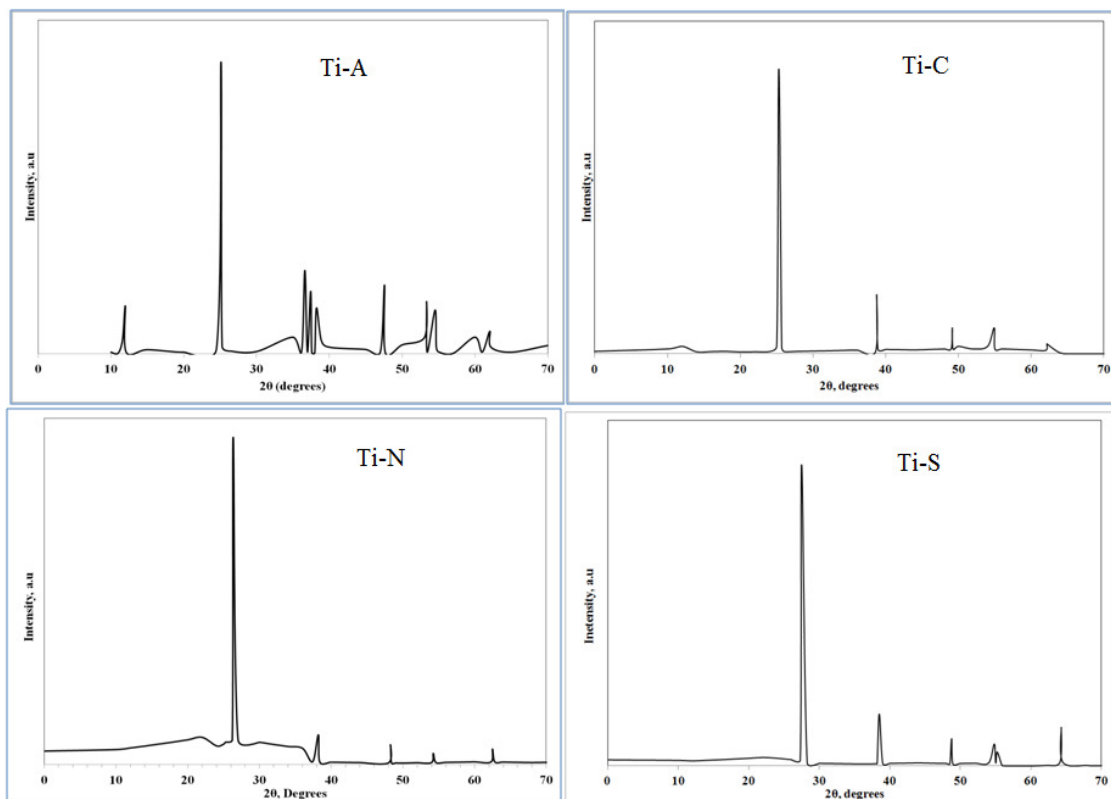


Fig. 1. XRD analysis of the prepared catalyst

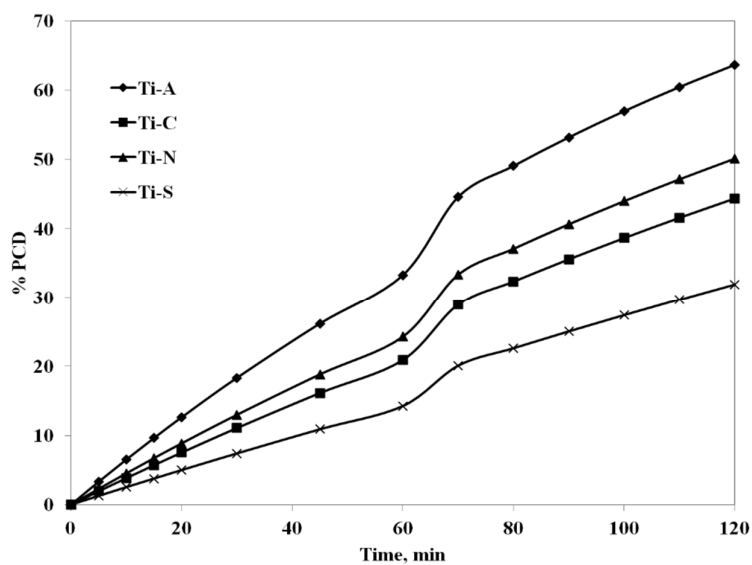
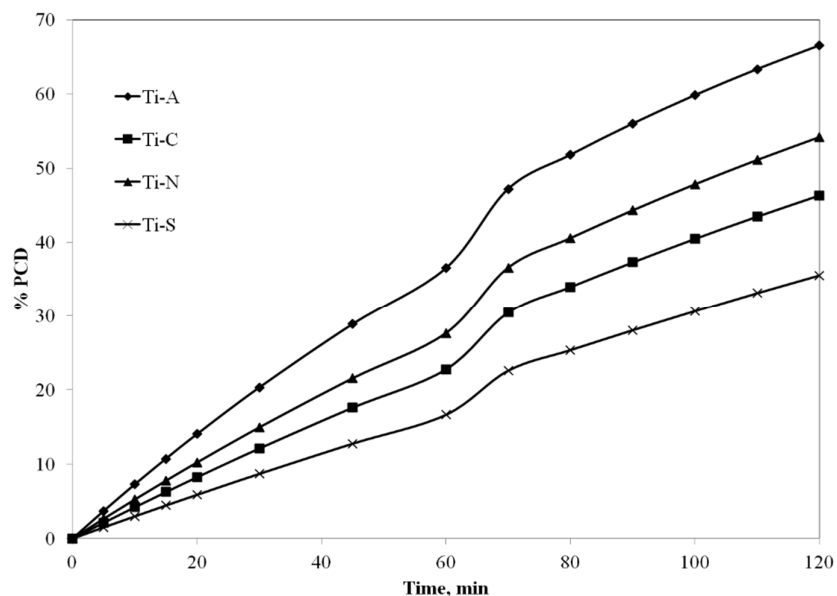
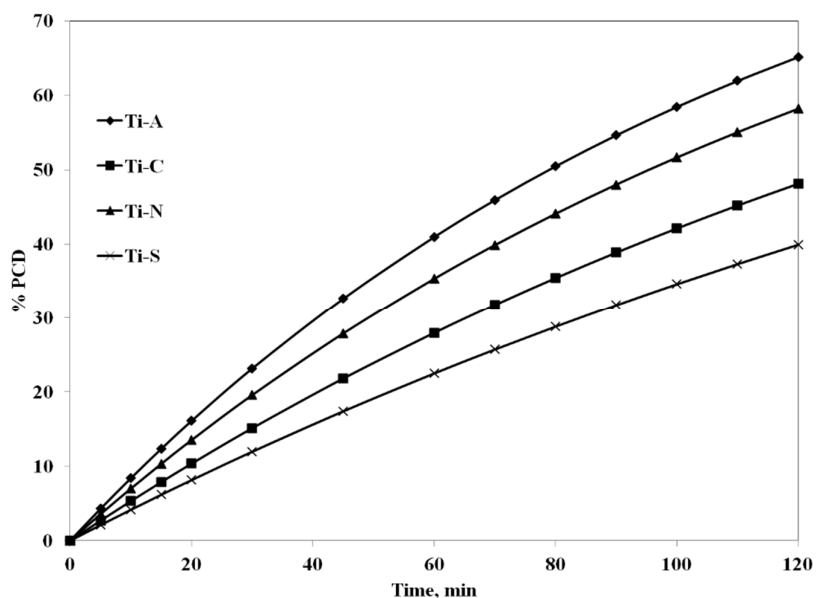


Fig. 2. Photocatalytic activity of different nanocrystalline catalyst on AR88 degradation in the presence of Visible light (AR 88 conc: 50 mgL<sup>-1</sup>, Catalyst dosage: 0.1 gL<sup>-1</sup>, Visible light irradiation: 120min, temp: 30°C)



**Fig. 3.** Photocatalytic activity of different nanocrystalline catalyst on DCA degradation in the presence of Visible light (DCA conc: 10 mgL<sup>-1</sup>, Catalyst dosage: 0.1 gL<sup>-1</sup>, Visible light irradiation: 120min, temp: 30°C)



**Fig 4:** Photocatalytic activity of different nanocrystalline catalyst on NB degradation in the presence of Visible light (NB conc: 50 mgL<sup>-1</sup>, Catalyst dosage: 0.1 gL<sup>-1</sup>, Visible light irradiation: 120min, temp: 30°C)

## CONCLUSION

The photocatalytic activity of semiconductor catalyst is dependent on surface and structural properties of semiconductor such as crystal composition, surface area, particle size distribution, porosity, band gap and surface hydroxyl density. Average crystal size is of primary importance in heterogeneous catalysis, because it is directly related to the efficiency of a catalyst through the definition of its specific surface area. Hence in this research an effort to prepare smaller particle size and high specific surface area was achieved by the addition of glacial acetic acid. PCD studies also proved that the particle size influences greatly the degradation of the compounds.

Table 2. Properties of the catalyst

Properties Catalyst	Average crystallite size, nm	Particle size, nm (BET method)	Pore volume, m <sup>3</sup> gm <sup>-1</sup>	Pore radius Å	Specific surface area m <sup>2</sup> gm <sup>-1</sup>	Anatase %
Ti-A	7.10	8.13	0.15	2.25	175.72	100.00
Ti-C	13.17	14.25	0.09	1.26	100.25	88.19
Ti-N	11.13	12.54	0.10	1.49	113.92	92.34
Ti-S	20.62	21.43	0.07	0.99	66.66	23.15

## REFERENCES

- Calza P, Pelizzetti E, Mogyorósi K, Kun R and Dékány I (2007). Size dependent photocatalytic activity of hydrothermally crystallized titania nanoparticles on poorly adsorbing phenol in absence and presence of fluoride ion. *Appl. Catal. B* 72: 314-321. doi:10.1016/j.apcatb.2006.10.019.
- Gartner M, Scurtu R, Ghita A, Zaharescu M, Modreanu M, Kokkoris M, Kordas G and Trapalis C. (2004) Spectroellipsometric characterization of sol-gel TiO<sub>2</sub>- CuO thin coatings. *Thin Solid Films* 455: 417-421 (2004). doi: 10.1016/j.tsf.2004.01.030
- Pavasupree S, Jitputti J, Ngamsinlapasathian S. and Yoshikawa S (2008). Hydrothermal synthesis, characterization, photocatalytic activity and dyesensitized solar cell performance of mesoporous anatase TiO<sub>2</sub> nanopowders. *Mater. Res. Bull* 43: 149-157. doi: 10.1016/j.materresbull.2007.02.028
- Pedraza F and Vasquez A (1999). Obtention of TiO<sub>2</sub> rutile at room temperature through direct oxidation of TiCl<sub>3</sub>. *J. Phys. Chem. Solids*, 60, 445-448 (1999). doi:10.1016/S0022-3697(98)00315-1
- Scolan E and Sanchez C (1998) Synthesis and characterization of surface-protected nanocrystalline titania particles. *Chem. Mater* 10: 3217-3223. doi: 10.1021/cm980322q
- Serpone N, Lawless D, Khairutdinov R and Pelizzetti E (1995) Subnanosecond Relaxation Dynamics in TiO<sub>2</sub> Colloidal Sols (Particle Sizes R<sub>p</sub> = 1.0-13.4 nm). Relevance to Heterogeneous Photocatalysis. *J. Phys. Chem.*, 99: 16655-16661. doi: 10.1021/j100045a027.
- Su C, Lin KF and Lin YH (2006) Preparation and characterization of high-surface-area titanium dioxide by sol-gel process. *J. Porous Mater* 13: 251-258. doi: 10.1007/s10934-006-8012-7.
- Tahiri H, Serpone N and Le van Mao R (1996). Application of concept of relative efficiencies and surface characterization of a new titania photocatalyst designed for environmental remediation. *J. Photochem. Photobiol. A*, 93: 199-203. doi:10.1016/1010-6030(95)04195-8.
- Wang G (2007) Hydrothermal synthesis and photocatalytic activity of nanocrystalline TiO<sub>2</sub> powders in ethanol-water mixed solutions. *J. Mol. Catal. A: Chem.* 274: 185 -191. doi:10.1016/j.molcata.2007.05.009.
- Zhang Z, Wang CC, Zakaria R and Ying JY (1998). Role of Particle Size in Nanocrystalline TiO<sub>2</sub>-Based Photocatalysts. *J. Phys. Chem. B* 102:10871-10878. doi: 10.1021/jp982948+

## INTERACTION OF ENGINEERED MATERIALS WITH MICROBIAL BIOFILMS AND ITS POTENTIAL APPLICATIONS

**Hengye Jing**, and George A. Sorial (University of Cincinnati, Cincinnati, OH, USA)  
Endalkachew Sahle-Demessie\* (US Environmental Protection Agency, Cincinnati, OH, USA)

Biofilms are surface-associated and highly-stratified microbial communities, existing in water distribution systems. Biofilms are mainly composed of extracellular polymeric substance (EPS), which act as a protective layer for bacteria. Pathogenic EPSs are critical in host-microbe interactions, where they aid in adherence and colonization within a host and function in immunomodulation or in water distribution systems. Different strategies have been applied to control waterborne pathogens. For instance, surface modification, or using engineered nanoparticles as anti-bacterial agents to manage their growth associated with biofilm in the water distribution system. Carbon nanotubes (CNTs) have been proven to have effective anti-bacterial and anti-biofilm properties and been widely used for making polymeric nanocomposites. In this study, the potential role of polyethylene (PE) nanocomposite containing 0%, 2 wt% and 4wt% of multi-walled carbon nanotubes (MWNTs) on inhibiting biofilm growth was studied. Two types of bacteria, *Pseudomonas fluorescens* and *Mycobacterium smegmatis* biofilms were investigated. Laser scanning microscopy (LSM) and FilmTracer™ LIVE/DEAD biofilm viability kit were used to trace the biofilm growth between the different surfaces on a time course. PE nanocomposites containing 2 wt% and 4 wt% MWNTs were observed to have less biofilm growth during first four weeks for both two types of biofilms. The nanocomposite containing 4 wt% MWNTs showed a stronger anti-bacterial effect during the first few weeks than the one with 2 wt% MWNTs. Further studies are conducted to explore this reason. Scanning electron microscope (SEM) provided a micro view of surface property of the PE/MWNTs nanocomposite such as surface roughness while atomic force microscopy (AFM) provided topographical mapping of the surface. Contact angle goniometer was also used to determine the surface energy of the different polymeric nanocomposites. SurPASS electrokinetic analyzer determined the streaming surface zeta potential of both PE/MWNTs nanocomposite and biofilms.

## **UNDERSTANDING THE FORMATION OF NATURALLY OCCURRING SILVER NANOPARTICLES IN AQUATIC ENVIRONMENT**

***Nathaniel F. Adegboyega***-, William C. Hockaday (Baylor University, Waco, TX, USA )  
Virender K. Sharma (Texas A&M, College Station, TX, USA)

Silver nanoparticles (AgNPs) as an emerging contaminant in the environment is of concern to society due to the potential for long-range transport, and the potential for ecological and human toxicity. Aquatic humic substances (HS) can influence AgNP transport, reactivity, removal, dissolution and formation. Therefore, understanding of the nature of HS-AgNP interactions would be essential to environmental behavior and identifying best-practices for AgNP removal from municipal waters. However, knowledge on the detail interactions between AgNPs and silver ion ( $\text{Ag}^+$ ) and aquatic humic substances (HS) at the molecular level is scant due to the limited number of analytical tools capable of detecting formation or transformation of AgNPs in the presence of HS.

We applied several analytical techniques including UV-visible spectroscopy, Fourier Transform-Ion Cyclotron Resonance mass spectrometry (FT-ICR MS) and several characterization techniques to investigate the formation of silver nanoparticles in the environment. Our results show that the spontaneous formation of silver nanoparticle in the environment is directly linked to the reduction of silver ions by naturally occurring humic substances. The formation of these silver nanoparticle is particularly controlled by environmental factors such as pH, temperature and light. The presence of  $\text{Fe}^{2+/3+}$  redox systems were found to influence the amount of silver nanoparticle formation.

An electrospray ionization technique equipped with a Fourier Transform-Ion Cyclotron Resonance mass spectrometry (FT-ICR MS) was also used as an analytical tool to monitor the direct interactions between humic substance and  $\text{Ag}^+$ . Our preliminary characterization of  $\text{Ag}^+$ -HS mixtures suggest a high preference of  $\text{Ag}^+$  for low molecular species of humic substances.



## **OPTIMIZED SYNTHESIS OF POLYMER-BASED GRAPHENE OXIDE NANOCOMPOSITES FOR HEAVY METAL ADSORPTION USING RESPONSE SURFACE METHODOLOGY**

***Jem Valerie D. Perez*** and Maria Lourdes P. Dalida  
(University of the Philippines, Quezon City, Philippines)  
Debora F. Rodrigues  
(University of Houston, Houston, TX, USA)

Nanocomposites containing graphene oxide (GO), polyethyleneimine (PEI), and chitosan (CS) were synthesized for chromium (VI) and copper (II) removal from water. Response surface methodology (RSM) was used for the optimization design of the synthesis of the CS-PEI-GO beads formed with different concentrations of PEI (1.0 – 2.0%), GO (500 – 1500 ppm), and glutaraldehyde (GLA) (0.5 – 2.5%) as cross-linking agent. Batch adsorption experiments were performed to obtain responses in terms of percentage removal of both Cr (VI) and Cu (II) ions. A second-order polynomial equation was used to model the relationship between the synthesis conditions and the adsorption responses. Analysis of Variance (ANOVA) showed that GLA concentration has opposite effects on Cr (VI) and Cu (II) adsorption due to different uptake mechanisms by the CS-PEI-GO beads for the two heavy metals. High  $R^2$  values of 0.9848 and 0.8327 for Cr (VI) and Cu (II) removal were obtained from the regression analyses, suggesting good correlation between observed and predicted values. Removal of up to 91.10% Cr (VI) and 78.18% Cu (II) were achieved by the beads composed of 2.0% PEI, 1500 ppm GO, and cross-linked with 2.08% GLA. Finally, the structure and surface properties of the CS-PEI-GO beads were characterized using X-ray diffraction (XRD), porosity and BET surface area analysis, Scanning electron microscopy (SEM), Fourier transform infrared spectroscopy (FTIR), and X-ray photoelectron spectroscopy (XPS). Overall, the synthesized CS-PEI-GO beads were proven to be effective in removing both cationic and anionic heavy metal pollutants.

## ORGANIC RADICAL INTERMEDIATE-SPARKED HIGHLY FENTON-CATALYTIC EFFICIENCY OF DANDELION-LIKE TiCuAl-SiO<sub>2</sub> NANOSPHERES FROM ORGANIC CONTAMINANT DEGRADATION

Lai Lyu, Lili Zhang and Chun Hu  
(Chinese Academy of Sciences, Beijing, China)

**INTRODUCTION.** Triggered by growing water pollution issues, research aiming at a more efficient water purification technology has been thriving. Fenton reaction as a typical advanced oxidation process is especially powerful, since it can rapidly and nonselectively degrade various organic pollutants via  $\bullet\text{OH}$ . However, in the conventional Fenton process, the reduction of the oxidation state ( $\text{M}^{(n+m)+}$ ) to the reduction state ( $\text{M}^{n+}$ ) of the metal by oxidizing  $\text{H}_2\text{O}_2$  is the rate-limiting step, and  $\text{H}_2\text{O}_2$  is decomposed with the formation of  $\text{O}_2$  as a reaction product in addition to superoxide radical ( $\text{O}_2^{\bullet-}$ ), which leads to excessive consumption of  $\text{H}_2\text{O}_2$ . Due to these deficiencies, most heterogeneous Fenton catalysts exhibited low activity and utilization efficiency of  $\text{H}_2\text{O}_2$ . Recently, we prepared a fibrous Fenton catalyst consisting of dandelion-like titanium-copper-aluminium trimetal-doped silica nanospheres (*d*-TiCuAl-SiO<sub>2</sub> Ns) for the first time. We found that a novel electron supply pathway from the generated organic radical intermediates ( $\bullet\text{R}$ ) sparked by Ti-Cu system could address the problems for activity and the utilization efficiency of  $\text{H}_2\text{O}_2$ . In this system, *d*-TiCuAl-SiO<sub>2</sub> Ns exhibited strong Fenton-catalytic activity and supreme utilization efficiency of  $\text{H}_2\text{O}_2$  in the degradation of persistent organic compounds under neutral pH conditions.

**OBJECTIVES.** The main objective of this study was to verify the generation of the organic radical intermediates and clarify the inducement mechanism of the high utilization efficiency of  $\text{H}_2\text{O}_2$ .

**METHODS.** The dandelion-like TiCuAl-SiO<sub>2</sub> nanospheres (*d*-TiCuAl-SiO<sub>2</sub> Ns) was synthesized via an *in situ* hydrothermal process. The characterization of the catalysts were studied via SEM, TEM, XPS, UV-Vis DRS, EPR and cyclic voltammetry. The analysis methods included HPLC, TOC, ICP-OES and ESR. The reaction process was analyzed by ATR-FTIR and *in situ* Raman.

**RESULTS AND CONCLUSIONS.** The XPS revealed that both  $\text{Cu}^+$  and  $\text{Cu}^{2+}$  existed on the surface of *d*-TiCuAl-SiO<sub>2</sub> Ns and  $\text{Ti}^{4+}$ ,  $\text{Ti}^{3+}$  and  $\text{Ti}^{2+}$  coexisted on the surface of *d*-TiCuAl-SiO<sub>2</sub> Ns with the percentage of 80.7%, 7.4% and 11.9%, respectively. The cyclic voltammetry data suggested that the introduction of Ti into the framework of *d*-TiCuAl-SiO<sub>2</sub> Ns reduced the reduction potential of  $\text{Cu}^{2+}$  and accelerated the electron transfer rate of  $\text{Cu}^+/\text{Cu}^{2+}$ . Therefore, the electrons of the produced  $\bullet\text{R}$  from the contaminant degradation could be successfully transferred to  $\text{Cu}^{2+}$  due to the lower reduction potential of  $\text{Cu}^{2+}$  in the Cu-Ti system, which eventually led to the rapid reduction of  $\text{Cu}^{2+}$  to  $\text{Cu}^+$  on the surface of the catalyst. In addition, the ATR-FTIR and *in situ* Raman results suggested that Ti greatly promoted the rapid contact between  $\text{H}_2\text{O}_2$  and Cu sites on the surface of *d*-TiCuAl-SiO<sub>2</sub> Ns, which was not affected by the pollutants. In this case, *d*-TiCuAl-SiO<sub>2</sub> Ns exhibited an exceptional performance in contaminant degradation. The BPA (25 ppm) could be completely degraded within 60 min and around 70.5% of TOC was degraded within 180 min in the suspension of *d*-TiCuAl-SiO<sub>2</sub> Ns, which is much higher than the 10-30% of TOC removal for BPA degradation in the reported Fenton processes under similar conditions, indicating the excellent activity of *d*-TiCuAl-SiO<sub>2</sub> Ns. After the reaction, no Ti and Al were detected in the solutions and the concentration of total dissolved Cu was only  $0.136 \text{ mg L}^{-1}$ , which was much below the limitation of Cu in EU directives

( $<2 \text{ mg L}^{-1}$ ) and USA regulations ( $<1.3 \text{ mg L}^{-1}$ ). The activity of *d*-TiCuAl-SiO<sub>2</sub> Ns did not decrease after eight successive cycles of degradation testing, which suggested that *d*-TiCuAl-SiO<sub>2</sub> Ns was a stable catalyst for heterogeneous Fenton reactions. In addition, the utilization efficiency of H<sub>2</sub>O<sub>2</sub> was maintained at more than 80% prior to the disappearance of BPA and this value did not decrease sharply after that due to the effect of the generated  $\bullet\text{R}$ , indicating the highly catalytic efficiency of *d*-TiCuAl-SiO<sub>2</sub> Ns.

## **ELECTROSPUN RECTORITE/TiO<sub>2</sub>/POLYMER NANOFIBROUS MATS FOR ADSORPTION OF HEAVY METALS**

***Yingfei Zhan*** and ***Hongbing Deng***  
(Wuhan University, Wuhan, China)

TiO<sub>2</sub> and rectorite (REC) doped cellulose acetate (CA) based nanofibrous mats were fabricated via electrospinning method, a young nanotechnology. These organic-inorganic composite had enhanced specific surface area, mechanical strength and thermal stability. REC/TiO<sub>2</sub>/CA composite nanofibrous mats had good three-dimensional structure just like pure polymer nanofibrous mats, and their fiber diameter range from 200 to 835 nm. The tensile strength of nanofibrous mats increased distinctly with the addition of TiO<sub>2</sub>, which changed from 2.09±0.47 MPa to 4.93±0.72 and 6.75±1.09 MPa. The TGA and DCS curves showed that the thermal stability of nanofibrous mats was enhanced with inorganic doping. And interestingly, the surface areas of TiO<sub>2</sub>/CA and REC/TiO<sub>2</sub>/CA (containing 1% wt REC) composite nanofibrous mats were 1.011 and 3.509 m<sup>2</sup>/g, respectively. Because REC is a kind of layered silicate with super large surface area and interlayer distance. TiO<sub>2</sub>, the adsorption agent, could remarkably improve the adsorption effect of the nanofibrous mats. And the more REC were added, the higher copper adsorption capacities were obtained. With favorable tensile strength and thermal stability, the REC/TiO<sub>2</sub>/CA composite nanofibrous mat can serve as a strong thin film for copper adsorption and obstruction in water.

**MULTIFUNCTIONAL GRAPHENE-BASED NANOCOMPOSITE MODIFIED MEMBRANE  
FILTERS FOR HEAVY METALS AND BACTERIA REMOVAL FROM WATER**

**Yvonne Ligaya F. Musico** and Maria Lourdes P. Dalida  
(University of the Philippines, Diliman, Quezon City, Philippines)  
Debora F. Rodrigues and Catherine M. Santos  
(University of Houston, Houston, TX, USA)

Commercially available membrane filters were modified with different polymers, nanomaterials and nanocomposites, namely, poly(*N*-vinylcarbazole (PVK), graphene (G), poly(*N*-vinylcarbazole)-graphene (PVK-G), graphene oxide (GO), and poly(*N*-vinylcarbazole)-graphene oxide (PVK-GO). The presence of graphene-based nanomaterials on the filter surfaces significantly improved the antibacterial property and heavy metal removal capacity of commercial membrane filters. The desorption process of lead (II) from the modified membrane filters using hydrochloric acid indicates that the filters can be reused. The results show that PVK-GO modified membrane filters consistently exhibited superior antimicrobial properties, metal removal capacity, desorption capacity and reusability among all the graphene-based membrane filters investigated. This research demonstrates that PVK-GO modified membrane filters, along with other graphene-based nanocomposite membrane filters, have efficient antibacterial property and high Pb<sup>2+</sup> removal capacity that can be ideal for water and wastewater treatment applications.

## **STUDY ON THE PHOTOCATALYTIC DEGRADATION OF MICROCYSTINS BY TiO<sub>2</sub> IMMOBILIZED ON FIBERGLASS CLOTH**

Deqiang Chen\*, Yiqun Chen

(Key Laboratory of Integrated Regulation and Resource Development on Shallow Lakes, Ministry of Education, College of Environment, Hohai University, Nanjing, 210098, China)

The TiO<sub>2</sub> immobilized on fiberglass cloth (FGC) was prepared through sol-gel method followed by daubing and coating process to improve the photocatalytic activity and overcome the difficulty of reuse of catalyst and the photodegradation of microcystins-LR (MC-LR) by the prepared catalyst was investigated. The morphology and microstructure of TiO<sub>2</sub> loaded on FGC were characterized via XRD and SEM, respectively. The result revealed that the crystalline structure of immobilized TiO<sub>2</sub> was nearly unchanged compared with commercial titanium dioxide (P25), and the average size of TiO<sub>2</sub> particles was about 15 nm. The process of sol-gel method followed by twice daubing and coating exhibited the relatively high TiO<sub>2</sub> loading amount. The TiO<sub>2</sub>/FGC system can effectively degrade the MC-LR in water under UV light and be effected by pH and initial concentration of MC-LR. The degradation rates of MC-LR reached to 91% and 57% at pH of 4 and 9, respectively. As the initial concentration increased from 50 µg/L to 300 µg/L, the MC-LR removal decreased from 87% to 60%. Addition of Fe<sup>3+</sup> can accelerate the decomposition of MC-LR by TiO<sub>2</sub>/FGC system.

**ELECTROSPUN CARBON NANOFIBERS WITH ZERO VALENT IRON NANOPARTICLES  
(ZVINPs@ECNFs) FOR HEAVY METALS REMEDIATION IN GROUND AND  
WASTEWATER**

Nikhil. R. Mucha, Lifeng Zhang

(Joint School of Nanoscience and Nanoengineering, North Carolina A&T State University, Greensboro,  
NC 27401, USA)

**Ramesh Ravella**, Muchha, R. Reddy

(North Carolina A&T State University, Greensboro, NC 27401, USA)

Rapid worldwide industrialization and population growth is leading to extensive environmental pollution. The discharge of wastewater from commercial and industrial wastes, untreated domestic sewage, and chemical contaminants into surface waters leads to a catastrophe. Industrial activities have led to elevated concentrations of a wide range of heavy metal ions in soil and groundwater. Heavy metal ions such as Chromium Cr (VI), Copper and Nickel are highly toxic. Various methods have been attempted to remove heavy metals from water including filtration, chemical precipitation, electrodeposition etc., but these methods suffer from limitations such as disposal of metal residual sludge, membrane clogging, intensive energy consumption, and high cost. Zero Valent Iron nanoparticles (ZVINPs) possess large capacity for remediating Cu (II) in water owing to their large surface area; high reactivity, non-toxicity, and ease of production. In this study, ZVI nanoparticles (ZVINPs) were synthesized using reduction method followed by deposition on electrospun carbon nanofibers (CNFs) and reached a hierarchical nanostructure, i.e. electrospun carbon nanofibers with surface attached ZVI nanoparticles (ZVINPs@CNFs). Zero Valent Iron (ZVI) nanoparticles possess high capacity for remediating heavy metal ions in water owing to their large surface area, high reactivity, non-toxicity, and ease of production. In this study, ZVI nanoparticles (ZVINPs) were synthesized using reduction method followed by deposition on electrospun carbon nanofibers (CNFs) and reached a hierarchical nanostructure, i.e. electrospun carbon nanofibers with surface attached ZVI nanoparticles (ZVINPs@CNFs). This novel nanomaterial has been evaluated for heavy metal removal from a series of solutions with varying concentrations, ZVI loading and pH of the solution. ZVINPs@CNFs outperformed pure ZVINPs in all cases. 0.04 g ZVINPs@CNFs could remove 94.2% Cu (II) ions from 50 ppm Cu (II) solution at pH 5.5 and 0.04 g of standalone ZVI could remove 60% of Cu(II) from 50 ppm solution at pH 5.5. It is envisioned that ZVINPs@CNFs is going to serve as a novel ZVI based nanomaterial for efficient heavy metal remediation in contaminated groundwater as well as in waste water treatment.

**AIR POLLUTION  
AND  
AIR QUALITY CONTROL**



## **PM<sub>2.5</sub> CHEMICAL CONSTITUENTS AT A RURAL SITE OF AGRA IN INDO-GANGETIC PLAIN: SOURCES AND TRANSPORT**

**Aparna Satsangi**, Nidhi Verma, Anita Lakhani and K. Maharaj Kumari\*

\*Email: maharajkumari.k@rediffmail.com

(Dayalbagh Educational Institute, Agra, UP, India)

**ABSTRACT:** Fine particulate matter (PM<sub>2.5</sub> aerosols) has been observed to adversely affect human health, visibility and climate change. PM<sub>2.5</sub> aerosol samples were collected from January to December 2015 during summer and winter seasons at Sikandarpur, Agra. The samples were analysed for carbonaceous aerosols (Organic and Elemental Carbon- OC and EC) and water soluble ions (F<sup>-</sup>, Cl<sup>-</sup>, NO<sub>3</sub><sup>-</sup>, SO<sub>4</sub><sup>2-</sup>, Na<sup>+</sup>, NH<sub>4</sub><sup>+</sup>, K<sup>+</sup>, Mg<sup>2+</sup> and Ca<sup>2+</sup>). PM<sub>2.5</sub> mass concentrations showed higher concentration during winter (109.6±17.8 µg m<sup>-3</sup>) as compared to summer (73.6±20.2 µg m<sup>-3</sup>). Carbonaceous aerosols (Organic Carbon: OC and Elemental Carbon: EC) and most of the water soluble ionic constituents (NO<sub>3</sub><sup>-</sup>, SO<sub>4</sub><sup>2-</sup>, NH<sub>4</sub><sup>+</sup> and K<sup>+</sup>) also showed enhanced concentrations during winter season while Ca<sup>2+</sup> high concentrations in summer season. The variation in summer and winter concentrations is due to the difference in meteorological parameters and different sources of emissions in both the seasons. This is further supported by air mass back trajectory analysis. In summer, long range transport from north western region was prominent while in winter season localized contributions dominated which could be due to enhanced biomass burning and other anthropogenic activities that occur in winter season to combat cold.

## **INTRODUCTION**

Atmospheric aerosols mainly consist of particles derived from natural sources and have a pronounced impact on global climate system (Poschl, 2005). The enhancement of atmospheric particles in present day due to anthropogenic activities substantially alters the aerosol burden of the atmosphere (Andreae, 2001). Such aerosols are laden with fine particles especially those which have aerodynamic diameter less than 2.5. This fine particulate matter is known to adversely affect human health, visibility and climate change. The direct and indirect effects of aerosol may change the radiation process (Liu et al., 2016). In order to limit the adverse impacts and to develop efficient strategies for air quality control, chemical composition of PM<sub>2.5</sub> needs to be studied. The study of variation of atmospheric composition with transport pathways may also help us to understand the influence of long range transport of pollutants on the atmospheric environment.

Very few studies have been carried out in the Indo-Gangetic plain (IGP) to characterize PM<sub>2.5</sub> aerosol which covers a vast area of Indian subcontinent and experiences extreme variability in the climate over the annual seasonal cycle (Ram et al., 2010b; Pachauri et al., 2013; Rastogi et al., 2014; Srinivas et al., 2016). It is one of the most populated and polluted regions of India due to large scale urbanization, changes in land use, industrial activities, and regional emission sources. These activities contribute a significant fraction to high aerosol loading over the entire region. As Agra lies in the IGP, it is also influenced by its variable climatic conditions.

## **SAMPLING SITE**

Agra lies in the Indo-Gangetic plain. It is in a semi-arid zone adjacent to the Thar Desert. It falls in the subtropical climatic belt and is about 1500 km away from the sea. Its borders touch Rajasthan to its west and south, the district of Firozabad to its East and the district of Mathura to its North. The Mathura oil refinery is about 40 km to the north and is in the upwind direction as winds are mostly from west and

northwest sector. Industrial activities of Agra include rubber processing, engineering and a few ferrous casting industries based on natural gas. It shows extreme variation in temperature with hot summers and chilly winters. May and June are the hottest months having maximum temperature over 40 °C. Dust storms are most frequent in May and can also occur in April and June which last for a period of 30 minutes to 2 hours. The frequency of dust storms in northern and north western India is high with wind speed ranging from 8 – 12 m s<sup>-1</sup>. The increased wind speed causes uplifting and transport of desert dust. These dust storms cause reduced visibility (800 m – 1 km) and severe air pollution. In winter, temperatures may fall as low as 0°C. The year's coldest months are December and January, when temperature averages around 10–15°C. The season frequently experiences heavy fog which disrupts daily life and hinders visibility.

The site under study is a rural area located in the north eastern region of Agra district in Uttar Pradesh, India. This village, Sikandarpur Mustkil (longitude and latitude: 27.26° N and 78.00° E) is about 15 km away from Agra city and does not have any industrial establishment within a diameter of about 10 kms and the major roads are more than 2 kms away from the site. It is surrounded by agricultural fields where mainly rice, wheat and seasonal vegetables are cultivated. Most of the people in the village cook food on *chulhas* using cowdung cakes and wood. The location of sampling site is shown in Figure 1.

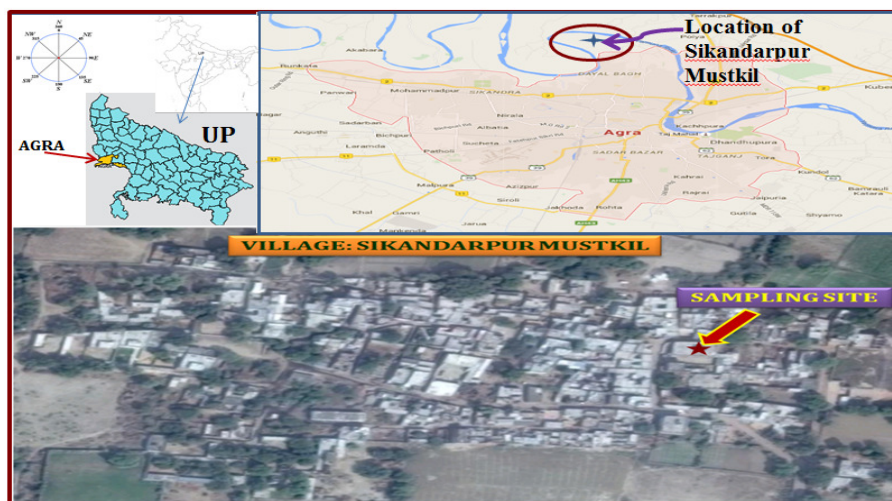


FIGURE 1. Map showing Sampling site

## SAMPLING

In 2015, PM<sub>2.5</sub> aerosol samples were collected during summer (March to June) and winter (January and February) seasons on the roof of a house in Sikandarpur at about 10 m above the ground level. For sample collection, quartz fiber filters (QFF, 47 mm, Pallflex) were weighed and placed in Fine Particulate Sampler (Model: APM 550EL; Make: M/s Envirotech Instruments Private Limited) for 24 hours at a flow rate of 1.0 m<sup>3</sup> hr<sup>-1</sup>. The flow meter of the sampler was calibrated with Air Flow Calibrator with an accuracy of 2%. QFFs were pre-annealed for 3 hours at 900°C in a muffle furnace. These filters were wrapped in aluminium foil within sealed polythene plastic bags before and after sampling. The exposed filters were stored in a refrigerator at ~4°C until extraction for chemical analysis to avoid contamination.

## SAMPLE ANALYSIS

**Gravimetric Analysis of PM<sub>2.5</sub> Mass Concentrations.** PM<sub>2.5</sub> mass concentration was determined by the gravimetric analysis of exposed filters using electronic microbalance. Each filter was stabilized at constant temperature (25±1°C) and relative humidity (50±1%) for 48 hours before and after sampling, and the net particle loading was obtained as PM<sub>2.5</sub> mass in µg m<sup>-3</sup> by the subtraction of pre-sampling weights from post-sampling weights. The typical uncertainty of gravimetric analysis is ±20 µg which represents ±5% of the total aerosol mass of the field samples.

**Carbonaceous Aerosol Analysis.** The OC and EC concentrations were determined using OCEC Laboratory instrument (Model 2000), Sunset Laboratory, Forest Grove, USA using NIOSH-5040 protocol based on thermal-optical transmittance (TOT). A punch of 1.5 cm<sup>2</sup> was placed in the sample boat of OCEC Analyzer. Detailed description of the method employed has been given in Satsangi et al. (2012).

**Chemical Analysis of Water Soluble Inorganic Ions (WSIIs).** Atmospheric aerosols were quantified for their water soluble inorganic ions (WSIIs). One-half of each filter paper was cut and extracted in 10 ml deionised water by ultra-sonication for 45 minutes. The extract was then divided into two parts: one part was treated with chloroform to prevent decomposition and was used for the analysis of anions while another part was preserved with 1% nitric acid (v/v) and used for the cation analysis. The concentration of major ions (F<sup>-</sup>, Cl<sup>-</sup>, NO<sub>3</sub><sup>-</sup>, SO<sub>4</sub><sup>2-</sup>, Na<sup>+</sup>, NH<sub>4</sub><sup>+</sup>, K<sup>+</sup>, Mg<sup>2+</sup> and Ca<sup>2+</sup>) was quantified by ion chromatography using Dionex ICS 1100 Ion Chromatograph system. The extracts were filtered with 0.45 µm PTFE syringe filter (Pall Co. Ltd., USA). Anions were analysed using 6mM NaOH as eluent on the system equipped with guard column (AG11), analytical column (IonPac AS11), and anion self-regenerating suppressor (ASRS 300, 4 mm) while cations were analysed on the system equipped with guard column (CG12A), analytical column (IonPac CS12A), and cation self-regenerating suppressor (CSRS 300, 4 mm) using 20 mM methane sulphonic acid (MSA) as eluent. The recoveries of ions were in the range of 80-90%.

All the reported ion concentrations were corrected for field blanks. Field blanks were the filters brought to the field and installed in the samplers but no air was pumped through the filters. Analytical uncertainties were estimated by calibrating the Dionex ICS 1100 Ion chromatograph with a fresh working standard solution of 1 ppm, prepared from a 1000 ppm stock solution by serial dilution. The variation in peak area was found to be less than 5%. The detection limit for every ion was calculated as three times the standard deviation of the blank. Detection limits (ng m<sup>-3</sup>) of the ionic species were as follows: F<sup>-</sup>: 5.0, Cl<sup>-</sup>: 17.2, NO<sub>3</sub><sup>-</sup>: 9.5, SO<sub>4</sub><sup>2-</sup>: 12.8, Na<sup>+</sup>: 2.5, NH<sub>4</sub><sup>+</sup>: 8.7, K<sup>+</sup>: 16.8, Mg<sup>2+</sup>: 3.2 and Ca<sup>2+</sup>: 7.2.

## TRANSPORT BY AIR MASS TRAJECTORIES

The sources and transport pathways of the chemical components in the atmospheric aerosols may be identified by the simulation of air mass backward trajectory analysis. These air mass back-trajectories were simulated using the National Oceanic and Atmospheric Administration (NOAA) Hybrid Single-Particle Lagrangian Integrated Trajectory (HYSPLIT) model which is based on the GDAS Meteorological Data. Three day back trajectories were calculated at 10:00 hours at a height of 1000 m above the ground level and have been represented in Figure 2. The average mixing height was also calculated every 6 hour for each sampling day by using HYSPLIT model (Draxler and Rolph, 2003).

## METEOROLOGICAL PARAMETERS

Surface meteorological parameters like temperature, relative humidity, wind direction and wind speed were recorded using an automatic weather monitoring system, Envirotech Wind Monitor WM271. The instrument was programmed to collect meteorological data at an interval of 1 minute which was downloaded and computed through software (Metlog, version 1). Average temperature varied from 8.3 to 39.5 °C during the sampling period from January to December 2015. Relative humidity ranged from 16.0 to 94.2% while the wind speed varied from 0.6 to 2.8 m sec<sup>-1</sup> with an average of 1.7 m/sec. The flow of wind direction was mostly from north or northwest and at other times it was observed to originate from southwest and east directions.

## RESULTS

**PM<sub>2.5</sub> Mass Concentrations.** PM<sub>2.5</sub> concentrations varied from 31.5 to 131.5 µg m<sup>-3</sup> with an average of 94.5 µg m<sup>-3</sup>. Almost 90% of the concentrations were above NAAQS standard value of 60 µg m<sup>-3</sup>. PM<sub>2.5</sub> mass showed higher concentration during winter (109.6±17.8 µg m<sup>-3</sup>) as compared to summer (73.6±20.2 µg m<sup>-3</sup>).

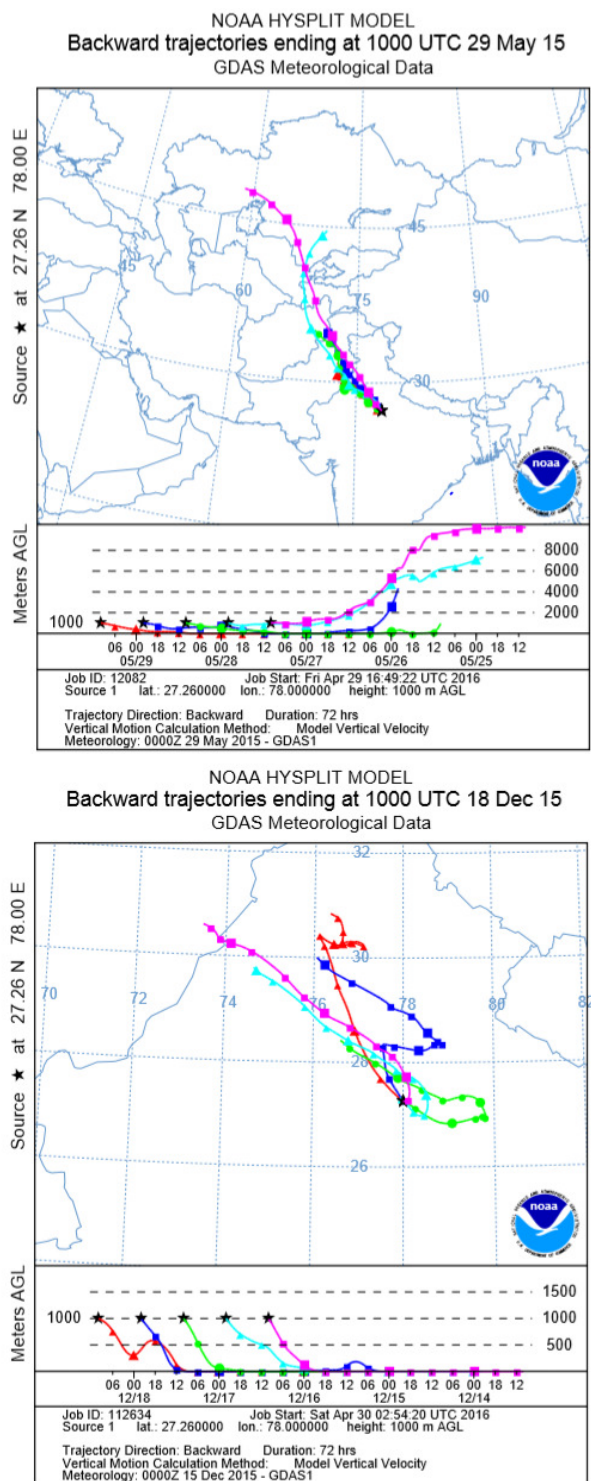


FIGURE 2. Air mass back trajectories at different heights

**Concentrations of Carbonaceous Aerosols.** Average OC and EC concentrations were estimated to be  $27.9 \pm 11.0 \mu\text{g m}^{-3}$  and  $4.6 \pm 2.0 \mu\text{g m}^{-3}$ , respectively. Total carbonaceous aerosols (TCA) accounted for about

45% of total PM<sub>2.5</sub> mass. OC/EC ratios suggest about transformation and sources of carbonaceous aerosols. In the present study, OC/EC ratios were 6.0±1.7.

OC and EC showed distinct seasonal variation in summer and winter seasons. Both OC and EC recorded higher concentrations in winter season as compared to summer. OC and EC concentrations were 18.3 and 3.5 µg m<sup>-3</sup> in summer and 30.6 and 4.9 µg m<sup>-3</sup> in winter season, respectively. OC and EC concentrations are comparable to the values reported from an earlier study, Lal Gadi, a rural site in Agra (OC=30.3 µg m<sup>-3</sup> and EC= 4.0 µg m<sup>-3</sup>; Pachauri et al., 2013). OC/EC ratios were 6.3±1.9 and 5.4±1.2, in winter and summer seasons, respectively. This indicates greater OC and hence, suggests secondary aerosol formation. In addition, burning activities might also be responsible for high ratios.

**Estimation of Secondary Organic Carbon (SOC).** On the basis of EC tracer method, Turpin and Huntzicker (1995) proposed an equation to estimate SOC formation by using the minimum OC/EC ratio.  $SOC = OC_{total} - EC \times (OC/EC)_{min}$

where SOC is the secondary organic carbon, OC<sub>total</sub> is the total OC in PM<sub>2.5</sub>, and (OC/EC)<sub>min</sub> is the minimum ratio observed in all samples. Castro et al. (1999) stated that for primary emissions, OC/EC ratio should be ~2. OC/EC ratios greater than 2.0 indicate secondary aerosol formation. For the estimation of SOC in the present study, lowest OC/EC ratios in the respective seasons were: [(OC/EC)<sub>min</sub> in summer=3.3; (OC/EC)<sub>min</sub> in winter=3.0]. The relative amount of SOC ranged from 20.0 to 47.0% (average=28.0%) in summer and from 32.0 to 65.0% (average=49.0%) of the total organic carbon in winter. This suggests greater SOC formation in winter.

**K<sup>+</sup>/OC and K<sup>+</sup>/EC ratios.** K<sup>+</sup> is considered as the index of biomass burning due to its release during combustion processes. Hence, K<sup>+</sup>/OC and K<sup>+</sup>/EC ratios may be used to characterize whether the emission source of carbonaceous aerosols is biomass burning or fossil fuel combustion. Relatively high K<sup>+</sup>/EC ratios have been reported for biomass burning (range: 0.21-0.46) and low ratios for fossil-fuel emissions (range: 0.025–0.09). This is because fossil-fuel emission produces very little potassium (Yang, He et al., 2005; Yang, Jian et al., 2005). At Agra, average of K<sup>+</sup>/EC and K<sup>+</sup>/OC ratios are 0.56±0.26 and 0.13±0.05 in winter season. These ratios are similar to those observed at Kanpur and Allahabad (Ram and Sarin, 2010a; 2010b) and indicate biomass burning may be the major source of carbonaceous aerosols in winter at Agra. Earlier studies have also reported biomass burning emissions from wood fuel, agriculture-waste and cow dung as a major source of carbonaceous aerosols in India (Venkataraman et al., 2005; Ram and Sarin, 2010a).

**Water Soluble Ionic Constituents.** Average ionic concentrations of major water soluble ions that were analysed have been shown in Table 1. Highest concentrations were of SO<sub>4</sub><sup>2-</sup> followed by Cl<sup>-</sup>, NO<sub>3</sub><sup>-</sup>, NH<sub>4</sub><sup>+</sup>, Na<sup>+</sup>, K<sup>+</sup> and Ca<sup>2+</sup>. F<sup>-</sup> and Mg<sup>2+</sup> showed low concentrations.

**TABLE 1. Average and Seasonal Variation of Water Soluble ions (µg m<sup>-3</sup>)**

	F <sup>-</sup>	Cl <sup>-</sup>	NO <sub>3</sub> <sup>-</sup>	SO <sub>4</sub> <sup>2-</sup>	Na <sup>+</sup>	NH <sub>4</sub> <sup>+</sup>	K <sup>+</sup>	Mg <sup>2+</sup>	Ca <sup>2+</sup>
<b>Winter</b>	0.3	9.6	9.7	10.6	4.2	6.6	5	0.8	3
<b>Summer</b>	0.3	6.5	4.7	5.5	4.4	2.9	3.4	0.6	3.6
<b>Average</b>	0.3	7.4	6.3	8	4.2	4.7	4.2	0.7	3.3

Most of the ions showed high concentrations in winter season as compared to summer. NO<sub>3</sub><sup>-</sup>, SO<sub>4</sub><sup>2-</sup> and NH<sub>4</sub><sup>+</sup> were almost double the concentrations recorded in summer, Cl<sup>-</sup> and K<sup>+</sup> concentrations were also higher as compared to summer concentrations. This also indicates formation of secondary inorganic aerosol in winter. Contrarily, Ca<sup>2+</sup> was higher in summer season. Mg<sup>2+</sup> was also higher in winter while F<sup>-</sup> did not show any seasonal change. Winter/Summer ratio has been depicted in Figure 3.

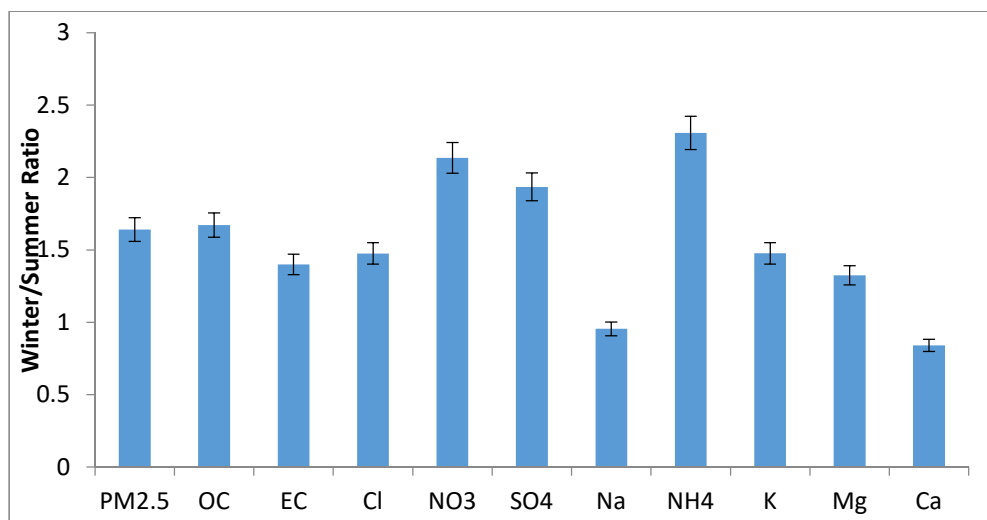


**Figure 3. Winter/Summer ratios of concentrations of selected chemical species.**

WSIS in fine particulate matter is mainly composed of  $\text{NH}_4^+$ ,  $\text{K}^+$ ,  $\text{NO}_3^-$  and  $\text{SO}_4^{2-}$ .  $\text{NH}_4^+$ ,  $\text{NO}_3^-$  and  $\text{SO}_4^{2-}$  are formed from precursor gases through chemical reactions that occur in the atmosphere. Gaseous  $\text{NH}_3$  first reacts with  $\text{H}_2\text{SO}_4$  to form  $(\text{NH}_4)_2\text{SO}_4$  and the rest combines with  $\text{HNO}_3$  to form  $\text{NH}_4\text{NO}_3$ . Molar  $\text{NH}_4^+/\text{SO}_4^{2-}$  ratios suggest formation of  $(\text{NH}_4)_2\text{SO}_4$  when the ratio is 2.0 or more. In the present study, molar ratios are 2.7 which suggest formation of both  $(\text{NH}_4)_2\text{SO}_4$  and  $\text{NH}_4\text{NO}_3$  salts.

**Source Characterization.** The probable reason for the difference in summer and winter seasons could be due to variation of meteorological parameters and different sources of emissions in both the seasons. This is supported by air mass back trajectory analysis. In summer, long range transport from north western region was noticed. High  $\text{Ca}^{2+}$  may be the result of dust events that predominate in May and June. When the wind speed exceeds  $18\text{ km hr}^{-1}$ , dust events occur and bring heaps of sand to the present site causing enhanced concentrations of crustal ions especially,  $\text{Ca}^{2+}$  and  $\text{Na}^+$ . Such an effect was absent in winter season where localized contribution dominated due to enhanced biomass burning and other anthropogenic activities. In order to combat cold, people burn wood, coal and cowdung cakes to keep themselves warm as the temperature becomes very low.  $\text{K}^+$  is an indicator of biomass burning while  $\text{SO}_4^{2-}$  and  $\text{Cl}^-$  indicate coal burning. Concentrations of OC, EC,  $\text{K}^+$ ,  $\text{SO}_4^{2-}$  and  $\text{Cl}^-$  are enhanced in winter due to the dominance of burning activities. Another reason for increase in winter time concentrations of most of the ions may be stagnant meteorological conditions (low wind speed, low mixing height, low temperature and high relative humidity) as compared to summer. Stable atmospheric conditions in winter prolong the residence time of the atmospheric pollutants and strengthen atmospheric oxidation. In summer, long periods of solar radiation favour the dispersion of pollutants due to convective mixing. This is further enhanced by high temperature and low relative humidity during this period. The average mixing height increases which leads to greater dispersion of primary pollutants.

## CONCLUSIONS

The concentrations of carbonaceous and inorganic aerosol components were reported from Sikandarpur, Agra. Average OC and EC concentrations were estimated to be  $27.9 \pm 11.0 \mu\text{g m}^{-3}$  and  $4.6 \pm 2.0 \mu\text{g m}^{-3}$ , respectively. Both OC and EC recorded higher concentrations in winter season as compared to summer. OC/EC ratios suggest secondary aerosol formation. The relative amount of SOC ranged from 20.0 to 47.0% (average=28.0%) in summer and from 32.0 to 65.0% (average=49.0%) of the total organic carbon in winter.  $\text{K}^+/\text{OC}$  and  $\text{K}^+/\text{EC}$  ratios suggest that biomass burning may be the major source of carbonaceous aerosols. Water soluble cations had higher concentrations as compared to anions.  $\text{SO}_4^{2-}$  showed highest concentrations followed by  $\text{Cl}^-$ ,  $\text{NO}_3^-$ ,  $\text{NH}_4^+$ ,  $\text{Na}^+$ ,  $\text{K}^+$  and  $\text{Ca}^{2+}$  while  $\text{F}^-$  and  $\text{Mg}^{2+}$  showed low concentrations.

Molar  $\text{NH}_4^+/\text{SO}_4^{2-}$  ratios of 2.7 suggest formation of both  $(\text{NH}_4)_2\text{SO}_4$  and  $\text{NH}_4\text{NO}_3$  salts. Most of the ions showed high concentrations in winter season as compared to summer. In winter season,  $\text{NO}_3^-$ ,  $\text{SO}_4^{2-}$  and  $\text{NH}_4^+$  were almost double the concentrations recorded in summer. This also suggests secondary aerosol formation in winter season. Results are further supported by air mass back trajectories.

## ACKNOWLEDGEMENTS

This work is financially supported by Women Scientist Scheme (Department of Science and Technology), India. The authors also thank Director of Dayalbagh Educational Institute and Head, Department of Chemistry for providing necessary facilities.

## REFERENCES

- Andreae, M. O. 2001, "The dark side of aerosols", *Nature*, 409: 671–672.
- Andreae, M. O.; Merlet, P. 2001. "Emission of trace gases and aerosols from biomass burning". *Glob. Biogeochem. Cycle*. 15: 955– 966.
- Draxler R.R. and Rolph G.D. 2003. HYSPLIT (HYbrid Single-Particle Lagrangian Integrated Trajectory) Model access via NOAA ARL READY Website (<http://www.arl.noaa.gov/ready/hysplit4.html>) NOAA Air Resources Laboratory Silver Spring MD.
- Liu, S., M. Chen, and Q. Zhuang. 2016. "Direct radiative effects of tropospheric aerosols on changes of global surface soil moisture." *Climatic Change*: 1-13.
- Pachauri T., A. Satsangi, V. Singla, A. Lakhani, K. Maharaj Kumari. 2013. "Characteristics and Sources of Carbonaceous Aerosols in  $\text{PM}_{2.5}$  during Wintertime in Agra, India". *Aer. Air Qual. Res.*, 13: 977–991.
- Pöschl, U. 2005. *Atmospheric Aerosols: Composition, Transformation, Climate and Health Effects*. Angew. Chem. Int. Ed., 44, 7520 – 7540.
- Ram K. and Sarin M.M. 2010a. Spatio-temporal variability in atmospheric abundances of EC, OC and WSOC over Northern India. *J. Aer. Sci.* 41(1): 88–98.
- Ram K. and Sarin M.M. 2010b. "Day-night variability of EC, OC, WSOC and inorganic ions in urban environment of Indo-Gangetic Plain: Implications to secondary aerosol formation". *Atmos. Environ.* 45(2): 460-468.
- Rastogi, N., A. Singh, D. Singh, M.M. Sarin. 2014. "Chemical characteristics of  $\text{PM}_{2.5}$  at a source region of biomass burning emissions: Evidence for secondary aerosol formation". *Environ. Poll.* 184: 563–569.
- Satsangi, A., Tripti Pachauri, Vyoma Singla, Anita Lakhani & K. Maharaj Kumari. 2012. "Organic and Elemental Carbon Aerosols at a Suburban site". *Atmos. Res.* 113: 13–21.
- Srinivas, B., N. Rastogi, M.M. Sarin, A. Singh, D. Singh. 2016. "Mass absorption efficiency of light absorbing organic aerosols from source region of paddy-residue burning emissions in the Indo-Gangetic Plain". *Atmos. Environ.* 125: 360–370. South Asian Aerosols and Anthropogenic Emissions: Regional And Global Climate Implications.
- Venkataraman C, G. Habib, A. Eiguren-Fernandez, A. H. Miguel and S. K. Friedlander. 2005. "Residential biofuels in South Asia: Carbonaceous aerosol emissions and climate impacts". *Science* 307(5714): 1454–1456.
- Yang F., K. He, B. Ye X. Chen, L. Cha, S. H. Cadle et al. 2005. "One-year record of organic and elemental carbon in fine particles in downtown Beijing and Shanghai". *Atmos. Chem. Phys.* 5(1): 1449–1457.
- Yang H., Z. Y. Jian, H. Ho, J. Xu, W. S. Wu, H. W. Chun et al. 2005. "The chemical composition of inorganic and carbonaceous materials in  $\text{PM}_{2.5}$  in Nanjing, China". *Atmos. Environ.* 39(20): 3735–3749.



## **AN INNOVATIVE APPROACH TO USE MODIS AOD DATA FOR PM<sub>2.5</sub> MONITORING**

**Zhiming Yang**, Harris Williams

(North Carolina Central University, Durham, NC 27707, U.S.A)

**ABSTRACT:** Current air particulate matter (PM) 2.5 monitoring in U.S. is limited in spatial resolution due to high operation and maintenance costs. Satellite-based monitoring could serve as an alternative for PM<sub>2.5</sub> monitoring. New aerosol optical depth (AOD) product derived from Moderate Resolution Imaging Spectroradiometer (MODIS) imagery offers a spatial resolution (3km) which is suitable for urban PM<sub>2.5</sub> monitoring. The purpose of this study was to develop a new approach to employ MODIS AOD data for PM<sub>2.5</sub> monitoring in NC. In this study, Terra MODIS AOD data (Collection 6) collected from 2010 to 2012 were downloaded from the United States Geological Survey (USGS) web site. Hourly PM<sub>2.5</sub> data for each PM<sub>2.5</sub> station was downloaded from the EPA AirNow web site. After the extraction of AOD values, a temporal AOD-PM<sub>2.5</sub> correlation was examined for each PM<sub>2.5</sub> station annually. Results suggest that the temporal correlation between MODIS AOD value and ground PM<sub>2.5</sub> concentration was statistically significant for majority of PM<sub>2.5</sub> monitoring stations in NC from 2010 to 2012. This significant AOD-PM<sub>2.5</sub> relationship can be used to develop a practical method for PM<sub>2.5</sub> monitoring using MODIS AOD. The similar approach could also be applied in other states in U.S.

## **INTRODUCTION**

Long-term exposure to high concentrations of fine particulate matter (particles with aerodynamic radius less than 2.5 micrometers, or PM<sub>2.5</sub>) may cause several health issues such as asthma, respiratory infections, lung cancer, and cardiovascular problems (Zanobetti et al. 2009). Current PM) 2.5 monitoring in U.S. is limited in spatial resolution due to high operation and maintenance costs of air monitoring instruments. No PM<sub>2.5</sub> monitoring station exists in many urban areas. Also, the PM<sub>2.5</sub> data collected from fewer fixed monitoring stations in a city does not fully represent the condition of an entire city, especially in a big city. Satellite-based monitoring could serve as an alternative for PM<sub>2.5</sub> monitoring because of its ability to provide more cost-effective observation on spatial pattern and gradient of PM<sub>2.5</sub> than traditional air quality monitoring.

New aerosol optical depth (AOD) product derived from Moderate Resolution Imaging Spectroradiometer (MODIS) imagery offers a spatial resolution (3km) which is suitable for PM<sub>2.5</sub> monitoring in urban areas. There have been several published studies on the evaluation of the new 3km MODIS AOD product (Munchak et al. 2013, Strandgren et al. 2014, Li et al. 2015). Strandgren et al. (2014) reported that the correlation between PM<sub>2.5</sub> and AOD was improved significantly with increasing spatial resolution of the AOD from 10km to 3km while Li et al. (2015) discovered the 3 km AOD had nearly the same correlation with the PM<sub>2.5</sub> as the 10 km AOD.

It was noticed that a large area was covered in aforementioned studies in which spatial-temporal AOD-PM<sub>2.5</sub> correlation was examined. Seldom has there been any study conducted at a station level, which is essential to test the relationship of AOD-PM<sub>2.5</sub> for real applications of MODIS AOD. The purpose of this study is to examine the AOD-PM<sub>2.5</sub> correlation in the state of North Carolina at a station level in order to develop an effective method to use MODIS AOD for PM<sub>2.5</sub> monitoring in NC.

## **MATERIAL AND METHODS**

In this study, Terra MODIS AOD data (Atmosphere level 2 Aerosol Product in HDF format, Collection 6) collected in 2010, 2011 and 2012 were ordered and downloaded from the United States



Geological Survey (USGS) web site. HDF data processing procedures include the reprojection of MODIS AOD data to a universal traverse Mercator (UTM) projection and conversion of file format to Geo TIFF. Hourly PM<sub>2.5</sub> data for each PM<sub>2.5</sub> station in North Carolina was downloaded from the EPA AirNow web site. There were seventeen PM<sub>2.5</sub> stations providing hourly measurements in NC in during 2011-2012 (Fig 1). The latitude and longitude of each station was used to create a shape file containing all hourly PM<sub>2.5</sub> monitoring stations in North Carolina. To match overpass time of Terra satellite, the average of PM<sub>2.5</sub> concentration measured at 11 am and 12 pm for each day was selected for the correlation testing.



Figure 1. Map of study area and PM<sub>2.5</sub> stations

In ArcMap, both the shape file of PM<sub>2.5</sub> stations and downloaded MODIS AOD images were overlaid. AOD value at each PM<sub>2.5</sub> station was extracted using a function tool entitled as “Extract values to points” in ArcTool Box. The attribute table of each newly generated shape file was exported as a txt file and then transferred into Microsoft Excel format. The temporal correlation between MODIS AOD value and ground PM<sub>2.5</sub> concentration was examined for each AirNow PM<sub>2.5</sub> station. The significance of all correlations was tested at 95% confidence level.

## RESULTS AND DISCUSSION

Annual temporal AOD-PM<sub>2.5</sub> correlation was examined for each AirNow PM<sub>2.5</sub> station from 2010 to 2012. The results are shown on Table 1. It can be seen that the temporal correlation between MODIS AOD and ground PM<sub>2.5</sub> was statistically significant for 13 out of 17 stations in NC in 2010. In 2011, temporal correlation between MODIS AOD and ground PM<sub>2.5</sub> was statistically significant for every AirNow PM<sub>2.5</sub> station in NC. In 2012, the temporal correlation between MODIS AOD and ground PM<sub>2.5</sub> was statistically significant for majority of AirNow PM<sub>2.5</sub> stations in NC. Furthermore, each correlation coefficient for the correlation between MODIS AOD and ground PM<sub>2.5</sub> was positive except Millbrook in 2012. If significant, most stations showed medium to strong AOD-PM<sub>2.5</sub> correlations in each year. These results suggested that it is promising to use temporal AOD-PM<sub>2.5</sub> correlation to develop a method used to retrieve PM<sub>2.5</sub> concentration using MODIS AOD data.

Linear equations were developed for stations whose temporal correlations were statically significant for all three years and results are shown Table 2. The slope and intercept of linear equations ranged 0.0079-0.0309 and 1.3689-6.7012 respectively for PM<sub>2.5</sub> stations in NC. In the same year, each station has different slope and intercept. Also, no spatial pattern was observed in slope and intercept. These results suggest each PM<sub>2.5</sub> station may have its own unique AOD-PM<sub>2.5</sub> correlation in NC. This explains why a spatial correlation between AOD and PM<sub>2.5</sub> was not significant for almost all days in which both AOD and PM<sub>2.5</sub> were sampled. It is likely that mixed AOD values from different stations would lead to failure in setting up significant spatial AOD-PM<sub>2.5</sub> correlation in NC.

**TABLE 1. Annual temporal correlation coefficients of AOD-PM2.5 from 2010 to 2012**

Station Name	2010	2010	2012
BRDED	0.3127	0.3753*	0.2295
Brryson	0.6123*	0.6281*	0.3445*
Clemmons Middle	0.8190*	0.6083*	0.5688*
Durham Armory	0.8205	0.8496*	0.2687
Garinger	0.6247*	0.7949*	0.8887*
Grier Middle	0.7222*	0.7704*	0.1657
Hattieaven	0.7942*	0.5488*	0.8591*
Hickory	0.7912*	0.6137*	0.8819*
Hopedale	0.9192*	0.7530*	0.3760
Leggett	N/A	0.7855*	0.6553*
Lwattowr	0.8827*	0.5809*	0.2692
Marion	0.5193*	0.8692*	0.7459*
Mendnhal	0.3655	0.7333*	0.5655
Millbrook NCore	0.8561*	0.4570*	-0.7785
Montclair	0.7967*	0.8184*	0.8596*
Rockwell	0.7558*	0.7694*	0.6685*
W Owen Sch	0.1524	0.4558*	0.2324

**TABLE 2. Linear equations for some AirNow PM2.5 stations in NC**

Station Name	2010	2011	2012
BRYSON	$PM_{2.5} = 0.0302AOD + 6.2954$	$PM_{2.5} = 0.026 AOD + 5.0558$	$PM_{2.5} = 0.0079AOD + 5.4894$
CLEMMONS	$PM_{2.5} = 0.019AOD + 5.6951$	$PM_{2.5} = 0.0157AOD + 4.1755$	$PM_{2.5} = 0.0134AOD + 4.3906$
GARINGER	$PM_{2.5} = 0.0206AOD + 5.1603$	$PM_{2.5} = 0.0222AOD + 1.9847$	$PM_{2.5} = 0.0235AOD + 2.24$
HATTIEAVEN	$PM_{2.5} = 0.0196AOD + 5.3961$	$PM_{2.5} = 0.0172AOD + 1.8613$	$PM_{2.5} = 0.0192AOD + 1.6052$
HICKORY	$PM_{2.5} = 0.0117AOD + 6.7012$	$PM_{2.5} = 0.0156AOD + 4.5604$	$PM_{2.5} = 0.0148AOD + 4.3314$
MARION	$PM_{2.5} = 0.0128AOD + 6.5031$	$PM_{2.5} = 0.0283AOD + 2.1746$	$PM_{2.5} = 0.0168AOD + 2.2938$
MONTCLAIRE	$PM_{2.5} = 0.0309AOD + 2.4352$	$PM_{2.5} = 0.0269AOD + 1.7902$	$PM_{2.5} = 0.0307AOD + 1.3689$
ROCKWELL	$PM_{2.5} = 0.0373AOD + 4.1406$	$PM_{2.5} = 0.0213AOD + 3.9573$	$PM_{2.5} = 0.0211AOD + 3.2748$

The relationship between ground-level PM2.5 and satellite-based AOD is highly associated with optical properties of local aerosols and their vertical distribution (van Donkelaar et al. 2010). In past decade,

many researchers have successfully improved correlations between MODIS AOD and ground PM<sub>2.5</sub> by incorporating vertical distribution (Boyouk et al. 2010; Chu et al. 2013) or inclusion of meteorological parameters (Koelemeijer et al. 2006; Gupta and Christopher 2009). However, significant amount of money and time are needed to develop a reliable method for the real application of MODIS AOD. The method based on temporal correlations might be more practicable to develop a method for PM<sub>2.5</sub> monitoring.

For reliable PM<sub>2.5</sub> monitoring by the MODIS satellite in NC, it is necessary to examine the number of days during which both MODIS AOD and PM<sub>2.5</sub> were sampled at each station. The results were summarized in Table 4, 5 and 6. In 2010, both AOD and PM<sub>2.5</sub> were sampled for less than six days per month and thirty one days per year for every PM<sub>2.5</sub> station. In 2011, with the exception of November and December, both AOD and PM<sub>2.5</sub> were sampled for less than five days per month and sixty days per year for every PM<sub>2.5</sub> station. In 2012, both AOD and PM<sub>2.5</sub> were sampled for less than six days per month and thirty seven days per year for every PM<sub>2.5</sub> station.

According to results above, there were significant number of days in which both AOD and PM were not sampled for almost all stations in all three years. In most cases above, AOD value did not exist while PM<sub>2.5</sub> value was available for each PM<sub>2.5</sub> station. This is a well-known “low sampling” problem mentioned in the literature (Gupta and Christopher 2008; Christopher and Gupta 2010). It was caused by the lower number of cloud-free days in the state of North Carolina from 2010 to 2012 since MODIS AOD values were only available during cloud-free days. There are usually a low number of cloud-free days (average 213 sunny days per year) in any given year in NC. Thus it is practicable to use MODIS AOD for PM<sub>2.5</sub> monitoring at a weekly level.

**TABLE 3. Number of days in which both AOD and PM<sub>2.5</sub> existed in North Carolina in 2010**

<b>Name</b>	<b>Jan</b>	<b>Feb</b>	<b>Mar</b>	<b>Apr</b>	<b>May</b>	<b>Jun</b>	<b>Jul</b>	<b>Aug</b>	<b>Sep</b>	<b>Oct</b>	<b>Nov</b>	<b>Dec</b>	<b>Total</b>
BDED	0	0	3	5	0	0	3	1	4	3	5	1	25
Bryson	4	0	3	3	0	0	4	4	3	1	3	0	25
Clemmons	2	2	2	2	2	2	2	2	5	2	6	2	31
Durham Arm	0	1	1	0	0	0	0	0	0	0	1	2	5
Grainger	3	1	2	5	1	4	3	1	2	3	4	2	31
Grier Middle	3	0	4	3	0	1	2	1	0	1	1	2	18
Hattieaven	2	0	2	3	1	0	2	1	2	0	4	1	18
Hickory	1	0	0	1	0	1	1	1	2	2	0	3	12
Hopedale	2	1	1	1	0	0	1	1	0	4	5	2	18
Lwattowr	0	2	1	1	0	0	1	0	1	2	1	1	10
Marion	0	1	2	0	0	2	3	2	3	0	4	1	18
Mendnhal	1	1	1	2	0	0	2	1	1	1	2	0	12
Millbrook	0	1	1	1	0	1	1	0	2	0	2	2	11
Montclair	3	1	3	1	2	0	3	0	2	1	2	1	19
Rockwell	3	2	3	3	1	2	2	1	4	3	3	2	29
W Owen sch	0	1	1	2	1	0	0	1	1	2	2	2	13

To be effective in PM<sub>2.5</sub> monitoring, the use of station-specific temporal correlation is an alternative approach to develop the application of MODIS AOD for PM<sub>2.5</sub> monitoring. The key step is to develop a reliable equation based on temporal AOD-PM<sub>2.5</sub> correlation for each PM<sub>2.5</sub> station. Also it is feasible to fill spatial PM<sub>2.5</sub> gaps based on temporal correlations in NC. For locations near current AirNow PM<sub>2.5</sub> stations, PM<sub>2.5</sub> concentrations could be retrieved from their corresponding AOD values using the linear equation developed for a nearby AirNow PM<sub>2.5</sub> station. For a location which is far from any existing AirNow PM<sub>2.5</sub> station, its PM<sub>2.5</sub> concentration could be interpolated from PM<sub>2.5</sub> concentrations at surrounding locations using various spatial interpolation techniques such as Kriging

**TABLE 4. Number of days in which both AOD and PM2.5 existed in North Carolina in 2011**

Name	Jan	Feb	Mar	Apr	May	Jun	Jul	Aug	Sep	Oct	Nov	Dec	Total
BDED	2	1	2	3	1	1	2	1	2	3	4	11	33
Bryson	1	1	4	2	2	3	5	7	3	5	4	6	43
Clemmons	2	2	2	4	5	4	3	4	3	5	8	7	49
Durham Armory	2	0	0	1	0	1	0	0	2	0	3	9	19
Garinger	4	1	3	2	1	3	0	3	2	5	7	4	36
Grier Middle	2	1	1	1	2	2	2	2	1	4	4	6	28
Hattieaven	2	2	1	3	3	3	1	3	3	1	7	8	39
Hickory	0	2	1	0	0	1	0	0	0	1	5	6	18
Hopedale	3	0	2	1	0	3	0	1	2	2	9	10	35
Leggett	0	0	0	0	0	0	2	0	3	4	7	13	30
Lwattowr	0	0	1	0	2	1	0	1	1	1	4	8	19
Marion	2	1	3	1	0	4	0	1	2	5	2	9	31
Mendnhal	2	1	2	2	2	0	1	3	1	0	4	11	27
Millbrook	3	0	1	1	0	0	1	1	3	0	5	7	22
Montclair	1	0	2	2	0	1	1	3	1	2	5	7	25
Rockwell	4	1	3	5	2	4	3	4	3	6	9	11	56
W Owen sch	3	1	0	0	2	1	0	0	0	3	10	10	25

**TABLE 5. Number of days in which both AOD and PM2.5 existed in North Carolina in 2012**

Name	Jan	Feb	Mar	Apr	May	Jun	Jul	Aug	Sep	Oct	Nov	Dec	Total
BDED	1	1	1	0	0	1	2	1	1	2	1	0	11
Bryson	0	4	3	1	4	5	2	4	2	5	5	0	35
Clemmons	3	2	2	4	2	4	4	2	3	5	3	3	37
Durham Armory	1	1	0	0	1	0	1	0	1	0	1	0	6
Garinger	2	0	0	0	0	1	3	0	1	3	1	2	13
Grier Middle	1	2	1	0	3	0	1	0	3	1	3	2	17
Hattieaven	1	2	1	0	1	1	1	1	2	3	2	0	15
Hickory	1	1	2	0	2	0	1	0	0	0	0	1	8
Hopedale	2	2	3	2	0	0	0	0	0	1	1	1	12
Leggett	5	3	5	3	0	2	5	3	4	2	2	3	37
Lwattowr	0	0	1	1	0	0	1	0	1	2	2	2	10
Marion	3	2	1	3	2	2	1	1	0	1	1	2	19
Mendnhal	1	2	2	1	1	1	1	1	1	2	2	1	16
Millbrook	0	0	1	1	1	0	0	0	0	0	1	0	4
Montclair	1	2	1	2	1	2	1	0	3	0	1	1	15
Rockwell	3	4	1	3	3	2	3	0	4	2	4	3	32
W Owen sch	1	0	1	1	1	1	1	0	1	1	2	0	10

Despite the limitations of this work, our findings revealed that there is an alternative approach to develop a practical method to use MODIS AOD data for PM2.5 monitoring. This new way would help in better understanding the characteristics of AOD-PM2.5 correlation at city and state level and its applications from an innovative perspective. Further studies are needed to develop a robust retrieval AOD-PM2.5 equation for each AirNow PM2.5 station in North Carolina for a real application of MODIS AOD data.

## CONCLUSIONS

Our results show that no significant spatial correlations between MODIS AOD at daily level were found in the state of North Carolina in 2010, 2011 and 2012. But there was statistically significant temporal correlation between MODIS AOD values and ground PM<sub>2.5</sub> concentration for most stations from 2010 to 2012. This significant temporal correlation can be used to develop a practical method for PM<sub>2.5</sub> monitoring using MODIS AOD in NC and other states in the United States.

## REFERENCES

- Boyouk, N., J. F. Leon, H. Delbarre, T. Podvin and C. Deroo. 2010. Impact of the mixing boundary layer on the relationship between PM<sub>2.5</sub> and aerosol optical thickness. *J Atmos. Environ.* 44: 271-277.
- Christopher, S.A. and P. Gupta. 2010. Satellite remote sensing of particulate matter air quality: the cloud-cover problem. *J Air Waste Manag Assoc.* 60(5): 596-602.
- Chu, D. A., T. Tsa, J. Chen, S. Chang, Y. Jeng, W. Chiang. and N. Lin. 2013. Interpreting aerosol lidar profiles to better estimate surface PM<sub>2.5</sub> for columnar AOD measurements. *Atmospheric Environment* 79: 172-187.
- Gupta, P. and S.A. Christopher. 2009. Particulate matter air quality assessment using integrated surface, satellite, and meteorological products: multiple regression approach. *J. Geophys. Res.* 114, D14205. <http://dx.doi.org/10.1029/2008JD011496>.
- Koelemeijer RBA, C.D. Homan, and J. Matthijsen. 2006. Comparison of spatial and temporal variations of aerosol optical thickness and particulate matter over Europe. *Atmos Environ* 40:5304; doi:10.1016/j.atmosenv.2006.04.044
- Li, R., J. Gong, L. Chen, and Z. Wang. 2015. Estimating Ground-Level PM<sub>2.5</sub> using fine-resolution satellite data in the megacity of Beijing, China. *Aerosol and Air Quality Research* 15 1347–1356.
- Munchak, L. A., R.C. Levy, S. Mattoo, L.A. Remer, B.N. Holben, J.S. Schafer, C. A. Hostetler, and R.A. Ferrare. 2013. MODIS 3 km aerosol product: applications over land in an urban/suburban region, *Atmos. Meas. Tech.*, 6, 1747–1759, doi:10.5194/amt-6-1747-2013.
- Strandgren, J., L. Mei, M. Vountas, J.P. Burrows, A. Lyapustin, and Y. Wang. Study of satellite retrieved aerosol optical depth spatial resolution effect on particulate matter concentration prediction. *Atmos. Chem. Phys. Discuss.*, 14, 25869-25899, doi:10.5194/acpd-14-25869-2014.
- van Donkelaar A, R.V. Martin, M. Braue, R. Kahn, R. Levy, and C. Verduzco, et al. 2010. Global estimates of ambient fine particulate matter concentrations from satellite-based aerosol optical depth: development and application. *Environ Health Perspect* 118:847–855.
- Zanobetti, A., N. Franklin, P. Koutrakis and J. Schwartz. 2009. Fine particulate air pollution and its components in association with cause-specific emergency admissions. *Environmental Health* 8:58–70.

## **STUDY ON AEROSOL FORMATION PROPERTIES IN AMMONIA-BASED WFGD PROCESSES**

**Huang Rongting**, Pan Danping, and Yang Linjun  
(Southeast University, Nanjing, China)

An ammonia-based wet flue gas desulfurization (WFGD) experimental platform was built to simulate separately the two different aerosol formation processes in the ammonia WFGD system of the heterogeneous reaction mechanism and the entrainment mechanism. The concentrations, the size distributions, the morphology features and the chemical composition of the aerosols formed after WFGD system were tested and investigated with the electrical low pressure impactor (ELPI), the pollutant PM sampler, the field emission scanning electron microscope (FESEM), and the aerosol mass spectrometer (AMS). The comparison was made of the numerical concentration size distributions of aerosols generated under the two formation mechanisms and the typical ammonia WFGD process. The results showed that the heterogeneous reaction mechanism is the dominating one of the two aerosol formation mechanisms in ammonia-based WFGD, which produced the majority of the aerosols emitted from the scrubber, which, if counted in numerical concentration, were mainly submicron particles, with the chemical ingredients consisting mainly of sulfates and ammonium and the size distribution based on numerical concentration being a bimodal one. While the entrainment mechanism had less influences on the aerosol formation in the ammonia WFGD, the aerosols generated under which condition were much larger than those formed under the heterogeneous reaction mechanism. Great differences were found between the aerosols formed under the two mechanisms.

## AIR FLOW SIMULATION AROUND AIRCRAFT

Jianfeng Liu<sup>\*1</sup>, Baoqing Wang<sup>2</sup>, Ronghui Chen<sup>3</sup>, and Zihui Ren<sup>4</sup>

<sup>1</sup>nkliujf@126.com, <sup>2</sup>wangbaoqing@nankai.edu.cn, <sup>3</sup>361970816@qq.com, <sup>4</sup>renzihuink@163.com  
(College of Environmental Science and Engineering, Nankai University, Tianjin 300071, China)

**ABSTRACT:** Ambient environmental quality measurement by using aircraft becomes more and more important. In this paper, the air flow around aircraft is studied and analyzed through CFD numerical simulation method. The results show that the airflow and pressure field around aircraft is obvious different in different position. The suitable position of the instruments on the aircraft can be found by simulation. So, It is suggested that CFD simulation can be useful for obtaining the optimum position of aerosol sampling inlet.

**Keywords:** Flow analysis; Aircraft; CFD simulation

## INTRODUCTION

An aerosol is defined as a suspension of liquid or solid particles in a gas. In reviewing aerosol measurement it is important to remember the gas. Average particle compositions vary with size, time, and location, and the bulk compositions of individual particles of a given size also vary significantly, reflecting the particles' diverse origins and atmospheric processing[1]. Air quality in China is getting worse following the economic expansion, which has continued to increase in the past decades. Around 20-30% of carbonaceous aerosols in the global atmosphere are generated in China[2]. These aerosols, together with the soil dusts originated from the deserts in the north/west regions, are occasionally transported to the western United States across the North Pacific Ocean[3]. A great variety of measurement systems, ranging from bulk filters to particle sizing instruments, are used on aircraft to examine ambient aerosols. For accuracy of aircraft measurements, a more fundamental question concerns the location of the instruments on the aircraft[4-5]. In this study, the suitable location will be discussed.

## DESCRIPTION OF THE MODEL

In this study, the sampling instrument is designed to be carried by an aircraft which cruises with a speed of 180~220km/h at 1~3km altitude. A photograph of aircraft shown in Fig. 1. Its length of wing is 17.24 m, the length and height is 14.86 m and 5.58 m. Its maximum flying height is 7000 m, maximum velocity is 292 km/h.

A computational fluid dynamics (CFD) program, FLUENT 14.0 (ANSYS Inc.), was used to air flow around aircraft. As a professional pre-processors software, ICEMCFD can provide a high efficient and reliable analysis model for CAE software. This research adopts the RANS (Reynolds Averaged Navier-Stokes) equation combined with the RNG  $k-\epsilon$  model, which is the most appropriate model that characterizes the flow field around aircraft. Numerical simulation of the airflow was performed with CFD assuming (1) the flow is incompressible, isothermal and turbulent, (2) the mean flow is symmetric about the centerline of the system and (3) a steady-state solution exists.

Fig. 2 shows computational domain and boundary conditions of aircraft. For analyzing an external flow, it is necessary to have a computational domain as large as possible, in order to ignore upstream and downstream effects. Considering these effects, 10 times of length of extra space is provided for the aircraft, and 8 times of height and width of aircraft. Three dimension surface mesh of aircraft shown Fig. 3.



FIG.1. The Photograph of Aircraft

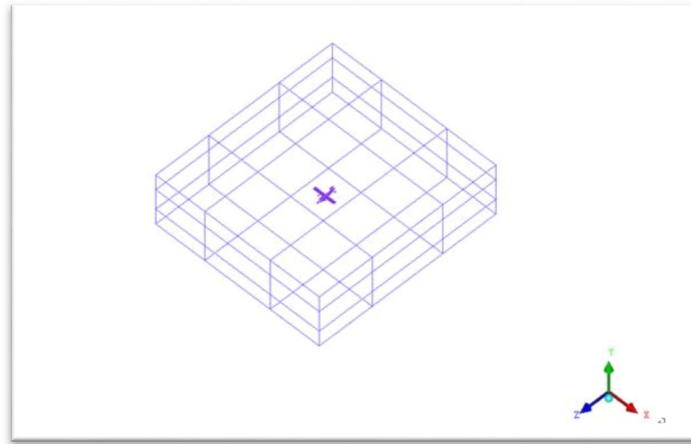


FIG. 2. Computational Domain and Boundary Conditons of Aircraft



FIG. 3. Three Dimention Surface Mesh of Aircraft

Longitudinal profile velocity and pressure distribution of aircraft surface shown in Fig. 4 and Fig.5. From Fig.4 and Fig.5, it is obviously different for flow fields around various shapes at reasonable distances



from the boundary and away from regions of high curvature, the flow fields are determined primarily by the overall radius of the cylindrical portion of the fuselage. It can be seen that the lifting of a finite wing generates line vortices which are shed from the trailing edge of the wing. Due to different curvature around aircraft, the depletion zone and enhancement zone will generated. The steady flow zone located in the bottom of the aircraft. So it is suitable position mounted the sampling instruments.

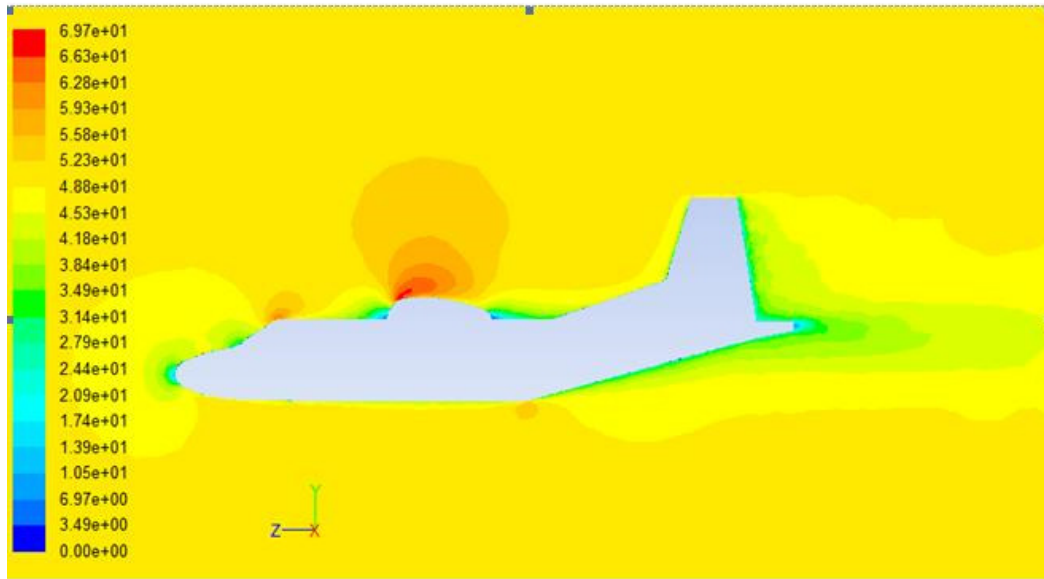


FIG. 4. Longitudinal Profile Velocity Distribution of Aircraft Surface

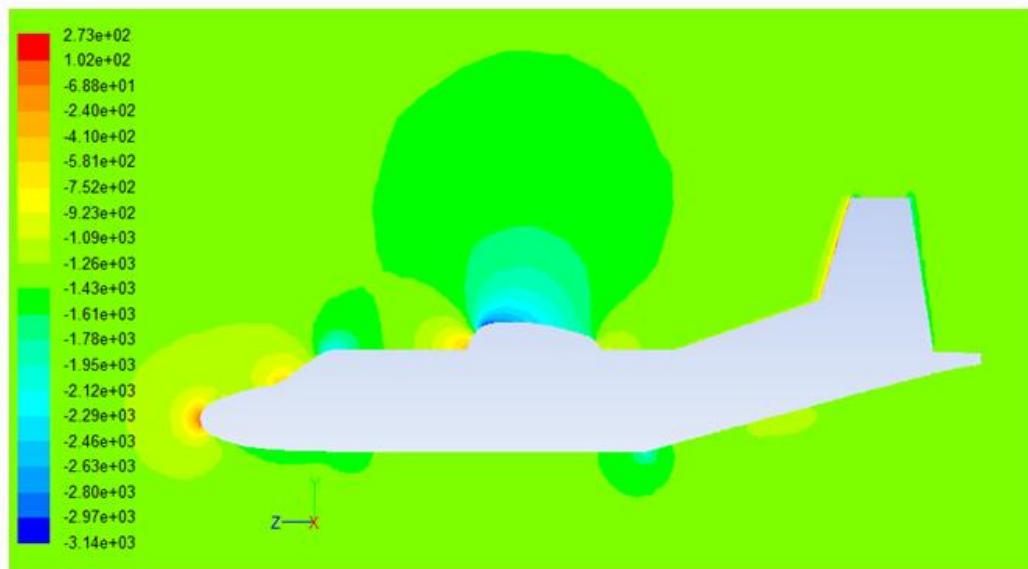


FIG. 5. Longitudinal Profile Pressure Distribution of Aircraft Surface

## CONCLUSIONS

In this paper, it is shown that the dominant features of the flow around shapes similar to aircraft fuselages can be obtained using CFD simulation applied to flows around aircraft. The flow of the bottom around aircraft is steady flow, So it is suitable position mounted the sampling instruments in order to avoid

flow disturbance around aircraft. At the same time, particles trajectory will be simulated by CFD to determined the depletion zone and enhancement zone around aircraft.

#### **ACKNOWLEDGMENT**

This work was financially supported by National major scientific instrument equipment development special (2011YQ060111).

#### **REFERENCES**

- [1] Peter H. McMurry. "A review of atmospheric aerosol measurements." *Atmospheric Environment* 34 (2000) 1959-1999.
- [2] Gehui Wang et al.. "Aircraft Measurement of Organic Aerosols over China." *Environ. Sci. Technol.* 41 (2007) 3115-3120.
- [3] Wilkening, K. E. et al.. "Trans-Pacific air pollution." *Science* 290 (2000): 65-67.
- [4] W.D. King. "Air Flow and Particle Trajectories around Aircraft Fuselages. I:Theory." *Journal of Atmospheric and Ocean Technology* 1(1984) 5-13.
- [5] B. Dix et al. "Airborne multi-axis DOAS measurements of atmospheric trace gases on CARIBIC long-distance flights." *Atmos. Meas. Tech.* 2(2009) 639–652.

## **BLACK CARBON AND SIZE-RESOLVED PARTICLE NUMBER CONCENTRATIONS DURING OPEN-FIELD BURNING OF CORN STRAW**

***Yu-Hsiang Cheng*** and Li-Sing Yang  
(Ming Chi University of Technology, New Taipei, Taiwan)

**ABSTRACT:** Information on the effect of open-field burning of agricultural residues on ambient black carbon (BC) mass and particle number concentrations is scarce. In this study, the real-time variation of BC mass and size-resolved particle number concentrations was monitored during a period of corn straw burning at a rural site to understand the effect of such open-field burning on short-term air quality. The measurement results showed that the hourly BC mass, total particle number, and ultrafine particle (UFP) number concentrations during the corn straw burning period could reach  $3775 \text{ ng m}^{-3}$ ,  $3.99 \times 10^4 \text{ \# cm}^{-3}$ , and  $2.03 \times 10^4 \text{ \# cm}^{-3}$ , respectively, which were 3.2, 5.3, and 3.8 times the reference values at the site, respectively. Field measurements showed that the hourly absorption Ångström exponent value during the corn straw burning period was 2.0. Furthermore, the measurement results showed a single-mode pattern for the particle number size distribution, and the dominant mode corresponded to 100 nm. Additionally, the measurement results suggested that most of the BC mass concentrations in fresh aerosols during the corn straw burning period were significantly and positively correlated with particle number concentrations in the size range of 56–320 nm.

## **INTRODUCTION**

A large amount of PM is produced during uncontrolled burning of agricultural residues, immediately degrading the air quality in the surrounding areas and causing acute symptoms in people with chronic respiratory conditions (Ryu et al., 2007; Zhang et al., 2011). Epidemiological studies have consistently reported that short-term exposure to high concentrations of PM can increase cardiovascular morbidity and mortality (Pope et al., 2011; Rice et al., 2013). Therefore, short-term air pollution episodes resulting from open-field burning of agricultural residues could pose a serious public health hazard.

Particularly, toxicological studies have suggested that ultrafine particles (UFPs) may be more harmful to health than large particles are because small particles have a considerably larger adsorbed or condensed surface area than large particles with the same mass do and can be deposited in the alveoli, where they interact with epithelial cells (Oberdörster et al., 2005). Additionally, black carbon (BC) is a major constituent of atmospheric aerosols, and it has an appreciable impact on global climate change, apart from adversely affecting human health (Rich et al., 2005; Jacobson, 2010). Therefore, the risk to human health from exposure to high BC mass and high particle number concentrations within a short period could be more serious than that from exposure to high  $\text{PM}_{2.5}$  concentrations.

However, information on the effect of open-field burning of agricultural residues on ambient BC mass and particle number concentrations is scarce. In this study, to understand the effect of open-field burning on short-term air quality, real-time variations of the BC mass and size-resolved particle number concentrations were monitored before and during a corn straw burning episode at a rural site. Correlations between the BC mass and size-resolved particle number concentrations during the episode were investigated. Moreover, the particle number size distribution and absorption Ångström exponent were determined for obtaining the characteristics of aerosol emissions from the corn straw open-field burning. The results can be used to address public health concerns and as a reference for managing similar episodes of open-field burning of agricultural residues.

## **MATERIALS AND METHODS**

In this study, the monitoring location was in the downtown area of Yanshui in southern Taiwan. There are a lot of corn fields in the vicinity of this small town. In this study, the monitoring instruments were set up on the rooftop of a building of Yanshui Junior High School (23°19'17.5"N, 120°15'50.3"E). Two Rack Mount Aethalometer instruments (Model AE31; Magee Scientific Corp., Berkeley, CA, USA) were used to measure the BC mass concentrations in parallel at two different aerosol sampling flow rates. The instruments can be used to evaluate BC mass concentrations at seven wavelengths: 370, 470, 520, 590, 660, 880, and 950 nm. Furthermore, a correction algorithm developed by Cheng and Yang (2015) was applied for minimizing artifacts in determining BC mass concentrations. In the current study, the BC mass concentrations determined at the wavelengths of 370 and 880 nm were treated as ultraviolet BC (UVBC) and BC, respectively, to distinguish particles bound to ultraviolet-absorbing organic compounds (Sandradewi et al., 2008). Additionally, a scanning mobility particle sizer (SMPS) spectrometer (TSI Model 3938; TSI, Inc., Shoreview, MN, USA) was employed to measure particle number size distributions of particles with diameters in the range of 13–750 nm. Local meteorological data were recorded using a Vantage Pro2™ weather station (Davis Instruments Corp., Hayward, CA, USA). The instruments were operated continuously from February 11 to 19, 2014, and the logging interval for all measurements was set at 5 min.

During the whole monitoring period, a remarkable open-field burning of corn straw upwind of the monitoring location was observed between 17:00 and 19:00 (2 h) on February 16, 2014. During this period, the ambient air was filled with smoke. Therefore, the data obtained during this period were considered to correspond to a short-term air pollution episode for agricultural residue burning (episode period). Furthermore, the data monitored at the same time and for the same duration on February 12 (Wednesday), 2014, were considered to represent the reference air quality status (nonepisode period) for this monitoring site because the wind speed and principal wind direction on this day were similar to those on February 16, 2014.

## RESULTS AND DISCUSSION

During the whole monitoring period, the average wind speed, temperature, and relative humidity were 1.7 m s<sup>-1</sup>, 15.9 °C, and 71.4%, respectively. Despite the irregular wind direction patterns on February 17 and 18, 2014, the principal wind direction was NNW–NNE. The daily average wind speed, principal wind direction, temperature, and relative humidity were 1.5 m s<sup>-1</sup>, NNW–NNE, 14.3 °C, and 68.9%, respectively, on February 12, 2014. On February 16, 2014, the daily average wind speed, principal wind direction, temperature, and relative humidity were 1.2 m s<sup>-1</sup>, NW–NE, 17.8 °C, and 73.2%, respectively. During open-field burning of corn straw (episode duration), the 5-min wind speed was between 0.9 and 1.8 m s<sup>-1</sup> (1.1 m s<sup>-1</sup> on average), and the principal wind direction was between NW and N.

The average UVBC and BC mass concentrations were 1652 and 1345 ng m<sup>-3</sup>, respectively, and the interquartile ranges were 799–1921 and 681–1641 ng m<sup>-3</sup> for UVBC and BC mass concentrations, respectively, during the whole monitoring period. Figure 1 shows the diurnal variations of the 5-min and 1-h UVBC and BC concentrations at the monitoring site on February 12 and 16, 2014. The daily average BC mass concentrations on February 12 and 16, 2014, were 1074 and 2013 ng m<sup>-3</sup>, respectively. The daily average BC mass concentration on February 16, 2014, was significantly higher than that on February 12, 2014, because obvious open-field burning was performed on February 16, 2014.

During the episode, the 5-min UVBC concentration can reach 47500 ng m<sup>-3</sup>, and remarkably, it is approximately three times the BC concentration, suggesting that ambient particles in this period were bound to ultraviolet-absorbing organic compounds, which were abundant. The hourly UVBC concentration during the episode increased to 11932 ng m<sup>-3</sup>, which was 8.3 times the value in the nonepisode period. The hourly BC concentration during the episode could increase to 3775 ng m<sup>-3</sup>, which was 3.2 times the value in the nonepisode period.

The absorption Ångström exponent has been used as an index for determining the type of BC emission source (Sandradewi et al., 2008). In this study, the daily average absorption Ångström exponent value for February 12, 2014 was 1.2, which was same as the value on February 16, 2014. The BC concentrations at this rural monitoring site on normal days were lower, and the measurement results

indicated that vehicular traffic was the main source of BC aerosols. Nevertheless, the hourly absorption Ångström exponent value during the episode was 2.0, implying that the source of BC aerosols during the episode was related to agricultural residue burning.

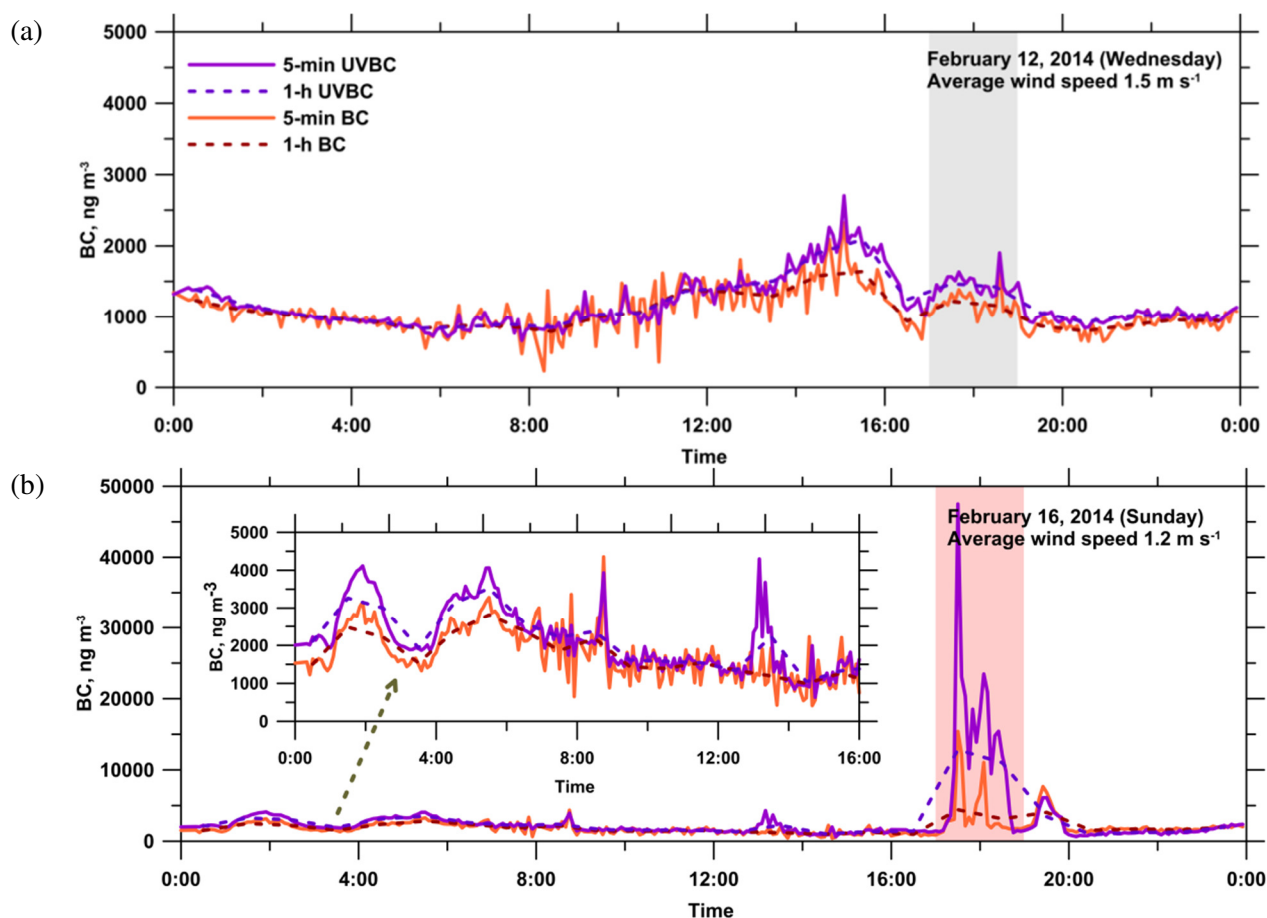


**FIGURE 1.** Diurnal variations of 5-min and 1-h UVBC and BC concentrations at the monitoring site on (a) February 12, 2014 and (b) February 16, 2014.

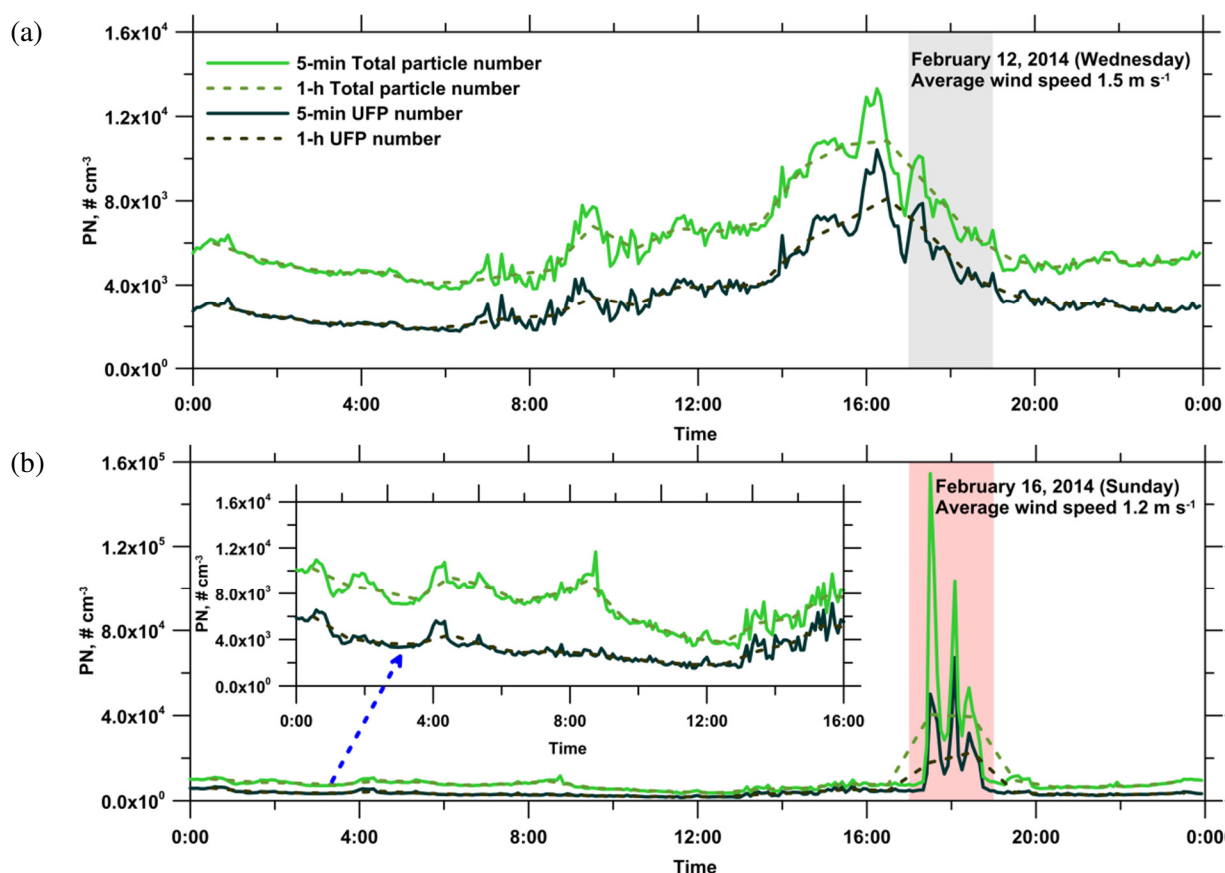
In this study, the total particle and UFP number concentrations in the size ranges of 13–750 and 13–100 nm were calculated from the raw data of the SMPS, respectively. During the whole monitoring period, the average total particle and UFP number concentrations were  $7.06 \times 10^3$  and  $3.76 \times 10^3$  # cm<sup>-3</sup>, respectively. The interquartile ranges were  $4.18 \times 10^3$ – $8.13 \times 10^3$  and  $2.22 \times 10^3$ – $4.32 \times 10^3$  # cm<sup>-3</sup> for total particle and UFP number concentrations, respectively. The average ratio of UFP-to-Total particle was 55.1% during the whole monitoring period, and the interquartile range was 47.9%–63.4%. The relative high ratio value of the UFP-to-Total particle usually can be observed during noon to afternoon hours, corresponding to photochemical nucleation processes under higher temperature conditions. Otherwise, the relative low ratio value of the UFP-to-Total particle occurred during pre-dawn hours, which was due to the coagulation of aged aerosols. The low ratio value of the UFP-to-Total particle also could be observed after a couple hours of the agricultural residues burning.

Figure 2 shows the diurnal variation of the 5-min and 1-h total particle and UFP number concentrations at the monitoring site on February 12 and 16, 2014. Time variations similar to those of the BC concentrations were observed for the total particle and UFP number concentrations, indicating that the ambient particles could share a common source with BC aerosols in this rural area. The daily average total

particle and UFP number concentrations were  $6.13 \times 10^3$  and  $3.61 \times 10^3 \text{ # cm}^{-3}$  for February 12, 2014, respectively, and they were  $1.01 \times 10^4$  and  $4.83 \times 10^3 \text{ # cm}^{-3}$  for February 16, 2014, respectively.

On February 16, 2014, an abrupt increase in the total particle and UFP number concentrations was clearly observed during the open-field corn straw burning episode (17:00–19:00). During the episode, the 5-min total particle and UFP number concentrations could reach  $1.54 \times 10^5$  and  $6.72 \times 10^4 \text{ # cm}^{-3}$ , respectively. These particle number concentrations during the episode were comparable with those at a busy traffic site and could severely affect human health. Additionally, the hourly total particle and UFP number concentrations during the episode increased to  $3.99 \times 10^4$  and  $2.03 \times 10^4 \text{ # cm}^{-3}$ , respectively, which were 5.3 and 3.8 times the values in the nonepisode period, respectively.

Particles in the size range of 100–180 nm (38.1%) and 56–100 nm (37.6%) were dominant during the episode. By contrast, particles in the size range of 32–56 nm (28.7%) and 56–100 nm (28.3%) dominated during the nonepisode period. According to the measurement results, the particle number size distribution patterns for different periods were considerably different. During open-field corn straw burning, the dominant mode of the particle number size distribution was at 100 nm.



**FIGURE 2.** Diurnal variations of 5-min and 1-h total particle and UFP number concentrations at the monitoring site on (a) February 12, 2014 and (c) February 16, 2014.

## CONCLUSIONS

In this study, the hourly BC concentration during the corn straw burning period increased to  $3775 \text{ ng m}^{-3}$ , which was 3.2 times the value during the same period on the reference day. The 5-min UVBC concentration during this episode reached  $47500 \text{ ng m}^{-3}$ , and it was approximately three times greater than the BC concentration, suggesting that ambient particles were bound to ultraviolet-absorbing organic compounds. According to the field measurement results, the hourly absorption Ångström exponent value was 2.0 during the episode. Additionally, the hourly total particle and UFP number concentrations during

the episode increased to  $3.99 \times 10^4$  and  $2.03 \times 10^4 \text{ \# cm}^{-3}$ , respectively, which were 5.3 and 3.8 times the reference values at the rural monitoring site, respectively. During the episode, the 5-min total particle and UFP number concentrations reached  $1.54 \times 10^5 \text{ \# cm}^{-3}$  and  $6.72 \times 10^4 \text{ \# cm}^{-3}$ , respectively. These particle number concentrations were comparable with those at a busy traffic site and could severely affect human health. Furthermore, the particle number concentrations during the episode were dominated by particles in the size range of 56–180 nm. The measurement results showed a single-mode pattern for the particle number size distribution, and the dominant mode was at 100 nm.

## ACKNOWLEDGEMENTS

The authors would like to thank the Ministry of Science and Technology of the Republic of China, Taiwan, for financially supporting this research under Contract No. MOST 102-2221-E-131-002-MY3.

## REFERENCES

- Cheng, Y. H., and L. S. Yang, 2015. "Correcting aethalometer black carbon data for measurement artifacts by using inter-comparison methodology based on two different light attenuation increasing rates". *Atmospheric Measurement Techniques Discussions*. 8:2851-2879.
- Jacobson, M. Z., 2010. "Short - term effects of controlling fossil - fuel soot, biofuel soot and gases, and methane on climate, Arctic ice, and air pollution health". *Journal of Geophysical Research*. 115:D14209.
- Oberdörster, G., E. Oberdörster, and J. Oberdörster, 2005. "Nanotoxicology: An emerging discipline evolving from studies of ultrafine particles". *Environmental Health Perspectives*. 113:823-839.
- Pope, C. A., J. C. Hansen, R. Kuprov, M. D. Sanders, M. N. Anderson, and D. J. Eatough, 2011. "Vascular function and short-term exposure to fine particulate air pollution". *Journal of the Air & Waste Management Association*. 61:858-863.
- Rice, M. B., P. L. Ljungman, E. H. Wilker, D. R. Gold, J. D. Schwartz, P. Koutrakis, G. R. Washko, G. T. O'Connor, and M. A. Mittleman, 2013. "Short-term exposure to air pollution and lung function in the Framingham Heart Study". *American Journal of Respiratory and Critical Care Medicine*. 188: 1351-1357.
- Rich, D. Q., J. Schwartz, M. A. Mittleman, M. Link, H. Luttmann-Gibson, P. J. Catalano, F. E. Speizer, and D. W. Dockery, 2005. "Association of short-term ambient air pollution concentrations and ventricular arrhythmias". *American Journal of Epidemiology*. 161:1123-1132.
- Ryu, S. Y., B. G. Kwon, Y. J. Kim, H. H. Kim, and K. J. Chun, 2007. "Characteristics of biomass burning aerosol and its impact on regional air quality in the summer of 2003 at Gwangju, Korea". *Atmospheric Research*. 84:362-373.
- Sandradewi, J., A. S. H. Prévôt, E. Weingartner, R. Schmidhauser, M. Gysel, and U. Baltensperger, 2008. "A study of wood burning and traffic aerosols in an Alpine valley using a multi-wavelength Aethalometer". *Atmospheric Environment*. 42:101-112.
- Zhang, H., D. Hu, J. Chen, X. Ye, S. X. Wang, J. M. Hao, L. Wang, R. Zhang, and Z. An, 2011. "Particle size distribution and polycyclic aromatic hydrocarbons emissions from agricultural crop residue burning". *Environmental Science and Technology*. 45:5477-5482.

## **INTEGRATED ASSESSMENT OF PARTICULATE MATTER IN KPK AND BALUCHISTAN BY USING GAINS- SOUTH ASIA MODEL**

***Sheikh Saeed Ahmad*** and Aisha Khan  
(Fatima Jinnah Women University, Rawalpindi, Pakistan)<sup>104</sup>

Pakistan is a developing country existing geographically at a pivoted location between two of the world's largest pollution emitting countries (China and India) which adds to the severity of environmental issues faced by the country. These concerns include air pollution, especially the particulate matters, climate change and extreme weather situations prevailing in Pakistan. Particulate matter is specifically responsible for deteriorating the health and causing significance decrease in life expectancy. The initial step in devising a wide ranging, multifaceted, economically feasible and sustainable solution to deal with the severity of this issue is the quantification of the Particulate Matter. GAINS model is one of the most comprehensive tool, dealing with the air pollutants and greenhouse gases covered by the Kyoto Protocol. This study has utilized this model to analyze the source based anthropogenic emissions of Particulate Matter ( $PM_{2.5}$ ,  $PM_{10}$  and  $PM_{tsp}$ ), their impacts and abatement cost, for the duration of 1990-2030, in Khyber Pakhtunkhwa and Baluchistan regions of Pakistan. An overall increasing trend was observed during 1990-2030 for  $PM_{2.5}$  (103.21-405.31kT/Y);  $PM_{10}$  (132.02-558.52kT/Y) and  $PM_{tsp}$  (204.64-775.86kT/Y). The loss in life expectancy caused by the exposure to  $PM_{2.5}$  during 1990-2030 was projected to increase from 10.03 months to 20.07 months. Finally, the study calculated the abatement cost for the emissions was projected to reach 21.57 million dollars in 2030. Therefore, this increasing emissions calls for swiftly initiating an efficient, comprehensive and cost effective approach towards the diminution of these Particulate matters, for improving the environment, with the co-benefit of improving the life expectancy of the population of the area under study.



**HEAVY METALS IN ROAD DUST FROM XIANDAO DISTRICT, CHANGSHA CITY, CHINA:  
HARACTERISTICS, HEALTH RISK ASSESSMENT AND INTEGRATED SOURCE  
IDENTIFICATION**

Jingdong Zhang, *Fei Li*, Jun Yang

(School of Information and Safety Engineering, Zhongnan University of Economics and Law, Wuhan  
430073, China)

The dust properties (dust organic material and pH), the concentrations of metals (Cu, Zn, Pb, Cd, Cr and Fe) in 51 road dust samples from Xiandao District (XDD), China, were investigated. Enrichment factor (EF), multivariate statistics, geostatistics and health risk assessment model were adopted to study the spatial pollution pattern, sources of studied metals and to identify the priority pollutants and regions of concern. The mean EFs of the studied metals revealed the following orders:  $Cd > Zn \approx Pb \approx Cu > Cr$ . For non-carcinogenic effects, the exposure pathway which resulted in the highest levels of exposure risk for children and adults was ingestion, followed by dermal contact and inhalation. Hazard index (HI) values for the studied metals at each site were within the safe level of 1 except maximum  $HI_{Cr}$  (1.08) for children. The carcinogenic risk (CR) for Cd and Cr at each site were within the acceptable risk level ( $1E-06$ ) except  $CR_{Cr}$  ( $1.08E-06$ ) at sampling site 6 for children. Cr was identified as the priority pollutant to human exposure followed by Pb and Cd with simultaneous consideration of the local population distribution. Results based on the integrated source identification indicated Pb, Cr and Zn were probably sourced from traffic-related sources; Cd associated with the dust organic material mainly originated from industrial sources; Cu mainly derived from both sources. Spatially, northwest and northeast of XDD were regarded as the priority regions of concern which were proved to be in close relationship with the land use patterns.

## CHLORINATED PARAFFINS IN CANADIAN HOUSE DUST AND NIST SRM 2585 (ORGANIC CONTAMINANTS IN HOUSE DUST)

*Xinghua Fan*, Hongtao Shang, Cariton Kubwabo, and Pat E. Rasmussen  
(Health Canada, Ottawa, ON, Canada)

Chlorinated paraffins (CPs) have been widely used as both flame retardants and plasticizers in rubbers and textiles, in paints and coating, in leather processing, and also as metal working fluids and sealants. They can be roughly classified into three categories according to their carbon chain length: short-chain CPs (C10-C13, SCCPs), medium-chain CPs (C14-C17, MCCPs), and long-chain CPs (C18-C30, LCCPs). The worldwide production of CPs was estimated to be 916,000 tons per year. Animal studies show that CPs (C12, 60% chlorine content) are carcinogenic in rats and mice of both sexes. Although the underlying mechanisms are not clear, the major target organs are the liver, kidney, and thyroid. CPs have been classified as Group 2B - possibly carcinogenic to humans based on animal study results by International Agency for Research on Cancer. Due to their wide use, CPs are ubiquitous in the environment and have been detected in air, soil, sediment, water, and house dust.

House dust is a sink and repository of various contaminants including CPs; it has been recognized as an important source for human exposure, especially for children, to dust-bound contaminants via inhalation, dermal adsorption and unintentional ingestion. The objective of the current study was to develop a method for the determination of SCCPs and MCCPs in indoor dust samples collected under the Canadian House Dust Study (CHDS). The method was based on those reported by Reth et al. (2005) and Yuan et al. (2012) with some modifications. Dust sample (0.1 g, <80 µm) was subjected to sonication extraction, cleanup by solid phase extraction (SPE) (Florisil cartridge topped up with acidified silica gel), and separation and detection by gas chromatography–mass spectrometry (GC/MS) operated in electron capture negative ionization (ECNI) mode. The method demonstrated good sensitivity, with the method detection limits (MDLs) down to 0.21 µg/g for SCCPs and 0.70 µg/g for MCCPs. The overall recoveries of the method were good, with 104±11% and 108±16% for SCCPs and MCCPs, respectively. SCCPs and MCCPs were detected in every sample (n=48), with median concentrations (range) of 6.2 (4.0-58) µg/g for SCCPs and 20 (5.9-900) µg/g for MCCPs. These are the first CP concentration data reported for Canadian house dust, which are relatively lower compared with those reported in other countries. On average, the percentages of SCCP congeners were 16.5%, 21.7%, 33.8%, and 28.0% for C10, C11, C12, and C13, respectively; the percentages of MCCP congeners were 48.6%, 25.8%, 15.8%, and 9.8% for C14, C15, C16, and C17, respectively. The method was also applied to the analysis of SCCPs and MCCPs in NIST standard reference material (SRM 2585, organic contaminants in house dust). To the best knowledge of the authors, this study was the first to report the CP concentrations in SRM 2585, with 7.58±0.43 µg/g for SCCPs and 16.4±2.1 µg/g for MCCPs. These results could be useful for the comparison of the accuracy for CP analysis using different analytical methods.

## **BEIJING DUST STORM IN SPRING SEASON AND ITS SOURCE APPORTIONMENT**

**Liu Yan-Ju** (Beijing Milu Ecological Research Center, Beijing, China)

Tong-Lin Han, Qing-Yang Liu (Beijing Center for Physical and Chemical Analysis, Beijing, China)

Dust storm of Beijing, usually occurred in Spring, has been paid much attention due to its seriously adverse effect on environment, ecosystem, economy and especially on human health. It has been disturbing the capital city of Beijing in recent years, making its exact source as a hot topic of debate again. This study aims to designate source of the Beijing dust storm by investigating physical and chemical features of both deposit dust and particulate matter during typical dust storm period, together with surface soil dust features of possible source regions, which were classified into four types of soil surface including dry saline lake (also saline soil, etc.), hills (also the mountain, etc.), the agricultural land (also desertified land, grassland, degraded grassland, etc.), sand (also deserts, sand dunes, etc.) based on the specific characteristics of the soil surface, the terrain feature, surface water soluble salt and dust content under diameter of 200  $\mu\text{m}$ , and the topography and landforms.

The result shows that the Beijing storm dust is closely related to dry saline lake due to its higher dust content, yellow-brown color, water delicate slippery feeling, “dirty” particle appearance, higher water soluble salt content, anion and cation content, low water insoluble matter content. The dust is similar to the dry saline lake and the hills in their dry laser particle size and the variation range, and conductivity. The proportion and minimum wind speed of dust are far lower than those of sand.  $\text{MgO}$ ,  $\text{CaO}$ ,  $\text{MnO}$ ,  $\text{CO}_2$  content of dust followed the diluted characteristics of the saline Lake dust;  $\text{Fe}_2\text{O}_3$ ,  $\text{FeO}$ ,  $\text{H}_2\text{O}$  content has the features of diluted hilly dust; the  $\text{TFe}_2\text{O}_3$  content of storm dust showed the characteristics of diluted hilly and farmland dust; the content of  $\text{K}_2\text{O}$  has the characteristics of diluted agricultural land and sand dust. It implies that the Beijing Dust Storm features were closely related to the dry saline lake, followed by the agricultural land and the hills, and weakly correlated with the sand and desert.

Beijing Dust Storms in March 27-29, and April 27-30, 2012 in Beijing were investigated the Backward trajectory to find that first Storm passed by northwest of Inner Mongolia, Hebei and Shanxi in the north, and the second one passed by Inner Mongolia, northern Hebei, Tianjin, Beijing and surrounding areas. Lead isotope composition in  $\text{PM}_{10}$  were further compared with those from the soil of the regions which air mass passed by and found that the two storms might be from Dry Salt Lake areas such as Anguli Noel, Ha Natsu Tu Nord, Bai Yin stem Nur etc. Therefore, Inner Mongolia, North Hebei, Tianjin, Beijing and around including dry Saline Lake of Inner Mongolia, certainly contributed to Beijing Dust storm.

## **OBSERVABLE CHARACTERISTICS OF CLOUD-TO-GROUND LIGHTNING INDUCED NO<sub>x</sub> AND O<sub>3</sub> OVER THE PRD REGION, CHINA**

**Yonglin Liu**, Xinhui Bi, L. Y. Chan, Qin hao Lin, Leilei Fei, Xinming Wang, Ping'an Peng, Guoying Sheng

(Guangzhou Institute of Geochemistry, CAS, Guangzhou, China)

Ground level NO<sub>x</sub> and O<sub>3</sub> from respective air quality monitoring stations along with cloud-to-ground (CG) lightning characteristic parameters deduced from the lightning location system (LLS) for five differing microenvironmental areas relative to mega city, city, municipal town, hilly suburban area and mountainous rural area conditions were examined in Pearl River Delta (PRD) study. We observed NO<sub>x</sub> enhancement and significant O<sub>3</sub> decline on observable lightning stroke days (OLSDs) as compared to non-OLSDs. For observation sites in the upwind of lightning occurred, there were no correlation between lightning parameters and ground level NO<sub>x</sub> and O<sub>3</sub>. For stations in downwind, the lightning stroke frequency and average peak current were found to be positively related to ground level NO<sub>x</sub> after lightning and negatively related to O<sub>3</sub>. The lightning occurred distance and wind speed were negatively related to ground level NO<sub>x</sub>. Our LLS data analysis showed that there were high variation of lightning characteristics and phenomenal changes among these areas. Special features and phenomenal changes related to the lightning characteristic parameters, such as OLSDs and observable lightning stroke frequency and density for an OLSD, were also addressed. Observed variation of lightning stroke distribution and thunderstorm activity is used to analyze the corresponding changes in ground level NO, NO<sub>2</sub> and O<sub>3</sub> over five areas. The ground level NO<sub>x</sub> and O<sub>3</sub> were affected by the transport from the upper or middle troposphere affect by downdraft of the thunderstorm and local microenvironmental meteorology. Microenvironmental variation due to change in topography, degree of urbanization, urban effect, as well as thunderstorm strength was found to affect the spatial distribution of lightning stroke and the severity of lightning activities over the observation areas. This approach increases our understanding of lightning induced NO<sub>x</sub> and O<sub>3</sub> in subtropical China. It also tells us more about the behavior of lightning while the thunderstorm traverses through an observation area. This information is lacking in previous studies.

**ATMOSPHERIC AEROSOL COMPOSITIONS AND SOURCES AT TWO NATIONAL  
BACKGROUND SITES IN NORTHERN AND SOUTHERN CHINA**

***Qiao Zhu, Ling Yan He and Xiao Feng Huang***

(Key Laboratory for Urban Habitat Environmental Science and Technology, Peking University Shenzhen  
Graduate School, Shenzhen, China.)

Although China's severe air pollution has become a focus in the field of atmospheric chemistry and the mechanisms of urban air pollution there have been researched extensively, few field sampling campaigns have been conducted at remote background sites in China, where air pollution characteristics on a larger scale are highlighted. In this study, an Aerodyne high-resolution time-of-flight aerosol mass spectrometer (HR-ToF-AMS), together with other relevant instruments, was deployed at two of China's national background sites in northern (Lake Hongze site) and southern (Mount Wuzhi site) China in the spring season, in order to characterize submicron aerosol composition and sources. The campaign-average  $PM_{10}$  concentration was  $36.2 \pm 20.2 \mu g m^{-3}$  at the northern China background (NCB) site, which was far higher than that at the southern China background (SCB) site ( $10.9 \pm 7.8 \mu g m^{-3}$ ). Organic aerosol (OA) (27.1%), nitrate (27.0%), and sulfate (21.9%) contributed the most to the  $PM_{10}$  mass at NCB, while OA (43.5%) and sulfate (30.5%) were the most abundant components of the  $PM_{10}$  mass at SCB, where nitrate only constituted a small fraction (4.7%) and might have contained a significant amount of organic nitrates (8–18%). The aerosol size distributions and organic aerosol elemental compositions all indicated very aged aerosol particles at both sites. The OA at SCB was more oxidized with a higher average oxygen to carbon (O/C) ratio (0.98) than that at NCB (0.67), and was found to be the most aged OA in real ambient air ever reported in the literature. Positive matrix factorization analysis was used to classify OA components and only secondary components were identified at both sites, including a semi-volatile oxygenated organic aerosol (SV-OOA) component and a low-volatile oxygenated organic aerosol (LV-OOA) component. LV-OOA accounted for more of the total OA at both sites. Using the total potential source contribution function model, the likely source areas of the major  $PM_{10}$  components at both sites were a large regional scale in East Asia. The responsible sources may not only include emissions from the Chinese mainland but also significantly include emissions from ocean-going cargo ships and neighboring countries.

## **DECREASING EMISSION FACTOR OF POLLUTANTS IN ABADAN REFINERY BY RENOVATING THE FURNACE DESIGN**

**Abbas Zabihi** (Mazndaran Gas Company, Sari, Iran)

Mohammadreza Raazi Tabari (Azad Univesity of Ahvaz, Ahvaz, Iran)

The significant consumption of petroleum and gas by most industries in the world results in the emission of greenhouse gases into the atmosphere. Abadan refinery has always been the biggest and oldest in the Middle East and has a variety of refined products. After six months of collecting data about pollutant concentration emitted from a stack of old furnaces of units 75 and new unit 200, the emission factor of the pollutant was calculated. The result showed that the emission factor of some hazardous pollutants emitted from old unit 75 was tremendously higher than that of unit 200. This study suggests the installation of a forced fan to provide the excess air and a feed temperature controlling system to control fuel gas consumption. These would make the fuel combustion complete and decrease its consumption. Meanwhile, further results showed that the renovation of unit 75 could lead to a significant annual reduction of some pollutants such as CO, H<sub>2</sub>S, and C<sub>x</sub>H<sub>x</sub> to 66 ton, 3 ton, and 800 kg, respectively; this would increase the emission rate of pollutant SO<sub>2</sub> up to 150 ton annually. Finally, the new data of pollution coming from unit 75 were compared to that of American refineries units. Results showed that the emission factor of NO<sub>x</sub> emitting from renovated furnace of unit 75 was 55% more than that of American units. Moreover, the SO<sub>2</sub> emission of unit 75 was significantly higher than that of US refineries. The study suggested that NO<sub>x</sub> be used to reduce burners and refine fuel gas, in order to eliminate hydrogen sulfide, decrease nitrogen, and sulfur oxides.

## **MODELLING GROUND-LEVEL OZONE CONCENTRATION USING IMPROVED DATA-MINING ALGORITHMS**

**S. MOHAN<sup>1</sup>** and **P. SARANYA<sup>2</sup>**

(<sup>1</sup>Environmental and Water Resources Engineering, Department of Civil Engineering, Indian Institute of Technology Madras, Chennai – 600036, India; <sup>2</sup>Environmental and Water Resources Engineering, Department of Civil Engineering, Indian Institute of Technology Madras, Chennai – 600036, India)

Ground level Ozone Concentration is an air-pollutant that is harmful to human health and vegetation. Also, the Environmental risks caused by exposure to ground level ozone have significantly increased during recent years, in many parts of the world as evident from literature. Thus the accurate ozone prediction or forecasting is important for warning the public of potential risks associated with heightened ozone levels. One major producer of ozone is the photochemical reaction between volatile organic components and the anthropogenic nitrogen oxides created by vehicular traffic. Therefore the measurement and monitoring of atmospheric ozone concentration levels is important. In this paper, the use of state-of-the-art machine learning approaches, especially, data mining approach in modelling the concentration of ground level ozone, measured in an industrial environment in the city of Chennai, India, once in 15 minutes over a period of 3 months in a critical season. The prediction is based on concentrations of three gases (NO<sub>2</sub>, SO<sub>2</sub>, and VOCs (Benzene, Toluene, p-Xylene)) and three meteorological parameters (ambient temperature, wind speed, wind direction, global radiation, and relative humidity). The analysis of the results indicates that accurate models for the concentration of ground level ozone can be derived with the best performance accuracies indicated by the data mining algorithms. The analysis carried out compares the use of different machine learning classifiers and proved that the Ensemble classifier Bagging performs superior to standard single classifiers, namely Artificial Neural Networks and Support Vector Machines, that are commonly adopted used in this type of analysis. In addition, the performance of the proposed Ensemble classifier technique when different base classifiers are used in optimising the configurations has been compared and found that the ensemble classifier outperforms the other single classifier systems. WEKA software was extensively used for the analysis in the study reported. The research conducted definitely bridges an existing research gap in big-data analytics related to prediction of environmental data, where present research is largely limited to using standard learning algorithms such as Neural Networks and Support Vector Machines often used and also takes the advantages of the standard learning algorithms.

## ADVANCED BUFFER MATERIALS FOR CO<sub>2</sub> CONTROL: IMPROVED AIR QUALITY AND ENERGY CONSERVATION IN COMMERCIAL BUILDINGS

Pavithra Ethirajan, Glenn Morrison, Fateme Rezaei  
(Missouri University of Science and Technology, Rolla, MO, USA)

**ABSTRACT:** The following is novel approach to control the indoor CO<sub>2</sub> levels in closed spaces, majorly focusing on commercial buildings. Amine impregnated Silica were identified as suitable candidates and synthesized; the amine loading ratio was varied to create a range of materials. These samples along with other zeolite candidates have been tested at varying levels of CO<sub>2</sub> in various set ups to determine the theoretical and real time CO<sub>2</sub> adsorption capacity. The research work also focuses on the desorption capacity of the substance. The desorption is allowed to occur gradually over time having concentration gradient as its sole driving force; usually a pressure or temperature swing is applied to desorb the adsorbates out of adsorbent. Results have showed TEPA impregnated silica to have a good adsorption capacity (1.5 mmol/g); and on decreasing the amine content, the silica-TEPA samples showed good desorption rate (31%). At room temperature and pressure conditions, cyclic tests were conducted in a small chamber mimicking real time indoor space. The adsorbent aided in considerable reduction of the CO<sub>2</sub> concentration in the confined space.

**Keywords:** Indoor Air Quality; CO<sub>2</sub> control; Amino polymers; TEPA; APS; PEI; Adsorption; Desorption

### INTRODUCTION

The ambient CO<sub>2</sub> concentration in outdoor air is about 400 ppm and that of indoor air is typically about 650-700 ppm. American Society of Heating, Refrigerating and Air conditioning Engineers (ASHRAE) recommend safe levels of CO<sub>2</sub> to be 1000-1100 ppm<sup>[5]</sup>. Studies also show that CO<sub>2</sub> at increased levels are considered as pollutants and affect cognition and productivity. At slightly higher levels, CO<sub>2</sub> induces stiffness and drowsiness; at greater levels the functioning of central nervous system is damaged. This affects and impairs the decision making performance<sup>[1]</sup>.

Ventilation is required to dilute air pollution generated indoors, but the energy used to conditioning this air is responsible for a large fraction of energy consumption in the United States. While removing pollution sources is the best strategy, CO<sub>2</sub> that is generated by people cannot be removed. In this research, a novel *passive* CO<sub>2</sub> control system is developed that incorporates advanced sorbents into surface coatings. These coatings adsorb CO<sub>2</sub> during high-occupancy periods and release the CO<sub>2</sub> during lower occupancy periods, thereby reducing peak concentrations of CO<sub>2</sub>, improving air quality and reducing the ventilation requirements. Research and survey show that out of the total energy consumed in typical buildings, about 40-60% is consumed for maintenance of appropriate ventilation and air circulation<sup>[6]</sup>.

The first leg of this research work was about understanding and studying amine impregnated silica and their adsorption capacity. There are quite a few CO<sub>2</sub> sorbents typically preferred for these studies, activated carbon, zeolites, silica supported amino polymers, and several metal-organic frameworks are among those. Silica functionalized with amines are very promising sorbents for CO<sub>2</sub> capture. Amines owe their high adsorption capacities to the presence of high density of active sites per unit mass. silica-amines can be categorized into three groups: primary, secondary and tertiary amines<sup>[2]</sup>. Diamine functional groups and hyperbranched amino-silica were found to have good adsorption capacities<sup>[3][4]</sup>. The candidates selected suitable for this study were tetraethylenepentamine (TEPA), polyethyleneimine (PEI), (3-aminopropyl)triethoxysilane (APS) and a commercial silica (PD, from PQ-corporation) was used as a mesoporous support. Literature surveys showed TEPA-impregnated silica has been widely accepted as a



good candidate in studies involving CO<sub>2</sub> capture. The preliminary tests of this research also prove the above statement. Out of the three amine candidates synthesized, PD-TEPA samples have high adsorption capacities and also display good desorption rates. Other than the amine candidates, Mg-MOF-74 was also considered for this study. Although MOFs are typically very good adsorbents, they are expensive and have stability issues. As the main objective of this study is to compare different materials to select a few suitable candidates as buffer material, activated carbon and zeolite 13X were also considered as potential buffer materials.

The next phase was the synthesis and characterization of the selected candidates, which included testing them for their adsorptive performance. The silica - amine samples were synthesized at varying ratios to generate a wide set of materials. Characterization included inspecting all the potential buffer materials by Fourier Transform Infrared Spectroscopy (FTIR). The Thermogravimetric Analysis (TGA) helped find out the CO<sub>2</sub> equilibrium adsorption capacity of each sample. For this, the sample is exposed to CO<sub>2</sub> gas for a specific period of time. Consecutively, purging nitrogen after CO<sub>2</sub> gas, the desorption rate as well was studied. The samples were exposed at both low (500 ppm) and high (3000 ppm) concentration of CO<sub>2</sub>. The dynamic adsorptive performance of the material was assessed with the help of a fixed bed column by performing CO<sub>2</sub> breakthrough measurements. The material should adsorb CO<sub>2</sub> rapidly but also desorb readily. More importantly, this happens without the supply of heat or pressure.

In the next step, the sorbents are incorporated into surface coatings such as water-based latex paint and the performance of each sorbent is compared with that of the powdered form. Finally after identifying the best adsorbent candidates, they are applied to walls in a full-sized (8 m<sup>3</sup>) chamber. The chamber simulates a small room with appropriate ventilation rates, surface area, CO<sub>2</sub> source rates, temperature and humidity controls. In this chamber, high and low occupancy periods can be simulated and the dynamic CO<sub>2</sub> buffering capability of each coating can be assessed under full-scale, realistic conditions. The primary goal of this paper is to make a comparative study analyzing the adsorption and desorption capacities of promising amino polymers of differing classes. Cyclic runs are studied to study and analyze the change in capacity (if any) of the adsorbent with each cycle.

A small scale chamber test was arranged and run to check the working capacity of the selected adsorbents. This set up consisted of a small confined space (20 L) into which a mixture of CO<sub>2</sub> and air was first purged, followed by purging just air. On comparing runs with and without the adsorbent material, it was observed that a considerable amount of CO<sub>2</sub> was reduced in presence of adsorbents.

The novelty of this research is in studying the desorption capacities of the adsorbents along with the adsorption capacities; having concentration gradient is the sole driving force here. Also, studies at low concentrations of CO<sub>2</sub> are rare. This study generates data on CO<sub>2</sub> buffering under realistic conditions that allow for extrapolation to multiple building types and conditions and also generates predictions about the applicability and energy consequences of CO<sub>2</sub> buffering for building stock across the U.S.

## EXPERIMENTAL SECTION

**Material Synthesis.** The amine-silica samples and the MOF samples were synthesized in lab. The initial step for all amine sorbents was drying silica overnight in a vacuum oven at about 105 °C. Similar procedures were followed for the PEI and TEPA samples. 20 mL methanol/g amine was mixed and stirred for an hour. With silica added to this solution, it was left to react overnight. The methanol was then evaporated with the help of rotovap. The sample was recovered by drying in vacuum oven at 60 °C for 1-2 h. The APS sample had a slightly different procedure where 70 mL toluene/g silica was degassed first. After half an hour, 0.3 ml DI water/g silica was added and let to equilibrate for 2-3 hours. Silica (PD) was added to this solution and later attached to condenser and heat to reflux at 85 °C. This was left to react overnight; later, to be filtered with 100 mL toluene, 100 mL hexane, 100 mL ethanol. The sample was similarly recovered. The same procedures were followed for all the amine samples with different silica/amine ratio.

Solvothermal synthesis method was applied for synthesizing Mg-MOF-74. About 0.112 g of DHTA was dissolved along with 0.475 g of Mg(NO<sub>3</sub>)<sub>2</sub>·6H<sub>2</sub>O in a solution of 45 ml DMF, 3 ml ethanol, 3 ml DI water. This solution was mixed with the aid of sonication. This was sealed and placed in oven for 21

h at 125 °C. The mother liquor was decanted and replaced with methanol after cooling it down to room temperature. This methanol solvent was decanted 5 times repeatedly over the next 2 days. The product was then dried at 250 °C under vacuum. The sample was left to cool down gradually and then recovered. Commercial zeolite 13X and activated carbon were purchased and used in this study.

### Material Characterization

***N<sub>2</sub> physisorption.*** BET characterization was carried out to determine the physical characteristics such as surface area and pore volume of the adsorbents. Liquid nitrogen BET analysis was performed using 3Flex gas analyzer (Micrometrics). The samples are required to be degassed before analysis and the degassing step was done using Smartvec.

***FTIR.*** The synthesized amine samples were characterized for functional groups using Fourier Transform Infrared Spectroscopy. Nicolet Nexus 470 FTIR spectrometer was used for performing this analysis. EZ-OMNIC software was used to plot and observe the spikes/peaks of the samples. A preparatory step of mixing amines with KBr was carried out before analyzing the amines. This mixing was done at 1:50 ratio of amine: KBr. A spectrum of the background was collected and then the prepared samples of each amine were tested. Each sample was analyzed at 16 scans per test.

**Equilibrium Adsorption Measurements.** TGA was used to determine the equilibrium adsorption measurements. The very first step in TGA is degassing the sample. This pulls out any gas adsorbed on the surface of the adsorbent; completely clearing out the active sites. The TGA follows a series of steps which can be modified as per requirement. For this study, the procedure was such that the material tested, is initially exposed to CO<sub>2</sub> gas for 4 hours and then nitrogen is purged for 6 hours. While the first half determines the adsorption capacity of the adsorbent, the second half shows the desorption capacity of the adsorbent. All the potential buffer materials were initially tested at 500 ppm CO<sub>2</sub>. The amines were tested at 3000 ppm CO<sub>2</sub> as well and also with varying procedure. The procedures were varied to study the effect of desorption time, the effect of increasing the flow rate of nitrogen on the desorption capacity.

**Chamber Experiments.** The thermogravimetric analysis gives more of a theoretical adsorptive capacity. To understand how these materials function in real time, a small chamber set up was readied; this followed similar procedure as TGA. The only difference being, TGA uses change in weight over time to determine the capacity, the set-up was in such way that the outlet CO<sub>2</sub> concentration could be measured at regular intervals of time. The set-up consists of a small chamber (20 L). A slab of gypsum which acts similar to a wall in a room was placed inside this chamber. For preliminary tests, the adsorbent material was simply dusted on the slab. A mixture of air and CO<sub>2</sub> was let in, maintaining the level of CO<sub>2</sub> at about 3300-3500ppm. At the same time, the outlet is connected to a box having a CO<sub>2</sub> monitor. The sensors in the CO<sub>2</sub> monitor continuously pick up the levels of the gas and the data is stored in the computer attached to this monitor. On comparing runs with and without the adsorbent, the effect of the adsorbent can be studied.

## RESULTS AND DISCUSSION

**Physical Properties of Materials.** BET analysis helped in understanding the physical properties of the amine adsorbent. The volume of the pores in the material and the surface area of the adsorbent were calculated. Upon amine functionalization, both surface area and pore volume decreased. On comparing the pore volumes and surface area of all the three amine adsorbents, the TEPA impregnated silica sample showed better characteristics with 0.765 cm<sup>3</sup>/g pore volume and about 250 m<sup>2</sup>/g of surface area. Table 1 shows the compilation of the N<sub>2</sub> physisorption results.

Figure1 shows the peaks obtained from FT-IR tests. It was observed that all the silica – amine samples had similar peaks when compared with each other and against bare silica as well. The major peaks belonged to O-H stretching at about 3000 – 3100 cm<sup>-1</sup>; Si-O-Si at around 1200 cm<sup>-1</sup>; Si-CH<sub>3</sub> was recognized by sharp peaks at 1260 cm<sup>-1</sup> and 750-865 cm<sup>-1</sup>; the N-H of amines were observed at 1600-1650 cm<sup>-1</sup>; and Si peaks at 460-480 cm<sup>-1</sup>.

**Table 1.** Physical properties of amine adsorbents

Adsorbent	$S_{\text{BET}}$ ( $\text{m}^2/\text{g}$ )	$V_{\text{pore}}$ ( $\text{cm}^3/\text{g}$ )
PD-Bare	294.1	1.04
PD - TEPA	247.4	0.76
PD - PEI	20.0	0.09
PD - APS	63.1	0.23

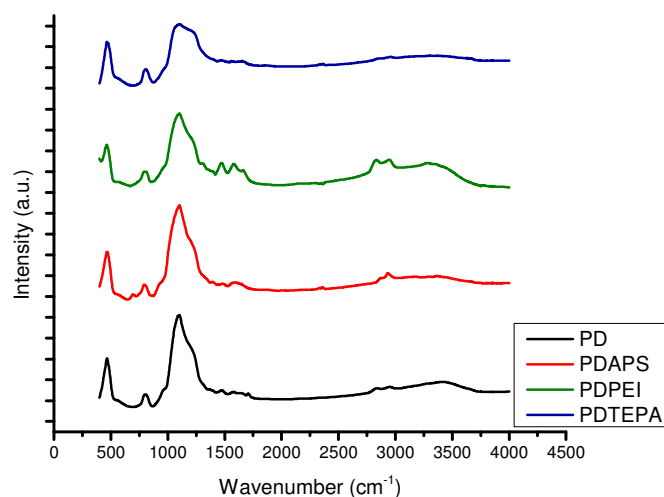


**Figure 1.** FTIR analysis of amine adsorbents

**Table 2.** Equilibrium adsorption measurements at 500 ppm  $\text{CO}_2$

Adsorbent Material	Adsorption capacity ( $\text{mmol/g}$ )	Desorption capacity ( $\text{mmol/g}$ )
PD-TEPA	2.1	0.021 (10%)
PD - PEI	1.2	0.102 (8.5%)
PD - APS	0.7	0.211 (30%)
Mg-MOF-74	19	-

**Equilibrium Adsorption Measurements.** The equilibrium adsorption measurements were initially carried out at 500 ppm  $\text{CO}_2$  for all the buffer materials. The sample to be tested was first degassed for 30 minutes and then cooled down to room temperature. Once in equilibrium at room temperature, the samples were first subjected to  $\text{CO}_2$  at a concentration level of 500 ppm for 4 h. At the end of 4 h, the  $\text{CO}_2$  supply is cut and nitrogen is supplied instead, for 6 h. This pattern helps understand the adsorption and desorption patterns of the samples tested. The same procedure has been followed to test all samples to have a common ground of comparison. It was found that only the amine impregnated silica samples showed desorption along with adsorption (2.1 mmol/g; 10% desorption capacity). The metal organic framework (Mg-MOF-74) though had a very high adsorption capacity (1.9 mmol/g), there was no desorption noticed. Table 1 discusses the adsorption and desorption capacities of various adsorbents considered as potential buffer

materials for this study. Figure 2 shows the normalized weight change during adsorption and desorption in the TGA runs.

As observed from the initial results, amine impregnated silica samples are more promising and suitable for this particular study. This is because along with adsorption, the desorption capacity too important. On identifying this category of adsorbents, several samples were synthesized by altering the ratio of amine: silica. Also, from the preliminary tests, it can be observed that the silica-TEPA sample is the most ideal adsorbent as it has a very high adsorption capacity (2.1 mmol/g). Samples of silica-TEPA were synthesized by gradually varying the amine content in each PD-TEPA sample.

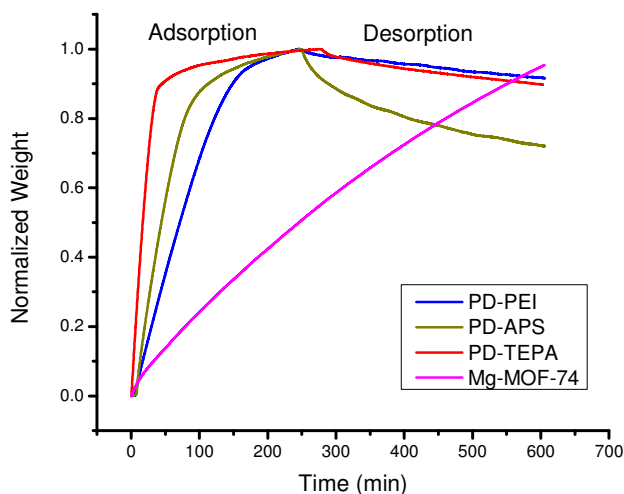


**Figure 2.** TGA plot for adsorption – desorption curves of amine adsorbents at 500pm CO<sub>2</sub>

**Table 3.** Effect of amine load on adsorption – desorption capacities

Adsorbent Material	PD:Amine ratio	Adsorption capacity (mmol/g)	Desorption capacity (%)
PD-TEPA_100%	1:1	2.1	8
PD-TEPA_50%	1:0.5	1.4	31
PD-TEPA_30%	1:0.3	1.08	40
PD-TEPA_1%	1:0.01	0.2	89

The first PD-TEPA sample synthesized contained equal ratio of silica and TEPA (1:1). The consecutive samples were at 1:0.5 (ML1) and 1:0.3 (ML2). Reduction in the amount of amine added to the zeolite reduces the overall adsorption capacity of the adsorbent. But, lower amine content helps increase the desorption capacity. At 1:1 ratio, the sample was observed to have very high adsorption capacity, 2.1 mmol/g, but had a very low desorption capacity, of just about 10%. On reducing the amine content by half, at 1:0.5, the sample now adsorbs a lower quantity of CO<sub>2</sub>, 1.4mmol/g, but the desorption capacity has gone up to 31%. On further reducing the amine content, to a ratio of 1:0.3, the same pattern is observed. The adsorption capacity is just about 1.08mmol/g and desorption rate has gone up to 40%. The same pattern

would be observed of the amine content is continued to reduce, a reduction in the overall adsorption capacity but an increase in the overall desorption rate.

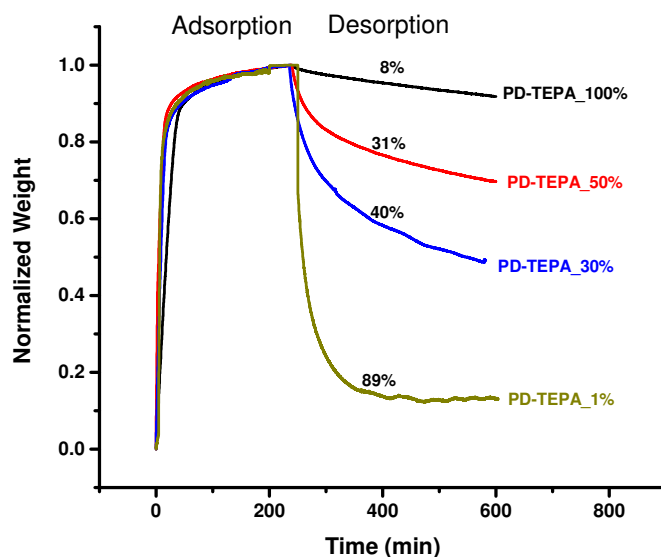


**Figure 3.** TGA plot for adsorption – desorption curves of PD-TEPA samples with varying TEPA loading.

**Table 4.** Effect of varying desorption conditions on desorption capacity

PD-TEPA (desorption condition)		Desorption capacity (%)
Time (h)	Flow rate (mL/min)	
6	40	31
10	40	37
15	40	39
6	80	34

Among the three PD-TEPA samples, the sample with 1:0.5 ratio of PD:TEPA is of interest as it is more suited for further studies. To understand the properties and functioning of these adsorbents, the chosen sample was used to carry out the same TGA experimental procedure, but with varying conditions. The effect of duration of desorption time and the effect of flow rate of gas on the adsorbent was studied.

As it can be observed from the above plots and table, desorption capacity increases with longer desorption duration and with higher flow rate of gas. The amount of CO<sub>2</sub> desorbed increases with increase in desorption time; but the rate at which desorption occurs, decreases. Also, though there is an increase in desorption, on increasing the flow rate of nitrogen, the difference is considerably small. From these results, it can be concluded that the chamber tests can be run at 8-16 cycles (8 hour adsorption; 16 hour desorption).

All the tests so far conducted were based on 1 cycle of adsorption – desorption. Hence it was decided that cyclic runs needed to be tested in the TGA to understand how the adsorption and desorption

capacity work when run consecutively. And it was observed that the adsorption and desorption of CO<sub>2</sub> in the first cycle was similar to the previous results, but on the second and the third runs, the material adsorbed to its initial capacity and desorbed the entire amount adsorbed in that cycle. This too is promising as the overall adsorption and desorption capacities have not varied much

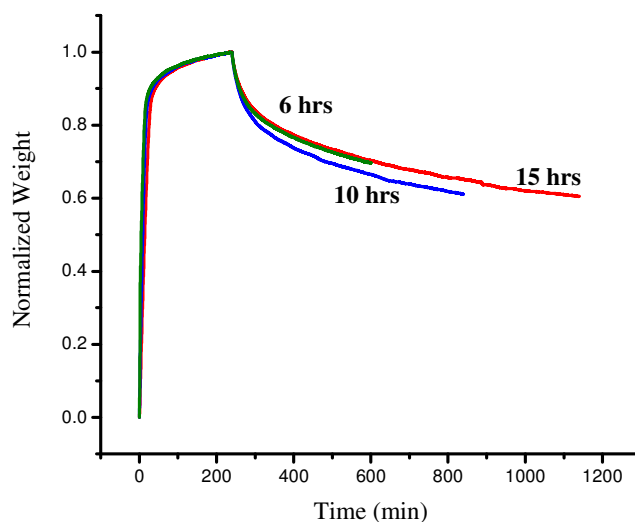


**Figure 4(a).** Effect of time on desorption capacity

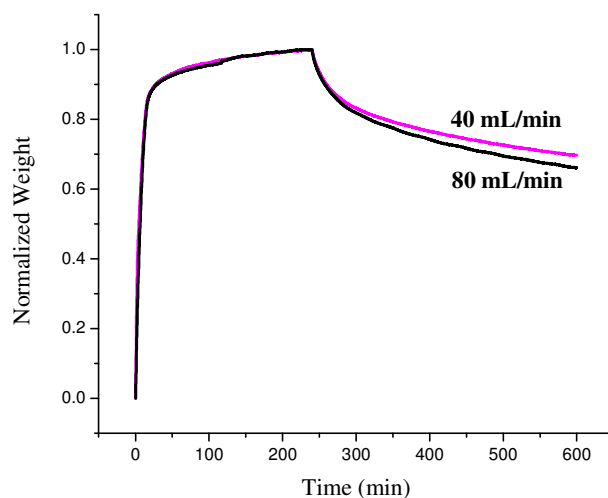


**Figure 4(b).** Effect of air flow rate on desorption capacity

**Chamber Experiments.** The initial chamber tests showed a very slight reduction in the levels of CO<sub>2</sub> with the presence of adsorbents. But this is promising as some reduction in the level of CO<sub>2</sub> has been observed; however small the reduction is. This leads to new exploration possibilities. The quantity of adsorbent material used, the flow rate at which the gas enters the chamber are few of the conditions that can be altered to understand the working of the adsorbent.

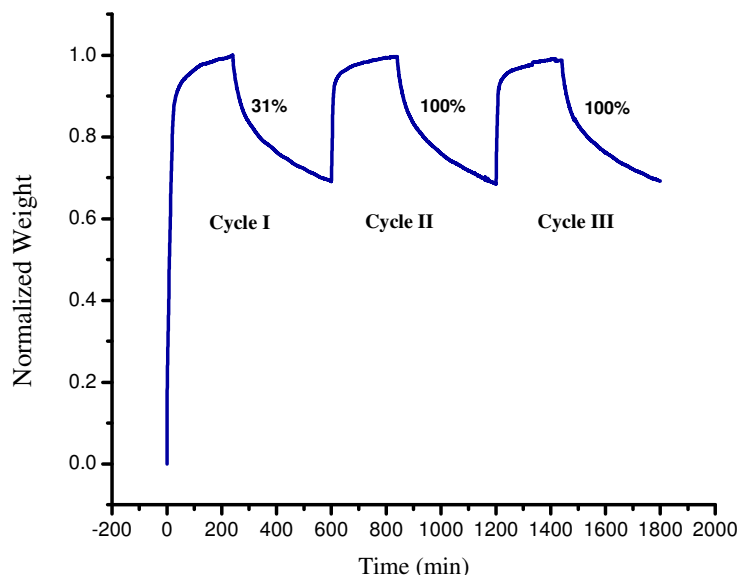


**Figure 5.** TGA plots for cyclic runs of adsorption – desorption

**Table 6.** Effect of varying inlet air conditions on adsorption – desorption

Adsorbent quantity (g)	Inlet gas flow rate (mL/min)	Adsorption capacity (mmol/g)
0.2	1000	0.68
1	1000	1.21
1	100	1.91
1	50	2.19

The first set of experiments was to determine an apt amount of adsorbent material to be used. A no-sample run was conducted for comparative purpose. Each run consisted of 3 cycles and each cycle consisted of 8 hr – adsorption and 16 hr – desorption. Runs were conducted at 0.2g and 1g adsorbent quantities. It is evident from the results that, increasing the amount of adsorbent material increases the adsorption capacity. This is because of the availability of more active sites on increasing the amount of the substance. And, we observe that the CO<sub>2</sub> levels do not rapidly fall after turning off the CO<sub>2</sub> supply; this is because, the CO<sub>2</sub> adsorbed by the material will be released back in to the air and then is flushed out of the chamber. With increase in the amount of material, longer shift occurs as more CO<sub>2</sub> is stored. Results indicated that 1.0 g adsorbent runs were more successful. Hence, the next set of runs – to determine the effect of inlet gas rate, was conducted with 1.0 g adsorbent material in the chamber. It was observed that on decreasing the flow rate of inlet gas, the adsorption capacity increased. A similar shift in the adsorption – desorption curves are noticed. Over here, as the over-all gas flow rate is reduced, the pace at which CO<sub>2</sub> is flushed out also decreases. Hence at lower flowrates, we find longer shifts. The adsorption capacity of the adsorbent is influenced by the inlet gas flowrate and the amount of adsorbent present.

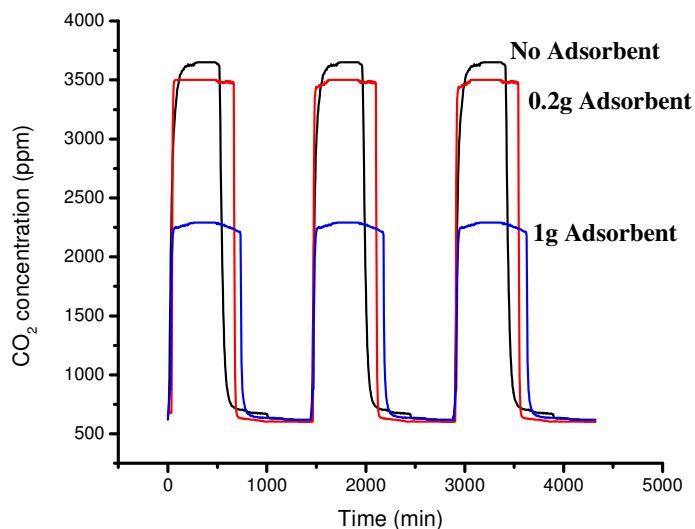


**Figure 6(a).** Effect of amount of adsorbent on adsorption – desorption

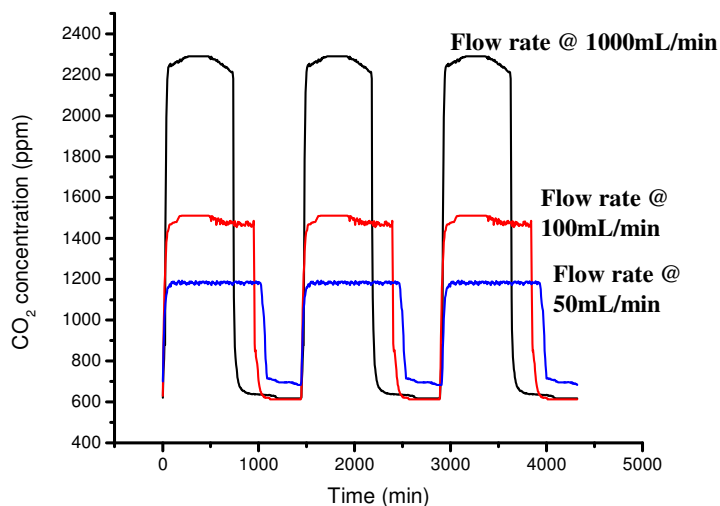


**Figure 6(b).** Effect of inlet flow rate of air on adsorption – desorption

## CONCLUSION

Amine impregnated silica have always been considered as suitable adsorbents for controlling CO<sub>2</sub> levels. It has been predicted and proved in this work that concentration gradient can be a sole driving force for desorption to occur. Also, this study creates a platform on which further studies and experiments related to control of indoor CO<sub>2</sub> could be performed. The chamber tests mentioned in the study are small scale testing. A bigger chamber/room should be considered for further studies. Results from bigger chamber/room will help shape the project such that this idea can be implemented shortly.

## ACKNOWLEDGEMENTS



This work was supported by the National Science Foundation (NSF CBET-1549736). We acknowledge the Environmental Research Center (ERC) and the Department of Chemical Engineering of Missouri S&T for the opportunity and the lab facilities.

## REFERENCES

- [a] Department of Civil, Architecture and Environmental Engineering, Missouri University of Science and Technology, 1404, N Pine Street, Rolla, MO 65409, USA
- [b] Department of Chemical and Biochemical Engineering, Missouri University of Science and Technology, 1404, N Pine Street, Rolla, MO 65409, USA
- [1] Cindy Frei, Harvard Study: Carbon Pollution Impairs Cognitive Function. 2015
- [2] Lee, Hsieh, et.al, CO<sub>2</sub> Adsorption by Y-type Zeolite Impregnated with Amines in Indoor Air
- [3] Wurzbacher, Gebald, et.al, Separation of CO<sub>2</sub> from Air by Temperature - Vacuum Swing Adsorption using Diamine Functionalized Silica Gel
- [4] Choi, Drese, Application of Amine Tethered Solid Sorbents for Direct CO<sub>2</sub> Capture from Ambient Air
- [5] ASHRAE Standard 62.1-2013, "Ventilation for Acceptable Indoor Air Quality", plus ASHRAE BOD approved addenda.
- [6] Distribution of Energy Consumption, Energy Data Book, US Department of Energy, 2006.

## **AMINE IMPREGNATED ACTIVATED CARBON IS A NOVEL MATERIAL FOR CO<sub>2</sub> CAPTURE**

**Dipa Das**, Debi Prasad Samal, and B. C. Meikap.

(Indian Institute of Technology Kharagpur, West Bengal, India – 721302)

**ABSTRACT:** The quality of the adsorbents is decided by its textural characteristics and surface chemistry. Prepared activated carbons surfaces are usually nonselective and lack of reactive groups. By suitable modification of their surfaces the quality of adsorption increases. Impregnation is one of the most suitable modifications techniques used for activated carbons. Monoethanol amine (MEA) and diethanol amines (DEA) solutions were selected for impregnation on the surface of the activated carbon with impregnation ratio 0.4. CO<sub>2</sub> adsorption test was performed to investigate the effect of the modification on CO<sub>2</sub> capture at standard temperature and pressure. Characterizations of the prepared samples have been done by physical and chemical analysis method. Amine impregnated sample leads to more CO<sub>2</sub> uptake at flue gas temperature. This property of amine impregnated activated showed more CO<sub>2</sub> uptake with a higher efficiency as compared to simple activated carbon. Among the two activated carbon, the maximum CO<sub>2</sub> adsorption capacity ( $q_e$ ) for monoethanolamine impregnated activated carbon (MEA-AC) was found out to be 36.83668 mg/g as compared to diethanol amine impregnated activated sample due to stronger carbamate formation and high stability.

## **INTRODUCTION**

Nowadays, large concentration of carbon dioxide, is emitted into the atmosphere. 60 percent of the global warming is caused by carbon dioxide (Houghton et al., 2001). Carbon captures and storage (CCS) process involves the separation of the CO<sub>2</sub> from either stack gas or other intermediate gas streams. Absorption, adsorption, cryogenic distillation and membrane separations are the current methods for CO<sub>2</sub> capture from flue gas. Absorption, by using an amine-based solution is frequently used in the industrial processes. The major disadvantages of this process are large amount of energy required for regeneration (Gray et al., 2004; Plaza et al., 2007) and it is very expensive. Adsorption is considered as one of the most important methods for CO<sub>2</sub> capture (Reynolds et al., 2005). The solid adsorbent used for adsorption should have high CO<sub>2</sub> selectivity and capacity for CO<sub>2</sub> capture. Among different porous materials, activated carbons are suitable adsorbents for CO<sub>2</sub> capture (Siriwardane et al., 2005) due to its well developed micro- and mesoporosities. In case of activated carbon, the adsorption capacity decreases when the temperature is high and also water competes with CO<sub>2</sub> for adsorption (Wang et al., 2007; Plaza et al., 2010; Plaza et al., 2009; Pevida et al., 2008; Maroto-Valer et al., 2005). For efficient capture of CO<sub>2</sub> from flue gas, the adsorbent used should operate at high temperatures and also high adsorption capacity and selectivity (Maroto-Valer et al., 2008). Introduction of amines on the surface of the activated carbon offers more absorption and due to solids it is easy to handle, and no corrosion of the process equipment occurs (Gray et al., 2004; Zhao et al., 2007). Selective adsorption of CO<sub>2</sub> of amine impregnated activated carbon was much more than the activated carbon adsorbents (Przepiorski et al., 2004; Wei et al., 2009). The main objective of our work is the development of an amine impregnated activated carbon adsorbent with high adsorption capacity. Impregnation of amine solution on the surface of activated carbon is a suitable modification technique to improve their capture performance for adsorption of CO<sub>2</sub>. For our current work, green coconut shell based ACs was used as adsorbents for gas adsorption. Monoethanol amine solution and diethanol amine solution were used to impregnate the surface of activated carbon. Carbon dioxide adsorption capacity was studied at standard temperature and pressure for the impregnated activated carbon material.

## MATERIALS AND METHODS

**Preparation of Adsorbents.** Fresh green coconut shells were collected from the nearby local market of IIT Kharagpur and then cut into small pieces followed by washing with tap water for removal of dirty material attached to it. Those washed green coconut shells were kept in the sunlight for 15-20 days till it becomes completely dry. Dried materials were kept inside the oven at 105°C for 48 hours for removal of moisture and other volatile impurities. Then the dried samples were crushed with a locally made crusher and sieved to a size of 512  $\mu\text{m}$ . Chemical activation was done with  $\text{ZnCl}_2$ . 20 gm. of dried precursor was well mixed with 100 ml of the concentrated solution of  $\text{ZnCl}_2$  that contains 20 gm. of  $\text{ZnCl}_2$  with impregnation ratio (activating agent/precursor) 1:1. The powdered material in slurry form was properly mixed and kept for 24 hours for proper soaking of  $\text{ZnCl}_2$  on the surface of powdered precursor. The slurry was kept inside the oven at 100 °C for 24 hours. The resulting chemical impregnated samples were placed inside galvanized iron pipe of dimensions of length 8 cm and inner diameter of 1.5 cm and kept inside the furnace; The material inside the furnace was heated (10 °C  $\text{min}^{-1}$ ) to the final carbonization temperature of 600 °C under the nitrogen flow rate of 120  $\text{cm}^3 \text{min}^{-1}$  at STP. The material was kept inside the furnace for one hour at 600 °C. Then it was cooled under the constant flow of nitrogen gas till the temperature reaches the room temperature. The dried material was washed with 0.5 N HCl for 2-3 times followed by washing with warm distilled water for removal of any kinds of residual organic and mineral matter. Finally the material was washed with cold water till the solution becomes neutral. The sample was dried for 24 hours at 100 °C inside an airoven till it becomes completely dry to form activated carbon. The dried activated carbon was impregnated with diethanol amine solution ( $\text{HO-CH}_2\text{-CH}_2\text{-NH-CH}_2\text{-CH}_2\text{-OH}$ ) and monoethanol amine solution ( $\text{OH-CH}_2\text{-CH}_2\text{-NH}_2$ ) in the impregnation ratio of 0.4. Two different amine-impregnated activated carbon samples were prepared and then dried in the hot air oven at the temperature of 100 °C for 48 hrs till it became completely dry and kept inside an air tight container for our experimental purpose.

**Characterization of Adsorbents.** Before the use of the adsorbents for specific purpose, physical and chemical characterization has been done by different methods that are discussed in the following section. Density of the amine impregnated activated carbons were found to be 2.85  $\text{gm/cm}^3$  and 2.97 $\text{gm/cm}^3$  for monoethanolamine impregnated activated carbon(MEA-AC) and diethanolamine impregnated activated carbon(DEA-AC) with impregnation ratio 0.4.

## RESULTS AND DISCUSSION

**Proximate and Ultimate Analysis.** Proximate analysis of the sample has been done for determination of the amount of percentage of moisture, volatile matter, fixed carbon and ash content. The result of proximate analysis was shown in Table 1.

**TABLE 1. Results of Proximate Analysis**

Sample	Proximate Analysis			
	Moisture (%)	Volatile Matter (%)	Ash (%)	Fixed Carbon (%)
RAW	13.834	44.969	2.564	38.633
AC	12.983	7.208	1.902	77.907
MEA-AC(0.4)	11.338	17.528	0.5	70.634
DEA-AC(0.4)	12.439	17.12	0.45	69.991

From this analysis it has been observed that the fixed carbon content of AC and amine impregnated AC was very high as compared to raw precursor, which results in better adsorbent for adsorption purpose.

From the Table 1, it has been observed that the raw precursor has high volatile matter and low ash content, so it can be a good starting material for preparation of activated carbon (Singh et al., 2008). During carbonization and activation process, the coconut shell has been decomposed as a result of which the volatile matters were removed from the coconut shell and carbon content increases. H<sub>2</sub>O and H<sub>2</sub> are removed by ZnCl<sub>2</sub> (Yorgunet et al., 2009) instead of removal of hydrocarbons. Elemental analysis of the sample has been done by CHNS analyser and the corresponding values of the different adsorbents were shown in Table 2. It has been seen that due to the amine impregnation the nitrogen content of the samples were more as compared to activated carbon and the raw precursor.

**TABLE 2. Elemental Analysis**

Sample	Ultimate Analysis				
	C (%)	H (%)	N (%)	O (%)	S (%)
<b>RAW</b>	46.185	9.416	0.99	33.385	10.024
<b>AC</b>	69.04	2.963	1.16	26.791	0.046
<b>MEA-AC(0.4)</b>	66.15	2.595	7.66	23.329	0.266
<b>DEA-AC(0.4)</b>	66.09	2.888	5.062	25.824	0.136

**Pore Structure and Surface Area of the Adsorbents.** The textural properties of the prepared samples have been determined by nitrogen adsorption and desorption isotherm at 77K. Before adsorption, the samples were degassed at 300°C under vacuum for 5 hr. The total surface area, micropore surface area, and the total pore volume of the prepared samples were found by applying Brunauer-Emmett-Teller (BET) and t-plot method in the relative pressure (P/P°) range of 0.05-0.30 (Brunauer et al., 1938). Micropore volume was found out by DR method. Mesopore volume was found out from deducting micro pore volume from total pore volume. The pore size distributions of the prepared samples have been determined by BJH model (Barrett et al., 1951). The pore structure parameters of the different samples were shown in Table 3. It is observed from the Table 3 that surface area and pore volume of the amine impregnated activated samples, were decreases due to pore blockage by functional groups attached on the surface as widely reported in the literature (Gorgulho et al., 2008).

**TABLE 3. Pore Structure Parameters**

Samples	S <sub>BET</sub> (m <sup>2</sup> /g)	v <sub>T</sub> (cm <sup>3</sup> /g)	M.P.V (cm <sup>3</sup> /g)	Avg. Pore Radius (Å°)	Micro Pore Area (m <sup>2</sup> /g)
<b>RAW</b>	59.728	0.05031	0	16.8461	0
<b>AC</b>	995.799	0.4487	0.372	9.01198	921.71
<b>MEA-AC(0.4)</b>	569.352	0.2795	0.201	9.81965	488.716
<b>DEA-AC(0.4)</b>	552.776	0.2621	0.198	9.79635	471.324

**CO<sub>2</sub> Capture Performance of Amine Impregnated Sample.** CO<sub>2</sub> batch adsorption analysis was carried out by autosorbiQ manufactured by Quanta chrome instrument. The samples were out-gassed at 523K for 6 hours upto atmospheric pressure. After degassing, under a vacuum, the carbon dioxide adsorption of the sorbents at relative pressure (P/P<sub>0</sub>) was evaluated at 298K. From the Figure 1, it has been seen that the adsorption of CO<sub>2</sub> was carried out till the relative pressure (P/P<sub>0</sub>) reaches the atmospheric pressure. The maximum volume of CO<sub>2</sub> adsorbed for MEA-AC (0.4) and DEA-AC (0.4) at atmospheric pressure was found out to be 18.7464 and 13.8062 cc/g. Similarly, the maximum CO<sub>2</sub> adsorption capacity (q<sub>e</sub>) for MEA-AC (0.4), and DEA-AC (0.4) was found out to be 36.83668 and 24.08795 mg/g. From the Figure 1 it can be observed that MEA-AC (0.4) has better adsorption capacity than DEA-AC (0.4). Amines are the

important source of basic sites for acidic carbon dioxide gas adsorption. Due to their acid-base properties, amine on the AC surfaces increases the adsorption capacity and selectivity of carbon dioxides. Typically, CO<sub>2</sub> is lewis acid and amines are lewis base. There is the presence of a lone pair of electrons on a nitrogen atom on amine functional groups.

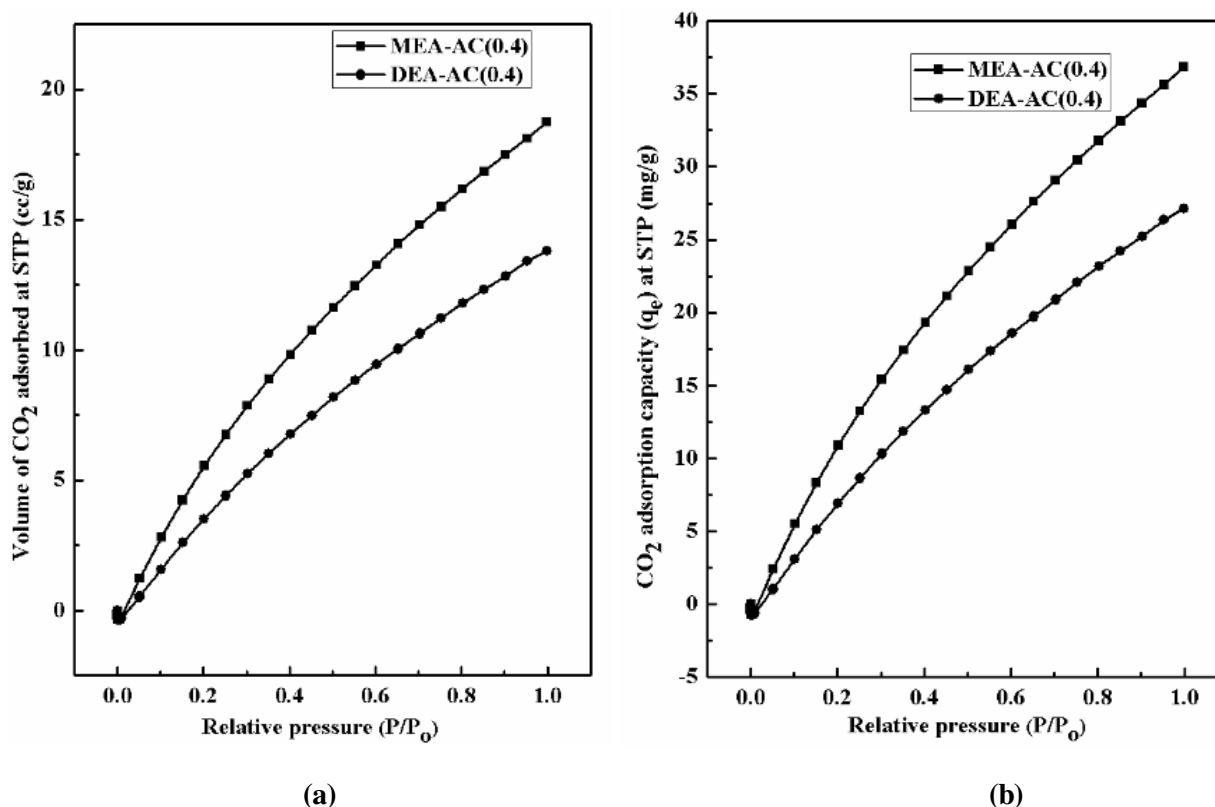


**FIGURE 1. (a)Volume of CO<sub>2</sub> adsorbed vs. Relative pressure and (b)CO<sub>2</sub> adsorption capacity vs. Relative pressure for amine impregnated activated carbon adsorbents**

So by which there is nucleophilic attack on the acidic carbon dioxide as a result of which there is formation of carbamate through the carboxyl group (Danckwerts et al.,1979; Caplow et al., 1968).The adsorption between the active site of amine and carbon dioxide is the driving force for capture of carbon dioxide by amine-modified carbon materials. It is observed from the Figure 1 that MEA modified samples have a higher capacity than DEA due to the effect of chemisorptions. 1° amine was more stable than 2° amine because MEA is of less viscous than DEA that affects the CO<sub>2</sub> reaction to a greater extent. The main reason can be described because of the -I effect of two alcohol groups present in 2° amine which acts as electron repellent to the existent electron deficient N<sup>+</sup> ion present in carbamate. Hence, the stability of 1° amine is more compared to 2° amine (Danckwerts et al., 1979) and thus MEA containing adsorbents shows greater adsorbent capacity than DEA containing adsorbent. As amine anchoring decreases surface area and increases the amine content. From the graph it can be seen that at same impregnation ratio of the amine impregnated carbon the volume of CO<sub>2</sub> adsorption and CO<sub>2</sub> adsorption capacity ( $q_e$ ) of MEA-AC was more than that of DEA-AC.From these results, MEA-AC may act as better adsorbent than DEA-AC for CO<sub>2</sub> capture.

**Thermo Gravimetric Analysis.** Figure 2 shows the plot of original weight versus temperature for MEA-AC (0.4) and DEA-AC (0.4). When the temperature was raised from room temperature 27 °C to a very high temperature 800 °C, amine impregnated activated carbons have high thermal stability and three zones of the profile are obtained. 1st stage, accounts for removal of volatile matter, moisture and other impurities. 2nd stage shows the decreasing slope accounts for slow decomposition. In 3rd stage with further rise in temperature the downward slope again increases rapidly for both cases that account to severe erosion of material. Clearly with respect to increasing the temperature from 27-800 °C, the total weight loss for MEA-AC(0.4) and DEA-AC(0.4) obtained are 36.102 % and 42.876 % . By analyzing both graphs we observed that the MEA-AC (0.4) has very high resistant to weight loss compared to the other for the same rise in temperature change. From this result we understand that impregnating activated carbon with monoethanol amine solution results high thermal stability in comparison to diethanol amine solution and it is thermally stable and resistant to surface erosion with rise in temperature and can be used in industrial scale application.

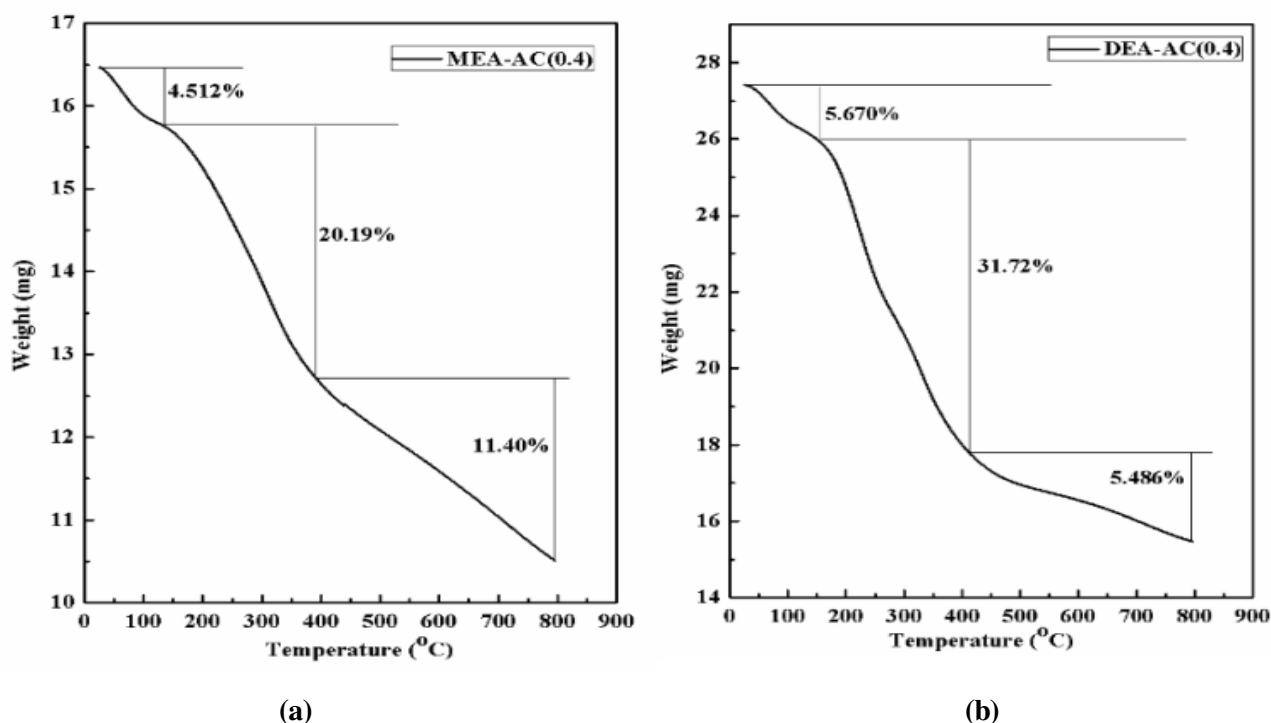


FIGURE 2. Thermal gravimetric analysis of (a) MEA-AC (0.4) and (b) DEA-AC (0.4)

**FTIR Analysis of the Amine Impregnated Activated Sample.** The FTIR spectra of amine impregnated activated carbon of impregnation ratio 0.4 at the absorption band 4000–400  $\text{cm}^{-1}$  intervals, has been shown in Figure 3. From the graph, we observe all kinds of functional groups such as carboxylic acid, alcohol, ether, ester, phenols, aliphatic amine, nitro, C-H groups and other aliphatic groups present in amine impregnated activated carbon. The bands at 609.42 and 607.09  $\text{cm}^{-1}$  have been assigned to N-H group. At 1320-1000 $\text{cm}^{-1}$ (strong) the functional group presents are alcohol, carboxylic acid, esters and ethers. A band at 1100  $\text{cm}^{-1}$  is attributed to C-O stretching. The band at 1054  $\text{cm}^{-1}$  may be due to the C-N stretching vibration. The bands at 1735 $\text{cm}^{-1}$  are due to N-H deformation vibration (Tang et al., 2012)

## CONCLUSIONS

In this work, activated carbons were impregnated by monoethanol amine and diethanol amine solutions with impregnation ratio 0.4. Carbon dioxide adsorptions of the samples were performed. From the ultimate analysis it was found that the nitrogen content of the amine impregnated ACs was higher than that

of raw material and activated carbon. Due to the presence of nitrogen group of the amine modified material the carbon dioxide adsorption capacity was more than that of simple activated carbon. From the results of the BET surface area, it has been seen that amine impregnated ACs have less specific surface area, pore volume and pore diameter, due to their blocking of pores by amine functional groups. But at the same time creating many active sites for CO<sub>2</sub> adsorption by chemisorptions method. Many active sites have been created on impregnated activated carbon particles and inside the micropores. The MEA impregnated AC shows higher CO<sub>2</sub> adsorption capacity. The maximum CO<sub>2</sub> adsorption capacity ( $q_e$ ) for monoethanolamine impregnated activated carbon (MEA-AC) was found out to be 36.83668 mg/g than DEA-AC due to stronger carbamate formation. Among the impregnated activated carbon samples, MEA-AC (0.4) is the more suitable adsorbents for CO<sub>2</sub> capture.

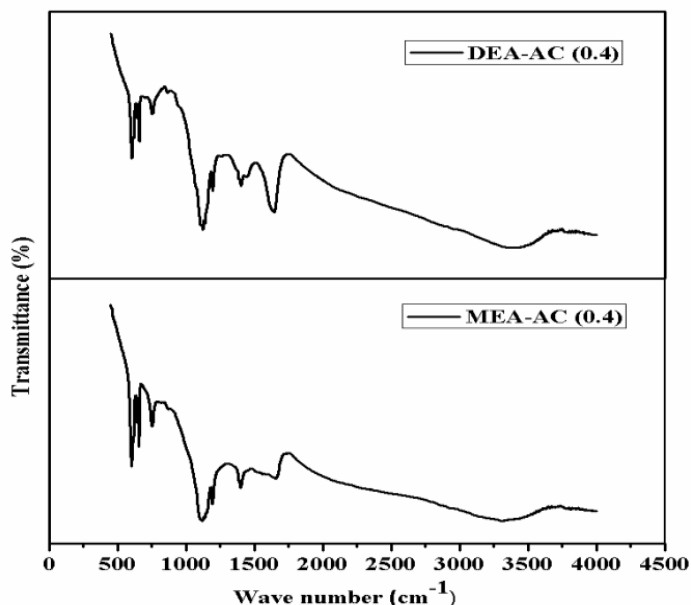


FIGURE 3. FTIR spectra of MEA-AC (0.4) and DEA-AC(0.4)

## ACKNOWLEDGEMENTS

This work was supported by the Chemical Engineering Department, Indian Institute of Technology, Kharagpur

## REFERENCES

- Barrett, E. P., L. G. Joyner, P. P. Halenda. 1951. "The determination of pore volume and area distributions in porous substances. I. Computations from nitrogen isotherms". *J. Am. Chem. Soc.* 73(1): 373-380.
- Brunauer, S., P. H. Emmett, and E. Teller. 1938. "Adsorption of gases in multimolecular layers". *J. Am. Chem. Soc.* 60(2): 309-319.
- Caplow, M. 1968. "Kinetics of carbamate formation and breakdown". *J. Am. Chem. Soc.* 90(24): 6795-6803.
- Danckwerts, P. V. 1979. "The reaction of CO<sub>2</sub> with ethanolamines". *Chem. Eng. Sci.* 34(4): 443-446.
- Gorgulho, H. F., J. P. Mesquita, F. Goncalves, M. F. R. Pereira, and J. L. Figueiredo. 2008. "Characterization of the surface chemistry of carbon materials by potentiometric titrations and temperature-programmed desorption". *Carbon.* 46(12): 1544-1555.
- Gray, M. L., Y. Soong, K. J. Champagne, J. Baltrus, R. W. Stevens, P. Toochinda, S. S. C. Chuang. 2004. CO<sub>2</sub> capture by amine-enriched fly ash carbon sorbents. *Sep. Purif. Technol.* 35(1): 31-36.

- Houghton, J. T., Y. D. J. G. Ding, D. J. Griggs, M. Noguer, P. J. van der Linden, X. Dai, and C. A. Johnson. 2001. Climate change 2001: the scientific basis.
- Maroto-Valer, M. M., Z. Lu, Y. Zhang, and Z. Tang. 2008. "Sorbents for CO<sub>2</sub> capture from high carbon fly ashes". *Waste Management*. 28(11): 2320-2328.
- Maroto-Valer, M. M., Z. Tang, and Y. Z. Zhang. 2005. "CO<sub>2</sub> capture by activated and impregnated anthracites". *Fuel. Proc. Technol.* 86(14): 1487-1502.
- Pevida, C., M. G. Plaza, B. Arias, J. Feroso, F. Rubiera, and J. J. Pis. 2008. "Surface modification of activated carbons for CO<sub>2</sub> capture". *Appl. Surf. Sci.* 254(22): 7165-7172.
- Plaza, M. G., C. Pevida, B. Arias, J. Feroso, M. D. Casal, C. F. Martn, and J. J. Pis. 2009. "Development of low-cost biomass-based adsorbents for postcombustion CO<sub>2</sub> capture". *Fuel*, 88(12): 2442-2447.
- Plaza, M. G., C. Pevida, A. Arenillas, F. Rubiera, and J. J. Pis. 2007. "CO<sub>2</sub> capture by adsorption with nitrogen enriched carbons". *Fuel*. 86(14): 2204-2212.
- Plaza, M. G., C. Pevida, C. F. Martn, J. Feroso, J. J. Pis, and F. Rubiera. 2010. "Developing almond shell-derived activated carbons as CO<sub>2</sub> adsorbents". *Sep. Purif. Technol.* 71(1): 102-106.
- Przepiórski, J., M. Skrodzewicz, and A. W. Morawski. 2004. High temperature ammonia treatment of activated carbon for enhancement of CO<sub>2</sub> adsorption. *Appl. Surf. Sci.* 225(1), 235-242.
- Reynolds, S. P., A. D. Ebner, and J. A. Ritter. 2005. "New pressure swing adsorption cycles for carbon dioxide sequestration". *Adsorption*, 11(1): 531-536.
- Singh, C. K., J. N. Sahu, K. K. Mahalik, C. R. Mohanty, B. R. Mohan, and B. C. Meikap. 2008. "Studies on the removal of Pb (II) from wastewater by activated carbon developed from Tamarind wood activated with sulphuric acid". *J. Hazard. Mater.* 153(1): 221-228.
- Siriwardane, R. V., M. S. Shen, E. P. Fisher, and J. Losch. 2005. "Adsorption of CO<sub>2</sub> on zeolites at moderate temperatures". *Energy Fuel*. 19(3): 1153-1159.
- Tang, Y. B., Q. Liu, and F. Y. Chen, 2012. "Preparation and characterization of activated carbon from waste ramulusmori". *Chem. Eng. J.* 203, 19-24.
- Wang, N., L. Ma, A. Wang, Q. Liu, T. Zhang. 2007. "CO<sub>2</sub> adsorption on SBA-15 modified by aminosilane". *Chin. J. Catalysis*. 28 (9): 805.
- Wei, J., J. Shi, H. Pan, Q. Su, J. Zhu, and Y. Shi. 2009. "Thermal and hydrothermal stability of amino-functionalized SBA-16 and promotion of hydrophobicity by silylation". *Microporous and Mesoporous Materials*. 117(3): 596-602.
- Yorgun, S., N. Vural, H. Demiral. 2009 Preparation of high-surface area activated carbons from Paulownia wood by ZnCl<sub>2</sub> activation. *Microporous Mesoporous Mater.* 122(1): 189-194.
- Zhao, H., J. Hu, J. Wang, L. Zhou, and H. Liu. 2007. "CO<sub>2</sub> capture by the amine-modified mesoporous materials". *Acta Physico-Chimica Sinica*. 23(6), 801-806.



## **CATALYTIC OXIDATION OF VOCS AND CO OVER OCTAHEDRAL LAYERED BIRNESSITES SYNTHESIZED BY DIFFERENT METHODS**

Zhidan Fu, Qing Ye\*, Heng Lu, Shuiyuan Cheng, Wang Dao  
(Laboratory of Beijing on Regional Air Pollution Control, College of Environmental and Energy Engineering, Beijing University of Technology, Beijing 100124, China)

Catalytic oxidation of volatile organic compounds (VOCs) and CO is one of the most effective technologies. Manganese oxide shows good catalytic performance in a number of oxidation processes. The manganese oxides have long been used as an active catalyst for the oxidation of carbon monoxide, methane, and hydrocarbons. The aim of the present work is to make manganese oxide octahedral layered (OL) birnessites using different methods and compare the catalytic performance of these materials.

The octahedral layered nanofiber-like birnessite (OL-1) was prepared via the oxidation  $\text{Mn}^{2+}$  by  $\text{MnO}_4^-$  in the KOH solution. The octahedral layered wool ball-like birnessite (OL-2) catalyst was prepared using the method similar to that for OL-1 fabrication but adding  $\text{HNO}_3$  instead of KOH to the mentioned. Moreover, the mixed solution was hydrothermally treated in Teflon-lined autoclave for at 170 °C for 4 days. The OL catalysts were prepared via the reduction  $\text{MnO}_4^-$  by ethanol or glucose aqueous in solution, and the obtained catalysts were denoted as OL-3 and OL-4, respectively. The obtained OL-1, OL-2, OL-3, and OL-4 precursors were filtered, washed, and calcined in air at 300 °C for 2 h. The OL catalysts were characterized by the XRD, BET and  $\text{H}_2$ -TPR techniques. Catalytic activities of the OL samples for the oxidation of CO, benzene or toluene. The reactant mixture was (1% CO + air), (2000 ppm benzene +air) or (2000 ppm toluene +air), the corresponding space velocity was 15,000 mL/(g h), and 40,000 mL/(g h).

The results show that the preparation method significantly had an important influence on the property of the OL catalyst. It is found that all of the samples have birnessite-type octahedral layered structure and an interlayer spacing of ca. 0.72 nm. The surface areas of the OL-1, OL-2, OL-3, and OL-4 samples were 7.6, 13.4, 63.2, and 42.6 m<sup>2</sup>/g, respectively. Obviously, surface areas and pore volumes of the OL-3 and OL-4 samples were much higher than those of the OL-1 and OL-2 samples. There was co-presence of  $\text{Mn}^{3+}$ ,  $\text{Mn}^{4+}$  and/or  $\text{Mn}^{2+}$  on the surface of these samples. Based on the manganese ion contents, the average oxidation states of surface Mn species in the birnessite samples were in the range of 3.2-3.5, which was lower than those (3.5-3.9) obtained from the  $\text{H}_2$ -TPR studies. The amounts of oxygen vacancies and lattice oxygen mobility of the OL-1 and OL-4 samples were higher than those of the OL-2 and OL-3 samples. Either in CO oxidation or in benzene or toluene oxidation, the catalytic activity decreased in the order of OL-1 > OL-4 >> OL-3 > OL-2, with the OL-1 sample showing the best performance ( $T_{50\%} = 115$  and  $T_{100\%} = 150$  °C for CO oxidation at 15,000 mL/(g h),  $T_{50\%} = 200$  °C and  $T_{95\%} = 240$  °C for benzene oxidation, and  $T_{50\%} = 190$  °C and  $T_{95\%} = 230$  °C for toluene oxidation at 40,000 mL/(g h)).

**PHOTOCATALYTIC OXIDATION OF FUEL VAPORS: A NOVEL METHOD FOR  
REDUCING FUEL VAPOR EMISSIONS FROM AUTOMOBILES**

**Catherine B. Almquist**

(Department of Chemical and Paper Engineering, Miami University, 650 E High Street, Oxford, Ohio  
45056, USA)

Fuel vapor recovery systems on automobiles are required on all models in the US since the year 2000. On each automobile is a carbon canister that recovers fuel vapors during refueling. When the automobile is turned on, air is passed through the carbon filters to desorb the fuel vapors, which are directed to the engine and burned. However, a parked automobile is exposed to temperature swings throughout the day and night, and the fuel vapors from the gasoline tank are continuously challenging the carbon filters. Eventually, the carbon canisters become saturated with fuel vapors while the automobile is not in operation, and the fuel vapors pass through the carbon filter and, thus, are emitted to the environment. This is especially problematic on warm sunny days, when volatile organic carbon emissions contribute to urban smog.

Photocatalytic oxidation of fuel vapors is being investigated for application in fuel vapor recovery systems. The idea is to destroy volatile organic compounds that escape from the carbon filters in an automobile before they are emitted to the environment. With the development of ultraviolet light emitting diodes (UV LEDs), it is possible to incorporate battery-powered UV light sources that are small enough for very niche applications, such as fuel vapor recovery systems. UV LEDs and a suitable photocatalyst, then, can be used to degrade VOCs within the automobile's fuel vapor recovery system. Results of this study include effects of humidity, temperature, and concentration of selected organic compounds on the efficiency and effectiveness of photocatalytically degrading fuel vapors within the fuel vapor recovery system in an automobile.

## **SYNTHESIS OF $\text{LiAl}_2$ -LAYERED DOUBLE HYDROXIDES FOR $\text{CO}_2$ CAPTURE OVER A WIDE TEMPERATURE RANGE**

**Liang Huang**, Junya Wang, Yanshan Gao, Yaqian Qiao, Qianwen Zheng and Qiang Wang  
(Beijing Forestry University, Beijing, China)  
Zhanhu Guo (Lamar University, TX, USA)  
Yufei Zhao (Chinese Academy of Sciences, Beijing, China)  
Dermot O'Hare (University of Oxford, Oxford, UK)

Although there have been many reports on layered double hydroxide (LDH) derived  $\text{CO}_2$  adsorbents, none of them have studied the special case of  $\text{LiAl}_2$  LDHs. Here we report the first detailed investigation of the performance of  $\text{LiAl}_2$  LDHs as novel  $\text{CO}_2$  adsorbents.  $\text{LiAl}_2$  LDHs were synthesized using both traditional coprecipitation and gibbsite intercalation methods. All the materials were thoroughly characterized using XRD, SEM, TEM, FTIR, BET, and TGA. The  $\text{CO}_2$  capture performance of these LDHs were investigated as a function of the charge compensating anions, Li/Al ratio in preparation solution, calcination temperature, adsorption temperature, and doping with  $\text{K}_2\text{CO}_3$ . The data indicated that  $\text{LiAl}_2$  LDHs derived compounds can be used as  $\text{CO}_2$  adsorbents over a wide temperature range (60–400 °C), with a  $\text{CO}_2$  capture capacity of 0.94 and 0.51 mmol g<sup>-1</sup> at 60 and 200 °C, respectively. By doping  $\text{LiAl}_2\text{-CO}_3$  LDH with 20 wt%  $\text{K}_2\text{CO}_3$ , the  $\text{CO}_2$  adsorption capacity was increased up to 1.27 and 0.83 mmol g<sup>-1</sup> at 60 and 200 °C, respectively.  $\text{CO}_2$  adsorption/desorption cycling studies showed that both pure  $\text{LiAl}_2$  LDH and the  $\text{K}_2\text{CO}_3$  promoted  $\text{LiAl}_2$  LDH had stable  $\text{CO}_2$  capture performance even after 22 cycles. Considering its high  $\text{CO}_2$  capture capacity and good cycling stability,  $\text{LiAl}_2$  LDH based novel  $\text{CO}_2$  adsorbents have significant potential for  $\text{CO}_2$  capture applications.

**NOVEL DeNO<sub>x</sub> AND DeSO<sub>x</sub> TECHNOLOGIES FOR FLUE GAS TREATMENT FOR BOILERS AND FURNACES**

***Jian Luo***

(KL Chemical Technologies, Inc., Tianjin Binhai EnviroTechnologies, Inc., Tianjin Key Lab of Heavy Metal Containing Waste water Treatment and Resources Recovery)

***Qihua Zhang***

(Tianjin Key Lab of Heavy Metal Containing Waste water Treatment and Resources Recovery, Tianjin, 300350, China)

Luo's Tehnologies for flue gas treatment, including a fabric filter device for particulate (as well as a part of heavy metal elements) removal, a fixed bed reactor for integrated removal of NO<sub>x</sub>, SO<sub>x</sub>, and heavy metals have been employed for treating flue gas for industrial and municipal boilers and furnaces. A novel oxidation catalyst for NO oxidation and subsequent removal, a reactant for SO<sub>x</sub> removal has been included for DeNO<sub>x</sub> and DeSO<sub>x</sub>, respectively. Two case studies, the applications of above-mentioned technologies and related devices combination for an industrial boiler with a capacity of 35 t/h in Langfang, Hebei Province and a municipal furnace for home heating in Tianjin (both in China) were shown. In both cases, the emission levels in terms of particuates, NO<sub>x</sub>, SO<sub>x</sub>, and heavy metals are well below those stipulated by Chinese nationals standards and are below those for natural gas firing boilers and furnaces. Pictures for devices, monitoring results, and comparison to other technologies will be shown in presentations.

## **IMMOBILIZATION OF SELF-STABILIZED PLASMONIC Ag-AgI ON MESOPOROUS Al<sub>2</sub>O<sub>3</sub> FOR NO ELIMINATION UNDER LED ILLUMINATION**

**Chun He**, Xiuqin Tan, Jiawei Zeng and Yaohua Hou (Sun Yat-sen University, Guangzhou, China)  
Dong Shu (South China Normal University, Guangzhou, 510006, China)

Nitrogen oxides (NO<sub>x</sub>), which result from automobile exhaust gas and industrial combustion of fossil fuels, are a major source of air pollution and cause ozone depletion, acid rain and photochemical smog. This has serious implications on the environment and health of the mankind. Till now, many conventional techniques have been developed to eliminate NO in industrial emission. However, these technologies were not economically feasible for removal of air pollutants at the parts per million (ppm) levels. The ideal process should be developed with further decreasing the economic and environmental costs of potential secondary pollution. Visible light driven (VLD) photocatalysis as a green technology that could use natural sunlight or artificial light to purify air pollutants at ambient condition, provides an attractive alternative to conventional approaches. Currently, the localized surface plasmon resonance (SPR) effect of noble-metal nanoparticles (e.g. Ag, Au, Pt) has become a research focus in the development of VLD photocatalysts. For practical application, the powdery photocatalyst would be simply blown away and time-consuming for nano-photocatalysts recycle. Therefore, to apply photocatalytic techniques in waste gas purification, it is essential to develop a facile process to effectively immobilize the powdery photocatalyst on a proper support

In this work, the plasmonic Ag-AgI with photoinduced self-stability was successfully immobilized on mesoporous Al<sub>2</sub>O<sub>3</sub> by a wet impregnation-precipitation and in-situ photoreduction method. The immobilized Ag-AgI/Al<sub>2</sub>O<sub>3</sub> was applied for photocatalytic removal of ppm-leveled NO under illumination of indoor LED tubes, which could obtain 100% NO removal in minutes at optimized conditions. The large dispersion of Ag-AgI on mesoporous Al<sub>2</sub>O<sub>3</sub> was firmly enough to overwhelm the continuous air flowing, and the enlarged surface area of Ag-AgI could efficiently enhance NO removal efficiency than pure Ag-AgI powder. Most importantly, the plasmonic Ag-AgI/Al<sub>2</sub>O<sub>3</sub> was stable in activity and can be used repeatedly without deactivation. On the basis of reactive species trapping and reaction intermediate monitoring, the responsible reactive species of photogenerated •OH, •O<sub>2</sub><sup>-</sup>, H<sub>2</sub>O<sub>2</sub> and h<sup>+</sup> were confirmed and the possible reaction mechanism of photocatalytic NO oxidation by Ag-AgI/Al<sub>2</sub>O<sub>3</sub> was revealed. The present work could provide new perspectives for promoting large-scale environmental applications of supported plasma photocatalysts.

## **TARGET-SPECIFIC CAPTURE OF RELEVANT GASEOUS POLLUTANTS USING BIODEGRADABLE POLYMERIC NANOPARTICLES**

***Fernanda Delbuque Guerra***, McKenzie L. Campbell, Frank Alexis and Daniel C. Whitehead  
(Clemson University, Clemson, SC, USA)

According to the World Health Organization (WHO), as urban populations grow, the quality of urban environments affects the public health with regards to issues ranging from waste disposal, water sanitation and air pollution. Anthropogenic and biogenic sources of chemical compounds can contribute to millions of deaths worldwide annually. Air pollution accounts for 1 in 8 deaths worldwide, corresponding to approximately 7 million deaths in 2012, according to data from the WHO. EPA has set National Ambient Air Quality standards for six principal pollutants; carbon monoxide, lead, nitrogen dioxide, ozone, particle pollution and sulfur dioxide. In regards to ozone levels, volatile organic compounds (VOCs) are of concern along with nitrogen oxides (NO<sub>x</sub>), once the reaction between these two classes of compounds, in the presence of light, is responsible for emission of ground level ozone. Major sources of NO<sub>x</sub> and VOCs include industrial facilities and electric utilities, motor vehicle exhaust, gasoline vapors, and chemical solvents. Many VOCs are also hazardous air pollutants and also known for their low, often unpleasant, threshold odor, which can be below parts per billion in some cases. Different nanotechnology approaches have been investigated in an effort to remediate such pollutants from the air. Among the many challenges preventing the global use of many nanomaterials are the high costs of fabrication, on-site recovery, limited scale-up, potential toxicity since many of them rely on metallic nanomaterials, the low off-targeting specificity responsible for decreasing the effectiveness of the material and the limited applicability to few classes of contaminants.

A rendering plant was used as a case study for the determination of the relevant compounds present at an industrial site. The sample analysis revealed different classes of chemical compounds, but aldehydes and carboxylic acids were predominant. Therefore, we developed biodegradable functional nanoparticles comprised of poly(d,l-lactic acid)-poly(ethylene glycol)-poly(ethyleneimine) (PDLLA-PEG-PEI) block co-polymers that are capable of capturing aldehydes and carboxylic acids by simple chemical reaction. Polymeric nanoparticles (NPs) were prepared using nanoprecipitation and surface functionalization with branched PEI was done by conjugation reaction using EDC. Aldehydes were captured by a condensation reaction forming imines, whereas carboxylic acids were captured by acid/base reaction. Our material has shown reductions of aldehyde and carboxylic acid vapors greater than 69% and 76%, respectively, reaching up to 98% in some cases. Further, we successfully demonstrated that a simultaneous capture of mixtures of aldehydes and carboxylic acids is possible, as well as the simultaneous capture of a mixture of two aldehydes. The nanoparticles reacted selectively with target contaminants obviating off-target binding when challenged by other VOCs with orthogonal reactivity. In additions to competition assays we have successfully demonstrated that our material outperforms activated charcoal, a well-known sorbent material widely used for various applications including flue gas treatment processes. The significant advantage of our strategy relies on the ability to tailor the surface functionality of the nanomaterials for a specific target analyte from vapormixtures.

## **WATER SCRUBBING OF H<sub>2</sub>S GAS IN DUAL-FLOW SIEVE PLATE COLUMN SCRUBBER**

**Swamy Kurella**, Pavan Kishan Bhukya and B. C. Meikap  
(IIT Kharagpur, West Bengal, India)

Plate scrubbers can be used for the removal of acid gases from the exhaust gas streams which are being released into the environment from many chemical process industries. The raw syngas which leaves from coal gasification units is having particulate matter and acid gases majorly hydrogen sulfide (H<sub>2</sub>S) and hydrogen chloride. A three stage lab scale dual-flow sieve plate column scrubber has been designed, fabricated and installed. In this work, the experiments were conducted to observe the removal of H<sub>2</sub>S using water as absorbing solution in the dual-flow sieve plate column wet scrubber. The H<sub>2</sub>S removal efficiencies were estimated at different liquid to gas ratios for 50 ppm, 100 ppm, 200 ppm and 300 ppm inlet H<sub>2</sub>S concentrations. The operated gas flow rates were from  $1.93 \times 10^{-3}$  Nm<sup>3</sup>/s to  $2.76 \times 10^{-3}$  Nm<sup>3</sup>/s and the liquid flow rates were from  $27.53 \times 10^{-6}$  m<sup>3</sup>/s to  $48.18 \times 10^{-6}$  m<sup>3</sup>/s. The removal efficiency increased with the liquid flow rate, gas flow rate and inlet H<sub>2</sub>S concentration. The maximum percentage removal of H<sub>2</sub>S is observed at  $2.76 \times 10^{-3}$  Nm<sup>3</sup>/s gas flow rate and  $48.183 \times 10^{-6}$  m<sup>3</sup>/s liquid flow rate for 300 ppm. A model has also been developed to predict the H<sub>2</sub>S gas removal by using the results from the experiments and adding the variables which show impact on the scrubber performance.

## **INDUSTRIAL AIR POLLUTION IN SAUDI ARABIA AND THE INFLUENCE OF METEOROLOGICAL VARIABLES**

***Jamal A. Radaideh***

(Civil and Environmental Dept., King Faisal University, Saudi Arabia. jalradaideh@kfu.edu.sa)

**ABSTRACT:** This survey study focuses on major air pollutants at the second industrial city in Dammam/Eastern province of Saudi Arabia, which was carried out in two following weeks during April 2015, and aims to estimate the degree of air pollution arise from industry and to determine the influence of meteorological variables on concentrations of air pollutants. The study investigated the distribution of major air pollutants including, carbon monoxide (CO), sulfur dioxide (SO<sub>2</sub>), nitrogen dioxide (NO<sub>2</sub>), volatile organic compounds (VOCS), ozone (O<sub>3</sub>), hydrogen sulfide (H<sub>2</sub>S), Carbon dioxide (CO<sub>2</sub>) and respirable particulate matter (PM<sub>2.5</sub> and PM<sub>10</sub>) in ambient air of Dammam industrial estate. Correlation analyses have been used to examine the association of air pollutants with each other and with meteorological variables. It was found that TVOC, PM<sub>10</sub>, TPS have a positive relationship with relative humidity, but negatively correlated with ambient temperatures. NO<sub>2</sub> in contrast, has a reverse correlation with relative humidity and a positive relationship with ambient temperatures. Ozone concentrations vary slightly in dependence of changing meteorological factors (temperatures and relative humidity). Our results suggest that appropriate industrial air pollution control should be applied to coarse particulate (PM<sub>10</sub>) and gaseous pollutants in the study area.

**Keywords:** Air pollution monitoring, air pollutants, meteorological variables, 2nd industrial city of Dammam, Saudi Arabia.

### **INTRODUCTION**

Recently, air pollution has become a major issue in Saudi Arabia and the neighboring GCC (Gulf corporation countries) because of accelerating urban development and growing industrialization. While Saudi Arabia's economic growth continues to be dominated by oil, the Kingdom has taken steps to diversify its economy. Heavy dependence on petroleum revenue continues, but industry and agriculture now account for a larger share of economic activity. Today, industrial products make up more than 90 percent of the Kingdom's non-oil exports. Saudi Arabia exports petrochemicals, plastics, metal goods, construction materials and electrical appliances to some 90 countries [1]. Petrochemical and other oil-based industries are concentrated at industrial cities in major urban centers. These plants use natural gas and natural gas liquids that were previously flared, as well as refined products from the oil industry to manufacture products that would in turn feed non-oil industries. Concentration on industrial plants in specific areas also facilitates the provision of vital support services, such as water, power and transportation. Since the mid-1970s, attention has centered on industrial development, primarily in the downstream activities of the petroleum sector and on import substitution. In fact, one of the most significant Kingdom's development strategies is the varying selection of industries. Steel plants, fertilizer plants, domestic and export-oriented refineries, and a series of major petrochemical complexes form the basis of the government's attempt to diversify the economy.

One of the problems that occur in Kingdom of Saudi Arabia like other countries in the world is air pollution. Air pollution in Saudi Arabia is now recognized as a significant environmental impact of intensive anthropogenic activities. Heavy traffic in the streets of urban areas increases emissions of O<sub>3</sub> as a result of the increased emissions of precursors (NO<sub>x</sub> and VOCS). Also, the local Saudi climatic conditions (high temperature, intense solar radiation, clear sky) lead to enhanced formation of



photochemical pollutants. Hence, the air pollution is the cause of many risks on health and environment, many of the people not realize it, but air pollution impacts our everyday life, causing grave health and environmental damages.

Air pollution is a main environmental risk to health. Through reducing air pollution levels, countries can reduce the trouble of disease from emphysema, heart disease, lung cancer, and both chronic and acute respiratory diseases, including asthma. WHO estimates that some 80% of outdoor air pollution-related premature deaths were due to ischemic heart disease and strokes, while 14% of deaths were due to chronic obstructive pulmonary disease or acute lower respiratory infections; and 6% of deaths were due to lung cancer. The 2005 "WHO Air quality guidelines" offer global guidance on thresholds and limits for key air pollutants that pose health risks. The Guidelines indicate that by reducing particulate matter (PM<sub>10</sub>) pollution from 70 to 20 micrograms per cubic meter (µg/m<sup>3</sup>), we can cut air pollution-related deaths by around 15% [4].

The multiple sources of air pollution and the heavy load of pollutants are a normal result of accelerated economic growth Saudi Arabia witnessed over the past three decades. Higher rates of air pollution are becoming strongly correlated with economic progress and style of living. Saudi Arabia's energy consumption has climbed dramatically over the past two decades. The energy consumption was 1.7 quadrillion Btu (quads) in 1980, and it was 4.6 quads in 2000. Overall, Saudi Arabia consumes about 1.1% of the world energy consumption. Therefore, Saudi Arabia's carbon emissions from transport sector have jumped in the past 40 years from 3.29 million metric tons in 1971 to 104.42 million metric tons in 2010. In addition the value for CO<sub>2</sub> emissions from gaseous fuel consumption (ktonn) in Saudi Arabia was recorded as much as 140,500 ktonn in 2009, while a minimum value of 0.00 ktonn was recorded in 1960 [3]. In the Gulf Cooperation Council (GCC) countries total atmospheric emission loads are about 3.85 million tons per year, made of 28% CO, 27% SO<sub>2</sub> and 23% particulates. Recent studies have indicated that the Gulf countries emit about 50% of the total of Arab countries' (254 million metric tons of carbon) emissions of CO<sub>2</sub> [5]. In terms of per capita carbon emissions, Saudi Arabia is still a regional leader. In 2000, the country's per capita carbon emissions were 3.7 metric tons [4].

The multiple sources of air pollution and the heavy load of pollutants are but a normal consequence of accelerated economic growth Saudi Arabia witnessed over the past three decades. Higher rates of air pollution are becoming strongly correlated with economic progress. Therefore, the Kingdom of Saudi Arabia has paid special attention to monitoring and reducing such emissions through concerted efforts under taken at both national and international levels alike.

Given the widespread concern of ambient air pollution in Saudi Arabia and its broad ranging impacts, the present study is focused on investigation of air pollution in one of the densest industrial areas of the region. The objective of this study is to present the spatial distributions of selected gaseous pollutants (SO<sub>2</sub>, NO<sub>2</sub>, CO, H<sub>2</sub>S, CO<sub>2</sub>, TVOC and Ozone) and particulate matter (PM<sub>2.5</sub>, PM<sub>10</sub> and PM<sub>1</sub>) within the study area and to identify the major impacts of air pollutants. Evaluation of existing air quality findings is occurring using limits recommended by available local and global air quality standards and guidelines, in particular NAAQS of USEPA [6], WHO air quality guidelines [2 and 3], PME standards [7], RCER for Jubail & Yanbu [8] and the European standards [9] will be reference standard for this survey study.

## **MATERIALS AND METHODS**

The 2nd industrial city in Dammam is one of the highest areas of industrial cities in kingdom of Saudi Arabia, which contain 340 of factories occupied a total area of 25,520,000 m<sup>2</sup>. It was established in (1978) and has 75,000 of workers distributed over the different factories involving food and drinks, manufactured metal products, machineries and equipment's, chemical products, building materials, textiles, wood products and furniture.

Air sampling using Air quality monitoring mobile station used to conduct the measurements of potential air pollutants.

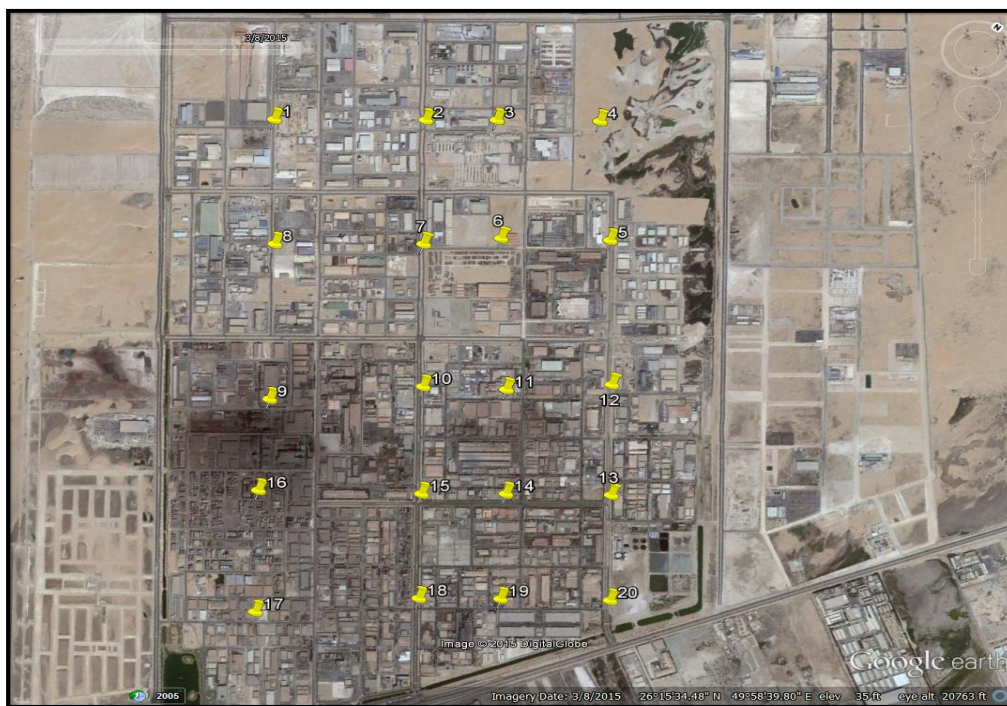


Figure 1. Boundary of 2<sup>nd</sup> industrial city of Dammam as shown by google map showing assigned location points for measurements and sampling (L1 - L20).

The survey study was conducted during two following weeks with noticeable change in ambient outside temperature and varying relative humidity. A total of 200 measurements and samples are collected over the course of study at selected points outside factories and workshops. Data of particulate matter (PM<sub>2.5</sub>, PM<sub>10</sub> and PM<sub>1</sub>) and gaseous air pollutants such as nitrogen dioxides (NO<sub>2</sub>), ozone (O<sub>3</sub>), carbon monoxide (CO), sulfur dioxide (SO<sub>2</sub>), carbon dioxide (CO<sub>2</sub>) and total organic compounds (TVOC) are measured. Meteorological parameters like temperatures and relative humidity are also collected during this survey. Levels of gaseous pollutants are analyzed using Wolf Pack AAQ Instrument. The PM levels are obtained using a particulate matter monitor (AEROCET 531S). The samplers draw air through a filter paper at a known constant rate for 24 hours. The resulting increase in the weight of the filter paper is expressed as the particulate concentration.

## STUDY AREA

The second industrial city of Dammam is located outside the urban boundaries of the city. The area with the coordinates, Latitude: 26°15'31"N Longitude: 49°58'5"E has a length of 15.57 kilometers and houses about 340 different factories.

The sampling station is installed at all points assigned for data collection (L1 – L20). Each point is supposed to represent a specific area from the whole study area. Factories are distributed randomly and equally over the area in a way that any measured air pollutant couldn't be referred to any specific industry.

When instrument is turned on, it starts to record concentrations of gaseous pollutants and particulate matter. After 6-8 minutes the recorded levels of concentrations are displayed on screen for all considered pollutants. The average value of all readings (60-65 readings) for each potential pollutant is presented in Table 1.

## DATA COLLECTION AND ANALYSIS

As soon as the measuring devices are calibrated and turned on to record pollution levels at each assigned location, recorded data pass through rectify units and an average value is displayed. For each

potential pollutant about 60 – 65 values are registered during the measuring period ranging from 7-8 minutes. The hourly mean concentrations of the measured pollutants during the two periods of study are presented in Table 1. In addition meteorological parameters such as temperature and relative humidity are recorded continuously and simultaneously.

Table 1: Results of air quality monitoring survey at 2<sup>nd</sup> industrial city/Dammam

Location	SO <sub>2</sub>	NO <sub>2</sub>	TVOC	CO <sub>2</sub>	Ozone	CO	PM1	PM2.5	PM10	TSP
points	ppm	ppm	µg/m <sup>3</sup>	ppm	ppm	ppm	(µg/m <sup>3</sup> )	(µg/m <sup>3</sup> )	(µg/m <sup>3</sup> )	(µg/m <sup>3</sup> )
L1	0.622	0.104	76.94	541.29	0.088	1.35	17.050	64.525	385.750	527.650
L2	0.630	0.130	54.27	561.98	0.081	1.43	14.800	56.067	159.933	170.867
L3	0.660	0.087	74.77	548.27	0.080	1.39	15.333	65.767	438.733	612.567
L4	0.500	0.100	58.80	541.09	0.082	1.34	15.700	60.250	264.800	309.150
L5	0.490	0.067	27.73	520.08	0.084	1.28	14.875	56.500	198.825	221.000
L6	0.512	0.083	33.51	559.22	0.080	1.26	14.067	61.633	491.133	710.033
L7	0.420	0.080	37.23	554.80	0.080	1.24	13.300	57.800	384.900	497.867
L8	0.380	0.102	89.51	602.16	0.086	1.23	14.067	62.067	405.233	539.833
L9	0.390	0.060	8.34	567.42	0.068	1.39	13.467	62.867	421.000	578.000
L10	0.400	0.064	42.92	560.59	0.086	1.28	15.933	64.633	434.867	611.233
L11	0.569	0.010	164.02	531.93	0.069	1.18	26.567	209.167	1409.767	1904.967
L12	0.476	0.021	141.59	537.02	0.090	1.80	26.133	204.800	1525.000	2196.700
L13	0.461	0.030	155.40	558.55	0.096	1.37	25.800	199.167	1470.533	2129.167
L14	0.524	0.035	135.84	538.58	0.089	1.58	27.900	218.000	1858.350	2737.900
L15	0.532	0.037	207.29	554.00	0.103	1.63	22.500	168.125	1229.550	1752.350
L16	0.692	0.027	256.40	584.13	0.092	1.56	29.033	226.133	1806.367	2767.333
L17	0.541	0.060	158.66	611.66	0.104	1.47	31.067	239.367	1717.633	2417.700
L18	0.674	0.069	118.52	631.18	0.103	1.41	31.967	234.700	1495.667	2009.000
L19	0.817	0.053	115.73	606.75	0.093	1.63	29.700	229.400	1742.550	2634.200
L20	0.800	0.067	67.78	546.20	0.099	1.57	30.600	228.033	1398.233	1740.700

Conversion factors: CO: 1 ppm  $\approx$  1.15 mg/m<sup>3</sup>, NO<sub>2</sub>: 1 ppm  $\approx$  378.5 ppb  $\approx$  1880 µg/m<sup>3</sup>, SO<sub>2</sub>: 1 ppb  $\approx$  2.6 µg/m<sup>3</sup> and 1ppm  $\approx$  2760 µg/m<sup>3</sup>, CO<sub>2</sub>: 1 ppm  $\approx$  1.83 mg/m<sup>3</sup>, Ozone: 1 ppm  $\approx$  1966 µg/m<sup>3</sup>  $\approx$  1.143 mg/m<sup>3</sup>.

## RESULTS AND ANALYSIS OF DATA COLLECTION

**Analysis of TOVC Concentrations.** As Table 1 and the derived Figure 3 show that the concentrations of TVOC are in the range of 27.73 – 89.51 µg/m<sup>3</sup> with an average of 53.39 µg/m<sup>3</sup> for first measurement batch conducted at locations L1 to L10, while during the second measurement period values are ranging from 115.73 – 256.40 µg/m<sup>3</sup> with an average of 152.123 µg/m<sup>3</sup> found at locations L11- L20. It is clearly observed that significantly higher TVOC levels are obtained during the second measurement batch at locations L11 – L20 against those recorded at locations L1 – L10 during the first measurement period.

The higher concentration of TVOC at these sampling sites is attributed to decrease in temperatures and relative humidity. The ambient temperatures during the first period were ranging from 35.81°C to 38.60 °C and the relative humidity values were in the range of 9.95% – 15.93%. During the second period the temperatures were in range of 29.56°C to 36.90 °C and the relative humidity values were in the range of 21.24% – 45.08%. The magnitude of air pollution in regard to TVOC couldn't be evaluated because there are no available standards for TOVC to compare with.

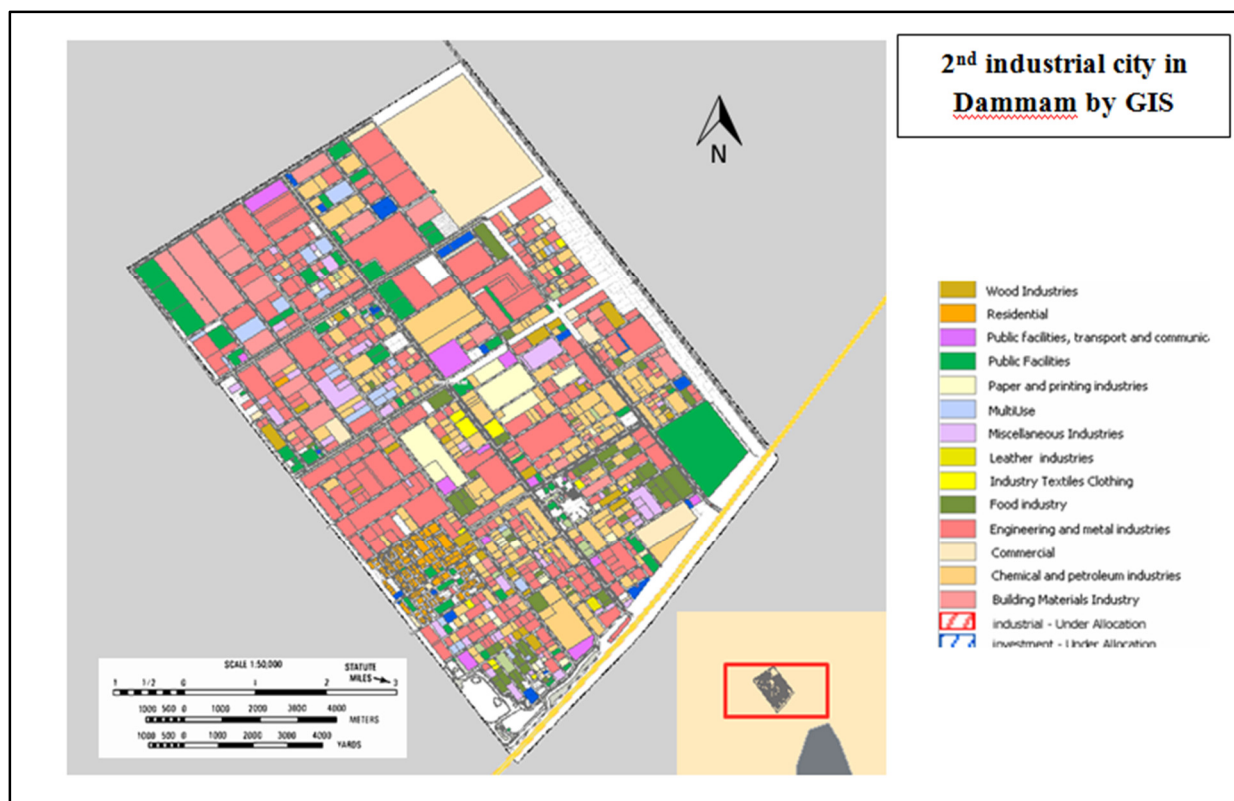


Figure 2. Distribution of factories over the area 2<sup>nd</sup> dammam industrial city and the location of sampling points (L1-L20).

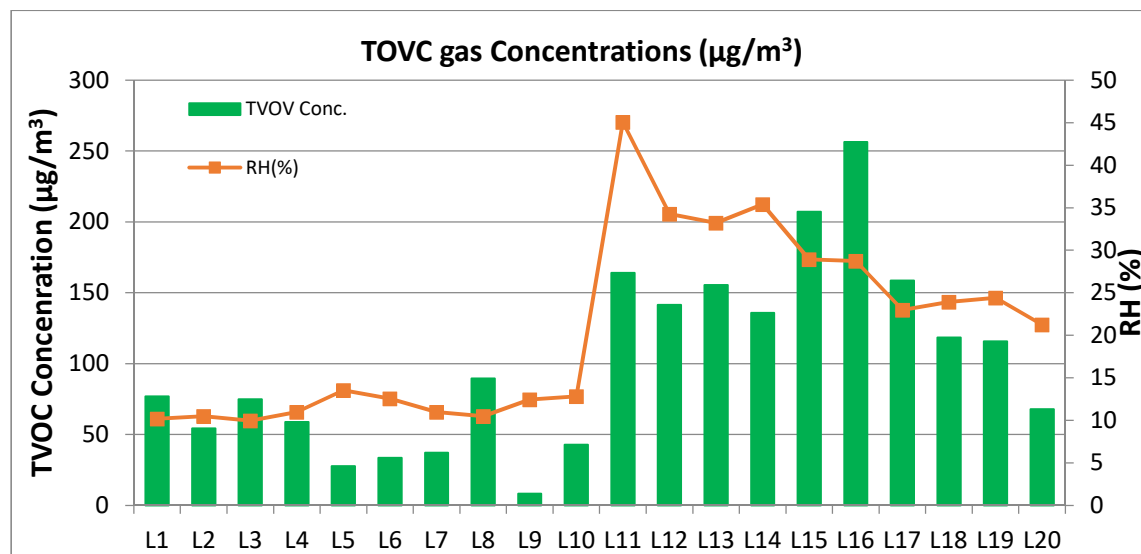


Figure 3. TVOC concentrations monitored at locations L1 – L20.

**Analysis of CO Concentrations.** For all Locations L1- L20, the hourly carbon monoxide concentrations ranged from 1.18 to 1.80 ppm with an overall hourly average of 1.42 ppm as shown in table 1. It is clear from the results also that all the measurements were below 2 ppm. The recorded 1-h measurements were compared with the available national and global standards: this comparison showed that almost all recorded results of the current study were below the 1-h average standards. As shown in table

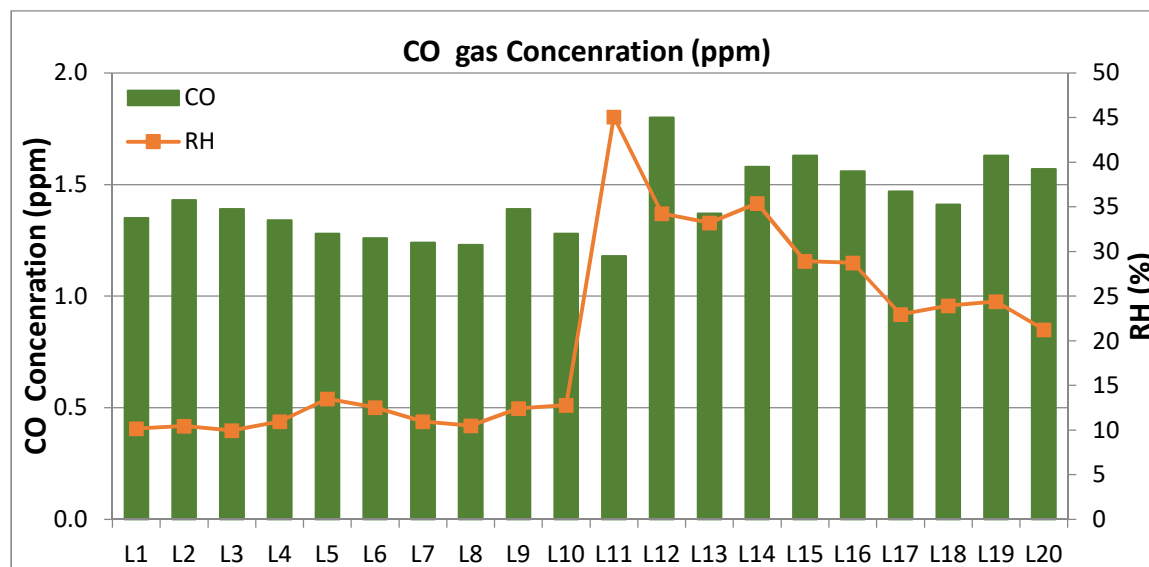


Figure 4. CO concentrations monitored at locations L1 – L20.

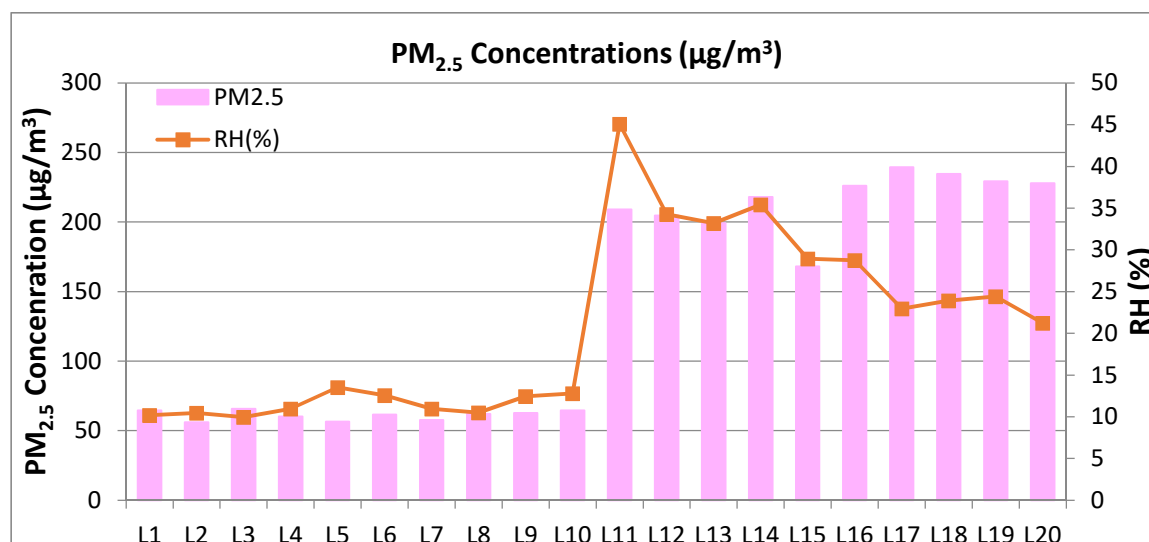


Figure 5. Average values of PM<sub>2.5</sub> recorded during both survey periods

**Analysis of PM<sub>2.5</sub> Levels.** As shown in Table 1, the concentration of PM<sub>2.5</sub> was in the range of 56.5 – 65.77 µg/m<sup>3</sup>, in average of 61.21 µg/m<sup>3</sup> for the first measurement period and in the range of 168.12– 239.37 µg/m<sup>3</sup> with an average of 215.69 µg/m<sup>3</sup> for the second period. The variation of particulate concentrations during this period was found to be minimal and below USEPA standards. Significantly higher PM<sub>2.5</sub> values were obtained at locations L11 to L20 compared to those obtained at locations L1-L10 during second period. The higher concentrations of particulate pollution at these sampling sites may be attributed to re-suspension of dust (road dust, entrainment of dust into the air from nearby areas and vehicular traffic around the study area) and to decrease in temperatures and associated relative humidity. Comparing values of PM<sub>2.5</sub> with allowable limits, it is clear that the quality of ambient air is below air quality standards defined available standards as shown in table.



**Analysis of PM<sub>10</sub> Concentrations.** Table 1 presents the average PM<sub>10</sub> concentrations found at sampling sites during both sampling periods. The average concentrations at locations L1 – L10 were found in the range of 159.93 – 491.13  $\mu\text{g}/\text{m}^3$ , while the average concentrations at locations L11 – L20 were found significantly higher and ranging from 1229.55 – 1858.35  $\mu\text{g}/\text{m}^3$ . Comparing the 1-h results at locations L1 – L10 with the available standards showed that they fluctuating around the highest allowable standards value defined by PME [7] standards. However, all of the individual recorded results were far beyond the desired value recommended by national and international standards as Table 1 indicates.

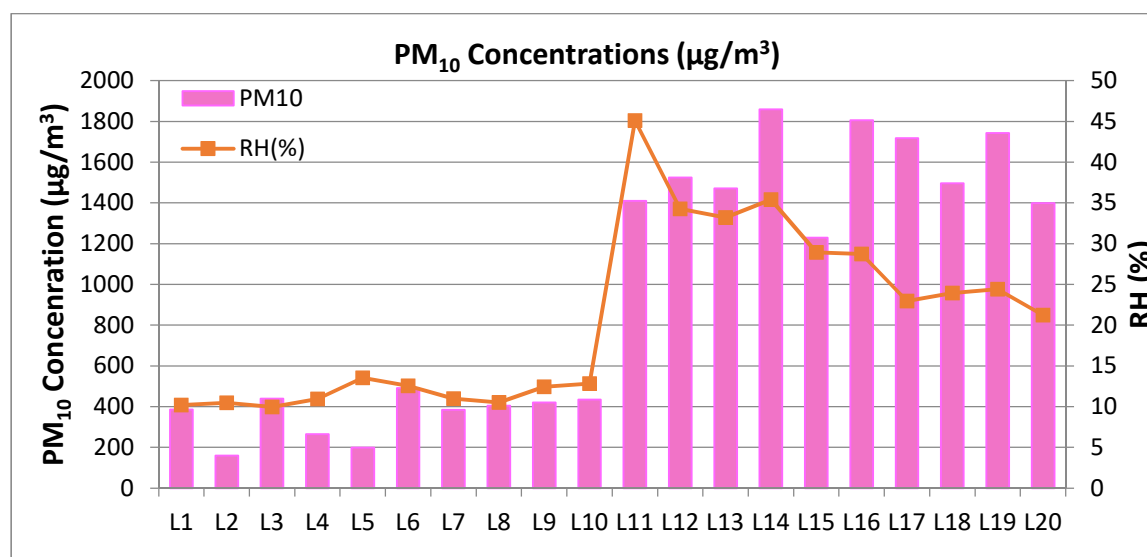


Figure 6. Average values of PM<sub>10</sub> recorded during both survey periods

**Analysis of Total Suspended Particles (TSP) Concentrations.** (TSP) are tiny airborne particles or aerosols that are  $\leq$  than 100 micrometers are collectively referred to as total suspended particulate matter (TSP). These particles constantly enter the atmosphere from many sources include human activities (combustion products, industrial processes and power generation) and from natural sources (soil, bacteria and viruses, fungi, mold and yeast, pollen, vapors and aerosols).

Table1 presents the average values of TSP concentrations found at sampling sites during both survey periods. The average concentrations at locations L1 – L10 were found in the range of 170.87 – 710.03  $\mu\text{g}/\text{m}^3$ , while the average concentrations at locations L11 – L20 were found significantly higher and ranging from 1740.70 – 2767.33  $\mu\text{g}/\text{m}^3$ . The higher levels of suspended particulates at locations L11 – L20 recorded during the second sampling period may be attributed to noticeable decrease in temperatures and relative humidity.

Comparing the 1-h results at locations L1 – L10 with the available standards showed that they fluctuating around the highest allowable standards value defined by PME standards. However, all of the individual recorded results were far beyond the desired value recommended by NAAQS of USA, WHO, and the European standards.

**Analysis of Ozone Concentrations.** The results of ozone monitoring are presented in Table1. As Figure 8 shows, average ozone concentrations are in range of 0.068 to 0.088 ppm for samples taken at locations L1 – L10 during the first sampling period. The overall average for these readings is (ppm). Concentrations taken during the second period are ranging from 0.069 to 0.104 ppm, with an average of (ppm). The ozone concentrations vary slightly among sampling locations and with varying meteorological variables during sampling periods. Comparing obtained levels for ozone with the available standards [6, 7, 8, 9 and 10], it is conclude that measured ozone is matching the reference standards used as evaluation basis for air quality.

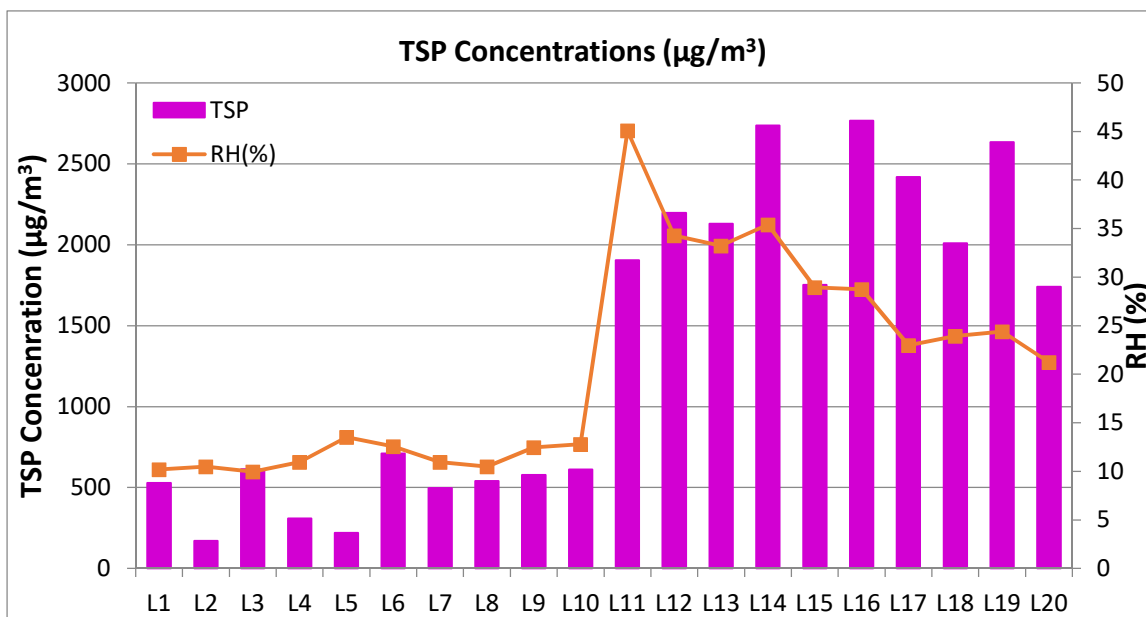


Figure 7. Average values of TSP concentrations recorded during survey periods.

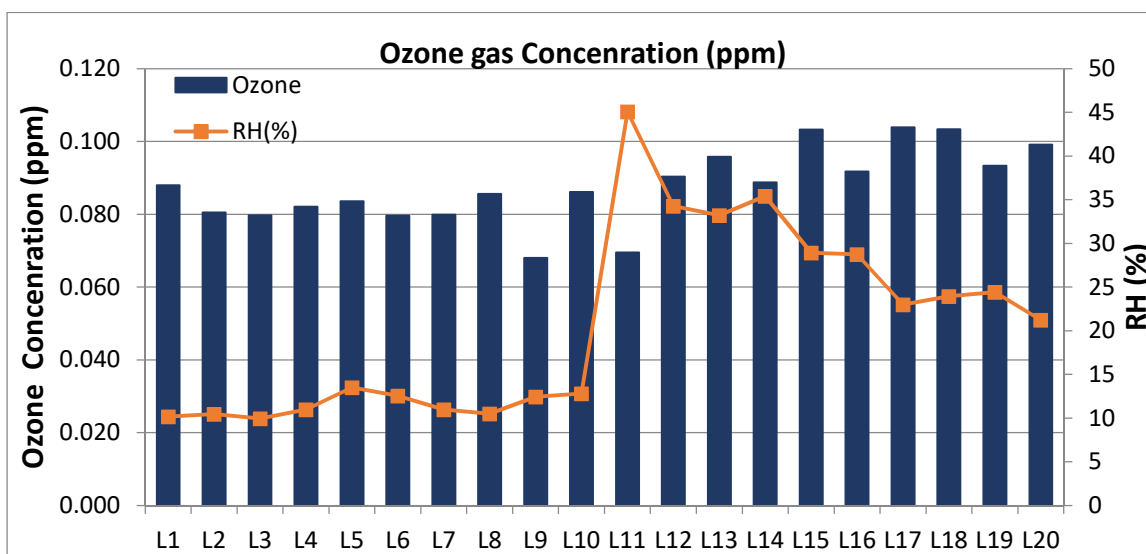


Figure 8. Average values of Ozone concentrations monitored during survey periods.

As indicated in figure 8 the correlation between relative humidity and ozone levels couldn't be clearly demonstrated. However a slight increase in ozone levels at locations L11 – L20 is noticeable and could be referred to the increase in ambient relative humidity during the sampling period.

**Analysis of NO<sub>2</sub> Concentrations.** It is apparent from Table 1 and Figure 9 that the average NO<sub>2</sub> concentrations ranged from 0.06 ppm to 0.104 ppm for samples taken at locations L1 – L10 during the first measuring period with an overall average of (0.88 ppm). The NO<sub>2</sub> concentrations taken during the second period at Locations L10 – L20 are ranging from 0.01 to 0.069 ppm with an overall average of (0.41 ppm) for this sampling batch. It has been noticed that the results were fluctuating among locations. Comparing existing concentrations taken during both sampling periods with available standards as shown in table, it is obvious that the quality of ambient air is below air quality defined by available standards. In addition,

Figure 9 shows clearly the decrease of NO<sub>2</sub> levels taken during the second sampling batch (at L11 – L20) against those monitored during the first sampling period taken at locations L1 –L10). Variations in meteorological parameters (temperatures and relative humidity) could be seen as cause for this concentration drop. Therefore, it is to conclude that NO<sub>2</sub> concentrations decrease as relative humidity increase, but decrease as temperature decrease. The negative correlation indicates that probably high temperatures result in higher dispersion and dilution of air pollutants, probably linked with vertical and horizontal turbulence [11].

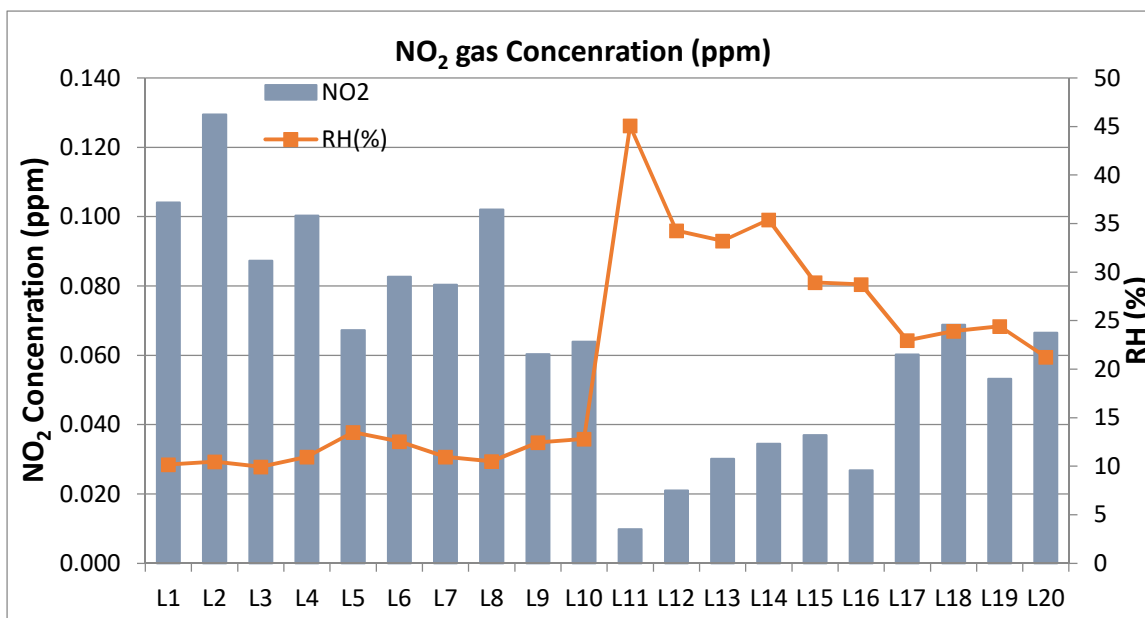


Figure 9. Average values of NO<sub>2</sub> concentrations monitored at locations L1 – L20.

**Analysis of SO<sub>2</sub> Concentrations.** The concentrations of SO<sub>2</sub> in the first measuring period at locations (L1 –L10) are in the range (0.38 – 0.66 ppm) with a daily average equals 0.50 ppm, while in the second period the concentrations ranging from 0.461 – 0.817 ppm with an average 0.53 ppm, slightly higher than during first period, as shown in Table 1 and Figure 10. A clear dependency of this result with the relative humidity couldn't be established. However, the small increase in concentrations at locations L11-L20 compared to levels of SO<sub>2</sub> monitored at L1-L10 could be referred to increase in relative humidity.

**Analysis of CO<sub>2</sub> Concentrations.** As presented in Table 1, Concentration levels of CO<sub>2</sub> are ranging from 541- 602 ppm with an of 555.7 ppm for measurements taken at L1 – L10 while the values of CO<sub>2</sub> levels ranged from 531- 631 ppm with an average 570.00 ppm for the points L11-L20. The concentration of CO<sub>2</sub> is almost constant at all points throughout the study area and don't experience any change in relation change of meteorological parameters (temperature and relative humidity). Although carbon dioxide is naturally present in the atmosphere as part of the Earth's carbon cycle, monitored levels came as high as it is expected in industrial areas. The main human activity that emits CO<sub>2</sub> is the combustion of fossil fuels (coal, natural gas, and oil) for energy and transportation, although certain industrial processes and land-use changes also emit CO<sub>2</sub>.



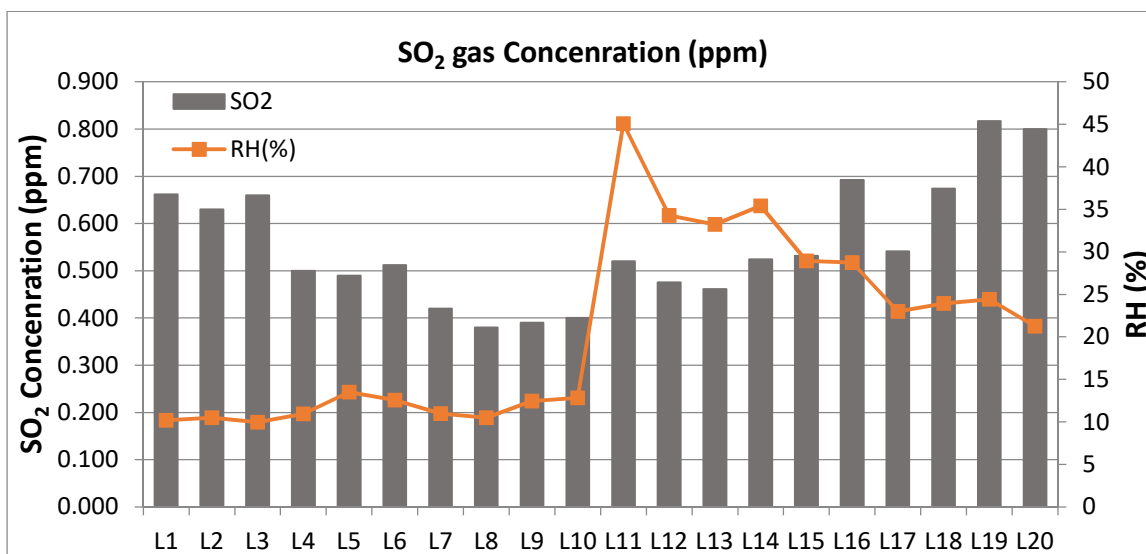


Figure 10. Average values of SO<sub>2</sub> concentrations monitored at locations L1 – L20.

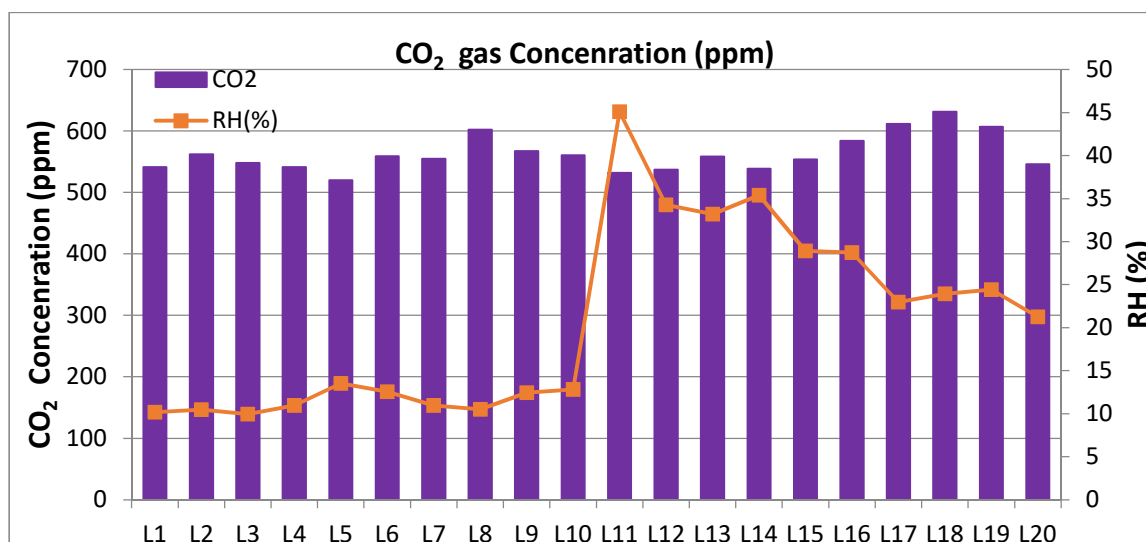


Figure 11. Average values of CO<sub>2</sub> concentrations monitored at locations L1 – L20.

## DISCUSSION

Air in the Kingdom of Saudi Arabia is generally not polluted. However, there are certain locations where the concentration of some pollutants could and do reach levels above the acceptable limits. This country is developing rapidly and the volume of imported and domestically produced chemicals and other products are on the increase which will all contribute to various types of air pollutants.

The study thought to examine the relationship between potential air pollutants (gaseous and particulate) among each other and with selected meteorological variables, emitted from factories distributed over the area of 2<sup>nd</sup> industrial estate of Dammam during 2 weeks in April, 2015. From the results presented for potential air pollutants and with considering Table 2 as basis for evaluation, it is quite evident that the quality of air in and around industrial cities might well be different from that of the rest of the Kingdom.

The analysis and comparison of collected data indicates that particulate matter in form of PM<sub>10</sub> and PM<sub>2.5</sub> contributes most to the highest levels of pollution. The recorded levels of these air pollutants reach ranges that exceed limit values adopted by all jurisdictions. For particulate matter, it is a major problem in Saudi Arabia, especially, in eastern province of Saudi Arabia that occasionally experience high particulate

and suspended matter concentrations as high as 900 – 1000  $\mu\text{g}/\text{m}^3$  [13]. Concentrations as high as monitored (215.69 and 1565.36)  $\mu\text{g}/\text{m}^3$  are detrimental to infrastructure and are a health hazard to human beings.

Table 2. Comparison of monitored air pollutants at 2<sup>nd</sup> industrial city based on the available air quality standards. All values are given either in ppm or in  $\mu\text{g}/\text{m}^3$ .

Pollutant		PM <sub>2.5</sub>	PM <sub>10</sub>	SO <sub>2</sub>		NO <sub>2</sub>		CO	O <sub>3</sub>
Air quality standards		$\mu\text{g}/\text{m}^3$	$\mu\text{g}/\text{m}^3$	ppm	$\mu\text{g}/\text{m}^3$	ppm	$\mu\text{g}/\text{m}^3$	ppm	$\mu\text{g}/\text{m}^3$
NAAQSs (USA) [6]		12***	150***	0.12*	-	0.246*	-	35*	0.075**
CAAQSs (Canada) [12]		-	-	0.335*	-	0.213*	-	30.6*	0.082
WHO [10]		25***	50***	0.13*	20*	0.07*	200***	26*	100**
EU guideline [9]		25	50***	0.28*	350*	-	200	0.14*	120**
PME + (RCER) [6] + [7]		35***	340***	0.28*	-	0.35*	-	32*	0.15*
Exist. value	L1 - L10	61.21*	358.52*	0.504*	-	0.088*	-	1.319*	0.081*
	L10 - L20	215.69*	1565.36*	0.604*	-	0.041*	-	1.52*	0.094*

\*: averaged over 1-hr      \*\*: averaged over 8-hr      \*\*\*: averaged over 24-hr      Conversion factors: CO: 1 ppm  $\approx$  1.15 mg/ $\text{m}^3$ , NO<sub>2</sub>: 1 ppm  $\approx$  378.5 ppb  $\approx$  1880  $\mu\text{g}/\text{m}^3$ , SO<sub>2</sub>: 1 ppb  $\approx$  2.6  $\mu\text{g}/\text{m}^3$  and 1 ppm  $\approx$  2760  $\mu\text{g}/\text{m}^3$ , CO<sub>2</sub>: 1 ppm  $\approx$  1.83 mg/ $\text{m}^3$ , Ozone: 1 ppm  $\approx$  1966  $\mu\text{g}/\text{m}^3 \approx$  1.143 mg/ $\text{m}^3$ .

The observed CO level (1.32 and 1.52 ppm) fell below the limit values adopted by NAAQS (USA, Canada), WHO and PME + RCER, but higher than EU allowable limits of 0.14 ppm. Ozone concentration measurements showed that in the study area, moderate ozone concentrations were measured. The recorded average values (0.081 and 0.094) and over 1-hr averaged slightly exceed the selected guideline values, in particular, are higher than the value of (0.075, 8-hr average) adopted by NAAQS of USA.

SO<sub>2</sub> maintains higher levels than required indicating a pollution. NO<sub>2</sub> maintains levels very close to the WHO guideline value around the world. For particulate matter, it is a major problem in almost all of Asia, exceeding 300  $\mu\text{g}/\text{m}^3$  in many cities.

## CONCLUSIONS

The present study analyzed the concentrations of potential air pollutants including SO<sub>2</sub>, NO<sub>2</sub>, TVOC, CO<sub>2</sub>, CO and O<sub>3</sub> measured at the 2<sup>nd</sup> industrial city/Dammam over 2 weeks in April 2015 and shows the daily average of monitored air pollutants are above the permissible limits suggested by available national and international jurisdictions such as PME and RCER, NAAQS of USA and Canada and the WHO guidelines. This result indicates that there are some areas suffering from air pollution and require immediate action plans to deal with the problem.

The interaction between various air pollutants and meteorological parameters is confirmed through the results of study and concluded that levels of observed air pollutants not only depend on the amount of pollutants emitted from various sources but also on meteorological parameters.

Analysis of temperatures and relative humidity clearly demonstrated that air pollutants concentrations increase with increase in relative humidity and decrease of temperatures.

## REFERENCES

- [1] "The Petrochemicals and Plastics Sector in the Kingdom of Saudi Arabia". U.S.-Saudi Arabian Business Council. Retrieved 12 February 2015.
- [2] The World Health Organization, (2011) air quality in countries around the globe.
- [3] WHO Factsheet N 313, March 2014. [WWW.who.int/mediacentre/factsheets/fs303/en/](http://WWW.who.int/mediacentre/factsheets/fs303/en/)
- [4] Abdallah, Kathleen. "Health and Environmental Benefits of Clean Fuels and Vehicles. "Keynote presentation. Cairo, Egypt: UN DESA, May 24, 2006.
- [5] Karin B. Yeatts, et.al. Indoor Air Pollutants and Health in the United Arab Emirates. *Environmental Health Perspectives* • volume 120, issue 5, May, 2012 . *Environ Health Perspect*; DOI:10.1289/ehp.1104090.
- [6] U.S. Environmental Protection Agency, (2011) National Ambient Air Quality Standards (NAAQS).
- [7] Ambient Air Quality, Presidency of Meteorology and Environment. Kingdom of Saudi Arabia National Environmental Standard.
- [8] Kingdom of Saudi Arabia National Environmental Standard. Ambient Air Quality Standards. Royal Commission Environmental regulations RCER for Jubail & Yanbu, 2004, Vol.I.
- [9] Air Quality standards, European Community 2014. New Air quality Directive (The Directive2008/50/EC). <http://ec.europa.eu/environment/air/quality/legislation/directive.htm>
- [10] WHO, Public Health Environment (PHE), Air Quality Guidelines 2005. [http://www.who.int/phe/health\\_topics/outdoorair/outdoorair\\_aqg/en/](http://www.who.int/phe/health_topics/outdoorair/outdoorair_aqg/en/)
- [11] EPA, 2010. US Environmental Protection Agency, air pollution control orientation course. Control emissions technologies. Transport and dispersion of air pollutants. <http://www.epa.gov/apti/course422/ce1>
- [12] Canadian Air Quality Standards CAAQS of Canada.. [http://www.ccme.ca/en/current\\_priorities/air/caaqs.html](http://www.ccme.ca/en/current_priorities/air/caaqs.html).
- [13] B.H. Alharbi, M.J.Pasha, and N. Tapper. Assessment of ambient air quality in Riyadh City, Saudi Arabia. *International Research Journal of environment science*. ISSN: 0973-4229

## **MONITORING OF HAZARDOUS ATMOSPHERIC RELEASES UNDER EMERGENCY SITUATION BY RADAR TRACER METHOD**

*Boris S. Yurchak* (EPA, Arlington, VA, USA)

**ABSTRACT:** In the case of an accident at nuclear or chemical facilities accompanied with emission of hazardous pollutants into the atmosphere, the lack of information about the spatial distribution of pollutants in the vicinity of an enterprise-emitter during approximately an hour after the accident in air and on the ground is experienced, i.e., within the local spatial scale. This makes it difficult to manage the emergency situation on the initial stage of the accident. To get more detailed information at this stage, the Radar Tracer Method (RTM) is suggested. RTM is based on marking aerosol-like pollution with radar light reflectors (chaff) that makes it possible to distinguish the markers and consequently to locate the pollution pattern reliably by radar. The features of this method and its possible fields of application are discussed.

### **INTRODUCTION**

Bhopal chemical and other similar accidents (e.g., MacKenzie, 1985), Chernobyl and Fukushima nuclear accidents in 1986 and 2011, respectively, highlighted the necessity to have a system for monitoring dispersion and transport of hazardous atmospheric releases (HAR) from potentially dangerous enterprises (PDE) of nuclear and chemical industries in real-time scale. This requirement is due to the health protection issues of enterprise employees and inhabitants in nearby located places as well as to target the logistic measures (e.g., evacuation). Currently, a forecast of the contamination is conducted using the models of pollutant dispersion in the Atmospheric Boundary Layer (ABL). However, the input information for these models is extracted from regular meteorological network and aerological (upper-air) observations with data acquisition frequency of only several times per day. The network of aerological stations is rare. Due to that, the prognostic wind field of scale ~ 30-50 km differs from the actual one, particularly in the transient period of a day, under the stable stratification, and during different inclement weather events. To support and improve systems of decision making under accidents at the PDE, the Radar Tracer Method (RTM) was suggested to be exploited (Zhukov and Yurchak, 1993). The objective of the current paper is to discuss the main features of the method and possible fields of its application.

### **PRIMARY PRINCIPLE OF THE RTM**

The RTM is aimed for radar "visualization" of footprint and path of a cloud of hazardous pollutants in the atmosphere. The pollutants can be radiation or chemical in nature. In this method the gas-aerosol impurity produced, for example, during an accident at a hazardous object, is marked with passive radar reflectors (chaff) which are then observed in the atmosphere by means of radar. The chaff was primary used to study the physics of the atmosphere as part of a research designed to monitor the modification of warm clouds and fogs and to study the diffusion of a passive impurity inside and around a cloud (e.g., Skhirtladze and Yurchak, 1979) and in the lower part of the ABL (e.g., Hildebrand, 1977; Zhukov and Yurchak, 1994). A characteristic feature of this study was use of chaff consisting of carbon-graphite materials "Uglen" (Girs et al., 1979) with a sedimentation rate of 10-30 cm/s and "Metka" with sedimentation rate of about 3 cm/s (Bessonov et al., 1987). These materials have a lower inertia than metallized materials containing a glass or polymer base. Although they produce a weaker radar signal, it can be detected on a distance of several tens of kilometers by ordinary weather radars. The advantage of tracking a hazardous impurity by the RTM is its sensitivity to wind shear and entrainment into a cloud. The basic characteristics of the RTM were provided in (Zhukov and Yurchak, 1993). Assuming Gaussian diffusion for time much longer than the Lagrangian time scale  $\tau_L$  of turbulence, the following

radar equation was obtained for finding the maximum range (in time and distance) for tracking chaff as a function of the diffusion parameters  $x_L = \bar{u} \tau_L$  (the spatial scale in the direction of transport,  $\bar{u}$  is average wind-direction transport velocity) and  $r_L = \tau_L \sqrt{\langle v^2 \rangle}$  (the diffusion scale,  $\langle v^2 \rangle$  is the variance of the pulsations of the velocity of a moving particle):

$$\lg \xi = \frac{1}{7} \left[ 2 \lg \sigma_\Sigma + \frac{1}{5} \left( \frac{P_t}{P_r} \right)_{dB} + 2 \lg \Pi - 3 \lg 4\pi - 6 \lg r_L - 4 \lg x_L \right] \quad (1)$$

where  $\xi = t/\tau_L = \bar{u}t/\bar{u}\tau_L = r/x_L$  is dimensionless range;  $\sigma_\Sigma$  is the initial effective scattering surface area of the chaff emission;  $\Pi$ ,  $P_t$  and  $P_r$  are the radar potential, transmitted pulse power, and radar receiver sensitivity, respectively. This form of the radar equation takes into account the dependence of the dimensionless range on meteorological situation (through the Lagrangian time scale and diffusion scale). The equation is a basis for designing the RTM system for different applications. It should be noted also that chaff can be detected not only by ground-based radars but airborne and satellite Synthetic Aperture Radars (SAR). The SAR application seems very perspective for HAR tracking due to possibility of having the plan position image of chaff clouds. Although the documentary proof cases of chaff tracking by SAR in the atmosphere are currently unknown, there are several papers describing detection of rain clouds over land and ocean by satellite SAR (e.g., Weinmann et al., 2008). It might be expected that radar detection of chaff is more reliable in comparison with rain drops due to anisotropic shape of an elementary scatterer of chaff that is a half-wavelength dipole. Effective chaff detection can be performed with the polarimetric radar (e.g., Martner et al., 1992).

## TRACKING AND MAPPING CLOUDS OF HAR DURING AN ACCIDENT

As depicted in Figure 1, during an accident or planned emission of toxic and/or radioactive gases and aerosols, the reflectors from dispersing devices are mixed by operator command or automatically with the radioactive impurity and are transported together with the impurity into the atmosphere, making it possible to estimate the average transport and transformation of the cloud by wind and turbulent diffusion in the layer of the atmosphere near the ground. At the enterprises, which are not equipped with containers holding the reflectors or with dispersing systems, the radar markers can be introduced into the area of the source of contamination by other methods, for example, dumped from flight vessels or shot in using pyrotechnic or pneumatic systems. In the RTM, the "visualization" of a radioactive cloud is accomplished by observing passive reflectors, which mark the cloud, by means of a radar (e.g., weather radar) located near an enterprise or group of enterprises being monitored. Information about the position and configuration of reflectors is fed into a computer which is coupled with the radar for preliminary processing of the echo signals and data compression. Next, the information is transmitted to the crisis center at the enterprise, where it is displayed on a monitor and serves for in situ calculations of the trajectory and geometric characteristics of the radioactive cloud in real time scale. The data are used to reconstruct the track of the cloud in the atmosphere and on the ground, to give instructions for airborne and ground-based sampling, to predict the spreading of the cloud during the immediate future period in time, and to make recommendations to the public health service (Yurchak, 1998). The working mobile prototype of such system is described in (Gariyants et al., 2006). The mapping of air and ground footprints of chaff releases from 300-metre meteorological tower has been performed during many field simulation experiments.

It should be noted additionally that the RTM can be used for training the personnel of the PDE by means of the natural imitation of HAR. This creates conditions of the simulated emergency situation very close to the real one and increases the capacity of the RTM-based monitoring system installed in the vicinity of the PDE.

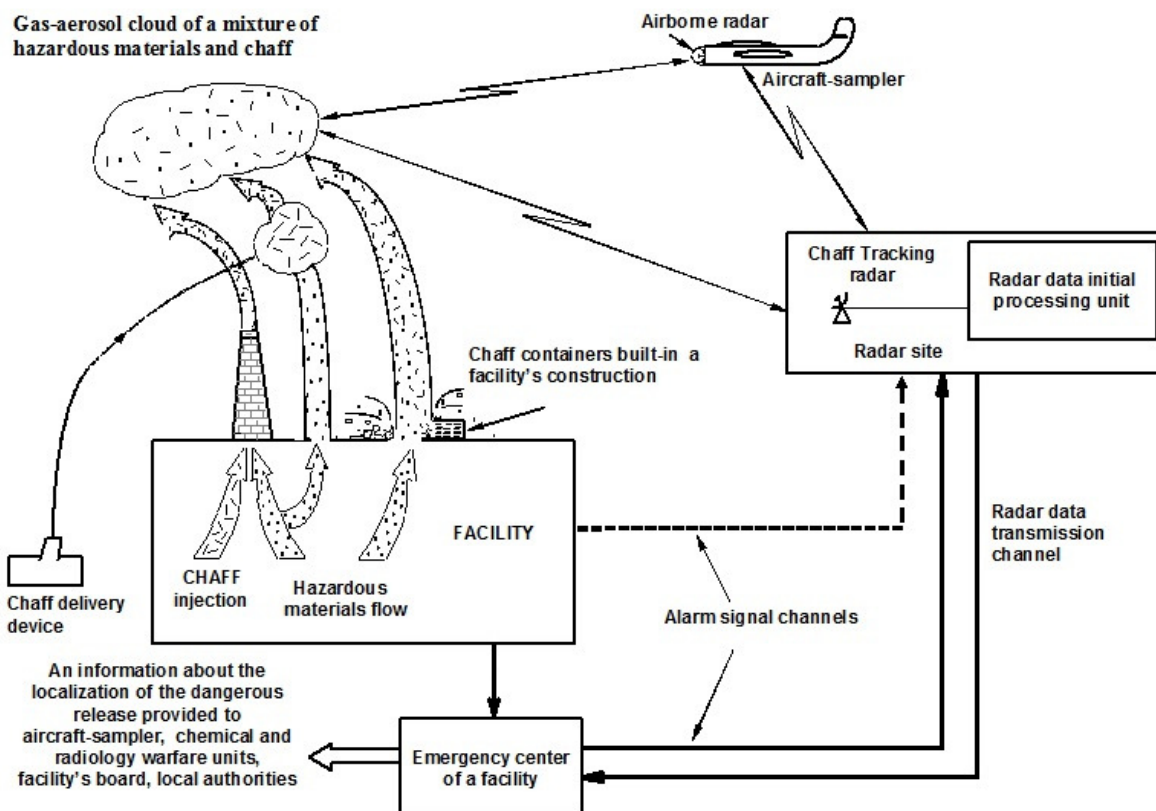


**FIGURE 1. An illustrative scheme of the RTM for tracking and mapping clouds of hazardous atmospheric releases from potentially dangerous facilities/enterprises**

### COMPILATION OF THE RTM WITH THE RADIOLOGICAL MEASUREMENTS

The most efficient known methodology for determining the radioactive contamination of the atmospheric HAR is  $\gamma$ -spectrometry performed by the ground-based spectrometers with their detectors upward. That data are essentially important for the source term assessment. The practical implementation of this method demands knowledge of emission geometry, i.e., the configuration of the cloud (plume) of radioactive substances, the position of the cloud in space relative to the  $\gamma$ -spectrometer, and the distribution of activity within the cloud. Using the RTM, it is shown that carbon chaff are subjected to atmospheric transport and diffusion process to nearly the same degree as the contamination of interest (Bessonov et al., 1987). It results the distribution of the concentration of chaff and HAR can be assumed to be similar, i.e., identical to within a dimensional factor. The isotopic ratio is assumed to be constant for all parts of HAR. Based on these conditions, the spatial distribution of radar reflectivity from chaff  $Z(\mathbf{R})$ , which marks the HAR cloud, within the radar volume is proportional to the volume activity of an elementary radionuclide source  $C(\mathbf{R})$  and differs only by a constant dimension factor  $D = C(\mathbf{R})/Z(\mathbf{R})$  at any radius-vector  $\mathbf{R}$  of the source relative to the radar. Once the coefficient  $D$  has been determined, the desired radioactivity distribution  $C(\mathbf{R})$  can be found from the distribution, measured by the radar method. Other radiation characteristics of the radioactive cloud can be calculated from the activity distribution. Practically, the factor  $D$  is determined from the formula:

$$D = [I_{ph}(E)] \left[ \frac{1}{\eta(E)} \right] \left[ \frac{1}{\varepsilon(E)} \right] \left[ \frac{1}{G(E)} \right], \quad (2)$$

where the square brackets represent the following parameters (from left to right): the spectrometer-measured quantity, the physical constant, the instrumental function of the detector and, the dimensional geometrical factor, respectively. All parameters are functions of energy  $E$  of unscattered gamma-rays. The last one,  $G(E)$ , is the subject of determination by the RTM:

$$G(E) = \int_{\tilde{V}} d\mathbf{R} \frac{Z(\mathbf{R})}{4\pi r^2} \exp[-\mu(E)r], \quad (3)$$

where  $\mu(E)$  is a liner attenuation factor for photons attenuated by air;  $\tilde{V}$  is the volume of HAR (chaff) cloud;  $\mathbf{R}$  and  $\mathbf{R}_0$  are the radius vector of the source and location of the detector relative to the radar, respectively,  $r = |\mathbf{R} - \mathbf{R}_0|$ . Since the distribution  $Z(\mathbf{R})$  can be determined by radar, the geometrical factor is determined as well. Analytical expressions for  $G(E)$  at different patterns of radar probing and other details of the methodology is provided in (Martinenko and Yurchak, 2001). At the light of contemporary achievements in exploiting of Unmanned Aerial Vehicles (UAV) for environmental monitoring including radiological survey (e.g., Torii and Sanada, 2015), it might be expected that the deployment of described above combined radar-radiometer system on UAV platform after corresponding adaptation will further improve the characteristics of the information support system.

## VALIDATION OF MESOSCALE MODELS

The analysis of results of the ETEX experiments indicates that even the initial material cloud development close to the source decides on the its future behavior (Graziani et al., 1997). The importance of correct determination of the tracer in the mesoscale region is therefore enhanced. This requires that experiments be conducted with increased density of the measurement network close to the source. There are estimates suggesting that the optimal number of samplers, even at 4 km range from the source, must be not less than about 80 (Kummel, 1984). Certainly, in real experiment such demands cannot be met and it is necessary to find other methods for registration of space-temporal characteristics of tracer. The validation procedure compares the prognostic results of theoretical models evaluated with the current meteorological parameters as input data and results of real pattern of impurity dispersion simulated by chaff dispersion under the same meteorological situation, Figure 2. The chaff dispersion is described in terms of the statistical diffusion theory at homogeneous turbulence with allowance for possible wind shifts (Byzova et al., 1991). The governing equation for chaff standard spatial deviations of concentration along axes of Cartesian coordinate system (x, y, z) in this approach is as follow:

$$S_i^2 = a_i \left[ b_i t - \frac{3}{2} + 2 \exp(-b_i t) - \frac{1}{2} \exp(-2b_i t) \right] + c_i t^3, \quad (4)$$

where  $i=x, y, z$ ;  $a_i = 2K_i \tau_{L,i}$ ;  $b_i = \tau_{L,i}^{-1}$ ;  $c_i = 1/6 \Gamma_i^2 K_z$ ;  $c_z=0$ ;  $t$  is diffusion time;  $\tau_{L,i}$  and  $K_i$  are integral time of Lagrangian turbulent scale and the diffusion factor in  $i$ -th direction, respectively;  $\Gamma_i$  is vertical gradient of the  $i$ -th component of the mean wind velocity;  $K_z$  is vertical diffusion coefficient. The first term in equation (4) describes the regime of the impurity cloud expansion with homogeneous turbulence, the second –accounts for the influence of vertical diffusion on longitudinal and lateral ones, given a wind

velocity shift. The approximation of field dependences  $S_i^2(t)$  by the least square method using (4) permits estimating parameters  $a_i$ ,  $b_i$  and  $c_i$ . These parameters are used to determine the diffusion coefficients and integral time scale of turbulence. The mixing layer height is determined as an upper bound of chaff cloud image at radar Range-Height Indicator. The complete description of measuring diffusion parameters of chaff releases from 300-metre meteorological tower is in (Zhukov and Yurchak, 1994) and field validation experiment - in (Golubenkov et al., 1998). In particular, results of comparison of experimental  $S_i$  with calculations by the RIMPUFF model (Mikkelsen et al., 1984) suggest considerable

difference, particularly for  $S_z$  and  $S_y$ . Therefore, the applicability of relations for calculating dispersions  $S_i$  recommended by that model calls for further studies. The study of applicability of the model based on the Monte-Carlo method (e.g., Hanna, 1984) for calculating diffusion indicates that the features of cloud dispersion derived from this model are in satisfactory agreement with known theoretical results for relative diffusion.

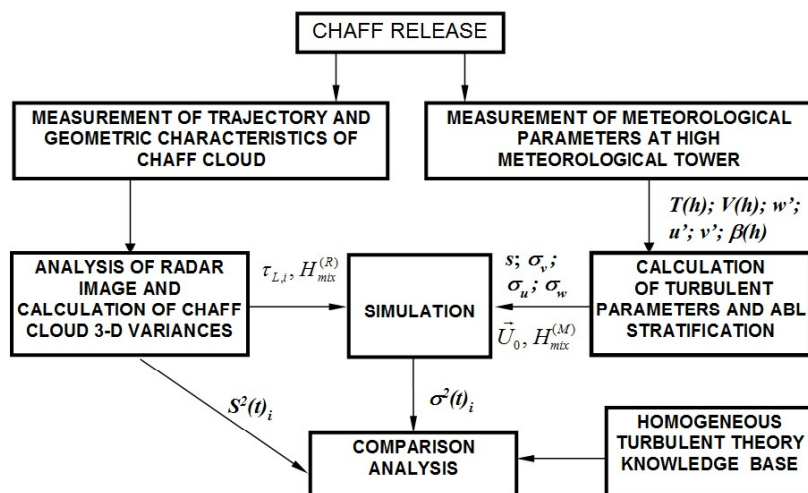


FIGURE 2. Scheme of validation of meso-scale models using the RTM. Designations are in the text.

## SUMMARY

The Radar-Tracer Method exploiting the radar chaff was presented. It is based on the well-known principle of marking a difficult-to-detect substance with materials one of whose properties is the same as that of the substance to be detected (for example, aerodynamic properties) while other properties differ so sharply that they make it possible to distinguish the markers reliably by technical means. Several useful attributes of the RTM technique are briefly demonstrated in the cases presented here. These include: (1) Tracking and mapping clouds of harmful atmospheric releases (HAR) during an accident; (2) Determination of the geometrical factor of the radioactive HAR to estimate its irradiation rate; (3) Validation of mesoscale models of dispersion of passive impurity in the atmosphere; (4) Training the personnel of environmental dangerous enterprises. The first two items are the direct actions of the countermeasure procedure in support of decision making person. The last two ones are aimed to improve the preparedness for the possible accident. Feasibility of the RTM was proved during many field experiments which primary feature was the usage of super light carbon chaff.

## REFERENCES

- Bessonov, V.A., Yu. P. Grishin, and M.A. Iordansky. 1987. "Product "Metka" for study of structure and dynamics of air fluxes in the near-cloud area" (in Russian). *Meteorol. Hydrol.*, 1:118-120.
- Byzova, N. L., E.K. Garger, and V.N. Ivanov. 1991. *Experimental studies of atmospheric diffusion and calculation of dispersion of material* (in Russian). Hydrometeoizdat, Leningrad, USSR.
- Gariyants, A.M., V.G. Bulgakov, V.M. Shershakov, and G.P. Zhukov. 2006. "Mobile measurement facilities for the real-time interaction with the RECASS NT system in antiterrorism actions." In S.



- Apikyan and D. Diamond (Eds.), *Countering Nuclear and Radiological Terrorism*, pp. 191-198. NATO Security through Science Series. Springer, Netherlands.
- Girs, S.P., V.N. Kamentsev, M.N. Serova, G.I. Skhirtladze, and B.S. Yurchak. 1979. "On the possibility of using electrically conducting carbon fibers for investigating air flows in clouds" (in Russian). *Trudy GGO*, 420: 82-88.
- Golubrnkov A. V., O.I. Vozzhenikov, G.P. Zhukov, and B.S. Yurchak. 1998. "Validation of meso-scale models using radar chaff data." Unpublished manuscript.
- Graziani G., W. Klug, S. Galmarini, G. Grippa. 1997. *Real Time Long Range Transport Model Evaluation.-ETEX second release*. Draft report for modelers meeting. Vienna. Joint Research Center, Ispra, Italy.
- Hanna, S.R. 1984. "Applications in air pollution modeling." In F.T Nieuwstadt and H. van Dop (Eds.), *Atmospheric turbulence and air pollution modelling*, pp. 275-307. D. Reidel Publishing Company, Holland.
- Hildebrand, P.H. 1977. "A radar study of turbulent diffusion in the lower atmosphere." *J. Appl. Meteorol.*, 21(11): 493-510.
- Kummel, M. 1984. "Development of optimal measuring network for environmental monitoring at NPP" (in Russian). In: *The radiation safety support of NPP maintenance*, Book 5, pp. 78-89. Vilnius. Energoatomizdat, Moscow, USSR.
- MacKenzie, D. 1985. "After Bhopal, everybody loves factory inspectors." *New Scientist*, Oct. 31, 1985.
- Martinenko, V.P., and B.S. Yurchak. 2001. "Radar-spectrometric method for determining the characteristics of radioactive emission." *Atomic Energy*, 91(2): 676-682.
- Martner, B.E., J.D. Marwitz, and R.A. Kropfi. 1992. "Radar observations of transport and diffusion in clouds and precipitation using TRACIR." *J. Appl. Meteorol.*, 9(6): 226-241.
- Mikkelsen, T., S.E. Larsen and S. Thykier-Nielsen. 1984. Description of the RISO Puff Diffusion Model. *Nuclear Technology*, 67: 55-65.
- Skhirtladze, G.I. and B.S. Yurchak. 1979. "Measurements of coefficient of horizontal turbulent diffusion in cumulus clouds by the radar method." *Izv. of USSR AS, FAO*, 15(2): 146-153.
- Torii, T., and Yu. Sanada. 2015. "Radiation measurement by unmanned aircraft after Fukushima Daiichi nuclear power plant accident." *Remotely Piloted Aircraft Systems Symposium*, ICAO Headquarters, Montreal, Canada.
- Weinmann, J.A., and F.Z. Marzano. 2008. "An exploratory study to derive precipitation over land from X-band Synthetic Aperture Radar measurements." *J. Appl. Meteorol. Clim.*, 47(2): 562-575.
- Yurchak, B.S. 1998. "Radar support for radiation conditions monitoring and survey systems." *Atomic Energy*, 84(5): 335-341.
- Zhukov, G.P., and B.S. Yurchak. 1994. "Diffusion of passive material in the atmospheric boundary layer by radar data." *Izv. of USSR AS, FAO*, 30(4): 451-457.
- Zhukov, G.P., and B.S. Yurchak. 1993. "An assessment of the possibility of determining the location and configuration of a cloud of harmful atmospheric emissions from industrial enterprises by the radar method" (in Russian). *Meteorol. Hydrol.*, 12: 94-100.

## **AN ALTERNATIVE ON-LINE METHOD FOR EVALUATING BROWN CARBON IN THE ATMOSPHERE**

**Guohua Zhang**, Xinhui Bi, and Xinming Wang

(Guangzhou Institute of Geochemistry, Chinese Academy of Sciences, Guangzhou, 510640, PR China)

While the dominant light-absorbing aerosol species is thought to be BC, other light absorbing species are also present in atmospheric aerosols, which were recently revealed to be of potentially important in the absorption of near-UV light, and thus the radiative forcing. High contribution of brown carbon (BrC) to light absorption at near-UV wavelength is reported worldwide from satellite and ground observations, and modeling studies. However, On-line estimation of light absorption properties of BrC still presents challenges. In this study, a multi-wavelength (370–950 nm) Aethalometer was applied to obtain the wavelength dependent light absorption coefficient ( $\sigma_{\text{abs}}$ ) of aerosols, before and after heated to 250 °C on a 5 minute cycle. An alternative method was developed to evaluate the contribution of BrC to light absorption at 370 nm ( $\sigma_{\text{abs,BrC}}/\sigma_{\text{abs,370nm}}$ ) by subtracting the measured  $\sigma_{\text{abs}}$  to  $\sigma_{\text{abs,BC}}$  at 370 nm. The  $\sigma_{\text{abs,BC}}$  at 370 nm was extrapolated using field measured absorption Ångström exponent (AAE) over the wavelength of 880–950 nm with one-hour resolution. The simultaneous measurements of heated aerosols provided evidence that the influence of BrC on the  $\sigma_{\text{abs}}$  over 880–950 nm is negligible. Meanwhile,  $\sigma_{\text{abs,BrC}}/\sigma_{\text{abs,370nm}}$  was also estimated by the previously reported methods by assuming AAE to be one (Method I) and based on the light absorption enhancement (Method II). While the estimated  $\sigma_{\text{abs,BrC}}/\sigma_{\text{abs,370nm}}$  based on our developed method and Method I was highly correlated ( $r^2 = 0.78$ ), the difference could be as large as > 20% on average. However, the mean contribution was obtained to be negative with Method II, indicative of net production of BrC when the aerosols were heated. The difference between the obtained  $\sigma_{\text{abs,BrC}}/\sigma_{\text{abs,370nm}}$  was ~40% on average and much higher (> 50%) during noon hours, when there were higher abundance of secondary organic aerosols (SOA) and sulfate. This developed method in this study is beneficial for future studies on the light absorption and climate forcing of BrC. The result indicates a potentially important contribution of light absorption from BrC at UV wavelength in the PRD region, which should not be neglected in the climate model.

## **ENVIRONMENTAL IMPACT OF BIOMASS BURNING FOR CIVIL USES ONTO A MOUNTAIN AREA**

***F. Petracchini, C. Balducci, M. Perilli, A. Cecinato, F. Liotta, V. Paolini, L. Paciucci.***  
(National Research Council of Italy, Monterotondo RM, Italy)

The impact of biofuel combustion for civil uses onto the environment was investigated through determining a list of air toxicants at Leonessa, a town lying in Apennines mountain region, Central Italy, and in its surroundings (Terzone). Attention was focussed on suspended particulate matter (PM<sub>10</sub>), polycyclic aromatic hydrocarbons (PAHs) and regulated pollutants (nitrogen dioxide, ozone and benzene). Two in-field campaigns, each lasting two weeks, were carried out in summer 2012 and winter 2013. Contemporarily, air was monitored in downtown Rome and in other localities of the province. In the summer all pollutants were more abundant in Rome (e.g., PAHs, 0.93 ng/m<sup>3</sup>, vs. 0.37 ng/m<sup>3</sup> at Leonessa and 0.14 ng/m<sup>3</sup> at Terzone; benzene, 0.9 µg/m<sup>3</sup> in Rome vs. 0.2 µg/m<sup>3</sup> at Leonessa), apart from ozone (73 µg/m<sup>3</sup> in Rome and >100 µg/m<sup>3</sup> at Leonessa). By contrast, in the winter PAHs were more at Leonessa (15.8 ng/m<sup>3</sup>) than in the capital city (7.0 ng/m<sup>3</sup>), and benzene was similar (2.3 µg/m<sup>3</sup>), despite suspended particulates were less (22 vs. 34 µg/m<sup>3</sup>). Due to lack of other important sources and the scarce impact of transport at mid (inter-regional) scale, biomass burning was identified as the major emitter of PAHs at Leonessa during the winter. Its importance was confirmed by the molecular signatures, pictured by PAH concentration ratios distinct from those of Rome. Other towns too experienced PM levels similar to capital city but higher PAH loads (~9.6 ng/m<sup>3</sup>), suggesting that uncontrolled biomass burning contributed to pollution across the Rome province. Important differences among PAH diagnostic ratios were observed at the sites also in the summer; nevertheless, in this case the ageing of air masses could play a role. As results of the two in field campaign can be concluded that biomass burning was the major emitter of PAHs at Leonessa during the winter. In summer period important differences among PAH diagnostic ratios were observed. Despite, the suspended particulates were less than in Rome suggesting the lack of other important sources and the scarce impact of transport at mid scale.

## **A PRELIMINARY ASSESSMENT OF MAJOR AIR POLLUTANTS IN THE CITY OF URUMQI, CHINA**

F. Petracchini, A. Cecinato, L. Paciucci, **V. Paolini\*** and F. Liotta  
(Institute of Atmospheric Pollution Research, National Research Council of Italy, Monterotondo, RM, Italy)

Nitrogen oxides (NO<sub>2</sub> and NO<sub>x</sub>), ozone (O<sub>3</sub>), sulphur dioxide (SO<sub>2</sub>), benzene, toluene, ethylbenzene and xylene (BTEX) and ammonia (NH<sub>3</sub>) in ambient air were preliminarily assessed, by diffusive sampling technique, in the years 2010-2012 through four measurement campaigns in Urumqi, the capital of Xinjiang in NW China. This is a heavily industrialized area where, up to date, very few air pollution studies are available. Impacts of pollutants have been assessed in the various critical areas affected by industrial activity and traffic. Principal component analysis (PCA) was also performed to understand the pollution sources and the correlation between the several pollutants monitored.

Considerably high mean annual pollutants concentrations have been observed, which ranged between, 46 and 158 µg m<sup>-3</sup> (SO<sub>2</sub>), 33 and 126 µg m<sup>-3</sup> (NO<sub>2</sub>), 82.5 and 140.5 µg m<sup>-3</sup> (NO<sub>x</sub>) and 46 and 82 µg m<sup>-3</sup> (BTEX).

It was found that nitrogen oxides, benzene and xylene were mostly emitted from industrial sources and motor vehicles. Very high consumption rates of fossil fuels for energy generation and domestic heating are mainly responsible for high annual pollution levels. The concentration values of the pollutants measured during different seasonal periods show remarkable differences: in winter period the coal burning in domestic heating facilities was found as the major contributor to SO<sub>2</sub> and BTEX pollution. Ammonia pollution was also found in the city area where are located a slaughter facility and a meat treatment facility. Predominant factors influencing pollutions were associated to those elements conditioning air pollutant diffusion: meteorology (wind speed and direction), air stagnation and inversion events, relevant emission sources (especially for BTEX and NO<sub>x</sub>), emission seasonality and photochemistry.

The analysis conducted can be a consistent pollution control policy framework to reduce emissions and critical pollution episodes.

## **METHODOLOGIES FOR A BETTER INTERPRETATION OF THE PRELIMINARY ASSESSMENT: IAPMS PANČEVO**

**L. Paciucci\***, F. Petracchini, A. Cecinato, **P. Romagnoli\***, V. Paolini, F. Liotta, F. Vichi  
(Institute of Atmospheric Pollution Research, National Research Council, Monterotondo, RM, Italy)  
M. Biscotto (Politecnico di Torino, Torino, Italy)

Air quality preliminary assessment was carried out in Pančevo, through eight two-week campaigns, one for each season, were carried out starting from August 2005 up to May 2006 by means of passive samplers for nitrogen dioxide, nitrogen oxides, sulphur dioxide, ozone, ammonia, benzene, toluene, xylenes, and total non methanic hydrocarbons exposed in 35 sites.

The sampling sites were divided into three categories, i.e.: (1) background - B, including both urban and suburban locations; (2) traffic - T, including traffic locations and hot spots; and (3) industrial - I.

By performing statistical analysis was found a high correlation between organic pollutants (benzene, toluene and xylenes; BTX) due to same source origin. In the T category sampling sites, the correlation between benzene and nitrogen dioxide was good as expected from sites close to traffic areas. This result substantiates the categorization of the sites. In the B category the correlation coefficient ( $R^2$ ) between  $\text{NO}_2$  and BTX was lower than in the other two categories (T and I categories) suggesting that some of the sites may not have background characteristics (they are outliers). As expected, after the removal of the outliers, the correlation coefficients raised up. This correlation is similar to that found in the T category, thus showing an affinity between these two categories (B and T categories). In the I category, unlike in the above mentioned categories, there was a lack of correlation between the organic pollutants and nitrogen dioxide (since traffic is not the major source). Considering the data set for the entire year it was found that sulphur dioxide (regional source) was rather uniform over all categories, nitrogen dioxide was slightly higher for T category, benzene and ammonia showed much higher concentrations in the I category due to the presence of sources in the area.

Regarding the sampling sites, the industrial areas strongly differ from the others because of the prevalence of BTX (Benzene, Toluene and Xylenes) emissions from inner sources, in particular near or inside the refinery. The B and T sites seemed to have the same chemical distribution, thus suggesting a similarity of sources. The overall conclusion was that all sites could be split up in two big clusters: an industrial and an urban one. The I cluster is strongly influenced by the facility emissions, while the urban cluster is less influenced by the industrial emissions and is affected by local emissions, such as traffic and domestic heating. The contribution of traffic sources to BTX and nitrogen oxides concentrations was not negligible, taking into account the differences between T and B values.

## **BIOLOGICAL TREATMENT OF CHLOROFORM IN A CONTROLLED AEROBIC TRICKLE BED BIOFILTER**

***Keerthisaranya Palanisamy\****, Bineyam Mezgebe and George A. Sorial  
(University of Cincinnati, Cincinnati, Ohio, USA)<sup>127</sup>

Endalkachew Sahle-Demessie (United States Environmental Protection Agency, Cincinnati, Ohio, USA)

Chlorination disinfection forms harmful disinfection byproducts (DBPs) when chlorine reacts with the naturally occurring humic and fulvic like substances present in water. DBPs are a group of halogenated organic compounds such as Trihalomethanes (THMs), haloacetic acids (HAAs), chlorophenols, chloral hydrate, and haloacetoneitriles (HANs) found in disinfected water that is released into the distribution system. Trihalomethanes are the commonly reported DBPs at environmentally relevant concentrations and chloroform constitutes 68% of the total THMs detected in drinking water. Under the SDWA, the USEPA establishes a MCL of 70 ppb for chloroform stating that people consuming chloroform in excess of this limit could experience adverse effects in liver, kidney, or central nervous system and increased risk of cancer. The level of chloroform detected in public water supplies range from 2 to 88 ppb and reaches as high as 300 ppb in ground water contaminated by landfill leachate. Since chloroform is a volatile organic compound (VOC), it readily evaporates into the atmosphere from disinfected water surface, where it is non-reactive at gaseous state causing long range air pollution. As a result, human exposure through inhalation is reported at an average concentration of 2 to 200  $\mu\text{g/day}$ . Current treatment technologies that counter the problem of DBPs in water treatment facilities such as air stripping, adsorption, ozonation, and advanced oxidation processes are reported to be energy intensive and generate secondary pollutants. Air stripping is a non-destructive mechanism commonly used by water utilities to remove VOCs post disinfection, however it releases concentrated off-gas streams into the atmosphere. Biofiltration is one of the most proven techniques for the removal of gas phase VOCs and is a widely applied off-gas control mechanism in Europe and Japan, but only recently been investigated in the United States.

In this paper, a trickle bed air biofilter (TBAB) is subjected to the biodegradation of chloroform under acidic conditions. TBAB has been shown to efficiently remove both hydrophobic and hydrophilic VOCs such as Methyl Ethyl Ketone, Methyl Isobutyl Ketone, Benzene and n-Hexane and achieves stable removal performance for a wide range of feed concentrations. In this study chloroform is subjected to cometabolic degradation with ethanol. The aerobic biofilter is operated at acidic conditions to benefit the growth of filamentous fungi as the principle media for biodegradation. The reason behind using fungi is that its aerial mycelia largely improve the surface hydrophobicity resulting in high partition of the VOCs by increasing its mass transfer from the gas phase to microorganisms in the solid phase. The objectives of the research are to: (1) determine the critical loading rate of chloroform that achieves stable removal efficiencies; (2) generate a carbon mass balance closure for the biofilter; (3) evaluate the biodegradation removal rate kinetics and (4) determine the amount of nitrogen consumed for biomass growth. The biofilter is constructed using cylindrical glass sections and packed with pelletized diatomaceous earth to support biological media. Compressed air transfers chloroform and ethanol from calibrated syringe pumps into the biofilter where buffered nutrients are sprayed intermittently to facilitate the activity of the micro-organisms. The biodegradation of chloroform is measured by the decrease in its initial concentration based on Pseudo first order kinetics. The experiment is carried out in five different phases of operation with each phase constituting a different feed ratio of the contaminant and the cometabolite. The biofilter is subjected to treat 5 ppm<sub>v</sub> of chloroform mixed with 200, 150, 100, 50 and 25 ppm<sub>v</sub> of ethanol. The removal efficiency obtained for chloroform was above 70% for four feed ratios studied. Degradation of chloroform peaked at 82% efficiency for influent chloroform and ethanol concentrations of 5 and 200 ppm<sub>v</sub> respectively. This

dechlorination process is expected to achieve a sustainable removal of atmospheric chloroform released from aerated disinfected water.

## **EFFECT OF METHANOL AND TOLUENE ON REMOVAL OF TRICHLOROETHYLENE IN A FUNGI SEEDED BIOTRICKLING FILTER**

***Dhawal Chheda\**** and George Sorial  
(University of Cincinnati, Cincinnati, OH, USA)

Trichloroethylene (TCE) is a chlorinated solvent which has several applications in the metal degreasing, plastics, dry cleaning, rubber and refrigerant industries. It is listed as a potential mutagenic and carcinogenic compound and when in contact, TCE can affect our nervous, reproductive and immune systems. It is one of the most detected chemicals in the Superfund sites and is therefore ranked at 16<sup>th</sup> position in the 2005 CERCLA List published by US E.P.A. More than 95% of US rural areas depend on groundwater which is contaminated by TCE and thus, its remediation is of utmost importance. Several technologies like ozonation, oxidation and adsorption have been suggested for removal of TCE from air and water resources. But such methods are either expensive, energy intensive or produce toxic by-products like furans. This research focuses on removal of trichloroethylene in a biotrickling filter (bioremediation) which is seeded with fungi strains and operated at an acidic pH.

TCE is in a highly oxidized state and not a competent carbon source for the microbes. Therefore, methanol is added along with TCE as a primary substrate or a “co-metabolite”. Two ratios of methanol-to-TCE are tested: 80% methanol to 20% TCE and 70% methanol to 30% TCE. TCE loading rates ranging from 3.22 g/m<sup>3</sup>/hr to 12.88 g/m<sup>3</sup>/hr are tested for each ratio. Thus, methanol loading ranges between 103.71 g/m<sup>3</sup>/hr and 711.14 g/m<sup>3</sup>/hr depending on the ratio. This assessment helps in establishing which ratio and what concentration range provides higher elimination capacities for TCE while avoiding the inhibitory effect of methanol at higher concentrations. For a loading rate of 3.22 g/m<sup>3</sup>/hr, average TCE removal efficiency of 81.4% was achieved in the 80:20 system while it was 79.9% for the 70:30 ratio. For a loading of 6.44 g/m<sup>3</sup>/hr, the efficiencies attained were 79% and 87.1% for the 80:20 and 70:30 systems respectively. For methanol, removal efficiencies achieved were consistently over 95%. Further analysis of TCE elimination is under examination for different residence times and co-metabolite concentrations.

In 2006, more than 82% of TCE was released from the above mentioned industries. When released from these industries, TCE is often accompanied by methanol and toluene. Therefore, a study is performed to test the biofilter performance for an inlet of a ternary blend of TCE, methanol and toluene. Again, two ratios are tested: 50% toluene to 26% TCE to 24% methanol and 45% toluene to 15% TCE to 40% methanol. Inlet concentration ranges from 10 to 20 ppmv TCE, 23 to 118 ppmv methanol and 17 to 50 ppmv toluene. This study is currently under investigation to check how the dynamics of TCE removal are disrupted in a ternary mixture of organic compounds in a fungi seeded biotrickling filter.



## **EVALUATIONS OF THE REMOVAL OF TRIHALOMETHANES BY TWO INDEPENDENT BIO-TRICKLING FILTERS UNDER DIFFERENT OPERATING CONDITIONS**

***Bineyam Mezgebe***, George Sorial, Keerthisaranya Palanisamy  
(University of Cincinnati, Cincinnati, OH 45221-0012, USA)  
Endalkachew Sahle-Demessie

(US EPA National Risk Management Research Laboratory, Cincinnati, OH 45268, USA)

Disinfection resulted from the reactions between the chlorine and natural organic substances increased the formation of chlorinated by-products including trihalomethanes (THMs). Since chlorination by-products are classified as potential carcinogenic by EPA, they are of importance for human health. THMs have the highest concentration of chlorination by products in drinking water and chloroform is the most abundant of all THMs with a maximum contaminant level (MCL) of 0.070 mg/L. Several physical and chemical removal methods are used to treat chloroform which are expensive and could generate secondary pollutants. Biofiltration is one of the most proven technologies for VOC control as it is environment-friendly, cost effective and releases fewer byproducts. In this study, an integrated technology is proposed by taking chloroform as a model THMs. This integrated technology consists of nitrogen stripping followed by anaerobic Bio-trickling Filter (BTF) or air stripping followed by aerobic BTF. Two independent and parallel aerobic and anaerobic BTFs with similar chloroform (5 ppmv) concentrations were investigated. In the anaerobic BTF, a co-metabolite and surfactant were utilized to enhance the biodegradation process. Upon the addition of Ethanol (co-metabolite) and Tomadol 25 - 7 (surfactant), the performance of the anaerobic reactor improved from an initial 49% to over 64% removal efficiency. Alternatively, the aerobic BTF was investigated under acidic environment to enhance fungi growth. The average removal efficiency under this acidic condition was 80%. The significance of the anaerobic compared to aerobic BTF was the generation of methane (0.32 mg / day) and carbon dioxide (147.4 mg/day) as the end products where as the main end product for aerobic BTF was carbon dioxide (169.7 mg/ Day). The study will further investigate the microbial diversity within the BTFs in order to get an insight of the BTFs' performances.

## **REMOVAL OF VAPOUR PHASE METHANOL IN THE PRESENCE OF THIOSULPHATE USING ANAEROBIC BIOTRICKLING FILTER**

***Mekonnen M. Tarekegn***

(School of post graduate studies, Department of Urban Environment and Climate Change Management, Ethiopian Civil Service University, 26148 Addis Ababa, Ethiopia)

Eldon Raj Rene Jack van de Vossenberg and Piet N. L. Lens

(Environmental Engineering and Water Technology (EWT) Department, UNESCO-IHE Institute for Water Education, Westvest 7, 2611 AX, Delft, The Netherlands)

The feasibility of methanol removal using an anaerobic biotrickling filter (BTF) was studied under different operational conditions. Anaerobic BTF experiments were performed by changing the empty bed residence times (EBRT) and inlet methanol (gas-phase) concentrations for ~66 days.

The nutrient medium containing thiosulphate was fed to the BTF in trickling mode (pH - 8.0). The methanol removal efficiencies of the BTF at EBRTs of 5 and 3 min were 96.7% and 90.5%, respectively. Concerning concentration effects, the methanol removals at an inlet concentration of  $1.4 \times 10^3 \text{ ppm}_v$  and  $5.2 \times 10^3 \text{ ppm}_v$  were 90.5% and 80.2%, respectively. A maximum methanol elimination capacity (EC) of  $1.5 \times 10^2 \text{ gMeOH/m}^3 \cdot \text{h}$  was achieved at an inlet loading rate (ILR) of  $1.7 \times 10^2 \text{ gMeOH/m}^3 \cdot \text{h}$ . The average growth rate of biomass observed in the BTF reactor under steady state operation during phase V (EBRT 5 min and inlet MeOH concentration  $1.0 \times 10^3 \text{ ppm}_v$ ), phase VI (EBRT 3 min and inlet MeOH concentration  $1.41 \times 10^3 \text{ ppm}_v$ ) and phase VII (EBRT 3 min and inlet MeOH concentration  $5.2 \times 10^3 \text{ ppm}_v$ ) were 0.13, 0.20 and  $0.10 \text{ d}^{-1}$ , respectively.

The average biodegradation rate of methanol in the BTF was  $0.63 \text{ d}^{-1}$  at a maximum methanol biodegradation rate of  $2.0 \text{ d}^{-1}$ . While the average biodegradation rate of thiosulphate was  $0.34 \text{ d}^{-1}$ . The average biomass yield coefficient observed in the BTF reactor at steady state condition was  $0.32 \text{ gbiomass} \cdot (\text{gMeOH})^{-1}$ . The mass balance calculation ascertained that ~27% of the incoming carbon and ~53% of sulphur was retained within the BTF reactor. Methanol is a hydrophilic VOC and thus it is easily scrubbed by the trickling liquid or it can be stripped by the incoming gas containing methanol. This reduced the total amount of carbon stored in the BTF reactor. It was ascertained that anaerobic biodegradation of gas phase methanol and liquid phase thiosulphate can be achieved within one bioreactor configuration which is promising for practical applications.

## **INTERFACE EFFECTS FOR CO<sub>2</sub> HYDROGENATION ON Pt<sub>4</sub>/γ-Al<sub>2</sub>O<sub>3</sub>.**

**Yulu Liu**, Wanglai Cen and Jianjun Li  
(Sichuan University, Chengdu, Sichuan, China)

Anthropogenic greenhouse gases which mainly consist of CO<sub>2</sub> have brought about climate change and are considered as a major threat faced by mankind. However, CO<sub>2</sub>, a very natural C1-resource, is being paid close attention as a substitute of toxic CO in C1-chemistry hopefully to keep carbon resources recycling. And CO<sub>2</sub> recycle to useful chemicals or liquid fuel will also help to remit the greenhouse effects. Selective hydrogenation of CO<sub>2</sub> to methanol or methane has been widely studied. In this work, density functional theory (DFT) was applied to investigating the hydrogenation of CO<sub>2</sub> over Pt<sub>4</sub>/γ-Al<sub>2</sub>O<sub>3</sub>(110) catalyst. HCOO and CO are the important intermediates in CO<sub>2</sub> hydrogenation. From our results, CO formation is kinetically and thermodynamically more favorable than HCOO formation, indicating that Pt-based catalysts benefit the formation of methane. Furthermore, based on the analysis of CO<sub>2</sub> hydrogenation on Pt(111) surface, we found that the supported catalysts has a lower activation barrier (0.34 eV) than that of metal catalyst (0.59 eV) in the first step, i.e. the process of trans-COOH species formation, showing that the interfacial sites between Pt<sub>4</sub> cluster and γ-Al<sub>2</sub>O<sub>3</sub>(110) slab can promote CO<sub>2</sub> hydrogenation. However, the cis-COOH species of the supported catalyst has a larger activation barrier (0.91 eV) than that of metal catalyst (0.56 eV), which means that dissociation of the former one is more difficult. Finally, further study is required to find an appropriate interface on the supported catalyst so that the compromise between activation barriers of CO<sub>2</sub> hydrogenation and COOH species dissociation could be achieved.

## **A NOVEL SnO<sub>2</sub>-CoO<sub>x</sub> CATALYST FOR NO OXIDATION WITH H<sub>2</sub>O**

**Huazhen Chang** and Mingguan Li (Renmin University of China, Beijing, China)  
Junhua Li (Tsinghua University, Beijing, China)

Noble metal catalysts have been comprehensively studied for NO oxidation which shows high catalytic activity. However, high cost limits their large-scale industrial application. In recent years, it was widely reported that cobalt-based catalysts were potential candidate for NO oxidation. Tin dioxide has been widely used as an oxidation catalyst as it can reversibly switched between Sn<sup>4+</sup> and Sn<sup>2+</sup> at a relatively low temperature. In this study, the Sn-Co-O mixed oxides catalysts were prepared by the coprecipitant method and the obtained samples were studied by means of XRD, BET, H<sub>2</sub>-TPR, XPS, in situ DRIFTS and NO + O<sub>2</sub> model reaction. The influences of H<sub>2</sub>O were also investigated.

A series of SnO<sub>2</sub>-CoO<sub>x</sub> catalysts prepared by a co-precipitation method were investigated for NO oxidation reaction. The catalyst with a molar ratio of Sn:Co=3:1 (denoted as Sn(0.75)-Co-O) exhibited excellent catalytic activity in a temperature range of 250-350 °C. In the presence of H<sub>2</sub>O, much better NO oxidation performance was also obtained over the same catalyst. NO-TPD showed that Sn(0.75)-Co-O the amounts of adsorbed NO were larger comparing with CoO<sub>x</sub> in the absence /presence of H<sub>2</sub>O. It indicated that the NO adsorption capacity was improved by addition of Sn. More active sites are available for NO adsorption even in the presence of H<sub>2</sub>O. XPS spectra showed that the ratio of chemisorbed oxygen increased, which contributed to enhance the redox property of Sn(0.75)-Co-O catalyst. Moreover, BET results revealed that the specific BET surface area increased over Sn(0.75)-Co-O catalyst, which are favourable for the adsorption and oxidation of NO.

**ENVIRONMENT-FRIENDLY AND HIGHLY EFFICIENT RARE EARTH BASED CATALYST  
FOR SELECTIVE CATALYTIC REDUCTION OF NO<sub>x</sub>**

Shemin Zhu, Yuesong Shen and Zhiwei Xue

(Jiangsu Collaborative Innovation Center for Advanced Inorganic Function Composites, Jiangsu National Synergetic Innovation Center for Advanced Materials (SICAM), College of Materials Science and Engineering, Nanjing Tech University, Nanjing, Jiangsu, China)

Zhimin Wang

(Shandong Gemsy Environmental Technology Co. LTD, Zibo, Shandong, China)

Nitrogen oxides (NO<sub>x</sub> for short), as one of the main causes of fog and haze and acid rain, has become the emphasis of current air pollution control. At present, selective catalytic reduction (SCR for short) of NO<sub>x</sub> has become the mainstream deNO<sub>x</sub> technology, whose technological core is the deNO<sub>x</sub> catalyst, and the major component system of the commercial deNO<sub>x</sub> catalysts is V<sub>2</sub>O<sub>5</sub>(WO<sub>3</sub>)/TiO<sub>2</sub>. Because the V<sub>2</sub>O<sub>5</sub> is a toxic and water-soluble substance, once the V<sub>2</sub>O<sub>5</sub> invasion into the human body, the health of the human body will be seriously damaged. Consequently, not only the catalyst production process will cause pollution, waste catalyst will once again threaten the safety of the environment, thereby research and development of an environment-friendly and highly efficient deNO<sub>x</sub> catalyst technology has become the great demand of the world environmental protection. Through more than ten years of scientific research, by using collaborative innovation of chemical catalysis and materials science, our R & D team successfully invented an environment-friendly and highly efficient rare earth based deNO<sub>x</sub> catalyst technology, which fills the gaps in the domestic and foreign industrial flue gas non-toxic deNO<sub>x</sub> catalyst technologies. So far, in research and development of the rare earth based deNO<sub>x</sub> catalyst, our R & D team already applied for more than 30 invention patents, published more than 60 academic papers, and obtained the original innovation intellectual property rights of China deNO<sub>x</sub> catalyst technology. The rare earth based deNO<sub>x</sub> catalyst technology successfully achieved industrialization in Shandong Gemsy Environmental Technology Co. LTD, which built the world's largest deNO<sub>x</sub> catalyst production line with a productivity of 5 million m<sup>3</sup> per year, and become the world's first and only enterprise that is able to produce environment-friendly and highly efficient deNO<sub>x</sub> catalyst. The new rare earth based deNO<sub>x</sub> catalyst exhibit better comprehensive performances and lower cost than those of the commercial vanadium-titanium system deNO<sub>x</sub> catalyst, with merits of environment-friendly chemical component, high deNO<sub>x</sub> efficiency (>90%), broad active temperature window (250°C–450°C), low conversion rate from SO<sub>2</sub> to SO<sub>3</sub> (<0.4%), high side crush strength (3MPa–15MPa), strong anti-humidity and water-resistance, strong anti-poisoning ability, reproducible for recycling use after deactivation, and waste catalyst without secondary pollution. Until now, the rare earth based deNO<sub>x</sub> catalyst has been successfully applied in over 60 actual deNO<sub>x</sub> projects in power, chemical, glass and cement industries, and take the lead in setting up the NO<sub>x</sub> "near zero emissions" project in coal-fired power plant in China. The new rare earth based deNO<sub>x</sub> catalyst technology was selected into "the directory that the State encourages the development of major environmental protection technology and equipment" of China in 2014, possessing broad prospects for international deNO<sub>x</sub> market.

## **INFLUENCE OF FE LOADINGS ON DESULFURIZATION PERFORMANCE OF ACTIVATED CARBON TREATED BY NITRIC ACID**

***Jiaxiu Guo***, Song Shu and Xiaoli Liu  
(Sichuan University, Chengdu, Sichuan, China)

SO<sub>2</sub> is one of the major pollutants in China because of coal burning and causes several environmental problems, such as acid rain and abrasion of buildings. Therefore, removal of SO<sub>2</sub> from emission sources is a great interesting and becomes a more urgent task. Activated carbon (AC) is a major porous material. The porous structure controls the availability of surface active sites and the degree of catalyst dispersion. Fe is easy to obtain and lose electron, promoting the redox cycle and showing a good oxidation performance. In the catalytic process, this obtainment and loss of electron transfer is the key to form the active intermediate. A series of Fe supported on activated carbon treated by nitric acid are prepared by incipient-wetness impregnation with ultrasonic assistance and characterized by N<sub>2</sub> adsorption-desorption, X-ray diffraction (XRD), Fourier transform infrared spectrum (FTIR) and X-ray photoelectron spectroscopy (XPS). It has shown that Fe loadings significantly influence the desulfurization activity. Fe/NAC5 exhibits an excellent removal ability of SO<sub>2</sub>, corresponding to breakthrough sulfur capacity of 323 mg/g and breakthrough time of 545 min. With the increase of Fe loadings, the generated Fe<sub>3</sub>O<sub>4</sub> and Fe<sub>2</sub>SiO<sub>4</sub> increase, but some generated H<sub>2</sub>SO<sub>4</sub> can react with Fe<sub>2</sub>SiO<sub>4</sub> and Fe<sub>3</sub>O<sub>4</sub> to produce Fe<sub>2</sub>(SO<sub>4</sub>)<sub>3</sub> when Fe<sub>2</sub>SiO<sub>4</sub> and Fe<sub>3</sub>O<sub>4</sub> are exposed to H<sub>2</sub>SO<sub>4</sub> for a long time. Fe/NAC1 has BET surface area of 925 m<sup>2</sup>/g with micropore surface area of 843 m<sup>2</sup>/g and total pore volume of 0.562 cm<sup>3</sup>/g including a micropore volume of 0.300 cm<sup>3</sup>/g. With the increase of Fe loadings, BET surface area and micropore volume decrease. When the Fe loadings increase to 10%, BET surface area and micropore volume decrease to 706 m<sup>2</sup>/g and 0.249 cm<sup>3</sup>/g. The Fe loadings influence the pore size distribution, and SO<sub>2</sub> adsorption mainly reacts in micropores at about 0.70 nm.

## **MINIMIZING ENVIRONMENTAL POLLUTION AND THE EFFECTS IN NIGERIA THROUGH GREEN DESIGN AND GREEN BUILDINGS**

*Iwuagwu, Ben Ugochukwu.* Dept of Architecture, Abia State Polytechnic, Nigeria  
Ikechukwu onyegiri. Dept of Architecture, Imo State University, Nigeria  
Iwuagwu, Ben Chioma M. Dept of Statistics, Abia State Polytechnic, Nigeria

**ABSTRACT:** The environmental impacts of buildings are enormous. Conventional buildings use large amounts of energy, land, water, and raw materials for their construction and operation. They are responsible for large amount of greenhouse gas (GHG) emissions as well as emissions of other harmful air pollutants. They also generate large amounts of construction and demolition (C&D) waste and have serious impacts on plants and wildlife. Considering the statistics, reducing the amount of natural resources buildings consume and the amount of pollution given off is seen as crucial for future sustainability. Over 40 percent of the energy used in Nigeria goes to heating, cooling, and power our buildings. And because much of this energy comes from dirty and dangerous sources like coal, oil, natural gas, and nuclear power, this accounts for nearly half of global warming pollution in the country. This high level of energy consumption pumps billions of tons of global warming pollution into the atmosphere causing ill health and depletion of the ozone layer. Green building is a high-performing, thoughtfully designed building that is very energy and water efficient, reduces its footprint on the planet, and provides a safer, healthier environment for the builders and future occupants throughout a building's life-cycle: from sitting to design, construction, operation, maintenance, renovation, and deconstruction. There are a number of motives to building green, including environmental, economic, and social benefits. However, this paper calls for an integrated and synergistic green design (GD) to both new construction and in the retrofitting of existing structures using renewable resources like sunlight through passive solar, active solar and photovoltaic techniques, using plants and trees through green roofs, rain gardens for reduction of rainwater run-off to minimize environmental pollution in Nigeria

### **INTRODUCTION**

Environmental pollution is one of the most pressing environmental problems and is among the critical challenges facing modern societies today. However, human activities directly or indirectly affect the environment adversely. By the activities of a stone crusher, he adds a lot of suspended particulate matter and noise into the atmosphere. Automobiles emit from their tail pipes oxides of nitrogen, sulphur dioxide, carbon dioxide, carbon monoxide and a complex mixture of unborn hydrocarbons and black soot which pollute the atmosphere. Domestic sewage and run off from agricultural fields, laden with pesticides and fertilizers, pollute water bodies. Buildings, however, contribute to environmental pollution and their environmental impacts are enormous. Conventional buildings use large amounts of energy, land, water, and raw materials for their construction and operation. They are responsible for large greenhouse gas (GHG) emissions as well as emissions of other harmful air pollutants. They also generate large amounts of construction and demolition (C&D) waste and have serious impacts on plants and wildlife. The International Energy Agency (2008) estimated that existing buildings are responsible for more than 40 percent of the world's total primary energy consumption and for 24 percent of global CO<sub>2</sub> emissions. This implies that the building sector uses more energy than other sectors like the industrial and transportation sectors. Due to increase in urban population and attendant residential pressures, energy consumption is projected to rise in buildings especially in fast growing countries (Odebiyi, Subramanian and Braimoh; 2010). This case of rise in energy consumption in buildings as a result of increase in urban population and residential pressure is also applicable in Nigeria. With the increasing building impact on energy

consumption and pollution in Nigeria, it is necessary, according to Iwuagwu and Azubuine (2015) to address these challenges of unsustainable building practices by adopting more sustainable building approach such as 'green architecture to reduce the amount of pollution generated by buildings and its adverse effects on our environment.

Buildings are the dominant energy consumers in modern cities but their consumption according to IEA, (2004) can be largely cut back through improving efficiency, which is an effective means to lessen greenhouse gas emissions and slow down depletion of non-renewable energy sources. The designs of the architects and building construction methods are very important in reducing the problem of climate change. Reducing the amount of natural resources buildings consume and the amount of pollution generated and given off is seen as crucial for future sustainability. Careful selection of environmentally sustainable building materials is the easiest way for Architects to begin incorporating sustainable design principles in buildings. Design decisions regarding the selection of less environmental impact building components according to Kim and Rigdon (1998) need careful consideration during the building design process. Careful building design and materials selection can substantially reduce environmental impacts of buildings. Despite the major efforts that have been made over recent years to clean up the environment, pollution remains a major problem and poses continuing risks to health and the environment. This paper highlights the effects of pollution and climate change, stressing the significant roles buildings, designs, construction methods and material specification play in creating and reducing environmental pollution and climate change. However, this paper calls for an integrated and synergistic design to both new construction and in the retrofitting of existing structures. It concludes by recommending the use of renewable resources like sunlight through passive solar, active solar and photovoltaic techniques, using plants and trees through green roofs, rain gardens for reduction of rainwater run-off to minimize environmental pollution in Nigeria.

## **EFFECTS OF ENVIRONMENTAL POLLUTION**

Rise in fossil fuel burning, construction and demolition waste, transportation, general land use changes etcetera have emitted and continuing to emit increasing quantities of greenhouse gases into the Earth's atmosphere and pollute our environment. The greenhouse gases include: carbon dioxide (CO<sub>2</sub>), methane (CH<sub>4</sub>) and nitrogen dioxide (N<sub>2</sub>O) etcetera. A rise in these gases and other environmental pollutants has increased the amount of heat from the sun withheld in the Earth's atmosphere, heat that would have been normally radiated back into space. This increase in heat has led to the greenhouse effect, resulting to climate change. The climate change as a result of increase in greenhouse gas emission has led to a lot of anomaly in our environment. In 2012, about 70 percent of major global droughts occurred in Africa. Kenya, Somalia, Sudan, Malawi, Angola, Chad and Ethiopia were particularly hit hard, and more than 16 million people in those countries were affected. In the same year, floods claimed 363 lives in Nigeria and 65 lives in Niger. In 2013, heavy rains continued with major flooding in Sudan, South Sudan, Mali, South Africa, Zimbabwe, Botswana and Mozambique. Despite the major efforts that have been made over recent years to clean up the environment, pollution remains a major problem and poses continuing risks to health. Even in developed countries, however, environmental pollution persists, most especially amongst poorer sectors of society (Samet, Dearry and Eggleston, 2011; Sexton and Adgate, 2001).

## **BUILDINGS AS A CONTRIBUTOR TO ENVIRONMENTAL POLLUTION**

Buildings consume a significant amount of our natural resources and have a wide range of environmental impacts. Considering what buildings are made of – steel, concrete, glass, and other energy-intensive materials – buildings have a high level of embodied energy. Producing and using these materials for construction depletes non-renewable resources and has environmental effects, these effects intensify the more frequently buildings are constructed, demolished and replaced. Buildings contribute to environmental pollution through:

**Energy Use.** Conventional building materials have high embodied energy. This includes the energy of the fuel used to power the harvesting or mining equipment, the processing equipment, and the transportation devices that move raw material to a processing facility. This energy typically comes from the burning of fossil fuels, which are a limited and a non-renewable resource. The greater a material's



embodied energy, the greater the amount of energy required to produce it, implying more severe ecological consequences.

**Construction Materials.** Building construction requires the constant production and harvesting of millions of tons of a variety of raw materials especially non-renewable, to meet world-wide demand. The amount of raw materials used in buildings construction is very large. Analysis of building products, from the gathering of raw materials to their ultimate disposal, provides a better understanding of the long-term costs of materials. These costs are paid not only by the client, but also by the occupants, and the environment. Careful selection of environmentally sustainable building materials, like timber, bamboo, earth and other low embodied energy building materials, is the easiest way for architects to begin incorporating sustainable design principles in buildings. Jong-Jin (1998) asserts that, price has been the foremost consideration when comparing similar materials or materials designated for the same function. However, the price of a building component represents only the manufacturing and transportation costs, but not social or environmental costs.

**Improper Land Use.** Millions of acres of land in Nigeria have buildings constructed on them. Buildings use large amounts of land; although the problem is the poor siting of buildings which leads to large amounts of land use. For instance, buildings built in the outskirts of existing residential or commercial areas require the construction of new roads, drainage, utility poles, and other infrastructure, which lead to, habitat destruction, land disturbance and erosion, among other things.

**Construction, Operation and Demolition Waste.** Tons of waste is typically deposited into a landfill during the construction of new homes. Construction waste consists primarily of timber and manufactured wood products, drywall, and masonry materials. Others are a mix of roofing materials, metals, plaster, plastics, foam, insulation, textiles, glass, and packaging. Even as these materials are recyclable, in Nigeria most of it is deposited into landfills causing environmental pollution.

## **OVERVIEW OF GREEN BUILDINGS.**

Nowadays, human beings pay great attention to environmental protection, thus develop a new trend — the Green Buildings. It is not about the color green, but has something to do with a new architectural concept. While the definition of what constitutes a green building is constantly evolving, the Office of the Federal Environmental Executive offers a useful working definition. This agency defines this green building as: the practice of increasing the efficiency with which buildings and their sites use energy, water, and materials, and reducing building impacts on human health and the environment, through better siting, design, construction, operation, maintenance, and removal—the complete building life cycle. Environmental Protection Agency (EPA) also defines green building as the practice of creating structures and using processes that are environmentally responsible and resource-efficient throughout a building's life-cycle from siting to design, construction, operation, maintenance, renovation and deconstruction. This practice expands and complements the classical building design concerns of economy, utility, durability, and comfort. Green building is also known as a sustainable or 'high performance' building. According to Iwuagwu and Azubuine (2015), green building is an outcome of a design, which focuses on increasing the efficiency of resource use- energy, water, and materials-while reducing building impacts on human health and the environment during the building life-cycle, through better siting, design, construction, operation, maintenance, and removal.

Buildings can incorporate many green features, but if they do not use energy efficiently, it is difficult to demonstrate that they are truly green. "Green building" is a concept that includes the design of the structure, site selection, building construction methods, building materials and landscaping practices. Green building is also referred to as "sustainable design" or "high-performance building." Green buildings offer an array of social benefits such as improved health, comfort, and productivity of occupants (Kats, Alevantis, Berman, Mills and Perlman, 2003). Economic benefits include reduction of building materials and operations costs. Social benefits include improvements in quality of life and equitable access to infrastructure services such as transportation, healthy indoor environments. Green buildings conserve vital natural resources and help to preserve fragile ecosystems, by reducing pollution and waste generation. In contrast to conventional buildings, green buildings seek to use land and energy efficiently, conserve water

and other resources, improve indoor and outdoor air quality, and increase the use of recycled and renewable materials.

## **HOW ENVIRONMENTAL POLLUTION IN NIGERIA COULD BE MINIMIZED USING GREEN BUILDINGS.**

***Through Construction Materials.*** Building construction requires the constant production and harvesting of millions of tons of raw materials to meet demand. The amount of raw materials used in buildings is very much and has been estimated that the construction industry consumes half of all products produced by volume (Hansen, 2004). A crucial part of green buildings is the material that is used in their construction. Green building materials are generally composed of renewable rather than non-renewable resources and are environmentally responsible because their impacts are considered over the life of the product. Green building materials can be selected by evaluating characteristics such as reused and recycled content, low off-gassing of harmful air emissions, low toxicity, sustainably and rapidly renewable materials, high recyclability, durability, longevity, and local production. In Nigeria today there are a lot of green building materials available but have not been effectively utilized. These materials are abundant in nature and include, earth, thatch, bamboo, stone etcetera; they are all sustainable and have characteristics that do not pollute our environment. Using earth as a case, according to iwuagwu and eme-anele (2012), characteristics of earth include: Durability, Energy Efficiency, reusability, among others.

***Through Architectural Design.*** A major element of green building design is increased energy efficiency through incorporation of passive design, efficient lighting, renewable energy technologies, and improved thermal performance of building shells. The goal is optimization of energy performance and integration of renewable energy options. Green buildings have large glazing for proper ventilation and lighting, reducing dependency on artificial ventilation and lighting reduces energy use and invariable reduces environmental pollution. Glazing allows increased daylight (without excess heat), reducing electrical lighting need. Increasing the thermal envelope allows for as much solar heat gain during cold weather, and shading during hot weather, while minimizing heat loss. Green buildings are designed to use low embodied energy materials and renewable building materials, these renewable materials are sustainable and reduces environmental impact.

***Through Sustainable Siting.*** A sustainable site approach optimizes land use and development density using site compatibility, protection of wetlands and natural habitats, transportation access and proximity to amenities in the decision-making process. In combination, these factors can significantly reduce adverse development impacts and minimize the building's ecological footprint. Landscape elements should include native plants as alternatives to conventional grass lawns, which often depend on irrigation and pesticides. Native plants are adapted to the natural hydrology, climate, and geography of the region and have evolved in relation to other local plants. This allows native plants to provide habitat for local species. Also, native plants normally require less watering, fertilizers.

***Construction, Operation, and Demolition Waste.*** Green buildings generally seek to minimize the amount of Construction & Demolition waste they generate by recycling or reusing the C&D waste. For sites that include the demolition of existing structures, plans can be developed early in the design process to manage and reuse as much material as possible through the deconstruction, demolition, and construction processes. Demolition generates large amounts of materials that can be reused or recycled—principally wood, concrete and other types of masonry, and drywall. Rather than demolishing an entire building, all or part of a building can be deconstructed. In contrast to building demolition, deconstruction involves taking apart portions of buildings or removing their contents with the primary goal being reuse. This reduces more material production and their use, reducing the energy use in their extraction, production and transportation to the site. It also reduces destruction of natural habitats and land disturbances which encourages environmental pollution.

Minimal construction waste during installation reduces the need for landfill space and also provides cost savings. According to Jong-Jin (1998) Designing floor intervals to coincide with the standard lengths of lumber or steel framing members also reduces waste. Taking advantage of the standard sizes of building

materials in the design phase reduces waste produced by trimming materials to fit, as well as the labor cost for installation.

**Local Materials.** Using locally produced building materials shortens transport distances, thus reducing air pollution produced by vehicles. Often, local materials are better suited to climatic conditions, and these purchases support area economies. It is not always possible to use locally available materials, but if materials must be imported they should be used in a small volume.

## **BENEFITS OF GREEN DESIGN AND GREEN BUILDINGS**

Environmental benefit from greening buildings that can be fairly easily estimated is lower air pollutant and CO<sub>2</sub> emissions. Emissions are reduced by decreasing energy use through energy-efficient design, use of renewable energy. Green building seek to rectify impacts of Energy Use in Buildings, Greenhouse Gas Emissions and Indoor Air Pollution, Building Water Use, Land Use and Consumption, Construction Materials and Construction, Operation, and Demolition Waste in conventional buildings. Reducing fuel and electricity consumption also lowers CO<sub>2</sub> emissions, a greenhouse gas that is linked to climate change. Decreased use of natural gas should also reduce methane emissions to the atmosphere (methane is another greenhouse gas). The effects of the build-up of greenhouse gases in the atmosphere may include sea level rise, weather changes (e.g., increase in violent weather patterns), and impacts on agriculture. Although climate change is likely to occur gradually over a long time period, energy-efficiency measures implemented now will slow the pace of the greenhouse gas build-up and its potential effects. The major benefits include:

**Sustainable Siting.** A sustainable site approach optimizes land use and development density using site compatibility, protection of wetlands and natural habitats, transportation access and proximity to amenities in the decision-making process. In combination, these factors can significantly reduce adverse development impacts and minimize the building's ecological footprint.

**Water Efficiency.** Green building designs emphasize water efficiency through landscaping, and reduced wastewater generation. Some examples include integration of rainwater catchments, gray water recycling and waste water treatment systems. These sustainable technologies significantly decrease the fresh water demands on local aquifers and at the same time reduce generation of waste water compared to conventional building designs.

**Energy Efficiency.** A major element of green building design is increased energy efficiency through incorporation of passive design, efficient lighting, renewable energy technologies, and improved thermal performance of building shells. The goal is optimization of energy performance and integration of renewable energy options.

**Building Materials.** Green buildings use sustainable construction materials and resources with low environmental impact minimizing consumption and depletion of material resources. This includes reduction, re-use and recycling of construction materials and generated waste, rehabilitation of existing structures, and explicit attention to building durability, adaptability and disassembly. The result is a reduction of extraction, processing, transportation, and solid waste.

**Healthy Indoor Environmental Quality.** Green buildings utilize efficient heating, ventilation and cooling systems (HVAC), low emissions paints and materials, and maximize use of natural day lighting to enhance indoor environmental quality. The result is improved health and comfort.

## **BARRIERS TO GREEN BUILDINGS.**

While the benefits of green buildings and sustainable development continue to show promising results, there are a number of barriers affecting realization of their full environmental, economic and social potential in Nigeria. Cost, industry awareness, and availability of green design technical capacities are the most significant operational barriers to green building design and construction. Knowledge and familiarity about green building practices has spread relatively slowly across the building industry.

## **RECOMMENDATIONS**

Having critically analysed the effects of environmental pollution, advantages of green buildings and the barriers to green buildings in Nigeria, the paper recommends the following, in the part of building professionals and government, to help facilitate awareness and construction of green buildings in Nigeria. Architects designing Buildings should design to eliminate waste by eliminate unnecessary finishes and make choices that use standard-sized or modular materials. Designers should consider product durability, availability, reusability, recyclability and biodegradability in the design process. Locally produced building materials are highly encouraged. Government should create more awareness on green buildings by making it a condition in all government projects. Government should also create an enabling ground for training and retraining of architects and other professional in the built industry to embrace green designs and green buildings. Government should also make it a condition for approval in the planning authorities all over Nigeria to help save our environment.

## **CONCLUSION**

The rate with which we pollute our environment through our practices; if efforts are not quickly made we will suffer more severe weather as a result of our activities. Even as reducing environmental pollution as a result of construction will not correct the anomaly in our climate, it will go a long way in relieving our climate. If recommendations of this paper are followed, we achieve a better climatic condition.

## **REFERENCES**

- Hansen, O. 2004. "Green Buildings" Small Business Innovation Research Special Solicitation Workshop, EPA
- IEA. 2004. "Oil Crises and Climate Challenges: 30 Years of Energy Use in IEA Countries." International Energy Agency, Paris, France.
- International energy agency. 2008. "Promoting Energy Efficiency Investments: Case Studies in the Residential Sector." International Energy Agency, Paris, France.
- Iwuagwu, B.U & N.C. Eme-Anele. 2012. "Earth Construction Technology and Design: A Positive Solution to Mass Housing In Africa". International Journal of scientific innovations and sustainable development. Vol. 2, Number 2, 2012.
- Iwuagwu, B.U & C.E. Azubuine. 2015. "Global Warming Versus Green Architecture: African Experience". Proceedings of International Conference on IT, Architecture and Mechanical Engineering (ICITAME'2015) May 22-23, 2015 Dubai (UAE).
- Jong-Jin, K. (1998). "Qualities, Use, and Examples of Sustainable Building Materials". National Pollution Prevention Center for Higher Education, Ann Arbor, Michigan
- Kats, G., L. Alevantis, A. Berman, E. Mills and J. Perlman. 2003. "The Costs and Financial Benefits of Green Buildings". A Report to California's Sustainable Building Task Force.
- Kim, J. and B. Rigdon. 1998. "Sustainable Architecture Module: Qualities, Use, and Examples of Sustainable Building Materials". Sustainable Architecture Compendium, National Pollution Prevention Center, University of Michigan.
- Odebiyi S O, S. Subramanian and A. K. Braimoh. 2010. "Green Architecture: Merits for Africa: Nigerian Case Study". Journal of Alternative Perspectives in the Social Sciences. Vol. 2 (2) 746 -767.
- Samet J. M, A. Dearry, P. A. Eggleston. 2001. "Urban air pollution and health inequities". A workshop report. Environ Health Perspect 109 (3): 357-74
- Sexton K, and J. L. Adgate. 2000. "Looking at environmental justice from an environmental health perspective". J Expos Anal Environ Epidemiol. 9: 3-8

## **ENHANCING ALGAL BIOHYDROGEN PRODUCTION USING FLUE GAS DERIVED BICARBONATE AND NUTRIENT LIMITATION**

*Sai Sameer Pusapaty* and K. Sata Sathasivan (The University of Texas at Austin, TX, USA)

**ABSTRACT:** Biohydrogen generated from algal cultures can be an effective solution as cleaner alternative fuel to reducing greenhouse gas emissions. Most of the related research is focused on limited strains and little has been known so far about improving hydrogen production. Flue gas derived bicarbonate generated from the Carbon Mineralization technique can be instrumental in boosting algal growth. If it can also enhance the hydrogen production capabilities, the algal system integration can lead to sustainable biohydrogen production. In this study, the hydrogen production capabilities of 5 macro algae that were collected using standard field techniques and 6 microalgae strains obtained from the UTEX culture collection have been studied. The experiment was conducted under anaerobic conditions/dark incubation after inducing nutrient limitation through dilution. Algal growth, cell count, starch amount and hydrogen concentrations were measured before and after the dark incubation period of 7 days per batch. Results obtained from batches of algal strains grown without bicarbonate and grown with 0.1M and 0.2M flue gas derived bicarbonate over 14 days were compared. Preliminary results indicate that in 8 out of 11 algal strains bicarbonate resulted in an increased hydrogen production of up to approximately 406 ml of gas per liter of algae.

### **INTRODUCTION**

Extreme climate changes that are being witnessed today are the very proofs of the global warming. A major cause of the greenhouse effect is due to anthropological activities. The significant response to this complex problem is to reduce emissions. Carbon capture and storage (CCS) is a major strategy to reduce GHG emissions. Novel Carbon mineralization technology offers many advantages over the traditional CCS methods. Integrating it with algal system by using the flue gas derived bicarbonate solution as the algal feedstock can stimulate the algal growth and rapidly absorb CO<sub>2</sub>, lower the overall cost and encourage widespread adaption.

Based on the existing literature, some algal strains have the ability to photosynthetically produce H<sub>2</sub> under anaerobic conditions. Hydrogen gas is seen as a future energy carrier by virtue of the fact that it is renewable, does not evolve the CO<sub>2</sub> in combustion, liberates large amounts of energy per unit weight in combustion and easily converted to electricity by fuel cells.

Algal Biohydrogen production from the integrated carbon mineralization will enable us to create a sustainable, carbon negative system. Current research is to study the effects of flue gas derived bicarbonate and nutrient depletion methods on the selected algal strains to increase the algal hydrogen production rates.

### **MATERIALS AND METHODS**

**Algal Strains and Cultivating Conditions.** 5 field macro algae samples and 6 micro algae strains are applied in this study. Field algae strains (TABLE 1) are collected from various water bodies around the town and the microalgae strains (TABLE 2) are obtained from the UTEX Culture Collection at the University of Texas. All the 11 strains of algae are maintained in the growth chamber with 12 hours of light and 12 hours dark cycles and kept under constant air bubbling at 20°C.

Experiments were conducted for the batches of 500 mL algal cultures (controls), 350mL algal cultures with 150mL of 0.1M flue gas derived sodium bicarbonate, 350mL algal cultures with 150mL of 0.2M flue gas derived sodium bicarbonate.

Algal cells were separated using filtering and added to DI water to induce nutrient depletion and were bubbled with Nitrogen to create anaerobic atmosphere and maintained in a dark chamber for 7 days to trigger Hydrogen production. Algal growth and starch quantification studies were conducted before and after dark incubation.

TABLE 1. List of Field Macro Algae strains collected for experimentation

ID	DATE	LOCATION GPS COORDINATES	WATER TEMPERATURE °C	COLLECTION TIME	WATER PH
1	8/20/15	Latitude : 30.513036   Longitude : -97.689046	26.1	10:18 AM	7.71
4	8/20/15	Latitude: 30.52023581558653   Longitude: -97.73501336574554	26.8	11:14 AM	7.31
5	8/20/15	Latitude: 30.52023581558653   Longitude: -97.73501336574554	26.8	11:30 AM	7.32
6	8/20/15	Latitude : 30.49648006306532   Longitude : -97.76916861534119	27.1	12:20 PM	7.71
7	8/20/15	Latitude: 30.49812559017617   Longitude: -97.76886820793152	27.2	12:45 PM	7.12

TABLE 2. List of microalgae cultures obtained from UTEX Culture Collection of Algae

ID	UTEX ID	ALGAE STRAIN
1	2168	<i>Chlorella vulgaris</i>
2	1785	<i>Chlorococcum rugosum</i>
3	90	<i>Chlamydomonas reinhardtii</i>
4	2016	<i>Scenedesmus obliquus</i>
5	755	<i>Porphyridium aerugineum</i>
6	LB 1355	<i>Kirchneriella cornuta</i>

**Bicarbonate for Photosynthesis.** Algae's efficiency at pulling inorganic carbon out of the environment is dependent on growth condition which implies the presence of an inducible carbon dioxide-concentrating mechanism in algal cells.  $\text{NaHCO}_3$  is a salt which consists of the ions  $\text{Na}^+$  and the bicarbonate anion,  $\text{HCO}_3^-$ . In aqueous solution, these ions are separated. Most algae can import both  $\text{CO}_2$  and  $\text{HCO}_3^-$  through the cell membrane. Once imported into the cell,  $\text{CO}_2$  or  $\text{HCO}_3^-$  accumulate mainly as  $\text{HCO}_3^-$ . In the carboxysome, where carbonic anhydrase (CA) exists, rapid equilibration between  $\text{CO}_2$  and  $\text{HCO}_3^-$  occurs. Corresponding with the accumulated  $\text{HCO}_3^-$ , this rapid equilibration leads to a high concentration of  $\text{CO}_2$  around ribulose-1,5-bisphosphate carboxylase oxygenase (Rubisco) in carboxysomes. Carbonic anhydrase is an enzyme that interconverts carbon dioxide and hydrogencarbonate which supply Rubisco with carbon dioxide from the pool of  $\text{HCO}_3^-$ . In the presence of this high substrate concentration, Rubisco fixes  $\text{CO}_2$  in the Calvin cycle, converting it into organic carbon (Chi, Zhanyou et al. 2011). The major antenna pigments in algae include chlorophylls, phycobiliproteins and carotenoids and the variation in the composition and relative abundance of these pigments give algae their distinctive color. Antenna complexes

are proteins with many bound antenna pigments which are important in absorbing light energy. If the algal photosynthesis would **increase** more carbon dioxide would be removed from the environment.

**Growth quantification.** Algae cultures were maintained for 4 weeks in the growth chamber with 12 hour light and 12 hour dark cycles at 20°C. Separated test batches were moved to continuous light chamber and kept for 2 weeks prior to filtration and re-suspending into DI water and analysis via spectrophotometry, cultures were evenly mixed using sterilized stir bars. Spectrophotometry readings were taken at 680nm wavelength.

**Starch Quantification.** Starch within the algal cells is measured before and after dark incubation. To measure the starch, 30 mL of algae samples are collected and centrifuged at the highest setting (8850 Xg) for 15 min (Z, Xioa et al. 2006). Liquid is drained out and samples are stored in the freezer. Once frozen the samples are crushed with mortar and pestle to break down the cells. Using 80% ethanol the crushed cells are transferred to a tube and are boiled till the ethanol is gone removing any impurities. To 2.5mL of the algal extract, 2.5mL of amylase solution is added and kept in the incubator at 37 degrees Celsius for 30 min. 5 mL of 1M Acetic Acid is mixed and the solution is transferred to 250mL flask. 200mL of DI water is added to the flask and 5mL of iodine reagent (0.2% iodine and 2% potassium iodide) is added. Absorbance values are measured at 580nm using Spectrophotometer to estimate the starch present in the sample.

**Algal Hydrogen Production.** Algal samples are sealed in Erlenmeyer flasks using rubber corks with 1 hole and 5mm flexible airline tubing. Pinch clamps were used to seal the rubber tubes. Nitrogen is bubbled through each sample before sealing it tightly. Samples are placed in a dark incubator without any apertures for light to pass through to prevent photosynthesis. Anaerobic conditions and Sulphur deprivation eventually trigger hydrogenase and Hydrogen production (B, Tamburic et al. 2011).

**Hydrogen Quantification.** Algal samples keep using up any available oxygen in the dark anaerobic atmosphere using respiration and depending upon the algal strain at some point of time hydrogenase enzyme gets triggered and that leads to hydrogen production. Eventually algal strain adapts and repairs the PSII system to resume the photosynthesis halting the Hydrogen production. So the produced gas contains oxygen, nitrogen and possibly hydrogen and carbon dioxide in the vent of delays during sealing the rubber cork. About 3mL gas samples are collected using Gas syringe and analyzed using Shimadzu Gas Chromatograph. Percentage values of the gases are derived and approximate volumes are estimated.

To quantify the chromatogram peak areas as moles, a calibration was created. 5 ml of pure hydrogen gas was created. Pressure was also recorded using a pressure sensor. The sample was then injected into the GC and the area for the hydrogen peak was measured. Using the measured values, the volume of gas was calculated using Van der Waal Equation with the average attraction constant (a) and mole volume constant (b) were taken from literature..

$$\left(P + \frac{n^2a}{V^2}\right)(V - nb) = nRT \quad (1)$$

## RESULTS AND DISCUSSION

**Algal Growth with Bicarbonate.** Analysis of algal chlorophyll (FIGURE 1) and starch growth (FIGURE 2) with bicarbonate using spectrophotometer absorbency values at 680nm and 580nm respectively revealed that the responses are species specific.

**Hydrogen Production.** Gas Chromatography analysis revealed the composition and the concentrations of different elements & compounds present in the injected 3mL gas samples. Hydrogen peaks in the chromatograms are easy early indicators. In figure 4, the increase in the number and length of the green

bars (Batch 3 with 0.2M NaHCO<sub>3</sub>) clearly indicate the positive response of algal strains with higher concentration of bicarbonate in producing biohydrogen. (0.2M) Bicarbonate triggered hydrogen production or an increase in the output in 8 out of 11 selected algal strains.

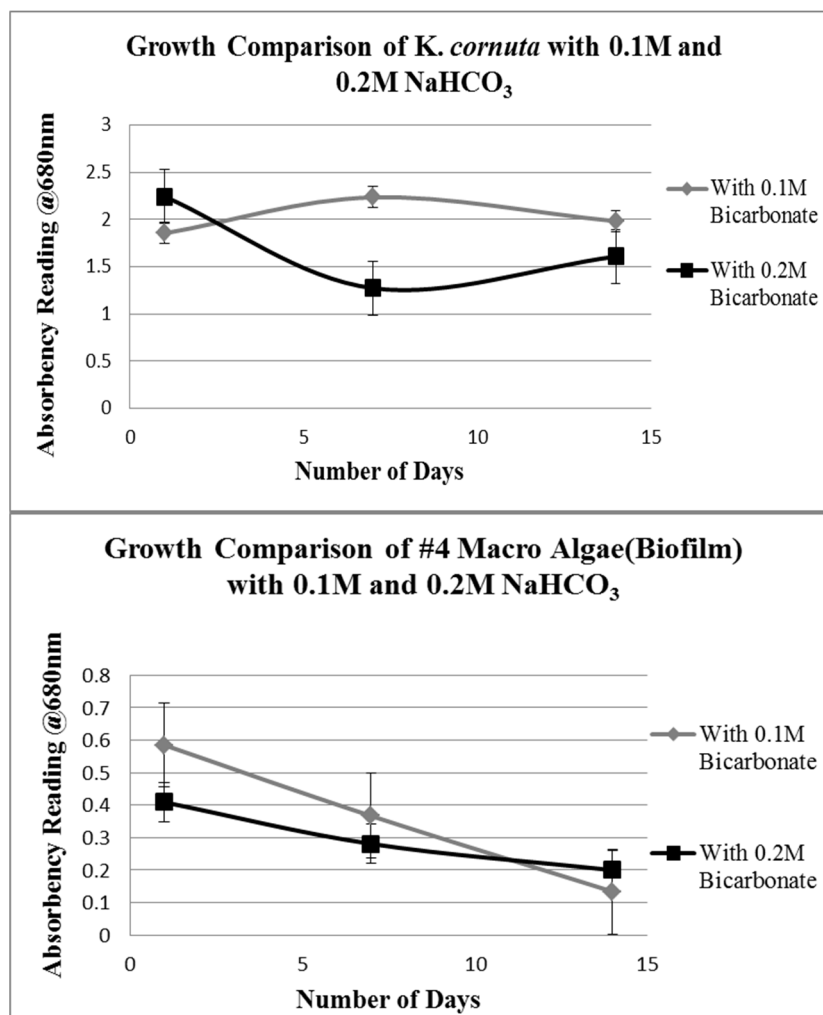


FIGURE 1. Absorbency values comparison with bicarbonate for *K. cornuta* and #4 (Biofilm)

*K. cornuta*, *C. vulgaris*, *C. reinhardtii* and the macro strains #1, #4 (biofilm), #5 showed significant increase in hydrogen production compared to other strains. Increased hydrogen yield observed for #1, #4 (biofilm) & #7 with 0.1M bicarbonate compared to higher concentration indicates that macro algae may have a threshold to the bicarbonate tolerance. It is also interesting to see that #6 macro algae produced significant hydrogen without bicarbonate and there was no hydrogen yield when grown with bicarbonate.



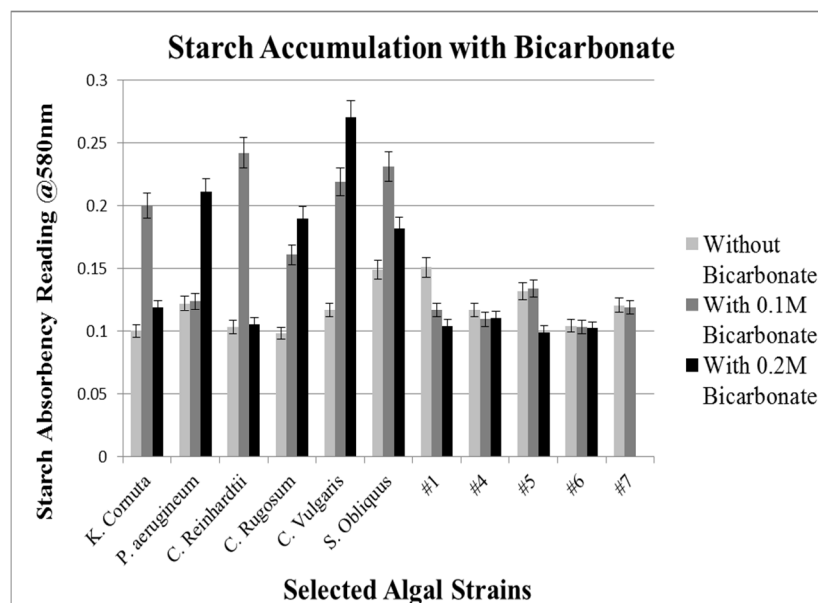
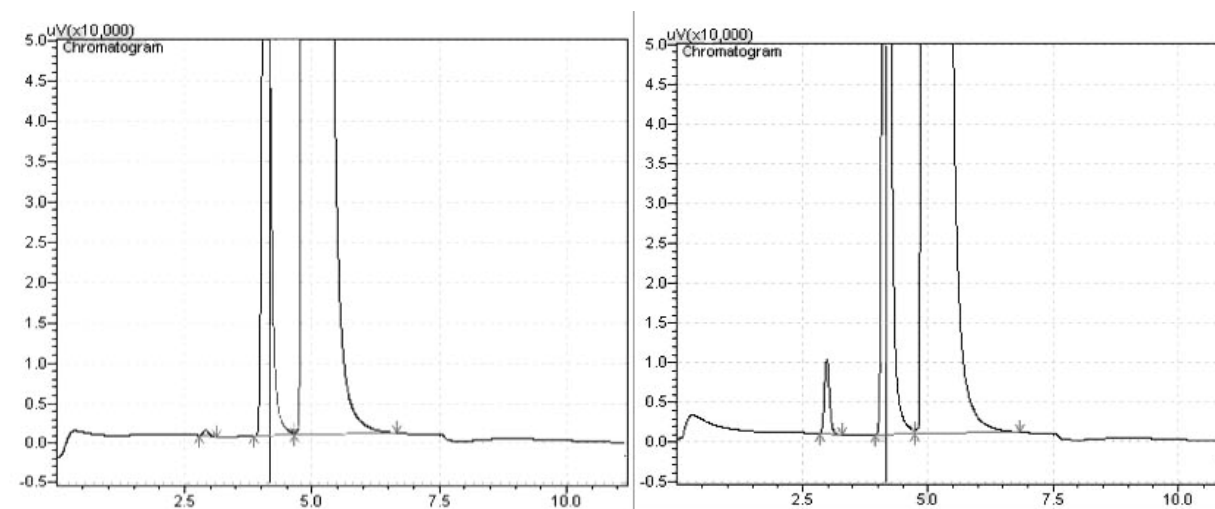


FIGURE 2. Comparison of starch absorbency values with Bicarbonate

FIGURE 3. Chromatograms of *K. cornuta* before and after the dark incubation

**Algal Growth and Starch Reduction during Anaerobic Dark Incubation.** The following Scatterplots depict the correlation between the cell growth, starch reduction and Hydrogen production. Overall trend shows that an increased bicarbonate concentration led to an increased starch reduction and an increased hydrogen production.

So far most of the research was focused on *C.reinhardtii*. This study indicates that other strains like *C. vulgaris*, *K. cornuta* and certain macro algae strains also have hydrogen production capabilities under dark anaerobic conditions and this is further enhanced by flue gas derived bicarbonate. These promising results achieved at the expense of minimum energy and with the utilization of atmospheric CO<sub>2</sub> can lead to more fascinating findings and eventually leading to a successful carbon negative system.

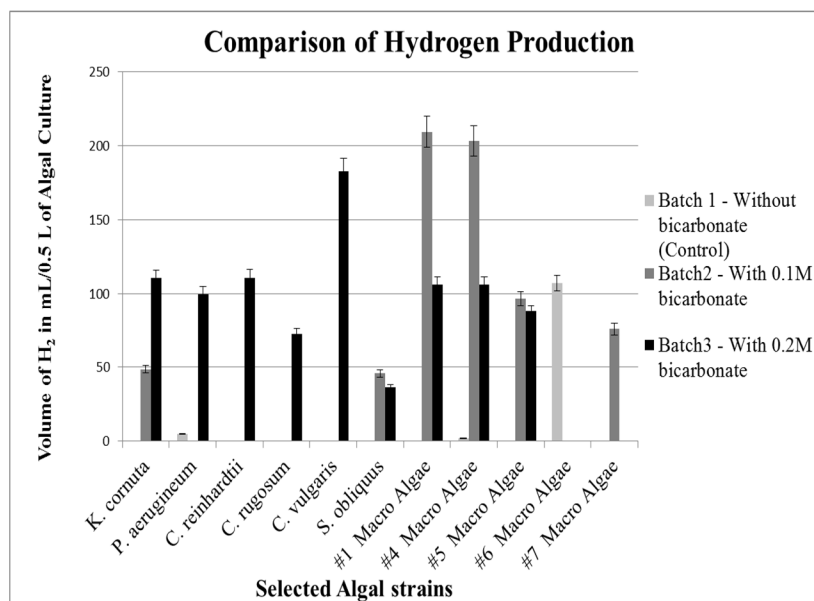


FIGURE 4. Comparison of Algal biohydrogen production in selected strains.

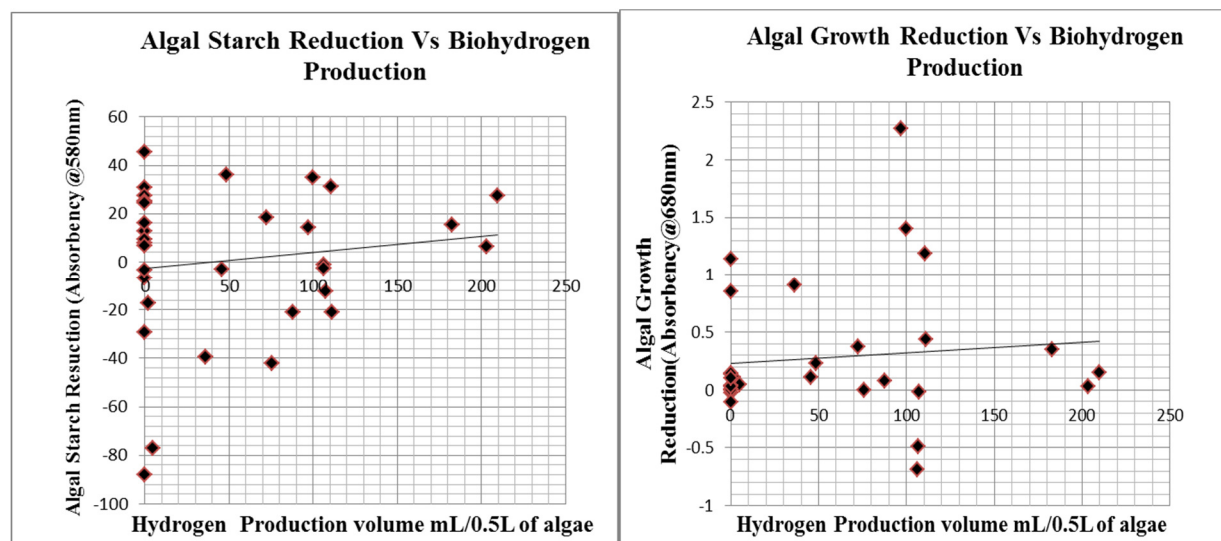


FIGURE 5. Effect of Starch & Growth Reduction on Hydrogen production

## CONCLUSIONS

This study demonstrates that bicarbonate addition can significantly affect the algal hydrogen production capability micro and macro algae, although the responses are species specific when compared under similar conditions.

Algal system integrated with Carbon Mineralization CCS Technology can utilize bicarbonate solution as algae feedstock, generate biohydrogen and other valuable byproducts from the harvested algal mass, and to recirculate the regenerated carbonate for carbon capture without spending energy. Cultivating strains of algae with higher bicarbonate absorption and growth rates have the potential to make the CCS process effective and more adaptable. Biohydrogen with 3 times the energy density as fossil fuels and water vapor as the only emission can aid in effectively remediating air pollution from flue gas emissions.

## REFERENCES

- Carrieri, D., Wawrousek, K., Eckert, C., Yu, J., & Maness, P. C. 2011. "The role of the bidirectional hydrogenase in cyanobacteria." *Bioresource Technology*, 102(18), 8368–8377.
- Chi, Z., O'Fallon, J. V., & Chen, S. 2011. "Bicarbonate produced from carbon capture for algae culture." *Trends in Biotechnology*, 29(11), 537–541.
- Dragone, G., Fernandes, B. D., Abreu, A. P., Vicente, A. a., & Teixeira, J. a. 2011. "Nutrient limitation as a strategy for increasing starch accumulation in microalgae." *Applied Energy*, 88(10), 3331–3335. <http://doi.org/10.1016/j.apenergy.2011.03.012>
- Fernandes, B., Dragone, G., Abreu, A. P., Geada, P., Teixeira, J., & Vicente, A. 2012. "Starch determination in *Chlorella vulgaris*-a comparison between acid and enzymatic methods." *Journal of Applied Phycology*, 24(5), 1203–1208. <http://doi.org/10.1007/s10811-011-9761-5>
- GEA Mechanical Equipment. (n.d.). Separation technology for Algae Production, 8.
- Hallenbeck, P. C., Abo-Hashesh, M., & Ghosh, D. 2012. "Strategies for improving biological hydrogen production." *Bioresource Technology*, 110, 1–9. <http://doi.org/10.1016/j.biortech.2012.01.103>
- Hallenbeck, P. C., & Benemann, J. R. 2002. "Biological hydrogen production; Fundamentals and limiting processes." *International Journal of Hydrogen Energy*, 27(11-12), 1185–1193. [http://doi.org/10.1016/S0360-3199\(02\)00131-3](http://doi.org/10.1016/S0360-3199(02)00131-3)
- Hemschemeier, A. C. 2005. "The anaerobic life of the photosynthetic alga *Chlamydomonas reinhardtii*," (August), 141 pp.
- Hunt, P. P. 1960. "Gas Chromatography of Hydrogen-Deuterium Mixtures."
- Kapdan, I. K., & Kargi, F. 2006. "Bio-hydrogen production from waste materials." *Enzyme and Microbial Technology*, 38(5), 569–582. <http://doi.org/10.1016/j.enzmictec.2005.09.015>
- Kim, D.-H., & Kim, M.-S. 2011. "Hydrogenases for biological hydrogen production." *Bioresource Technology*, 102(18), 8423–8431. <http://doi.org/10.1016/j.biortech.2011.02.113>
- Kim, S.-K., & Lee, C.-G. 2015. *Marine Bioenergy Trends and Development*. CRC Press.
- Marx, F., Training, O., Training, P., Darin, C., Training, R. O., Kimberly, M., ... Co-investigator, N. (2014). No Title No Title. *Igarss 2014*, (1), 1–5. <http://doi.org/10.1007/s13398-014-0173-7.2>
- Melis, A., & Happe, T. 2001. "Hydrogen Production ." Green Algae as a Source of Energy. *Plant Physiology*, 127, 740–748. <http://doi.org/10.1104/pp.010498.740>
- Mertens, R., & Liese, A. 2004. "Biotechnological applications of hydrogenases." *Current Opinion in Biotechnology*, 15(4), 343–348. <http://doi.org/10.1016/j.copbio.2004.06.010>
- Rumpel, S., Siebel, J., Farès, C., Duan, J., Reijerse, E., Happe, T., ... Winkler, M. 2014. "Enhancing Hydrogen Production of Microalgae by Redirecting Electrons from Photosystem I to Hydrogenase." *Energy & Environmental Science*, 1–10. <http://doi.org/10.1039/C4EE01444H>
- Scoma, A., Giannelli, L., Faraloni, C., & Torzillo, G. 2012. "Outdoor H<sub>2</sub> production in a 50-L tubular photobioreactor by means of a sulfur-deprived culture of the microalga *Chlamydomonas reinhardtii*." *Journal of Biotechnology*, 157(4), 620–627. <http://doi.org/10.1016/j.jbiotec.2011.06.040>
- Skjånes, K., Rebours, C., & Lindblad, P. 2012. "Potential for green microalgae to produce hydrogen, pharmaceuticals and other high value products in a combined process." *Critical Reviews in Biotechnology*, 33(January 2012), 1–44. <http://doi.org/10.3109/07388551.2012.681625>
- Srirangan, K., Pyne, M. E., & Perry Chou, C. 2011. "Biochemical and genetic engineering strategies to enhance hydrogen production in photosynthetic algae and cyanobacteria." *Bioresource Technology*, 102(18), 8589–8604. <http://doi.org/10.1016/j.biortech.2011.03.087>
- Tamburic, B., Zemichael, F. W., Crudge, P., Maitland, G. C., & Hellgardt, K. 2011. "Design of a novel flat-plate photobioreactor system for green algal hydrogen production." *International Journal of Hydrogen Energy*, 36(11), 6578–6591. <http://doi.org/10.1016/j.ijhydene.2011.02.091>
- Tamburic, B., Zemichael, F. W., Maitland, G. C., & Hellgardt, K. 2011. "Parameters affecting the growth and hydrogen production of the green alga *Chlamydomonas reinhardtii*." *International Journal of Hydrogen Energy*, 36(13), 7872–7876. <http://doi.org/10.1016/j.ijhydene.2010.11.074>

- Tamburic, B., Zemichael, F. W., Maitland, G. C., & Hellgardt, K. 2012. “A novel nutrient control method to deprive green algae of sulphur and initiate spontaneous hydrogen production.” *International Journal of Hydrogen Energy*, 37(11), 8988–9001. <http://doi.org/10.1016/j.ijhydene.2012.02.043>
- Vítová, M., Bišová, K., Kawano, S., & Zachleder, V. 2015. “Accumulation of energy reserves in algae: From cell cycles to biotechnological applications.” *Biotechnology Advances*, 33(6), 1204–1218. <http://doi.org/10.1016/j.biotechadv.2015.04.012>
- Xiao, Z., Storms, R., & Tsang, A. 2006. “Corrigendum to A quantitative starch – iodine method for measuring alpha-amylase and glucoamylase activities.” *Analytical Biochemistry*, 362(MAY 2006), 146–148. <http://doi.org/10.1016/j.ab.2006.01.036>

## HOW DO PLANT LEAVES REMOVE DUST AND ITS ATTACHED METALS ON THE ROADSIDE OF BEIJING?

Yang Zheng, Liu Yanju

(Beijing Milu Ecological Research Center, Beijing, China)

Air pollution is a global urban environmental problem. As the capital of China, Beijing is keeping facing the disturbance of high concentration of air dust, thus is necessary to find improve method. Taking advantage of phytoremediation, an ecological and friendly way to improve air quality, this study aims to investigate how the urban green plants remove air dust and its attached metals by their leaves. In harvest season, leaves samples of 32 plant species were collected from heavy traffic roadsides, then their dust and dust attached metals were analysed to select those plant species which could well accumulate or remove dust and metals. The result shows that per square meter plant leaves could remove 0.52 to 23 g dust with the average of 7.50 g, follows the sequence from high to low of *Koelreuteria paniculata*, *Ulmus pumila*, *Syringa oblata*, *Malus micromalu*, *Weigela florida* cv. *Red Prince*, *Ailanthus altissima*, *Salix babylonica*, *Robinia pseudoacacia*, *Ligustrum* × *vicaryi*, *Euonymus japonicus* etc.. The comparison of Cd, Cr, Cu, Fe, Mn, Ni, Pb, Zn content in diswashed leaves among plant species indicates that different species could best accumulate the certain metals. *Chaenomeles speciosa* accumulated the highest Cd of 9.48 µg per gram leaf. The highest Cr value of 19.80 µg per gram leaf was observed in *Sorbaria kirilowii*. The highest Cu content of 34.12 and Fe of 867.96 µg per gram leaf both was in *Sophora japonica*. Highest Mn content of 168.77 µg per gram leaf was in *Rosa chinensis*, and highest Ni of 18.72 µg per gram leaf was in *Prunus cerasifera* f. *atropurpurea*. *Populus trichocarpa* accumulated the most Pb of 6.57 µg per gram leaf, and *Populus tomentosa* accumulated the most Zn of 141.95 µg per gram leaf. By comparing the metal contents in same species leaves diswashed and washed, some species was found to remove a certain metal more efficiently than the others. The difference between Cd in diswashed and washed leaves of *Jasminum nudiflorum* was the highest of 0.80 µg per gram leaf. Cr of 3.65 was in *Ulmus pumila*, Cu of 13.31 in *Sophora japonica*, Fe of 407.73 in *Ulmus pumila*, Mn of 20.97 in *Rosa chinensis*, Ni of 4.89 in *Prunus cerasifera* f. *atropurpurea*, Pb of 4.46 in *populus trichocarp*, and Zn of 80.23 in *Amygdalus triloba*. The difference between metals in diswashed and washed leaf was divided by washed leaf metal for the same species to get a relative metal removable ability, and the result shows that *Jasminum nudiflorum* could remove 150.5% of its total accumulated Cd, *Ulmus pumila* do 66.89% of Cr, *Sophora japonica* do 63.96% of Cu, *Weigela florida* cv. *Red Prince* do 220.7% of Fe, *Amygdalus triloba* do 81.8% of Mn, *Koelreuteria paniculata* do 90.5% of Ni, *Parthenocissus tricuspidata* do 2023.4% of Pb, and *Amygdalus triloba* do 245.10% of Zn.

## **FUTURE PERSPECTIVE AND MITIGATION OPTIONS FOR ATMOSPHERIC MERCURY (Hg) EMISSIONS IN CHINA**

***Qingru Wu*** and Shuxiao Wang  
(Tsinghua University, Beijing, China)

We have presented atmospheric Hg emissions in China for the year 2020 and 2030 in this study. We develop two socioeconomic scenarios to project future energy consumption and industrial products production, including a business as usual scenario (BAU) and an alternative policy scenario (PC). For each scenario, we develop two end-of-pipe pollution control measures, including progressive (PGC) and stringent control case (SCC). We find that atmospheric Hg emissions are projected to be similar as the emissions in 2010 (approximately 539 t) under the BAU-PGC scenario. This indicates that the Hg removal by the progressive end-of-pipe pollution control measures will be offset by the Hg input from increased energy consumption and products production. In other scenarios, atmospheric Hg emissions are all less than the emissions in 2010. By using the stringent control technologies, atmospheric Hg emissions can be reduced by up to 76.9% in 2030. The share of elemental Hg will decline from 55% in 2010 to 39–41% in 2030 under PGC scenarios. However, it will still be the dominant species in 2030 under SCC scenarios.

Future emission scenarios imply different mitigation options for the convention-regulated sectors. Current legislations and progressive pollution control (eg., dust collection, desulfurization and denitration measures) will be the primary mitigation options for controlling emissions from coal-fired power plants, coal-fired industrial boilers, and nonferrous metal smelting, which will reduce 87%, 55% and 74% of current emissions (compare to 2010), respectively. Large-scale deployment of dedicated Hg removal technologies (eg., activated carbon injection and Boliden-Norzink technology) will aid to additional 2%, 35% and 15% of Hg reductions in these three sectors, respectively. For cement production, unless the stringent control measures (eg., dust shuttling) are fully applied, Hg emissions will increase by up to 22% in 2030 under the PC-PGC scenario. For municipal solid wastes incineration sectors, due to the sharp increase of incinerated solid wastes, Hg emissions will increase to 5.7–11.7 t in 2030, all larger than the emissions of 0.7 t in 2010. Thus, stringent control measures should be used in this sector. Moreover, although most of the primary emission sources in 2010 will still contribute to large amount of emissions in 2030, attention should also be paid to the emissions from non-convention-regulated sources, such as iron and steel production sector. Emission from this sector will head the emission inventory in the PC-SCC scenario in 2030.

**BIO-ASSESSMENT  
AND  
TOXICOLOGY**

## **RESPIRATORY SYSTEM EMERGENCY SERVICE VISITS IN ADANA, TURKEY (2007-2011)**

Ertan Kara<sup>1</sup>, Hasan Goksel Ozdilek<sup>2</sup>, Emine Erman Kara<sup>3</sup>

<sup>1</sup> Cukurova University, Faculty of Hecicine, Dept. of Public Health, Adana, Turkey

<sup>2</sup> Canakkale Onsekiz Mart University, Faculty of Engineering, Environmental Engineering Dept., Terzioğlu Campus, 17020 Canakkale, Turkey<sup>139</sup>

<sup>3</sup> Nigde University, Faculty of Engineering, Environmental Engineering Dept., 51245 Nigde, Turkey

**ABSTRACT:** The center of the province of Adana is located on a flat area, yet being a metropolitan area it has some ambient air quality issues. In this study, a comprehensive evaluation was completed on the effects on health, exemplified by the emergency respiratory system and asthma diagnoses, which are triggered with urban air pollution chiefly caused by motor vehicle traffic nowadays. The air pollution data that exist between 2007 and 2011 and the upper respiratory and asthma diagnosed emergency room admittances to Cukurova University Balcali Hospital were evaluated. For this purpose the official records collected for four consecutive years from Adana Cukurova University Balcali Hospital and ambient air quality monitoring stations were evaluated. The relationships between asthma and air quality parameters as well as between respiratory system diagnoses and air quality parameters were statistically evaluated using trend analysis. It is found that there is a significantly decreasing trend in the number of emergency visits due to asthma problems in Adana. However, an insignificantly changing trend in respiratory system diagnoses was determined.

**Key words:** Air pollution, asthma, PM<sub>10</sub>, SO<sub>2</sub>, Adana-Turkey.

## **INTRODUCTION**

Urbanization plays a key role in human health. Turkey has transferred itself into an urban society over the last 30 years, and it has taken big steps towards becoming one of the world's fastest growing economies. However, at the same time it has experienced air pollution related health problems. The air quality monitoring system has been automated since the late 1990s. A majority of the automated air quality monitoring stations report only particulate matter (PM<sub>10</sub>) and sulphur dioxide (SO<sub>2</sub>) in the country. Prior to this automation only some health institutions and concerned scientists collected data on air quality in Turkey. Although serious episodes of air pollution have been reported in such places as London in 1952 (Bell et al., 2004), Los Angeles in 1965 and 1984, and in New York City in 1953 (Nazaroff and Alvarez-Cohen 2001; Masters and Ela 2008), the link between air pollution and health has not been strongly established in Turkey, despite the fact that many urban centres experience air pollution related health problems (Özdilek, 2006). Özdilek (2006) compared urban centres that use natural gas and those that use mostly coal for heating purposes during winter months. He reported that pneumonia is strongly linked to urban air quality impairment (Özdilek 2006). Tomac et al. (2005) linked asthma and air quality in Zonguldak, the country's only hardcoal mining area, where the Catalagzi hard coal fired power plant has been into operation for a very long time. Berktaş and Bircan (2003) examined atmospheric sulphur dioxide and particulate matter and their effects on asthma symptoms recorded at emergency rooms in Ankara, the capital of Turkey. Over the past few decades, heating systems in many Turkish cities have shifted from using conventional heating resources (primarily coal and wood) to imported natural gas. However, a dramatic increase in the number of motor vehicles, the addition of new fossil-fuel power plants, and changes in local climatic conditions (such as the urban heat island effect and the construction of new dam lakes) have had an effect. Recently,



a ban on the use of sulphur containing diesel for diesel type motor vehicles and leaded gasoline for regular motor vehicles was implemented in Turkey in order to improve ambient air quality.

PM<sub>10</sub>, defined as particulate matter with a mass median aerodynamic diameter not greater than 10 µm, is responsible for health effects diagnosed in the upper respiratory tract (Cheremisinoff, 2002) upper airways. As Nawrot et al. (2007) indicated fine particulate matter is responsible for deaths reported in summer than in winter. Sulphurous air pollution affects public health as a result of coal burning and the operation of diesel engines. Asthma and bronchitis are the main consequences of sulphur dioxide type air pollution (Stephens and Stair, 2007). These pollutants are common in the urban environment because of meteorological conditions, the intensity of traffic, fossil fuel use, and buildings that hinder air circulation. Carlslaw et al. (2007) modeled nitrogen oxide concentrations on a busy road in central London and found a decreasing nitrogen oxide concentration due to a decrease in overall traffic and meteorological circumstances not from nitrogen oxide emissions.

The metropolitan area of Adana has a population of 1,637,053 (based on 2010 data) and its annual population growth rate is 1.41% (Turkish Statistical Association, 2011). The city is approximately 215 km away from Turkey's largest coal-fired energy production plant (Afsin-Elbistan, in the province of Kahramanmaraş) (Say, 2006). Adana has another fossil fuel power plant, the Sugoza coal-fired energy plant, which is 50 km away from the city of and is situated by the Mediterranean Sea. The Sugoza Power Plant utilizes imported low-level sulphur-type coal. Although Adana is located on a flat plain, the city's traffic load is thought to emit a significant amount of particulate matter and other traffic-related air pollutants into the atmosphere. The area of Adana city encompasses an east-west distance of 16 km and a north-south distance of 7 km. The urbanized area is nearly 88 km<sup>2</sup>. The population density is 17,746 people per km<sup>2</sup> in the city. As of 2011, the metropolitan area has five counties: Seyhan (population 723,277), Karaisalı (population 22,981), Yüreğir (population 422,529), Sarıçam (population 120,325), and Cukurova (347,941) (TUIK, 2011).

This study examines ambient air pollution and respiratory system disease cases in Adana. We studied the temporal change in ambient air quality in Adana. The purpose of this study is to evaluate the relationship between air pollution and the number of asthmatic patients seen in the center of Adana between 2007 and 2011.

## **MATERIALS AND METHODS**

Meteorological data was taken from the Turkish Meteorological Institution. Air pollution data was collected from the Turkish Meteorological Institution's automated system. The data includes sulfur dioxide and particulate matter above 10 micrometer in diameter. In addition to ambient air quality, vehicular traffic-related carbon monoxide (CO<sub>2</sub>), sulfur dioxide (SO<sub>2</sub>), and nitrous oxide (NO<sub>x</sub>) emissions between 2004 and 2010 (on an annual basis) were estimated using data about the number of motor vehicles and specifications within Adana. Both monthly and quarterly means were computed. A parametric statistical analysis was completed.

From traffic related air contaminants' emissions, the base concentrations of SO<sub>2</sub> and NO<sub>x</sub> were computed for dates when/during times when inversion occurred. Traffic-related emissions were computed from the counted number of motor vehicles and their types (using diesel or regular fuel) and their estimated years of production. While newer motor vehicles emit approximately 110 g CO<sub>2</sub> per km, older motor vehicles in Turkey emit more than 200 g CO<sub>2</sub> per km. Similarly, NO<sub>x</sub> emissions were computed. Stoichiometric computations were done using such figures. The city centre was assumed to be elliptical on the ground and a dome on vertical axis. For the thermal inversion layer, the following formula was utilized:

$$V = \pi ab \left[ \left( \frac{2c}{3} \right) - x + \left( \frac{x^3}{3c^2} \right) \right] \quad (1)$$

where,

V: the volume of air above the city under conditions where atmospheric inversion exists (m<sup>3</sup>)

a : half-length of the city from the city centre to the y axis (m)

b : half-width of the city from the city centre to the x axis (m)

c : length of the top point from the ground to the vertical (z) axis (assumed to be 100 m)

$x$  : length of the inversion layer from the ground to the vertical ( $z$ ) axis (assumed to be 80 m)

The nonparametric correlation coefficient (Spearman) was computed based on seasonal median  $PM_{10}$  and emergency visits diagnosed as respiratory system-related and seasonal  $PM_{10}$  and emergency visits diagnosed as asthma. Finally, the Mann-Kendall trend test was applied for the same aforementioned parameters to determine whether  $PM_{10}$ , respiratory system diagnoses and recorded asthma cases were increasing or decreasing at the emergency room at Çukurova University Faculty of Medicine.

The variance of the Mann-Kendall trend test was computed by using the following formula:

$$\text{Var}(S) = 1/18 [(n(n-1)(2n+5)) - (\sum t_p(t_p-1)(2t_p+5))] \quad (2)$$

where,

$n$ : the number of data points ( $n=16$  between Spring 2007 and Winter 2010)

$t_p$ : the number of data points in the  $p^{\text{th}}$  group.

Then  $Z$  was computed by using the following formulas:

$$Z = (S-1)/[(\text{Var}(S))^{0.5}] \text{ if } S \text{ is greater than } 1 \quad (3)$$

$$\text{or } Z = (S+1)/[(\text{Var}(S))^{0.5}] \text{ if } S \text{ is a negative number} \quad (4)$$

## RESULTS AND DISCUSSION

According to the 2007-2011 data, examined on a daily basis, air pollution on more than half of the days each year exceeded the limit established for particulate matter ( $PM_{10}$ ), which is set at  $50 \mu\text{g m}^{-3}$  by the European Union. For example, in 2009, 64 days exceeded the limit value for  $PM_{10}$  at the Çatalan air quality monitoring station, which is approximately 20 km away from Adana city center, and 247 days exceeded the limit value for  $PM_{10}$  at the Adana Governorate Building site that is situated in the city center of Adana. For 2007 a total of 161 days were above the  $50 \mu\text{g m}^{-3}$  limit value. For 2008, this total was 145 days. For 2009, a total of 172 days, for 2010, a total of 187 days, and for 2011, a total of 208 days were above the  $50 \mu\text{g m}^{-3}$  limit value.

Table 1. Respiratory system and asthma morbidities (2007-2011) in Adana metropolitan area

Season	Respiratory system morbidity (emergency room admittance per million)		Asthma morbidity (emergency room admittance per million)	
	Average	Standard deviation	Average	Standard deviation
Spring	1449	520	71	21
Summer	852	300	45	10
Autumn	1402	529	62	17
Winter	1873	230	86	18

An aging population an increase in motor vehicles, urban sprawl, and traffic congestion are all important factors influencing health effects related to air quality. Depending on the size of the urban area, commuting distances tend to be lengthier in larger cities. In many metropolitan areas it might be hard to wean residents off their dependency on automobiles in the future as cities grow. This is expected to affect the seriousness of motor vehicle-related air pollution in such areas.

In Adana, the highest increase in patients suffering from upper respiratory system diseases occurred between September and October of 2007. Although particulate matter is the highest in August, our study shows that particulates showed no effect on the number of patients that suffered from respiratory system problems (Figure 1). Sulphur dioxide emissions at this time, however, were some of the highest for the days that data was available, and the monthly mean was  $2.5 \mu\text{g m}^{-3}$  in August 2007. For March, April, October, November and December, there were more than 300 patients diagnosed each month with upper respiratory system failure at Çukurova University Faculty of Medicine (Balcali Hospital). The median number of upper respiratory system failure patients treated at Çukurova University Faculty of Medicine between March and December 2007 on a seasonal basis was computed to be over 900 (Figure 1). The number of patients with

upper respiratory system failure, on a monthly basis, in March and April, as well as from October to the end of the year, was above the median value. As related to the number of days on which 24-hour limit values for PM<sub>10</sub> were exceeded at the Adana Meteorological Station's air quality monitoring station (shown in Figure 2), it seems after September the number of patients increases remarkably, although the PM<sub>10</sub> monthly statistical mean is not correlated with the number of patients diagnosed with upper respiratory system failures in Adana in 2007. Not surprisingly, the highest total respiratory system emergency room visits occurred in the winter of 2011, when SO<sub>2</sub> concentration was 7 µg m<sup>-3</sup>.

The decrease in the number of patients diagnosed with upper respiratory system-related diseases started in March and ended in August. In September, there is a remarkable increase in the number of patients diagnosed with upper respiratory system failures. The highest increase was recorded from September to October, and close to a 50% increase in the number of patients suffering from upper respiratory disease was recorded during that time period. The increase in patients diagnosed with upper respiratory diseases diagnosed at Çukurova University Faculty of Medicine's Balcalı Hospital from October to November and from November to December is almost the same. This could be explained by the decreased strength of the immune system as the temperature changes in winter. Because local people are accustomed to hot weather and a relatively low level of air pollution, people tend not to become sick easily. However, sudden changes in temperature might weaken the immune system. It is found that there was no trend in the ambient seasonal PM<sub>10</sub> mean between spring 2007 and winter 2010.

According to the seasonal Mann-Kendall trend test for 19 consecutive seasons from spring 2007 (starting in March 2007) to winter 2011 (ending in November 2011), a significant decreasing trend was found for asthma in terms of emergency room admittances ( $S=-57$ ,  $\text{Var}(S)=817$ ,  $Z=-1.959 < Z_{\text{critical}}=-1.645$ ). It was found that the level of PM<sub>10</sub> is closely linked to asthma (Boubel et al. 1994) despite the fact that emergency asthma cases and ambient PM<sub>10</sub> are not linked as being statistically significant in this study.

Table 2. Pearson correlation among variables examined in Adana between 2007 and 2011 (based on seasonal median values)

	RSM	AM	PM <sub>10</sub>	SO <sub>2</sub>	WS	WD	AT	RH	AP
RSM	1								
AM	<b>0.661</b>	1							
PM <sub>10</sub>	-0.170	-0.052	1						
SO <sub>2</sub>	0.192	0.147	-0.053	1					
WS	0.058	0.184	-0.057	0.073	1				
WD	0.304	0.133	0.228	0.165	0.141	1			
AT	-0.330	<b>-0.577</b>	0.188	-0.324	0.038	0.176	1		
RH	-0.255	<b>-0.445</b>	0.056	-0.022	0.345	0.197	<b>0.447</b>	1	
AP	-0.172	-0.214	-0.175	-0.172	-0.240	-0.132	0.153	0.310	1

RSM: respiratory system morbidity

AM: Asthma morbidity

PM<sub>10</sub>: particulate matter (µg m<sup>-3</sup>)

SO<sub>2</sub>: sulphur dioxide (µg m<sup>-3</sup>)

WS: wind speed (m s<sup>-1</sup>)

WD: wind direction (degrees)

AT: air temperature (°C)

RH: relative humidity (percent)

AP: air pressure (mb)

Based on the Mann-Kendall trend test, respiratory system morbidities recorded as emergency cases experienced a statistically insignificant change between spring 2007 and autumn 2011. The test result was found as  $Z=0.419 < Z_{\text{critical}}=1.645$  ( $S=13$ ,  $\text{Var}(S)=817$ ), which indicates a non-significant change in emergent respiratory system admittances to Çukurova University Faculty of Medicine Balcalı Hospital.

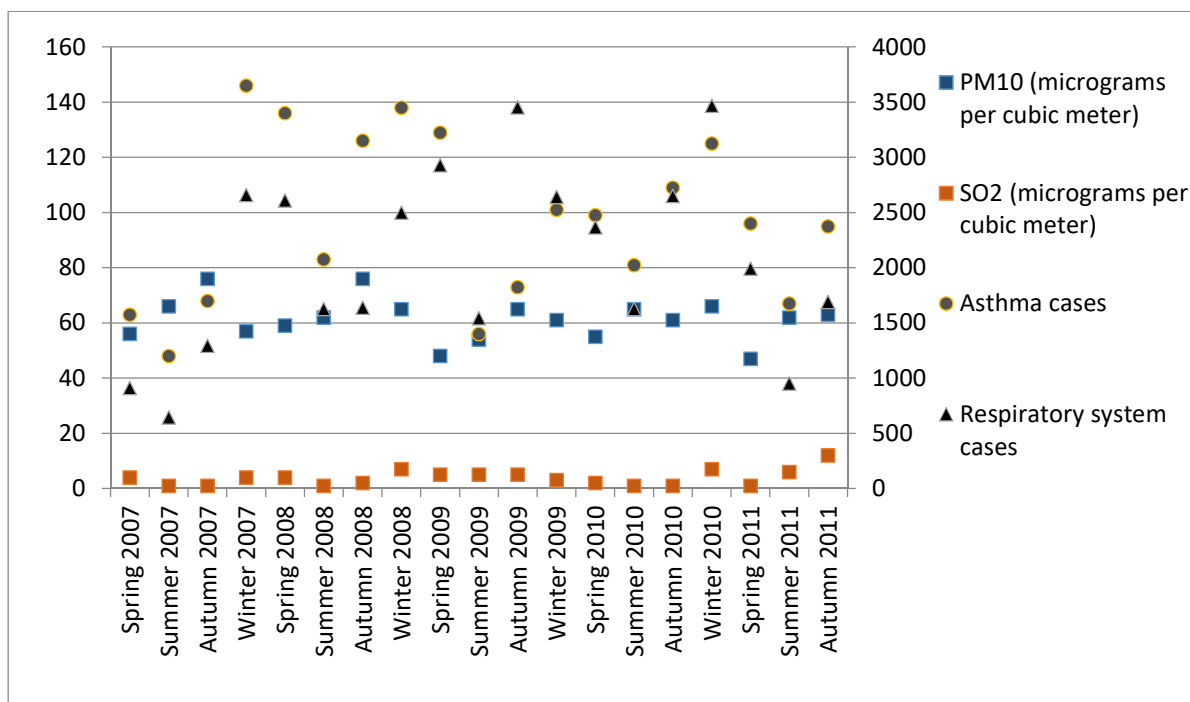


Figure 1. PM<sub>10</sub>, SO<sub>2</sub>, asthma and respiratory system emergency room admissions time series recorded at Adana Cukurova University Balcali Hospital (only respiratory system emergency cases are on secondary y axis)

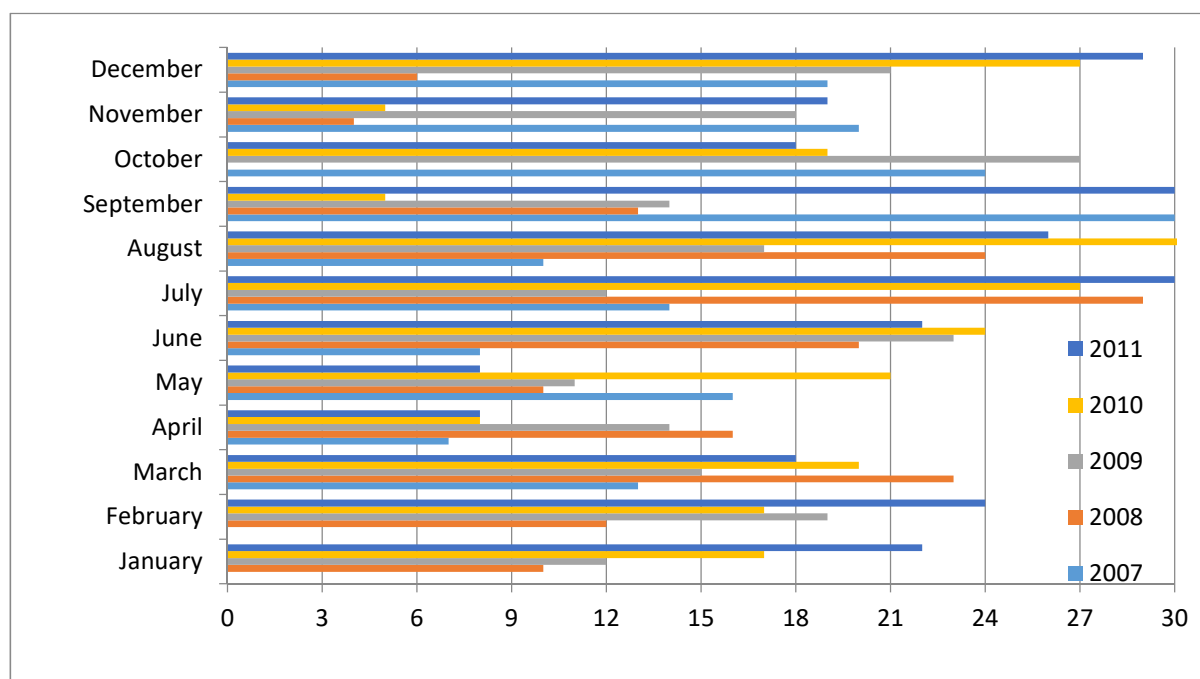


Figure 2. Number of days on which 24 hour limit values for PM<sub>10</sub> were exceeded at Adana Meteorological Station's air quality monitoring station. For 2007 total 161 days, for 2008 total 145 days, for 2009 total 172 days, for 2010 total 187 days, and for 2011 total 208 days are above 50 µg/m<sup>3</sup> limit value.

In our study it was found that ambient air quality has not improved over the period of the analysis. Ambient air quality improvement might be seen some time in the future, despite the fact that, in the future, traffic related emissions in both CO<sub>2</sub> and NO<sub>x</sub> is expected to be higher mainly due to a potential increase in private cars and traffic congestion in Adana. Adana in the 1990s underwent a transformation from an industrial to a post-industrial local economy, although in fact the air quality in Adana is somewhat less susceptible to industrial emissions than in other cities, due to the local environmental conditions. Agardy, for example, underlines that stoichiometrically computed air emissions for the mass load discharge from industrial stacks are mostly lower than the actual measured emissions (Agardy, 2005).

It is known that particles in ambient air can be problematic for the human respiratory system. The European Union recommends that the number of days on which one-day limit value for PM<sub>10</sub> (50 µg m<sup>-3</sup>) is met should not exceed 35 days each year (SYKE, 2008). However, problems associated with the effect of ambient air quality on respiratory health arise due to factors such as the ever-increasing traffic, meteorological variables (such as the transport of desert sand from northern Africa), construction activities, and other factors affecting air quality.

## REFERENCES

- Agardy, F. J. (2005). Environmental Solutions. Agardy, F. J. and Nemerow, N.L. (editors). Elsevier Academic Press: Burlington, MA.
- Bell, M.L., Davis, D.L., Fletcher, T. (2004). "A Retrospective Assessment of Mortality from the London Smog Episode of 1952: The Role of Influenza and Pollution". *Environ Health Perspect* 112 (1): 6–8.
- Berktaş, M. and Bircan, A. (2003). Effects of Atmospheric Sulphur dioxide and particulate matter concentrations on emergency room admissions due to asthma in Ankara. *Tüberküloz and Toraks Dergisi*. 51: 231-238.
- Boubel, R. W., Fox, D. R., Turner, B., Stern, A. C. (1994). Fundamentals of Air Pollution (3rd ed.). Academic Press: San Diego, CA.
- Carslaw, D. C., Beevers, S. D., Tate, J. E. (2007). Modelling and Assessing Trends in Traffic-Related Emissions Using a Generalised Additive Modelling Approach. *Atmospheric Environment*, 41: 5289-5299.
- Cheremisinoff, N.P. (2002). Handbook of Air Pollution Prevention and Control. Butterworth-Heinemann, Amsterdam, the Netherlands.
- Masters, G.M. and Ela, W.P. (2008) Introduction to Environmental Engineering and Science (3<sup>rd</sup> Edition) Pearson International Edition, Prentice Hall: Upper Saddle River, NJ.
- Nawrot, T.S., Torfs, R., Fierens, F., De Henauw, S., Hoet, P.H., Van Kersschaever, G., De Backer, G. Nemery, B. (2007). Stronger associations between daily mortality and fine particulate air pollution in summer than in winter: evidence from a heavily polluted region in western Europe. *J. Epidemiol Community Health*. 61 (2): 166-149.
- Nazaroff, W.W. and Alvarez-Cohen, L. (2001). Environmental Engineering Science. John Wiley and Sons, Inc: New York, NY.
- Özdilek, H.G., (2006). "An Analogy on Assessment of Urban Air Pollution in Turkey over the turn of the new Millennium (1992-2001)" *Environmental Monitoring and Assessment* **123/1-3**: 95-112.
- Say, N.P. (2006). "Lignite fired thermal power plants and SO<sub>2</sub> pollution in Turkey" *Energy Policy* **34**: 2690-2701.
- Stephens, C. and Stair, P. (2007). Charting a New Course for Urban Public Health. In: State of the World: Our Urban Future. Starke L. (editor). WW Norton and Company: New York, NY.
- SYKE (Finnish Environment Institute SYKE) (2008). Finland – State of the Environment. Putkuri, E., Lindholm, M. And Lyytimäki, J. (editors) 20 pp. Helsinki, Finland.
- Tomac N, Demirel F, Acun C, Ayoglu F. (2005). Prevalence and risk factors for childhood asthma in Zonguldak, Turkey. *Allergy Asthma Proc*. 26: 392-402.
- TUIK (2011). Address based population data (in Turkish). Accessed from the internet on January 25, 2012 from <http://rapor.tuik.gov.tr>.

## CARCINOGENICITY AND MUTAGENICITY ASSESSMENTS OF DIETARY EXPOSURE TO PAHs IN IMPORTED FISH PRODUCTS IN NIGERIA

**Nsikak U. Benson**, Akan B. Williams, Winifred U. Anake, Kelechi P. Eke, Adebunayo E. Adedapo  
(Covenant University, Ogun State, Nigeria)

Abaas A. Olajire (Ladoke Akintola University of Technology, Ogbomoso, Nigeria)

Polycyclic aromatic hydrocarbons (PAHs) occurrence and assessment of dietary exposure from imported canned sardines (*Sardinops sagax*) commercially marketed in local stores and supermarkets in Nigeria were evaluated for the first time. PAHs determinations were performed using high performance liquid chromatography (HPLC) (Agilent 1290 model) equipped with UV-VIS diodes array detector (DAD) at  $\lambda = 210$  nm and 214 nm. The percentages recoveries were higher than 96%. The degree of contamination expressed as total concentrations of PAH (TPAHs) congeners ranged between 2.53 and 35.55  $\mu\text{g kg}^{-1}$  dry weight (d.w.) at  $\lambda = 210$  nm, and 1.30 and 27.93  $\mu\text{g kg}^{-1}$  (d.w.) at  $\lambda = 214$  nm. The carcinogenic (BaP-TEQ) and mutagenic toxicities (BaP-MEQ) of eight priority PAHs were evaluated. Benzo(a)pyrene, benzo(b)fluoranthene, benzo(k)fluoranthene and indeno(1,2,3-d) pyrene contributed significantly to the total carcinogenic equivalents of PAHs. The mutagenic equivalents were largely influenced by equivalence factors of benzo(a)anthracene, and benzo(a)pyrene and indeno(1,2,3-d) pyrene. The estimated daily intake (EDI) and excess cancer rate (ECR) were evaluated for adults and children exposure related risks.

## **DOSE RESPONSE CURVES DERIVED FROM CLINICAL OZONE EXPOSURES CAN INFORM PUBLIC POLICY**

**Sabine S. Lange\*** and Michael E. Honeycutt (Texas Commission on Environmental Quality, TX, USA)  
Ge Tao, Lorenz R. Rhomberg, and Julie E. Goodman (Gradient, MA, USA)  
Michael L. Dourson (University of Cincinnati, OH, USA)

Ozone is one of six criteria air pollutants for which regulations are set by the US Environmental Protection Agency using the National Ambient Air Quality Standards (NAAQS). The ozone NAAQS level was recently changed to 70 parts per billion (ppb) from 75 ppb, but debate is ongoing about the public health protection afforded by this change. Our study used data from human clinical studies to inform policy decisions about a protective ozone level. We plotted mean forced expiratory volume (FEV<sub>1</sub>) response versus total inhaled ozone dose (calculated from ozone concentration, duration of exposure and ventilation rate) from clinical studies of 1-8 hour durations. There were clear thresholds of effect, which were consistent with the known ozone mode of action. The initial plot used data from healthy young adults; additional analyses incorporated data from children and asthmatics, but results did not differ. We estimated expected ozone doses that would be experienced by the population based on known exercise ventilation rates and durations, at ambient ozone concentrations of 75, 70 or 65 ppb (8-hour maximum average). Doses were similar at these three concentrations, and most doses were below those associated with an adverse FEV<sub>1</sub> decrement, even when different exposure times and ventilation rates were assessed. Ozone doses were estimated in Texas in 2013 at monitors that would have attained a 75 ppb or 70 ppb standard, and again found that the doses were very similar. This type of analysis can determine thresholds of ozone toxicity and realistic exposure doses, which can be crucial for choosing an ambient ozone concentration that is protective of human health.

**MITOCHONDRIAL INJURY-REGULATED JOINT HEPATOTOXICITY INDUCED BY  
COMBINED EXPOSURE OF PCB77 AND Cd**

***CUI Jiansheng GAO Yu WANG Lixin***

(Institute of Environmental Science and Engineering, Hebei University of Science and Technology;  
Hebei Key Laboratory of Molecular Chemistry for Drug, Shijiazhuang, 050018, China)

Extensive research indicated that both Polychlorinated biphenyls (PCBs) and heavy metal Cadmium (Cd) could induce multiple toxicities including hepatotoxicity. However, the joint toxic effects and mechanisms caused by the combined exposure of PCBs and Cd have been rarely investigated. We here addressed their separate and joint hepatotoxicity with assessments *in vitro* in a representative human hepatic cell line SMMC-7721. Obvious joint toxicity of these two kinds of pollutants was observed through cell viability assay after 48 h combined exposure with 25  $\mu\text{mol}\cdot\text{L}^{-1}$  PCB77 and 20  $\mu\text{mol}\cdot\text{L}^{-1}$   $\text{Cd}^{2+}$ . Without impact on the integrity of cell membrane, combined exposure significantly decreased mitochondrial transmembrane potential and increased mitochondrial membrane permeability followed by induced cell apoptosis. Our results also showed the increased cellular ROS level upon combined exposure. In short, we demonstrated that the combined exposure of PCB77 and Cd can incur joint hepatotoxicity, and the toxicity mechanism is that the change of the mitochondrial transmembrane potential induces cell apoptosis.



## **PROTECTIVE ROLE OF CICHORIUM INTYBUS AGAINST MANGANESE TOXICITY IN LIVER AND KIDNEY**

***Ram Prakash***

(Department of Zoology, Dr. A.G.D Bendale Mahila Mahavidyalaya, Jalgaon-425001, India)

Manganese is an essential trace element and involves widely in biological reactions. It activates numerous enzymes such as Kinases, esterases, mutases, peptidases, dehydrases etc. However higher intake of manganese was recorded hazardous to cell/tissues. It was recorded in our laboratory that manganese cause hepatic cell necrosis, fibro-proliferation, bi-nucleated cells, pycnosis of nuclei, glomerulo-nephritis, glomerular damage and disturbances in plasma membrane of PCT and DCT. Manganese also decreased activity of some key enzymes such as alkaline and acid phosphatase, cholinesterase and glucose-6-phosphatase. Recently we designed experiments on rats as first were exposed with manganous chloride for thirty days and then post exposed with the extract of *Cichorium intybus* for fifteen more days. Observations were made on liver and kidney for histological and histochemical parameters. It was recorded that most lesions were reversed towards their normal conditions. Therefore it was concluded that *Cichorium intybus* has therapeutic values against manganese toxicity in liver and kidney. The observations on other parameters also support present data.

**URINARY METABOLOMICS REVEALED ARSENIC EXPOSURE-RELATED METABOLIC ALTERATION: A PROOF-OF-CONCEPT STUDY IN A CHINESE MALE COHORT**

**Jie Zhang**, Weipan Xu, Heqing Shen  
(Institute of Urban Environment, CAS, Xiamen, Fujian, China)

The general population may be exposed to arsenic through various sources. Although targeted urinary biomonitoring of arsenic species provides the most accurate assessment of arsenic exposure, the arsenic-related metabolic perturbations are required to be evaluated. The objective of this proof-of-concept study is to investigate arsenic-induced phenotypic metabolome changes. Urinary arsenic species such as inorganic arsenic, methylarsonic acid, dimethylarsinic acid and arsenobetaine were quantified in a Chinese adult male cohort using high performance liquid chromatography (HPLC)-inductively coupled plasma-mass spectrometry. Urinary metabolomes were analyzed using HPLC-quadrupole time of flight mass spectrometry (qTOF-MS) and the arsenic-related metabolic changes were investigated by using a partial least squares discriminant analysis model. After adjustment for age, BMI, smoking and drinking, five potential biomarkers of testosterone, hippurate, acetyl-N-formyl-5-methoxykynurenamine (AFMK), serine and guanine were identified from 61 candidate metabolites, which indicated the exposure to arsenic induced endocrine disruption and oxidative stress in humans. Some dose-dependent trends have been also observed. The combined pattern of testosterone, hippurate, serine and guanine gave an AUC of 0.91 with sensitivity and specificity = 88% and 80%, respectively. We have demonstrated that metabolomics can be used to identify arsenic-related changes at the biomolecular level. The nature of the arsenic-related metabolic changes and trends may be used to further refine population based risk analysis of arsenic exposure.

## **ASSESSING OCCUPATIONAL EXPOSURE IN BLACK HAIR SALONS**

***Sarah Lemelman, Raymond Trott***, Anna Abrams, Allison Marill, Alexis J. Cooper, Ramya Ramakrishna, Jay Feinstein, Teleah Slater, Annie Fortnow, Cassidy Tatun, Omkar Kulkarni, Sandra Waternberg (Student Group, Environmental Studies Program, Brandeis University, Waltham, MA, United States); Faculty and instructors: Laura J. Goldin, Theodore A. Myatt, Joseph G. Allen, James H. Stewart, Matthew A. Fragala (Faculty and instructor Group, Environmental Studies Program, Brandeis University Waltham, MA, United States)

This purpose of this study was to investigate air quality in Black hair salons. Black hair salons are generally small, enclosed spaces that use different products marketed for particular types of hair styling. These products may not receive same amount of research or environmental review that other more widely marketed products would encounter and may result in exposures of consumers and salon workers to potentially harmful chemicals. We collected short-term air samples of VOCs, aldehydes, and ketones in ten salons in the greater Boston area, along with fine particulate matter (PM<sub>2.5</sub>) and carbon dioxide. Seven out of the ten salons had fine particulate matter levels well above the National Ambient Air Quality Standards outdoor limit. A follow-up time-series investigation into sources of PM<sub>2.5</sub> in salons identified PM<sub>2.5</sub> spikes during the use of irons and hair dryers. Regarding chemical exposures, five salons had chloroform concentrations above EPA's screening level carcinogenic target risk value, and all ten salons had benzene concentrations above EPA's carcinogenic target risk level. Elevated levels of carbon dioxide in all salons also suggested inadequate ventilation. This study reveals higher than expected levels of PM<sub>2.5</sub> inside salons, and two carcinogens/chemicals above EPA screening levels. Further evaluation is recommended to: determine if these findings are consistent in a wider range of the salons, assess the potential health implications of these exposures, and identify which products and services are contributing to the exposures and identify controls to reduce exposures.

**DIOXIN-LIKE RATHER THAN NON DIOXIN-LIKE PCBs PROMOTE THE DEVELOPMENT OF ENDOMETRIOSIS THROUGH THE STIMULATION OF IMMUNE-ENDOCRINE INTERACTION**

***Qiansheng Huang***, Yajie Chen, Sijun Dong

(Key Lab of Urban Environment and Health, Institute of Urban Environment, Chinese Academy of Sciences, Xiamen, China)

Endometriosis is an estrogen-dependent and inflammation-dependent disease with high prevalence and severe health outcome. Epidemiological studies showed the association between polychlorinated biphenyls (PCBs) and endometriosis. In contrast, little evidence is available in terms of molecular toxicology. In this study, Dioxin-like CB126 and non-dioxin-like CB153 within human exposure regimen were used to treat primary cultured eutopic endometrial stromal cells (ESCs) and EM mice model. CB126 rather than CB153 significantly enhanced the biosynthesis of 17 $\beta$ -estradiol (E2) secretion from ESCs in a dose-dependent way. 17 $\beta$ -hydroxysteroid dehydrogenase 7 (HSD17B7) was the responding gene to PCBs exposure among genes related to estrogen metabolism. CB126 decreased the methylation of HSD17B7 promoter. The elevated levels of HSD17B7 expression was also observed in the eutopic endometrium of EM patients. CB126 rather than CB153 triggered the inflammatory response through directly stimulating the secretion of inflammatory factors and indirectly inhibiting the level of lipoxin A4. Furthermore, the increasing level of inflammatory factors positively enhanced the expression of HSD17B7. Antagonism of aryl hydrocarbon receptor (AhR) diminished the endocrine and inflammatory effects by CB126. *In vivo* EM mice model confirmed the promotion of CB126 on the endometriotic lesion. The peritoneal fluid levels of E2 and inflammatory factors both increased in the EM mice treated with CB126. Taken together, we demonstrated that

CB126 instead of CB153 triggered the EM development through stimulating the estrogen biosynthesis, inflammation and their positively interaction by AhRreceptor.

**BACTERICIDAL AND ANTIOXIDANT PROPERTIES OF ESSENTIAL OILS OF THE FRUITS  
*Dennettia tripetala* G. BAKER**

**Sunday O. Okoh**, B.C. Iweriegbor, O.O. Okoh and U.U. Nwodo and A. I. Okoh  
(University of Fort Hare, Alice, South Africa)

Bactericidal and antioxidant properties of unripe and ripe fruits of *Dennettia tripetala* and their potentials for the management of infectious and oxidative-stress diseases were investigated *in-vitro* in the research. Essential oil obtained from the fruit using Clevenger modified apparatus, was characterized by high resolution GC-MS, while antioxidant and bactericidal properties were investigated by spectrophotometric and agar diffusion methods respectively. The essential oils demonstrated strong antibacterial property when subjected to *Enterococcus faecium*, *Escherichia coli*, and *Staphylococcus aureus*. Unripe fruit oil (UFO) was more active than the ripe fruit oil (RFO) against test bacteria with minimum inhibition concentration (MIC) ranging between 0.05-0.15 mg/mL and that of ripe fruit oil (RFO) ranging between 0.10–0.20 mg/mL. The IC<sub>50</sub> for RFO (0.42 mg/mL) showed that it has higher antioxidant strength than UFO and vitamin C (0.74 and 3.38 mg/mL) and comparable to  $\beta$ -carotene (0.37 mg/ mL) in inhibiting 2, 2'-diphenyl-1-picrylhydrazyl radicals (DPPH<sup>•</sup>). Antiradical property of both oils against DPPH<sup>•</sup>, 2, 2'-azinobis-(3-ethylbenzothiazolin - 6-sulfonic acid) diammonium salt (ABTS<sup>•+</sup>), lipid peroxide (LP<sup>•</sup>) and nitric oxide (NO<sup>•</sup>) radicals were in concentration-dependant manner. Findings from this research indicates that in addition to the local uses of the UFO and RFO, the essential oil has strong bioactive compounds and have good antibacterial and antioxidant properties and may be alternative to synthetic antibiotics on future investigations.

## AFLATOXIN CONTAMINATION OF SOME EDIBLE GRAINS FROM LAGOS AND OTA MARKETS, NIGERIA

Mary Oloyede, Akan Williams and Nsikak Benson  
(Department of Chemistry, Covenant University, Ota, Ogun State, Nigeria)

**ABSTRACT:** Levels of aflatoxin in maize, sorghum, millet, wheat and rice obtained from Lagos and Ota markets in Nigeria are reported. Aflatoxin determination was carried out using high performance liquid chromatograph coupled with diode array detector (HPLC-DAD). The concentrations of aflatoxins in the grains obtained from Mile 12 market, Lagos ranged between 34.3 µg/kg and 300.1 µg/kg while the concentrations in the grains obtained from Dada market, Ota ranged between 42.3 µg/kg and 1245 µg/kg. The levels of total aflatoxins were generally higher in the grains sampled from Lagos market. These values exceed the maximum limits of 10 µg/kg set by regulatory bodies in Nigeria, thus posing a great health risk for consumers. Recovery studies indicated that the method was efficient as recovery of the residue ranged between 82.2% and 96.2%. There is need for the creation of awareness on aflatoxin in order to sensitize people on health hazards associated with its contamination. In addition, there is need to promote proper practices of grain production and storage to prevent its contamination and reduce exposure.

**Keywords:** Aflatoxin, Grains, Contamination, Nigeria.

### INTRODUCTION

Aflatoxins are by-products of fungal metabolism mainly synthesized by fungus of the genus *Aspergillus*. In Nigeria, the risk of chronic exposure to aflatoxins from susceptible foods, especially maize, a staple food, is of great concern owing to the health hazards associated with it. Dietary exposure to low doses of aflatoxins is a known risk cause of liver cancer and may also affect protein metabolism and immunity thereby leading to low immunity and malnutrition (Williams *et al.*, 2004). Consumption of highly contaminated foods results in severe, acute hepatitis also known as aflatoxicosis. Symptoms of this disease include vomiting, jaundice, abdominal pain, liver failure and sometimes death. Four different aflatoxins, B<sub>1</sub>, B<sub>2</sub>, G<sub>1</sub> and G<sub>2</sub> have been identified with B<sub>1</sub> being the most toxic. Human exposure to aflatoxins can result directly from ingestion of contaminated foods or indirectly from consumption of foods from animals previously exposed to aflatoxin in feeds (Odoemelam and Osu, 2009).

Grains are small, hard, dry seeds with or without attached hulls or fruit layers harvested for human or animal consumption. After being harvested, dry grains are more durable than other staple foods and this durability has made grains well suited to industrial agriculture, since they can be mechanically harvested, transported by rail or ship, stored for long periods in silos, and milled for flour or pressed for oil. Sorghum, millet, maize, wheat and rice are the most important cereals in Nigeria (Omotosho and Muhammadu-Lawal, 2008; Obatolu, 2002). Millet is the cereal of the dryer regions with little rainfall. Sorghum crops are the cereals of the savannah and stretch into the sub-humid environments. Maize and rice are crops of the humid tropic- areas with high rainfall, swamps and areas with or without water for irrigation. Rice can grow in upland areas, such as those suitable for maize. Other types of rice grow in swamps, requiring lots of water. While maize is found across Nigeria's upland and irrigated lands, rice also grows well wherever there is adequate water/irrigation (Ekwuruke, 2005).

In Nigeria, the use of cereals range from preparation of "Akamu" and "Agidi" to preparation of "Nrioka", "Tuwoshinkafa" and "Tuwomasara". Roasted corn, boiled corn or popcorn is also consumed as

snacks. Cereals are also used in preparation of animal feed and fodder. They are used in the production of alcoholic beverages and fermentation products (Ekwuruke, 2005).

Storage is an important activity, which enhances marketing efficiency by providing utility. Storage is particularly important in agriculture because agricultural production is seasonal while the demands for agricultural commodities are evenly spread throughout the year. There is need to meet average demand of agricultural products by storing excess supply during the harvesting season for gradual release to the market during off-season periods thereby stabilizing food prices. Postharvest facilities or appropriate storage technology has been the major problem of Nigerian agriculture for a long time (Adejumo *et al.*, 2007). Aflatoxins are found in many countries of the world, especially in tropical and subtropical region where the warm and humid weather provides optimal conditions for the growth of aflatoxigenic molds. The optimum temperature for the growth of the moulds is 24 – 35°C, thus crops grown in tropical and subtropical conditions are more prone to aflatoxin contamination than those in temperate regions. Being a tropical country, Nigeria's conditions of temperature and humidity favour pre-harvest and post-harvest contamination of stored grains by the fungi (Odoemelam and Osu, 2009).

## EXPERIMENTAL

**Sample Collection.** This study examined two popular grocery markets namely Ota market and Mile 12 market in Lagos. Both markets are located in South West, Nigeria. Stratified random sampling was carried out to obtain 5 kg from the bulk of stored grains (rice, wheat, sorghum, millet and corn) in stores and open markets. The samples obtained were put in paper bags and refrigerated in the laboratory at 4°C. A laboratory size of 500g was obtained from the grounded sample and analysed.

**Apparatus and Reagents.** All glasswares used were thoroughly washed with distilled water, rinsed with acetone and dried in an oven prior to use. The apparatus used included High Performance Liquid Chromatography (HPLC) from Agilent technologies, top loading balance, orbital shaker, hot plate, hot oven, Erlenmeyer flasks, filter paper, pipette, test tubes, funnel, beaker, micro syringe, measuring cylinder and vials with TFE caps. The standards were obtained from Sigma –Aldrich. All reagents used were of HPLC grade. Acetonitrile was obtained from Lichrosolv, Germany and methanol was obtained from Tedia Company, USA.

**Materials and Methods.** Determination of Aflatoxins in the grains was carried out in accordance with the standard methods outlined in AOAC Official Method 994.08 with some modifications. It involved solid phase extraction with HPLC analysis. 25 g of each ground sample was weighed into a 250 mL Erlenmeyer flask and 100 mL of a mixture of acetonitrile and water (84:16 v/v) was added. The mixture was shaken for one hour on an orbital shaker and then filtered through a fast qualitative filter paper. 4 mL of the filtrate was passed through a Supelco Aflazea SPE cartridge. The toxin was eluted with 2 mL of HPLC grade methanol. The eluate was evaporated to dryness and reconstituted with deionized water. The mixture was constituted using a vortex mixer and 20 µL was injected into the HPLC. The HPLC was set for analysis of total aflatoxins at ambient temperature, with a flow rate of 0.8 mL/min, injection volume of 20 µL and run time of 13 minutes. The mobile phase used was an isocratic mixture of water: methanol: acetonitrile (50:40:10); analytical column: ZORBAX Eclipse XDB C18 Column, 4.6 mm × 250 mm. The diode array detector was set at a wavelength of 365 nm.

## RESULTS AND DISCUSSION

The mean levels of aflatoxins in grains from Ota and Lagos markets are shown in Tables 1 and 2 while recovery studies of some selected samples are shown in Table 3. Total aflatoxins in grains from Ota market was highest in maize with a concentration of 300.1 µg/kg while the level in sorghum from Mile 12 market was the highest. Even though AFB<sub>1</sub> was not detected in millet and sorghum samples from Ota market and in maize, sorghum and rice from Mile 12 market Lagos, it is worrisome that the level of AFB<sub>1</sub> was beyond the permissive limit of 5 ppb in all the other grains sampled (Commission Regulation, 2006).

This is because AFB<sub>1</sub> is carcinogenic and the most potent of the aflatoxins. The levels of total aflatoxins were generally higher in the grains sampled from Lagos market. This might be due to poor storage conditions and a higher level of exposure to contaminants. From the study, it is observed that sorghum has high concentrations in both markets (220.5 µg/kg and 1245.1 µg/kg). These values indicate that sorghum is highly susceptible to aflatoxin infestation. Also, it is observed that the concentration of aflatoxin in millet obtained from Ota is relatively low with a mean concentration of 34.3 µg/kg compared with 120.3 µg/kg obtained from Lagos. Generally, the absence of AFB<sub>1</sub> and AFB<sub>2</sub> in samples of sorghum obtained from both markets is remarkable. Recovery Studies of some selected samples ranged from 82.2% to 96.2% indicating that the method used was satisfactory.

**Table 1. Mean Levels (mg/kg) of Aflatoxins in Grains from Ota, Ogun State**

	AFB <sub>1</sub>	AFB <sub>2</sub>	AFG <sub>1</sub>	AFG <sub>2</sub>	Total AFs
Maize	10.4	143.9	ND	145.7	300.1
Millet	ND	11.8	ND	22.5	34.3
Sorghum	ND	ND	130.3	90.1	220.5
Wheat	13.0	23.5	ND	86.5	123.1
Rice	11.5	18.6	8.2	47.2	85.7

**Table 2. Mean Levels (mg/kg) of Aflatoxins in Grains from Mile 12 Market, Lagos State.**

	AFB <sub>1</sub>	AFB <sub>2</sub>	AFG <sub>1</sub>	AFG <sub>2</sub>	Total AFs
Maize	ND	567.6	13.6	21.3	602.6
Millet	20.3	12.9	ND	87.2	120.5
Sorghum	ND	ND	1203.8	41.3	1245.1
Wheat	9.1	5.9	ND	27.2	42.3
Rice	ND	ND	60.2	13.4	73.6

ND- Not Detected

**Table 3. Recovery Studies of some samples**

Sample	Recovery (%)
Corn	82.2
Rice	96.2

This study reports levels of total aflatoxins that are not within the acceptable limits of 10 ppb (EMAN, 2006). The levels of aflatoxins obtained in this study was in consonance with earlier reports and studies conducted (Bankole and Adebajo, 2003; Gwaryet *al.*, 2012; Aroworaet *al.*, 2012). The aflatoxin levels in grains obtained from open markets are, therefore, unsafe for human consumption and could pose a health risk to consumers.

## CONCLUSION

Results of this study showed that there is presence of high levels of the toxin in grains obtained from the selected markets, which exceeds the permissible limits set by regulatory bodies for consumers. The toxin was detected in all the samples with maize having the highest concentrations. Therefore, there is need to prevent aflatoxin contamination in the grains by adoption of moisture-control measures that promote improved storage and educating farmers on the importance of Good Agricultural Practices during planting, harvesting and postharvest handling of crops.

## REFERENCES



1. Adejumo, T.O.; Hettwer, U. and Karlovsky, P. (2007). Survey of maize from south-western Nigeria for zearalenone,  $\alpha$ - and  $\beta$ -zearalenols, fumonisin B1 and enniatins produced by *Fusarium* species. *Food Additives* 24: 993-1000.
2. Arowora, K.A.; Abiodun, A.A.; Adetunji, C.O.; Sanu, F.T.; Afolayan, S.S, and Ogundele, B.A. (2012). Levels of Aflatoxins in Some Agricultural Commodities sold at Baboko Market in Ilorin, Nigeria. *Global Journal of Science Frontier Research Agriculture and Veterinary Sciences* 12.
3. Bankole, S.A. and Adebajo, A. (2003). Mycotoxins in food in West Africa: current situation and possibilities of controlling it. *African Journal of Biotechnology* 2: 254-263.
4. Ekwurike, H. (2011). Cereals: Grains that feed the World. *Panorama*
5. EphremGuch (2015). Implication of Aflatoxin Contamination in Agricultural Products. *American Journal of Food and Nutrition* 3(1), 12-20.
6. European Mycotoxin Awareness Network (2006). Annual Report retrieved from [www.mycotoxin.org](http://www.mycotoxin.org)
7. Ezekiel, C.N. and Sombie, J.I. (2014) Survey of aflatoxins and fungi in some commercial breakfast cereals and pastas retailed in Ogun State, Nigeria. *Nature and Science*, 12(6); 27-32.
8. Fapohunda, S.O.; Soler C.; Ezekiel, C.N.; Manes, J.; Kayode F. and Rubert J. (2013). A survey of mycotoxins in random street-vended snacks from Lagos, Nigeria, using QuEChERS-HPLC-MS/MS. *European Mycotoxins Awareness Network* 32: 673-677.
9. Gwary, O.M.; Hati, S.S.; Dimari, G.A. and Ameh, J. A. (2012).Assessment of Mycotoxins (Total Aflatoxins and Ochratoxin-A) Contamination of Staple Cereals. *International Journal of Chemical and Biochemical Sciences* 2: 1-6.
10. IARC (2002). International Agency for Research on Cancer Monographs on the Evaluation of carcinogenic risks to humans, 80
11. Obatolu, V.A. (2002). Nutrient and sensory qualities of extruded malted or unmalted millet/soybean mixture. *Food Chem*76: 129-133.
12. Odoemelam, S.A. and Osu, C.I (2009). Aflatoxin B<sub>1</sub> Contamination of Some Edible Grains Marketed in Nigeria. *E- Journal of Chemistry* 6(3): 308-314.
13. Omotosho, O. A. and Muhammad-Lawal, A. (2010).Optimal food plan for rural households' food security in Kwara State, *Nigeria: The goal programming approach*.
14. RASFF (2011). Retrieved from [http://ec.europa.eu/food/safety/rasff/index\\_en.html](http://ec.europa.eu/food/safety/rasff/index_en.html)
15. Whitlow, L. W. and Hagler, W. M. (2008). Mould and Mycotoxin Issues in Dairy Cattle: Effects, Prevention and Treatment. *WCDS Advances in Dairy Technology*. 20: 195-209.
16. Williams, J. H.; Phillips, T. D.; Jolly, P. E.; Stiles, J. K.; Jolly, C. M. and Aggarwal, D. (2004). Human aflatoxicosis in developing countries: a review of toxicology, exposure, potential health consequences, and interventions. *The American journal of clinical nutrition* 80: 1106–1122.

## GENOTOXIC EFFECTS OF COAL FLY ASH IN *TRIGONELLA FOENUM GRAECUM* (L.)

Rucha U. Raval, Kailash P. Patel and Mariya J. Jairajpuri

(Department of Biosciences, Veer Narmad South Gujarat University, Surat, Gujarat, India)

E-mail: [kailash.patel@yahoo.com](mailto:kailash.patel@yahoo.com)

**ABSTRACT :** The aim of this research is to study the effects of different concentration (20%, 50%, 80%, and 100%) of Fly Ash with Vermicompost and Pressmud on the root meristems of *Trigonella foenum graecum*. 10 seeds were grown in pot at 20%, 50%, 80% and 100% concentration of FlyAsh. It was determined that FlyAsh increased the rate of the mitotic division at different concentration with the increase in mitotic anomalies. Very rare anomalies were encountered in the control group and at the concentration of 20% but at concentration of 50%, 80% and 100% of FlyAsh chromosomal aberration such as sticky metaphase, laggard chromosome, bridge chromosome, vagrant chromosome etc. were observed. Mitotic index increases from control to lower concentration of Fly Ash, while at higher concentration mitotic index gets lower and chromosomal aberrations get higher. At higher concentration frequency of chromosomal bridge were very high while at lower concentration sticky metaphase normally appeared.

**Keyword:** FlyAsh, Vermicompost, Abnormalities, Mitotic index, Chromosomal aberration.

## INTRODUCTION

Energy requirements for the developing countries are met from coal-based thermal power plants. The disposal of the increasing amounts of solid waste from coal-fired thermal power plants is becoming a serious concern. Coal ash is mostly made up of fine particles that is known as FlyAsh. In India, nearly 90 Mt of FlyAsh is generated per annum and is largely responsible for environmental pollution.

Soil application of fly ash waste has both beneficial and adverse effect on crop yield. The adverse effect is common at high rates of fly ash due to increased salinity and accumulation of toxic levels of elements. To overcome these adverse effects of fly ash, it can be supplemented by Vermicompost and additional source of organic matter like Pressmud(PM). Pressmud is a by product of sugar industries, that generates intense heat, foul odour and takes long time for decomposition. Vermicomposting is a biological technique of composting wide ranges of organic wastes with the help of the gut micro organisms of surface living earthworms. The final product of Vermicompost is a very good organic fertilizer, it reduces levels of contaminations and tends to hold more nutrients over a longer period, without causing any adverse effect on environment. India is the largest producer of fenugreek in the world(Zohary, D. and M. Hopf, 2000).

The aim of this study was to investigate the chromosomal abnormalities induced by fly ash on the root tips of *Trigonella foenum graecum* L. and also to determine the relation between mitotic index and chromosome abnormalities.

*Trigonella foenum-graecum* L (fenugreek) is cultivated as annual, winter legumes in India. The species can be grown easily in low-input, minimal environment and are good sources of calories, seed proteins, B-vitamins and minerals.

Present study was particularly carried out to evaluate whether fly ash, along with Vermicompost and pressmud can be effective for betterment of the plants.

## MATERIALS AND METHODS

10 seeds of *Trigonella foenum-graecum* were germinated in pots. 50 ml of distilled water was supplied every alternate day. The total mixture of Fly Ash, Vermicompost and Pressmud was 50gm and from that different concentrations were made as Table 1. Photomicrographs were taken on Axioscope.

**Table 1.** Parameters in the Experiments

% Concentration	Fly Ash(gm)	Vermicompost (gm)	Pressmud (gm)
Control	0	25	25
20%	10	20	20
50%	25	12.5	12.5
80%	40	5	5
100%	50	0	0

## RESULTS

The staining procedure followed was that of (Fiskesjo G 1988). Mitotic index and percentage of aberrant cells were calculated using following formula.

$$\text{Mitotic Index (\%)} = \frac{\text{No. of divided cells}}{\text{Total no. of cells studied}} \times 100$$

$$\text{Aberrant cells (\%)} = \frac{\text{No. of aberrant cells}}{\text{No. of dividing cells}} \times 100$$

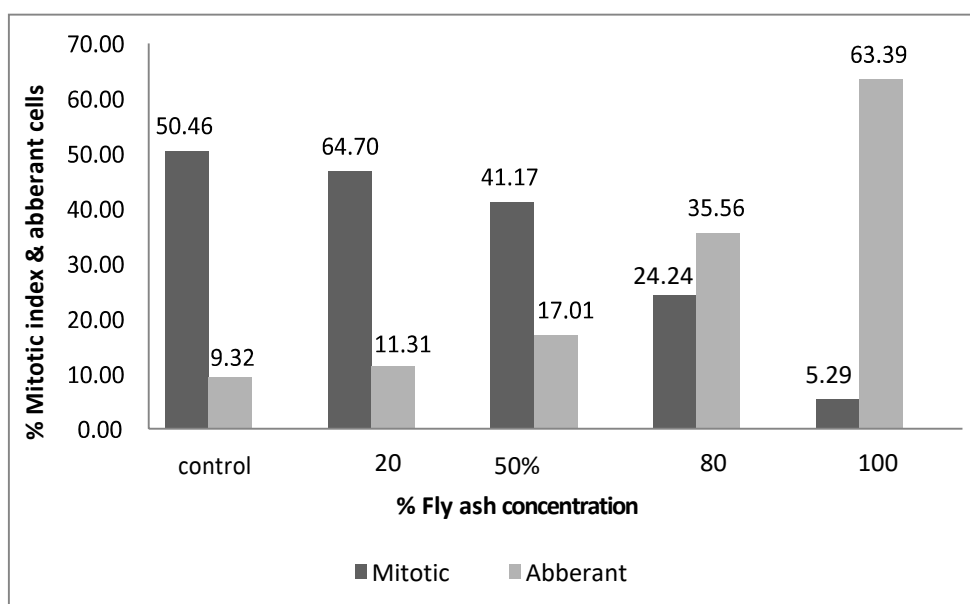


**FIGURE 1.** Mitotic Index

**Table 2.** Effect of Thermal Effluent on Root Tip Cells of *Trigonella foenum graecum*.

Concentration (%)	Mitotic Index (%)	Aberrant cells (%)
Control	50.46	4.34
20	64.70	2.31
50	41.17	17.01
80	24.24	35.56
100	5.29	63.39

The Mitotic Index is summarized in Figure 1 and Table 2. Normal chromosomes and Chromosomal abnormality caused by Fly ash are shown in Figure 2.

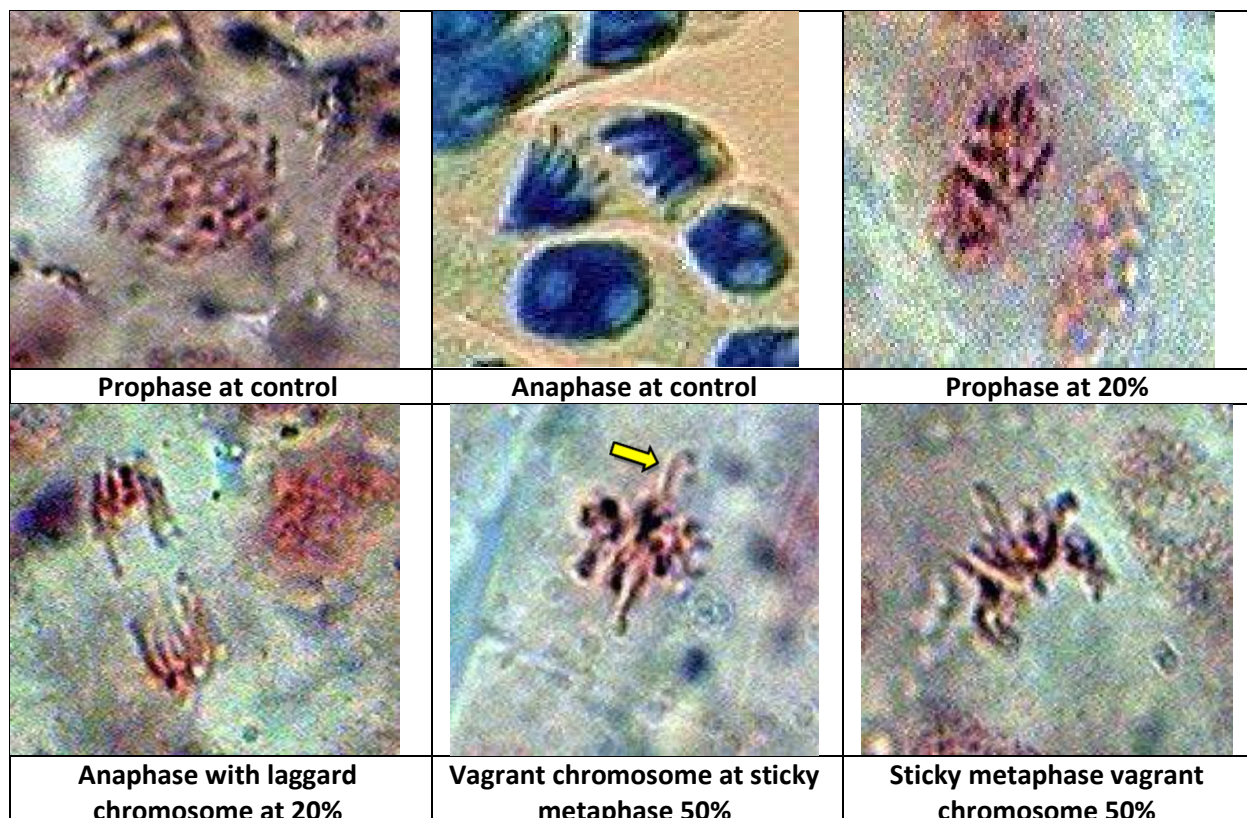


**FIGURE 2a.** Normal chromosomes and Chromosomal abnormality caused by Fly ash.

## DISCUSSION

The research revealed that fly ash increased the mitotic division creating very high chromosomal abnormalities in the root meristem of *Trigonella foenum graecum* at higher concentration. This suggests the presence of certain cytotoxic/genotoxic substances in the fly ash. At lower concentration no chromosomal abnormality is observed but at higher concentration chromosome bridges were frequently observed. Other aberration included vagrant chromosome, laggard chromosome, disturbed anaphase, sticky metaphase, micronuclei and nuclear degeneration.

Mitotic bridge at higher concentration is commonly observed abnormality, most probably formed by the breakage and fusion of chromosomes (Egypt J Bot, 1990 and Gomurgen AN, 2000). Presence of chromosome bridges may be due to stickiness or formation of dicentric chromosomes caused by breakage and reunion (Bempong AM, 1973).

Laggard chromosome resulted due to failure of the chromosomes to get attached to the spindle fibre and to move to either of the two poles (Namita Khanna\*and Sonia Sharma).

Disturbed metaphase and anaphase are another most frequently observed abnormality observed in treated cells. It may be caused by the loss of activity of microtubules in spindle fibres leading to complete inhibition of spindle formation (El-Khodary S, Habib A, Haliem A, 1990).

Sticky chromosomes indicate a highly toxic, irreversible effect probably leading to cell death (Fiskesjo G 1985 and 1988). There is a hypothesis that stickiness of chromosomes may cause incomplete separation of daughter chromosomes as a result of cross-linkage chromo proteins (Kong MS, Ma TH 1999).

Stickiness in chromosomes is a result of partial dissociation and altered pattern of organization of nucleoprotein (Evans HJ, 1962). The stickiness of chromosomes makes their separation and free movement



incomplete and thus they remain connected by bridges (Kabarity A, El-Bayourni AA & Habib AA 1974). This may also be due to the defective formation of the spindle apparatus (Badr A 1986 and Abraham S & Rajalakshmy BN 1989).

Also nuclear degeneration was observed with “cavity like” space, which is a starting point of apoptosis resulting in cell death due to the accumulation of heavy metals in the plants. Chromatid breaks, asymmetrical exchanges and incomplete symmetrical exchanges would give rise to acentric fragments at mitosis and at the later stage these fragments appear as micronuclei. ( Kailash P. Patel *et al*, March 2013)

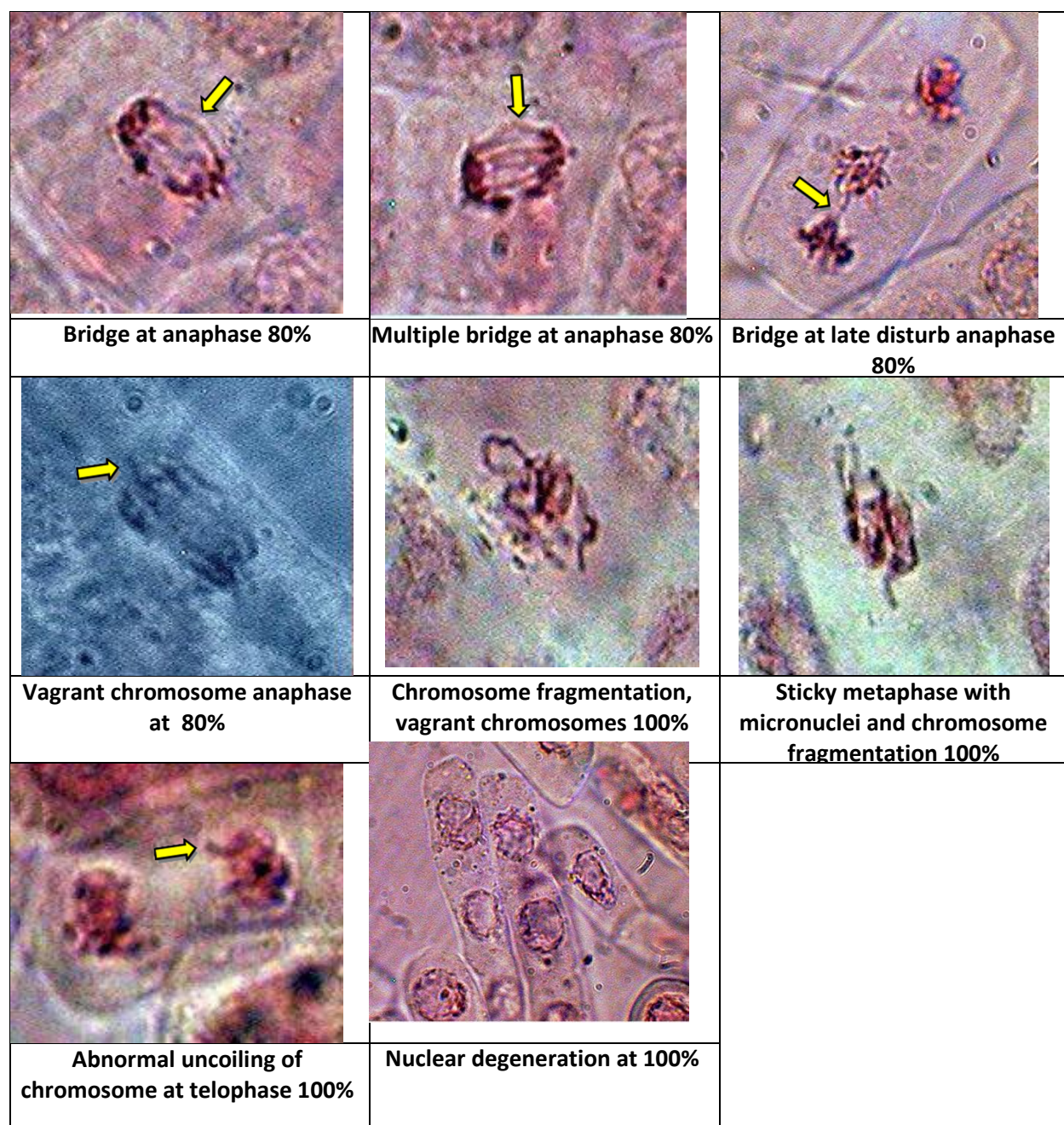


**FIGURE 2b.** Normal chromosomes and Chromosomal abnormality caused by Fly ash.

## CONCLUSION

We can conclude that the lower concentration of fly ash mixed with vermicompost and pressmud increases the mitotic index and do not cause toxic effects, whereas higher concentration of fly ash works as a toxic material for the plant.

## REFERENCES

- Abraham S & Rajalakshmy BN (1989). Production of mitotic abnormalities by magnesium sulphate in *Vicia faba* L. *Cytologia* 54: 559-563.
- Anis M, Aijas AW. Caffeine induced morpho-cytological variability in fenugreek, *Trigonella foenum-graecum* L. *Cytologia* 1997; 62: 343-349.
- Badr A (1986). Effects of the S-Triazine herbicide tubutryn on mitosis chromosomes and nucleic acids in root tips of *Vicia faba*. *Cytologia* 51: 571-577.
- Bempong AM (1973). Cytological effects of nogalmycin in *Tradescantia paludosa* microsporocytes. *Mutation Res* 21: 323-326.
- Darlingtonand, C.D., L.F. La Cour, *The Handling of Chromosomes*, 6th Edn, George Allen and Unwin Ltd, 1976.
- El-Khodary S, Habib A, Haliem A. Effect of herbicide Tribunil on root mitosis of *Allium cepa*. *Cytologia* 1990; 55: 209-215.
- Evans HJ (1962). Chromosomal aberrations induced by ionizing radiations. *Int Rev Cytol* 13: 221-321.
- Fiskesjo G (1985). The *Allium* test as a standard in environmental monitoring. *Hereditas*, 102: 99 – 112.
- Fiskesjo G (1988). The *Allium* test – an alternative in environmental studies: The relative toxicity of metal ions. *Mutat. Res.* 197: 243 – 260.
- Gomurgen AN. Cytological effect of the herbicide 2, 4-D Isooctylester 48% on root mitosis of *Allium cepa*. *Cytologia* 2000; 165: 383-388.
- Haliem AS. Cytological effects of the herbicide sencor on mitosis of *Allium cepa*. *Egypt J Bot* 1990; 33: 93-104.
- Kailash P. Patel and Kalpesh M. Patel. Cytological Changes in *Trigonella Foenum-graecum* (L.) under the Cadmium Stress. *Journal of Life Sciences and Technologies* Vol. 1, No. 1, March 2013.
- Kabarity A, El-Bayourni AA & Habib AA (1974). Effect of morphine sulphate on mitosis of *Allium cepa* L. Root Tips. *Biol Plant* 16: 275- 282.
- Kong MS, Ma TH (1999). Genotoxicity of contaminated soil and shallow well water detected by plant bioassays. *Mutat. Res.*, 426(2): 221.
- Manas Ranjan Senapati, Fly Ash from Thermal Power Plants – Waste Management and Overview
- O. Timothy \*, M. Idu, D.I. Olorunfemi, O. Ovuakporie-Uvo] Cytotoxic and genotoxic properties of leaf extract of *Icacina trichantha* Oliv South African Journal of Botany 91 (2014) 71–74.
- Rahat Niyazi and Sadhana Chaurasia Vermistabilization of Fly Ash Amended With Pressmud By Employing *Eisenia Foetida*
- S. Shylaja, —Effect of certain physical and chemical mutagens on plant chromosomes,|| Ph.D. Thesis, South Gujarat University, Surat. Gujarat, India, 1994.
- Solomon M, Belenghi B, Delledonne M, Menachem E, Levine A 1999. The involvement of cysteine proteases and protease inhibitor genes in the regulation of programmed cell death in plants. *Plant Cell* 11: 431-443.
- Sugimura T S Kondo & H Takebe.1982. Environmental mutagens and carcinogens. University of Tokyo, Press and Alan R Liss Inc.New York.

## HISTOLOGICAL EFFECTS OF BISPHENOL A ON GILLS, DIGESTIVE GLANDS AND ADDUCTOR MUSCLES OF LABORATORY-REARED *Corbicula fluminea* Mull.

**Kimberly B. Benjamin**, Jessmine L. Competente and Dyan Gabrielle H. de Guzman  
(University of the Philippines Manila, Ermita, Manila, Philippines)

**ABSTRACT:** Bisphenol A (BPA) is a commonly occurring industrial chemical that is present in polycarbonate plastics and epoxy resins. In this study, the toxicity of BPA was analyzed through its histological effects on the gills, digestive glands and adductor muscles of *Corbicula fluminea*, a freshwater bivalve. Forty laboratory-reared *C. fluminea* were exposed to set-ups with 1 µg/L, 2 µg/L and 3 µg/L of BPA for twenty-one days. Histological alterations such as vacuolations, necrosis, lamellar deformation, hyperplasia, loss of epithelium, necrosis, tubular alteration, neoplasia, hemocyte infiltration, hypertrophy and pyknosis were observed. These characteristics were then scored using a modified histological index. Post-hoc analysis revealed that there was a significant difference in the histological alterations observed between the tissues of exposed and unexposed clams. Moreover, it has been shown that the degree of histological damage among the tissues is as follows: digestive gland > gills > adductor muscles.

### INTRODUCTION

Bisphenol A (BPA) is a chemical commonly used in the production of polycarbonate plastics and epoxy resins- both of which are utilized in applications that makes our lives easier and convenient (Flint et al., 2014). Polycarbonate plastics are used in compact discs, medical devices as well as food and beverage containers. Epoxy resins on the other hand, are used to coat metal products such as food cans and pipes of water supply (Stahlhut et al., 2009). BPA enters freshwater ecosystems through effluents from sewage treatment plants, plastic factories and landfill leachate (Oelmann et al., 2000). According to Crain et al., (2007), BPA concentration in freshwater ecosystems may vary and can reach up to 21 µg/l with the sediments containing an even greater concentration compared to the water column. BPA quickly disperse and disappear from natural water systems and this is highly attributed to adsorption by suspended materials and sediments as well as absorption of aquatic animals and plants (Oelmann et al., 2009; Flint et al., 2014). BPA is a toxic compound and its effects on vertebrates and invertebrates have been thoroughly described (Ike et al., 2000; Kang, 2007; Oelmann et al., 2009; Flint et al., 2014). Mechanistically, it has been shown to affect lipid peroxidation, endocrine function and production of reactive oxygen species in vertebrate and invertebrate organisms (Lehmann, 2007; Flint et al., 2014). However, bibliographic data report limited information about the histological effects of BPA on mollusk in particular the bivalves, which are considered as suitable organisms for biomonitoring purposes due to their filter-feeding behavior, sessile status and ability to concentrate pollutants to several orders of magnitude above ambient levels in aquatic environment (Oliveira et al., 2014). Moreover, histological effects of this compound is only limited to the gonads of invertebrates and not on gills, digestive glands and adductor muscles which are also essential in their survival (Santos and Martinez, 2014). The digestive gland being involved in pollutant detoxification, homeostasis and bioaccumulation (Mantecca et al., 2006); the gills are used for respiration and filtration (Beltran and Pocsidio, 2010); and, the adductor muscles are involved in regulating the opening of the valves of clams (Beltran and Pocsidio, 2010).

The Asiatic clam or *Corbicula fluminea* was utilized in this study, because of their wide distribution, high density as well sensitivity to pollutants such as BPA (Colombo et al., 1995, Labrot et al., 1999; Fournier et al., 2005; Lehmann, 2007). These characteristics qualify them as a good sentinel organism for monitoring the status of aquatic environment. The exposure of the clams to environmentally-relevant concentrations of 1 µg/L, 2 µg/L and 3 µg/L BPA (Hatel et al., 2012; Yang et al., 2014) under controlled laboratory conditions aims to give data on the actual histological effects of this compound on the adductor

muscles, digestive gland and gills of the test organism .

## MATERIALS AND METHODS

**Experimental Design.** *C. fluminea* clam with a shell length of 20-30 mm, were obtained from a local unimpacted watershed (La Mesa, Watershed, Quezon City, Philippines). The clams were acclimatized in the laboratory for period of two weeks prior to toxicity test. During acclimatization, the clams were maintained under a 12h:12h photoperiod in a glass aquarium containing 1000L of clean aerated and dechlorinated water with sand. Further, filtration system for waste removal, constant zooplankton supply and replacement as well as quality testing of water was done every seven days.

After acclimatization, ten clams were randomly placed in a 5-L glass container labeled as control, S1, S2, and S3- the *control* set-up containing only depurated water and sand and the experimental set-ups containing depurated water, sand and 1.0 µg/L, 2.0 µg/L, and 3.0 µg/L of BPA, respectively. Exposure period lasted for twenty-one (21) days along with proper maintenance measures being observed.

**Histological Analysis.** After 21 days, five *C. fluminea* from each of the 4 set-ups were randomly selected. The specimen were prepared for histological analysis by prying open the shells and inserting a toothpick between the valves. The clams were euthanized and their adductor muscles, digestive glands and gills were excised and were separately placed in properly labeled vials containing Davidson's fixative for 24 hours. After the 24-hour period, the tissues were immediately transferred to 70% ethanol-containing vials until histological processing.

The tissues were processed, embedded in paraffin, sectioned at 5 microns, stained with Hematoxylin-Eosin at the National Kidney and transplant Institute and examined via and Olympus light microscope. A modified index adapted from Costa et al., (2013) was used to evaluate the intensity of cellular and morphological alterations among the fields of view. The categories for the gills and the adductor muscles were cellular and morphological changes and neoplasia while that of the digestive glands were tubular alterations, intertubular changes and neoplasia. The scores range from 0 to 3, 0 indicating 0-20%; 1 indicating 21-40%; 2 indicating 41-60% and 3 indicating 61-100% tissue aberration.

**Statistical Analysis** The Kruskal-Wallis test for non-parametric data utilizing a Mann Whitney post hoc analysis was performed to analyze the scores. Statistical comparisons were considered significant at 5% level ( $p < 0.05$ ).

## RESULTS

No mortality was observed both in the control and experimental groups during the 21-day exposure.

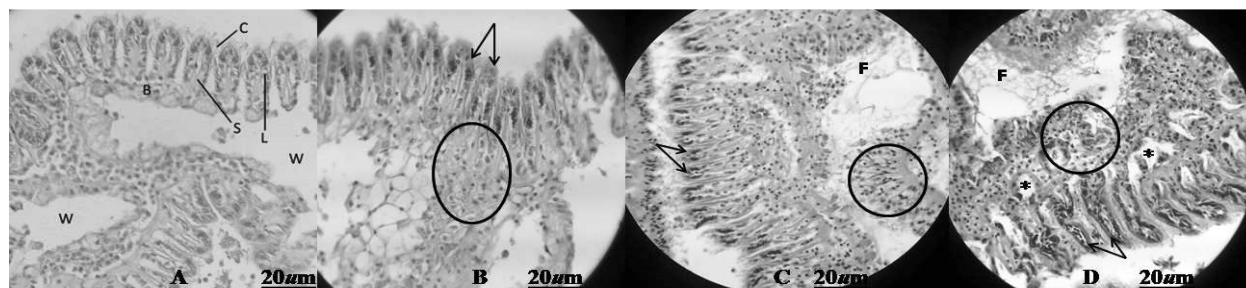


FIGURE 1. Photomicrographs of gills in control and BPA-exposed *C. fluminea* clams after 21 days. (A) Unexposed control clam showing regular arrangement of the gill filaments with a single layer of epithelial cells (C) supported by skeletal rods (S) forming a well-defined lamellae (L). (B) Clams exposed to 1 µg/L BPA; (C) Clams exposed to 2 µg/L; and, (D) Clams exposed to 3 µg/L BPA. Circle=hypertrophy; F=fibrosis; arrow=hyperplasia; asterisk=necrosis.



**Gill Histopathology.** Figure 1A shows the optimal histological characteristics of the clam gills. This is characterized by a well-defined lamellae made up of skeletal rods which supports a single layer of ciliated epithelial cells. Figure 1B-C on the other hand, show the alterations brought about by varying concentrations of BPA on the tissues of the gills of *C. fluminea*. Common histological aberrations that were seen in the exposed groups include vacuolation, hypertrophy, hyperplasia, lamellar deformations and necrosis. Occurrences of other alterations such as loss of epithelium, lipofuscin aggregations, fibrosis and hemocyte infiltration were also observed as concentration increases. Statistical analysis of the median score for cellular and morphological characteristics in gills revealed that clams from all groups are statistically different from each other as shown by differences in number (Table 2). Moreover, mean ranks showed that the highest intensity of damage was seen in 3ug/L while the least was seen in the control group (Table 1). No significant neoplasia was seen in all groups.

TABLE 1. Medians and mean ranks of the cellular, morphological and neoplastic changes in the tissues of the gills of *C. fluminea* across 1, 2 and 3  $\mu\text{g/L}$  of BPA. . Differences in number of median denotes significant difference using Mann Whitney Test at  $p < 0.05$  with  $n = 150$ .

Treatment	Cellular and Morphological Changes		Neoplasia	
	Median	Mean Rank	Median	Mean Rank
Control	0	4	0	4
1 $\mu\text{g/L}$	1	3	0	3
2 $\mu\text{g/L}$	2	2	0	2
3 $\mu\text{g/L}$	3	1	0	1

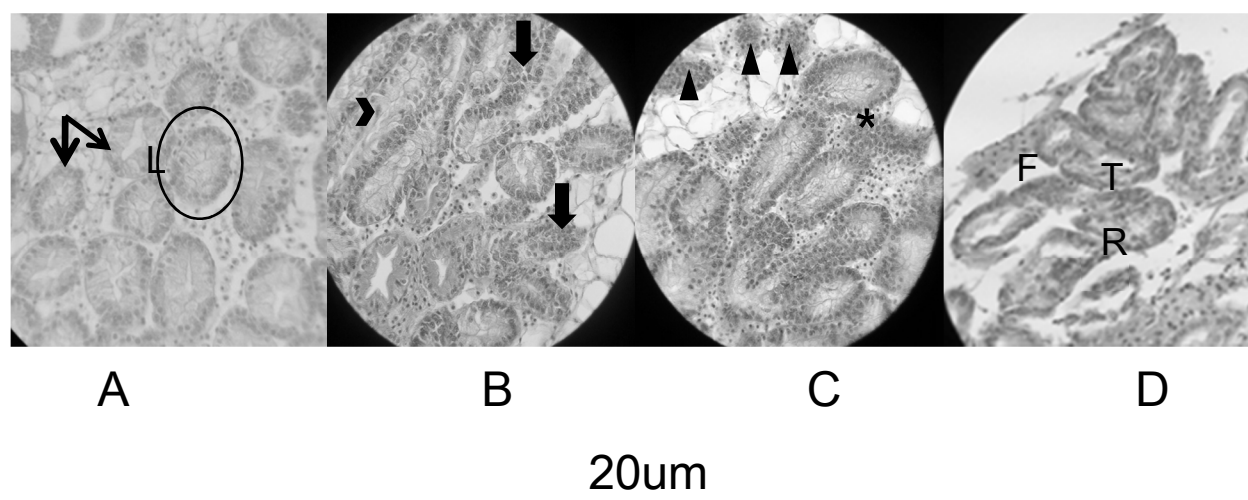


FIGURE 2. Photomicrographs of digestive gland in control and BPA-exposed *C. fluminea* clams after 21 days. (A) Unexposed control clam showing intact digestive tubules (encircled), surrounded by regular epithelium (thin arrow); (B): Clams exposed to 1  $\mu\text{g/L}$  BPA; (C) Clams exposed to 2  $\mu\text{g/L}$ ; and, (D) Clams exposed to 3  $\mu\text{g/L}$  BPA. Arrowhead=hypertrophy; thick arrow= hyperplasia; triangle= granulocytoma; F=fibrosis; asterisk= necrosis; TR=tubular regression.

**Digestive Gland Histopathology.** Figure 2A shows the normal digestive gland of clams from the control group. In its normal state, the digestive gland shows intact digestive tubules with regular epithelium surrounded by a well-defined basement membrane. Moreover, intertubular spaces consist of connective tissues without sign of neoplasia and fibroma. Figure 2B-D illustrates the effects of a 21-day exposure of clams to different concentrations of BPA. The digestive glands of the treated groups exhibited high instances of hyperplasia, hypertrophy, necrosis and granulocytoma. Moreover, few incidences of fibrosis, neoplasia and lipofuchsin aggregation were also observed. Statistical analysis revealed that in terms of tubular alterations, clams exposed to 2 $\mu$ g/L and 3 $\mu$ g/L BPA rendered similar histological effects, while the clams in the control and those exposed to 1 $\mu$ g/L BPA are significant. Analysis on the intertubular and neoplastic changes in digestive gland however revealed that only the control group is statistically significant (Table 2).

**Adductor Muscles Histopathology.** Figure 3A shows the adductor muscles of clams from the control group. They displayed muscle fibers that are uniformly organized and adhering with each other. The cells are fusiform in shape with a central nucleus. Figures 3B-D illustrates the effect of varying concentration of BPA on the adductor muscles. Histological examination of the tissues revealed the occurrence of necrosis, loss of surface adherence and loss of muscle organization among the exposed group. Statistical analysis of the median value of cellular and morphological damage revealed that only the control group is different. Moreover, in terms of neoplasia, no significant difference was seen across all groups (Table 3).

TABLE 2. Medians and mean ranks of the tubular alterations, intertubular and neoplastic changes in the tissues of digestive gland of *C. fluminea* across 1, 2 and 3  $\mu$ g/L of BPA. Differences in number denotes significant difference using Mann Whitney Test at  $p < 0.05$  with  $n = 150$ .

Treatment	Tubular Alterations		Intertubular Changes		Neoplasia	
	Median	Mean Rank	Median	Mean Rank	Median	Mean Rank
Control	0	4	0	4	0	4
1 $\mu$ g/L	2	3	1	2	1	3
2 $\mu$ g/L	3	2	1	3	1	1
3 $\mu$ g/L	3	1	1	1	1	2

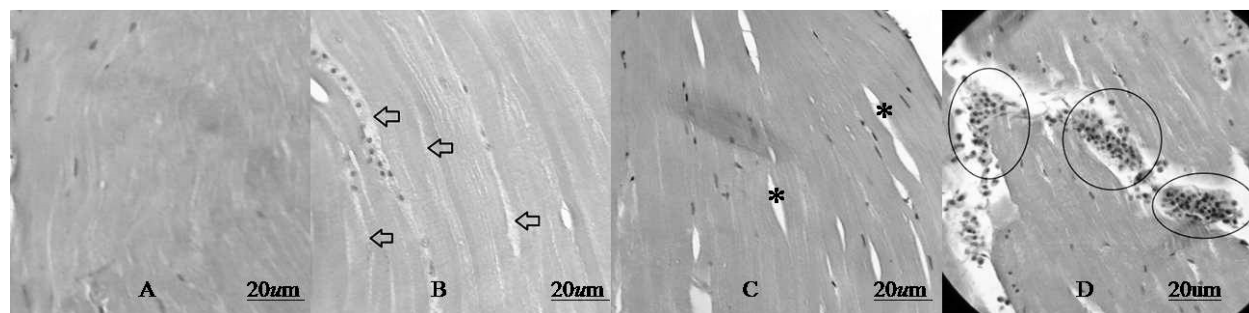


FIGURE 3. Photomicrograph of adductor muscles in control and BPA-exposed *C. fluminea* clams after 21 days. (A) Unexposed control clam showing organized muscle fibers; (B): Clams exposed to 1  $\mu$ g/L BPA; (C) Clams exposed to 2  $\mu$ g/L; and, (D) Clams exposed to 3  $\mu$ g/L BPA. Asterisk=loss of surface adherence ; thick arrow= necrosis; solid ring= haemocytosis

TABLE 3. Medians and mean ranks of the cellular, morphological and neoplastic changes in the tissues of the gills of *C. fluminea* across 1, 2 and 3 µg/L of BPA Differences in number denotes significant difference using Mann Whitney Test at  $p < 0.05$  with  $n = 150$ .

Treatment	Cellular and Morphological Changes		Neoplasia	
	Median	Mean Rank	Median	Mean Rank
Control	1	4	0	4
1 µg/L	2	2	0	3
2 µg/L	2	3	0	2
3 µg/L	2	1	0	1

## DISCUSSION

Different organs have varying responses to different types of toxic compounds. In this study, the toxic effects of environmentally relevant concentrations of BPA on the histology of gills, digestive gland and adductor muscles of laboratory-reared *C. fluminea* were established. Based on the results, the gills, digestive glands and adductor muscles showed differential responses to the presence of BPA. Among the three organs, it was found out that the digestive gland was the most affected organ histologically and statistically due to significant tubular and intertubular alterations as well as incidences of neoplasia even at the lowest concentration. According to Hayashi et al. (2008), BPA are often directed particularly in the lumen of the tubules where they are metabolized substantiating the greater histological damage seen in the tubules. Its high sensitivity is directly attributed to its role in homeostasis, contaminant uptake, digestion, metabolism as well as detoxification process (Kanapala & Arasada, 2013; Costa et al., 2012). Next to the digestive gland, the gills of exposed clams were significantly affected as well. The gills showed a concentration- dependent response towards BPA as seen by an increasing median score in its cellular and morphological attributes. Further, the statistically significant difference in histological scores seen among concentrations would show that gills have specific responses to specific amount of BPA.

The increase in vacuolation and hypertrophy in clams exposed to 1µg/L is a physiological adaptation to limit damage (Flint, 2014). Vacuolation and hypertrophy are essential in confinement, isolation and sequestration of materials that could pose harm to the organism (Costa et al., 2012; Flint et al., 2014). At higher concentrations, vacuolations and hypertrophy prove to be inefficient as a response to the slowed metabolism of the organism. According to Leonard et al., (2014) a concentration of 2µg/L of BPA slows the metabolic processes of the cells causing them to die, thus hyperplasia or increase in cellular number take place as an adaptation to an increasing functional demand. Further, fibrosis was also common in gill tissues exposed to 2µg/L. According to Payan et al., (2014), it is a degenerative response to exposure to harmful chemicals characterized by deposition of connective tissue that can obliterate the architecture of the tissues thereby leading to loss of physiological function. At the highest concentration of 3µg/L, epithelial detachment, lamellar deformation and loss of epithelia and necrosis were seen. These mechanisms serve as barrier to prevent further entry of contaminants to damage other organs. Similar mechanism was also observed by Kumar et al., (2012) in gills of *Lamellidens marginalis*, a freshwater bivalve. Such stringent response has to be employed by the gills since it plays significant role in respiration, acid-base balance, ionic and osmotic regulation, food capture and maintenance of water current which greatly affects the physiological well-being of the organism. (EI-Shenawy et al., 2007, 2009; Beltran and Pocsidio, 2010).

The least affected among the organs is the adductor muscles with alterations limited to loss of surface adherence, haemocyte infiltration, loss of muscle organization and necrosis. Statistical analysis showed that all the exposed groups had a similar median score corresponding to only 41-60% damage. The high endurance of the adductor muscles even at high concentrations of BPA is due to its function of regulating the closing and opening of the shell (Beltran and Pocsidio, 2010). In addition, Hayashi et al. (2008) noted that the adductor muscles have a very low bioaccumulation rate to BPA and its metabolites.

## CONCLUSIONS

It is concluded that digestive gland was the most affected tissue followed by the gills then adductor muscles. The differential histological responses of the tissues of *C. fluminea* in different concentrations of BPA proves that they are good indicators of environmental stressors such as BPA. Future studies on the effects of lower concentrations (<1 ug/L) on digestive gland and higher concentrations (>3ug/L) on the adductor muscles.

## REFERENCES

- Beltran, K.S. and Pocsidio, G.N. 2010. Acetylcholinesterase activity in *Corbicula fluminea* Mull., as a biomarker of organophosphate pesticide pollution in Pinacanauan River, Philippines. *Environ Monit Assess* 165:331-340
- Colombo, J. C., Bilos, C., Campanaho, M., Presa, M. J. R., and Catoggio, J. A. 1995. Bioaccumulation of polychlorinated-biphenyls and chlorinated pesticides by the Asiatic Clam *Corbicula fluminea*—its use as sentinel organism in the Rio-De-La-Plata Estuary, Argentina. *Environ Sci Technol* 29 : 914–27
- Costa, P. M., Carreira, S., Costa, M. H. and Caeiro, S. 2012. Development of histopathological indices in a commercial marine bivalve (*Ruditapes decussatus*) to determine environmental quality. *Aquat Toxicol* 126: 442-454.
- Crain, D. A., Eriksen M., Iguchi T., Jobling, S., Laufer, H., LeBlanc, G. A. and Guillette, L. J. 2007. An ecological assessment of bisphenol-A: Evidence from comparative biology. *Reprod Toxicol* 24, 225-239.
- Flint, S., Markle, T., Thompson, S., and Wallace, E. 2012. “Bisphenol A exposure, effects and policy: A wildlife perspective- a Review” *J. of Environ Mngt* 104:19-34.
- Fournier, E., Adam, C., Massabuau, J. C., and Garnier-Laplace, J. 2005. Bioaccumulation of waterborne selenium in the Asiatic clam *Corbicula fluminea*: influence of feeding-induced ventilatory activity and selenium species. *Aquat Toxicol* (Amsterdam, Netherlands) 72:251-260.
- Hatel, A., Alavi, S.M.H., Abdulfatah, A., Fontaine, P., Rodina, M., Linhart, O. 2012. Adverse effects of Bisphenol A on reproductive physiology in male goldfish at environmentally relevant concentrations. *Ecotoxicology and Environmental Safety* 76:56-99
- Hayashi, O., Kameshiro, M., Masuda, M., and Satoh, K. 2008. Bioaccumulation and metabolism of [<sup>14</sup>C]bisphenol a in the brackish water bivalve *Corbicula japonica*. *Biosci. Biotechnol. Biochem.*, 72(12): 3219-3224.
- Ike, M., Jin, C.S., Fujita, M., 2000. Biodegradation of bisphenol A in aquatic environment. *Water Sci. Technol* 42: 31-38.
- Kanapala, V. & Arasada, S. 2013. Histopathological effect of paraquat (gramoxene) on the digestive gland of freshwater snail *Lymnaea luteola* (Lamarck: 1799) (mollusca: gastropoda). *International Journal of Scientific Research in Environmental Sciences*, 1(9): 224-230.
- Kang, J. H., Aasi, D. and Katayama Y. 2007. Bisphenol a in the aquatic environment and its endocrine-disruptive effects on aquatic organisms. *Crit Rev Toxicol* 37: 607-25.
- Klecka, G.M., Staples, C.A., Clark, K.E., van der Hoeven, N., Thomas, D.E. and Hentges, S.G. 2009. Exposure Analysis of Bisphenol A in Surface Water Systems in North America and Europe. *Environ Sci Technol* 43(16):6145-6150
- Kumar, S., Pandey, R. K., Das, V.K. 2012. Dimethoate alters respiratory rate and gill histopathology in freshwater mussel *Lamellidens marginalis* (Lamarck). *Journal of Applied Bioscience* 38 (2): 154-158.
- Labrot, F., Narbonne, J. F., Ville, P., Saint Denis, M., and Ribera, D. (1999). Acute toxicity, toxicokinetics, and tissue target of lead and uranium in the clam *Corbicula fluminea* and the worm *Eisenia fetida*: comparison with the fish *Brachydanio rerio*. *Arch Environ Contamin Toxicol* 36:167-178.
- Lehmann, D.W., Levine, J.F. and Law, J.M. 2007. Polychlorinated bisphenyl exposure causes gonadal atrophy and oxidative stress in *Corbicula fluminea* Clams. *Toxic Path* 35:356-365.
- Leonard, J.A., Cope, W.G., Barnhart, M.C. and Bringolf, R.B. 2014. Metabolomic, behavioral, and reproductive effects of the synthetic estrogen 17  $\alpha$ -ethinylestradiol on the unionid mussel *Lampsilis fasciola*. *Aquatic toxicology*, 150, 103-116

- Mantecca, P., Vailati, G. Bacchetta, R. 2006. Histological changes and Micronucleus induction in the Zebra mussel *Dreissena polymorpha* after Paraquat exposure. *Histol Histopathol* 21: 829-840.
- Oehlmann J., Schulte-Oehlmann U., Tillmann M. and Markert B. 2000. Effects of endocrine disruptors on prosobranch snails (Mollusca: Gastropoda) in the laboratory. Part I: Bisphenol A and octylphenol as xeno-estrogens. *Ecotoxicology* 9: 383-397.
- Oehlmann, J., Schulte-Oehlmann, U., Kloas, W., Jagnytsch, O., Lutz, I., Kusk, K.O., Wollenberger, L., Santos, E.M., Paull, G.C., Van Look, K.J., Tyler, C.R., 2009. A critical analysis of the biological impacts of plasticizers on wildlife. *Phil. Trans. R. Soc. B* 364: 2047e-2062.
- Oliveira, L.F., Silva, S.M.C.P. and Martinez, C. 2014. Assessment of domestic landfill leachate toxicity to the Asian clam *Corbicula fluminea* via biomarkers. *Ecotoxicol. Environ. Saf* 103:17-23.
- Pavan, P. G., Stecco, A., Stern, R. & Stecco, C. (2014). Painful connections: Densification versus fibrosis of fascia. *Curr Pain Headache Rep* 18(441), 1-8.
- Stahlhut, R.W., Welshons, W.V., Swan, S.H. 2009. Bisphenol-A data in NHANES suggest longer than expected half-life, substantial nonfood exposure, or both. *Environ. Health Perspect* 117: 784e-789.
- Santos, K.C. and Martinez, C.B.R. 2014. Genotoxic and biochemical effects of atrazine and Roundups, alone and in combination, on the Asian clam *Corbicula fluminea*. *Ecotoxicol. Environ. Saf.* 100: 7-14
- Yang, Y., Kim, S., Hong, Y., Ahn, J., Park, M. 2014. Environmentally relevant levels of Bisphenol A may accelerate the development of Diabete mellitus in adolescent Otsuka Long Evans Tokushima fatty rats. *Toxicol. Environ. Health. Sci.* 61(1): 41-47.

## BIO-ASSESSMENT AND TOXICOLOGICAL EFFECTS OF BIOLARVICIDES ON TARGET AND NON-TARGET ORGANISMS IN RIVERS STATE, NIGERIA

Wachukwu, C.K., Ollor, O.A., Ganabel, C.B, and Azike, C. A.

(Department of Medical Laboratory Science, Rivers State University of Science and Technology, Nkpulu-Oroworukwo, Port Harcourt, Nigeria)

Two biolarvicides (Bactivec and Griselesf) were used to control mosquito larvae in Rivers State, Nigeria. The aim of this study was to assess the health and environmental risks associated with the application of biolarvicides on target and non-target organisms. A total of ten (10) target organisms (mosquito larvae) and non-target organisms (tadpoles) were each exposed to different concentrations of biolarvicides (*Bacillus thuringensis* var *israelensis* (Bti)(Bactivec) and *Bacillus sphaericus* (Bs)(Griselesf) respectively. Ten-fold serial dilutions of the biolarvicides were made up to  $10^3$ . Thereafter, ten (10) target and non-target organisms each were added into the diluted samples and allowed to remain at both room temperature (20-28°C) and atmospheric temperature (30 – 35°C) for 14 days. They were also exposed to the undiluted biolarvicides and given the same treatment like the diluted ones. The viability or duration of the biolarvicides effect were also tested by exposing them to the environment for 7 days. Thereafter, the organisms were added to determine the effect of biolarvicides on them. Five milliliter (5ml) each of the undiluted biolarvicides (Bactivec and Griselesf) were mixed together and the organisms were added to it to check the synergistic effect on the organism. The pH and temperature were determined using the digital pH meter (model PHS-3C, UK) and the mercury thermometer. Two hundred and sixty (260) blood samples were collected and analyzed from the sprayed and control zones for malaria parasite and haematological parameters. The result showed that the undiluted biolarvicides killed the entire target and non-target organisms at ten (10) minutes of exposure, while the combined biolarvicides killed the non-target organism within 5 minutes of exposure and the target organisms were killed after 10 minutes of exposures to the biolarvicide. One in ten ( $10^1$ ) dilution killed over 50% of the same organisms after 60 minutes exposure. At  $10^2$  dilutions, the organisms were all killed after 48 hours exposure, while  $10^3$  dilutions had no effect on the organisms. The results also showed that the undiluted and  $10^1$  dilution can persist in the environment for long period of over seven days. The pH of the biolarvicides ranged from 6.0 and 6.9. The results of the haematological and malaria parasite showed that 162 (81%) had malaria parasites, while 38(19%) had no malaria parasites. There were no changes in the haematological parameters such as Hb, WBC and differential cell count. Therefore, it can be inferred that appropriate concentration of a given biolarvicide be used to avoid causing potential harm to other members of the ecosystem.

**ENANTIOSELECTIVE PHYTOTOXICITY OF  $\gamma$ -HEXABROMOCYCLODODECANE  
ENANTIOMERS TO MAIZE**

***CUI Jiansheng, LIU Ying, WU Tong***

(School of Environmental Science and Engineering, Hebei University of Science and Technology;  
Hebei Key Laboratory of Molecular Chemistry for Drug, Shijiazhuang, 050018, China)

In the present study, two enantiomers of  $\gamma$ -hexabromocyclododecane ( $\gamma$ -HBCD) were prepared by preparative liquid chromatography. To investigate the selective oxidative damage of HBCD to maize, young seedlings were exposed to solutions of HBCD enantiomers and racemate with different concentrations. The root biomass, shoot biomass, and root and shoot elongation of maize were inhibited after exposure with the inhibition rates following the order (+) $\gamma$ -HBCD > (rac) $\gamma$ -HBCD > (-) $\gamma$ -HBCD. The antioxidant enzyme activities of superoxide dismutase (SOD) and peroxidase (POD) both in roots and shoots were significantly upregulated by exposure to lower concentrations of (+) and (rac) $\gamma$ -HBCD than (-) $\gamma$ -HBCD. In contrast to (-) $\gamma$ -HBCD, the activities of SOD and POD were all decreased by higher exposure concentrations of (+) and (rac) $\gamma$ -HBCD. The intensities of histone H2AX phosphorylation were increased at first with an increasing exposure concentration of all  $\gamma$ -HBCD enantiomers and racemate and then decreased, indicating the enantio-specific induction of DNA damage in maize. All of these results provide solicited evidence of the significant enantioselectivity phytotoxicity of  $\gamma$ -HBCD to maize with a higher toxicity of (+) $\gamma$ -HBCD than (rac) $\gamma$ -HBCD and (-) $\gamma$ -HBCD.

## **EFFECTS ON LENGTH, WEIGHT AND ORIENTATION RESPONSES OF EARTHWORMS EXPOSED TO MAN-MADE ELECTROMAGNETIC NOISE**

**Şükran Yalçın Özdilek**, Sevil Yalçın and Rukiye Altaş  
(Çanakkale Onsekiz Mart University, Çanakkale, Turkey)

Earth has a natural magnetic field about 60  $\mu\text{T}$  at the poles and 30  $\mu\text{T}$  at the equator and many animals use this natural phenomenon for orientation and navigation. With the development of technology, the natural systems have to expose high electromagnetism because of heavy usages of electric and electrical devices. This man-made electromagnetic noise has increased dramatically above the natural magnetic fields in human occupied areas in the last two decades. In general, many scientists consider possible negative and positive effects of electromagnetism on human life and living system. The experimental studies indicate that magnetic and electromagnetic fields cause same changes on the living activities, such as, oxidative, genotoxic effects, survival, metabolic rates. The studies about the effects of man-made electromagnetic noise also focus on the behavioural patterns of organisms such as deviation on the migration route. The present study aimed to understand the possible effects of man-made electromagnetic noise as physiological and behavioural response on the earthworm as a model organism in laboratory conditions. The triplet experimental groups (each were composed of 20 earthworms) were exposed to 1.5 mT to 8 mT electromagnetic field using 1.5V current in a solenoid coil during one hour in a vivarium. The experimental and control designs were kept in a similar conditions and the length and weight of earthworms were measured before and after seven-day experimental design. The positions of earthworms were recorded by a photograph machine in every five minutes. The angles in terms of mean vector of each position of each earthworm beginning from the centre of vivarium were recorded by Adobe Photoshop CS6 program. The mean vectors and angles of different experimental designs and controls were compared by circular statistics. The results indicate that while the mean length of experimental group was decreased ( $F=16.4$ ;  $df=118$ ;  $p<0.001$ ) the mean weight of the earthworms had not changed ( $F=2.01$ ;  $df=118$ ;  $p>0.05$ ). The orientation of the earthworms in control and experimental groups were statistically different ( $p<0.005$ ).



**ASSESSMENT OF POLLUTION BIOMARKER AND STABLE ISOTOPE DATA IN  
*Mytilus galloprovincialis* TISSUES**

**Şükran Yalçın Özdilek\*** and Neslihan Demir

(Çanakkale Onsekiz Mart University, Faculty of Science and Arts, Department of Biology, Çanakkale, Turkey)

Mussels, *Mytilus galloprovincialis* give a rapid response to pollutants as an enzymatic antioxidant defenses with their oxidative potential. Superoxide dismutase (SOD) is one of the antioxidant defenses enzymes in mussels and converts the superoxide anion into hydrogen peroxide and this enzyme is used as biomarkers of oxidative damage. As well as many topics in ecology, stable isotopes are also signature for organic and heavy metal pollution in aquatic ecosystems. Particularly, the carbon isotopic signature is suggested as a proper sewage indicator for mussels, which filter particular organic matter from the water for feeding. Both method use different indicators for chronic response of pollution. This study aims to compare the stable carbon and nitrogen values of different mussel tissues and the changes on the SOD values of the same tissues in order to understand the relationship between two mechanisms of bio indicator processes of physiological response of mussel to pollution. The change on the level of superoxide dismutase (SOD) in the gill, hepatopancreas and mantle tissues of *M. galloprovincialis* with  $\delta^{13}\text{C}$  and  $\delta^{15}\text{N}$  isotopes were assessed in different locations (Kepez and Güzelyalı) in Çanakkale. The SOD values of mussel samples were found as Gill > hepatopancreas > mantle collected from Kepez and gill > hepatopancreas collected from Güzelyalı. There were significant differences among the mean SOD values of different tissues both in Kepez and Güzelyalı samples ( $p<0.05$ ). However, there were not any significant differences among the mean SOD values of different tissues of control group. There were enrichment both in nitrogen and carbon isotope values of hepatopancreas tissues both in Kepez and Güzelyalı samples. The mean  $\delta^{13}\text{C}$  value of hepatopancreas tissue and the mean  $\delta^{15}\text{N}$  value of gill tissue were a distinct group for Kepez samples and the mean  $\delta^{13}\text{C}$  and  $\delta^{15}\text{N}$  values of hepatopancreas and gill tissues were different for Güzelyalı samples ( $p<0.001$ ). There were a negative correlation between  $\delta^{13}\text{C}$  values and SOD values in Kepez samples ( $p<0.001$ ).

## **GRAPHENE INDUCED EPITHELIAL-MESENCHYMAL TRANSITION IN A549 CELLS *In Vitro***

***Yanyan Liao, Ziyang Zhang***

(Institute of Urban Environment, Chinese Academy of Sciences, Xiamen, Fujian Province 3361021, China)

With the deep research of the carbon nano-materials, especially the graphene was firstly discovered since 2004, it has gradually become a "superstar material" in the region of materials science. Nano-graphene are two-dimensional structures of carbon. Due to their unique physical and chemical properties, they have been widely used in biomedical, electronic devices and composite materials research fields. They also have a very bright application prospects, such as biosensors, biological imaging, gene delivery, photothermal therapy of tumor and cancer, hydrophobic anticancer drugs, and antibacterial materials and organization of material and other fields. However, the toxicity of graphene on health remains unknown and is of great concern.

One of the most important impacts on physiological pathology is the transfer of tumor invasion. This process is called Epithelial-Mesenchymal transition (EMT). The process mainly occurred in the polarity of epithelial cells, which will be changed into mesenchymal cells and they have invasiveness and migration capability. It exists in multiple physiological and pathological processes in human body. Many studies have shown that EMT and tumor cell invasion and metastasis are closely related. Thus, this experiment was designed to observe graphene stimulate EMT mechanisms to promote the metastasis of human lung adenocarcinoma epithelial cell line (A549).

A549 cells were plated in the 6-well plates and incubated for 48 h and 72 h. Graphene samples were introduced to the cells with final concentrations of 20ug/ml, 10ug/ml, 5ug/ml and 1ug/ml. Cells without graphene exposure were taken as the control. Wound healing assay showed that cell migration rate was obviously higher in graphene treatment groups. Transwell assay demonstrated that the invasion rate was increased in graphene-treated A549 cells. The expression levels of E-cadherin,  $\beta$ -catenin, TIMP-1, Wnt5a, ICAM-1, vimentin and Twist1 in A549 cells were examined by Western blotting, and reverse transcription(RT)-PCR. The results showed that the expression level of epithelial markers (E-cadherin,  $\beta$ -catenin, TIMP-1 and Wnt5a) was reduced after exposure to graphene for 48h and 72h, while the expression of mesenchymal markers (ICAM-1, vimentin and Twist1) were significantly increased after exposure to graphene for 48h and 72h. Our data suggest that graphene may promotes A549 cells invasion, migration and tumorigenesis ability. EMT is involved in graphene treated A549 cells.

## **DEVELOPING AN ASSOCIATION NETWORK FROM PROTEOME CHANGES TO ROOT PHENOTYPIC PROPERTIES FOR ALUMINUM TOLERANCE IN SWITCHGRASS**

**Mahesh Rangu**, Zhujia Ye, Sarabjit Bhatti, Suping Zhou  
(Tennessee State University, Nashville, TN, 37209, USA)  
Theodore W. Thannhauser

(Robert W. Holley Center for Agriculture and Health, USDA-ARS, Cornell University, Ithaca, New York)

Aluminum (Al) stress is a major problem causing reduction in plant growth in acidic soil. The most noticeable symptom of Al toxicity is the development of stunted root systems on sensitive plants. Plants were grown hydroponically in Al-treated and control cultures and a proteomic analysis of plants root tissue (Switchgrass) was carried out to document differential protein expression as a function of the Al status. During short-term treatment (<1 month), plant root length was not affected, even though there was some reduction in photosynthetic activity, leaf number, plant height and biomass yield. 7614 proteins in root tip protein extract and 7097 proteins in elongation protein extract were identified. Out of these proteins 1274(17%) root tip proteins and 891 (13%) elongation proteins were showed significant differences (t-test, p-value <0.05) with low fold change. Quantitative proteomics analysis of the root-tip and the root elongation zone have identified proteins encoded by Al tolerance genes, such as homologs of AtSTAR1, proteins for heavy metal transport/detoxification, vacuolar sorting receptor 3, and NRAMP metal ion transporter 6, which were induced in both root tips and/or elongation zones. The phosphate transporter was greatly induced, but the K transporter was repressed. Various transcription factors were identified and found to be both repressed or induced depending upon their functional context. Several proteins related to root hair initiation and development were induced which may affect the total surface area for nutrient uptake including Al ions. Proteins for suberin biosynthesis and Casperian strip formation on endodermis were induced in the elongation zone, which suggests a mechanism for tighter control of mineral flux of into the stele. Proteins affecting chromatin status, gene transcription, and protein translation activity were also affected by the Al treatment. Long term Al treatments (> 2 months) also carried out with longer exposure whereby the root structure started to show the typical Al-stress phenotype. Mass spectrometry, employing tandem mass tag (TMT) labeling used to identify protein changes in plant tissues due to Al stress.

**SITE-SPECIFIC SOIL ARSENIC BIOAVAILABILITY: THE 21<sup>ST</sup> CENTURY NEXUS  
BETWEEN SITE CHARACTERIZATION AND RISK ASSESSMENT.**

***N.T. Basta\****, S.D. Whitacre (The Ohio State University, Columbus, OH, USA)

V. M. Hanley and P. Myers (California Department of Toxic Substances Control, Sacramento, CA, USA)

A.L. Foster (USGS, Menlo Park, CA, USA)

S.W. Casteel (University of Missouri, Columbia, MO, USA)

Risk assessment methodologies provide conservative approaches to estimate the potential for adverse effects on human health from exposure to contaminants in soil. Risk assessment often establishes reference doses and cancer slope factors based on highly bioavailable forms of chemicals. Soil often interact with chemicals reducing their potential solubility in the environment and bioavailability for absorption by humans. Often the most important risk pathway associated with human exposure to arsenic-contaminated soils is incidental soil ingestion. We studied 18 soils collected from arsenic-contaminated gold mining sites throughout California. Soil As ranged from 200 to 12,000 mg/kg and relative bioavailability, measured by soil dosing trials using Juvenile Swine, ranged from 1% to 40% which were below the USEPA default value of 60%. In vitro Bioaccessibility (IVBA) As was measured by three in vitro gastrointestinal (IVG) methods. Arsenic RBA and IVBA were greatly reduced by adsorption to reactive Fe minerals including goethite and ferrihydrite. In vitro–in vivo correlation analysis found one IVG method conservatively predicted As RBA in all study soils and provided a good estimate (within 90% CI) of RBA As ( $RBA\ As = 0.8\ IVG + 4.39$ ,  $r^2=0.82$ ). Use of RBA As was able to identify high risk soils that require remedial action. Bioavailability and/or bioaccessibility methods can be used to measure site-specific arsenic bioavailability characterize risk at thousands of abandoned gold mining sites with elevated levels of soil arsenic throughout the state of California and elsewhere where the primary risk pathway of concern is incidental soil ingestion.

## **COMPREHENSIVE EVALUATION OF IN VITRO BIOACCESSIBILITY METHODS TO PREDICT BIOAVAILABILITY OF ARSENIC IN CONTAMINATED SOILS.**

**Brooke N Stevens\***, Nicholas T Basta, Shane D Whitacre

(The Ohio State University, Columbus, OH, USA)

Aaron R Betts, Kirk G Scheckel, (US EPA, Cincinnati, OH, USA)

Karen D Bradham, (USEPA, Triangle Park, NC, USA)

Soil arsenic (As) is a primary human health risk driver at many DoD, DOE, and USEPA sites. Often the calculated risk can be reduced when the bioavailability of arsenic in the soil is included in the risk calculations. In vitro bioaccessibility (IVBA) methods can be used to predict in vivo relative bioavailability (RBA). In order to determine the ability of an in vitro method to predict RBA, a correlation is done producing an in vitro-in vivo correlation (IVIVC). Due to the high cost of in vivo studies the importance of in vitro method's ability to predict RBA is growing. We report the most comprehensive IVIVC study for twenty nine soils with a range in soil properties, contamination sources, and solid phase As speciation.

Arsenic sources in study soils included orchards, glass works, copper mining, smelter, pesticide, and gold mining. The ability of five international published in vitro methods to predict animal RBA As (adult mouse and juvenile swine models) was determined. IVBA As vs. RBA As was fitted using linear regression and evaluated for goodness of fit, slope, y-intercept, prediction error, and compared against proposed acceptance criteria. Soil properties relevant to As solubility and bioaccessibility were determined; including total As, reactive Fe and Al, pH, organic carbon content and clay content. Solid phase speciation was determined using Extended X-Ray Absorption Fine Structure spectroscopy and linear combination fitting (LCF). Eighteen different As mineral phases were identified by LCF analyses, the most dominant phases were As (V) adsorbed to soil minerals such as ferrihydrite and goethite. Arsenic bioavailability and bioaccessibility ranged from 4 to 80 % and < 5 to > 90% respectively. Arsenic bioaccessibility was strongly correlated ( $r^2 > 0.7$ ) with RBA As, however the methods that most resemble human physiology were better at predicting RBA As according the proposed criteria. Results from this study will help support the adoption of methods to measure bioaccessible As that predict RBA As.

## MODELLING OF ARSENIC REMOVAL FROM GROUNDWATER BY ELECTRODIALYSIS

**Rose Marie O. Mendoza** (Far Eastern University-NRMF, Institute of Medicine, Quezon City, Philippines)

Meng-Wei Wan and Chi-Chuan Kan (Chia Nan University of Pharmacy and Science, Department of Environmental Engineering and Science Tainan Taiwan, ROC)

Maria Lourdes P. Dalida (National Graduate School of Engineering, Department of Chemical Engineering, University of the Philippines, Diliman, Quezon City)

**ABSTRACT:** A model for Arsenic removal from ground water was evaluated. At varying experimental conditions, the second order homogeneous ordinary differential equation model proposed by Yu and Admassu on ion removal (from pulp and paper mill process stream) was able to predict the concentration, current utilization and removal of As ions from ground water samples efficiently. Two model parameters specifically for arsenic systems was derived: A is a parameter used to describe the characteristics of the solution, while  $\lambda^2/B$  is a parameter that is related to the stack electrical field strength. Post hoc analysis of the model and  $R^2$  values of 0.9899 and above was obtained for all parameters considered which indicate that the model can adequately describe the removal of arsenic from contaminated waters. The model was used to determine the effects of experimental parameters on Arsenic removal from ground water samples in terms of applied potential, feed flow velocity and initial feed concentration. A very satisfactory agreement between model predicted and experimental values of concentration, current utilization and removal efficiencies were obtained.

## INTRODUCTION

Arsenic-related incident covers almost majority of Asia. Bangladesh, Cambodia, China, India, Myanmar, Nepal, Pakistan, Taiwan and Vietnam are countries recently has been identified to use arsenic (As) contaminated ground water for irrigation. This poses serious health hazard to people eating food from the crops irrigated with arsenic contaminated water, in addition to the fact As accumulating in irrigated soils poses a serious threat to sustainable agriculture in affected areas (Brammer and Ravensoft, 2009). Bangladesh's As-contaminated groundwater has been extensively used to irrigate paddy rice, during dry season of 75% of the total area given to rice cultivation with arsenic levels of 4-8  $\mu\text{g/g}$  and reaches to 83  $\mu\text{g/g}$  (Rahman and Hasegawa, 2011). Because of the similar agro-ecological and hydrogeological conditions of these South East Asian regions the threat of arsenic contamination can easily reach neighboring countries. So far, arsenic contamination is widely detected to the alluvial plains of South and South East Asia where rice (paddy) is the main crop irrigated with ground water. According to Ravensoft (2007a,b), the GIS-based-geological-geochemical-hydrological models predict widespread pollution of ground waters in Indonesia, Malaysia and the Philippines – where water supplies were not yet tested for Arsenic.

Mendoza et al. (2014) in their study mentioned the viability of Electrodialysis (ED) as a process to remove inorganic As from contaminated waters. The study also stressed that experiments on arsenic systems should be carefully modelled and optimized to yield higher removal rates, while generating lesser waste by-products which can be more toxic than its source. Galvanin et al. (2015) opined that model-based design of experiment is a satisfactory approach to minimize the number of trials required for actual experimental runs.

To date, there is very less attention focused on model parameters for natural aqueous systems, particularly on arsenic removal and separation using electrodialysis (ED). The Nernst-Planck equation is

one of the most utilized and widely-used model for a time-dependent transport and conversion on mass through the motion of charged chemical species in fluid medium (Kirby et al., 2010). Galvanin et al. (2015) utilized the Nernst-Plank approach to model the electrodialytic recovery of multi-valent electrolytes to accomplish desalination using NaCl while Zourmand et al. (2015) combined the Nernst-Plank model with that of Navier-Stokes model to develop a mass transfer model for the prediction of ion transport through electrodialysis (ED) cell using also NaCl solution. Mohammadi et al. (2005) as well as Sadrzadeh and Mohammadi (2007) provided a statistical model of metal ion removal from textile and semiconductor effluents using electrodialysis and electrodialysis reversal by a Taguchi L9 OA design. It was only Mendoza et al. (2014) who used the electrodialysis (ED) process in removing arsenic from as-spiked water and come up with an optimum experimental conditions based on maximized As removal or separation. Thus, the burden of treating arsenic contaminated waters that will produce streams of higher arsenic concentration is one of the drawback of the study. The need to initially model arsenic systems to predict its removal from contaminated water will be of great contribution to the environmental sustainability of the said process. Through a model that will mimic the removal of arsenic from aqueous systems and with several related studies, lesser concentrated wastes will be generated which can gear the ED process towards zero-waste technology.

This paper investigates the removal of As from actual groundwater samples through the determination of the concentration and limiting current profile using the Yu and Admassu model (2000) for metal ions removal (from pulp and paper industry) and to come up with an model-generated predictions on arsenic removal at varied experimental conditions. The study also includes the model determination of the effect of experimental parameters such applied potential, feed flow velocity, initial feed concentration and operating time which is then later compared to the actual experimental data.

## MATERIALS AND METHODS

**Materials.** Groundwater samples used in this experiment were obtained from raw water source, well no. 9 and 10 of Taiwan Water Corporation's Water Treatment Plant in Beigang Township, Yunlin, Taiwan. Characteristics of the groundwater used for this study was presented in Table 1. The samples were filtered immediately through a 0.45 $\mu$ m pore size cellulose acetate syringe filter to minimize arsenic III oxidation with air. To further preserve arsenic species in the filtered sample, ethylenediaminetetraacetic acid (EDTA) was added immediately to the filtrate. This preserves the distribution of arsenic species by chelation to metal ions, prevents drastic changes in sample pH and minimizes microbial activity. Filtered samples were stored in PET containers at reduced head space and refrigerated at 4°C (Bednar et al., 2004).

**TABLE 1. Characteristics of the ground water used in this study**

Cations	Concentration mg/L	Anions	Concentration mg/L
Na <sup>+</sup>	145.50	Cl <sup>-</sup>	130.559
K <sup>+</sup>	34.515	NO <sub>3</sub> <sup>-</sup>	<0.1
Mg <sup>2+</sup>	18.97	SO <sub>4</sub> <sup>2-</sup>	2.285
Ca <sup>2+</sup>	20.75	HCO <sub>3</sub> <sup>-</sup>	119.70
Mn <sup>2+</sup>	0.093	PO <sub>4</sub> <sup>3-</sup>	6.299
Fe <sup>tot</sup>	<0.01	TOC	1.19 mg. C
As <sup>tot</sup>	0.702		

*Others: E<sub>h</sub> = -162.2 mV; pH = 7.68; T = 23°C; EC = 1388  $\mu$ S/cm*

(Obtained from: Taiwan Water Corporation's Water Treatment Plan, Well no. 9 and no. 10, Beigang County, Yunlin, Taiwan)

The ORP and pH of the solutions was monitored using Suntex pH-ORP meter model SP-300. Current and Voltage measurements were performed using a Hao Ling HL 833 digital ammeter and voltmeter, respectively. The total As, As III and As V concentrations and concentrations of cations (Na, Mg, Ca, K, Mn and Fe) of the feed, diluate stream and concentrate stream was determined using a Perkin Elmer 2000 Optima DV Inductively Coupled Plasma - Optical Emission spectrophotometer equipped with a hydride generator (HG-ICP-OES). Anion concentration in the form of nitrates, nitrites, phosphates, sulphates and chlorides, were analyzed using a Dionex DX-120 ion chromatograph (IC) equipped with a Reagent Free Controller (RFC), carbonates were obtained by titrimetric methods and TOC by direct method for drinking water and wastewaters (Method 10129) using Hach DR 500 UV-VIS Spectrometer. Conductivities of the solution were determined using Suntex EC-410 digital conductivity meter attached to the control panel.

**Methods.** The tailor-made electrodialysis (ED) provided by Shell Kwong Sir Enterprise Co., was used to conduct As removal experiments in the recirculating batch mode. The ED stack is composed of a single hydraulic and single electrical stack with 20 cell pairs situated 0.9 mm apart. Operating temperature for the whole system was set at  $25^{\circ}\text{C} \pm 1^{\circ}\text{C}$ . Maximum parameters for the ED stack as recommended by the manufacturer were indicated in the study of Mendoza et al. (2014). Optimum experimental settings such as applied voltage of 17V, initial feed concentration ( $C_0$ ) of 700 ppb, feed flow rate of 0.033 l/s and a minimum operating time of 92 minutes used by Mendoza et al. (2014) in their study on As-spiked water was considered for model experimental runs. Groundwater samples were pre-treated in the pre-oxidation tank to transform  $\text{As}^{3+}$  to  $\text{As}^{5+}$ , then fed into the feed tank. From the feed tank, contaminated groundwater sample was introduced in the ED stack at an optimum feed flow velocity, and the sample was desalted in 92 minutes using 17V as the applied voltage. As the feed was introduced, the tap water as the electrode flush solution was circulated into the anodic and cathodic compartments. The concentrate stream was dumped into the electrode flush tank and eventually became part of the electrode flush solution.

The samples from the diluate stream were immediately digested with 5% potassium iodide (KI), 5% vitamin C and concentrated HCl. The mixture was set aside for 25 minutes for stabilization and diluted to its marked volume using Ultrapure 18.2 m $\Omega$  deionized water. A solid phase extraction membrane, Supelco LC-SAX strong anion resin was used to immediately separate As III from As V at an elution time of 1 minute (Jang et al., 2011). The total As, As III and As V of the sample was analyzed using a Perkin Elmer Inductively Coupled Plasma-Optical Emission Spectrophotometer (HG-ICP-OES) Optima DV2000 at 228.812 nm, using Hydride Generation. A reducing agent in the form of 5% sodium borohydride ( $\text{NaBH}_4$ ) in 0.5% sodium hydroxide (NaOH) was used counter current with the sample to prevent further sample oxidation or metal complexation phenomena. Calibration standards of 1, 5, 10, 50, 100 and 700 ppb are freshly prepared during sample analysis. Two 2 sample replicates, check samples and standards are included to countercheck the accuracy and precision of the determination of the concentrations using HG-ICP-OES.  $R^2$  for each analysis was established at 0.999 or higher. Cations and anion content as well as TOC and bicarbonate were also evaluated.

## RESULTS AND DISCUSSION

In a published paper in 2000 by Z.Yu and W. Admassu, a model for the concentration and current profile was evaluated and used in removing metal ion from pulp and paper mill process stream. The model describes the transport of metal ions in the boundary layers at membrane surfaces and the limiting current density as a function of low velocity and removal efficiency. The general transport equation for the molar flux ( $J$ ) driven by diffusion, migration and convection in the ED channels is governed by the Nernst-Planck equation (Yu and Admassu, 2000):

$$J_{\pm} = -z_{\pm}v_{\pm}FC_{\pm}\nabla\phi - D\nabla C_{\pm} + C_{\pm}u \quad (1)$$



The model was anchored on the following assumptions: (1) the potential is a function of location due to a constant current supply, and the external applied potential is considered constant thus potential gradient will also be considered constant. Thus, equation (1) becomes:

$$\frac{\partial C_{\pm}}{\partial t} + u \nabla C_{\pm} = z_{\pm} v_{\pm} F \nabla \cdot (C_{\pm} + \nabla \phi) + D_{\pm} \nabla^2 C_{\pm} \quad (2)$$

The motion of the charged particles will bring current into the system. The current intensity for the solution is defined as  $i = F \sum z_j J_j$  which gives the equation for the aqueous solution as:

$$i_{\pm} = -F^2 \nabla \phi \sum z_{\pm}^2 v_{\pm} C_{\pm} - F \sum z_{\pm} D_{\pm} \nabla C_{\pm} + F u \sum z_{\pm} C_{\pm} \quad (3)$$

To simplify the model equations the following assumptions were made: (1) for a quasi-steady state the time variation of concentration and the diffusion term along the flow direction is negligible compared to convection; and (2) neutrality of charge is satisfied in the whole channel which makes  $z_+ C_+ + z_- C_- = 0$  and (3) the influence of the flow profile of fluid is negligible which allowed the system to be considered as a plug flow fluid. The dilute nature of the solution makes its viscosity as that of water which will now flow the schematic flow in Figure 1 (Yu and Admassu, 2000). This follow that:

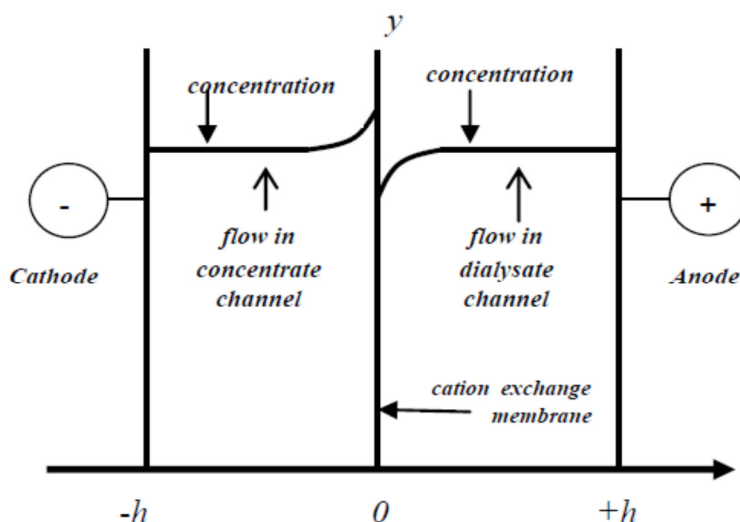


**FIGURE 1. Flow scheme of the solution in the ED stack**

Simplifying equation (3) and inserting it to equation (2) results in:

$$u \frac{\partial C_{\pm}}{\partial y} = D_{\pm} \frac{\partial^2 C_{\pm}}{\partial x^2} + z_{\pm} v_{\pm} F \frac{d\phi}{dx} \frac{\partial C_{\pm}}{\partial x} \quad (4)$$

For the current density and simplification of equation (3) is based on the assumption previously expressed considering a constant potential gradient within the stack. This makes the effect of convection in equation  $u C_{\pm}$  negligible. The current in the anionic membrane  $i = 0$  since the current density in the cation exchange membrane is the only one being considered in the model. Thus, the current in the cationic membrane is:

$$i_+ = -D_+ F z_+ \frac{dC_+}{dx} - \frac{F^2 z_+^2 D_+ C_+}{RT} \frac{d\phi}{dx} \quad (5)$$

and by principle of electroneutrality and non-ideality on membranes,

$$\frac{dC_+}{dx} = \frac{F z_+ C_+}{RT} \frac{d\phi}{dx} \quad (6)$$

Equation (2) is simplified by setting  $A = u/D_+$  and another parameter as

$$B = z_+ v_+ F / D_+ \cdot d\phi / dx \quad (7)$$

from a deduced dimensionless reduced concentration  $C^* = C_w/C_0$ , equation (2) becomes

$$A \frac{\partial C^*}{\partial y} = \frac{\partial^2 C^*}{\partial x^2} + B \frac{\partial C^*}{\partial x} \quad (8)$$

where  $C_0$  is the initial concentration and  $C_w$  is defined as the wall concentration in the boundary layers near the interface as shown in Figure 3 (Yu and Admassu, 2000). Analyzing Figure 2, the boundary conditions for equation (16) are set as:  $x = 0$ ,  $C^* = C_s$  ( $C^*|_{x=0}$ ),  $x \rightarrow h$  ( $x > x_a$ ),  $C^* = C_h$  ( $C^*|_{x=h}$ ) and  $y = 0$ ,  $C^* = 1$  for  $x > x_a$ .

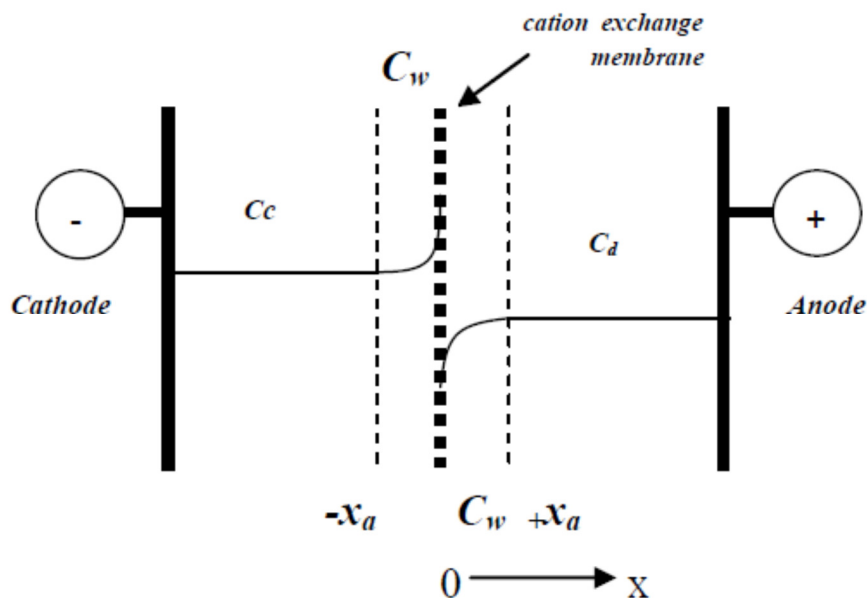


**FIGURE 2. Boundary layer used in this study for the ED process**

The transport of ions in this model assumes that it occurs and only significant along the boundary layers, which is in the region where  $x$  is greater than 0 but less than  $x_a$ . From Figure 3 we can say that  $x_a \ll h$  when  $x > x_a$  and  $x \rightarrow h$ , then  $x \rightarrow \infty$ . This analysis of the boundary layers generates a general solution for equation (8) as:

$$C^*(x, y) = f(y)g(x) \quad (9)$$

which can be written as:

$$\frac{A}{f} \frac{df}{dy} = \frac{1}{g} \left( \frac{d^2g}{dx^2} + B \frac{dg}{dx} \right) \quad (10)$$

In the dialysate channel, the cation transport decreases along the flow direction (y). Introducing a constant  $-\lambda^2$  to represent separation constant in the dialysate channel based on the boundary conditions set, equation (10) becomes:

$$\frac{df}{dy} + \frac{\lambda^2}{A} f = 0 \quad (11)$$

which is a second-order homogeneous ordinary differential equation with the form;

$$\frac{d^2g}{dx^2} + B \frac{dg}{dx} + \lambda^2 g = 0 \quad (12)$$

And an auxillary equation (Kreyzig, 2006):

$$K^2 + BK + \lambda^2 = 0 \quad (13)$$

Equation (13) has two roots:

$$K_{1,2} = -\frac{B}{2} \left\{ 1 \mp \left( 1 - \frac{4\lambda^2}{B^2} \right)^{1/2} \right\} \quad (14)$$

The general solution for Equation (12) (Kreyzig, 2006) is:

$$g(x) = N_1 \exp(K_1 x) + N_2 \exp(K_2 x) \quad (15)$$

Combining equation (11) and equation (13), the reduced concentration in the dialysate channel is:

$$C^*(x, y) = f(y)g(x) = \{m_1 \exp(K_1 x) + m_2 \exp(K_2 x)\} \exp\left(-\frac{\lambda^2}{A} y\right) \quad (16)$$

The integration constants  $m_1$  and  $m_2$  was determined using boundary conditions. For the purpose of simplification of equation (16) the following assumptions were made:  $4\lambda^2/B^2 \ll 1$  and  $\lambda^2/B \ll B$  so that  $K_2 \approx -B$ ; at  $y = 0$ ,  $C^* = 1$  for  $x > x_a$ ,  $x$  becomes large,  $\exp(-Bx) \rightarrow 0$  faster than  $\exp(-\lambda^2/Bx)$  because  $\lambda^2/B \ll B$ . This yields,

$$m_1 = \exp\left(\frac{\lambda^2}{B} h\right) \quad (17)$$

and

$$m_2 = \frac{\exp\left(\frac{\lambda^2}{B} h\right) \left\{ \frac{\left(\frac{d\phi}{dx}\right)_{m,d}}{\frac{d\phi}{dx}} + \left(\frac{RT}{z+F}\right) \left(\frac{\lambda^2}{B}\right) \left(\frac{d\phi}{dx}\right) \right\}}{1 + \left(\frac{d\phi}{dx}\right)_{m,d} / \left(\frac{d\phi}{dx}\right)} \quad (18)$$

and gives the concentration profile at any location in the ED dialysate and concentrate channel, respectively as :

$$\frac{C_w}{C_0} = \left[ 1 - \frac{\left(\frac{d\phi}{dx}\right)_{m,d} \frac{d\phi}{dx}}{1 + \left(\frac{d\phi}{dx}\right)_{m,d} \frac{d\phi}{dx}} \exp(-Bx) \right] \exp\left(-\frac{\lambda^2}{A}y\right) \quad (19)$$

For the current density profile equations (5), (6) and (19) yields:

$$i_{w,d} = -2D_+Fz_+C_0 \left[ B \frac{\left(\frac{d\phi}{dx}\right)_{m,d} \frac{d\phi}{dx}}{1 + \left(\frac{d\phi}{dx}\right)_{m,d} \frac{d\phi}{dx}} \right] \exp(-Bx) \exp\left(-\frac{\lambda^2}{A}y\right) \quad (20)$$

Equation (19) and (20) is then simplified by integrating both sides with the boundary condition  $C_s = C_w|_{x=0}$  which results to:

$$C_w - C_s = -\frac{i_+}{2D_+Fz_+} x_a \quad (21)$$

where  $i_+$  is the current flowing in the opposite direction of  $x$ ,  $F$  is the Faraday's constant (96,480 C/mol),  $D_+$  diffusion coefficient ( $\text{cm}^2/\text{s}$ ) of cation in the solution,  $z$  is the charge of ion and  $x_a$  (mm) average thickness of the boundary layer.  $C_w - C_s$  will be greater than 0 which is considered as the concentration of in the diluate compartment when boundary conditions  $C_s = C_w|_{x=0}$  is considered. When  $C_s \rightarrow 0$ ,  $i_+ = i_{lim}$  and :

$$i_{lim} = \frac{2D_+Fz_+}{x_a} C_w|_{x \rightarrow 0} \quad (22)$$

From Kocherginsky (2010), equation (22) has a form:

$$i_{lim} = C_0 e^{\frac{-u^*}{u}} \quad (23)$$

where  $u^* = D_+ \lambda^2 y$ . Equation (23) indicates the limiting current density is a function of both initial concentration  $C_0$  and flow velocity  $u$ . The magnitude of the parameter  $\lambda^2$  is a function of initial concentration ( $C_0$ ) removal efficiency (R%) and physical ED stack characteristics.

For equations (19), in the boundary layers, when  $x \approx 0$ , the concentration becomes independent of  $x$  as  $x \rightarrow h$ . This means that the significant removal or separation of ions mainly occurs at the membrane walls/surfaces. As a function of  $y$ , the decrease in the concentrate channel results to an increase in concentration of the concentrate channel. Due to the transport of ions in the boundary layer, the system will tend to polarize when  $y = L$  as  $x \rightarrow 0$ . This makes the field strengths at membrane surface different in the cationic and anionic membrane surfaces. In this model, the field strengths are estimated using the continuity condition of electrical current at specified locations.

From equation (20), the value of current at entrance ( $y=0$ ) is at maximum and decreases continuously as it approaches  $y = L$ . At the membrane surface ( $x=0$ ), the current density also reaches the maximum value. In the boundary layer, the current density decreases as  $x \rightarrow x_a$ , beyond the boundary layer,  $x \rightarrow h$  and  $i \rightarrow 0$ . This strongly suggests that concentration or concentration gradient is one of the factors that can influence current and current density.

From Ohms Law, the intensity of current is directly proportional to the electric field. As such there is a direct variation that can be observed between current density and the surface electrical field  $(d\phi/dx)_{m,d}$  which in turn show a direct relationship between ion transport. This resulted in the direct proportionally between current density and initial concentration.

For parameter estimation of the model equations for concentration profile and current density at any location in the ED channel, R% is defined based on as a function of  $\lambda$  is obtained as:

$$S\% = R\% = \frac{c_o - c}{c_o} \times 100 = \left( 1 - \exp\left(-\frac{\lambda^2}{A} L\right) \right) \times 100 \quad (24)$$

**TABLE 2. Typical values used for model calibration and model parameters for the ED process**

Geometric Sizes	Symbol	Value	Source
Flow distance	L (mm)	360 mm	This study
Flow width	W(mm)	170 mm	This study
Half-channel width	h (mm)	5 mm	This study
Average film thickness	xa	0.45 mm	This study
Number of cell pairs		20	This study
<i>Characteristics of Feed Solution</i>			
Average flow speed	u (cm/s)	0.0033	This study
Valence (as H <sub>2</sub> AsO <sub>4</sub> )	z	1	Clifford and Ghurye, 2005
Initial Concentration	Co (ppb)	700	This study
Diffusion Coefficient	D (cm <sup>2</sup> /s)	0.809x10 <sup>-5</sup>	Leaist (2007)
Density	ρ (g/cm <sup>3</sup> )	1	
Viscosity of water	μ( kg/ m s)	900 x 10 <sup>-6</sup>	Leaist (2007)
<i>Applied Conditions</i>			
Temperature	T (K)	298	This study
Constant electrical field	dθ/dx (vol/m)	100 kg-m/s <sup>2</sup> C	Yu and Admassu (2000)
Removal Efficiency	E%	99.56	This study
<i>Physical Constant</i>			
Faraday Constant	F (C/mol)	96480	
Gas Constant	R (J/K mol)	8.413	

Equation (20) is true only when  $0 < (R\%) < 100$ . An evaluation of the concentrate channel, though not so significant in this study must also be performed to facilitate transport equation facilitation. For the concentrate channel, the bulk concentration increases along the flow direction (Yu and Admassu, 2000). To compare the separation of concentrate to that of the dialysate channel, another separation constant in the form of  $\xi$  is defined related to the gain efficiency in the concentrate channel which leads to:

$$R\% = \frac{c_L - c_o}{c_o} \times 100 = \left[ \exp\left(\frac{\xi^2}{A} y\right) - 1 \right] \times 100 \quad (25)$$

and yields,

$$\xi^2 = \frac{A}{L} \ln\left(1 + \frac{R'\%}{100}\right) \quad (26)$$

Non-ideality of membrane assumption ensures that there is no retention of cations at the membrane surfaces and in the membrane and indicate that the amount cations removed from the dialysate channel (R%) is equal to the amount of ions gained in the concentrate channel (R'%) which makes the magnitude of  $\lambda^2 > 0$ .

To estimate the magnitude of  $\lambda^2/B$ , model parameters based on typical values in ED process for KCl is used by the paper (Yu and Admassu, 2000), which gives an initial value for for Co and an average R% of 50 for batch ED process (Mc Neil and McCoy, 1989). This follows that:

$$\frac{\lambda^2}{B} = \frac{1}{L} \left| \ln \left( 1 - \frac{R\%}{100} \right) \right| \frac{uRT}{z_+ D_+ F (d\phi/dx)} = 0.018/\text{mm}. \quad (27)$$

$$B = \frac{z_+ v_+ F}{D_+} \frac{d\phi}{dx} = \frac{z_+ F}{RT} \frac{d\phi}{dx} = 3.823/\text{mm} \quad (28)$$

$$\frac{\xi^2}{B} = 0.011/\text{mm}. \quad (29)$$

For the model calibration, Table 2 presents the nown physical parameters of the ED stack as well as the physical and chemical properties of the solution and the membranes while to facilitate model parameter estimation, typical values for ED process in the table below is used.

**TABLE 3. Parameters obtained for Yu and Admassu Model**

<b>Varied Parameters</b>	<b>Correlation Coefficient, R<sup>2</sup></b>	<b><math>\lambda^2/B</math> mm<sup>-1</sup></b>	<b>A cm<sup>-1</sup></b>
<b>Initial Feed Concentration<sup>a</sup></b>			
200 ppb	0.993	0.63690	42.0272
500 ppb	0.966	0.67654	42.0272
700 ppb	0.981	0.73093	42.0272
<b>Feed Flow Velocity<sup>b</sup></b>			
0.0025 m <sup>3</sup> /s	0.994	1.30843	30.9024
0.0033 m <sup>3</sup> /s	0.999	1.30843	42.0272
0.0042 m <sup>3</sup> /s	0.999	1.30843	51.9160
<b>Applied Potential<sup>c</sup></b>			
5V	0.980	0.03133	42.0272
10V	0.993	0.00084	42.0272
17V	0.993	0.00004	42.0272

<sup>a</sup> Applied Potential (E)=3-20V; feed flow rate = 0.0033 m<sup>3</sup>/s; Time = 92 min.

<sup>b</sup> Applied Potential (E)=17V; Initial feed concentration = 700 ppb; Time = 92 min.

<sup>c</sup> Feed flow rate = 0.0033 m<sup>3</sup>/s; Initial feed concentration = 700 ppb; Time = 92 min.

The very good agreement between the experimental and model predicted values was dictated by the R<sup>2</sup> values indicated in Table 3 which was found to be greater than 0.98 on all parameters set for the study. Two model parameters were considered for this study; A is a parameter used to describe the characteristics of the solution, while  $\lambda^2/B$  is a parameter that is related to the stack electrical field strength. The increasing values of  $\lambda^2/B$  with respect to increase in initial feed concentration indicate efficient current utilization in the stack and efficient collision of ions during desalination within the stack channel while a

constant value of  $A$  as the initial concentration increases indicates that ion transport is not limited to solution characteristics, rather it is more dictated by current and potential. Figure 3a shows that the removal of As ions from the feed for both experimental and predicted values are more efficient at applied potentials above 10V.

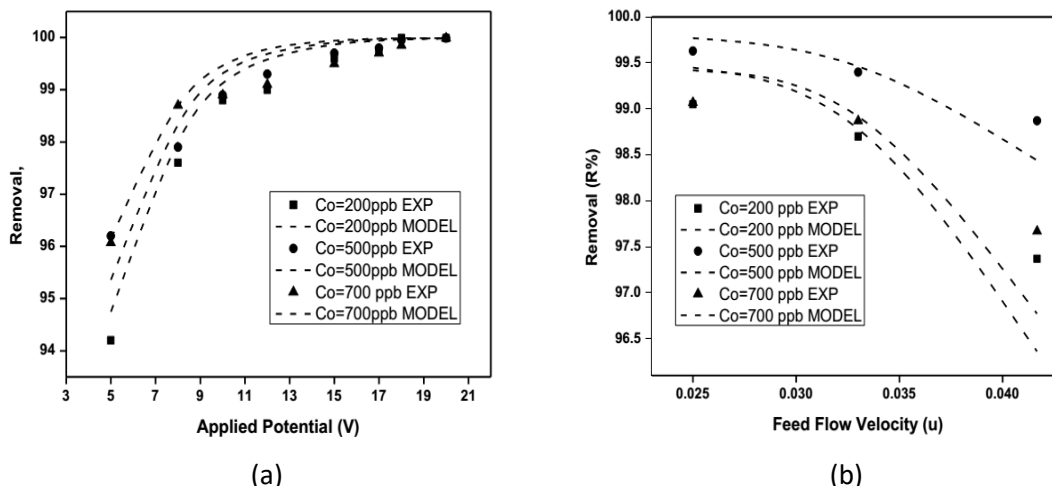


**FIGURE 3. (a) Experimental and model predicted values on the effect of applied potential on As removal efficiency at variable concentrations; (b). The comparison between experimental values on the effect of feed flow velocity ( $u$ ) to removal efficiency at varied initial feed concentration and constant applied potential of 15V and feed flow velocity of 0.033 l/s (2.0 l/min) and retention time of 92 minutes.**

**Effect of experimental parameters on Arsenic removal from groundwater using ED.** Model predicted values was compared with that of the experimental values in evaluating the effect of experimental parameters on arsenic removal. From Figure 3a model predicted values agrees satisfactorily with that of experimental values, confirming a direct relationship between applied potential %removal at variable concentration. The %removal was found to increase as the applied potential is increased at high or low initial feed concentrations. The same satisfactory agreement was found between % removal and feed flow velocity at high and low concentrations. However, an inverse relationship was found between %removal and feed flow velocity at varied concentrations as illustrated in Figure 3b. This can be due to the fact that the initial feed flow velocity was complemented by the applied potential resulting in a very fast transit of ions to the boundary layers, which indicates that in an ED system, very low or very high feed flow velocity are both non ideal conditions that may lead to neither increased energy consumption or polarization. Higher removal rate was found to at feed flow velocity of 0.033 l/s.

As observed from Figure 4, an increase in removal rate corresponds to decreases in current utilization. An increase in the electrical field strength parameter as applied potential is increased is a result of stack current utilization. The current in the stack is utilized to transport ions and co-ions across the membrane surfaces. As the ions are transported across, the ions in the diluate stream also decrease which results in the lesser current requirement. As shown in Figure 4, as the removal rates approaches the 90% and above region as current utilization approaches to minimum, and as expected electrical field strength is reduced. The reduction in the electrical field strength in this manner does not necessarily indicate polarization since it can also mark as the end of the desalination process. Both model generated vales and experiment a values accounts for such trend.

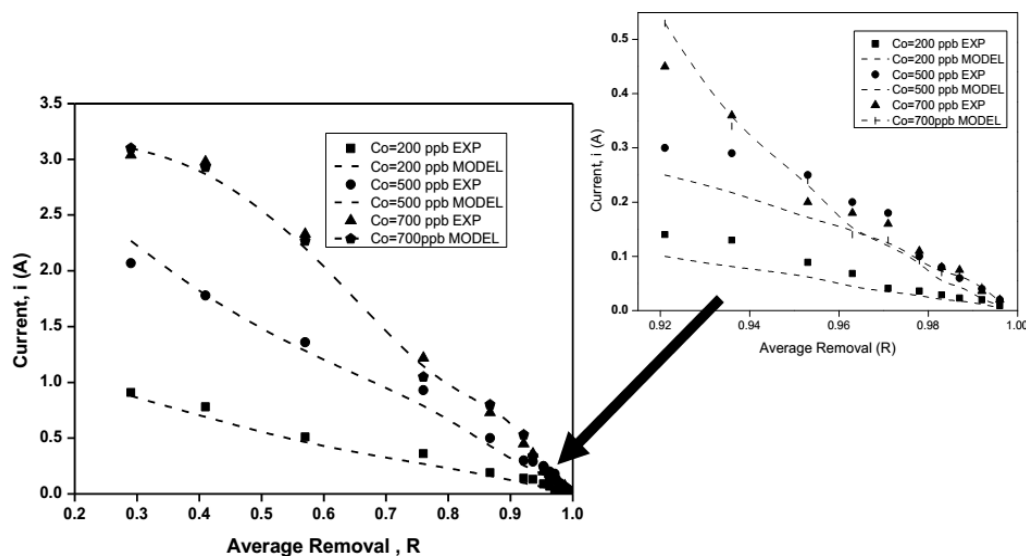


**FIGURE 4.** The experimental and model predicted values of current utilization and removal efficiency at a constant applied potential of 17V and feed flow velocity of 0.033 l/s (2.0 l/min) at variable concentrations.

## CONCLUSIONS

The Yu and Admassu model which was initially used to model the concentration and current density profile for the removal of metal ion from pulp and paper mill process stream was evaluated and found to satisfactorily predict removal of arsenic from contaminated water streams and determine the effect of experimental parameters on arsenic removal. Two model parameters were derived:  $A$  is a parameter used to describe the characteristics of the solution, while  $\lambda^2/B$  is a parameter that is related to the stack electrical field strength. The increasing values of  $\lambda^2/B$  with respect to increase in initial feed concentration indicate efficient current utilization in the stack and efficient collision of ions during desalination within the stack channel while a constant value of  $A$  as the initial concentration increases indicates that ion transport is not limited to solution characteristics, rather it is more dictated by current and potential. Results of this study has been found to support several literature on ED process indicating that removal rate increases as applied voltage and current density increases. In terms of initial feed concentration, the remarkably high removal rates from 500 – 700 ppb is brought about by the increase in ionic particles that intensifies the current in the stack. Medium feed flow velocity was known to be ideal for arsenic systems. The experimental data generated yielded 2 parameters that can be utilized for arsenic systems.

## ACKNOWLEDGEMENT

This paper acknowledges the Taiwan National Science Council for financially supporting this research under Contract No. NSC 101-2221-E-041-010-MY3 in collaboration with the Commission on Higher Education-Higher Education Development Program (CHED-HEDP), Republic of the Philippines.

## REFERENCES

- Bednar, A.J., Gabarino, J.R., Burkhardt, M.R., Ranville, J.F., Wildeman, T.R. (2004). "Field and laboratory arsenic speciation methods and their application to natural-water analysis". *Water Research* **38** (2). 355-364.
- Brammer, H. Ravenscroft, P. (2009). "Arsenic in groundwater: A threat to sustainable agriculture in South and South East-Asia." *Environmental International*. **35**, 647-654.
- Chekioua, A., Delimi, R. (2015). "Purification of  $H_2SO_4$  by Pickling Bath by Fe (II) ions using Electrodialysis process." *Energy Procedia*. **74**, 1418-1433.



- Galvanin, F., Marchesini, R., Barolo, M., Bezzo, F., Fidaleo, M. (2015). "Optimal design of experiments for parameter identification in electrodialysis models." *Chem. Eng. Res. Design*. **In press, accepted manuscript**, Available on line 12, November 2015.
- Ghurye, G., Clifford, D.,(2004). "As(III) Oxidation using chemical and solid-phase oxidants." *J.AWWA*. **96**(1)84-96.
- Kirby, B.J. (2010). "Micro- and Nanoscale Fluid Mechanics: Transport in Microfluidic Devices: Chapter 11:Species and Charge Transport" [www.Kirbyresearch.com/index.cfm/wrap/textbook/microfluidicsnanofluidicsch11.html](http://www.Kirbyresearch.com/index.cfm/wrap/textbook/microfluidicsnanofluidicsch11.html) retrieved on line December 22, 2015.
- Mendoza, RM. O., Kan, C-C., Dalida, ML. P., Wan, M-W. (2014). "Feasibility studies on arsenic removal from aqueous solutions by Electrodialysis." *J. Environmental Science and Health, Part A*. **49**, 545-554.
- Mohammadi T., Moheb A., Sadrzadeh M., Rasmi A. (2005). "Modelling of metal ion removal from waste water by electrodialysis." *Separation Purification Technology*, **41**, 73-82.
- Rahman, M.A., Hasegawa, H. (2011). "High levels of inorganic arsenic in rice in areas where arsenic-contaminated water is used for irrigation and cooking." *Science of Total Environment*,**409** (22), 4645-4655.
- Sadrzadeh, M., Rami A., Mohammadi, T., (2007). "Separation of different ions from Waste water at various operating conditions using electrodialysis." *Desalination*. **54**,147-156.
- Zourmand, Z., Faridirad, F., Kasiri, N., Mohammadi, T. (2015). "Mass transfer modelling of desalination through and electrodiaysis cell." *Desalination*. **359**, 41-51.

**ANAEROBIC BIODEGRADATION OF PARA-TOLUENE SULFONIC ACID, SULFANILIC ACID AND THIOPHENE-2-ACETIC ACID BY THE SULFATE REDUCING BACTERIUM *DESULFOVIBRIO PSYCHROTOLERANS*, STRAIN JS1<sup>T</sup> IN LIQUID CULTURES, SOIL AND SLUDGE MICROCOSMS**

<sup>1</sup>Sasi Jyothsna, T.S. <sup>1</sup>Sasikala, Ch.\* and <sup>2</sup>Ramana, Ch.V.

<sup>1</sup>Bacterial Discovery laboratory, Centre for Environment, Institute for Science & Technology, Jawaharlal Nehru Technological University Hyderabad, Hyderabad-500086, India

<sup>2</sup>Department of Plant Sciences, School of Life Science, University of Hyderabad, Hyderabad-500046, India

\*E-mail: sasi449@yahoo.ie; sasikala.ch@gmail.com

**ABSTRACT:** A sulphate reducing bacterium *Desulfovibrio psychrotolerans*, strain JS1<sup>T</sup> could biodegrade three aromatic sulphur compounds namely p-toulene sulfonic acid (PTSA), Sulfanilic acid (SFA) and Thiophene – 2 – acetic acid (TPA) when provided as sole source of carbon under strict anaerobic conditions. The biodegradation of these compounds was studied using spectrophotometer and HPLC. The strain JS1<sup>T</sup> could grow in 25 mM and could tolerate (with feeble growth) up to 50 mM of all the three test compounds supplemented as sole carbon source however, optimum growth was at 3 or 4 mM concentration. Though none of the tested compounds were completely metabolised within the experimental period of three months, PTSA was degraded up to 82%, SFA up to 65.5% and TPA was degraded up to 72% in liquid culture. The soil and sludge microcosm studies conducted with a) the pure culture of strain JS1<sup>T</sup> alone and b) Strain JS1<sup>T</sup> along with native microbiota (as consortium) revealed that strain JS1<sup>T</sup> could degrade the test compounds more efficiently as pure culture when compared to that with its consortium. The role of native microorganisms in degradation of these compounds was insignificant. The biodegradation of PTSA and TPA was significantly reduced in sludge microcosm when compared to that in soil while, SFA degradation was similar in both soil and sludge microcosms the reasons for which are unknown. A 66%, 38% degradation of PTSA, 65%, 64% degradation of SFA and 72%, 31% degradation of TPA was noted in soil microcosm and in sludge microcosm respectively by the pure culture of JS1<sup>T</sup>. The present work in laboratory scale is a preliminary study conducted at ambient, natural conditions of soils and sludge which thus indicated the potential of *D. psychrotolerans*, strain JS1<sup>T</sup> for biodegradation of contaminated soils and sludge, which could be potentially useful in bioremediation of contaminated soils.

**Key words:** Anaerobic biodegradation, Aromatic sulphur compounds, Microcosm studies, Sulfate reducing bacteria, *Desulfovibrio psychrotolerans*, para- toluene sulfonic acid, Sulfanilic acid, thiophene-2-acetic acid.

**Abbreviations:**SRB = Sulfate Reducing Bacteria, PTSA = para-Toluene Sulfonic Acid, SFA = Sulfanilic Acid, TPA = Thiophene-2-acetic acid.

## INTRODUCTION

Aromatic compounds form the second largest group of organic compounds in nature after carbohydrates (Shinoda *et. al.*, 2005). Hazardous aromatic compounds get into the environment in the form of diverse detergents, with oil spills, sewage from petroleum refineries and chemical plants, and with municipal waste waters. Many environments are anoxic or rapidly become anoxic due to contamination with carbon rich compounds like wastes from industrial effluents, gasoline, crude oil etc. Removal of such

recalcitrant compounds becomes important as these potentially hazardous molecules may enter into drinking water supplies (El-Ashtoukhy *et al.* 2013).

As a major part of natural environment has little or no access to atmospheric oxygen, anaerobic microbes hold a major role in the processing of the nutrient cycles in nature and also in waste treatment plants where the aerobic processes may not completely remove aromatic compounds, turning researchers' interest to the study of the anaerobic metabolism of these compounds (Harwood *et al.*, 1999). In this regard, sulfate reducing bacteria (SRB) have been extensively recognized and studied due to their ubiquitous distribution and capability in anaerobic biodegradation and biotransformation of a number of environmental pollutants under sulfate reducing conditions (Ensle and Suflita, 1995).

The aim of the present investigation was to study the ability of a sulfate reducing bacterium, *Desulfovibrio psychrotolerans*, strain JS1<sup>T</sup> (Jyothsna *et al.*, 2008) to degrade three aromatic sulfur compounds namely para-toluene sulfonic acid (PTSA), sulfanilic acid (SFA) and thiophene-2-acetic acid (TPA) under strict anaerobic conditions. These pollutants enter into environment through effluents from textile, dye and chemical industries and petroleum products. The aerobic degradation pathway of toluene was demonstrated in *Pseudomonas testosterone* (Locher *et al.*, 1989). A 40% degradation of sulfanilic acid under aerobic conditions by fungal strains *Phanerocheate chrysosporium* (Paszezynski *et al.*, 1992) and *Aspergillus niger* RH19 (Faryal, 2006) were demonstrated. *Sphingomonas subartica* strain was reported to utilize sulfanilic acid as sole carbon, nitrogen and sulfur source indicating its degradation by the strain (Perei *et al.*, 2001). Aerobic microbiological conversion of thiophenes has been studied extensively (Kobayashi *et al.*, 2001; Hirasawa *et al.*, 2001). However, very little information is available concerning the anaerobic conversion of these aromatic sulfur compounds.

Microcosm studies were conducted in sludge and soil microcosms to understand the degradation of test compounds under the influence of environmental and other biological interferences.. The present study demonstrating the degradation of aromatic sulfur compounds by *D. psychrotolerans*, JS1<sup>T</sup> in liquid culture and in microcosms is the first such study of degradation, by any pure culture of SRB under obligately anaerobic conditions.

## MATERIALS AND METHODS

**Growth Medium for Degradation Studies.** The pure culture of *D. psychrotolerans* strain JS1<sup>T</sup> was grown in Postgate's B medium (PBM) (Postgate, 1984) consisting of (gL<sup>-1</sup>) KH<sub>2</sub>PO<sub>4</sub>.7H<sub>2</sub>O, 0.5; NH<sub>4</sub>Cl, 1.0; Na<sub>2</sub>SO<sub>4</sub>, 4.5; CaCl<sub>2</sub>.2H<sub>2</sub>O, 0.06, MgSO<sub>4</sub>.7H<sub>2</sub>O, 2.0, Yeast extract, 1.0, FeSO<sub>4</sub>.7H<sub>2</sub>O, 0.004, Sodium citrate, 0.3, Sodium Lactate, 3.5, Sodium ascorbate solution (1M), 1 ml and Na<sub>2</sub>S.9H<sub>2</sub>O solution (1M), 1ml. A one percent (v/v) inoculum of pure culture of strain JS1<sup>T</sup> washed twice in sterile saline, centrifuged and the culture pellet was inoculated into Postgate's B medium with the aromatic sulfur test compounds namely, para-toluene sulfonic acid [PTSA], Sulfanilic acid [SFA] and Thiophene 2-Acetic acid [TPA] supplemented as either sole source of carbon (3mM) replacing lactic acid or electron acceptor (0.5mM) replacing FeSO<sub>4</sub> respectively in 7.5 ml screw capped tubes incubated at 30±2°C. The culture was frequently sub cultured in the same medium and used for the biodegradation studies.

Turbidometry was used to monitor the growth of *D. psychrotolerans*, strain JS1<sup>T</sup>. Increase in optical density (OD) (turbidity) was measured for every 24 h starting from time 0 h, up to 96 h. Optical density of the bacterial suspension was directly measured in a Systronics make (model 112) colorimeter at 540 nm (filter 7) against un-inoculated medium blank.

**Maximum Biodegradability and Biosorption Test.** Different concentrations of the test compounds (i.e. 0, 1, 2, 3, 4, 5, 10, 25 and 50 mM) were supplemented as sole carbon source replacing lactic acid. Growth as increase in optical density was measured colorimetrically at 24 h interval starting from time 0 h (i.e., 0, 24,48,72,96 and 120 h). For reading the degradation of the test compounds, two ml of the liquid culture was taken in 2.0 ml eppendorf tube, centrifuged at 8000 rpm for 15 minutes, 0.5 ml of the culture supernatant was diluted 10 times with deionized water. The diluted sample was measured for absorbance at the λ maxima of 229nm for PTSA, 280nm for SFA and TPA on a Spectron Genesys 2 Spectrophotometer.

Cells were simultaneously observed under phase contrast light microscope (Olympus BH-2) for viability from each test sample.

In order to see whether the aromatic sulfur compounds PTSA, SFA and TPA under test were being adsorbed or truly utilized by the strain JS1<sup>T</sup>, live and dead (heat killed) culture/biomass of strain JS1<sup>T</sup> were separately inoculated into Postgate's B medium supplemented with 3mM of the test compound as sole carbon source and incubated at 30±2°C. Growth in terms of increase in OD was measured colorimetrically and concentrations of each of the test compounds were estimated by U.V. absorption at their respective absorption maxima of the test compounds.

**HPLC Analysis for Biodegradation of Test Compound.** The HPLC analysis of aromatic sulfur test compounds, PTSA, SFA and TPA in culture supernatants was performed at room temperature using a Shimadzu SPD-10AVP isocratic system. Luna 5µ C<sub>18</sub> (2) 100A column (250 x 4.6 mm) was used for the detection of metabolites in a UV-VIS detector. SFA and PTSA were detected in a solvent system containing methanol:Potassium Phosphate buffer 0.05M at pH 6.5 (40:60) at 1.0 ml.min<sup>-1</sup> flow rate with the detection done at 280nm, PTSA was detected in a solvent system containing methanol:water (40:60) at 1.0 ml.min<sup>-1</sup> flow rate with the detection done at 229nm. The retention times (T<sub>R</sub> in minutes) of SFA, PTSA and TPA were 2.6, 3.2 and 3.4 respectively in their specific solvent systems and flow rates as mentioned above.

The degradation/disappearance of three aromatic sulfur compounds PTSA, SFA and TPA by the strain JS1<sup>T</sup> was determined though HPLC at regular intervals from 0 hr, up to 15 days of incubation. Three months (90 days) old inoculated sample was also analyzed for each test compound.

**Soil and Sludge Microcosm Studies for Biodegradation.** The microcosm studies were carried out in soil collected from JNTU (Jawaharlal Nehru Technological University Hyderabad) campus and anaerobic sludge collected from the sedimentation tank of JETL (Jeedimetla Effluent Treatment Limited), Hyderabad. The sludge used in this experiment had a pH of 7.58, EC (Electrical conductivity) of 16.42 µSeimens, alkalinity of 440 mg/l, COD of 4200 mg/l (for 10 times diluted sample), TDS (Total Dissolved Solids) of 4308 mg/l. These parameters were analyzed according to the methods suggested in the standard methods for determination of water and waste water. The soil used had a pH of 7.2. The carbon, nitrogen, hydrogen and sulfur content in the soil were analyzed by Elementar make CHNS analyzer comprising Vario Micro software. The soil contained 1.8% organic carbon, 0.2% hydrogen, 0.4% nitrogen and 0.02% sulfur and had a pH of 8.2.

The strain JS1<sup>T</sup> grown in PBM supplemented with 3 mM of the test compound as sole source of carbon, was centrifuged and the cell pellet was suspended in the PBM without any carbon source. This was used as inoculum in the soil and sludge microcosms spiked with the test compound. Microcosms were carried out in test tubes (25 X 150 mm) with 20g soil and/or 20 ml sludge spiked with one aromatic sulfur test compound in each at 3 mM concentration supplemented with 2 ml PBM without any carbon source in two sets of tubes. One set was autoclaved which indicated the degradation of test compound by the inoculated strain JS1<sup>T</sup> alone and another set was left unautoclaved to assess the degradation of the test compound by the native microorganisms if any. Within the autoclaved and unautoclaved sets of tubes, one set was inoculated with 2 ml of the strain JS1<sup>T</sup> and another was left uninoculated. The culture was thoroughly mixed with the soil and sludge and closed with rubber seal and flushed with Argon gas to maintain anaerobic conditions and incubated at 28 ± 2°C for 20 days. Soil and sludge samples (1g and/or 1ml) were drawn and analyzed for concentrations of each test compound at 5 days intervals.

For extraction of PTSA, SFA and TPA from soil and for sludge, 1g of soil or sludge was suspended in 10ml of deionized water and vortexed thoroughly followed by centrifugation at 10000 rpm for 10 min. The supernatant was extracted and diluted 10 times (10 µl supernatant in 90 µl milli Q water) and was analyzed by HPLC as mentioned in the previous segment.

## RESULTS

**Growth of JS1<sup>T</sup> on Aromatic Sulphur Compounds.** The strain JS1<sup>T</sup> grew in all media with the tested aromatic sulphur compounds with a gradual increase in growth within the tested period of 10 days.. Growth in terms of OD at 540 nm was maximum (1.98) in positive control where PBM (with 3 mM lactate as carbon source and 0.5 mM FeSO<sub>4</sub> as electron acceptor) was used and the growth was minimum (0.1 & 0.3) where PBM without any carbon or electron acceptor source was used respectively. The three test compounds were better utilized as carbon source (CS) rather than electron acceptor (EA) by the strain JS1<sup>T</sup> as evident from the result measured in terms of OD at 540 nm after 10 days of incubation as PTSA-CS (1.64) > TPA-CS (1.54) > SFA-CS (1.38) > PTSA-EA (0.97) > SFA-EA (0.90) > TPA-EA (0.63) (Fig. 1). Further experiments were carried out by supplementing these test compounds as sole carbon source.

The effect of increasing concentrations (from 0 mM to 50 mM) of each of the three aromatic sulfur test compounds, i.e., PTSA, SFA and TPA when given as sole carbon source on the growth of strain JS1<sup>T</sup> within a time course of 5 days showed that the strain JS1<sup>T</sup> grew optimally in all three test compounds at 3 or 4 mM concentration. Growth was feeble at and above 25 mM concentration of PTSA, while the strain could tolerate up to 50 mM concentration of SFA and TPA (Fig. 2).

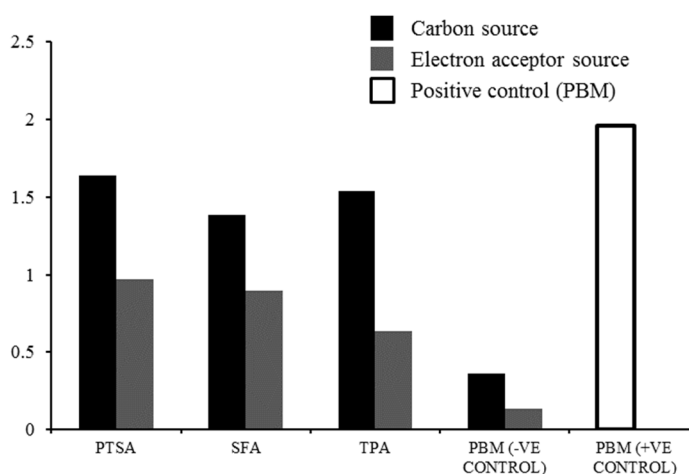
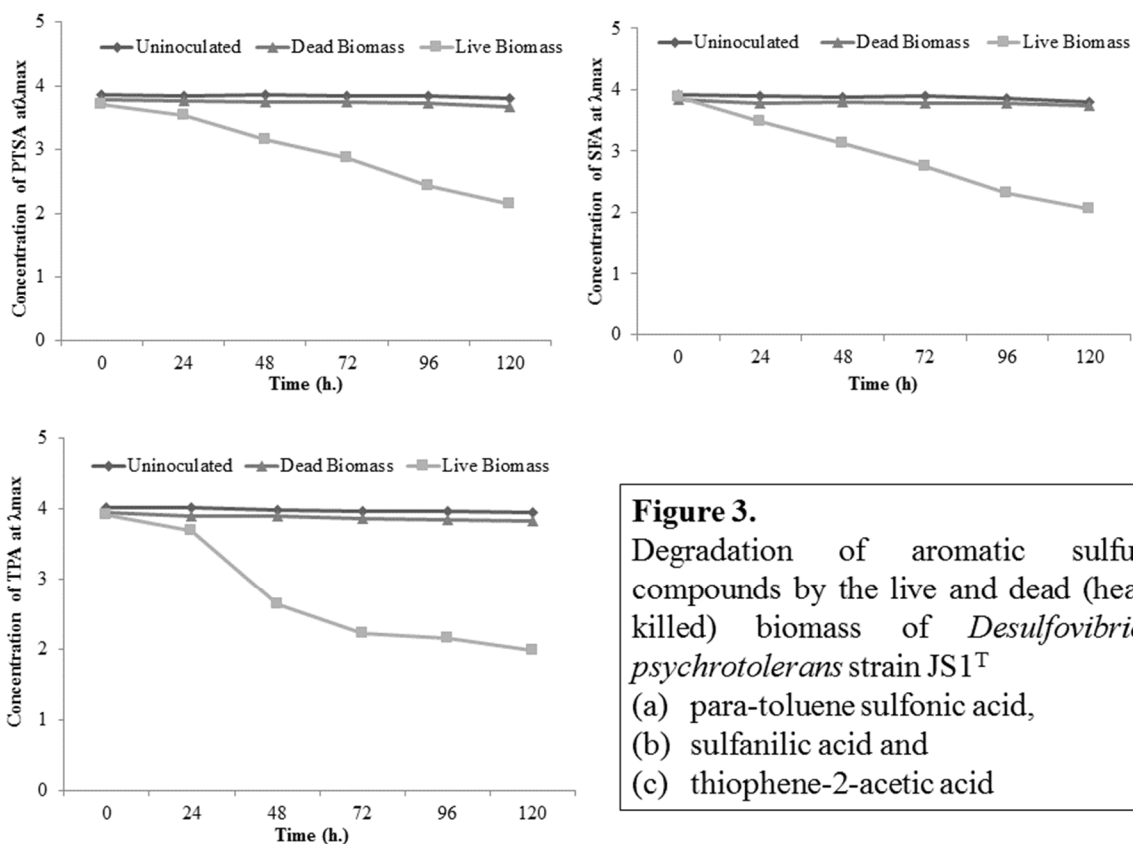
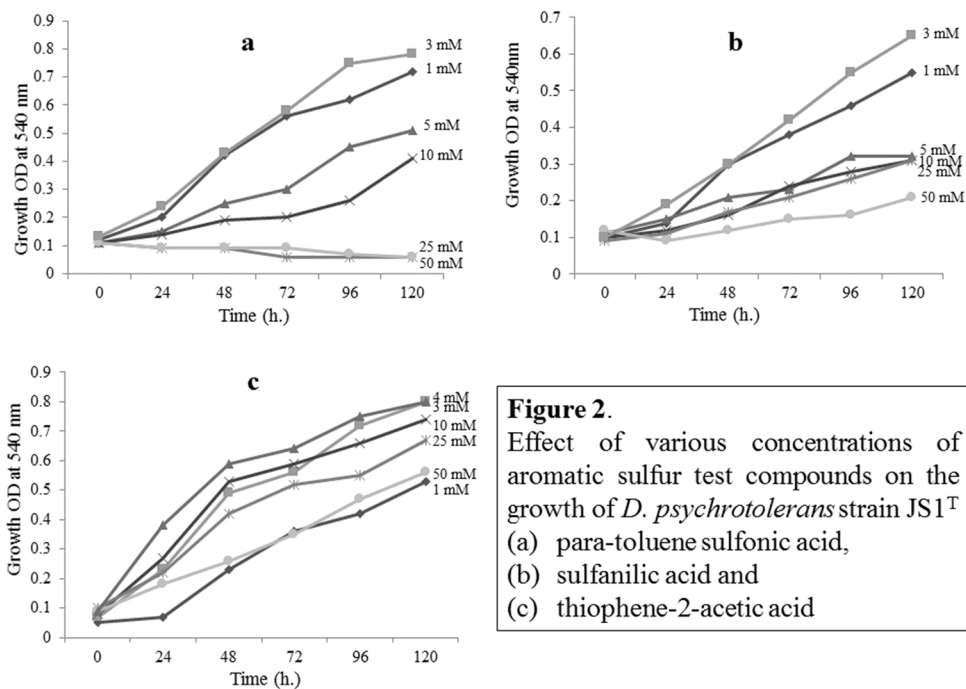


**Figure 1.** Growth of *Desulfovibrio psychrotolerans* strain JS1<sup>T</sup> on the three aromatic sulfur compounds supplemented as either sole carbon source or electron acceptor source with reference to the positive and negative controls

### Degradation of Aromatic Sulfur Compounds by Live and Dead Biomass of Strain JS1<sup>T</sup>

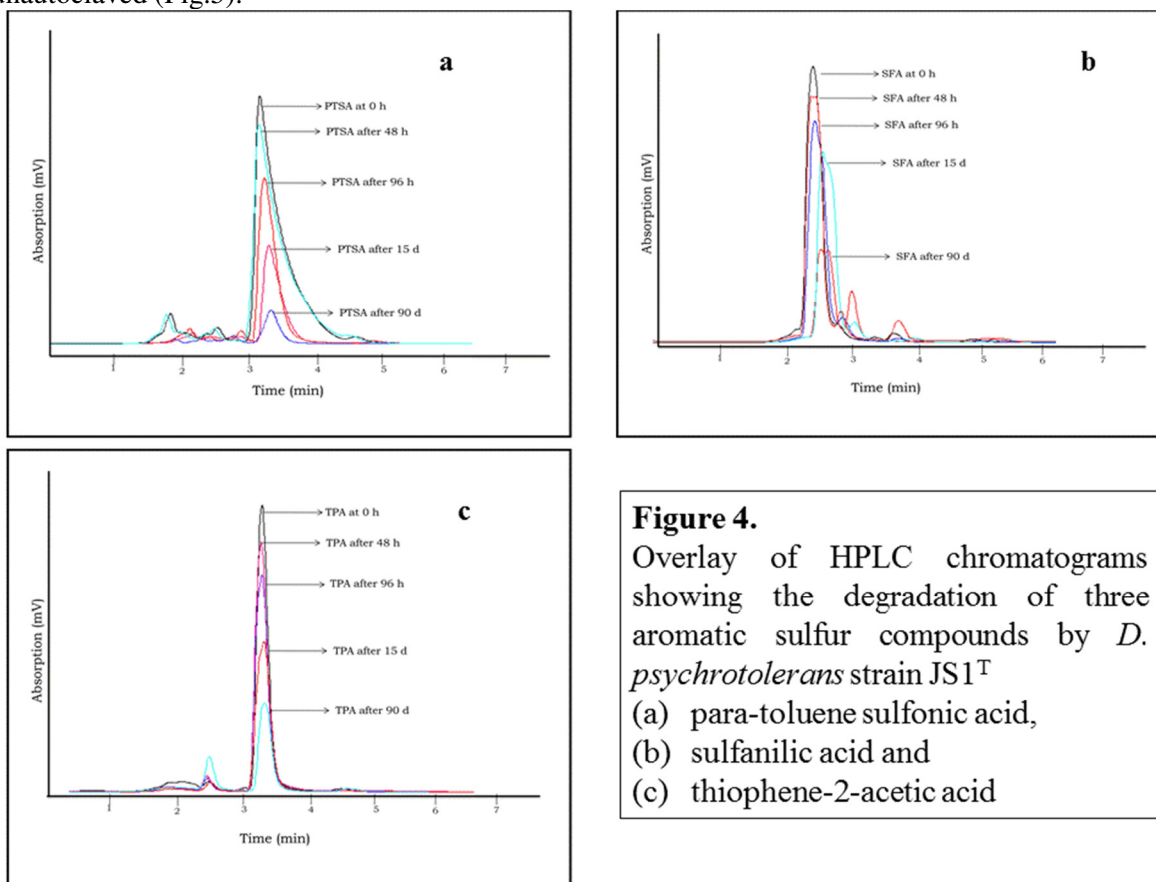
In the experiment conducted with live and dead biomass of JS1<sup>T</sup> to understand the loss of each test compound in the course of degradation, due to passive adsorption, if any, it was observed that the compound adsorbed was ignorable in all the three cases. There was no decrease in concentration of the test compounds inoculated with dead biomass of JS1<sup>T</sup> until 5 days of observation. Among the three test compounds, 42% of PTSA (Fig. 3-a), 47% of SFA (Fig. 3-b) and 49% of TPA (Fig. 3-c) were degraded after 5 days of incubation by the strain. None of the tested compounds were completely degraded by strain JS1<sup>T</sup> within 5 days of incubation. The compounds PTSA and SFA were gradually degraded up to day 5 while the degradation of TPA was rapid up to day 2 after inoculation and then the degradation slowed down gradually till the end of day 5 (Fig. 3).



**HPLC Determination of Degradation of Aromatic Sulfur Compounds.** The HPLC analysis of degradation of the aromatic sulfur test compounds by the strain JS1<sup>T</sup> showed a decrease of PTSA by 13%,

34% and 60% after 2, 4 and 15 days of incubation respectively and a maximum decrease of 83% after 90 days of incubation. Neither additional peaks nor peak shift was observed up to 15 minutes of run of the test compound in HPLC (Fig. 4-a). A decrease in concentration of SFA by 10%, 20% and 33% after 2, 4 and 15 days of incubation respectively and a maximum decrease of 75% were observed after 90 days of incubation. The decrease in the SFA peak ( $T_R$  2.6) was associated with an increase in an unknown peak ( $T_R$  3.0). But the increase in the unknown peak was not proportional to the decreasing SFA peak (Fig. 4-b). A decrease in concentration of TPA was observed by 11%, 23% and 47% after 2, 4 and 15 days of incubation respectively and a maximum decrease of 68% was observed after 90 days of incubation. The decrease in the TPA peak ( $T_R$  3.4) was associated with an increase in an unknown peak ( $T_R$  2.6). But the increase in the unknown peak was not proportional to the decrease in TPA peak (Fig.4-c). None of the test compounds were degraded completely within the tested period of three months.

**Sludge and Soil Microcosm Studies on Degradation of The Selected Aromatic Sulfur Compounds by *Desulfovibrio psychrotolerans*, JS1<sup>T</sup>.** The degradation of aromatic sulfur compounds in sludge microcosms due to the individual and combined activities of *D. psychrotolerans*, JS1<sup>T</sup> and the native microorganisms (if any, present in the sludge sample) analyzed through HPLC observed after 10 days of incubation revealed a degradation of PTSA up to 38% by strain JS1<sup>T</sup> alone (Fig. 5-1a) and up to 47% by the combined activity of JS1<sup>T</sup> and native microbes of the sludge (Fig. 5-1b). SFA was degraded up to 64% by strain JS1<sup>T</sup> alone (Fig. 5-2a) and 58% by the combined activity of JS1<sup>T</sup> and native microbes of the sludge (Fig. 5-2b). TPA was degraded up to 31% by strain JS1<sup>T</sup> alone (Fig. 5-3a) and 48% degradation was observed by the combined activity of JS1<sup>T</sup> and native microbes of the sludge (Fig. 5-3b). However, no significant decrease in concentrations of PTSA, SFA and TPA was observed in uninoculated sludge samples either autoclaved or unautoclaved (Fig.5).



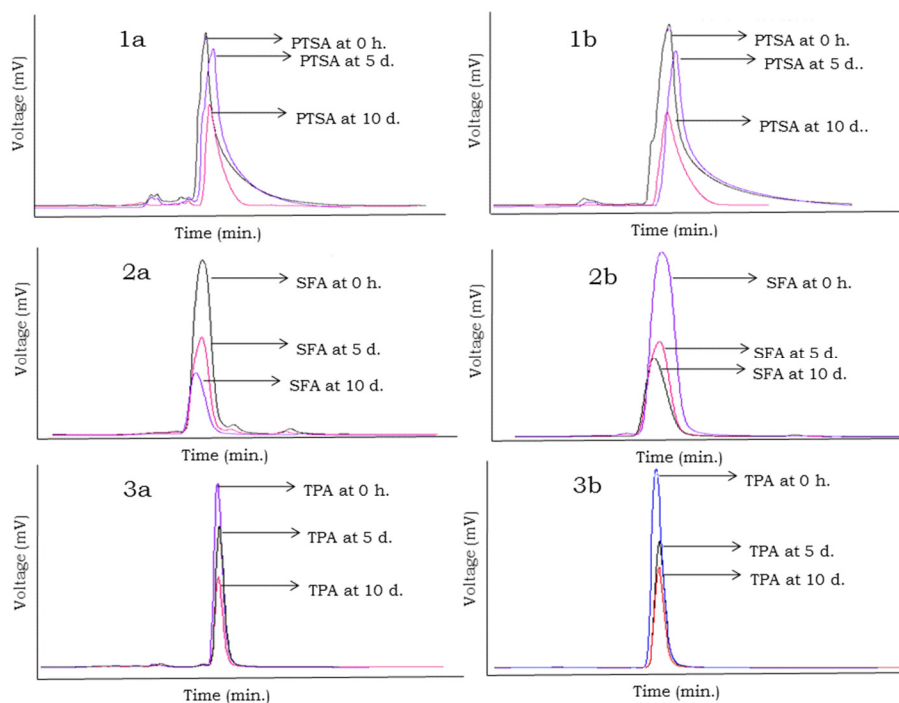


**Figure 5. Overlay of HPLC chromatograms showing the degradation of the three aromatic sulfur test compounds by *Desulfovibrio psychrotolerans* strain JS1<sup>T</sup> in sludge microcosms.**

- (a) = autoclaved sludge inoculated with 2 ml log phase culture of JS1<sup>T</sup>  
 (b) = un-autoclaved sludge inoculated with 2 ml log phase culture of JS1<sup>T</sup>

Similarly, the degradation of aromatic sulfur compounds in soil microcosms revealed a PTSA degradation of up to 66% by strain JS1<sup>T</sup> alone (Fig. 6-1a) and 63% degradation by the consortium of JS1<sup>T</sup> and native microbes of the soil (Fig. 6-1b). SFA was degraded up to 65% by strain JS1<sup>T</sup> alone (Fig. 6-2a) and 40% degradation was observed by the consortium of JS1<sup>T</sup> and native microbes of the soil (Fig. 6-2b). TPA was degraded up to 72% by strain JS1<sup>T</sup> alone (Fig. 6-3a) while only 30% degradation was observed by the consortium of JS1<sup>T</sup> and native microbes of the soil (Fig. 6-3b). However, no significant decrease in concentrations of PTSA, SFA and TPA was observed in uninoculated soil samples either autoclaved or unautoclaved (Fig. 6).

## DISCUSSION

Sulfate reducing bacteria are phylogenetically and physiologically diverse group of bacteria, characterized by their versatile metabolic capabilities to use various electron acceptors and donors (Widdel, 1998). They are generally considered as the terminal oxidizers in the natural recycling of organic compounds to CO<sub>2</sub> in anoxic environments. Due to these exceptional capabilities, SRB are studied and applied in various bio-degradative tasks under anoxic regions (Widdel, 2007). In the present study, three test compounds were selected for biodegradation studies, namely para-toluene sulfonic acid (PTSA), sulfanilic acid (SFA) and thiophene-2-acetic acid (TPA). These pollutants enter into environment through effluents from textile, dye and chemical industries and petroleum products. These compounds were used as sole sulfur source or as sole carbon/electron donor source in many previous reports (Locher *et al.*, 1993; Yemashova, *et al.*, 2004 and Yamada *et al.*, 2001).

In the present study, the biodegradability of these compounds by strain JS1<sup>T</sup> was tested by supplementing them as either sole carbon source and/or sole electron acceptor. Shcherbakova *et al.*, (2003) reported that a sulfate reducing strain *Desulfovibrio* sp. SR1 utilized PTSA as an electron acceptor. PTSA and SFA have reducible sulfur moiety in the chemical structure, and hence can also serve as electron



acceptor in addition to being utilized as carbon source. TPA on the other hand was reported to undergo degradation in soil under oxygen limiting conditions when no other external electron acceptor was added (Anjana and Pranav, 2006) and dibenzothiophene served as an electron acceptor in anaerobic respiration in a report by Annweiler *et. al.*, (2001). Hence the degradation of TPA was also tested in the absence of any electron acceptor.

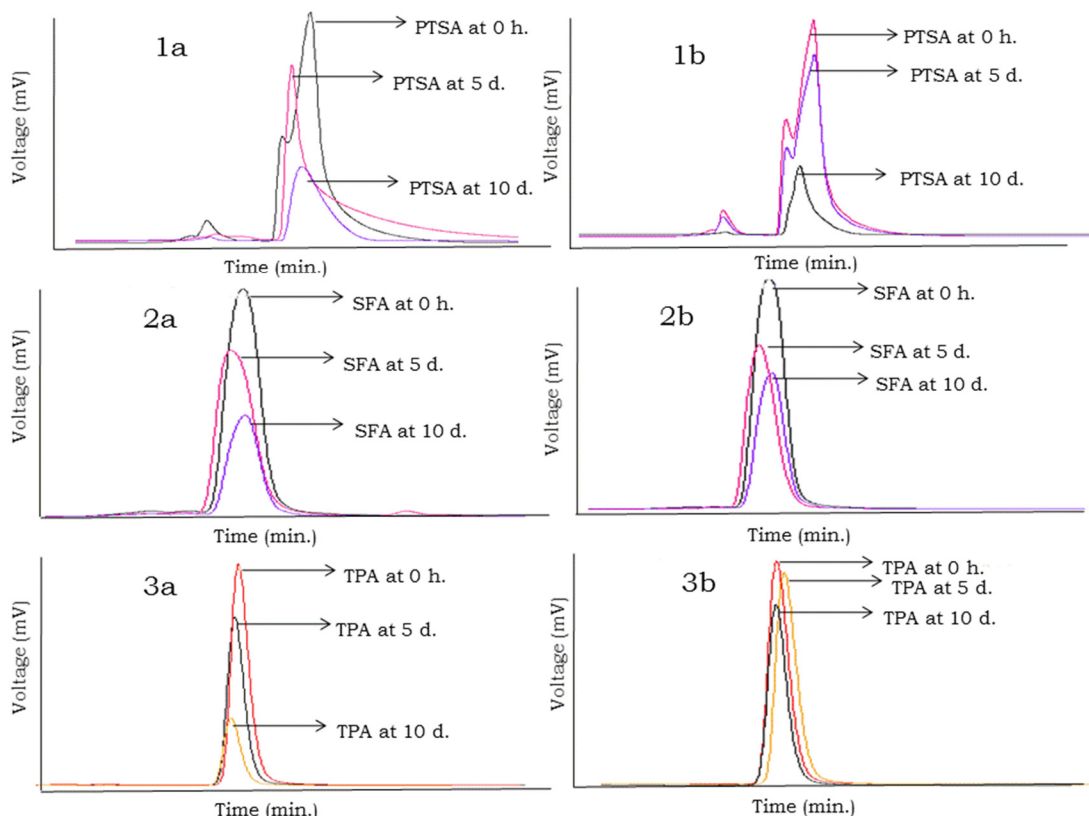


**Figure 6. Overlay of HPLC chromatograms showing the degradation of the three aromatic sulfur test compounds by *Desulfovibrio psychrotolerans* strain JS1<sup>T</sup> in soil microcosms**

(a)= autoclaved soil inoculated with 2 ml log phase culture of JS1<sup>T</sup>

(b)= un-autoclaved soil inoculated with 2 ml log phase culture of JS1<sup>T</sup>

*Desulfovibrio psychrotolerans*, JS1<sup>T</sup> was selected as the test organism for studying the degradation of aromatic sulfur compounds, as this was the only bacterium among 5 cultures tested, that could grow in a medium supplemented with the test compounds. Our efforts to enrich SRB degrading these compounds from 20 different environmental samples also were not successful (data not shown). The *D. psychrotolerans*, JS1<sup>T</sup> could grow in medium with the aromatic sulfur compounds supplemented as either sole carbon source or as sole electron acceptor. But as the strain JS1<sup>T</sup> could grow well in medium with these compounds supplemented as sole carbon source further degradation studies were conducted with the test compounds as carbon supplements. This result also supports the earlier report that aromatic compounds are metabolized by SRB much efficiently when they are supplemented as sole carbon source (Harms, 1993).

Hulshoff Pol, (1998) has reported that many SRB are quite resistant to overloads of certain organic compounds and to toxic upsets from aromatic compounds like alkanes, ethylbenzene, toluene, chloroform and other long chain fatty acids and can dominate in growth by competing with other anaerobic bacteria. A

similar observation was made with respect to the tolerance of the test compounds by strain JS1<sup>T</sup>. The *D. psychrotolerans*, JS1<sup>T</sup> was not sensitive to even very high concentrations of the test compounds. PTSA was tolerated up to a concentration of 25 mM while SFA and TPA were tolerated even up to the highest concentration of 50 mM tested compound. However, optimum growth was observed when the aromatic sulfur compounds were supplemented as sole carbon sources within a concentration of 3 and 4 mM. The pattern of degradation of the test compounds by *D. psychrotolerans*, JS1<sup>T</sup> was similar to that of its growth on these compounds.

A few SRB have been reported to adsorb certain metals and pollutants especially in activated sludge. (Byrns, 2001 and Machemer, 1992). Hence, it was essential to understand whether disappearance of the compound observed in the presence of *D. psychrotolerans*, JS1<sup>T</sup> was due to the biodegradation or simple passive adsorption. It was concluded that passive adsorption did not play a significant role since there was no significant loss (<5% loss) in the concentration of the compounds when inoculated with dead biomass (heat killed), while there was rapid decrease in their concentration when inoculated with live biomass within 5 days of incubation.

Though there are no reports of degradation of aromatic sulfur compounds by any SRB, *Desulfobacula toluolica* and *Desulfobacula phenolica* (Rabus *et al.*, 1993), *Desulfosarcina cetonica* (Harms *et al.*, 1999) have been demonstrated to degrade toluene completely to CO<sub>2</sub>. The mixed cultures of SRB and other methanogenic bacteria were reported to degrade toluene. Degradation of PTSA under anaerobic conditions by mixed cultures was reported by Shcherbakova *et al.*, (2003). Also, anaerobic degradation of dibenzothiophene (Yamada *et al.*, 2001) and anaerobic desulfurization of benzothiophene and dibenzothiophene (Marcelis, 2003) have been reported in mixed cultures of SRB earlier, no reports exist on the anaerobic degradation of either PTSA, SFA or TPA by pure cultures of SRB. Hence, the present study on degradation of aromatic sulfur compounds by *D. psychrotolerans*, JS1<sup>T</sup> is the first such study of degradation by any pure culture of SRB. However, none of the aromatic sulfur compounds were completely degraded within the experimental period of three months (PTSA was degraded by 82%, SFA by 65.5% and TPA by 72%).

In general, laboratory studies are not accurate predictors of field degradation rates (Di *et al.*, 1998). Bioremediation via environmental introduction of degradative microorganisms requires that microbes survive in substantial numbers and effect an increase in the rate and extent of pollutant removal in these natural habitats (Krumme *et al.*, 1994). Measuring biodegradative activity and efficiency of the selected microbes in natural habitats is difficult due to limited accessibility of samples as well as sorption and abiotic transformation of contaminants (Margesin and Schinner, 1997). Due to these reasons, microcosm studies are generally used to understand these important parameters before switching on to on-site studies.

Microcosm studies are also known as the biofeasibility studies. Microcosms are artificial, simplified ecosystems that are used to simulate and predict the behaviour of natural ecosystems under controlled conditions (Kassen, *et al.*, 2000). These studies are useful in understanding the effect caused due to a pollutant or to determine the role of microbes in eliminating or reducing the effect of these pollutants in natural systems. The microcosm studies of degradation of pollutants by SRB conducted till now have mainly concentrated on degradation by mixed populations. An example is the degradation of toluene by SRB in oil contaminated soils (Noh *et al.*, 2003).

In the present study the degradation of aromatic sulfur compounds and their subsequent degradation by pure culture of *D. psychrotolerans*, JS1<sup>T</sup> was carried out in both soil and sludge microcosms that mimic the naturally existing environments of contaminants. *D. psychrotolerans* JS1<sup>T</sup> was employed independently (in sterile soil and/or sludge) and also in consortium with the native microbiota (unsterile soil and/or sludge) inhabiting the soil and sludge samples. The viability of spiked pure culture of strain JS1<sup>T</sup> in soil and sludge microcosm could be checked by streaking the spiked samples on to PBM at regular time intervals during the experiment and observing for the pure colonies of the strain JS1<sup>T</sup>.

The role of native microbiota alone in the degradation of the test compounds was insignificant as observed in the unsterile and uninoculated microcosms of soil and sludge spiked with the aromatic sulfur compounds. PTSA was degraded by strain JS1<sup>T</sup> much efficiently in soil microcosm (66%) than in sludge microcosm (38%). Degradation of PTSA by indigenous soil and sludge microbiota in consortium with JS1<sup>T</sup>

was not very significant, but a slight increase of degradation to 47% (from 38%) in sludge and a slight decrease of degradation to 63% (from 66%) in soil were observed. The degradation of SFA by pure culture of JS1<sup>T</sup> was almost similar in sludge and soil microcosms (64 and 65% respectively) but the degradation in consortium with soil and sludge microflora was lowered to 58% (from 64%) in sludge and 40% (from 65%) in soil microcosms respectively. The degradation of TPA was the least in sludge microcosm (31%) while the highest in soil microcosm (72%). There was a significant decrease in degradation to 30% (from 72%) due to contribution of soil consortia and an increase to 48% (from 30%) due to contribution of sludge consortia.

The present work in lab scale is a preliminary study conducted at ambient conditions (pH, temperature, nutritional conditions etc.) of naturally occurring soils and sludge and thus indicates the potential of *D. psychrotolerans*, JS1<sup>T</sup> for bioremediation of contaminated soils and sludge.

## SUPPLEMENTARY

The cultures were grown in Postgate's B medium (PBM) supplemented with the aromatic sulfur compound para-toluene sulfonic acid (PTSA) or Sulfanilic acid (SFA) or Thiophene-2-acetic acid (TPA) as sole source of carbon (\*CS) at 3mM concentration or electron acceptor (+EA) at 0.5 mM concentration. NH<sub>4</sub>Cl (0.1% w/v) was used as nitrogen source and yeast extract (0.05% w/v) as a source of growth factor(s).

S. No	Sulfate reducing bacteria used	Growth with PTSA		Growth with SFA		Growth with TPA	
		*CS	+EA	CS	EA	CS	EA
1	<i>Desulfovibrio psychrotolerans</i> JS1 <sup>T</sup>	+	+	+	+	+	+
2	<i>Desulfotomaculum ruminis</i> JS3	-	-	-	-	-	-
3	<i>Desulfovibrio dechloracetivorans</i> JS4	-	-	-	-	-	-
4	<i>Desulfovibrio marinisediminis</i> JS8	-	-	-	-	-	-
5	<i>Desulfovibrio carbinoliphilus</i> JS11	-	-	-	-	-	-

**Supplementary Table 1:** Utilization of aromatic sulfur compounds by Sulfate reducing bacteria

## REFERENCES

- Anjana, D. and Pranav, V. (2006). Petroleum and hydrocarbon microbiology. In Applied Microbiology. 12-22.
- Annweiler, E., Michaelis, W. and Meckenstock, R.U. (2001). Anaerobic cometabolic conversion of benzothiophene by a sulfate reducing enrichment culture and in a tar-oil contaminated aquifer. Appl. Environ. Microbiol. 67: 5077-5083.
- Byrns, G. (2001). The fate of xenobiotic organic compounds in wastewater treatment plants. Water Res. 35: 2523-2533.
- Di, H.J., Aylmore, L.A.G., and Kookana, R.S. (1998). Degradation rates of eight pesticides in surface and subsurface soils under laboratory and field conditions, Soil Science, 163: 404-411.

- El-Ashtoukhy SZ, El-Taweel YA, Abdelwahab O, Nassef EM (2013)** Treatment of petrochemical wastewater containing phenolic compounds by electrocoagulation using a fixed bed electrochemical reactor. *Int J Electrochem Sci* 8:1534–1550
- Ensley, B.D. and Suffita, J.M. (1995).** Metabolism of contaminants by mixed and pure cultures of sulfate-reducing bacteria. In: Larry, L. Barton., Tony Atkinson and Roger, F. Sherwood (eds.) *Biotechnology Handbooks-8. Sulfate Reducing Bacteria*. Plenum Press. New York. Pp. 294.
- Faryal, R., Ahmed, S and Hameed, A. (2006).** Biodegradation of 4-aminobenzene sulphonic acid by a local textile mill *Aspergillus niger* isolate Pak. J. Bot., 38: 1333-1340.
- Harms, G. (1999).** Anaerobic oxidation of *o*-xylene, *m*-xylene, and homologous alkylbenzenes by new types of sulfate-reducing bacteria. *Appl. Environ. Microbiol.* 65: 999–1004.
- Harwood, C.S., Burchhardt, G., Herrmann, H., and Fuchs, G. (1999).** Anaerobic Metabolism of Aromatic Compounds via the Benzoyl-CoA Pathway, *FEMS Microbiol. Rev.* 22: 439–458.
- Hirasawa, K., Ishii, Y., Kobayashi, M., Koizumi, K. and Maruhashi, K. (2001).** Improvement of desulphurisation activity in *Rhodococcus erythropolis* KA2-5-1 by genetic engineering. *Biosci. Biotechnol. Biochem.* 65: 239–246.
- Hulshoff Pol, L.W., Lens, P.N.L., Stams, A.J.M., and Lettinga, G. (1998). Anaerobic treatment of sulphate-rich wastewaters. *Biodegradation* 9: 213-224.
- Jyothsna, T.S.S., Sasikala, Ch. and Ramana, Ch.V. (2008).** *Desulfovibrio psychrotolerans* sp. nov., a psychrotolerant and moderately alkaliphilic sulfate-reducing deltaproteobacterium from the Himalayas. *Int. J. Syst. Evol. Microbiol.* 58: 821-825.
- Kassen, R., Buckling, A., Bell, G., Rainey and. Paul, B. (2000). Diversity peaks at intermediate productivity in a laboratory microcosm. *Nature* 406: 508–512.
- Kobayashi, M., Horiuchi, K., Yoshikawa, O., Hirasawa, K., Ishii, Y., Fujino, K., Sugiyama, H. and Maruhashi, K. (2001).** Kinetic analysis of microbial desulphurisation of model and light gas oil containing multiple alkyl dibenzothiophenes. *Biosci. Biotechnol. Biochem.* 65: 298–304.
- Krumme, M.L., Smith, R.L., Egestorff, J., Thiem, S.M., Tiedje, J.M., Timmis, K.N. and Dwyer, D.F. (1994).** Behaviour of pollutant-degrading microorganisms in aquifers: Predictions for genetically engineered organisms. *Environ. Sci. Technol.* 28: 1134-1138.
- Locher, H.H., Leisinger, T. and Cook, A.M. (1989).** Degradation of p-Toluenesulphonic Acid via Sidechain Oxidation, Desulphonation and *meta* Ring Cleavage in *Pseudomonas (Comamonas) testosteroni* T-2. *J. Gen. Microbiol.* 135: 1969-1978.
- Locher, H.H., Poolman, B., Cook, A.M. and Konings, W.N. (1993).** Uptake of 4-toluene sulfonate by *Comamonas testosteroni* T-2. *J. Bact.* 175: 1075-1080.
- Machemer, S.D. and Wildeman, T.R. (1992).** Adsorption compared with sulfide precipitation as metal removal processes from acid mine drainage in a constructed wetland. *J. Contaminant Hydrol.* 9: 115-131.
- Margesin, R. and Schinner, F. (1997).** Efficiency of indigenous and inoculated cold-adapted soil microorganisms for biodegradation of diesel oil in Alpine soils. *Appl. Environ. Microbiol.* 63: 2660-2664.
- Noh, S.L., Choi, J.M., An, Y.J., Park, S.S. and Cho, K.S. (2003). Anaerobic biodegradation of toluene coupled to sulfate reduction in oil-contaminated soils: optimum environmental conditions for field applications. *J. Environ. Sci. Health*, 38: 1087-97.
- Paszezynski, A., Pasti-Grigsby, M.B., Goszezynski, S., Crawford, R.L. and Crawford, D.L. (1992).** Mineralization of sulfonated azo dyes and sulfanic acid by *Phanerochaete chrysosporium* and *Streptomyces chromofuscus*. *Appl. Environ. Microbiol.* 58: 3598-3604.
- Perei, K., Rákhely, G., Kiss, I., Polyák, B. and Kovács, K.L. (2001).** Biodegradation of sulfanilic acid by *Pseudomonas paucimobilis*. *Appl Microbiol Biotechnol* 55: 101-107.
- Postgate, J.R. (1984).** *The sulphate-reducing bacteria*, 2<sup>nd</sup> ed. Cambridge University Press, Cambridge, England.

- Rabus, R., Nordhaus, R., Ludwig, W. and Widdel, F. (1993).** Complete oxidation of toluene under strictly anoxic conditions by a new sulfate-reducing bacterium. *Appl. Environ. Microbiol.* 59: 1444-1451.
- Shcherbakova, V.A., Chuvil'skaya, N.A., Golovchenko, N.P. Suzina, N.E., Lysenko, A.M. Laurinavichyus, K.S. and Akimenko, V.K. (2003).** Analysis of the Anaerobic Microbial Community Capable of Degrading *p*-Toluene sulfonate. *Microbiology.* 72: 666-671.
- Shinoda, Y., Akagi, J., Uchihashi, Y., Hiraishi, A., Yukawa, H., Yurimoto, H., Sakai, Y. and Kato, N. (2005).** Anaerobic degradation of aromatic compounds by *Magnetospirillum* strains, Isolation and degradation genes. *Biosci. Biotechnol. Biochem.* 69: 1483-1491.
- Widdel, F. (1998).** Microbiology and ecology of sulfate – and sulfur-reducing bacteria. *Biology of Anaerobic microorganisms.* A.J.B. Zehnder (ed.). John Wiley and Sons, Inc. New York. 469-585.
- Yamada, K.O., Morimoto, M. and Tani, Y. (2001).** Degradation of dibenzothiophene by sulfate reducing bacteria cultured in presence of only Nitrogen gas. *J. Biosci. Bioengineer.* 91: 91-93.
- Yamashova, N., Telegina, A., Kotova, I., Netrusov, A. and Kalyuzhnyi, S. (2004).** Decolorization and partial degradation of selected azo dyes by methanogenic sludge. *Appl. Biochem. Biotechnol.* 119: 31-40.

## RELATION AMONG TRIPHENYL TIN RECOGNITION, DEGRADATION, ION METABOLISM AND EFFECTIVE PROTEINS OF *BACILLUS THURINGIENSIS*

Jinshao Ye and Linlin Wang

(School of Environment, Jinan University, Guangzhou 510632, Guangdong, China; Joint Genome Institute, Lawrence Berkeley National Laboratory, Walnut Creek 94598, CA, USA)

**ABSTRACT:** Triphenyltin (TPT) is one of the organometallic endocrine disruptors that pollutes the natural environment with its worldwide use. Thus far, information on its recognition, combination and transformation by effective proteins is limited and needs to be revealed. To this end, TPT degradation, cellular ion metabolism and proteomics of *Bacillus thuringiensis* were investigated. TPT was successively transformed to diphenyltin, monophenyltin and tin. During this process,  $\text{Na}^+$ ,  $\text{NH}_4^+$ ,  $\text{Mg}^{2+}$  and  $\text{NO}_3^-$  were released. The results of two-dimensional gel electrophoresis verified that proteins with primary and secondary structures in IEF IPG-strip gels could recognize TPT and form complexes. The up-synthesis of ribosomal proteins associated with protein translation, acyl-CoA dehydrogenase related to fatty acid metabolism, and succinyl-CoA synthetase subunit beta, succinyl-CoA synthetase subunit alpha, ATP F0F1 synthase subunit alpha, glucose-6-phosphate isomerase and ferredoxin-NADP reductase involved in ATP synthesis were consistent with the results of the interaction between TPT and proteins in electrophoresis. This confirmed that effective proteins related to TPT transport, degradation and energy generation were also effective for TPT recognition even the active structures of these proteins were destroyed. The current findings developed a new approach for investigating interaction between proteins and target compounds, and presented a new insight into protein recognition of target compounds that the recognition by some effective proteins did not rely on their active quaternary structures.

## INTRODUCTION

Triphenyltin (TPT) is one of the endocrine disruptors that pollutes the natural environment with its worldwide use. Owing to its thermal stability, biodegradation is a major pathway accelerating the removal of TPT in the natural environments. Metabolite analysis has revealed its degradation pathway that TPT was initially triggered by benzene ring cleavage, which occurred individually and synchronously, producing diphenyltin (DPT), monophenyltin (MPT) and tin (Tang et al., 2016). Nevertheless, information concerning TPT binding and transformation by the effective proteins has remained scarce, which hinders the metabolic mediation of TPT biodegradation. To regulate TPT biodegradation and clarify the mechanism of TPT biosorption, transport and transformation, it is of critical importance to determine the relation among TPT recognition, TPT transformation and effective proteins.

As for protein identification, labeling-based mass spectrometry quantification technologies, including isotope-coded affinity tags, stable isotope labeling by amino acids in cell culture, and isobaric tag for relative and absolute quantification (iTRAQ), have been used to quantitatively analyze the proteomics in different organisms (Aebersold and Mann, 2003). To reveal the interaction between TPT and proteins at primary, secondary, tertiary and quaternary structures, both two-dimensional gel electrophoresis and iTRAQ technology were used to investigate the protein expression and identify the effective proteins involved in TPT recognition, transport and degradation in the current study.

Regarding the effective microbes for TPT degradation, *Bacillus thuringiensis* is a widespread species forming spore, which ensures the resistance of this species to a variety of stresses, including pollutant toxicity. The efficient degradation/transformation of some toxic xenobiotics, such as dimethyl phthalate (Brar et al., 2009), fipronil (Mandal et al., 2013) and uranium(VI) (Pan et al., 2015), by a portion of *B. thuringiensis* strains has been proved. A strain of this species isolated from organotins contaminated

sediment samples has also been confirmed that could effectively cleave the carbon-tin covalent bonds of organotins in our previous studies (Tang et al., 2016). Therefore, *B. thuringiensis* was selected in the current study to reveal the relation about the proteomics and TPT degradation.

## MATERIALS AND METHODS

**Materials.** *B. thuringiensis* GIMCC 1.817 was an effective strain for TPT degradation and was stored at the Microbiology Culture Centre of Guangdong Province. TPT was purchased from Sigma–Aldrich. The concentrations of  $\text{KH}_2\text{PO}_4$ , NaCl,  $\text{NH}_4\text{Cl}$ , and  $\text{MgSO}_4$  in the mineral salt medium (MSM) for TPT degradation were 30, 20, 30 and 10  $\text{mg L}^{-1}$ , respectively.

**TPT biotransformation.** Twenty microliters of MSM containing 1  $\text{mg L}^{-1}$  of TPT and 1  $\text{g L}^{-1}$  of cells were cultured in the dark on a rotary shaker at 130  $\text{r min}^{-1}$  for 24 h. After degradation, the cells were separated and washed using pure water for protein extraction.

**Protein preparation.** The cells were suspended in 1 mL lysis buffer added with 0.2  $\text{g L}^{-1}$  phenylmethylsulfonyl fluoride, 2% v/v IPG buffer, 0.6  $\text{g L}^{-1}$  DTT, and vibrated for 30 s. The samples were frozen in liquid nitrogen thrice for 15 min each time, and subsequently treated by ultrasonication for 20 min. Nucleasae was added to the lysate at a final concentration of 1%. After incubation at 4 °C for 30 min, the cell debris was removed at 4 °C by centrifugation at 13500  $\text{r min}^{-1}$ .

**Protein digestion, iTRAQ labeling and analysis.** Briefly, proteins from each sample were reduced with 10 mM DTT for 1 h at 37 °C. The cysteines were blocked with 1  $\mu\text{L}$  blocking reagent for 10 min at room temperature. The protein samples were added in 10 KD Amicon Ultra-0.5 centrifugal filter devices, followed by centrifugation at 12000  $\text{r min}^{-1}$  for 20 min. After removal the liquid, the samples in filter devices were digested by 50  $\mu\text{L}$  trypsin (Promega, V5280, USA) at 4% w/w overnight at 37°C. Subsequently, the samples were centrifuged, and 1  $\mu\text{g}$  trypsin was added to each filter for 2 h. After centrifugation, liquid in the collection tube was collected.

The tryptic peptides were labeled with iTRAQ reagent multiplex kit (Sigma, PN 4352135, USA) according to the manufacturer's instructions. Subsequently, the labeled peptides were dried in a vacuum concentrator. The samples were then resolved with solution containing 2% v/v CAN and 0.1% v/v formic acid, centrifuged at 12000  $\text{r min}^{-1}$  for 20 min, and detected by an AB Sciex TripleTOF 5600 mass spectrometer (AB Sciex, Framingham, MA, USA) equipped with a Nanospray III source.

**Two-dimensional gel electrophoresis.** Two-dimensional electrophoresis was performed to investigate the interaction between TPT and proteins with primary and secondary structures. After TPT degradation, the protein samples were diluted with hydration solution to the concentration of 400  $\text{g L}^{-1}$  added with 0.3  $\text{g L}^{-1}$  DTT, 0.5% v/v IPG buffer and 0.02% w/v bromophenol blue. The first dimension electrophoresis was conducted in isoelectric focusing (IEF) IPG-strip gels (13 cm, pH 4–7, GE Healthcare). Samples were first loaded by passive rehydration for 12 h. The IEF was run at 30 V for 12 h, 100 V for 1 h, 200 V for 1 h, 500 V for 1 h, 1000 V for 1 h, followed by a linear increase to and held at 8000 V until 32000 Vhr was obtained. Subsequently, the equilibrated strips were inserted on the top of 12.5% sodium dodecyl sulfate (SDS) separating polyacrylamide gel and covered with 0.5% w/v low melting point agarose. The gels were run in an electrophoresis system (Hoefer SE600, GE Healthcare) at a constant current of 5 mA  $\text{gel}^{-1}$  for 30 min, and then at 15 mA  $\text{gel}^{-1}$  until the marker dye reached the bottom of the gels. After in-gel digestion, the protein spots were identified.

## RESULTS AND DISCUSSION

**TPT Degradation.** To determine the dephenylation pathway, TPT, DPT and MPT at 1  $\text{mg L}^{-1}$  were degraded, respectively. Fig. 1a confirms that TPT was transformed to DPT and MPT, among which DPT

reached its maximal concentration of  $233 \mu\text{g L}^{-1}$  at 0.5 d, followed by an almost linear decline curve. This finding illustrates that the generated DPT was further degraded effectively. However, a little of MPT was produced at 0.5 d, which indicates that MPT transformation was a rapid process, or the degradation of TPT and DPT to MPT was a slow period. The PTs curve shows that  $107 \mu\text{g L}^{-1}$  of TPT was transformed to tin at this interval. These results confirm that MPT dephenylation was not a rate-limiting step in TPT degradation. The decreasing curve of DPT concentration over time accompanied with MPT accumulation at 2–4 d illustrates that TPT dearylation occurred successively (Fig. 1a). The concentration of DPT (Fig. 1b) was higher than that of MPT (Fig. 1c) in the entire degradation process.

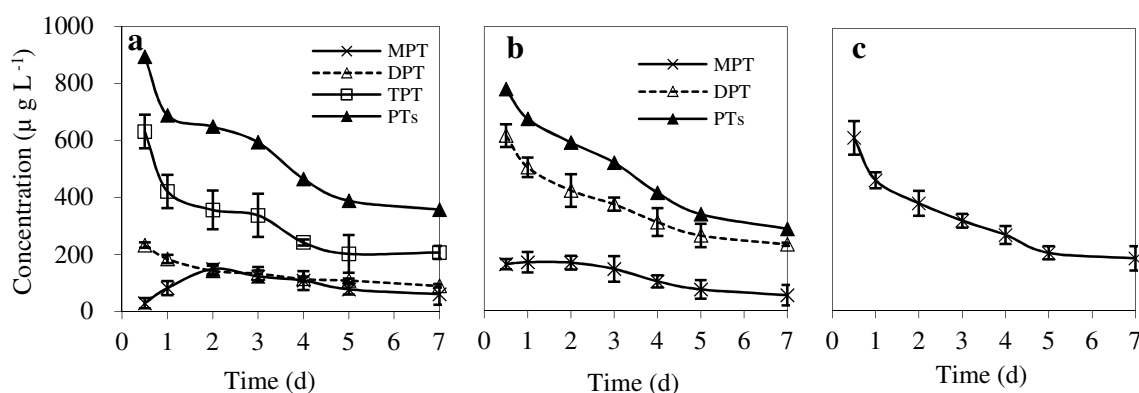


**Fig. 1** PT degradation by  $0.3 \text{ g L}^{-1}$  *B. thuringiensis* for 0.5–7 d. (a) TPT degradation and its metabolites, (b) DPT degradation and its metabolite, and (c) MPT degradation.

**Ion metabolism.** The negative and positive values of ion concentration shown in Fig. 2 represent ion assimilation and release, respectively.  $\text{Na}^+$ ,  $\text{NH}_4^+$ ,  $\text{Mg}^{2+}$ , and  $\text{NO}_3^-$  were released, whereas  $\text{K}^+$  and  $\text{PO}_4^{3-}$  were absorbed, but  $\text{Cl}^-$  varied between uptake and release during the TPT degradation process. TPT biodegradation is a metabolic process that is certainly related to ion transport. Ion metabolism is primarily attributed to ion channel transport, membrane alteration, ion exchange and cell metabolism. TPT can alter the membrane structure due to the interaction between TPT and membrane components, triggering cell permeability.  $\text{Na}^+$  is an essential cation for energy metabolism and ion homeostasis. Its flux is usually considered as a symbol of change in membrane permeability (Hite et al., 2015). Similar to ion exchange occurred during adsorbate binding (Ye et al. 2013), the release of  $\text{Mg}^{2+}$  and  $\text{Na}^+$  could balance the biosorption of PTs.

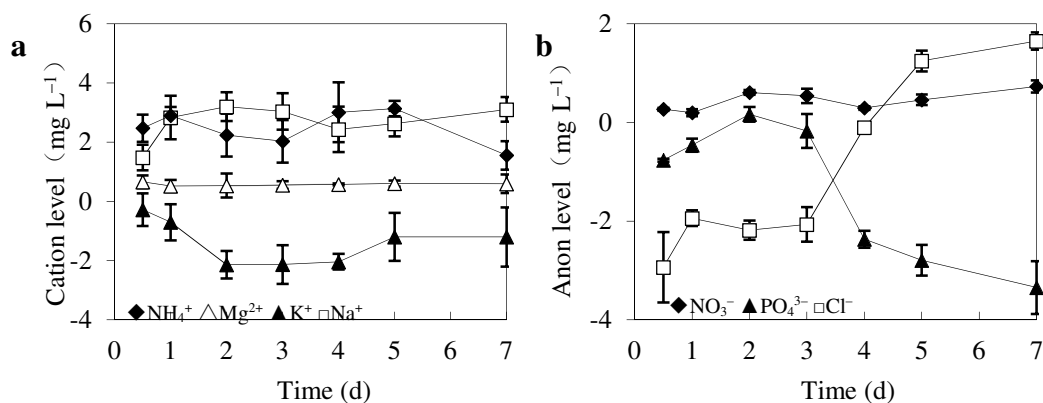


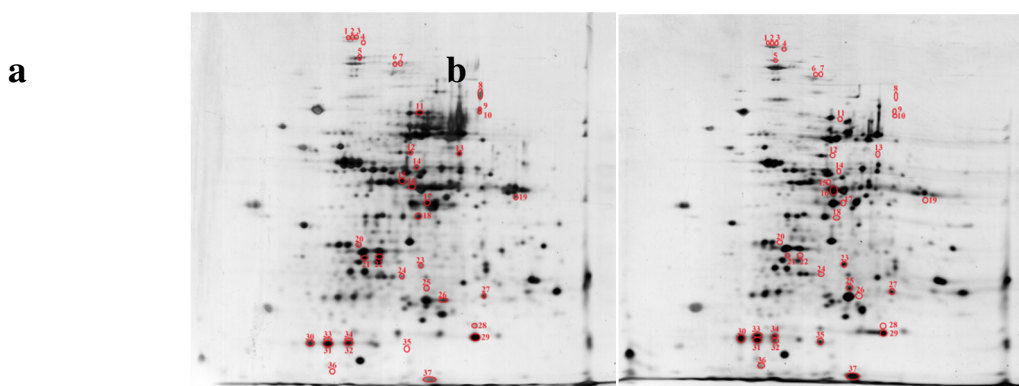
**Fig. 2** Change in (a) cation and (b) anion concentration in solution during degradation of  $1 \text{ mg L}^{-1}$  TPT by  $0.3 \text{ g L}^{-1}$  *B. thuringiensis*.



As a protein inhibitor, TPT depresses protein expression and triggers inactive protein degradation (D'Onofrio et al. 2013).  $\text{NH}_4^+$  is a common intracellular ion and a component of proteins. Its release is related to both rose membrane permeability and protein degradation.  $\text{NH}_4^+$  generated via protein and phospholipid photocatalysis was also gradually released by yeast (Thabet et al., 2013).

The accumulation of  $\text{K}^+$  and  $\text{PO}_4^{3-}$  might be related to their cellular functions (Fig. 2b).  $\text{K}^+$  is involved in various metabolic activities, and is transported by  $\text{Na}^+/\text{K}^+$ -ATPase in the opposite direction as  $\text{Na}^+$ .  $\text{PO}_4^{3-}$ , an important anion for metabolism in all forms of life, takes part in various metabolic processes. Therefore, high-energy phosphate conversion could account for  $\text{PO}_4^{3-}$  transport in the present study. The same direction of  $\text{K}^+$  and  $\text{PO}_4^{3-}$  flux during  $\text{PO}_4^{3-}$  uptake by *Leishmania infantum* is consistent with the current findings (Russo-Abrahão et al. 2013). These findings obviously confirmed that the exposure to TPT is the responsible cause contributing to the increased release of ions.

**Interaction between TPT and Proteins with Primary and Secondary Structures.** To determine whether TPT recognition depended on the active structures of proteins, TPT at  $1 \text{ mg L}^{-1}$  was added to the low melting point agarose. The immobilized nonlinear pH gradient strip separated proteins in the first dimension electrophoresis was located in front of this agarose. In contrast to proteins, TPT with small size in the migration process could move along the gel faster than the forward proteins. If a protein destroyed by the denaturing SDS-PAGE in the second dimension could recognize TPT, the generated complex would locate at different position in gel.



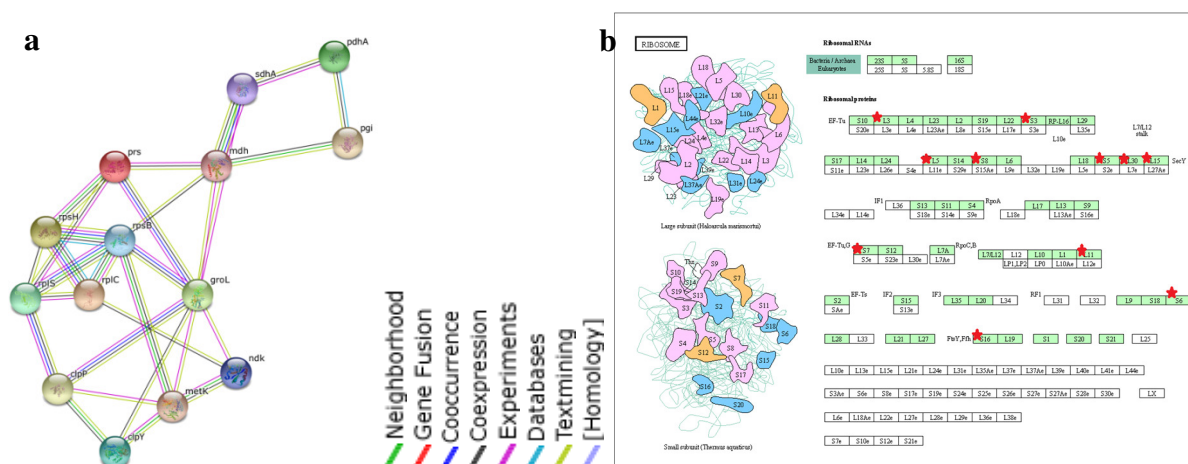
**Fig. 3** Interaction between TPT and inactive proteins during the vertical electrophoresis process. (a) control sample, and (b) experimental sample with TPT in a low melting point agarose gel.

Figure 3 exhibits that although the proteins in IEF IPG-strip gels were at inactive conditions, some of them in the 2-D electrophoresis process could recognize and combine with TPT, which revealed that pollutant recognition by some effective proteins did not rely on the active quaternary structures of proteins. The finding presents a new insight into protein recognition of target compounds. Protein identification and function category indicates that those proteins were primarily related to antioxidant defense (superoxide dismutase) and endogenous toxin transformation (glyoxalase), fatty acid metabolism and oxidation (propionyl-CoA carboxylase, enoyl-CoA hydratase, electron transfer flavoprotein subunit alpha), protein synthesis (amidotransferase, elongation factor Tu) and hydrolysis (ATP-dependent Clp protease), purine, nucleotide and fructose biosynthesis (adenylosuccinate synthase, ribose-phosphate pyrophosphokinase 1, fructose-bisphosphate aldolase). These results also infer that TPT degradation process tended to trigger the different expression of proteins associated with protein synthesis, pollutant degradation, membrane change and ATP synthesis.

**Interaction between TPT and active proteins.** The iTRAQ results show that 32 and 21 proteins were up- and down-regulated expression after TPT degradation. Among the up-regulation proteins, 14 of them enriched in a network with various functions (Fig. 4a), including biosynthetic process (GO:0009058),

generation of precursor metabolites and energy (GO:0006091), nitrogen compound metabolic process (GO:0006807), phosphate-containing compound metabolic process (GO:0006796), primary metabolic process (GO:0044238) and cellular process (GO:0009987).

The coexistence of ribosomal proteins RpsB, RpsH, RplC and RPlS associated with protein translation (Fig. 4b); and the up-synthesis of acyl-CoA dehydrogenase related to fatty acid metabolism; and the up-expression of succinyl-CoA synthetase subunit beta, succinyl-CoA synthetase subunit alpha, ATP FOF1 synthase subunit alpha, glucose-6-phosphate isomerase and ferredoxin-NADP reductase involved in ATP synthesis were consistent with the results of the interaction between TPT and proteins in two-dimensional gel electrophoresis, which confirmed that effective proteins related to TPT transport, degradation and energy generation were also effective for TPT recognition even the active structures of these proteins were destroyed by sodium dodecyl sulfate along with other reagents. Regarding the down-regulated synthesis proteins, none of them enriched in interaction network indicated that TPT degradation did not trigger significant inhibitory effects on cellular activities.



**Fig. 4 (a)** Network of up-regulation proteins after TPT degradation, and **(b)** ribosomal proteins mapped onto KEGG pathway.

## CONCLUSIONS

TPT degradation process tended to trigger different expression of proteins associated with protein synthesis, pollutant degradation, membrane change and ATP synthesis. Effective proteins related to TPT transport, degradation and energy generation could recognize TPT, even their active structures were destroyed. The current findings developed a new approach for investigating the interaction between proteins and target compounds, and presented a new insight into protein recognition of target compounds that the recognition by some effective proteins did not rely on their active structures.

## ACKNOWLEDGEMENTS

This research was supported by the National Natural Science Foundation of China (Nos. 21377047, 21577049), and the Science and Technology Project of Guangdong Province (No. 2014A020216013).

## REFERENCES

- Aebersold, R., and M. Mann. 2003. "Mass spectrometry-based proteomics." *Nature* 422:198-207.
- Brar, S.K., M. Verma. R.D. Tyagi. J.R. Valéro, and R.Y. Surampalli. 2009. "Concurrent degradation of dimethyl phthalate (DMP) during production of *Bacillus thuringiensis* based biopesticides." *J. Hazard. Mater.* 171, 1016-1023.
- Hite, R.K., P. Yuan, Z.L. Li, Y.C. Hsuing, T. Walz, and R. MacKinnon. 2015. "Cryo-electron microscopy structure of the Slo2.2 Na<sup>+</sup>-activated K<sup>+</sup> channel." *Nature* 527: 198-203.

- Mandal, K., B. Singh, M. Jariyal, and V.K. Gupta. 2013. "Microbial degradation of fipronil by *Bacillus thuringiensis*." *Ecotox. Environ. Safe.* 93: 87–92.
- Pan, X.H., Z. Chen, F.B. Chen, Y.J. Cheng, Z. Lin, and X. Guan. 2015. "The mechanism of uranium transformation from U(VI) into nano-uramphite by two indigenous *Bacillus thuringiensis* strains." *J. Hazard. Mater.* 297: 313–319.
- Russo-Abrahão, T., M. Alves-Bezerra, D. Majerowicz, A.L. Freitas-Mesquita, C.F. Dick, K.C. Gondim, J.R. Meyer-Fernandes. 2013. "Transport of inorganic phosphate in *Leishmania infantum* and compensatory regulation at low inorganic phosphate concentration." *BBA-Gen. Subjects* 1830, 2683–2689.
- Tang, L.T., L.L. Wang, H.S. Ou, Q.S. Li, J.S. Ye, and H. Yin. 2016. "Correlation among phenyltins molecular properties, degradation and cellular influences on *Bacillus thuringiensis* in the presence of biosurfactant." *Biochem. Eng. J.* 105: 71–79.
- Thabet, S., M. Weiss-Gayet, F. Dappozze, P. Cotton, and C. Guillard. 2013. "Photocatalysis on yeast cells: toward targets and mechanisms." *Appl. Catal. B–Environ.* 140–141: 169–178.
- Ye, J.S., H. Yin, D.P. Xie, H. Peng, J. Huang, and W.Y. Liang. 2013. "Copper biosorption and ions release by *Stenotrophomonas maltophilia* in the presence of benzo[a]pyrene." *Chem. Eng. J.* 219: 1–9.

**BACTERIAL COMMUNITY STRUCTURE CORRESPONDS TO PERFORMANCE IN A  
MICROAEROPHILIC SULFATE AND NITRATE CO-REDUCTION SYSTEM**

Xi-Jun Xu, **Chuan Chen**, Ai-Jie Wang, Duu-Jong Lee, and Nan-Qi Ren  
(Harbin Institute of Technology, Harbin, Heilongjiang, China)

The succession of complex internal sulfur cycles and sulfide-oxidizing bacteria community has been observed during wastewater treatment under microaerophilic conditions or denitrifying conditions. However, current knowledge of the microbial ecology and physiology of sulfur cycles under microaerophilic denitrifying conditions is scarce, and as a result more research dedicated to understand the microbial community is required. Here we characterized the microbiology of bacterial communities stimulated by microaerophilic conditions. The results of our study indicated the superior performance of the microaerophilic reactor in terms of enhanced sulfur production and COD removal rates. We hypothesized that phylogenetic or structural features of the microbial communities could explain the enhanced performance of the microaerophilic reactor. We used Illumina sequencing with 16S rRNA gene to characterize the bacterial communities and identified *Bacteroidetes*, *Firmicutes*, *Proteobacteria*, *Spirochaetae* and *Synergistetes* members that were dominant in microbial communities. Specifically, our study revealed that it was the structural component, in terms of bacterial richness and evenness, rather than the phylogenetic affiliation of dominant bacteria, that best corresponds to reactor performance.

**A NEW AHL MOLECULE GENERATED BY NITRITE-OXIDIZING BACTERIA.**

**Jie Gao** and Guoqiang Zhuang

(Research Center for Eco-Environmental Sciences, Chinese Academy of Sciences, Beijing, China)

Revealing regulatory mechanism of nitrification is a crucial step to understand nitrogen conversion in agricultural systems and wastewater treatment. In this study, the gene *nwiI* of *Nitrobacter* was confirmed to be a homoserine lactone synthase by heterologous expression in *Escherichia coli*, which synthesized several acyl-homoserine lactone signals with 7 to 11 carbon acyl groups. A novel signal 7, 8-*trans*-N-(decanoyl) homoserine lactone (C10:1-HSL) was identified both in *Nitrobacter* and the recombined *E. coli*. Furthermore, this novel signal also triggered variance in nitrification rate and transcriptional level of genes involved in nitrification process. These results indicate that quorum sensing may play a potential role in nitrogen metabolism regulation.

## EVIDENCE OF QUORUM QUENCHING AND INHIBITION OF BIOFILM FORMATION IN *Sphingomonas Spp*

**Parul Gulati** and Moushumi Ghosh

(Department of Biotechnology, Thapar University, Patiala-147004, Punjab, India)

*Sphingomonas* spp. is ubiquitous in the environment and can be frequently found in drinking water. Their amazing metabolic diversity, ability to survive in low nutrient conditions and oligotrophic niches qualifies its prevalence and biofilm formation. Recent reports indicate the biofilm forming capability of *Sphingomonas* in water distribution systems and therefore a hazard for human health necessitating intervention/controls. The purpose of this work was to obtain a polymeric material as a potential quorum quencher as a new strategy to control biofilm formation, through interference with the communication system. In the present study, we isolated 140 isolates of *Sphingomonas* spp. from twenty diverse municipal drinking water sites and characterized those capable of biofilm formation. Screenings of isolates were carried out by examining them on *Sphingomonas*- specific growth medium containing 100 and 50- µg/ml streptomycin and piperacillin, respectively. In addition, two sets of PCR primers targeting serine palmitoyl transferase gene (spt) were used (Yim *et al*, 2010). Growth and biofilm profiles of the positive isolate along with standard *Sphingomonas* strains were determined. N-acyl homoserine lactone (AHL) biosensors *Chromobacterium violaceum* CV026 and *Agrobacterium tumefaciens* A136 were used for detection of quorum sensing in *Sphingomonas* sp. For inhibition of quorum sensing, sublethal concentrations of quarternized polymer and standard 4-Nitropyridine -N-oxide were determined and used subsequently for quorum quenching studies. Results of our study suggest a potential of biofilm blocking by using the novel polymeric material and a possibility to further this approach for controlling *Sphingomonas* biofilms in drinking water systems.

## **IDENTIFICATION OF FUNGAL ENDOPHYTES FROM MAIZE SHOOTS WITH BIOTECHNOLOGICAL POTENTIAL IN AGRICULTURE**

Mashiane R.A and *Adeleke R.A*

(Agricultural Research Council, Pretoria, Gauteng, SA)

Bezuidenhout C.C

(North-West University-Potchefstroom campus, Potchefstroom, North-West, SA)

Plant-microbe interaction plays an important role in plant health and development. Studies have indicated that almost all plants host endosymbionts. Therefore, a better understanding of endophytic fungi in maize may help to elucidate their function and potential roles more effectively in developing sustainable systems of crop production.

Our study investigated fungal endophytes associated with transgenic and non-transgenic maize shoots. Fungi were isolated from stem, leaves, tassels and seeds of both transgenic MON810 (expressing cry1Ab proteins) and non-transgenic isogenic maize lines. The fungal isolates were characterised based on sequence analysis of the internally transcribed spacer (ITS) region. This survey further allowed us to identify candidate endophytes for introduction into commercial maize cultivars for biomass enhancement.

A total of 21 and 27 isolates were obtained from transgenic Bt maize and non-transgenic isogenic maize, respectively. The fungal diversity of Bt maize did not differ significantly from that of non-transgenic maize. Taxonomically, species of the genera *Epicoccum*, *Fusarium*, *Phoma*, *Alternaria* and *Nigrospora* were common to both maize lines. Species of the genera *Ampelomyces*, *Cladosporium*, *Pithomyces*, *Mucor* and *Acremonium* were uniquely associated with Bt maize while *Chaetomium*, *Peyronellaea* and *Trichoderma* with non-Bt maize. The most frequently isolated group were *Fusarium* from the tassels, *Epicoccum* and *Alternaria* from the leaves.

The abundance of taxa in the shoots were assigned to the order Hypocreales to which mutualistic clavicipitaceous endophytes of grasses belong, suggesting great potential for utilising these endophytes for enhancing biomass production of this important agricultural crop.

**PECTINASE FROM *BACILLUS SUBTILIS* STRAIN BTK-27: OPTIMIZATION OF CULTURAL CONDITIONS AND APPLICATION IN COFFEE PROCESSING**

*Oliyad Jeilu Oumer* (Ambo University, Ambo, Ethiopia)  
Dawit Abate (Addis Ababa University, Addis Ababa, Ethiopia)

The demand for enzymes in the global market is projected to rise at a fast pace in recent years. There has been a great increase in industrial applications of pectinase owing to their significant biotechnological uses. For this reason, this study was undertaken with aims of; isolating and screening microorganisms from coffee pulp, molecular identification of the potential pectinolytic isolates and optimizing pectinase production both on submerged fermentation and solid state fermentation. Moreover, characterizing the enzyme and proving its potential application in demucilisation of coffee. In the present investigation 95 isolates were isolated and screened for their pectinolytic activity from coffee pulp samples. The isolates with high potential pectinase activity were identified molecularly by sequencing 16s rDNA region of the isolates. The bacterium, *Bacillus subtilis* strain Btk27 was selected for production optimization of the enzyme based on its outstanding features. The production of pectinase was enhanced by 656% (in YEP) and 159% (in wheat bran) times on submerged fermentation and solid state fermentation, respectively. In addition, optimization steps were carried out to make the production of pectinase enzyme cost effective and commercially viable. The maximum pectinase production was observed using YEP (submerged fermentation) and Wheat bran (solid state fermentation) at initial pH of 6.5, at 37°C and by supplementing the medium with 3mM MgSO<sub>4</sub>·7H<sub>2</sub>O. The maximum Pectinase activity was achieved at pH 7.5 and 50°C. Also, the enzyme activity was found stimulated with Mg<sup>2+</sup> and Ca<sup>2+</sup> metal ions. Moreover, it was stable on EDTA, Triton-100, Tween 80 and Tween 20. The enzyme, K<sub>m</sub> and V<sub>max</sub> values were identified as 1.879mg/ml and 149.6 U respectively. The potential application of the enzyme for coffee processing was studied, and it is found that complete removal of mucilage from coffee beans within 24 hours of treatment indicating the potential application in coffee processing.



